Use of Physiologically-Based Pharmacokinetic Modelling To Support Dose Optimization in The Critically Ill

by

Samuel Dubinsky

A thesis
presented to the University of Waterloo
in fulfillment of the
thesis requirement for the degree of
Doctor of Philosophy
in
Pharmacy

Waterloo, Ontario, Canada, 2024

© Samuel Dubinsky, 2024

Examining Committee Membership

The following served on the Examining Committee for this thesis. The decision of the Examining Committee is by majority vote.

External Examiner	MARC SCHEETZ Associate Dean of Research, Midwestern University, College of Pharmacy
Supervisor	ANDREA N. EDGINTON Professor and Hallman Director, University of Waterloo School of Pharmacy
Internal Members	KEVIN M. WATT Adjunct Professor, University of Waterloo School of Pharmacy Professor, Division of Critical Care Medicine Department of Pediatrics Spencer Fox Eccles, School of Medicine University of Utah
	MICHAEL A. BEAZELY Professor, University of Waterloo School of Pharmacy
Internal-External Member	ELIZABETH IRVING Professor, University of Waterloo School of Optometry and Vision Science

Author’s Declaration

This thesis consists of material all of which I authored or co-authored: see Statement of Contributions included in the thesis. This is a true copy of the thesis, including any required final revisions, as accepted by my examiners.

I understand that my thesis may be made electronically available to the public.

Statement of Contributions

Samuel Dubinsky was the sole author of Chapters 1 and 8, which were written under the supervision of Dr. Andrea Edginton and were not written for publication.

This thesis consists in part of six manuscripts written for publication. Exceptions to sole authorship of material are as follows:

Research presented in Chapter 2:

Samuel Dubinsky conceptualized the idea and topic of this research under the supervision of Dr. Andrea Edginton and Dr. Kevin Watt. All research incorporated within this Chapter was conducted at the University of Waterloo. With help from Caitlin Carter, an initial search strategy was constructed. Steven Saleeb and Bilal Ahmed provided first-level and second-level screenings of included studies. Samuel Dubinsky provided resolution of any discrepancies from the independent screen. Cindy Yeung was consulted for assistance with methodology and review of final manuscript. The final version of this manuscript was reviewed by all authors.

Research presented in Chapter 3:

Samuel Dubinsky conceptualized the topic for this manuscript under the supervision of Dr. Andrea Edginton and Dr. Paul Malik. With assistance from Dr. Paul Malik, Samuel Dubinsky developed the healthy adult PBPK models for each investigative drug incorporated within this manuscript. Samuel Dubinsky conducted the CKD-PBPK model simulations and analyzed the results. Dr. Dagmar Hajducek was consulted for statistical analysis used to develop the OAT parameterization. The final version of the manuscript was written by Samuel Dubinsky, with approval from all authors. Contributions from Dr. Paul Malik were final as of June 11, 2021.

Research presented in Chapter 4, 5 and 6:

Dr. Kevin Watt is the primary investigator of a National Institute of Health (NIH) grant (R01HD097775) which supported conducting this work. With assistance from Carina Imburgia, Dr. Autumn McKnite, and Dr. Porter Hunt, Samuel Dubinsky performed the experiments while interpreting the analytical results. Dr. Joseph Rower and Dr. Cassandra Rice performed the drug analysis for anakinra and cefazolin. Dr. Autumn McKnite and Dr. Porter Hunt were instrumental in the construction of the anakinra PBPK model used throughout Chapter 6. Samuel Dubinsky wrote the final version of each manuscript, with review and approval being obtained from each author.

Research presenting in Chapter 7:

Samuel Dubinsky conceptualized the idea for this manuscript under the supervision of Dr. Andrea Edginton, with consultation from Dr. Mark McIntyre. Cefazolin model construction and validation was performed by Samuel Dubinsky under the supervision of Dr. Andrea Edginton. All authors approved final version of the manuscript written by Samuel Dubinsky.

Abstract

Critical care is a subspeciality of medicine that incorporates a multidisciplinary approach for patient care in a heterogeneous population. The wide array of etiologies to critical illness may result in disturbances to homeostasis and organ function. This variability in host-response may impact the pharmacokinetics (PK) of an individual, resulting in potential differences in drug exposure compared to a healthy counterpart. The high mortality rates of critically ill patients are thought in part to be due to altered drug exposure, resulting in suboptimal dosing or adverse effects.

The complexity and heterogeneity of critical illness limits the feasibility of conventional PK studies for dose determination in this population. Furthermore, current "one-dose-fits-all" approaches in pharmacotherapy overlook the interplay between drug physicochemical properties and pathophysiology towards altered PK in the critically ill. Methods incorporating pharmacometrics have advanced our understanding of this relationship, however current approaches may require robust data sets to inform dose-exposure relationships and limit extrapolations to untested clinical scenarios.

Methods incorporating physiologically-based pharmacokinetic (PBPK) modelling are encouraging to overcome some of the current challenges and knowledge gaps towards optimizing drug therapy in critically ill patients. PBPK models leverage mechanistic principles to incorporate knowledge of physiology and drug physicochemical properties to provide a simulation-based approach to drug PK. Knowledge of drug PK and physiology in healthy adults may be adjusted to account for differences in age (i.e adults to children), or disease (i.e. critical illness), to predict drug exposure. As these methods leverage known prior information, it enables a more proactive approach in predicting drug PK in clinical settings when data sampling is sparse, such as the critically ill.

This thesis aims to apply state-of-the-art mechanistic modelling strategies to advance pharmacotherapy in critically ill adults and in children receiving extracorporeal life-saving technology. The objectives are to (1) analyze the PK data in critically ill children receiving continuous renal replacement therapy (CRRT), (2) evaluate the extraction of drugs via CRRT utilizing a closed-loop *ex-vivo* study design, and (3) develop PBPK models to optimize drug

dosing in various presentations of critical illness. The first objective included a systematic review to evaluate our current understanding of drug PK in critically ill children receiving CRRT. Several knowledge gaps were identified, which were to be addressed within the second objective by incorporating a closed-loop study design to isolate the drug-CRRT circuit interaction. This *ex-vivo* approach was the first of the holistic methodological solution towards which this thesis aims to achieve. Knowledge gained from the *ex-vivo* studies may be integrated into a PBPK model structure to provide a mechanistic understanding of drug PK, allowing for prospective dose predictions in untested scenarios.

Within this work, it was identified that 40% of PK studies conducted in critically ill children receiving CRRT focused on antimicrobials. Furthermore, only 50% of studies included in the final analysis provided dosing guidance based upon PK findings in this population, representing several knowledge gaps to support clinicians in dosing guidance at the bedside. Anakinra and cefazolin were targeted as drugs of need for dosing guidance in patients receiving CRRT. *Ex-vivo* studies were conducted to investigate the drug-circuit interaction. Both anakinra and cefazolin, were efficiently removed from plasma upon the completion of the experiment, rendering a sieving coefficient of 0.34 and 0.31, respectively. A PBPK model for anakinra was developed to predict the PK in children receiving concurrent CRRT and extracorporeal membrane oxygenation (ECMO). Upon applying the results from the *ex-vivo* experiment, PBPK model predictions successfully described anakinra PK amongst critically ill children enrolled in a prospective, opportunistic study. Overall anakinra exposure was similar amongst children receiving ECLS compared to those who are not, supporting the hypothesis that renal dose adjustments in this population may not be required.

The work herein this thesis seeks to advance the application of PBPK in supporting pharmacotherapy to a diverse group of critically ill patients. In doing so, a mechanistic representation of cefazolin drug concentrations in the central nervous system (CNS) through PBPK was performed. Cefazolin cerebrospinal fluid (CSF) concentrations were accurately predicted, and simulated CSF:plasma ratios fell within a 1.5 fold-error compared to observed values. Dosing simulations demonstrate that a continuous infusion of 10 g/day may be required to achieve pharmacodynamic response towards methicillin-susceptible Staphylococcus *aureus* in treating infections in the CNS.

This thesis aims to articulate the multiplicity of PBPK to support dosing guidance in the critical care setting. Several knowledge gaps were identified, and the methods applied aim to address some of the current limitations of conventional PK studies in this population. PBPK modelling efforts such as these have the potential to improve generalizability, and efficiently conduct PK studies in a highly vulnerable patient population by reducing the number of participants required and applying a more proactive approach to dose determination in untested clinical scenarios.

Acknowledgements

I would like to acknowledge my supervisor, Dr. Andrea Edginton, for all her support and guidance throughout the years. Under her tutelage, I have diversified my skillset through teachings in theoretical concepts and practical application in advanced pharmacokinetics. Dr. Edginton has provided mentorship towards problem-solving and leadership, all of which will be pivotal during the next chapter of my career. Thank you for all your support.

To my Thesis Committee Members, Dr. Kevin Watt and Dr. Michael Beazely, your guidance and knowledge towards this thesis has been of paramount importance. Throughout this process you have challenged me to expand my methodological approach and analytical reasoning. For this, you have strengthened my skills that will enable me to become an independent researcher. I am forever grateful and eager to continue our professional relationship.

During my thesis I was fortunate enough to research abroad at the University of Utah, in Salt Lake City. On this visit, Dr. Kevin Watt and his research lab showed the utmost gratitude and support towards my research objectives. I specifically want to acknowledge, Dr. Autumn McKnite, Dr. Rachel Hudson, Dr. Porter Hunt, and Carina Imburgia for the assistance and long hours spent in the lab. I began this excursion meeting new colleagues and left with life-long friendships. Much of the work throughout this thesis would not have come to fruition without their support.

Finally, I would like to acknowledge past lab members, Dr. Paul Malik, Dr. Jacky Yu, and Dr. Cindy Yeung, and current lab members, Dr. Dagmar Hajducek, Dr. Abdullah Hamadeh, Dr. Pierre Chelle, Dr. Min-Soo Kim, Samantha Hirniak and Shirley Wang. Each of them has supported me throughout my graduate career. My sincerest gratitude goes to you all.

Dedication

I would like to dedicate this thesis to my wife, Jenny, for her love, support and patience over the past few years. When I proposed pursuing a PhD., as any Antimicrobial Stewardship Pharmacist would respond, Jenny said to me “as long as you focus on antimicrobials”. A simple enough request for me to uphold for what we were about to experience together over the next four years.

Jenny has always seen my potential, and the confidence she has instilled in me has motivated me to pursue goals that I thought were otherwise unachievable. As she navigates her own successful career, her support has remained constant throughout my academic journey. This quest towards achieving my PhD. is not possible without her.

Table of Contents

Examining Committee Membership ii
Author's Declaration iii
Statement of Contributions iiiv
Abstract vi
Acknowledgements ix
Dedication x
List of Figures xviii
List of Tables xxiii
List of Abbreviations xxv
Chapter 1: Background 1
1.1 Critical Care Medicine 1
1.1.2 Pediatric Critical Care 2
1.2 Pharmacokinetic Changes Due to Critical Illness 2
1.2.1 Absorption 3
1.2.2 Volume of Distribution 4
1.2.3 Clearance 5
1.2.4 Pathophysiological Changes 7
1.3 Extracorporeal Therapy 11
1.3.1 Continuous Renal Replacement Therapy 11
1.3.2 Pharmacokinetic Alterations in Patients Receiving Continuous Renal Replacement Therapy 14
1.3.3 Extracorporeal Membrane Oxygenation 18
1.4 Determining Drug Dosing on Extracorporeal Life-Support 19
1.4.1 Physiologically-Based Pharmacokinetic Modelling 20
1.5 Aim, Objectives, and Hypothesis 22
1.5.1 Objective 1: Analyze the Pharmacokinetic Data in Critically Ill Children Receiving Continuous Renal Replacement Therapy 22
1.5.2 Objective 2: Evaluate the Continuous Renal Replacement Therapy Extraction of Drugs *Ex-vivo* 22
1.5.3 Objective 3: Develop Physiologically-Based Pharmacokinetic Models to Optimize Drug Dosing in The Critically Ill 23

Chapter 2: Pharmacokinetics of commonly used mediations in children receiving continuous renal replacement therapy: a systematic review of current literature 24
2.1 Overview 25
2.2 Introduction 26
2.2 Methods 28
2.2.1 Search Strategy 28
2.2.2 Study Selection 28
2.2.3 Data Extraction 29
2.2.4 Quality Assessment 30
3. Results 30
3.1 Characteristics of Included Studies and Study Population 30
3.1.2 Quality Assessment 40
3.1.3 Alterations in Pharmacokinetic Parameters 40
3.1.4 Ex-vivo Studies 57
2.3 Discussion 84
2.4 Conclusion 87
Chapter 3: Determining the Effects of Chronic Kidney Disease on Organic Anion Transporter 1/3 Activity Through Physiologically-Based Pharmacokinetic Modelling 89
3.1 Overview 90
3.2 Introduction 91
3.3 Methods 92
3.3.1 Software 92
3.3.2 PBPK Models for Healthy Adults 93
3.3.3 PBPK Models for Chronic Kidney Disease 96
3.3.4 Organic Anion Transporter Parameterization 97
3.3.5 Non-Renal Clearance in CKD 98
3.3.6 Sensitivity Analysis 98
3.4 Results 99
3.4.1 PBPK Models for Healthy Adults 99
3.4.2 PBPK Models for Chronic Kidney Disease 100
3.4.3 Sensitivity Analysis 107
3.4. Discussion 108
3.5 Conclusion 112
Chapter 4: Anakinra Removal by Continuous Renal Replacement Therapy: An Ex-vivo Analysis 114

4.1 Overview 115
4.2 Introduction 116
4.2 Materials Methods 118
4.2.1 Institutional Review Board 118
4.2.2 Circuit Configuration 118
4.3.3 Continuous Renal Replacement Therapy Circuit Setup 119
4.3.4 Control Setup 120
4.3.5 Drug Administration and Sample Collection 120
4.3.6 Drug Analysis 121
4.3.7 Statistical Analysis 123
4.3 Results 123
4.3.1 CVVH Circuit 123
4.3.2 CVVHD Circuit 124
4.3.3 CVVHDF Circuit 124
4.4 Discussion 126
4.5 Conclusion 130
Chapter 5: Cefazolin Removal via Pediatric Continuous Renal Replacement Therapy: An Ex-vivo Analysis 131
5.1 Overview 132
5.2 Introduction 132
5.3 Materials and Methods 133
5.3.1 Circuit Configuration 133
5.3.2 Continuous Renal Replacement Therapy Circuit Setup 134
5.3.3 Control Setup 135
5.3.4 Drug Administration and Sample Collection 135
5.3.5 Drug Analysis 136
5.3.6 Statistical Analysis 138
5.4 Results 138
5.5 Discussion 140
5.6 Conclusion 143
Chapter 6: Physiologically-Based Pharmacokinetic Modelling in Critically Ill Children Receiving Anakinra While on Extracorporeal Life Support 145
6.1 Overview 146
6.2 Introduction 147

6.3 Methods 148
6.3.1 Software 148
6.3.2 Model Building Workflow 149
6.3.3 Adult PBPK Model 151
6.3.4 Pediatric PBPK Model 152
6.3.5 ECLS-PBPK Model 153
6.3.6 Dosing Simulations 154
6.3.7 PBPK Model Acceptance Criteria 155
6.4 Results 156
6.4.1 Adult IV PBPK Model 156
6.4.2 Adult Subcutaneous PBPK Model 157
6.4.3 Pediatric Subcutaneous PBPK Model 158
6.4.4 ECLS-PBPK Model 160
6.4.5 Dosing Simulations 162
6.5 Discussion 164
6.6 Conclusion 168
Chapter 7: Defining safe and effective cefazolin dosing regimens for MSSA infections in the CNS: leveraging sparse real-world data and PBPK modeling 169
7.1 Overview 170
7.2 Introduction 171
7.3 Methods 172
7.3.1 Software 172
7.3.2 Healthy Adult Cefazolin PBPK Model Development 173
7.3.3 Healthy Adult Cefazolin PBPK Model Evaluation 173
7.3.4 Adult Cefazolin CSF-PBPK Model Development 173
7.3.5 Adult Cefazolin CSF-PBPK Model Evaluation 174
7.3.6 Dose-Exposure Assessment 175
7.3.7 Safety Assessment 176
7.4 Results 176
7.4.1 Healthy Adult Cefazolin PBPK Model Evaluation 176
7.4.2 Adult Cefazolin CSF-PBPK Model Evaluation 177
7.4.3 Dose-Exposure Assessment 179
7.4.4 Safety Assessment 181

7.5 Discussion 184
7.6 Conclusion 187
Chapter 8: Discussion, Conclusions, and Future Directions 189
8.1 Discussion 189
8.2 Conclusion 196
8.3 Future Directions 197
Letters of Copyright Permission 201
References 214
Appendix A 267
1. Search Strategy 267
2. ClinPK Checklist 268
Appendix B 271
1. Building a Physiologically-Based Pharmacokinetic Model for Meropenem in Healthy Adults 271
1.1 Introduction 271
1.2 Methods and Results 271
1.2.1 Modelling Strategy 271
1.2.2 Intravenous model construction 272
1.2.3 Intravenous Model Verification 274
1.2.4 Population Verification 275
1.3 Discussion and Conclusion 276
1.4 Figures 277
2. Building a Physiologically-Based Pharmacokinetic Model for Acyclovir in Healthy Adults 283
2.1 Introduction 283
2.2 Methods and Results 283
2.2.1 Modelling Strategy 283
2.2.2 Intravenous Model Construction 283
2.2.3 Intravenous Model Verification 286
2.2.4 Population Verification 287
2.3 Discussion and Conclusion 288
2.4 Figures 288
3. Building a Physiologically-Based Pharmacokinetic Model for Ciprofloxacin in Healthy Adults 291
3.1 Introduction 291
3.2 Methods and Results 291

3.2.1 Modelling Strategy 291
3.2.2 Intravenous Model Construction 291
3.2.3 Intravenous Model Verification 294
3.2.4 Population Verification 294
3.3 Discussion and Conclusion 295
3.4 Figures 296
4. Clinical Studies Incorporated in the CKD-PBPK Model Validation 299
4.1 Ciprofloxacin 299
4.2 Acyclovir 299
4.3 Meropenem 300
4.4 Furosemide 300
5. Chapter 3 Appendix Figures 301
Appendix C 303
1. Supplementary Figures 303
2. Supplementary Tables 306
Appendix D 308
1. Supplementary Figures 308
2. Supplementary Tables 310
Appendix E 311
1. Building a PBPK Model for Intravenous Anakinra in Healthy Adults 311
1.1 Introduction 311
1.2. Methods and Results 312
1.3. Figures 317
2. Building a PBPK Model for Subcutaneous Anakinra in Healthy Adults 321
2.1 Introduction 321
2.2 Methods and Results 321
2.3 Figures 325
3. Building a PBPK Model for Anakinra in Adults with Chronic Kidney Disease 327
3.1 Introduction 327
3.2 Methods and Results 327
3.3 Figures 332
4. Supplementary Figures 335
Appendix F 340

1. Building a PBPK Model for Cefazolin in Healthy Adults 340
1.1 Introduction 340
1.2 Methods and Results 340
1.3 Figures 349
2. Building a PBPK Model for Cefazolin Cerebrospinal Fluid Concentrations 353
2.1 Introduction 353
2.2 Methods and Results 353
2.3 Results and Discussion 355
2.4 Figures 357
3. Additional Figures 359

List of Figures

Figure 1-1. Whole-body physiologically-based pharmacokinetic (PBPK) model adapted from Edginton et al. [149] Each organ (15) is connected by two blood compartments to represent an anatomical arrangement. The arrows between compartments mathematically described drug disposition through ordinary differential equations. 21

Figure 2-1. Preferred Reporting Items for Systematic Review and Meta-Analyses (PRISMA) diagram of included studies. 31

Figure 3-1. Parameterization of organic anion transporter 1and 3 functionality across varying stages of chronic kidney disease. Data investigating the relationship between *p*-aminohippuric acid extraction ratio (EPAH) and estimated GFR (eGFR) was extracted from several studies (black dots). [318–323] A Weibull function (blue-line) was determined to be the best representation of the relationship between EPAH and eGFR. 98

Figure 3-2. Simulated physiologically-based pharmacokinetic drug-drug interaction plasma concentration-time profiles after optimization compared to observed data for (A) furosemide, (B) ciprofloxacin, (C) acyclovir, and (D) meropenem. Observed data presented as mean (circles) with standard error of the mean (error bars) for each respective study. [296,297,327,328] The blue line represents the same dose of investigative drug administered after completion of probenecid dosing protocols. Details on dosing regimen and study populations may be found in each respective Appendix file (B1-3). 100

Figure 3-3. Simulated chronic kidney disease physiologically-based pharmacokinetic (CKD-PBPK) plasma concentration-time profiles compared to observed data for CKD stage 3. Observed data presented as mean (circles) with standard error of the mean (error bars) for each respective study. [329–333] The red line represents the simulated mean concentration-time profile facilitated by the population CKD-PBPK models in PK-Sim, while the shaded region indicates the corresponding standard deviation. Details on dosing regimen and study populations may be found in the Appendix B4. 103

Figure 3-4. Simulated chronic kidney disease physiologically-based pharmacokinetic (CKD-PBPK) plasma concentration-time profiles compared to observed data for CKD stage 4. Observed data presented as mean (circles) with standard error of the mean (error bars) for each respective study. [332,334] The red line represents the simulated mean concentration-time profile facilitated by the population CKD-PBPK models in PK-Sim, while the shaded region indicates the corresponding standard deviation. Details on dosing regimen and study populations may be found in the Appendix B4. 104

Figure 3-5. Simulated chronic kidney disease physiologically-based pharmacokinetic (CKD-PBPK) plasma concentration-time profiles compared to observed data for CKD stage 5 without administration of intermittent hemodialysis. Observed data presented as mean (circles) with standard error of the mean

(error bars) for each respective study. [329,331,333,334] The red line represents the simulated mean concentration-time profile facilitated by the population CKD-PBPK models in PK-Sim, while the shaded region indicates the corresponding standard deviation. Details on dosing regimen and study populations may be found in the Appendix B4. 104

Figure 3-6. Simulated chronic kidney disease physiologically-based pharmacokinetic (CKD-PBPK) plasma concentration-time profiles compared to observed data for end stage renal disease on intermittent hemodialysis. Observed data presented as mean (circles) with standard error of the mean (error bars) for each respective study. [329,332,333,336] The red line represents the simulated mean concentration-time profile facilitated by the population CKD-PBPK models in PK-Sim, while the shaded region indicates the corresponding standard deviation. Details on dosing regimen and study populations may be found in the Appendix B4. 105

Figure 3-7 Predicted vs. observed area under the concentration-time curve extrapolated to infinity (AUC_∞) of included simulations using chronic kidney disease physiologically-based pharmacokinetic (CKD-PBPK) simulations (A) in comparison to conventional scaling methods (B). Dashed line represented 1.25-fold error, while the dotted line represents 1.5-fold error. 106

Figure 3-8. Local sensitivity analysis for organic anion transporter 1/3 drug-drug interaction potential in healthy individuals compared to chronic kidney disease for each investigative drug. OAT transporter K_M and V_{max} was varied by ±10% to analyze the relative change in area under the concentration-time curve extrapolated to infinity (AUC_∞). 108

Figure 4-1. Illustration of the closed-loop ex-vivo continuous renal replacement (CRRT) circuit. Anakinra removal from plasma was determined with each modality of CRRT: A) continuous veno-venous hemofiltration (CVVH), B) continuous veno-venous hemodialysis (CVVHD), C) continuous veno-venous hemodiafiltration (CVVHDF). Standard control samples were analyzed with time matched plasma and hemofiltrate samples. 119

Figure 4-2. Percent anakinra remaining in plasma and standard control with standard deviation shown as error bars. Due to incomplete mixing of the circuit, anakinra percent remaining in plasma was determined at t= 15 minutes for A) hemofiltration (CVVH). Percent remaining in plasma was analyzed at time = 5 minutes for B) hemodialysis (CVVHD) and C) hemodiafiltration (CVVHDF). 125

Figure 4-3. Graphical representation of the determined anakinra sieving coefficient / dialysate saturation constant (A) and estimated transmembrane clearance (B). All data presented as mean with error bars representing the standard deviation. 126

Figure 5-1. Illustration of the closed-loop ex-vivo CRRT circuit. Cefazolin removal from plasma was determined for continuous veno-venous hemodiafiltration (CVVHDF). Standard control samples were analyzed with time matched plasma and hemofiltrate samples. 134

Figure 5-2. Percent cefazolin remaining in plasma and standard control with standard deviation shown as error bars. Percent remaining was analyzed at time = 5 minutes.....139

Figure 5-3. Graphical representation of the average (± standard deviation) cefazolin dialysate saturation constant over time.....140

Figure 6-1. A visual illustration of the workflow and model structure for predicting anakinra pharmacokinetics in children receiving extracorporeal therapy using physiologically-based pharmacokinetic (PBPK) modelling. In this workflow, an adult PBPK model was constructed and validated (Step 1), prior to scaling to children (Step 2). Upon evaluation of the pediatric PBPK model, ex-vivo parameters were incorporated to the whole-body structure for verification of the final pediatric anakinra ECLS-PBPK model (Step 3). 150

Figure 6-2. Anakinra IV PBPK model evaluation to observed concentrations from individuals in the study by Granowitz et al. [474] The solid line represents the average concentration vs. time profile of the virtual population while the observed data is presented as mean (circles) with standard deviation (error bars).....157

Figure 6-3. Predicted and observed plasma concentrations from the pediatric anakinra SC PBPK model. A virtual population (n=1000) individuals was created to correspond with the patient demographics in the pharmacokinetic study by Urien et al. [463] Individuals within this study received anakinra doses between 2-10 mg/kg daily, to a maximum of 100 mg. To simulate this, the 5th-95th prediction interval (shaded region) was simulated for the corresponding doses. Observed individual plasma concentrations is represented by the circles.....159

Figure 6-4. Predicted and observed plasma concentrations from the pediatric anakinra SC PBPK model. A virtual population (n=1000) individuals was created to correspond with the patient demographics in the pharmacokinetic study by Ilowite et al. [50] Individuals within this study received anakinra a dose of 1 mg/kg daily, to a maximum of 100 mg. To simulate this, the 5th-95th prediction interval (shaded region) was created for the corresponding dose. Observed individual plasma concentrations is represented by the circles. 160

Figure 6-5. Predicted versus observed anakinra plasma concentrations of the final ECLS-PBPK model. Observed concentrations (red circles) were prospectively collected from the ongoing Opportunistic PK Study of Commonly Used Drugs in Children on ECLS for an adolescent receiving anakinra subcutaneous 100 mg every 12 hours, while be treated with simultaneous continuous renal replacement therapy (CRRT) and extracorporeal membrane oxygenation (ECMO). A virtual population (n=1000) was created, and a prediction interval (shaded region) was generated to predict the anakinra plasma concentrations. For visual representation, simulations were conducted with no extracorporeal life support (blue), with the addition of CRRT (orange) and with the addition of CRRT and ECMO (pink).....161

Figure 6-6. Anakinra ECLS-PBPK model dosing simulations to compare the area under the concentration time curve (AUC) at steady state in virtual adolescents receiving extracorporeal life-support (ECLS) to healthy adolescents. Virtual populations (n=1000) of adolescents (age:12-17) were created to simulate anakinra subcutaneous doses of 100 mg every 6-12 hours. The AUC at steady state was determined for those individuals receiving continuous renal replacement therapy (red), concurrent ECLS (continuous renal replacement therapy and extracorporeal membrane oxygenation; blue) and compared to a virtual population of healthy adolescents (orange). The solid line represents the median, box represents the interquartile range, and the whiskers represent the 90th prediction interval. 162

Figure 6-7. Anakinra ECLS-PBPK model dosing simulations to compare the area under the concentration time curve (AUC) at steady state in virtual adolescents receiving extracorporeal life-support (ECLS) to those who are not. Virtual populations (n=1000) of adolescents (age:12-17) were created to simulate anakinra subcutaneous doses of 100 mg every 6-12 hours. The AUC at steady state was determined for those individuals receiving continuous renal replacement therapy (red), concurrent ECLS (continuous renal replacement therapy and extracorporeal membrane oxygenation; red) and compared to a virtual population of adolescents who were not (blue). The solid line represents the median, box represents the interquartile range, and the whiskers represent the 90th prediction interval. 163

Figure 7-1. Population verification of the observed cefazolin cerebrospinal fluid (CSF) concentrations from individuals within the study by Novak et al. [506] CSF concentrations of cefazolin were obtained at a median of 2.5 days after the first administered dose from a dosing protocol of intravenous cefazolin administered every 8 hours. Predicted cefazolin maximum, minimum and 4-hour post dose cefazolin concentrations were compared to the observed values (circles). The solid line represents the median CSF concentrations with the shaded region representing the 5th-95th percentile of the virtual population. 178

Figure 7-2. Population verification of the observed cefazolin cerebrospinal fluid (CSF) concentrations from individuals within the study by Le Turnier et al. [494] CSF concentrations of cefazolin (red dots) were obtained 24 hours after initiating a continuous infusion of 8 g/day. Data presented as a function of the EUCAST epidemiological cutoff (ECOFF) of 2 mg/L for methicillin-susceptible Staphylococcus aureus. The solid line represents the median, box represents the interquartile range, and the whiskers represent the 90th prediction interval. 179

Figure 7-3. Target attainment of several cefazolin dosing protocols to reach 100% fT>MIC in the cerebrospinal fluid for the virtual population of participants from the study by Le Turnier et al. [494] A range of cefazolin MIC values for methicillin-susceptible Staphylococcus aureus (MSSA) were tested as per CLSI and EUCAST breakpoints. An epidemiological cutoff of 2.0 mg/L was incorporated. A probability of target attainment of 90% was deemed appropriate. 180

Figure 7-3. Visual illustration of cefazolin safety assessment. A simulated dose of cefazolin IV every 6 hours after a 3-hour infusion time was conducted for illustration purposes. The simulated trough in plasma (A) and cerebrospinal fluid (B) was evaluated to neurotoxicity threshold suggested to increase the likelihood of cefazolin induced neurotoxicity (dotted red line). The simulated range of plasma

concentrations may be shown in the shaded region, with the solid black line representative of the 90th percentile in each reference fluid. 183

List of Tables

Table 1-1. Comparison of acute kidney injury classifications. 8

Table 2-1. Overview of study characteristics that met inclusion criteria. 33

Table 2-2 Pharmacokinetics of medications administered to pediatrics receiving CRRT..... 59

Table 2-3. Pharmacokinetics of medications administered to an ex-vivo CRRT circuit..... 77

Table 3-1. PBPK model parameters. 93

Table 3-2. Exposure predictions of drugs undergoing active tubular secretion via OAT in chronic kidney disease. 101

Table 4-1. Anakinra physicochemical properties and clearance mechanisms. 117

Table 4-2. Continuous renal replacement therapy circuit components. 118

Table 4-3. Continuous renal replacement therapy circuit setup. 123

Table 5-2. Continuous renal replacement therapy circuit setup. 135

Table 5-3. Cefazolin pharmacokinetic variables determined within a CVVHDF circuit. Data presented as mean, standard deviation and range. 140

Table 6-1. Drug specific parameters and ADME of anakinra for subcutaneous model development. 151

Table 6-2. Pharmacokinetic datasets for the pediatric subcutaneous anakinra model evaluation. 153

Table 7-1. Summary of pharmacokinetic studies used to evaluate the cefazolin-CSF PBPK model..... 175

Table 7-2. Pharmacodynamic target attainment of simulated cefazolin dosing protocols for methicillin-susceptible Staphylococcus aureus. Data presented as the probability of target attainment in which the unbound cefazolin concentrations are 100% above the minimum inhibitory concentration (% fT>MIC) in the cerebrospinal fluid. 181

Table 7-3. Cefazolin safety assessment. Data presented as trough concentrations of the 90th percentile within the virtual population for cerebrospinal fluid and plasma. 182

List of Abbreviations

AAFE	Absolute Average Fold-Error
AAG	α-1 Acid Glycoprotein
ADME	Absorption, Distribution, Metabolism, Elimination
AFE	Average Fold-Error
AKI	Acute Kidney Injury
AKIN	Acute Kidney Injury Network
ARC	Augmented Renal Clearance
AUC	Area Under The Concentration-Time Curve
C_D	Drug Concentration in Dialysate
CKD	Chronic Kidney Disease
CL_{CRRT}	Clearance due to Continuous Renal Replacement Therapy
CL_{NR}	Non-Renal Clearance
CL_{Renal}	Renal Clearance
$CL_{reabsorption}$	Clearance due to Passive Reabsorption
$CL_{secretion}$	Clearance due to Active Tubular Secretion
CLSI	Clinical and Laboratory Standards Institute
CL_{total}	Total Clearance
Cmax	Maximum Concentration
Cmax/MIC	Maximum Concentration to Minimum Inhibitory Concentration Ratio

Cmin	Minimum Concentration
CNS	Central Nervous System
C_p	Drug Concentration in Plasma
CSF	Cerebrospinal Fluid
C_{SS}	Concentration at Steady-State
CrCL	Creatinine Clearance
CRP	C-Reactive Protein
CRS	Cytokine Release Syndrome
CRRT	Continuous Renal Replacement Therapy
CVVH	Continuous Veno-Venous Hemofiltration
CVVHD	Continuous Veno-Venous Hemodialysis
CVVHDF	Continuous Veno-Venous Hemodiafiltration
C_{uf}	Drug Concentration in Ultrafiltrate
CYP-450	Cytochrome P450
DDI	Drug-Drug Interaction
DILI	Drug-Induced Liver Injury
ECLS	Extracorporeal Life-Support
ECMO	Extracorporeal Membrane Oxygenation
EMA	European Medicines Agency
ESRD	End-Stage Renal Disease
ER	Extraction Ratio
EVD	External Ventricular Device

EUCAST	European Committee on Antimicrobial Susceptibility Testing
FDA	Food and Drug Administration
*f*T>MIC	Time that the Unbound Concentration Remains Above The Minimum Inhibitory Concentration
fu	Fraction Unbound
GFR	Glomerular Filtration Rate
HF	Hemofiltrate
HLH	Hemophagocytic Lympohistiocytosis
ICU	Intensive Care Unit
IHD	Intermittent Hemodialysis
IL-1	Interleukin-1
IL-1RA	Interleukin-1 Receptor Antagonist
IM	Intramuscular
KDIGO	Kidney Disease: Improving Global Outcomes
k_e	Elimination Rate Constant
LLOQ	Lower Limit of Quantification
MAS	Macrophage Activation Syndrome
MARS	Molecular Adsorbent Recirculating System
MATE	Multidrug and Toxin Extrusion Transporters
MIC	Minimum Inhibitory Concentration
MODS	Multiple Organ Dysfunction Syndrome
MSSA	Methicillin-Susceptible Staphylococcus *Aureus*

MRP	Multidrug Resistance Proteins
OAT	Organic Anion Transporter
OATP	Organic Anion Transporting Polypeptide
OCT	Organic Cation Transporters
PAH	ρ-Aminohippuric Acid
PAN	Polyacrylonitrile
PBPK	Physiologically-Based Pharmacokinetics
PDA	4-Pyridoxic Acid
PFR	Patient Fluid Removal Rate
P-gp	P-Glycoprotein
PICU	Pediatric Intensive Care Unit
PK	Pharmacokinetics
PK/PD	Pharmacokinetics/Pharmacodynamics
pKa	Acid Dissociation Constant
PMA	Postmenstrual Age
PMMA	Polymethylmethacrylate
PNA	Post-Natal Age
popPK	Population Pharmacokinetics
PS	Polysulfone
pRIFLE	Pediatric Risk-Injury-Failure-Loss-ESKD
PTA	Probability of Target Attainment
Q_b	Blood Flow Rate
Q_D	Dialysate Flow Rate
Q_{eff}	Effluent Flow Rate

Q_{plasma}	Plasma Flow Rate
Q_{post}	Post-Replacement Fluid Flow Rate
Q_{pre}	Pre-Replacement Fluid Flow Rate
Q_{uf}	Ultrafiltration Flow Rate
SC	Subcutaneous
S_C	Sieving Coefficient
SCr	Serum Creatinine
S_D	Dialysate Saturation Constant
RIFLE	Risk-Injury-Failure-Loss-ESKD
RRT	Renal Replacement Therapy
t ½	Half-Life
VA-ECMO	Veno-Arterial Extracorporeal Membrane Oxygenation
V_D	Volume of Distribution
V_{ss}	Volume of Distribution at Steady-State
VV-ECMO	Veno-Venous Extracorporeal Membrane Oxygenation

Chapter 1: Background

1.1 Critical Care Medicine

Critical care, or intensive care is a subspecialty of medicine focused on providing comprehensive management to patients with, or at risk of acute, life-threatening conditions. This clinical specialty incorporates a multidisciplinary approach to patient care that differs from other subspecialities by implementation of higher nurse-to-patient ratios, standardized protocols, and use of advanced technologies to support failing organ systems. [1,2] Patient care is provided within designated areas of hospital institutions termed intensive care units (ICU). These high acuity medical units serve as the place for continuous monitoring of seriously ill patients. [3] Etiologies of acute illness for patients in the ICU are inherently heterogeneous. These may be the consequence of infection, failure of vital organ systems (i.e. kidney, lungs, cardiovascular), trauma or post-surgical complications. [1,4] What adds to the complexity of critical care, beyond the heterogeneity of the presenting syndrome, is that the physiological response that follows. This in of itself is inherently heterogenous between individuals. [1] Such heterogeneity presents challenges to the clinical team and despite advancements in practice, mortality and morbidity associated with critical illness remains high.

As ICU level care is extremely resource intensive, differences in global mortality rates range from 9% to upwards of 60%, [5,6] with disparities noted in the economic level of a country. [5] In Canada, mortality rates in the ICU approximate 9%. [7] The comparatively lower mortality rates in Canada may reflect access to care and differences in resource availability as there are approximately 12.5 ICU-level beds per 100,000 people compared to <1 per 100,000 in resource-limited countries. [8,9] While the overall mortality rates may be comparatively lower, ICU admissions in this country continue to rise at an exponential rate. Such a rise has exceeded that of the overall national hospitalization rate, and due to the costs associated with the level of resources required for complex care, a significant burden on the healthcare system in Canada remains. [7] To offset this burden and advance critical care practices, several advancements in institutional protocols, diagnostics and organ support have been implemented to improve patient care. However, advancements in drug delivery continues to be an area of need.

1.1.2 Pediatric Critical Care

Pediatric intensive care units (PICU) are specialized units designated to provide comprehensive care to children experiencing life-threatening conditions such as infections, trauma, or surgeries. [10,11] It is estimated that approximately 200,000 pediatric patients are admitted to a PICU each year in the United States and account for nearly 15% of all critical care admissions in Canada. [12,13] This increase may largely be attributed to advancements in medical practice and continual development of life-saving technologies. [14,15]

It is estimated that up to 20% of all children admitted to a PICU will experience various degrees of multiple organ dysfunction syndrome (MODS). [12] MODS encompasses failure of vital organ systems such as the respiratory, renal, neurological, hepatic and cardiovascular systems. [16] Epidemiological data suggests that respiratory and cardiovascular failure are most prevalent. [17,18] A complete understanding of the epidemiology has yet to be known due to the lack of large prospective data sets, however MODS has shown to be a significant predictor of mortality and poor long-term functional outcomes. [18] Complications that follow are associated with a severe inflammatory response that is commonly triggered by conditions such as shock, infection or trauma. [16,18] To prevent further complications and reduce mortality associated with MODS, many of these children will require life-saving extracorporeal technologies such as continuous renal replacement therapy (CRRT) or extracorporeal membrane oxygenation (ECMO).

1.2 Pharmacokinetic Changes Due to Critical Illness

Critically ill patients represent a unique population that may experience a heterogenous array of complications including widespread systemic inflammation due to infection, trauma, post-surgical complications, and organ dysfunction. Critical illness may be explained by disturbances in homeostasis, and organ function. The disturbances in homeostasis and organ function may affect the normal pharmacokinetic (PK) profile of an individual, resulting in potential differences in drug exposure compared to a healthy counterpart. Early recognition of the impact of disease states on PK has the potential to improve patient outcomes. For example, optimization of antimicrobial dosing based upon predefined pharmacokinetic/pharmacodynamic

(PK/PD) targets may decrease mortality and antimicrobial resistance. [19,20] It is important to conceptualize that the physiological response to critical illness is extremely variable, and that the potential for PK changes may not be uniform across individuals. However, understanding the potential consequences is of the utmost importance for optimizing safe and effective drug use in this population. The following sections will illustrate potential alterations in absorption, distribution, metabolism, and elimination (ADME) that may occur in a critically ill patient. Additionally, the effect of extracorporeal therapy on drug PK will be discussed further in **Section 1.3**.

1.2.1 Absorption

The degree of absorption after oral administration is highly dependent upon the physicochemical properties of the drug and the gastrointestinal environment. Such drug properties include molecular weight, solubility, lipophilicity, acid dissociation constant (pKa); while surface area, gastric motility, pH and blood flow account for the physiological parameters effecting oral drug absorption. [21,22] Extravascular drug administration does not only encompass oral routes, as drugs may also be administered via the subcutaneous (SC) or intramuscular (IM) route. Several physiological abnormalities during critical illness have the potential to impair drug absorption via extravascular administration.

During states of shock, regardless of the etiology, blood flow is redistributed from the liver, kidney, and gastrointestinal tract to more vital organs such as the brain, heart and lungs. [19,21,23] Redirection of blood from the periphery has potential to reduce the amount of systemic absorption from the gastrointestinal tract, muscular and subcutaneous tissues. [24,25] This natural physiological shunting of blood flow may be further compounded by the administration of vasoactive agents to maintain hemodynamic support.

Few drugs are often absorbed in the stomach due to the lower pH and surface area compared to the small intestine. Therefore, gastric emptying time is often a key determinant of oral drug absorption and bioavailability. [26] In response to critical illness, gastric emptying time is often delayed in up to 60% patients. [27] The causal is multifactorial, and likely a result of the physiological response to illness or use of medications such as opioids and sedatives. [27,28]

Slowing of gastric emptying time has the potential to delay the time to maximum drug concentration (t_{max}) and the onset of pharmacodynamic activity. [28–30]

As enzyme metabolism may also occur at the site of the gastrointestinal tract, cellular dysfunction due to atrophy has the potential to reduce drug metabolism. [21,31,32] Although limited evidence identifies the impact of critical illness on enzymatic activity in the gastrointestinal tract, it seems plausible that reduced function may occur similarly to that in other clearing organs (i.e. liver). [33] The impact of critical illness on drug metabolism in the liver will be discussed further in **Section 1.2.3**.

The blood flow redistribution in response to critical illness also affects the perfusion to additional sites of drug absorption, including the subcutaneous tissue and muscle compartment. Compounded with peripheral edema due to fluid shifting and use of vasoactive medications, the absorption of extravascular doses to these compartments are often altered. [34–36] This may be quite consequential and put patients at risk for suboptimal therapy if not accounted for. Due to the changes in physiology, it is often advised that intravenous drug administration be utilized when possible.

1.2.2 Volume of Distribution

Volume of distribution (V_d) is a primary (PK) parameter that may be defined as the apparent volume to which a drug is completely dissolved. It is a proportionality constant relating the concentration of a drug in plasma to the total amount in the body. The distribution phenomenon of drugs within body tissues is highly dependent on multiple factors such as degree of protein binding, permeability of tissue, lipid solubility (logP), pH of the environment and pKa. [21,37] Hydrophilic drugs primarily distribute in the plasma and blood compartments, therefore have a low V_d. While in contrast, drugs that are lipophilic distribute widely throughout the body into the tissue compartments. Understanding the degree of hydro/lipophilicity of a particular medication is important for conceptualizing the impact of critical illness of V_d.

Although there are several etiologies of critical illness, sepsis is the most common. It is characterized by a dysregulated host response to infection. [38] Endotoxins from bacteria or fungi may produce direct effects on the vascular endothelium, leading to vasoconstriction, vasodilation, endothelial damage and increase permeability. [23,39] The endothelial layer is

essential for maintaining tissue fluid homeostasis, therefore any dysregulation may result in fluid shifting intravascularly to the interstitial space. [39,40] This shifting of fluid, often termed "third spacing" creates a newly expanded compartment for which drugs may deposit into. [21,23,31] Larger than expected V_d for hydrophilic drugs such as β-lactams, aminoglycosides and vancomycin may be seen in critically ill patients compared to healthy counterparts. [41–43] Increases in Vd may impact the pharmacodynamics of concentration-dependent antibiotics (i.e. aminoglycosides), where peak plasma concentrations are correlated with response. [21,23,31] Therefore to compensate, higher initial loading doses may be required. The resulting response in V_d is less influential for lipophilic drugs as they inherently distribute beyond the plasma and blood compartments. [44,45]

Upon administration of a medication, it is important to consider that only the unbound fraction of a drug may migrate from plasma to body tissues. [97] The major plasma proteins, albumin and α-1 acid glycoprotein (AAG), are involved in drug sequestration within the plasma. [98,99] The affinity of a drug to these plasma proteins is associated with the molecule's acid-base characteristics, as acidic drugs have a higher affinity to albumin, whereas more basic molecules will bind to AAG. The pathophysiological changes due to critical illness described above have the potential to disrupt normal serum concentrations of such plasma binding proteins therefore affecting the V_d of highly bound compounds.

Opposing changes in the plasma proteins may be noted in critical illness. First, albumin levels may be reduced (hypoalbuminemia) in as many of 75% of individuals. [46,47] Impairment of synthesis due to direct hepatic injury or extravasation may reduce the amount of circulating plasma albumin. Although the implications of hypoalbuminemia may be more pronounced on drug clearance (**Section 1.2.4**), changes in unbound fractions may lead to altered V_d. This is evident with ceftriaxone, a highly protein bound cephalosporin, as the unbound fraction may be increased by approximately 90% in critically ill patients. [100] Oppositely, as AAG is an acute phase reactant, increases in plasma concentrations may be observed in response to critical illness. [48,49] This leads to a higher degree of protein binding sites for those drugs binding to AAG and a reduction in the unbound fraction.[48]

1.2.3 Clearance

1.2.3.1 Metabolism

Drug metabolism may occur in various body tissues, including the gastrointestinal tract, kidney and most commonly, the liver. Drug metabolism via the liver depends on three physiologic parameters: blood flow to the organ, enzymatic activity, and protein binding. Critical illness may affect each of these parameters to some degree, however when assessing the potential impact on hepatic clearance it is important to have context of the drug specific hepatic extraction ratio. The hepatic extraction ratio (ER) may be defined as the ratio of the rate of elimination to the liver to that of its presentation. [50,51] Drugs with a high ER (>0.70) have clearance approximating blood flow, therefore clearance may be altered with any perfusion abnormalities. [21,51] Conversely, clearance of drugs with a low ER (<0.30) are dependent upon the intrinsic clearance and fraction unbound. [21,51] As discussed in **Section 1.2.2**, changes in unbound fraction can fluctuate regardless of which plasma protein the drug is bound to.

Drug metabolism in the liver may occur via two processes: phase I metabolism, which cytochrome P450 (CYP 450) enzymes are largely responsible, and phase II metabolism via mechanisms such as glucuronidation, sulfonation and acetylation. [50] In response to the acute stress of critical illness there is often an increase in the production of stress hormones, acute-phase proteins, and proinflammatory cytokines.[1,52] This may have a direct impact on the expression of CYP 450 enzymes in the liver, resulting in extreme variability in hepatic clearance for substrate drugs. [53] Additionally, direct insult to the liver via ischemia, inflammatory endotoxins or drug-induced liver injury (DILI) may impair phase I metabolism to some degree. [21,53] The impact of critical illness on phase II metabolism remains less defined, however states of inflammation induce a downregulation of these processes. [53,54] Therefore, in critically ill individuals experiencing hyperinflammatory phenotypes, one would expect altered phase II metabolism.

1.2.3.2 Elimination

The previous sections have thoroughly discussed the implications of critical illness on several PK parameters. Although the evidence does support that careful consideration must be made to changes in absorption, distribution and metabolism, the most tangible PK process for clinicians and researchers that may be impacted is that of clearance. Such an importance is reflective of how clearance is inversely proportional to drug exposure or the area-under the concentration time curve (AUC). Any fluctuations in drug clearance will be reflective in fluctuations in drug AUC. Therefore, depending on the therapeutic window or toxicity thresholds of a particular drug, dose adjustments may be required. Renal clearance may be the most notable clearance process altered in critically ill patients and is one that requires specific attention as many of the commonly used drugs in this setting undergo a significant renal clearance. These include antibiotics such as beta-lactams, [105] aminoglycosides, [106] and vancomycin, [107] antifungals such as fluconazole, [107] and analgesics such as morphine. [108]

Renal clearance is the sum of three distinct processes: glomerular filtration (GFR), active tubular secretion and passive reabsorption. [55] Mathematically, this can be defined as:

Eq. 1-1

$$CL_{Renal} = (fu\ x\ GFR) + CL_{secretion} - CL_{reabsorption}$$

where CL_{renal} represents total renal clearance, *fu* is the fraction unbound, GFR is the glomerular filtration rate, and $CL_{secretion}$ and $CL_{reabsorption}$ represent active tubular secretion and passive reabsorption, respectively. Critical illness may impact each process specifically, however as GFR is the primary mechanism responsible, this parameter is most influential.

1.2.4 Pathophysiological Changes

1.2.4.1 Acute Kidney Injury

Acute kidney injury (AKI) is one of the most common complications to a critically ill patient and has been shown to result in significant increases in morbidity and mortality. [56,57] The incidence rate amongst critically ill individuals is extremely high, approaching 50% in adults, [58,59] and approximately 30% in children. [60,61] Currently, three widely used classification systems of AKI have been implemented into clinical practice and validated in

several patient populations. [62–64] The overall premise of such classifications focuses on changes in serum creatinine and urine output as surrogates for GFR. [65] A comparison of the three classifications may be found in **Table 1-1**. [65]

Table 1-1. Comparison of acute kidney injury classifications.

Criteria	RIFLE Creatinine Definition	Criteria	AKIN Creatinine Definition	Criteria	KDIGO Creatinine Definition	Urine* Output
Risk	Increase in SCr ≥1.5 x baseline or GFR decrease > 25%	Stage 1	Increase in SCr ≥26.4 µmol/L or increase ≥1.5 x baseline	Stage 1	Increase in SCr ≥26.4 µmol/L in 48 h or increase ≥1.5 x baseline	<0.5 mL/kg/h for ≥6 h
Injury	Increase in SCr ≥2 x baseline or GFR decrease > 50%	Stage 2	Increase in SCr ≥2 x baseline	Stage 2	Increase in SCr ≥2 x baseline	<0.5 mL/kg/h for ≥12 h
Failure	Increase in SCr ≥3 x baseline or SCr ≥354 µmol/L with an acute rise of at least 44 µmol/L or GFR decrease >75%	Stage 3	Increase in SCr ≥3 x baseline or SCr ≥354 µmol/L with an acute rise of at least 44 µmol/L or initiation of RRT	Stage 3	Increase in SCr ≥3 x baseline or SCr ≥354 µmol/L or initiation of RRT irrespective of SCr or in patients <18 years, decrease in eGFR to <35 mL/min/1.73m^2	<0.3 mL/kg/h ≥24h or anuria ≥12h
Loss	Complete loss of kidney function >4 weeks					
ESKD	Complete loss of kidney function >3 months					

AKIN; acute kidney injury network, eGFR; estimated glomerular filtration, ESKD; end stage, GFR; glomerular filtration rate, h; hour, KDIGO; kidney disease improving global outcomes, kg; kilogram, mL; millilitre, RRT; renal replacement therapy, SCr; serum creatinine, µmol/L; micromole per litre.

* Urine output criteria consistent amongst all three classifications

To ensure an adequate description of AKI for pediatric patients, Akcan-Arikan *et.al* constructed a modified version of the risk-injury-failure-loss-ESKD (RIFLE) criteria to account

for childhood growth and physiological maturation. [66] As opposed to using changes in serum creatinine concentrations, pediatric RIFLE (pRIFLE) incorporates estimated creatinine clearance (CrCL), which is a function of patient demographics such as age, height, and weight. [66] In comparison to the acute kidney injury network (AKIN) and the kidney disease: improving global outcomes (KDIGO) classifications, pRIFLE showed similar associations with pediatric morbidity and mortality. [66]

1.2.4.2 Pathophysiology of Acute Kidney Injury in The Critically Ill

Several potential causes have been known to contribute to AKI within a critically ill patient, with the most common being sepsis, ischemia related to hypoperfusion and/or use of nephrotoxic agents. [67] The pathology of AKI may range from decreases in GFR due to reversible injury, to tubular necrosis leading to chronic kidney disease (CKD) or renal failure. [67] It has been suggested that inflammation associated with critical illness results in apoptosis and non-specific changes of renal tubular cells or brush border membranes may be the primary pathological mechanism of AKI. [68]

Sepsis-induced AKI may occur in up to 50% of critically ill adults and 20% of children.[69–71] The pathophysiology has not been fully understood; however it has been described by heterogenous tubular injury without characteristic features of necrosis as seen in severe ischemic injury. [72,73] Circulating toxins may trigger a reduction in blood flow and infiltration of inflammatory cells. [72,74] Sepsis may also lead to the induction and release of apopoetin-2, and reduction in apopoetin-1 receptor expression, resulting in vascular capillary leakage. [75,76] Such consequences may result in apoptosis and necrosis, contributing to sustained AKI or progression to CKD in a small subset of patients. [75,76]

Redistribution of blood flow as previously described, results in a reduction in renal blood flow and is a significant contributor to AKI. Contributing factors to renal ischemia include reductions in intravascular volume, systemic hypotension, fluid retention and/or neurohormonal activation. [72] Under normal physiological conditions, the medullary region of the kidney receives poorly oxygenated blood and low blood flow, making this region susceptible to injury upon systemic hypoperfusion. [77,78] Systemic hemodynamic instability may lead to hemodynamic imbalances within the kidney, increasing the release of vasoconstrictive molecules

such as endothelin. [77,78] Simplistically, ischemic AKI may lead to alterations in renal processes, cell structure and gene expression.

Thirdly, one of the largest contributors of AKI to a hospitalized or critically ill patient is the use of nephrotoxic agents. Data suggests that the use of nephrotoxic agents may account for up to 60% of AKI cases in hospitalized adults and 25% in children. [77,79–81] The renal vasculature is highly subjected to the direct effects of blood circulating molecules due to the kidneys receiving a large percentage (25%) of blood flow from cardiac output. Nephrotoxic agents may induce kidney injury through several mechanisms, including alterations in kidney hemodynamics, direct cellular injury, or osmotic injury. [72,82]

1.3 Extracorporeal Therapy

Organ impairment or failure may be quite common in critically ill adults [83,84] and children. [16,85,86] Patients experiencing impairment to vital organs such as the lungs, kidneys, and heart are at high risk of mortality. [16,83,84] To offset the complications and improve patient outcomes, extracorporeal therapy is often required. This includes the use of CRRT and ECMO. Both act as artificial organs, supporting the kidneys and heart and lungs, respectively. As they provide non-specific exchanges of substances in the blood as a filtration mechanism, important PK considerations must be made.

1.3.1 Continuous Renal Replacement Therapy

Renal replacement therapy (RRT) was originally developed as a method of blood purification and solute removal in patients with chronic kidney disease. However, with advancements in technology it has become an application of great importance in critically ill patients experiencing renal dysfunction and/or fluid overload. [56] As previously discussed, a high percentage of critically ill patients may experience some degree of renal impairment. [58–61] Of these, 10% of adults and 5% of children require RRT to manage the consequences of kidney injury. [56,87] Due to the hemodynamic instability of critically ill patients, traditional forms of RRT (i.e. intermittent hemodialysis) may not be tolerated due to the rapid rate of solute and fluid removal. [56,87] With the ability to provide a more gradual removal of solutes and fluid over prolonged periods of time, CRRT has become the method of choice for renal support in critically ill adults and children.

Historically, CRRT was developed as an arteriovenous therapy, however more recent practices utilize pump-driven venovenous circuits. [56] Within these circuits, venous blood is removed from patient circulation through a large catheter and then passes through a peristaltic blood pump to generate enough perfusion pressure to enable ultrafiltration of plasma water through the circuit membrane. [88] Solute removal occurs differently depending on the modality of CRRT which includes: continuous veno-venous hemofiltration (CVVH), continuous veno-venous hemodialysis (CVVHD) or continuous veno-venous hemodiafiltration (CVVHDF). The overall objective of fluid and solute removal is similar between these modalities however the mechanistic function differs between each. [56,89] Each method of solute removal may have differential effects on the pharmacokinetics of medications administered. Additionally, circuit properties such as filters, membranes and flow rates may impact clearance of certain medications. [90–92] A thorough understanding of the interplay between circuit, drug and patient factors is important to describe the PK of medications administered to this population.

1.3.1.1 Continuous Veno-Venous Hemofiltration

Within a CVVH system, solute transport occurs through convective clearance. The concept of convective clearance is that solutes within the blood are forced across a semi-permeable membrane, a process referred to as “solvent drag”. [88,93] This process of mass transport differs from the random Brownian movement of solutes associated with diffusion due to the generation of a pressure gradient. [93,94] The high ultrafiltration rates applied for solute clearance requires the addition of physiologic replacement fluids to restore fluid volume and electrolytes. [87,88,94] Replacement fluids may be administered to the CRRT circuit either prior to or after the hemofilter. Prefilter administration of replacement fluids dilutes the blood which offers advantages in filter life preservation however reduces the effectiveness of solute clearance at a fixed ultrafiltration rate. [56]

1.3.1.2 Continuous Veno-Venous Hemodialysis

CVVHD circuits utilize a concentration gradient to perform solute removal. In these circuits, a counter current dialysate solution is administered across the external surface of the dialysis membrane, allowing for solutes to be removed from the blood down their concentration gradient. [56] Unlike CVVH, ultrafiltration rates are generally low, if used at all, allowing for adjustments in fluid balances without the need for replacement fluid administration. [56,88] Clearance of endogenous solutes or medications via a CVVHD is dependent on molecular weight. Diffusion provides efficient clearance of lower molecular weight solutes (<500-1500 Da) but decreases as molecular weight increases. [56] This differs in comparison to CVVH circuits where the rate limiting step in solute clearance is membrane porosity, rendering CVVH more efficient in clearance of solutes ranging from 1000 to 20,000 Da. [56,88] However, with advancements in circuit membrane technology, the use of "high-flux" or "high-cutoff" membrane filters have reduce the importance of molecular weight on solute clearance. [95,96]

1.3.1.3 Continuous Veno-Venous Hemodiafiltration

The third modality of CRRT, and the most common applied in both adult [97] and pediatric [98] intensive care units is that of CVVHDF. CVVHDF combines dialysis with filtration, resulting in solute clearance through both diffusion and convection. [56,99] The addition of dialysis within the CVVHDF circuit allows for an increase in small-molecule solute clearance compared to middle-to-large molecular weight solutes. As identified by Brunet *et.al*, clearance of small solutes such as urea and creatinine by CVVHDF approximated the sum of CVVH and CVVHD. [100] However, this concept did not hold true with larger endogenous solutes such as β2-microglobulin, suggesting that clearance via CVVHDF is difficult to predict and must consider circuit flow rates and molecular weight of solute. [100,101] An understanding of such mechanisms of extracorporeal clearance is imperative to understand the potential alterations of the PK of administered medications.

1.3.2 Pharmacokinetic Alterations in Patients Receiving Continuous Renal Replacement Therapy

As the purpose of CRRT is to provide support to the failing kidney, the non-specific mechanism of filtration has the potential to remove drugs from systemic circulation to various degrees. Intuitively, the filtration acts as a clearing organ and the CRRT circuit clearance (CL_{CRRT}) needs to be accounted for when assessing CL_{total} of a particular drug. Additionally, circuit specific properties such as flow rates and membrane composition, may directly impact drug PK. The PK of drugs in CRRT has been studied extensively in adults, and several reviews have been conducted to draw large conclusions. [89,102–107] Although, PK studies in children receiving CRRT have been conducted, no such review is available to assess the literature as a whole. The following sections will briefly describe the variables associated with PK alterations in these patients.

1.3.2.1 Mechanistic Differences

As previously discussed, the mechanisms for solute removal differ between CRRT modalities, rendering potential differences in drug PK. With a CVVH circuit, drug clearance is largely dependent upon the ultrafiltration rate and independent of molecular size.[89,99] To assess the potential for drug passage across the hemofilter in a CVVH circuit, a drug-specific constant referred to as the sieving coefficient (S_C) is considered. The S_C expresses the ratio of unbound drug concentration in the ultrafiltrate (waste; C_{uf}) to the concentration in plasma (C_p) (Eq. 1-2). [102,103]

$$S_c = \frac{C_{uf}}{C_p} \qquad \textbf{Eq. 1-2}$$

S_C values near 1 indicates free passing of drug across the hemofilter, while a SC of 0 indicates minimal transport. Drug clearance (CL_{CVVH}) may be estimated by the product of the ultrafiltration rate (Q_{uf}) and the S_C of a particular drug (Eq. 1-3). [102,103]

$$CL_{CVVH} = Q_{uf}\, x\, S_C \qquad \textbf{Eq. 1-3}$$

The high ultrafiltration rates often utilized require the addition of replacement fluids, either pre- or post-hemofilter, to ensure plasma water volume and electrolytes are being restored. [88,93,108] The dilutional effect may decrease the efficiency of solute removal. This has been shown with up to a 40% reduction in small solute clearance when a pre-filter replacement technique is used compared to post-filter replacement. [109] Clinically, Uchino *et.al* demonstrated that the CL_{CVVH} of vancomycin increased with post-filter replacement fluid administration compared to pre-filter. [110] In order to account for the dilution effect of pre-filter replacement, one can approximate with the use of a correction factor (Eq 1-4 & 1-5):

$$CL_{CVVH}(pre) = Q_{uf}\ x\ S_C\ x\ CF \qquad \textbf{Eq. 1-4}$$

$$CF = \frac{Q_{plasma}}{Q_{plasma+}\ Q_{pre}} \qquad \textbf{Eq. 1-5}$$

Where, Q_{plasma} and Q_{pre} represent the flow rates of plasma and pre-filter replacement fluids, respectively. [102,103] In this equation, Q_{plasma} is approximated by blood flow (Q_b) x 1-hematocrit (HCT). The application of this concept in Eq. 1-3 does not need to be considered for small solute clearance within a post-dilutional method of CVVH. As a result, CL_{CVVH} using post-filter replacement fluids may be described using Eq. 1-3.

The clearance of CVVHD differs through a diffusive process with the use of a countercurrent dialysate solution. The dialysate flow is substantially slower than blood flow, enabling sufficient time for the diffusive process to occur across circuit membranes. [108] The ability of a solute, or drug, to diffuse through a CVVHD circuit membrane may be quantified by the dialysate saturation constant (S_D). [102,103] This constant is mathematically equivalent to SC, as the ratio of drug concentration in dialysate (waste, C_d) to the drug concentration in plasma (C_p). The full equation may be found in Eq. 1-6.

$$S_D = \frac{C_d}{C_p} \qquad \textbf{Eq. 1-6}$$

Utilizing S_D along with the dialysate flow rate (Q_D), CVVHD clearance (CL_{CVVHD}) may be estimated (Eq. 1-7). [102,103]

$$CL_{CVVHD} = Q_D \, x \, S_D \qquad \textbf{Eq. 1-7}$$

With a countercurrent configuration, increased Q_D prevents dialysate saturation and improves the diffusion gradient.

The third modality of CRRT, CVVHDF, integrates a combination of convection and diffusion for fluid and solute removal. CVVHDF clearance (CL_{CVVHDF}) may be approximated by the sum of each respective process (Eq. 1-8). [102,103]

$$CL_{CVVHDF} = \left(Q_{uf} \, x \, S_c \, x \, CF\right) + \left(Q_D \, x \, S_D\right) \qquad \textbf{Eq. 1-8}$$

As CVVHDF incorporates ultrafiltration, replacement fluids are required. [102,103] Therefore, a correction factor (Eq. 1-5) based on replacement fluids may need to be applied when estimating CL_{CVVHDF}.

1.3.2.2 Flow Rates

Based upon the estimation equations presented above, flow rates of each CRRT modality affect both CL_{RRT} and CL_{total}. The effluent flow rate (Q_{eff}), or "dose" of the CRRT circuit is defined as the waste fluid per unit of time from the outflow port of the dialysate/ultrafiltrate compartment of the CRRT circuit. The effluent flow rate equates to the sum of all removal processes incorporated in the circuit, including the Q_{uf}, Q_D and patient fluid removal rate (PFR) (Eq. 1-9).

$$Q_{eff} = Q_{uf} + Q_D + PFR \qquad \textbf{Eq. 1-9}$$

Increases in effluent flow rates have been shown to significantly correlate with CL_{total} and CL_{RRT} of several antibiotics such as meropenem, piperacillin and vancomycin. [90] Furthermore, administration of vancomycin to patients receiving high effluent flow rates of CVVH have been shown to have a reduced probability of reaching target attainment. [111] Therefore, consideration of effluent flow rates within a CRRT circuit is of the utmost importance to ensure adequate dose.

1.3.2.3 Circuit Membrane Composition

CRRT circuit membranes have traditionally been categorized based upon composition (cellulose vs. synthetic) or permeability (low vs. high-flux). [92] Historically, cellulose membranes were used however advancements in technology to address the bio-incompatibilities have shifted towards the use of synthetic based membranes in modern circuits. [92,112,113] Examples of synthetic membranes used today in CRRT circuits include sulfonated polyacrylonitrile (PAN), polymethyl-methacrylate (PMMA) and polysulfone membranes (PS).[92,114,115]

To this point the concept of CL_{CRRT} has been thought of in the context of filtration mechanisms such as convection or dialysis. However, a third possible mechanism of drug removal from plasma may be that of drug adsorption to circuit materials. [116] Adsorption may be dependent on membrane specific properties such as the composition or charge, and drug specific properties including lipophilicity, protein binding and charge. [92,116,117] Comparisons between PAN and PS have shown that PS circuit membranes may reduce the adsorption and CL_{RRT} of several antibiotics. [117,118] A complex interaction, which may be explained by the Gibbs-Donan effect, between molecular charge and the negative charge of membranes have been suggested to explain this process.[103,117] As an example, adsorption of gentamicin, a positively charged molecule, may have significant adhesion to CRRT circuit membranes.[117,119]

Drug specific properties must also be accounted for when assessing the potential for adsorption. Drugs that are lipophilic and highly protein bound are less likely to be removed from plasma by filtration mechanisms, as only the unbound drug is cleared. [102,103,116] However, significant adsorption may occur, leading to high CLCRRT for molecules with these physicochemical properties. [117,120] It should also be noted that the drug-membrane interaction appears to be saturable and may be of significance during initial dosing and upon replacement of new filters. [121,122]

1.3.3 Extracorporeal Membrane Oxygenation

Extracorporeal membrane oxygenation (ECMO) is a form of life-support used in patients with cardiorespiratory failure. [123,124] Mechanistically, blood is drained from the patients venous system, oxygenated, and then returned to systemic circulation via the venous or arterial system. There are two forms of ECMO used in a critical care setting, veno-venous ECMO (VV-ECMO) and veno-arterial ECMO (VA-ECMO). [124,125] In a VV-ECMO circuit, the drained venous blood undergoes gas exchange and returned to the venous circulation, providing only respiratory support. In a VA-ECMO circuit, the venous blood is reinfused back to the arterial system, providing both cardiovascular and pulmonary support. [124,125] Regardless of which circuit is utilized, the components remain the same. [126] As with CRRT, one of the challenges clinicians face in providing pharmacotherapy to those on ECMO support is the potential impact of altered drug PK.

1.3.3.1 Pharmacokinetic Alterations in Patients Receiving Extracorporeal Membrane Oxygenation

Drug PK may be altered in critically ill patients receiving ECMO by one of three possible mechanisms: 1) drug extraction from the circuit, 2) changes in V_d and 3) changes in drug clearance (CL_{total}). As in CRRT circuits, drug extraction or adsorption in an ECMO circuit is dependent upon circuit materials and the physicochemical properties of the drug. In general drugs that are highly lipophilic, and protein bound are most likely to adsorb to ECMO circuit materials. [127,128] However, since adsorption may occur because of the hydrophobic interactions between drug and circuit polymers, the physicochemical properties of the drug and circuit composition should be assessed in tandem, rather than individually. [127,129,130] This has been evident with the use of fentanyl, as drug extraction may differ significantly with different circuit membranes [127] or membrane coatings. [131,132]

ECMO circuit use may alter the V_d of drugs through multiple mechanisms, including drug adsorption, hemodilution and the physiological response of critical illness. [133,134] As discussed above, drug adsorption to the circuit may initially decrease plasma drug concentrations. [127,133,134] To compensate for the apparent increase in V_d, higher loading

doses are often required. [133,134] However, the drug adsorption process may become saturated, and the adsorptive potential may decrease over time. [133] Secondly, the effect of hemodilution may be most influential to changes in drug V_d. When initiating ECMO therapy, the administration of priming solutions is often required. Furthermore, throughout the course of ECMO treatment blood transfusions and fluid administration are typically needed to manage any bleeding complications and maintain circuit flow, respectively. [133–135] This inherently increases blood volume and may be most pronounced on the V_d of hydrophilic drugs and young infants. [133,134] Additionally, the initiation of ECMO circuits may illicit an immediate and complex inflammatory response, [133,134,136] similar to that associated with critical illness (**Section 1.2.2).**

Changes in drug clearance during ECMO are a result of the direct physiologic response on clearing organs. Renal dysfunction is common, occurring in approximately 30% of patients receiving VV-ECMO and 50% of patients receiving VA-ECMO. [134,137,138] Reasoning for high rates of kidney injury are not entirely clear however it is likely a result of hypoxia and/or perfusion abnormalities that may be seen prior to ECMO initiation. [134] Due to the impact of renal impairment, CL_{total} of renally cleared drugs are altered. [128,133,134] As previously discussed, reductions in blood flow may impact hepatic clearance in states of critical illness. Due to perfusion fluctuations in patients on ECMO, similar reductions in hepatic blood flow may be expected. [133,134,139] Furthermore, the inflammatory response either prior to, or in result of ECMO initiation may impact hepatic enzyme activity through inhibition or downregulation. [134,139,140]

1.4 Determining Drug Dosing on Extracorporeal Life-Support

Drug dosing recommendations may be derived by conducting traditional PK studies, assessing the concentration vs. time profile, and analyzing the data using PK modelling techniques. Such modelling strategies may include noncompartmental and compartmental PK analyses, or population PK modelling (popPK). These methods apply mathematical concepts to fit a model to drug concentration vs. time profiles from individuals included within the PK study. The role of these methods for determining drug dosing in patients receiving extracorporeal life-support (ECLS) may be beneficial in optimizing pharmacotherapy. For example, popPK

modelling strategies enable assessments of covariates related to patient-specific or ECLS-specific factors that may be influential in drug PK. [116,141–143] However, limitations are present as these traditional approaches require more robust sampling strategies, may be limited in extrapolations to different patient populations (i.e. adults to pediatrics) and may become obsolete with advancements in circuit technology. [141,144] Strategies to overcome these limitations include the use of physiologically-based pharmacokinetic (PBPK) modelling. [141,144]

1.4.1 Physiologically-Based Pharmacokinetic Modelling

Physiologically-based pharmacokinetic (PBPK) models incorporate three components during model development such as: system-specific properties, drug properties and the structural model. [145,146] The structural PBPK model, or anatomical arrangement, consists of 15 organ compartments linked with two blood compartments. Drug disposition between each compartment is mathematically described using ordinary differential equations. A representation of the anatomical arrangement may be found in **Figure 1-1**. PBPK models have become well recognized for dose extrapolation in predicting pediatric exposure and have become an integral component of drug development. [145] As the model structure is mechanistically derived with known parameters attributed to physiology and drug PK, extrapolations to special populations (i.e. pediatrics, organ impairment) may be conducted by incorporating known physiological information of the target population. This approach may serve to be superior to alternative modelling strategies in children <2 years of age when maturational components of drug PK are not fully developed. [147,148]

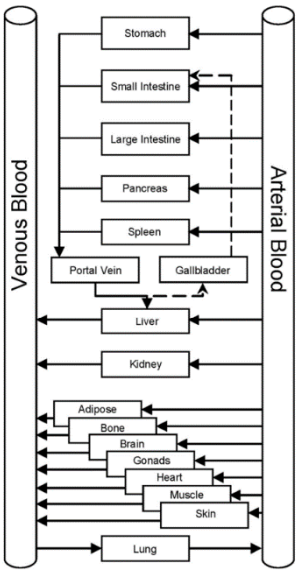


Figure 1-1. Whole-body physiologically-based pharmacokinetic (PBPK) model adapted from Edginton et al. [149] Each organ (15) is connected by two blood compartments to represent an anatomical arrangement. The arrows between compartments mathematically described drug disposition through ordinary differential equations.

Recently the use of PBPK modelling for guiding appropriate pharmacotherapy in patients receiving extracorporeal has been shown. [144,150] By incorporating the physiological alterations associated with critical illness with the results from *ex-vivo* extracorporeal analyses into the PBPK model structure, Watt *et al*. demonstrated feasibility in providing successful predictions of drug PK in critically ill children on ECMO. [144] These methods are adaptable to new circuit technology and can be altered to different forms of extracorporeal therapy (i.e. CRRT). In doing so, an ECLS compartment can be added to the whole-body PBPK structure to account for any changes in drug PK. The ECLS compartment is mathematically constructed by incorporating known volumes, circuit flows and manufacture specifications of circuit components for the purpose of predicting drug concentrations in the target population. This modelling approach may address some of the limitations of traditional PK studies in this population as it can reduce the number of participants required for data analysis, improve clinical trial efficiency and may be modifiable to new circuit technology, flow rates or target populations (i.e. adults vs. pediatrics). Although the results from the analysis by Watt *et al*.[144] demonstrate

success of this approach, further confirmation in different populations, different forms of ECLS and different drugs are required for widespread adoption into clinical practice.

1.5 Aim, Objectives, and Hypothesis

This thesis aims to apply state-of-the-art mechanistic modelling strategies to advance pharmacotherapy in critically ill adults and children on ECLS. Through applications in PBPK, this thesis seeks to inform drug dosing in critically ill patients experiencing heterogenous etiologies of illness. Different modelling techniques will incorporate disease associated pathophysiological alterations to be applied to specific clinical scenarios.

1.5.1 Objective 1: Analyze the Pharmacokinetic Data in Critically Ill Children Receiving Continuous Renal Replacement Therapy

Objective 1: To conduct a comprehensive systematic review for the purpose of summarizing the PK literature of critically ill children receiving CRRT. This objective will entail a comparison of PK between children on CRRT to critically ill children who are not, identify commonly used drugs with limited pediatric-specific dosing guidance, and assess the reporting quality of current studies.

Hypothesis 1: In critically ill children receiving CRRT, the PK of commonly used drugs will be largely similar to critically ill children who are not receiving CRRT.

1.5.2 Objective 2: Evaluate the Continuous Renal Replacement Therapy Extraction of Drugs *Ex-vivo*

Objective 2: Using established methods, the drug-CRRT circuit interaction will be investigated for anakinra and cefazolin. Furthermore, this thesis seeks to demonstrate how large molecule therapeutic proteins may be removed from plasma using modern CRRT circuit technology.

Hypothesis 2: Using modern CRRT circuit technology, both cefazolin and anakinra will be extracted from plasma.

1.5.3 Objective 3: Develop Physiologically-Based Pharmacokinetic Models to Optimize Drug Dosing in The Critically Ill

Objective 3: Develop PBPK models that account for altered physiology associated with critical illness for the purpose of optimizing pharmacotherapy.

Hypothesis 3: This approach to predicting drug concentrations in the critically ill will be successful upon evaluation with observed data.

Chapter 2: Pharmacokinetics of commonly used mediations in children receiving continuous renal replacement therapy: a systematic review of current literature

This chapter is reflective of an original manuscript published by the PhD candidate (Samuel Dubinsky) in *Clinical Pharmacokinetics*. All pertinent dialogue in this chapter was written by the PhD candidate.

Information regarding applicable letters of copyright permission is presented in the **Letters of Copyright Permission.**

2.1 Overview

Background:

The use of CRRT for renal support has increased substantially in critically ill children compared to intermittent modalities due to its preferential effects on hemodynamic stability. With the expanding role of CRRT, the quantification of extracorporeal clearance (CL_{RRT}) and the effect on primary pharmacokinetic parameters is of the utmost importance. Within this review we aimed to summarize the current state of the literature and compare published pharmacokinetic analyses of commonly used medications in children receiving CRRT to those who are not.

Methods:

A systematic search of the literature within electronic databases PubMed, EMBASE, Cochrane Library and Web of Science was conducted. Published studies that were included contained relevant information on use of commonly administered medications to children, from neonates to adolescents, receiving CRRT. Pharmacokinetic parameters that were analyzed included V_d, CL_{total}, CL_{RRT}, AUC and elimination half-life. Information regarding CRRT circuit, flow rates and membrane components were analyzed to investigate differences in pharmacokinetics between each modality.

Results:

45 studies met final inclusion within this systematic review, totaling 833 pediatric patients, with 586 receiving CRRT. Antimicrobials were the most common pharmacological class represented within the literature, representing 81% (35/43) of studies analyzed. Children receiving CRRT largely had similar V_d and CL_{total} to critically ill children not receiving CRRT, suggesting reno-protective dose adjustments may lead to subtherapeutic dosing regimens in these patients. Overall, there was a tendency for hydrophilic agents, with low protein binding to undergo elevated CL_{total} in these children. However, results should be interpreted with caution due to the large variability amongst patient populations and heterogeneity with CRRT modalities, flow rates and use of ECMO within studies. This review was able to identify that variation in solute removal, or CRRT modalities, properties (i.e. flow rates) and membrane composition may have differing effects on the pharmacokinetics of commonly administered medications.

Conclusion:

The current state of the literature of medications administered to children receiving CRRT largely focuses on antimicrobials. Significant gaps remain with other commonly used medications such as sedatives and analgesics. Overall reporting of patient clinical characteristics, CRRT settings and circuit composition was poor, with only 10% of articles including all relevant information to assess the impact of CRRT on CL_{total}. Changes in pharmacokinetics because of CRRT often required higher than labelled doses, suggesting renally adjusted, or reno-protective doses may lead to subtherapeutic dosing regimens. A thorough understanding of the interplay between patient, drug and CRRT-circuit factors are required to ensure adequate delivery of dosing regimens to this vulnerable population.

2.2 Introduction

The incidence of pediatric patients admitted to intensive care units continues to rise in North America, with approximately 200,000 annual admissions within the US. [12,13] Approximately 20% of critically ill children may experience various degrees of multiple organ dysfunction. [12] Multiple organ dysfunction, or MODS, encompasses failure of organ systems such as the respiratory, renal, neurological, hepatic and cardiovascular systems. [16] MODS is largely associated with a severe inflammatory response that is commonly triggered by conditions such as shock, infection, or trauma. [16,60] Of these, renal dysfunction has been shown to be one of the most common and one of the strongest predictors of mortality within a pediatric intensive care unit (PICU). [60]

Recent epidemiological data suggests that renal dysfunction amongst pediatric patients may be as high as 30% and associated with a mortality rate of nearly 15% within a PICU. [18,56,60,61] To prevent further complications and reduce mortality associated with renal dysfunction, many of these children will require extracorporeal technologies such as continuous renal replacement therapy (CRRT).

Renal replacement therapy (RRT) was originally developed as a method of fluid and solute removal in patients with chronic kidney disease. Due to preferential effects on hemodynamics compared to intermittent modalities, CRRT has become the treatment of choice for patients requiring renal support. [56] Multiple CRRT techniques have been used to aid in fluid and solute removal, including continuous veno-venous hemofiltration (CVVH), continuous veno-venous hemodialysis (CVVHD), and continuous veno-venous hemodiafiltration (CVVHDF). Depending on the modality chosen, drugs will be cleared differently.

Clearance through a convective process, as seen with CVVH, is largely dependent upon the ultrafiltration rate and independent of molecular size. [89,99] This differs from the diffusion process seen within CVVHD, as efficient clearance depends on molecular weight and the utilization of a concentration gradient for molecules to move from blood to dialysate. [103,108] Where as, CVVHDF combines both mechanisms (diffusion & ultrafiltration) to aid in solute removal. [103,108] The efficiency of drug removal is expected to be CVVHDF>CVVH>CVVHD. [56,89]

With the expanding data supporting the impact of CRRT on survival of critically ill children, the quantification of extracorporeal clearance (CL_{RRT}) has significant implications for alteration in the pharmacokinetic behaviour of medications. [151] Differences in method of RRT, circuit properties such as flow rates or membrane composition, in conjunction with patient clinical status and the physicochemical properties of a drug, may lead to suboptimal pharmacodynamic responses or toxicity based on alterations in volume of distribution (V_d) or total clearance (CL_{total}). [94,103,108] For example, the degree of CL_{RRT} is of particular importance for patients experiencing life-threatening infections as the consequences of suboptimal dosing has been shown to negatively impact mortality and increase antimicrobial resistance. [87,152,153] Current dosing recommendations are guided by a one-size-fits all approach, lacking patient, and circuit specificity. [154] To date there are no systematic reviews investigating the pharmacokinetic parameters for commonly used medications within pediatric patients receiving CRRT. The goal of this systematic review is to summarize the pharmacokinetic data and investigate the quality and validity, with the objective of providing a

guide for clinicians to develop optimal dosing regimens for pediatric patients and to identify knowledge gaps for future research.

2.2 Methods

The systematic review protocol has been previously registered on PROSPERO, CRD42021250070. [155]

2.2.1 Search Strategy

A systematic search of the literature within electronic databases PubMed(MEDLINE), Ovid EMBASE, Cochrane Library and Web of Science was conducted with assistance from an information specialist (CC). The search strategy was developed using keywords: *pharmacokinetics*, *drug dosing*, *pediatrics,* and *renal replacement therapy* within the pediatric patient population from birth to 18 years. Further refining was done to include articles published from 1990 to May 3, 2021. Researchers were alerted to additional results for the search after May 2021 to September 15th, 2021 by automatic email alerts. Articles during this period were screened and selected in a similar manner to the original search. Limitation of publication date was to ensure the search results only included pharmacokinetic analyses with widely used veno-venous CRRT circuits. To maximize inclusion, references of selected publications were reviewed, and all relevant articles were included. The full search strategy for PubMed(MEDLINE) can be found in **Appendix A1**.

2.2.2 Study Selection

The final search results from each database were imported within the software Covidence (Melbourne, Australia). [156] Two reviewers (SS + BA) independently screened each title and abstract to assess eligibility for inclusion. The systematic review process was conducted in accordance with the Cochrane Handbook for systematic reviews and interventions. [157] All discrepancies between reviewers were resolved by a third independent reviewer (SD). Studies were included if they met the following pre-defined inclusion criteria: 1) study population of ages 18 years and below, including neonates (0-28 days), infants (29 days – 1 year of age), children (>1-12 years) and adolescents (>12-18 years), 2) those receiving CRRT such as: CVVH,

CVVHD, and CVVHDF, 3) studies reporting results of primary pharmacokinetic parameters such as CL (CL_{total} & CL_{RRT}), V_d or AUC in patients receiving CRRT. No restrictions on the use of additional extracorporeal technologies such as ECMO were included within this review. *Ex-vivo* studies investigating the drug-CRRT circuit interaction were included to illustrate the impact on pharmacokinetics. All study designs, including case reports and case series were incorporated within this review. Studies that were excluded were: 1) Non-English publications, 2) animal studies and 3) studies including predominantly adult populations with no clear separation of pediatrics.

2.2.3 Data Extraction

All extracted data was contained within a pre-populated data extraction sheet developed using Microsoft Excel. Extracted data included study design, sample size, drug, dose, administration route (i.e. enteral or intravenous), and patient demographics including age, body weight (kg), and height (cm). Indicators of clinical status were also extracted if applicable, including serum creatinine (SCr), albumin, bilirubin, liver enzymes and presence or absence of residual renal function. As the study population included children receiving CRRT, all relevant CRRT circuit components were recorded such as: CRRT machine, circuit filter/tubing, including membrane porosity, flow rates (i.e. blood, dialysate, ultrafiltrate) and replacement fluid flow rate (i.e. prefilter vs. post-filter replacement). Additionally, the sieving coefficient (S_C) or dialysate saturation constant (S_D) was also extracted. This may simply be defined as the ratio between the drug concentration in the effluent fluid to plasma for a CVVH and CVVHD circuit respectively. The presence or absence of ECMO was also noted.

The pharmacokinetic parameters that were extracted included: CL_{total}, Vd, AUC, half-life (t ½), elimination rate constant (k_e) and peak/trough concentrations (Cmax & Cmin). Pharmacokinetic parameters were recorded as mean/median values as presented in each respective study. Additionally, the method of pharmacokinetic analysis and model structure was included within the extraction. For population pharmacokinetic (PopPK) models, covariates and final model equations were documented if applicable.

Probability of target attainment (PTA) was also recorded. PTA included time above the minimum inhibitory concentration (fT>MIC) for time-dependent antimicrobials, peak-concentration to MIC ratio (Cmax/MIC) for concentration-dependent antimicrobials and

AUC/MIC ratio for exposure-dependent antimicrobials. Pharmacodynamic targets for non-antimicrobials were also investigated if reported.

2.2.4 Quality Assessment

One of the main objectives of this review was to assess the quality of the current literature of pharmacokinetic analyses in children receiving CRRT. The ClinPK quality assessment tool constructed by Kanji *et al.* was developed to aid clinicians' ability to assess validity and quality of reporting for pharmacokinetic studies. [158] This 24-item checklist includes criteria such as study rationale, eligibility criteria, coadministration of study drugs, validation of quantitative bioanalytical methods, use of pharmacokinetic software, transparency of extracorporeal technology components and quality of reported results. [159] As a result, this tool was incorporated within the review to allow for better assessment of clinical application.

3. Results

3.1 Characteristics of Included Studies and Study Population

The literature search strategy identified 1713 non-duplicate records. After title and abstract screening, 129 were determined to be eligible for full-text review. Among these, 45 studies met inclusion criteria and included a total of 833 pediatric patients, with 586 receiving CRRT. Only one patient included within the review received peritoneal dialysis. Retrieval process of included studies is shown in **Figure 2-1**, in accordance with the PRISMA statement. [159]

Of the 45 included studies, 16 (36%) were prospective, [160–174] 6 (13%) were retrospective, [175–180] 19 (42%) were case reports or case-series, [181–199] and 4 (9%) were *ex-vivo* studies. [91,118,200–202] Of these 12 (27%) included a PopPK analysis. [161,162,165,167,171–176,179,180] Data on 33 different medications were reported within this analysis, including: 14 antibiotics (vancomycin, tobramycin, daptomycin, meropenem, doripenem, ticarcillin-clavulanic acid, teicoplanin, amikacin, clindamycin, piperacillin-tazobactam, cefepime, ceftriaxone, ceftolozane-tazobactam, linezolid), 4 antivirals (ribavirin, acyclovir, oseltamivir, peramivir), 4 antifungals (voriconazole, fluconazole, liposomal amphotericin B, caspofungin), 2 anticonvulsants (phenobarbital, phenytoin), 4 vasoactive agents (vasopressin, milrinone, dobutamine, dopamine), and others (clonidine, digoxin, theophylline,

midazolam, propafenone). Within this analysis, 20 out of 45 studies (44%) included children <1 year of age. [161,162,164,166–168,171–174,176–182,184–186,192] The clinical and methodological characteristics of included studies may be found in **Table 2-1**.

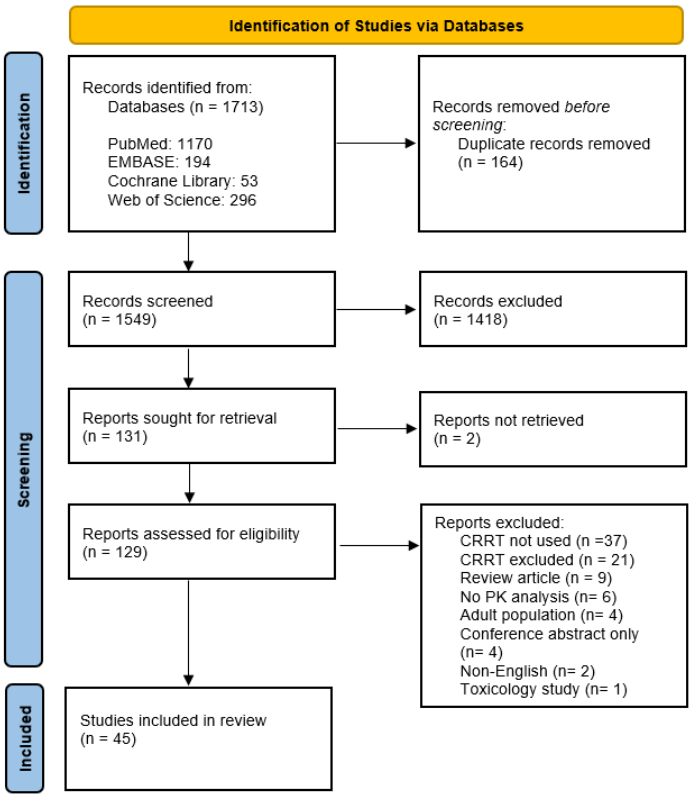


Figure 2-1. Preferred Reporting Items for Systematic Review and Meta-Analyses (PRISMA) diagram of included studies.
CRRT; continuous renal replacement therapy, PK; pharmacokinetics

The specific modality of CRRT used in the patient population was reported in 88% of included studies. All three methods of CRRT (i.e. CVVH, CVVHD, CVVHDF) were represented, with CVVH being the most common in 47% of studies. Information on specific CRRT modality, flow rates and filter components may be found in **Table 2-2**. At least one patient received ECMO in approximately half (53%) of the studies, with VA-ECMO being the most common method. To fully assess the impact of CRRT on clearance (CL_{RRT}), an understanding of blood, replacement fluid, dialysate and/or ultrafiltrate fluid flow rates is required. Within the studies incorporating CRRT, blood flow rate was reported in 24 (53%), replacement fluid was

reported in 14 (31%), dialysate flow rate was reported in 19 (42%) and ultrafiltrate flow rate was reported in 25 (56%) studies respectively. Only 18 (40%) studies reported all necessary mechanistic properties of CRRT to assess impact on CL_{RRT}. The specific filter used within the CRRT machine was reported in 27 (60%) studies, with the AN 69 polyacrylonitrile filter being the most common.

To assess certain confounding characteristics on the pharmacokinetic alterations within this patient population, information on baseline laboratory values (i.e. creatinine, albumin, liver enzymes), residual renal function and concurrent medications was analyzed. Baseline SCr, albumin and liver enzymes were reported in 53%, 24%, and 29% of studies, respectively. Reported information on residual renal function or urine output was included in 40% of the studies. The inclusion of a comparator group, children not receiving CRRT, was included in 4 (9%) out 45 studies. [166,173,178,193] Therefore to assess comparison of pharmacokinetic parameters in those studies that did not include a comparator, pharmacokinetic studies of age-matched historical controls not receiving CRRT were investigated.

Table 2-1. Overview of study characteristics that met inclusion criteria.

Reference (Year of Publication)	Country	Study Design	Drug	Participants (n)	Sex (F/M)	Age±SD (n) [range]	Weight (kg) [range]	Height (cm) [range]	Organ Dysfunction
Antibiotics									
Penicillins									
Lindsay *et al.* [187] (1996)	USA	Case-series	Ticarcillin-clavulanic acid	3 CRRT:3	F:1 M:2	9.2y ±2.4 [6-16y]	49.9 ±20.5 [22.1-100]	NR	NR
Tanggirdwood *et al.* [193] (2020)	USA	Case Report	Piperacillin/tazobactam	1 CRRT:1	F	13 y	42	NR	Renal, hepatic
Cephalosporins									
Stitt *et al.* [177] (2019)	USA	Retrospective	Cefepime	4 CRRT:4	F: 2 M:2	1.8 y [0.5-5y]	11.6 [5.4-25]	NR	NR
Butragueño-Laiseca *et al.* [173] (2020)	Spain	Population PK	Ceftolozane-Tazobactam	3 CRRT:1	NR	12 m [8-19 m]	8.5 [5.8-11]	NR	Renal, CV
Carbapenems									
Cies *et al.* [184] (2016)	USA	Case Report	Meropenem	1 CRRT:1	F	10 d	2.8	NR	Renal, hepatic, respiratory
Nehus *et al.* [171] (2014)	USA	Population PK	Meropenem	287 CRRT:287	NR	<1y: 52 1-5y: 58 5-12: 69 12-18y: 79 >18y: 29	Median: <1y: 3.7 (IQR 2.9-5.8) 1-5y :14 (IQR 11.3-16.5) 5-12y: 31.6 (IQR 22.0-37.8)	Median: <1y: 52.8 (IQR 48-58) 1-5y: 86.5 (IQR 79-98) 5-12y: 125 (IQR 114-138)	NR

							12-18y: 59.7 (IQR 44.6-70.4) >18: 55 (IQR 50.0-78.5)	12-18y:160 IQR 150-169) >18y: 165 (IQR 147-178)	
Nehus *et al.* [163] (2016)	USA	Prospective, open-label	Meropenem	7 CRRT:7	F:2 M:5	14.3y [5-21y]	18.59 [21.9-72.6]	147.04 [107.5-187.5]	Renal, respiratory
Rapp *et al.* [172] (2019)	France	Population PK	Meropenem	40 CRRT: 11	F: 20 M: 20	Median: 16.8 m [1.4-187.2 m]	Median: 9.1 [3.8-59]	NR	Renal, respiratory, CV
Saito *et al.* [190]53 (2020)	Japan	Case Report	Meropenem	1 CRRT:1	F	19 m	9.0	NR	Renal, respiratory
Tan *et al.* [165] (2021)	Singapore/USA	Prospective, open-label, population PK	Meropenem	9 CRRT:9	F: 5 M: 4	7.28y [0.1-18.9y]	24.52 [2.6-56.3]	NR	Renal, respiratory, hepatic, CV
Wang *et al.* [166] (2020)	China	Prospective, observational	Meropenem	27 CRRT:6	F: 13 M:14	Median: 1.29 y (IQR 0.67-3.25y)[d] 2.0 y (IQR 1.13-6.68y)[e] 2.50 y (IQR 0.5-5.25y)[f]	Median: 11 (IQR 7.75-12.63)[d] 12.50 (IQR 8.6-27.15)[e] 14.50 (IQR 6.53-21.50)[f]	NR	Renal, respiratory

Cies *et al.* [199] (2017)	USA	Case Report	Doripenem	1 CRRT:1	M	11 y	24.7	NR	Renal, respiratory
Aminoglycosides									
Armstrong *et al.* [182] (1993)	USA	Case Report	Tobramycin	1 CRRT:1	F	4 m	4.0	47	Renal
Glycopeptides									
Armstrong *et al.*[182] (1993)	USA	Case Report	Vancomycin	1 CRRT:1	F	4 m	4.0	47	Renal
Cies *et al.*[186] (2016)	USA	Case-series	Vancomycin	11 CRRT:11	F: 6 M: 5	8.38y [0.08-18y]	35.72 [3.1-61.7]	NR	Renal, respiratory, hepatic, CV
Moffett *et al.* [176] (2019)	USA	Retrospective, population PK	Vancomycin	138 CRRT:138	F: 37 M: 63	Median: 4.9 y (IQR 1.0-14.5y) GA: 40 w (IQR 39-40w) PMA: 297w (IQR 93-791w)	31.0 ±25.8	111 ±40	NR
Zylbersztajn *et al.*[178] (2018)	Chile	Retrospective	Vancomycin	29 CRRT:11	F: 10 M: 19	Median: 24 m (IQR 10-100m)[a] 42 m (IQR 12-99m)[b] 8 m (IQR 1-72m)[c]	Median: 12 (IQR 8-21)[a] 13.5 (IQR 8-23)[b] 8 (IQR 2.9-23)[c]	NR	Renal, respiratory

Lincosamides									
Poli *et al.* [196] (2019)	Switzerland	Case Report	Clindamycin	1 CRRT:1	NR	14 y	75	NR	Respiratory
Oxazolidinones									
Yang *et al.* [174] (2021)	China	Prospective, open-label, population PK	Linezolid	63 CRRT: 15	F: 20 M: 43	5.21y ±4.22 [0.10-15.3]	22.28±15 [4.20-70]	NR	Renal, respiratory, hepatic
Antivirals									
Aebi *et al.* [181] (1997)	USA	Case Report	Ribavarin	1 CRRT:1	M	10 d	3.3	NR	Renal, respiratory
Sargel *et al.* [192] (2018)	USA	Case Report	Ribavarin	1 CRRT:1	M	5 w	3.43	NR	Renal, respiratory
Cies *et al.* [185] (2015)	USA	Case Report	Acyclovir	1 CRRT:1	F	14 d	NR	NR	Renal, respiratory, hepatic
Karsch *et al.* [188] (2016)	Germany	Case Report	Oseltamivir	1 CRRT:1	F	9 y	NR	NR	Renal, respiratory, CV
Eyler *et al.* [198] (2012)	USA	Case Report	Oseltamivir	1 CRRT:1	M	6 y	28.2	NR	Respiratory
Wildschut *et al.* [169] (2010)	The Netherlands	Prospective, PK analysis	Oseltamivir	3 CRRT:3	F:1 M:2	11.67 y [6-15y]	45.19 [40-55.5]	NR	Respiratory
Dillon *et al.* [195]		Case report	Peramivir	1 CRRT:1	F	17 y	49.5	NR	Renal, respiratory
Antifungals									
Azoles									
Brüggeman *et al.* [183] (2008)	The Netherlands	Case report	Voriconazole	1 CRRT:1	M	5 y	NR	NR	Respiratory
Oualha *et al.* [189] (2019)	France	Case Report	Fluconazole	1 CRRT:1	NR	17 y	NR	NR	Renal

Watt *et al.* [168] (2012)	USA	Prospective, open-label,	Fluconazole	10 CRRT:3	NR	Median: GA: 37 w (IQR 36-390w) PNA: 19d (IQR 9-30d)	Median: 3.2 (IQR 2.6-3.4)	NR	Renal, respiratory
Watt *et al.* [167] (2015)	USA	Open-label, 3 prospective trials, population PK	Fluconazole	40 CRRT:7	F: 14 M: 26	Median PNA: 22d [1-6498d] GA: 38w [24-41w] PMA:41w [35-79w]	Median: 3.4 [1.9-77]	NR	Renal, respiratory
Anticonvulsants									
Michaličková *et al.*[162] (2020)	Czech Republic	Prospective, cohort, population PK	Phenobarbital	13 CRRT:1	F: 6 M:7	Median: 2 d (IQR 0-7d) GA: 38 w (IQR 38-41w)	Median: 3.23 (IQR 2.67-3.72)	NR	Respiratory
Suzuki *et al.* [197] (2019)	Japan	Case Report	Phenobarbital	1 CRRT:1	F	9 y	NR	NR	Renal
Thibault *et al.* [179] (2020)	USA	Retrospective, population PK	Phenobarbital	35 CRRT:8	F: 14 M: 21	Median: PNA: 14d [1-154d] PMA: 40.4w [35.7-55.9w]	Median: 3.4 [1.6-8.1]	Median: 50.4 [31.5-74.8]	Renal, respiratory, cardiac

Rosenberg *et al.*[194] (2014)	Sweden	Case Report	Phenobarbital	1 CRRT:1	M	14 y	41	140	Renal, respiratory, hepatic
Thibault *et al.* [180] (2020)	USA	Retrospective, population PK	Phenobarbital	38 CRRT:2	NR	Median: PNA: 5 d [0-26d] PMA: 39^{2} w [28^{2}-$42w^{6}$]	Median: 3.2 [1.3-3.8]	Median 49	Renal, respiratory, CV
Vasoactive Agents									
Baird [160] (2010)	USA	Prospective, cohort	Vasopressin	9 CRRT:9	NR	Median: 14 y [1-19y]	NR	NR	Renal
Gist *et al* [175] (2015)	USA	Retrospective, population PK	Milrinone	11 CRRT:3	F: 2 M:1	12 y	20	NR	Renal
Freter *et al.* [170] (1998)	USA	Prospective, PK analysis	Dopamine Dobutamine	3 CRRT:3	F: 2 M:1	NR	12.46 [8-16.4]	81 [75-85]	Renal
α-Adrenergic Receptor Agonist									
Kleiber *et al.* [161] (2017)	The Netherlands	Prospective, cohort, population PK	Clonidine	22 CRRT: 20	F: 11 M:11	Median: 1.0 m (IQR 6.4m) GA: 38.9 w (IQR 5.6w) PMA: 42.8 w (IQR 17.6w)	Median: 4 (IQR 3.1)	NR	Renal, respiratory, CV
Benzodiazepine									
Mulla *et al.*[164] (2003)	England	Prospective, cohort	Midazolam	20 CRRT:7	F: 9 M: 11	IV GA: 40.2 w ±1.2	IV: 3.6 ±0.6	NR	Renal, respiratory

						ECLS GA: 38.9 w ±2.4	ECLS: 3.2 ±0.5		
Anti-arrhythmics									
Seto *et al.* [191] (1999)	Canada	Case Report	Propafenone	1 CRRT:1	F	3 y	11	NR	Renal, hepatic

All data reported as mean [range] unless otherwise stated.

AKI; acute kidney injury, cm; centimeters, CRRT; continuous renal replacement therapy, CV; cardiovascular, d; days, ECMO; extracorporeal membrane oxygenation, F; female, GA; gestational age, IQR; interquartile range, kg; kilograms, M; male, m; months, NR; not reported, PMA; postmenstrual age, PNA; postnatal age, PK; pharmacokinetics, RRT; renal replacement therapy, SD; standard deviation, y; years.

a: ECMO no acute kidney injury (AKI)/RRT
b: AKI with or without RRT
c: ECMO with RRT without AKI
d: Non ECLS
e: CRRT
f: ECMO

3.1.2 Quality Assessment

Of the 24-items within the ClinPK checklist, >50% provided an explanation of the study rationale, objectives and hypotheses, eligibility criteria, drug preparation characteristics, pharmacokinetic modelling techniques and formulas for calculating pharmacokinetic variables. All detailed percentages of included studies within this review may be found in **Appendix A-2**. Only 26 of the 45 included studies (58%) provided background information on pharmacokinetic data of the drug used within each respective study. Additionally, 15 out of 45 studies (33%) reported a description of concurrent medications used within study population, therefore limiting the ability to assess for confounding drug-drug interactions. One of the main findings within this review was the paucity of reporting of patient demographics that may account for inter- and intra-patient pharmacokinetic variability. Of the 45 studies, only 16 (38%) described relevant patient demographics within this review. As this review was focused on the pharmacokinetic changes associated with CRRT, reporting of CRRT modality and settings were assessed. Eighteen (40%) studies reported all necessary mechanistic properties of CRRT modality to assess impact on CL_{RRT} and to allow for reproduction of methodology. [91,118,163,166,171,176,177,184,186,189–191,194,195,197,200,201]

3.1.3 Alterations in Pharmacokinetic Parameters

3.1.3.1 Antibiotics

3.1.3.1.1 Penicillins

3.1.3.1.1.1 Tircacillin-Clavulanic Acid

One study within this review included a case-series (n=3) investigating the pharmacokinetics of ticarcillin-clavulanic acid in pediatric patients receiving CRRT. [187] Study investigators demonstrated ticarcillin-clavulanic acid pharmacokinetics with a one-compartment, first order model. [187] Each patient received CVVH with an average ultrafiltration flow rate of 890 mL/h. [187] Two patients within this study received ECMO for a portion of study duration. Mean weight normalized CL_{total} was determined to be 0.038 L/h/kg and 0.184 L/h/kg for ticarcillin and clavulanic acid, respectively. [187] Weight normalized CLRRT for ticarcillin and clavulanic acid was 0.022 L/h/kg and 0.049 L/h/kg. [187] The differences in CLRRT between the

two molecules may be explained by the increased SC of clavulanic acid compared to ticarcillin (1.69 vs. 0.83). [187]

Total weight normalized clearance for ticarcillin within this population was lower than prior reports of critically ill premature infants (0.047-0.074 L/h/kg) [203–205] and full-term infants and children (0.126-0.150 L/h/kg) not receiving CRRT. [206,207] The recorded V_d is similar to what has been reported in the literature within pediatric patients not receiving CRRT (0.22-0.48 L/kg). [203,205–207] No dosing recommendations were provided by study investigators.

3.1.3.1.1.2 Piperacillin-Tazobactam

We identified one case-report analyzing the pharmacokinetics of piperacillin-tazobactam in a 13-year-old pediatric patient receiving CRRT. [193] Due to pre-existing liver failure, molecular adsorbent recirculating system (MARS) therapy was administered in conjunction with CVVHD to aid in fluid and albumin filtration. [193,208] Piperacillin-tazobactam was administered as an intermittent infusion over 30 minutes with a dose of 48 mg/kg/dose every 8 hours. [193] CL_{total} of piperacillin-tazobactam was determined prior to MARS and CVVHD, while on MARS/CVVHD and during CVVHD only. CL_{total} was 0.13 L/h/kg, 0.39-0.45 L/h/kg and 0.18 L/h/kg during each analytical period. [193] Interestingly, CL_{total} during MARS/CVVHD within this study was similar to prior analyses of critically ill patients with augmented renal clearance (ARC) or burns (0.18-0.299 L/kg/h). [209,210] CL_{total} of piperacillin-tazobactam in this patient receiving MARS/CVVHD was also similar to healthy infants and children (0.198-0.33 L/h/kg). [206] Investigators suggested that a piperacillin-tazobactam dose of 80 mg/kg/dose every 6 hours would be required to ensure 50% fT> 4xMIC while receiving MARS/CVVHD and 100% fT> 4xMIC while receiving CVVHD alone for the treatment of *Pseudomonas aeruginosa* (MIC 16 µg/mL). [193]

3.1.3.1.2 Cephalosporins

3.1.3.1.2.1 Cefepime

The investigation by Stitt *et al.* was a retrospective study analyzing the pharmacokinetics of cefepime in pediatric patients receiving CVVHDF. [177] Cefepime was administered as an intermittent infusion with doses of 48-64 mg/kg/dose every 6-12 hours. [177] CVVHDF settings may be found in **Table 2-2**. CL_{total} within this study was determined to be 0.056 L/h/kg, with a

V_d of 0.14 L/kg and an elimination t ½ of 1.93 h. [177] The weight normalized CL_{total} in this study was slightly reduced compared to previous investigations in neonates (0.07-0.20 L/h/kg), [211–214] and critically ill infants and children not receiving CRRT (0.19 L/h/kg). [215] In comparison, the V_d determined within this study was significantly lower than those recorded in neonates (Vd 0.41-0.43 L/kg), [212,213] and infants and children (V_d 0.33 L/kg). [215] Study investigators suggested that doses > 50 mg/kg/dose every 12 hours are required to achieve a pharmacodynamic target of 100% fT> 1-4xMIC, assuming MIC of 8 µg/mL for *Pseudomonas aeruginosa.* [177]

3.1.3.1.2.2 Ceftolozane-Tazobactam

Butragueño-Laiseca *et al*. reported the results of a pharmacokinetic analysis of 3 pediatric patients receiving ceftolozane-tazobactam. [173] Within this analysis, an intra-study comparison was conducted between patients with sepsis and no AKI, sepsis with AKI and sepsis requiring CVVHDF support. Ceftolozane-tazobactam was administered as an IV intermittent infusion of 40 mg/kg every 6 hours, 36 mg/kg every 8 hours and 30 mg/kg every 8 hours for each respective patient. [173] CL_{Renal} was 0.88 L/h, 0.27 L/h and 0.39 L/h in each patient. V_{SS} was 2-fold higher in the patient without renal dysfunction compared to CVVHDF (4.39 L vs. 1.91 L). [173] Interestingly, elimination t ½ was consistent between the patient receiving CVVHDF and that who didn't. Ceftolozane-tazobactam was determined to have a SC of 1.06 within the CVVHDF circuit.

Pharmacokinetic parameters reported in this study differed slightly than those determined in a single IV dose pharmacokinetic study conducted by Bradley *et al.* [216] Study authors determined that doses of 35 mg/kg IV Q8H, 10 mg/kg IV Q8H and 30 mg/kg IV Q8H would be sufficient to ensure 40% fT>MIC, assuming a MIC of 4 µg/mL for *Pseudomonas aeruginosa.* [173] However, due to the small sample size included within this analysis, further research is needed to confirm these findings.

3.1.3.1.3 Carbapenems

3.1.3.1.3.1 Meropenem

Meropenem was the most studied drug identified within the literature, with 7 studies included within this review. Within these 7 studies, 5 were prospective pharmacokinetic analyses [163,165,166,171,172] and 2 were case reports. [184,190] A total of 363 patients were analyzed, with sepsis being the most common reason for admission. CL_{total} of meropenem ranged from 0.09-0.474 L/kg/h within these patients across all CRRT modalities. In the studies that reported V_d it was quite heterogenous, ranging from 0.194 to 0.59 L/kg. Cies *et al.* reported the pharmacokinetics of meropenem administered as a 10 mg/kg continuous infusion to a 10-day old neonate weighing 2.8 kg receiving CVVHDF. [184] The authors concluded that a loading dose of 40 mg/kg, followed by a continuous infusion of 10 mg/kg/h would provide 100% fT>MIC up to the *Pseudomonas aeruginosa* breakpoint of 16 µg/mL. [184] The need for extended interval administration of meropenem in patients receiving CRRT was also reported by Saito *et al*. [190] The child within this report received CVVHD+ECMO with a blood flow rate of 50-80 mL/min, and a dialysate flow rate of 820-1500 mL/h. [190] It was determined that meropenem 200-300 mg/kg/day every 8 hours as a 1-hour infusion or meropenem 200-300 mg/kg/day every 8 hours as a 3-hour infusion would be necessary to achieve a pharmacodynamic target for *Escherichia coli* (MIC= 1µg/mL).

A popPK model of meropenem was simulated for pediatric patients receiving CRRT and then further validated by a prospective, pharmacokinetic analysis by Nehus *et al*. [171] Within this simulation, meropenem was administered as an intermittent infusion of 20 mg/kg/dose every 8-12 hours to patients <1-18 years of age. All modalities of CRRT were simulated, with 49% receiving CVVHD, 27% receiving CVVH and 24% receiving CVVHDF. [171] A popPK, four-compartment model was used in dosing simulations, final popPK model estimates may be found in **Table 2-2**. To obtain the pharmacodynamic target, it was determined that children (<5kg) receiving CRRT should receive meropenem 20 mg/kg every 8 hours and children (>5 kg) should receive meropenem 20 mg/kg every 12 hours.

These results were further validated in a prospective pharmacokinetic study (n=7) with participants receiving an average meropenem dose of 18.6 mg/kg/dose. [163] Two subjects received CVVH, while the remaining received CVVHDF for renal dysfunction and fluid

overload. [163] Administering a dose of meropenem 20 mg/kg every 12 hours achieved a pharmacodynamic target of 100% fT>MIC in 5/7 patients for *Pseudomonas aeruginosa* (MIC= 4 µg/mL. [163]

Rapp *et al.* conducted a prospective, pharmacokinetic analysis of 40 critically ill pediatric patients receiving meropenem. [172] A two compartment, first order elimination popPK model was used to describe the pharmacokinetics. [172] In those who did not receive CRRT, more than half were determined to have augmented renal clearance (ARC; eGFR >130 mL/min/1.73 m^2). [172,217] CRRT was determined to be an influential covariate for CL_{total} of meropenem in those children receiving therapy. [172] Upon popPK simulations, the authors concluded that intermittent infusions of meropenem 20 mg/kg/dose every 8 hours is adequate for treating bacteria with a MIC <2 µg/mL. [172] However, for bacteria with an elevated MIC (>4 µg/mL), meropenem should be administered as a continuous infusion of 60 mg/kg/day in pediatric patients receiving CRRT. [172]

The fourth prospective, pharmacokinetic analysis of meropenem in pediatrics receiving CRRT identified within this review was conducted by Tan *et al*. [165] A two-compartment model was used to determine meropenem pharmacokinetics. [165] Meropenem was administered as an intermittent infusion of 20-40 mg/kg/dose every 12 hours. Four children received CVVH, while 5 received CVVHDF. [165] Additionally, 4 children received concurrent ECMO during the study period. [165] Mean CLRRT of 1.4 L/h was determined in these patients, which was similar to that recorded by Nehus *et al.* (1.9 L/h). [163,165] The average SC of meropenem for CRRT was 0.96, demonstrating the ability for meropenem to pass across the CRRT circuit membrane. [165] The authors concluded that meropenem 20 mg/kg/dose every 8 hours administered as a 4 hour intermittent infusion or meropenem 40 mg/kg/dose every 8 hours as a 2 hour infusion would be sufficient to attain pharmacodynamic target in these patients receiving CRRT with an ultrafiltration rate of 1952 mL/1.73m^2/h. [165]

Wang *et al.* analyzed 27 pediatric patients receiving meropenem 20 mg/kg/dose every 8 hours as a 1-hour intermittent infusion. [166] Analyses were conducted in patients receiving CVVHDF, ECMO or neither. [166] CLtotal was similar between the 3 groups, 15.73 L/h in those children receiving CVVHDF, 11.59 L/h in those children on ECMO, and 13.51 L/h with no extracorporeal therapy. [166] Interestingly, V_d was decreased in patients receiving CVVHDF

(19.42 L) compared to those on ECMO (31.67 L) and those not receiving ECLS (34.41 L). [166] Elimination t ½ of meropenem was similar between the 3 cohorts. The authors concluded that meropenem 20 mg/kg/dose every 8 hours administered as a 1-hour infusion is appropriate for critically ill children receiving CVVHDF, ECMO or neither. [166]

Several pharmacokinetic analyses have been conducted with meropenem in critically ill children not receiving CRRT. There is substantial heterogeneity within the literature in terms of primary pharmacokinetic parameters. CL_{total} for meropenem in neonates has been shown to be 0.24 L/kg/h, [218] and 0.33-0.43 L/kg/h in critically ill children. [219–224] While Vd of meropenem in neonates has been shown to be 0.55 L/kg, [218] and 0.20-0.78 L/kg in critically ill children. [219–224] CL_{total} and V_d of meropenem in critically ill children appear to be similar regardless if CRRT is administered or not, suggesting higher than labelled doses may be required to ensure pharmacodynamic target attainment.

3.1.3.1.3.2 Doripenem

The use of doripenem in an 11-year-old pediatric patient was investigated by Cies *et al*. [199] Dorpienem was administered as a 2.5 mg/kg/h continuous infusion for the treatment of pneumonia due to multi-drug resistant organisms. At the time of CVVH administration, this patient maintained residual renal function with a urine output of 0.46 mL/min/kg. CL_{total} of doripenem was 10.5 mL/kg/min. [199] Administering doripenem as a 2.5 mg/kg/h continuous infusion ensured 100% fT>MIC for bacteria with a MIC <4 mg/L. [199] CL_{total} of doripenem in this patient was over 2-fold of what has been previously reported in pediatric patients not receiving CRRT (4.4-4.8 mL/min/kg). [225] The results of this case report demonstrate that CLtotal is substantially increased with CVVH and residual renal function, therefore alterations in dosing administration may be needed to ensure pharmacodynamic target attainment. Further studies are warranted to confirm these findings.

3.1.3.1.4 Aminoglycosides

3.1.3.1.4.1 Tobramycin

Despite the widespread use of tobramycin in neonates and infants, only one case-report was included within this review analyzing the pharmacokinetics in a 4-month-old anuric infant. [182] Tobramycin was administered as 1.8-2.5 mg/kg/dose, with the interval guided by therapeutic drug monitoring. As a result of renal dysfunction, CVVH was started with a blood

flow rate of 15 mL/min and an ultrafiltration flow rate of 20-30 mL/min. [182] CLRRT of tobramycin was determined to be 0.32-0.91 mL/min, while elimination t ½ decreased from 40-44 hours to 20-23 hours during CVVH. [182] The authors determined that 48-66% of the tobramycin dose was removed during a 24-hour CVVH study period. [182] Tobramycin elimination t ½ in healthy pediatrics has been reported to be 2.37 h, [226] and 1.2-2.32 h in adults. [226–230] Elimination t ½ of tobramycin has also been shown to be increased in critically ill adults not receiving CRRT (2.9-5.4 h). [229,230]

3.1.3.1.5 Glycopeptides

3.1.3.1.5.1 Vancomycin

Four studies within this review analyzed the pharmacokinetics of vancomycin in pediatrics receiving CRRT. These 4 studies included 179 patients, ranging from ages 4 months to 14.5 years. [176,178,182,186] Two studies were retrospective, [176,178] and two were case-reports/case-series. [182,186] Only one study within this analysis included patients receiving ECMO concurrently with CRRT. [178] Three studies included pharmacokinetic analyses, [176,178,182] while one study results were based on data from trough concentrations. [186]

Armstrong *et al.* conducted a pharmacokinetic analysis in a 4-month old neonate receiving vancomycin 11-15 mg/kg/dose as an intermittent infusion. [182] Due to renal dysfunction, CVVH was initiated with a blood flow rate of 15 mL/min and an ultrafiltration rate of 20-30 mL/min. [182] CL_{RRT} of vancomycin was determined to be 0.27-0.80 mL/min with an elimination t ½ of 20-24 h. [182] The SC of vancomycin within the CVVH membrane filter was 0.86-1.55. [182] The authors determined that 35% of the vancomycin dose was removed by CVVH. [182]

A novel vancomycin administration approach was investigated in a case-series of 11 pediatric patients by Cies *et al*. [186] Within this study, a 15-20 mg/kg loading dose followed by the addition of vancomycin into the CRRT solution at a final concentration of 18-30 mg/L was administered continuously. All three CRRT modalities were used within the analysis, with 4 patients receiving CVVH, 2 patients receiving CVVHD and 8 patients receiving CVVHDF. [186] Average vancomycin concentration at the time of analysis was 22.3 (±3.3) µg/mL, with 8/11 patients meeting therapeutic target within 8 hours. [186] The authors concluded that the application of administering vancomycin within the CRRT solution at a final concentration of

18-30 mg/L may be safe and effective in pediatric patients receiving CRRT, however further studies are needed to confirm these results. [186]

Moffet *et al.* conducted a retrospective, pharmacokinetic analysis of 138 patients receiving vancomycin while on CVVHDF. [176] Within this analysis, the mean vancomycin dose administered as a 1-hour intermittent infusion was 14.3 mg/kg/dose. A popPK, two compartment model was used to describe vancomycin pharmacokinetics within this population. [176] CL_{total} of vancomycin was 2.29 L/h, with V_d of central and peripheral compartments 81 L and 550 L, respectively. [176] Dialysate and ultrafiltration rates were found to be significant covariates for CL_{total} upon popPK analysis. It was determined that vancomycin 40-50 mg/kg/day every 8-12 hours dosed upon fat-free mass (FFM) would be necessary to achieve an AUC/MIC ratio ≥400 and a vancomycin trough < 20 mg/L in pediatric patients receiving CVVHDF. [176] Final popPK model and significant covariates for CL and V_d may be found in **Table 2-2**.

The final vancomycin pharmacokinetic study included within this review investigated 29 critically ill pediatric patients receiving extracorporeal therapy. [178] This analysis included a comparison of 3 groups, those receiving ECMO with no AKI/CRRT (1), those with AKI receiving ECMO ± CRRT (2) and those receiving ECMO and CRRT without AKI (3). [178] Vancomycin was administered as 40 mg/kg/day every 6 hours, 40 mg/kg/day every 8 hours and 40 mg/kg/day every 8 hours for the 3 respective groups. [178] CL_{total} of vancomycin was determined to be 1.67 mL/min/kg, 0.83 mL/min/kg and 1.17 mL/min/kg in the 3 groups, while V_d was 0.73 L/kg, 1.16 L/kg, 0.88 L/kg. [178] Final adjusted doses of vancomycin 40 mg/kg/day every 6 hours, 20 mg/kg/day every 12 hours and 40 mg/kg/day every 6 hours for each respective group to ensure an AUC/MIC ≥ 400. [178]

The pharmacokinetics of vancomycin in critically ill pediatric patients has been widely studied due to its broad spectrum of activity against gram-positive bacterial infections. CL_{total} in critically ill pediatric patients has been shown to be quite heterogenous. With a CL_{total} of 0.07-0.117 L/kg/h in patients with septic shock, [43,231] 0.11-0.19 L/kg/h in patients with cardiogenic shock and/or post-cardiac surgery, [232–234] 0.05-0.18 L/kg/h in children with malignancy, [235,236] and 3.24 L/kg/h in critically ill patients with ARC. [237] V_d of vancomycin may also change depending on patient population, as for critically ill pediatric patients the V_d may range from 0.40-0.91 L/kg, [43,231–233,237] with a slightly higher V_d in critically ill oncology

pediatric patients of 1.03-1.04 L/kg. [235,236] The identified studies within this analysis suggest that CL_{total} and V_d of vancomycin may be similar among critically ill pediatric patients, regardless of CRRT. Use of vancomycin should be guided by TDM to ensure efficacy and minimize toxicity.

3.1.3.1.6 Lincosamides

3.1.3.1.6.1 Clindamycin

This review identified only one case-report analyzing the pharmacokinetics of clindamycin administered to a 14-year-old pediatric patient receiving CRRT. [196] Within this study, clindamycin, at an unrecorded dose, was administered to a patient with septic shock while on concomitant CVVH and VV-ECMO. The pharmacokinetics were described with a one-compartment model, with a CLtotal of 3.6-15.5 L/h. [196] The authors concluded that no dose adjustments for clindamycin are necessary for pediatric patients receiving CVVH + ECMO. [196] CL_{total} within this analysis is consistent to what has been shown in pediatric pharmacokinetic studies of the same age not receiving extracorporeal therapy (4.17-14.25 L/h). [238]

3.1.3.1.7 Oxazolidones

3.1.3.1.7.1 Linezolid

A recent popPK analysis by Yang *et al*. investigated the pharmacokinetics of IV linezolid in pediatric patients with suspected or confirmed infection due to multi-drug resistant gram-positive cocci. [174] 63 children were included, with 15 receiving CRRT and 2 on ECMO. No information was reported on CRRT modality, flow rates, or filters used within this study. A dose of 10 mg/kg three times per day was given to patients <12 years of age (n=57) and 600 mg twice daily for children 12-18 years (n=6). The pharmacokinetics of linezolid were described with a two-compartment, first order model, with weight and AST being significant covariates for CL_{total}. CRRT and ECMO were included within popPK model analysis, however, were shown to be insignificant covariates on linezolid pharmacokinetics. The final popPK model may be found in **Table 2-2**. CL_{total} and V_C were estimated to be 2.34 L/h and 5.22 L, respectively. [174] CL_{total} and V_c estimates within this study were increased compared to those reported by an alternative popPK analysis in children of similar age. [239] Within this study, CL_{total} and V_d were 1.31 L/h and 4.24 L, respectively. [239] Characteristics of critical illness were not considered within this

analysis, as such future studies are needed to determine the influence of critical illness, CRRT and/or ECMO on the pharmacokinetic parameters of linezolid within pediatric patients.

3.1.3.2 Antivirals

3.1.3.2.1 Ribavarin

Two case-reports were identified within this review describing the pharmacokinetics of ribavirin in pediatric patients receiving CRRT. [181,192] In each case, CVVH and ECMO were administered to the patient for renal and respiratory support. [181,192] Ribavarin was administered as 5 mg/kg/dose intermittent infusion every 6 hours to a 10 year old pediatric patient within Aebi *et al.* [181] CL_{RRT} of CVVH was determined to be 0.046 L/kg/h with a V_d at steady state of 1.37 L/kg. [181] As 39% of the ribavirin dose was eliminated by CVVH+ECMO, the authors concluded that no dosing adjustments are necessary in patients receiving extracorporeal therapy. [181]

Within the case-report conducted by Sargel *et al.*, a higher dose of ribavirin was administered to this 5-week-old patient. [192] CL_{total} within this analysis was 0.31-0.76 L/kg/h. [192] CL_{RRT}, V_d and elimination t ½ were calculated to be 0.12 L/kg/h, 2.92-5.1 L/kg, and 2.68-10.7 h respectively. [192] The sieving coefficient of ribavirin was 1.17, slightly higher than the value recorded by Aebi *et al.* [181,192]

There is a paucity of pharmacokinetic data within the literature analyzing ribavirin in critically ill pediatric patients. CL_{total} for ribavirin in pediatric patients being treated for viral encephalitis and human immunodeficiency virus (HIV) infections were shown to be 0.29 L/kg/h and 0.39 L/kg/h respectively. [240,241] V_d in patients receiving CRRT + ECMO in the analysis by Sargel *et al.* were consistent with children not receiving extracorporeal therapy (5.1 L/kg vs. 4.64-7.7 L/kg). [192,240,241] Elimination t ½ was also similar between the two groups (10.7 h vs. 10.8-18.6 h). [192,240,241]

3.1.3.2.2 Acyclovir

One case-report investigated the pharmacokinetics of acyclovir in a critically ill pediatric patient receiving CVVH/CVVHDF in addition to ECMO. [185] Acyclovir was initially started as an intermittent infusion of 30 mg/kg/dose every 8 hours, then subsequently changed to be administered continuously within the CRRT dialysate solution to a final concentration of 5.5

μg/mL. [185] Plasma concentrations of acyclovir were determined to be 8.4 mg/L and 5.3 mg/L at 24 h and 72 h respectively. [185] Administering acyclovir as a continuous infusion within the dialysate solution may be safe and effective in pediatric patients receiving CRRT + ECMO, however further studies are needed to confirm these findings. [185]

3.1.3.2.3 Oseltamivir

Two case-reports and one prospective, pharmacokinetic study were included within this analysis. [169,188,198] Karsch *et al.* investigated the use of oral (75 mg twice daily) and intravenous (100 mg twice daily) oseltamivir in a 9-year old patient receiving CVVHDF and ECMO. [188] The ultrafiltration rate for CVVHDF administered to this patient was 1.2 $L/m^2/h$. [188] AUC_{0-12} was 1070 ng·h/mL for oseltamivir and 47,250 ng·h/mL for oseltamivir carboxylate (OSC). [188] The average SC during the sampling period of oseltamivir was 1.39 and 1.44 for OSC. [188] Despite target concentrations for oseltamivir not being well defined, the authors concluded that oral doses of 75 mg twice daily and intravenous doses of 100 mg twice daily for oseltamivir may be necessary to ensure antiviral activity in children receiving extracorporeal support. [188]

A similar analysis was conducted by Eyler *et al.* in a 6-year-old pediatric patient receiving CVVHD and ECMO. [198] Oseltamivir was administered as an oral dose of 90 mg (4 mg/kg) twice daily. CVVHD was administered using the AN-69 filter membrane with a dialysate flow rate of 1000 mL/h and a mean ultrafiltration rate of 304 mL/h. [198] Non-compartmental methods were used to describe the pharmacokinetics of oseltamivir and OSC. CL_{total} of oseltamivir and OSC was 0.33 L/kg/h and 0.23 L/kg/h respectively. [198] CL_{RRT} was 0.07 L/kg/h and 0.06 L/kg/h for oseltamivir and OSC. [198] AUC_{0-12} for oseltamivir was calculated to be 30.5 ng·h/mL, while OSC was 905 ng·h/mL, significantly lower than that analyzed by Karsch *et al.* and Wildschut *et al*. [169,188,198] Oseltamivir and OSC saturation coefficients for CVVHD were 0.99 and 0.85 respectively. [198] Based these results, it was recommended that oral oseltamivir 90 mg twice daily should be given to pediatric patients receiving CVVHD and ECMO. [198]

The pharmacokinetics of oseltamivir in patients receiving organ support identified within this review mirror previous pediatric pharmacokinetic reports. An analysis conducted by Oo *et al.* investigated the pharmacokinetics of oseltamivir suspension (2 mg/kg) administered to

children (1-12y) and adolescents (13-18y). [242] CL_{total} in this analysis was 0.63 L/kg/h for OSC in children and 0.32 L/kg/h in adolescents, consistent with Eyler *et.al.* [198,242] Elimination t ½ of OSC in pediatrics not receiving organ support are also similar to those that do, with an elimination t½ of 7.8 h in children and 8.1 h in adolescents. [242]

3.1.3.2.3 Peramivir

Dillon *et al.* reported the pharmacokinetics of peramivir in a 17-year old pediatric patient receiving CVVHDF. [195] Throughout hospital stay the patient experienced significant renal and respiratory dysfunction due to septic shock associated with H1N1 influenza. [195] CL_{total} in this patient was 0.032 L/kg/h, with a V_d 0.32 L/kg. [195] Elimination t ½ of peramivir was 11.6 h. [195] The case series conducted by Cies *et al.* analyzed the pharmacokinetics of peramivir in 11 patients admitted to the PICU. [243] Median CL_{total} was 0.31 L/kg/h, with a 0.58 L/kg V_d and a 1.7 h elimination t ½. [243] These results are slightly different than those determined by a popPK analysis in infants and children by Sugaya *et.al*. [244] CL_{total}, and V_d from the final model were 0.516 L/kg/h and 0.194 L/kg, respectively, [244] suggesting CL_{total} of peramivir is significantly lower in pediatric patients receiving CVVHDF. Further studies are needed to confirm these findings.

3.1.3.3 Antifungals

3.1.3.3.1 Azoles

3.1.3.3.1.1 Voriconazole

Brüggeman *et al.* reported the pharmacokinetics of voriconazole in a 5-year old patient receiving concurrent CVVH and VV-ECMO for an invasive aspergillus infection. [183] Voriconazole (IV) 7 mg/kg twice daily was started and further increased to 14 mg/kg twice daily based on TDM. [183] Information regarding CVVH prescription was not reported within this analysis. Based on the plasma concentrations, a non-compartmental pharmacokinetic analysis of voriconazole was conducted. CL_{total} was shown to be 0.22 L/h/kg, within an elimination t ½ of 4.7 h. [183] AUC0-12 of voriconazole in this patient was 64 mg·h/L. [183] The authors determined that pediatric patients receiving CRRT+ECMO should receive a voriconazole dose of 10-14 mg/kg twice daily to achieve target trough (Cmin) concentrations > 1mg/L. [183] TDM is recommended to ensure efficacy and safety.

Several PopPK models have been constructed to describe the pharmacokinetics in pediatric patients, including critically ill and immunocompromised. [245–247] CL_{total} identified within these analyses are quite heterogenous, ranging from 0.09-0.582 L/h/kg. [245–247] Elimination t ½ closely resembled that determined by Brüggeman *et al.*, with a range of 2.41-2.45 hr for voriconazole. [245,246] As V_d was not reported by Brüggeman *et al.*, no comparison can be made, however due to the use of ECMO in this patient one would assume an increased V_d due to the effects of ECMO on lipophilic drugs (logP voriconazole = 1.82). [127,248] Further analyses in pediatric patients receiving organ support are needed to confirm if higher doses are required to achieve pharmacodynamic targets.

3.1.3.3.1.2 Fluconazole

Fluconazole was the most studied antifungal agent in pediatric patients receiving CRRT identified within this review. One case report, [189] and 2 prospective analyses, [167,168] totaling 51 patients were analyzed. Oualha *et al.* reported the pharmacokinetics of a 17-year old patient receiving fluconazole IV 600 mg once daily as a 30-minute intermittent infusion. [189] As the patient developed anuric renal dysfunction, CVVHD was started with an ultrafiltration rate of 90 mL/h. [189] CL_{total} and CL_{RRT} of fluconazole in this patient were 2.79 L/h and 1.64 L/h, respectively. [189] V_d at steady state was shown to be 30 L, with an elimination t ½ of 7.4 h. [189] The authors concluded that a fluconazole loading dose of 900 mg IV, followed by maintenance doses of 600 mg IV twice daily would be required to achieve target attainment in pediatric patients receiving CVVHD for *Candida* infections with an MIC >2 mg/L. [189]

The first prospective, pharmacokinetic analysis conducted by Watt *et al.*, investigated fluconazole use in infants (<120 post-natal days; median GA 37 w). [168] Fluconazole was administered as a 25 mg/kg IV dose over 2-hours for prophylaxis and 12 mg/kg IV once daily over 1-hour for known or suspected fungal infection. [168] All patients were treated with ECMO, while only 2 received CVVH and 1 received CVVHD. Median CL_{total} of fluconazole in those who received one dose was 0.017 L/h/kg, and 0.022 L/h/kg in those were received multiple doses. [168] V_d and elimination t ½ were similar between the two groups. [168] The pharmacokinetics of fluconazole were described with a one-compartment model, with 7/9 infants achieving 50% T>MIC for prophylaxis. [168] The authors concluded that fluconazole 25 mg/kg

IV weekly would be sufficient for pharmacodynamic target attainment in prevention of fluconazole infections in patients receiving organ support. [168]

The second prospective, pharmacokinetic analysis conducted by Watt *et al.*, utilized prospective data from 3 open-label pharmacokinetic studies (n=40) in patients receiving ECMO ± CRRT. [167] Fluconazole was administered as a 25 mg/kg IV dose for prophylaxis, and a 25 mg/kg loading dose, followed by a 12 mg/kg daily maintenance IV dose for treatment of confirmed or suspected fungal infections. [167] Twenty-one patients received ECMO support, while only 7 received CRRT. A one-compartment popPK model was used to describe fluconazole pharmacokinetics within this population. [167] The final model may be found in **Table 2-2**. CL_{total} (0.018 L/kg/h) was similar in children irrespective of ECMO use. [167] Patients who received ECMO within this analysis had a slightly larger V_d compared to those who didn't (1.3 L/kg vs. 0.93 L/kg). [167] The authors concluded that a loading dose of 35 mg/kg, followed by maintenance doses of 12 mg/kg once daily would be required to achieve pharmacodynamic target attainment within this population. [167] Caution should be made when extrapolating these results to children receiving CRRT±ECMO due to the low number of children receiving CRRT support.

Several analyses have reported the pharmacokinetics of fluconazole in neonates, infants and children. CL_{total} ranges from 0.011-0.0312 L/kg/h in neonates, [249] 0.015-0.0378 L/kg/h in infants, [250–252] and 1.164-1.368 L/kg/h in children. [252] The V_d of fluconazole also ranges depending on age, with 1.17-1.84 L/kg in neonates, [249,252] 0.95-1.05 L/kg in infants, [249–252] and 0.70-0.95 L/kg in children. [249,252] Caution should be applied when interpreting these comparisons due to the low number of children receiving CRRT identified within this review.

3.1.3.4 Anticonvulsants

3.1.3.4.1 Phenobarbital

Phenobarbital was the only anticonvulsant identified within this review administered to patients receiving CRRT. This review included 2 case-reports, [194,197] 2 retrospective analyses, [179,180] and 1 prospective analysis, [162] including a total of 87 patients. CVVHDF was the most common CRRT modality used, while 3 studies included patients receiving concurrent ECMO. [162,179,180,194,197] Suzuki *et al.* presented the pharmacokinetics of a 9-

year old patient receiving phenobarbital for acute encephalopathy. [197] CVVHDF was administered to this patient for renal dysfunction with a blood flow rate of 60 mL/min, replacement fluid flow rate of 240 mL/h, a dialysate flow rate of 1000 mL/h and an ultrafiltration rate of 1300 mL/h. [197] CL_{total} and CL_{RRT} in this patient were 1.11 L/h and 0.85 L/h, respectively. [197] These results are similar to those determined by Rosenborg *et al.* in a patient receiving CVVHD. [194] The V_d of phenobarbital was 0.95 L/kg, with an elimination t ½ of 14.8 h. [197] The authors recommended that a phenobarbital dose of 20 mg/kg/day was needed to maintain therapeutic concentrations of 10-30 µg/mL in this patient receiving CVVHDF.

Thibault *et al.* conducted a retrospective, pharmacokinetic analysis of phenobarbital administered to neonates and infants receiving ECMO±CRRT. [180] Thirty-five patients were included, with a median PNA of 14 days and a median PMA of 40.4 weeks. [180] Only 5 patients received CVVHDF. Phenobarbital was administered with a loading dose of 10-60 mg/kg, followed by a maintenance dose of 3-8 mg/kg/day every 12 hours. [180] A one-compartment, popPK model was constructed to describe the pharmacokinetics of phenobarbital. [180] CL_{total} was calculated to be 0.011 L/h/kg in patients receiving ECMO and 0.069 L/h/kg in those receiving ECMO + CVVHDF. [180] V_d of phenobarbital in this population was 1.12 L/kg, similar to neonates post-cardiac surgery receiving ECMO±CVVHDF (0.95L/kg). [179,180] Based on popPK dosing simulations, to achieve a phenobarbital trough (Cmin) concentration of 20-40 mg/L, loading dose of 40 mg/kg, followed by a maintenance dose of 40 mg/kg/day divided every 6 hours is required in patients receiving ECMO+CVVHDF. [180]

The only prospective analysis identified within this review was conducted by Michaličková *et al*. [162] Only one patient received CRRT, while all 13 received ECMO therapy. [162] A one-compartment, popPK model was constructed to illustrate the pharmacokinetics of phenobarbital within this population. [162] CL_{total} showed a time-dependent increase in CL_{total}, ranging from 0.003-0.01 L/h/kg with a V_d of 0.85 L/kg for a typical neonate with median body weight 3.21 kg and median PNA of 2 days while on ECMO. [162] A loading dose of 20 mg/kg followed by a maintenance dose of 4 mg/kg/day divided twice daily, increasing by 0.25 mg/kg every 12 hours was required to maintain phenobarbital concentrations of 15-40 mg/L. [162]

The pharmacokinetics of phenobarbital in pediatric patients receiving CRRT±ECMO demonstrate that CL_{total} may increase in comparison to those who are not. CL_{total} in hospitalized

pediatrics has been shown to be 0.02 L/h in neonates, [253,254] and 0.37-0.67 L/h in young infants.[255,256] V_d of phenobarbital in infants not receiving organ support (0.64-0.98 L/kg) is similar to pediatric patients within this analysis.[255,256] Caution should be applied when interpreting these results due to the limited number of patients receiving CRRT. Dosing of phenobarbital should be guided by TDM, however more frequent and higher dosing may be needed in some cases to achieve therapeutic targets due to the impact of CRRT±ECMO on the pharmacokinetics.

3.1.3.5 Vasoactive Agents

3.1.3.5.1 Vasopressin

Baird published the only study of vasopressin administered to pediatric patients receiving CRRT. [160] Vasopressin was administered to these patients as a continuous infusion of 0.0003-0.0008 iu/kg/min. [160] Three patients received CVVH, while the remaining received CVVHDF. [160] The average effluent flow rate of CRRT used within this study was 30 mL/min. [160] CL_{RRT} for vasopressin was 48 mL/min, similar to the effluent flow rate administered to this study cohort. [160] The SC of vasopressin was 1.1. [160] This analysis suggested vasopressin CL_{total} mimics that of the effluent flow rate delivered to pediatric patients receiving CRRT. Higher doses may be required to elicit pharmacodynamic response based on increasing effluent flow rates.

3.1.3.5.2 Milrinone

The pharmacokinetics of milrinone were described in one retrospective analysis conducted by Gist *et al.* [175] Eleven patients with AKI were included within this analysis, however only 3 received CRRT. [175] Children within this cohort received a continuous milrinone infusion of 0.25-0.75 μg/kg/min. [175] There were no significant differences of CL_{total} between those children receiving CRRT and those who did not (5.3±3.4 L/h/70kg vs. 5.3±1.4 L/h/70kg; p=0.20). [175] CL_{total} was significantly reduced compared to previously published reports of critically ill children without AKI/CRRT (15.9-18.9 L/h/70kg), [257,258] demonstrating the impact of renal dysfunction on milrinone CL_{total}.

3.1.3.5.3 Dopamine & Dobutamine

The study published by Freter *et al.* investigated the pharmacokinetics of dopamine and dobutamine in 3 critically ill pediatrics with renal dysfunction and cardiac instability. [170] Each patient received CVVH, with an ultrafiltration flow rate of 10-100 mL/h. [170] Dopamine and

dobutamine were administered as continuous infusions of 5.0-25.0 µg/kg/min. Mean CL_{total} for dopamine and dobutamine in this study was 25.30 mL/min/kg and 48.20 mL/min/kg respectively. [170] While CL_{RRT} for dopamine was 0.078 mL/min/kg and 0.036 mL/min/kg for dobutamine. [170] Minimal drug was extracted by CVVH within this analysis (0.56% and 0.13%). [170] The SC within the CVVH system was 0.92 for dopamine and 0.59 for dobutamine. [170]

CL_{total} of dopamine within this study was significantly decreased to that observed by Eldadah *et al*. [259] Within this study, CL_{total} of dopamine in children admitted to a PICU ranged from 151 mL/kg/min in those with renal and hepatic dysfunction to 949 mL/min/kg in those with normal organ function. [259] CL_{total} of dobutamine identified by Freter *et al.* was similar to what has been reported in pediatric patients not receiving CRRT (40-130 mL/min/kg). [170,260]

3.1.3.6 α-Adrenergic Receptor Agonist

3.1.3.6.1 Clonidine

Kleiber *et al.* conducted a prospective, pharmacokinetic analysis of 22 pediatric patients requiring clonidine for sedation within the PICU. [161] Clonidine was administered as a 1-2 µg/kg bolus, followed by a continuous infusion of 0.1-1.0 µg/kg/h. [161] All patients included within this analysis received VV-ECMO, with 20/22 children receiving concurrent CRRT. [161] CL_{total} and V_d were determined to be 30 L/h/70 kg and 454 L/70kg respectively. [161] These results suggest CL_{total} and V_d may be increased for clonidine in pediatric patients receiving organ support compared to those who don't, as previous literature has shown a CL_{total} of 14.6-15.2 L/h/70kg, [261,262] and a V_d of 391 L/70kg. [262] Dosing recommendations presented within this study may be found in **Table 2-2**.

3.1.3.7 Benzodiazepines

3.1.3.7.1 Midazolam

Midazolam pharmacokinetics were described in one prospective analysis by Mulla *et al*. [164] Within this study, 20 patients received a continuous infusion of midazolam 50-2200 µg/kg/h, with additional bolus doses of 50-100 µg/kg as needed to target a sedation score of 4 defined by study authors. [164] All children received ECMO, with only 7 receiving concurrent CVVH. CL_{total} was 3.5 mL/min/kg [0.4-17.5] within these children. [164] CL_{total} of midazolam in healthy pediatric patients not receiving organ support or with hepatic dysfunction, have been

shown to be 9.11-11.3 mL/min/kg in young infants, [263,264] and 9.33-10.0 mL/min/kg in children. [264] de Wildt *et al.* demonstrated within a popPK study that CL_{total} of midazolam in critically ill children, including those with hepatic dysfunction, was 5.0 mL/min/kg. [265] This study demonstrates that CL_{total} and V_d of midazolam are significantly altered in pediatric patients receiving organ support within the first 24 hours. [164] Beyond 24 hours, there appears to be a reduction in CL_{total} and/or a change in V_d. [164] Higher doses of midazolam may be required acutely (~24 h) upon the initiation of organ support to achieve sedation targets within these children.

3.1.3.8 Anti-Arrhythmic Agents

3.1.3.8 Propafenone

Seto *et al.* presented a case-report of a 3-year-old patient receiving propafenone as a 1 mg/kg loading dose, followed by a maintenance continuous infusion of 2-4 µg/kg/min for complex congenital heart disease. [191] CL_{total} in this child was 0.94-1.08 L/h/kg. [191] Propafenone was undetectable within the ultrafiltration fluid, suggesting minimal clearance by CVVH. [191] CL_{total} in this patient was similar to what has been previously reported in pediatric patients not receiving CRRT, with 1.18 L/h/kg after oral propafenone and 1.21 L/h/kg after IV propafenone. [266] The results of this report suggest propafenone CL_{total} is not significantly affected by acute renal and hepatic impairment. [191]

3.1.4 Ex-vivo Studies

This review incorporated 4 studies of 14 different medications administered within an *ex-vivo* CRRT circuit. All three methods of CRRT were identified within these analyses. The purpose was to investigate the SC of medications and to determine the effects of flow rates and membrane circuit components (i.e. filter membranes) on CL_{RRT}. Purohit *et al.* demonstrated that increasing ultrafiltration rates lead to an increase in CL_{RRT} and SC for hydrophilic molecules with a high unbound fraction such as piperacillin and meropenem within a CVVHDF circuit. [91] This finding was further replicated with vancomycin in the study by Kroh *et al.*, [201] illustrating a positive correlation with k_e and increasing ultrafiltration rates. Shiraishi *et al.* concluded that drug-loss due to filter membrane adsorption differs based on membrane circuit composition as polysulfone (PS) and polymethylmethacrylate (PMMA) resulted in higher teicoplanin CL_{RRT} compared to a polyacrylonitrile membrane (PAN). [118] Differing albumin

concentrations were also shown to affect CL_{RRT} of ceftriaxone, a highly protein bound antibiotic, as CL_{RRT} increased with lower albumin concentrations. [201,202] These results suggest that differing albumin concentrations, often seen in critically ill patients, may impact CL_{RRT} for highly protein bound molecules. The pharmacokinetic results, along with CRRT settings of included *ex-vivo* studies may be found in **Table 2-3**.

Table 2-2 Pharmacokinetics of medications administered to pediatrics receiving CRRT.

Reference (Year)	Drug	Dose	CRRT, Received CRRT/ no. participants	Flow Rates	ECMO, Received ECMO/ no. participants	PK Parameters[a] [range]	Sieving Coefficient (Sc)[a] / Dialysate Saturation Constant (S_D)[a] [range]	PopPK Model/Covariates	PTA	Suggested Dose
Antibiotics										
Penicillins										
Lindsay *et al.* [187] (1996)	Ticarcillin - Clavulanic Acid	NR	CVVH: 3/3 Amicon D20 filter	Mean Ultrafiltration: 890 mL/h±31	ECMO: 2/3	Ticarcillin: CL_{total}: 0.038 L/kg/h, ↓ CL_{RRT}: 0.022 L/kg/h V_d: 0.26 L/kg, ↔ t ½: 4.6 h, ↑ Clavulanic Acid CL_{total}: 0.184 L/kg/h, ↓ CL_{RRT}: 0.049 L/kg/h V_d: 0.69 L/kg, ↑ t ½: 2.45 h, ↑	Ticarcillin: 0.83±0.11 [0.61-1.06] Clavulanic Acid: 1.69±0.19 [1.44-1.97]	NA	NA	Not given
Tang Girdwood *et al.* [193] (2020)	Piperacillin-Tazobactam	48 mg/kg IV Q8H over 30 minutes	CVVHD: 1/1 in addition to MARS	Blood: 150 mL/min Pre-filter: 150 mL/h	No	Prior to CRRT/MARS: $CL_{total:}$ 0.13 L/h/kg, ↓ CRRT/MARS: 0.39-0.45 L/h/kg, ↑ CVVHD: 0.18 L/h/kg, ↔	NR	NA	fT>4x MIC	80 mg/kg Q6H
Cephalosporins										
Stitt *et al.* [177] (2019)	Cefepime	48-64 mg/kg IV Q6-12H	CVVHDF: 4/4 HF 1000 filter	Blood: 75 mL/min	No	CL_{total}: 0.056 L/h/kg [0.012-0.08], ↓	NR	NA	100% fT>1xMIC: ¾ patients	Doses > 50 mg/kg Q12H may be required

				Pre-filter: 512.5 mL/h Post-filter: 50 mL/h Dialysate: 925 mL/h Effluent: 4986 mL/1.73m^2/h		V_d: 0.14 L/kg [0.04-0.23], ↓ t ½: 1.93 h [1-2.9], ↔			100% fT>4xMIC: ¼ patients	
Butragueño-Laiseca *et al*. [173] (2020)	Ceftolozane-Tazobactam	No AKI: 40 mg/kg IV Q6H AKI: 36 mg/kg IV Q8H CVVHDF: 30 mg/kg IV Q8H	CVVHDF: 1/3 Prismaflex	Blood: 30 mL/min Replacement: 160 mL/h Dialysate: 250 mL/h Effluent: 470 mL/h	No	CL_{Renal}: No AKI: 0.88 L/h, ↔ AKI: 0.27 L/h, ↓ CVVHDF: 0.39 L/h, ↓ V_{ss}: No AKI: 4.39 L, ↑ AKI: 2.49 L, ↔ CVVHDF: 1.91 L, ↔ t½: No AKI: 3.51 h, ↑ AKI: 6.62 h, ↑ CVVHDF: 3.51 h, ↑ AUC: No AKI: 397.73 mg·h/L	1.06 [0.99-1.14]	NR	40% fT>MIC: With MIC of 4 µg/mL	Sepsis no AKI: 35 mg/kg IV Q8H AKI: 10 mg/kg IV Q8H CVVHDF: 30 mg/kg IV Q8H

						AKI: 1481.48 mg·h/L CVVHDF: 448.72 mg·h/L				
Carbapenems										
Cies *et al.* [184] (2016)	Meropenem	40 mg/kg IV bolus, followed by 10 mg/kg/hr CI	CVVHDF: 1/1 AN 69 filter	Blood: 50 mL/min Pre-filter: 250 mL/h Post-Filter: 50 mL/hr Dialysate: 200 mL/hr Ultrafiltration: 0-40 mL/hr	ECMO: 1/1	CL_{total}: 0.474 L/kg/h, ↑ Css: 21 mg/L	NR	NA	100% fT>MIC	40 mg/kg bolus, followed by 10 mg/kg/hr CI
Nehus *et al.* [171] (2014)	Meropenem	20 mg/kg IV Q8-12H	CVVHD: 140/287 CVVH: 78/287 CVVHDF: 69/287 M100 0.9m^2 and M60 0.6m^2 polyacrylonitrile	Blood: <1y: 40 mL/min 1-5y: 62.5 mL/min 5-12y: 100 mL/min 12-18y: 150 mL/min >18y: 120 mL/min Ultrafiltration: <1y:	No	NR	NR	$CL = 8.2 \cdot 0.49 \cdot (\frac{WT}{75})^{0.75}$ $V_d = 8.2 \cdot (\frac{WT}{75})^{1.0} (1 + \frac{FO}{100})$	40% fT>MIC & 100% fT>MIC with MIC of 4 µg/mL	>5y: 20 mg/kg Q12H <5y: 20 mg/kg Q8H

				8.5 mL/kg/h 1-5y: 7.4 mL/kg/h 5-12: 4.7 mL/kg/h 12-18: 4.1 mL/kg/h >18: 2.8 mL/kg/h Total effluent: <1y: 107.6 mL/kg/h 1-5y: 57.4 mL/kg/h 5-12y: 43.3 mL/kg/h 12-18: 35.4 mL/kg/h >18y: 24.4 mL/kg/h					
Nehus *et al.* [163] (2016)	Meropenem	Mean: 18.6 mg/kg IV Q12H	CVVH: 2/7 CVVHDF: 5/7 AN 69 (0.6 or 0.9m^2) HF 1000 (1.1m^2)	**CVVH:** Blood: 175 mL/min Pre-filter: 1797 mL/min	ECMO: 1/7	CL_{total}: 3.7 L/h±2.3, ↓ CL_{RRT}: 1.9 L/h±0.5 63.4% removed	NR	NA	100% fT>MIC: 5/7 93% fT>MIC: 1/7	20 mg/kg Q12H

				Post-filter: 185 mL/min Ultrafiltration: 211 mL/min **CVVHDF:** Blood: 164 mL/min Pre-filter: 706 mL/min Post-filter: 50 mL/min Dialysate: 760 mL/min Ultrafiltration: 526.6 mL/min	Vss: 0.35 L/kg±0.085, ↔ t ½: 4.3 h±1.8, ↑			43% fT>MIC: 1/7 with MIC of 4 µg/mL	
Rapp *et al.* [172] (2019)	Meropenem	60 mg/kg/day IV Q8H or CI	CRRT: 11/40 Modality NR	NR	ECMO: 8/40 ECMO+CRRT: 2/40	NR	NR	$CL_i = 6.82\ x\ (\frac{BW_i}{70})^{0.75}\ x\ (\frac{eGFR_i}{100})^{0.3;}$ $CL_{iCRRT} = CL_{pop}\ x\ 0.9$ $CL_{pop} = 6.82$ (L/h) $V1_{pop}(L) for\ 70kg\ BW = 40.6$ $V2_{pop}\ (L) for\ 70kg\ BW = 9.2$	50% fT>MIC	50% fT>MIC (<2 µg/mL): 60 mg/kg/day Q8H 50% fT>MIC (>4 µg/mL): 60 mg/kg/day CI
Tan *et al.* [165] (2021)	Meropenem	20-40 mg/kg IV Q12H	CVVH: 4/9 CVVHDF: 5/9 <10kg: PAES (0.2m^2)	Dialysate: 737.4 mL/1.73m^2/h Ultrafiltration: 1952 mL/1.73m^2/h	VV-ECMO: 3/9 VA-ECMO: 1/9	CL_{total}: 0.091 L/h/kg±0.032 [0.04-0.157], ↓ CL_{RRT}: 1.4 L/h±0.93 [0.472-2.9]	0.962±0.137 [0.737-1.1]	$CL_i = (\theta_{(1)}) * (WT_i/70kg)^{0.75}$ $V_{ci} = (\theta_{(2)}) * (WT_i/70kg)^{1}$ $Q_i = (\theta_{(3)}) * (WT_i/70kg)^{0.75}$ $V_{pi} = (\theta_{(4)}) * (WT_i/70kg)^{1}$ $\theta_{(1)} = 4.1 L/hr$	100% fT>MIC with MIC 4 µg/L for > 90% of simulations	20 mg/kg Q8H over 4-hr infusion OR 40 mg/kg Q8H over 2-hr infusion

			11-30 kg: AN69 ($0.6m^2$) >30kg: AN69 ($0.9m^2$)			V_C: 0.194 L/kg±0.002 [0.193-0.2], ↔ V_P: 0.211 L/kg±0.002 [0.209-0.214], ↔ t ½: 3.9 h ±1.6 [2.1-7.5], ↑		$\theta_{(2)} = 13.6L$ $\theta_{(3)} = 9.0\ L/hr$ $\theta_{(4)} = 14.17\ L$		
Saito *et al.* [190] (2020)	Meropenem	300 mg/kg/day IV Q8H as a 3-h infusion	CVVHD: 1/1 UT filter 300S ($0.3m^2$)	Blood: 50-80 mL/min Dialysate: 820-1500 mL/h	VA-ECMO: 1/1	Median CL_{total}: 0.132 L/kg/h, ↓ Median V_d: 0.59 L/kg, ↔	NR	NA	100% fT>MIC with MIC of 1µg/mL	200-300 mg/kg/day Q8H as 1-hr infusion 200-300 mg/kg/day as 3-hr infusion
Wang *et al.* [166] (2020)	Meropenem	20 mg/kg IV Q8H as a 1-hr infusion	CVVHDF: 6/27 AN 69 filter	Blood: 4 mL/kg/min Pre-filter: 25 mL/kg/h Dialysate: 20 mL/kg/h Ultrafiltration: 2 mL/kg/h	VA-ECMO: 6/27	Median CL_{total} ECMO: 11.59 L/h, ↔ [5.92-20.19] CRRT: 15.73 L/h, ↔ [2.11-39.29] Non-ECLS: 13.51 L/h, [3.71-20.80] Median Vd: ECMO: 31.67 L [20.95-81.54], ↔ CRRT: 19.42 L[8.76-108.8], ↓ Non-ECLS: 34.41 L	NR	NA	NR	20 mg/kg Q8H as a 1-hr infusion

						[9.57-113.5] Median t ½ : ECMO: 2.27 h [1.76-3.55], ↔ CRRT: 2.22 h [1.77-3.76], ↔ Non-ECLS: 2.25 h [1.46-3.06]				
Cies *et al.* [199] (2017)	Doripenem	2.5 mg/kg/hr IV CI	CVVH: 1/1 AN69 filter	Blood: 180 mL/min Pre-filter: 900 mL/min Post-filter: 100 mL/min	No	CL_{total}: 10.5 mL/kg/min, ↑ Doripenem concentration: 4.01 mg/L	NR	NA		100% fT>MIC for MIC <4 mg/L	2.5 mg/kg/hr IV CI
Aminoglycosides										
Armstrong *et al.* [182] (1993)	Tobramycin	1.8-2.5 mg/kg/dose IV	CVVH: 1/1 Amicon dialfilter	Blood: 15 mL/min Ultrafiltration: 20-30 mL/min	No	CL_{RRT}: 0.626 mL/min [0.32-0.91] t ½: 20-23 h, ↑	1.13-1.42	NA		NR	NR
Glycopeptides										
Armstrong *et al.* [182] (1993)	Vancomycin	11-15 mg/kg/dose IV	CVVH: 1/1 Amicon dialfilter	Blood: 15 mL/min Ultrafiltration: 20-30 mL/min	No	CL_{RRT}: 0.586 mL/min [0.27-0.80] t ½: 20-24 h, ↑	0.86-1.55	NA		NR	NR
Cies *et al.*[186] (2016)	Vancomycin	15-20 mg/kg IV loading dose, followed by addition	CVVH: 7/11* CVVHD: 2/11* CVVHDF: 5/11*	**CVVH:** Blood: 215.39 mL/min	No	Cmin: 22.3 µg/mL±3.3 [12.9-28.7] 10/11 patients achieved	NR	NA		NR	15-20 mg/kg IV loading dose, followed by addition into CRRT solution at a

		into CRRT solution at a final concentration of 18-30 mg/L	AN69 filter *patients received multiple methods of CRRT	Pre-filter: 773.08 mL/h Post-filter: 159.01 mL/h **CVVHD:** Blood: 440 mL/min Pre-filter: 100 mL/h Post-filter: 50 mL/h Dialysate: 1100 mL/h **CVVHDF:** Blood: 218 mL/min Pre-filter: 977.5 mL/h Post-filter: 223.68 mL/h Dialysate: 800 mL/h		target Cmin in 8 h				final concentration of 18-30 mg/L
Moffett *et al.* [176] (2019)	Vancomycin	Average dose: 14.3 mg/kg/dose IV	CVVHDF: 138/138 HF 1000 filter	Blood: 102 mL/min Pre-filter: 464 mL/h Post-filter: 48 mL/h Dialysate: 598 mL/h Ultrafiltration: 289 mL/h	No	CL_{total}: 2.29 L/h, ↔ V_c: 81 L, ↑ V_p: 550 L	NR	CL = $2.24\ x\ \left(\frac{FFM}{70}\right)^{0.75}\ x\ 0.535^{LN\left(\frac{SCR}{0.56}\right)}\ x\ 0.92^{LN\left(\frac{BUN}{30}\right)} x\ 1.88^{\left(\frac{CRRTUF}{500}\right)x\ 1.12}$ V_d: $81.0\ x\ \left(\frac{FFM}{70}\right)$	AUC/MIC ≥ 400 Cmin < 20 mg/L	40-50 mg/kg/day Q8-12H based on FFM

Zylbersztajn *et al.*[178] (2018)	Vancomycin	ECMO no AKI/RRT: 40 mg/kg/day IV Q6H ECMO AKI with or without RRT: 40 mg/kg/d IV Q8H ECMO with RRT without AKI: 40 mg/kg/d IV Q8H	CRRT: 11/29 Modality NR	NR	VV-ECMO: 19/29* VA-ECMO: 20/29* *Patients may have received both methods of ECMO	Median CL_{total}: ECMO without AKI: 1.67 mL/min/kg [IQR 1-1.67], ↔ ECMO AKI with or without RRT: 0.83 mL/min/kg [IQR 0.38-1], ↔ RRT without AKI: 1.17 mL/min/kg [IQR 0.63-1.55], ↔ Median V_d: ECMO without AKI: 0.73 L/kg [IQR 0.7-0.9], ↔ ECMO AKI with or without RRT: 1.16 L/kg [IQR 0.68-1.6], ↑ RRT without AKI: 0.88 L/kg [IQR 0.68-0.92], ↔ Median t ½ : ECMO without AKI: 6.2 h [IQR 4.9-8.06], ↑	NR	NA	AUC/MIC ≥ 400	Final adjusted doses: ECMO without AKI: 40 mg/kg/day Q6H ECMO AKI with or without RRT: 20 mg/kg/day Q12H RRT without AKI: 40 mg/kg/day Q6H

						ECMO AKI with or without RRT: 23.6 h [IQR 16.2-31], ↑ RRT without AKI: 8.69 h [IQR 5.05-17.52], ↑				
Lincosamides										
Poli *et al.* [196] (2019)	Clindamycin	NR	CVVH: 1/1 Cytosorb cartridge	NR	VV/VA-ECMO: 1/1	CL_{total}: 3.6-15.5 L/h, ↔	NR	NA	NR	No dose adjustments needed
Oxazolidinones										
Yang *et al.* [174] (2021)	Linezolid	<12 y: 10 mg/kg IV Q8H 12-18y: 600 mg IV Q12H	CRRT: 15/63	NR	ECMO: 2/63	CL_{total}: 2.34 L/h, ↑ V_C: 5.22 L, ↑ V_p: 28.79 L, ↑	NR	$V_c = 5.22 \cdot e^{(\eta V)}$ $CL = 2.34 \cdot \left(\frac{wt}{15}\right)^{0.8} \cdot \left(\frac{AST}{45.9}\right)^{(-0.16)} \cdot e^{(\eta CL)}$	>90% PTA at an AUC/MIC value > 80 MIC: 0.125-32 mg/L	<12 y: 10 mg/kg IV Q8H with MIC ≤ 1 mg/L 12-18 y: 600 mg IV Q12H with MIC ≤ 1 mg/L <12y with AST >200 U/L: 10 mg/kg IV Q12H with MIC ≤ 1 mg/L 12-18y with AST >200 U/L: 600 IV Q48H with MIC ≤ 1 mg/L
Antivirals										
Aebi *et al.* [181] (1997)	Ribvarin	5 mg/kg IV Q6H	CVVH: 1/1 Amicon minifilter	Ultrafiltration: 178.3 mL/h	VA-ECMO: 1/1	CL_{RRT}: 0.046 L/kg/h	0.85 [0.67-1.04]	NA	NR	5 mg/kg IV Q6H

						V_{ss}: 1.37 L/kg, ↓				
Sargel *et al.* [192] (2018)	Ribavarin	33 mg/kg loading dose, 16 mg/kg/dose IV Q6H for 16 doses, then 8 mg/kg/dose IV Q8H for 9 doses	CVVH: 1/1	NR	VV-ECMO: 1/1	CL_{total}: 0.31-0.76 L/kg/h, ↔ CL_{RRT}: 0.12 L/kg/h V_d: 2.92-5.1 L/kg, ↔ t ½: 2.68-10.7 h, ↔	1.17 [1.07-1.37]	NA	NR	NR
Cies *et al.* [185] (2015)	Acyclovir	30 mg/kg/dose IV Q8H, then added to dialysate solution for final concentration of 5.5 ug/mL	CRRT: 1/1 Modality NR	NR	ECMO: 1/1	Acyclovir Concentrations: 24 h: 8.8 mg/L 72 h: 5.3 mg/L	NR	NA	>3 mg/L	NR
Karsch *et al.* [188] (2016)	Oseltamivir	75 mg PO BID 100 mg IV BID	CVVHDF: 1/1 Fresenius FX 60	Ultrafiltration: 1.2 $L/m^2/h$	ECMO: 1/1	t ½: OS: 2.2 h AUC_{0-last}: OS:1070 ng·h/mL OSC: 45,490 ng·h/mL AUC_{0-12}: OS: 1070 ng·h/mL OSC: 47,250 ng·h/mL	OS: 1.39 [1.04-2.09] OSC: 1.44 [1.15-2.12]	NA	NR	75 mg PO BID OR 100 mg IV BID
Eyler *et al.* [198] (2012)	Oseltamivir	90 mg PO Q12H	CVVHD: 1/1 AN 69 filter	Dialysate: 1000 mL/h Ultrafiltration: 340 mL/h	ECMO: 1/1	CL_{total}: OS: 0.33 L/kg/h OSC: 0.23 L/kg/h, ↔ $CL_{RRT:}$	$S_{D:}$ OS: 0.99 OSC: 0.85	NA	IC_{50}: 0.186 ng/mL	90 mg PO Q12H

						OS: 0.07 L/kg/h OSC: 0.06 L/kg/h t ½: OS: 25.9 hr OSC: 8.21 h, ↔ AUC_{0-12}: OS: 30.5 ng·h/mL OSC: 905 ng·h/mL				
Wildschut *et al.* [169] (2010)	Oseltamivir	< 15kg: 60mg/day PO Q12H 15-23 kg: 90 mg/day PO Q12H 23-40 kg: 120 mg/day PO Q12H >40 kg: 150 mg/day PO Q12H	CVVH: 3/3	NR	ECMO: 3/3	OS: AUC_{0-12}: 115.1 µg·h/mL OSC: AUC_{0-12}: 4943.7 µg·h/mL	NR	NA	NR	No dose recommendation provided
Dillon *et al.* [195]	Peramivir	600 mg IV x 1, followed by 200 mg IV daily	CVVHDF: 1/1 M100 filter	Blood: 250 mL/min Pre-filter: 500 mL/h Post-filter: 500 mL/h Dialysate: 1000 mL/h Ultrafiltration: 150 mL/h	No	CL_{total}: 0.032 L/kg/h, ↓ V_d: 0.32 L/kg, ↑ t ½: 11.6 h AUC: 126,000 ng·h/mL	NR	NA	NR	No dose recommendations provided
Antifungals										
Azoles										

Brüggeman *et al.* [183] (2008)	Voriconazole	7 mg/kg IV BID, increased to 14 mg/kg IV BID	CVVH: 1/1	NR	VV-ECMO: 1/1	CL_{total}: 0.22 L/h/kg, ↔ t ½: 4.7 h, ↑ AUC_{0-12}: 64 mg·h/mL	NR	NA	Cmin > 1mg/L	10-14 mg/kg IV BID
Oualha *et al.* [189] (2019)	Fluconazole	10 mg/kg/day IV	CVVHD: 1/1	Blood: 150 mL/min Dialysate: 4000 mL/h Ultrafiltration: 90 mL/h	No	CL_{total}: 2.79 L/h, ↑ CL_{RRT}: 1.64 L/h V_{ss}: 30 L, ↔ t ½: 7.4 h, ↓	NR	NA	fAUC/MIC > 100 Cmax: 16-32 mg/L Cmin: >10 mg/L	900 mg loading dose, followed by 600 mg IV BID
Watt *et al.* [168] (2012)	Fluconazole	Prophylaxis: 25 mg/kg IV Q7D Treatment: 12 mg/kg IV once daily	CVVH: 2/10 CVVHD: 1/10	NR	ECMO: 10/10	**Prophylaxis:** Median CL_{total}: 0.017 L/kg/h, ↔ Median V_d: 1.5 L/kg, ↔ Median t ½: 60 h, ↑ Median AUC_{0-24}: 322 mg·h/mL **Treatment:** Median CL_{total}: 0.022 L/h/kg, ↔ Median V_d: 1.9 L/kg, ↔ Median t ½: 56 h, ↑ Median AUC_{0-24}: 352 mg·h/mL	NR	NA	Prophylaxis: 50% T>MIC Treatment: AUC_{0-24}: >400 mg·h/mL	Prophylaxis: 25 mg/kg Q7D Treatment: Loading doses of 30-40 mg/kg may be required to meet PD target
Watt *et al.* [167] (2015)	Fluconazole	Prophylaxis: 25	CVVH: 5/40	NR	ECMO: 21/40	CL_{total}: ECMO:	NR	$CL = \theta_{CL} x\ wt\ x\ (\frac{creatinine}{0.4})^{-0.29}$	Prophylaxis:	Prophylaxis: 12 mg/kg IV x 1 dose,

		mg/kg IV Q7D Treatment: 12 mg/kg IV once daily	CVVHD: 2/40			0.018 L/h/kg [0.013-0.043], ↔ No ECMO: 0.018 L/h/kg [0.008-0.042] V_d: ECMO: 1.3 L/kg [0.81-1.8], ↔ No ECMO: 0.93 L/kg [0.55-1.4]		$Vd = \theta_V x\ wt\ x\ 1.39^{ECMO}$	50% T>MIC Treatment: AUC_{0-24}: >400 mg·h/mL	followed by 6 mg/kg daily while on ECMO Treatment: 35 mg/kg loading dose, followed by 12 mg/kg once daily
Anticonvulsants										
Suzuki *et al.* [197] (2019)	Phenobarbital	NR	CVVHDF: 1/1 PMMA membrane	Blood: 60 mL/min Replacement: 240 mL/h Dialysate: 1000 mL/h Ultrafiltration: 1300 mL/h	No	CL_{total}: 1.11 L/h, ↑ CL_{RRT}: 0.85 L/h V_d: 0.95 L/kg, ↔ t ½: 14.8 hr, ↓ k_e: 0.0467 h^{-1}	NR	NA	Therapeutic range: 10-30 µg/mL	20 mg/kg/day was needed to maintain therapeutic range
Rosenberg *et al.* [194] (2014)	Phenobarbital	135 mg PO per day; eventually transitioned to IV	CVVHD: 1/1	Blood: 60 mL/min Dialysate: 1400 mL/h	No	CL_{total}: 1.27 L/h, ↑ CL_{RRT}: 1.01 L/h V_d: 0.95 L/kg, ↔ AUC_{0-12}: 1718 µmol·h/L	S_D: 0.64	NA	NR	Phenobarbital 900-1000 mg/day needed to achieve Cmin of 100-120 µmol/L
Thibault *et al.* [179] (2020)	Phenobarbital	Loading dose: 10-60 mg/kg IV	CVVHDF: 5/35	NR	VA-ECMO: 35/35	CL_{total}: ECMO: 0.011 L/h/kg, ↔	NR	$CL = 0.038x\ (\frac{wt}{3.4})^{0.75}\ x\ \left(\frac{AGE}{[5.9 + AGE]}\right)$ $Vd = 3.83\ x\ \frac{wt}{3.4}$	Cmin: 20-40 mg/L	ECMO: LD: 30 mg/kg, MD 6-7 mg/kg/day Q12H

		Maintenance dose: 3-8 mg/kg/day IV Q12H				ECMO+CVVHDF: 0.069 L/h/kg, ↔ V_d: 1.13 L/kg, ↑				ECMO +CRRT: LD: 40 mg/kg/dose, MD 40 mg/kg/day divided Q6H
Thibault *et al.* [180] (2020)	Phenobarbital	Loading dose: 15-20 mg/kg IV Maintenance dose: 3-6 mg/kg/day IV	CVVHDF: 2/38 PD: 1/38 Included in model: 2/38	NR	ECMO: 13/38 Included in model: 12/38	CL_{total}: 0.005 L/h/kg, ↓ V_d: 0.95 L/kg, ↔	NR	$CL\left(\frac{mL}{hr}\right) = 14.4\ x\ \frac{wt}{3.2}^{0.75}\ x\ \left(\frac{postnatal}{6}\right.$ $Vd\ (mL) = 3050\ x\ \frac{wt}{3.2} x\ 1.21\ (if\ on\ ECM$	Cmin: 20-40 mg/dL	LD: 20-30 mg/kg MD: 4-5 mg/kg/day
Michaličková *et al.*[162] (2020)	Phenobarbital	Median LD: 7.5 mg/kg IV (IQR: 8.5-16) Median MD: 6.9 mg/kg/d IV (IQR:4.5-8.5)	CRRT: 1/13 Modality NR	NR	VV-ECMO: 1/13 VA-ECMO: 11/13 VV+VA-ECMO: 1/13	CL_{total}: 0.003-0.01 L/h/kg, ↓ V_d: 0.85 L/kg, ↔	NR	$CL\left(\frac{L}{hr}\right) = CLp\ x\ (1 + \theta bBWCL\ x\ [bBW - 2.59])\ x\ (1 + \theta AGE\ x\ [AGE - 4.50]) x\ (1 + \theta TE\ x\ \left[\frac{TE}{109}\right])^{ECMO\_on}$ $Vd\ (L) = Vp\ x\ (1 + \theta BWV\ x\ [BW - 2.70])$	Cmin: 15-40 mg/L	LD: 20 mg/kg MD: 4 mg/kg BID, increasing by 0.25 mg/kg Q12H
Vasoactive Agents										
Baird [160] (2010)	Vasopressin	0.0003-0.0008 iu/kg/min IV CI	CVVH: 3/9 CVVHDF: 6/9 AN 69 ($0.9m^2$)	Mean Dialysate: 30 mL/min Mean Ultrafiltration: 30 mL/min	No	CL_{RRT}: 36 mL/min [2-68]	1.1 [0.9-1.7]	NA	NR	No dose recommendation provided
Gist *et al* [175] (2015)	Milrinone	0.25-0.75 µg/kg/min IV CI	CRRT: 3/8 Modality NR	NR	No	CL_{total}: 5.3 L/h/70 kg ±3.4, ↓	NR	NR	NR	No dose recommendation provided
Freter *et al.* [170] (1998)	Dobutamine	5.0-25.0 µg/kg/min IV CI	CVVH: 3/3	Blood: 15-17 mL/min	No	CL_{total}:	0.59	NA	NR	No dose adjustment required

			Amicon diafilter (10,000 Da)	Ultrafiltration: 10-100 mL/h		48.20 mL/min/kg ±9.4, ↔ CL_{RRT}: 0.036 mL/min/kg ± 0.008				
Freter *et al.* [170] (1998)	Dopamine	5.0-25.0 µg/kg/min IV CI	CVVH: 3/3 Amicon diafilter (10,000 Da)	Blood: 15-17 mL/min Ultrafiltration: 10-100 mL/h	No	CL_{total}: 25.3 mL/min/kg±11, ↓ CL_{RRT}: 0.078 mL/min/kg± 0.06	0.92	NA	NR	No dose adjustment required
α-Adrenergic Receptor Agonist										
Kleiber *et al.* [161] (2017)	Clonidine	1-2 µg/kg IV bolus then 0.1-1.0 µg/kg/h IV CI	CVVH: 20/22 AN 69 filter ($0.9m^2$)	Median Ultrafiltration: 300 mL/min	VV-ECMO: 15/22 VA-ECMO: 7/22	CL_{total}: 30 L/h/70 kg, ↑ V_d: 454 L/70 kg, ↑	NR	$CL = CLpop\left(\frac{WT}{70}\right)^{0.75} x \left(\frac{PN}{T50pna^{\theta 1}}\right.$ $Vd = Vpop(\frac{WT}{70}) x (1 + Emax \cdot \frac{tec^{\theta 3}}{T50ec^{\theta 3} + tec^{\theta 3}})$	NR	3 day old (3kg): Bolus: 5 µg/kg x 3 followed by 0.12 µg/kg/h infusion 1-month old (4kg): Bolus: 5 µg/kg x 3 followed by 2 µg/kg/h infusion 12-year old (35kg): Bolus: 5 µg/kg x 3 followed by 1 µg/kg/h infusion
Benzodiazepine										
Mulla *et al.*[164] (2003)	Midazolam	50-2200 µg/kg/h IV CI	CVVH: 7/20	NR	VV-ECMO: 17/20	CL_{total}: 3.5 mL/min/kg ±4.9, ↔	NR	NA	Cmin: > 1 µg/mL	Higher doses may be needed within

					VA-ECMO: 3/20	Plasma Concentrations: 24 h: 1.4 µg/mL [0.08-3.2] 48 h: 1.8 µg/mL [0.1-4.9] 72 h: 2.6 µg/mL [0.2-7.5]			Target sedation score = 4	the first 24 hours
Anti-Arrhythmics										
Seto *et al.* [191] (1999)	Propafenone	LD: 1 mg/kg IV MD: 2-4 µg/kg/min IV CI	CVVH: 1/1 Fresenius F40 filter	Blood: 50-80 mL/min Pre-filter: 300-500 mL/h Ultrafiltration: 340-550 mL/h	No	CL_{total}: 1.0 L/h/kg [0.94-1.08], ↔ CL_{RRT}: Undetectable	NR	NA	Guided by clinical response	No dosage adjustments required

[a]: data reported as mean unless otherwise stated

AKI; acute kidney injury, ALB; albumin, AST; aspartate aminotransferase, AUC; area under the curve, bW; birth body weight, BUN; blood urea nitrogen, $\theta bBWCL$; increase in CL per kg of birthweight, θBWV; increase in volume of distribution per kg actual body weight,CL_i; individual clearance, CL_{pop}; median population clearance, CL_{total}; total clearance, CL_{RRT}; clearance as per CRRT circuit, CL_{Renal}, renal clearance, Cmax; maximum concentration, Cmin; minimum concentration, CRRT; continuous renal replacement therapy, CVVH; continuous veno-venous hemofiltration, CVVHD; continuous veno-venous hemodialysis, CVVHDF; continuous veno-venous hemodiafiltration, DIURETIC; refers to the use of diuretic, ECMO; extracorporeal membrane oxygenation, $Emax$; maximal effect, FFM; fat-free mass, FO; fluid overload, IQR; interquartile range, k_e; elimination rate constant, MARS; molecular adsorbent recirculating system, MIC; minimum inhibitory concentration, NA; not applicable, NR; not reported, OS; oseltamivir, OSC; oseltamivir carboxylate, PD; peritoneal dialysis, PK; pharmacokinetics, PNA; post-natal age; PopPK; population PK; PTA; probability of target attainment, Q; inter-compartment clearance, SCR; serum creatinine, t½; elimination half-life, $T50$; time to half maximal effect, tec; time on ECMO, θTE; increase in CL per hr time after ECMO cannulation, VA-ECMO; venoarterial

extracorporeal membrane oxygenation, V_d; volume of distribution, V_c; volume of distribution central compartment, V_p; volume of distribution in peripheral compartment, $V1_{pop}$; median population central volume of distribution, $V2_{pop}$; median population peripheral volume of distribution, VV-ECMO; venovenous extracorporeal membrane oxygenation, WT; weight, ↑; increased relative to non-CRRT controls, ↓; decreased relative to non-CRRT controls, ↔; equal to non-CRRT controls.

Table 2-3. Pharmacokinetics of medications administered to an ex-vivo CRRT circuit.

Reference	Drug	Concentration	CRRT	Flow Rates	PK Parameters[a] (±SD)	Sieving Coefficient (Sc)[a] / Dialysate Saturation Constant (S_D)[a] (±SD)	Adsorption Fraction[a] (±SD)
Antibiotics							
Penicillins							
Purohit *et al.* [91] (2019)	Piperacillin	420 µg/mL	CVVHDF HF1000 (1.1m^2) membrane	Blood: 50 mL/min Post-filter: Low: 100 mL/hr High: 200 mL/hr Dialysate: Low: 100 mL/hr High: 200 mL/hr Ultrafiltration: Low: 200 mL/hr High: 400 mL/hr	CL_{RRT}: Low: 2.61 mL/min ±0.4 High: 4.97 mL/min ±0.76	Low: 0.78 ±0.12 High: 0.75 ±0.11	0.26±0.13
Cephalosporins							
Harvey *et al.* [202] (2014)	Ceftriaxone	80 mg/kg Infant: 6kg Pediatric: 20kg	CVVH Infant: HF400 (0.4m^2) Pediatric: HF700 (0.7 m^2)	Blood: 6 mL/kg/min Pre-filter: 70% Ultrafiltration: 30 mL/kg/hr	CL_{RRT}: HF400 albumin: 1.97 mL/min HF400 blood: 5.65 mL/min HF400 Hartmann's: 3.58 mL/min HF700 albumin: 10.55 mL/min HF700 blood: 17.91 mL/min HF700 Hartmann's: 12.23 mL/min	HF400 albumin: 0.23 HF400 blood: 0.31 HF400 Hartmann's: 0.52 HF700 albumin: 0.64 HF700 blood: 0.51 HF700 Hartmann's: 0.49	NR
Kroh *et al.* [201] (1998)	Ceftriaxone	200 mg	CVVH	Blood: (1) 50-20 mL/min (2) 120 mL/min	k_e: ↑UF V_d: ↓UF	SC: ↑UF	NR

			FH77H hydrophobic polyamide matrix ($1.4m^2$) Experiment 1: ↑UF Experiment 2: ↑Albumin Experiment 3: Added FFP	(3) 120 mL/min Ultrafiltration: (1) 10-50 mL/min (2) 30 mL/min (3) 30 mL/min Post-filter replacement fluids: NR			
Carbapenems							
Purohit *et al.* [91] (2019)	Meropenem	150 µg/mL	CVVHDF HF1000 ($1.1m^2$) membrane	Blood: 50 mL/min Post-filter: Low: 100 mL/hr High: 200 mL/hr Dialysate: Low: 100 mL/hr High: 200 mL/hr Ultrafiltration: Low: 200 mL/hr High: 400 mL/hr	CL_{RRT}: Low: 2.48 mL/min ±0.55 High:7.66 mL/min ±1.1	Low: 0.74 ±0.17 High: 1.15 ±0.16	0.15 ±0.08
Aminoglycosides							
Kroh *et al.* [201] (1998)	Amikacin	20 mg	CVVH FH77H hydrophobic polyamide matrix ($1.4m^2$) Experiment 1: ↑UF Experiment 2: ↑Albumin Experiment 3: Added FFP	Blood: (1) 50-20 mL/min (2) 120 mL/min (3) 120 mL/min Ultrafiltration: (1) 10-50 mL/min (2) 30 mL/min (3) 30 mL/min Post-filter replacement fluids: NR	k_e: ↑UF	NC	NR

Glycopeptides							
Kroh *et al.* [201] (1998)	Vancomycin	30 mg	CVVH FH77H hydrophobic polyamide matrix ($1.4m^2$) Experiment 1: ↑UF Experiment 2: ↑Albumin Experiment 3: Added FFP	Blood: (1) 50-20 mL/min (2) 120 mL/min (3) 120 mL/min Ultrafiltration: (1) 10-50 mL/min (2) 30 mL/min (3) 30 mL/min Post-filter replacement fluids: NR	k_e: ↑UF	NC	NR
Shiraishi *et al.* [118] (2012)	Teicoplanin	50 µg/mL	CVVHDF Membranes: PAN, PS, PMMA	Blood: 100 mL/min Post- filter replacement: 500 mL/hr Dialysate: 500 mL/hr Ultrafiltration: 500 mL/hr	CL_{RRT}: **No Albumin** PAN: 12.6 mL/min ±1.0 PS: 50.6 mL/min ±2.6 PMMA: 60.8 mL/min ±4.7 **Albumin:** PAN: 6.7 mL/min ±0.9 PS: 27.8 mL/min ±0.7 PMMA: 26.7 mL/min ±1.0	NR	**No Albumin:** PAN: 0.004 ±0.003 PS: 0.698 ± 0.009 PMMA: 0.894 ±0.024 **Albumin:** PAN: 0.037 ±0.023 PS: 0.614 ±0.048 PMMA: 0.756 ±0.019
Kroh *et al.* [201] (1998)	Teicoplanin	30 mg	CVVH FH77H hydrophobic polyamide matrix ($1.4m^2$) Experiment 1: ↑UF Experiment 2:	Blood: (1) 50-20 mL/min (2) 120 mL/min (3) 120 mL/min Ultrafiltration: (1) 10-50 mL/min (2) 30 mL/min (3) 30 mL/min	k_e: ↑UF	NC	NR

			↑Albumin Experiment 3: Added FFP	Post-filter replacement fluids: NR			
Lipopeptide							
Churchwell *et al.* [200] (2006)	Daptomycin	4 mg/kg to achieve 50 mg/L	CVVH, CVVHD F-160NR Polysulfone ($1.5m^2$) AN 69 (M-100) ($0.9m^2$)	**CVVH** Blood: 200-400 mL/min Ultrafiltration: 1-6 L/hr **CVVHD** Blood: 200-350 mL/min Dialysate: 1-6 L/hr	**CL_{CVVH}:** Polysulfone: 2.84-19.0 mL/min AN69: 2.59-14.0 mL/min **CL_{CVVHD}:** Polysulfone: 2.59-14.86 mL/min AN69: 2.0-5.15 mL/min	**CVVH:** Polysulfone: 0.16-0.20 AN69: 0.14-0.16 **CVVHD:** Polysulfone: S_D: 0.15 AN69: S_D: 0.052-0.13	NR
Antifungals							
Azoles							
Purohit *et al.* [91] (2019)	Voriconazole	5 µg/mL	CVVHDF HF1000 ($1.1m^2$) membrane	Blood: 50 mL/min Post-filter: Low: 100 mL/hr High: 200 mL/hr Dialysate: Low: 100 mL/hr High: 200 mL/hr Ultrafiltration: Low: 200 mL/hr High: 400 mL/hr	CL_{RRT}: Low: 1.53 mL/min ±0.43 High: 2.67 mL/min ±0.70	Low: 0.46 ±0.13 High: 0.40 ±0.11	0.27 ±0.05
Echinocandins							
Purohit *et al.* [91] (2019)	Caspofungin	25 µg/mL	CVVHDF HF1000 ($1.1m^2$) membrane	Blood: 50 mL/min Post-filter: Low: 100 mL/hr High: 200 mL/hr Dialysate: Low: 100 mL/hr	CL_{RRT}: Low: 0.40 mL/min ±0.16 High: 0.40 mL/min ±0.16	Low: 0.12 ±0.05 High: 0.06 ±0.02	0.22 ±0.04

				High: 200 mL/hr Ultrafiltration: Low: 200 mL/hr High: 400 mL/hr			
Polyenes							
Purohit *et al.* [91] (2019)	Liposomal amphotericin B	120 µg/mL	CVVHDF HF1000 (1.1m^2) membrane	Blood: 50 mL/min Post-filter: Low: 100 mL/hr High: 200 mL/hr Dialysate: Low: 100 mL/hr High: 200 mL/hr Ultrafiltration: Low: 200 mL/hr High: 400 mL/hr	CL_{RRT}: Low: 0.025 mL/min ±0.05 High: 0.025 mL/min ±0.05	Low: 0.007 ±0.02 High: 0.004 ±0.01	0.13 ±0.08
Anticonvulsants							
Kroh *et al.* [201] (1998)	Phenobarbital	40 mg	CVVH FH77H hydrophobic polyamide matrix (1.4m^2) Experiment 1: ↑UF Experiment 2: ↑Albumin Experiment 3: Added FFP	Blood: (1) 50-20 mL/min (2) 120 mL/min (3) 120 mL/min Ultrafiltration: (1) 10-50 mL/min (2) 30 mL/min (3) 30 mL/min Post-filter replacement fluids: NR	k_e: ↑UF V_d: ↓UF Ae: ↓Alb	SC: ↓Alb	NR
Kroh *et al.* [201] (1998)	Phenytoin	20 mg	CVVH FH77H hydrophobic polyamide matrix (1.4m^2)	Blood: (1) 50-20 mL/min (2) 120 mL/min (3) 120 mL/min Ultrafiltration: (1) 10-50 mL/min (2) 30 mL/min	k_e: ↓UF	NC	NR

			Experiment 1: ↑UF Experiment 2: ↑Albumin Experiment 3: Added FFP	(3) 30 mL/min Post-filter replacement fluids: NR			
Cardiac Glycosides							
Kroh *et al.* [201] (1998)	Digoxin	2 µg	CVVH FH77H hydrophobic polyamide matrix ($1.4m^2$) Experiment 1: ↑UF Experiment 2: ↑Albumin Experiment 3: Added FFP	Blood: (1) 50-20 mL/min (2) 120 mL/min (3) 120 mL/min Ultrafiltration: (1) 10-50 mL/min (2) 30 mL/min (3) 30 mL/min Post-filter replacement fluids: NR	k_e: ↑UF V_d: ↑Alb	NC	NR
Phosphodiesterase Inhibitor							
Kroh *et al.* [201] (1998)	Theophylline	20 mg	CVVH FH77H hydrophobic polyamide matrix ($1.4m^2$) Experiment 1: ↑UF Experiment 2: ↑Albumin Experiment 3: Added FFP	Blood: (1) 50-20 mL/min (2) 120 mL/min (3) 120 mL/min Ultrafiltration: (1) 10-50 mL/min (2) 30 mL/min (3) 30 mL/min Post-filter replacement fluids: NR	k_e: ↑UF	SC: ↓Alb	NR

Ae; eliminated amount of drug, Alb; albumin, CL_{RRT}; clearance as per CRRT circuit, CRRT; continuous renal replacement therapy, CVVH; continuous veno-venous hemofiltration; CVVHD; continuous veno-venous hemodialysis; CVVHDF; continuous veno-venous

hemodialfiltration; FFP; fresh frozen plasma, k_e; elimination rate constant, NC; no correlation, NR; not reported, PK; pharmacokinetics, SC; sieving coefficient, S_D; dialysate saturation constant, SD; standard deviation, UF; ultrafiltration, V_d; volume of distribution, ↑; indicates a positive correlation ($p < 0.05$, ↓; indicates a negative correlation ($p < 0.05$).
[a]All data reported as mean unless otherwise stated.

2.3 Discussion

To our knowledge, this is the first systematic review focusing on drugs of all therapeutic classes administered to children across the age spectrum, from neonates to adolescents, receiving CRRT. A previous review conducted by Veltri *et al.* [154] provided an overview of medications administered to this population, however dose recommendations were largely based on adult extrapolations. Using a comprehensive search strategy, this review identified 45 studies evaluating 33 different medications. The current state of the literature largely focuses on the use of antibiotics, as 14 out of 45 studies analyzed the pharmacokinetics of antibiotics administered to pediatric patients receiving CRRT.

Most studies identified that V_d and CL_{total} may be similar in critically ill pediatric patients receiving CRRT compared to critically ill pediatric patients who did not. This suggests renally adjusted doses may lead to subtherapeutic dosing regimens. In the studies that included a comparator, CL_{total} was increased in those receiving CRRT compared to those who did not, especially in the presence of residual renal function. [166,178,193] These results were demonstrated with antibiotics (meropenem, piperacillin, vancomycin) where CL_{total} is largely dependent on renal clearance. [267–269] The SC of such medications approximated 1.0, suggesting free passage across the CRRT circuit membrane from blood to ultrafiltrate/dialysate fluid. [166,178,193,270] Meropenem, piperacillin and vancomycin all demonstrate similar physicochemical properties as they are hydrophilic agents with a relatively high unbound fraction (~50-98%). [267–269] Drugs with similar physicochemical properties result in high S_C within CRRT circuits, therefore being subjected to increased CLRRT. [271] Higher S_C and CL_{RRT} were also recorded for these molecules within the included *ex-vivo* analyses. [91,201] However, further studies with comparator arms would be needed to confirm the relationship between hydrophilicity and fraction unbound with CL_{total} in patients on and off CRRT. Furthermore, often higher doses were needed within these studies to achieve adequate pharmacodynamic target attainment. [166,178,193]

One of the objectives of this review was to investigate the pharmacokinetics of molecules administered to pediatric patients receiving CRRT and how these may differ between circuits.

Only one such comparison was made due to the paucity of studies and poor quality of reporting. CL_{total} of meropenem was greatest with CVVHDF (0.13 mL/kg/hr) and lowest with CVVHD (0.037 mL/hr/kg) when similar blood flow rates (50 mL/min) and membrane filters were used (AN 69). [184,190] Although these results do support greatest CL_{RRT} with CVVHDF within pediatrics, there may be high variability between compounds based on pharmacokinetic behaviour and physicochemical properties.

CRRT membrane composition have been shown to impact CL_{total} of medications due to the differences in adsorptive potential and surface area. [272,273] Commonly used semi-synthetic membranes such as PS, PAN, and PMMA contain different degrees of charge which affect adsorptive capacity based on the charge of molecule. [272,273] This concept was shown in the analysis by Shiraishi *et al.*, indicating a higher adsorption potential of the PAN filter, leading to a reduction in CL_{RRT} for teicoplanin. [118] The effects of membrane potential may differ based on the physicochemical properties of a drug as indicated by Lindsay *et al*. [118] Within this study, CL_{total} and CL_{RRT} was significantly greater for clavulanic acid, a negatively charged molecule, compared to piperacillin. [118] Increases in membrane porosity have the potential to increase CL_{RRT} of certain molecules as demonstrated by Harvey *et al*. [202] The surface area of the membrane filter is of particular importance when designing drug dosing regimens for pediatric patients receiving CRRT due to the smaller total blood volume seen in children. A thorough understanding of the physicochemical properties of both circuit membranes and molecules is needed to ensure adequate dosing regimens for pediatrics receiving CRRT.

This review had several limitations, first there was substantial heterogeneity in the patient populations identified. This heterogeneity may explain the large variability in primary pharmacokinetic parameters identified and may limit the ability to draw significant conclusions. CL_{total} of medications administered to patients receiving CRRT may also depend on non-renal CL mechanisms. Non-renal clearance may also be affected by critical illness due to inflammatory responses downregulating CYP-mediated enzymes, hepatic dysfunction, drug-drug interactions and AKI-mediated uremic toxins affecting metabolic enzymes and drug transporters. [274] Reporting of relevant clinical variables associated with renal and hepatic function was poor within the identified studies, therefore minimal conclusions can be drawn as to how acute illness

may affect non-renal CL in pediatrics. Secondly, nearly half (42%) of the studies identified were case-reports or case-series. Due to the high variability in pharmacokinetic parameters within critically ill children, the small sample sizes limit the generalizability of the results and should be interpreted with caution. Thirdly, >40% of studies included children <1-year of age. Age-related changes in metabolism and excretion of pharmacokinetics affecting V_d and CL_{total} has been well established. [275,276] Changes in body water composition in neonates and young infants results in higher percentages of total body water, affecting V_d. [275,276] Additionally, due to maturation in kidney size and metabolic enzymes, CL_{total} may be decreased in young infants compared to more mature children or adolescents. [275,276] As a result, more robust studies are warranted to describe the pharmacokinetics in pediatrics receiving CRRT across the age spectrum. Finally, 53% of studies included children receiving ECMO, accounting for 24% (197/833) of the total number of children included within this review. As previously mentioned, ECMO may induce alterations in pharmacokinetic parameters of certain medications, therefore a patient specific approach should be utilized when applying these results.

One of the primary objectives of this review was to assess the quality of reporting of pharmacokinetic research within this patient population. To fully assess the validity of such results, completeness and transparency in reporting is of the utmost importance. Overall, reporting of necessary information was generally poor as described by the ClinPK statement. [158] Significant under reporting was seen with the use of concurrent medications and patient demographics that may explain intra- and inter-patient pharmacokinetic variability. Although no formal validated tool has been developed to assess the quality of reporting of pharmacokinetic studies incorporating CRRT, Choi *et al.* illustrate suggestions for a complete data set that would allow clinicians to incorporate CRRT properties to bedside dosing recommendations. [103] Within this review approximately 10% of studies contained all necessary data required to describe mechanistic effects of CRRT, in conjunction with patient clinical characteristics on the pharmacokinetics of administered drugs. It is imperative that future pharmacokinetic studies in pediatrics receiving CRRT include specific details such as modality, flow rates and filters used, in addition to clinical patient characteristic to further enhance the applicability of such results.

Pediatric pharmacokinetic studies present significant challenges due to logistical and ethical considerations. Often challenges arise with obtaining informed consent, withdrawing blood and urine samples, and recruiting participants within studies. [277,278] Predictive simulations through the use of physiologically-based pharmacokinetic modelling (PBPK) may address these limitations with compartmental modelling by translating CRRT *ex-vivo* experiments into bedside dosing recommendations. Modelling of drug exposure in pediatrics on CRRT may occur through linking a CRRT "organ" within the PBPK model and parameterized with data from *ex-vivo* studies. [144] With the incorporation of volume, blood flow, and drug clearance of the CRRT circuit, the impact of CRRT on drug pharmacokinetics can be predicted *in-vivo* and the CRRT-PBPK model may be used to determine optimal dosing regimens within this patient population.

2.4 Conclusion

With the use of a comprehensive search strategy, this review was able to identify that primary pharmacokinetics in pediatric patients receiving CRRT are largely similar to critically ill children who are not. Over 50% of studies provided a dosing recommendation based on patient specific pharmacokinetics, however due to the substantial amount of heterogeneity within the patient populations, drugs analyzed, and doses administered, these results should be interpretated with caution. Renally adjusted or reno-protective doses often led to subtherapeutic dosing regimens within these patients, illustrating the impact of CRRT on primary pharmacokinetic parameters. However, upon future well designed, pharmacokinetic studies within this population, the use of TDM to guide prescribing practices, when applicable, will optimize PTA and minimize adverse events.

This review identified several *ex-vivo* CRRT analyses that provide mechanistic insight as to how extracorporeal clearance may be affected by variation in circuit settings (i.e. flow rates, membrane composition). Utilization of these analyses may provide a glance of the pharmacokinetics of certain medications administered to patients receiving CRRT. As such, further well-designed *ex-vivo* analyses incorporating commonly used CRRT circuit characteristics are required as a starting point to understand the pharmacokinetics within this population. However, a thorough understanding of the interplay between CRRT circuit

components, patient clinical status and drug physicochemical properties are required when designing safe and effective dosing regimens. Significant gaps remain within the literature, as a large majority of medications studied were antimicrobials. Minimal studies have been conducted on the use of analgesics or sedatives within this population despite widespread use within a PICU. This review highlights the urgent need for well-designed pharmacokinetic studies in children receiving CRRT and the incorporation of *ex-vivo* analyses in conjunction with PBPK modelling to provide a complete mechanistic understanding of the interplay between drug, circuit, and patient interactions.

Chapter 3: Determining the Effects of Chronic Kidney Disease on Organic Anion Transporter 1/3 Activity Through Physiologically-Based Pharmacokinetic Modelling

This chapter is reflective of an original manuscript published by the PhD candidate (Samuel Dubinsky) in the journal of *Clinical Pharmacokinetics*. All pertinent dialogue in this chapter was written by the PhD candidate.

Information regarding applicable letters of copyright permission is presented in the **Letters of Copyright Permission**.

3.1 Overview

Background:

The renal excretion of drugs via organic anion transporters (OAT1/3) is significantly decreased in patients with renal impairment. This study uses physiologically-based pharmacokinetic models to quantify the reduction in OAT1/3-mediated secretion of drugs throughout varying stages of chronic kidney disease.

Methods:

Physiologically based pharmacokinetic models were constructed for four OAT1/3 substrates in healthy individuals: acyclovir, meropenem, furosemide, and ciprofloxacin. Observed data from drug-drug interaction studies with probenecid, a potent OAT1/3 inhibitor, were used to parameterize the contribution of OAT1/3 to the renal elimination of each drug. The models were then translated to patients with chronic kidney disease by accounting for changes in glomerular filtration rate, kidney volume, renal blood flow, plasma protein binding and hematocrit. Additionally, a relationship was derived between the estimated glomerular filtration rate and the reduction in OAT1/3-mediated secretion of drugs based on the renal extraction ratios of *p*-aminohippuric acid in patients with varying degrees of renal impairment. The relationship was evaluated *in silico* by evaluating the predictive performance of each final model in describing the pharmacokinetics (PK) of drugs across stages of chronic kidney disease.

Results:

OAT1/3-mediated renal excretion of drugs was found to be decreased by 27-49%, 50-68% and 70-96% in stage 3, stage 4, and stage 5 of CKD, respectively. In support of the parameterization, physiologically based pharmacokinetic models of four OAT1/3 substrates were able to adequately characterize the PK in patients with different degrees of renal impairment. Total exposure after intravenous administration was predicted within 1.5-fold error and 85% of the observed data points fell within 1.5-fold prediction error. The models modestly under-predicted plasma concentrations in patients with end-stage renal disease receiving intermittent hemodialysis. However, results should be interpreted with caution due to the limited number of

molecules analyzed and the sparse sampling in observed chronic kidney disease pharmacokinetic studies.

Conclusion:

A quantitative understanding of the reduction in OAT1/3-mediated excretion of drugs in varying stages of renal impairment will contribute to better predictive accuracy for PBPK models in drug development, assisting with clinical trial planning and potentially sparing this population from unnecessary toxic exposures.

3.2 Introduction

Chronic kidney disease (CKD) affects nearly 10% of the global population. [279] Chronic kidney disease is defined by a reduction in kidney function as approximated by the glomerular filtration rate (GFR) below 60 mL/min/1.73m2 for 3 months or more. [64] Several equations to approximate GFR are used in clinical practice such as the Cockcroft-Gault, Modification of Diet in Renal Disease or the CKD Epidemiology Collaboration equations. [64] Stages of CKD are classified by the degree of renal impairment, with stage 3, stage 4 and stage 5 defined by estimated GFR values of 59 to 30, 29 to 15 and <15 mL/min/1.73m2, respectively. [64]

Patients with CKD may take more than twelve different prescription drugs per day to reduce morbidity and mortality associated with the disease. [280] It is a clinical challenge to ensure safe and effective dosing for each of these medications in patients with renal impairment because CKD affects many aspects of pharmacokinetics (PK) and drug disposition. Most intuitively, renal elimination pathways are compromised. About one-third of the most prescribed drugs in the US undergo renal elimination and 90% of these are actively secreted by the kidney. [281] While passive filtration of drugs into urine declines directly in proportion to the GFR, the progressive decline in secretory function in each stage of CKD remains poorly understood.

There are two common groups of transporters by which drugs can be actively secreted from the interstitial space of the nephron across the renal epithelium and into the urine. Cations may be taken up by organic cation transporters (OCT) and secreted into urine by P-glycoprotein (P-gp) and/or the multidrug and toxin extrusion transporters (MATE1, MATE2K). [282] Anions may be taken up by organic anion transporters (OAT1, OAT3) and secreted into the urine by the

multidrug resistance proteins (MRP1-4). [282] A recent review summarizes evidence that the activities of apical efflux transporters are largely preserved in CKD. [282] The renal clearances of drugs that are substrates for OCT tend to decline in parallel with GFR, suggesting that the activity of renal OCT transporters may not be significantly compromised by uremia. [283,284] However, there is convincing evidence that the activities or expression of renal OAT transporters may be significantly compromised in renal impairment, with this inhibition driven by high concentrations of circulating uremic toxins. [282,285,286] The progressive decline in renal clearance for most OAT1/3 substrates is more severe than the decline in GFR. [287,288]

In this work, a parameterization for the relative activity of OAT1/3 transporters across various stages of renal impairment is developed and evaluated using a mechanism-based modeling approach. Physiologically-based pharmacokinetic (PBPK) models represent drug absorption, distribution, metabolism, and excretion (ADME) within virtual individuals according to the actual mechanisms responsible, as far as can be feasibly identified. This exercise leverages recent advancements in PBPK modeling in patients with CKD that quantify the systemic impact of the disease on parameters related to renal, hemodynamic and gastrointestinal physiology. [284] Building on this foundation, we developed PBPK models for four drugs that are OAT substrates (acyclovir, meropenem, furosemide, ciprofloxacin) with the overall objective of using a physiological model to understand how OAT1/3 activity may be compromised in patients with varying degrees of renal impairment and evaluated their predictive accuracy when the parameterization for OAT activity is applied.

3.3 Methods

3.3.1 Software

All PBPK modeling was carried out using PK-Sim v9.1 as part of the Open Systems Pharmacology suite (www.open-systems-pharmacology.org). Parameter sets for healthy adults and aged persons in European and white American populations have been described previously. [289,290] Scientific data to inform the individual and population-level parameter changes in CKD were applied using MATLAB R2021a (Mathworks, Natick, Massachusetts) as published previously. [284] Noncompartmental analysis of observed PK datasets was conducted with the PKNCA package in R where necessary.

3.3.2 PBPK Models for Healthy Adults

Physiologically based pharmacokinetic models were constructed to mechanistically represent the pharmacokinetics of four drugs that are substrates of OAT1/3 in healthy adults. A detailed report of model development and verification for each molecule in healthy adults is available in **Appendix B, Section 1-3.** The final parameters for each molecule are presented in **Table 3-1**.

Table 3-1. PBPK model parameters.

Parameter	Ciprofloxacin	Furosemide	Meropenem	Acyclovir
Fraction unbound in plasma (f_u)	0.67 [291]	0.022 [292]	0.98 [268,293]	0.85 [294]
Lipophilicity (logP)	0.95 [291]	-0.24	-1.21[a] [-1.21- -1.21]	-0.69[a] [-0.69 - -0.69]
Molecular weight (g/mol)	331.30 [291]	330.74	383.46 [293,295]	225.21 [294]
Effective molecular weight (g/mol) ***accounting for halogens***	314.30	330.74	383.46	225.21
Fraction excreted in urine (*fe; %)*	61.2±7.2 [296]	74±7 [292]	79±2 [297]	86.2±11.4 [298]
Contribution of TS of CL_R[c] (%)	73	98	96	74
Partition coefficient algorithm	PK-Sim Standard	Schmitt	Rodgers and Rowland	Rodgers and Rowland
Cell permeability algorithm	PK-Sim Standard	Charge-dependent Schmitt	Charge-dependent Schmitt	Charge-dependent Schmitt
GFR fraction	1.0	1.0	1.0	1.0
OAT[b] concentration (µM)	0.0917 [292]	0.0917 [292]	0.0917 [292]	0.0917 [292]
OAT V_{max} (µM/min)[a]	5.96 (M/min) [5.60-6.30]	754.40 [292]	1262.57 [1248.49-1268.14]	25.75 (mM/min) [25.70-26.19]
OAT Km (µM)	70 [299]	21.50 [292]	847 [300]	342.30 [299]
Apical transporter type	TS[c]	MRP4 [292]	TS[c]	MATE [301]
Apical transporter[b] concentration (µM)	1.0	0.02 [302,303]	1.0	1.0
Apical transporter[b] V_{max} (µM/min)	58.39[a] [55.45-61.62]	163.09[a] [292]	116.11 [115.67-117.16]	0.99[a] (mM/min) [0.98-0.99]

Apical transporter[b] Km (µM)	1000	27.96 [292]	770 [304]	3480 [299]
Metabolizing enzyme	CYP 1A2[b]	UGT 1A9[b] [292]	Renal DHP-1[b] [21]	CMMG[d]
Metabolizing enzyme concentration (µM)	1.8	0.197 [292]	1.0	1.0
Metabolizing enzyme specific clearance[a] (L/µmol/min)	0.027 [0.027-0.027]	187.53 [292]	89.21 [88.99-89.90]	0.031 [0.031-0.031]

[a] Parameters optimized from their literature values
[b] Relative expression in human organs extracted from the PK-Sim Gene Database for Humans
[c] TS; generic apical transporter on the apical side of kidney cells
[d] CMMG; assumed first order metabolism within the liver
[e] Percentage of tubular secretion of renal clearance was calculated as $(CL_R - f_u*GFR)/CL_R$

Briefly, each model in healthy adults was developed by collecting and appraising the physiochemical properties of each molecule from literature. Organ specific partition coefficients were calculated with the PK-Sim standard, Schmitt, or the Rodgers and Rowland algorithms. [305–307] Information regarding expression and localization of renal transporters was extracted from Ivanyuk *et al.* and previously published PBPK-models. [292,301] It was assumed that basolateral uptake into renal epithelium by OAT1 and OAT3 occurs via one generic OAT transporter within the models since the processes are not uniquely identifiable.

Previous PBPK models for drugs with active tubular secretion often simplified the two processes of basolateral influx and apical efflux with 'global' renal drug transporters to represent the net flux into urine. Such assumptions were largely due to the absence of *in vitro* and *in vivo* data to parameterize each process separately. [284,288,308] In this work, uptake via OAT transport was mathematically identified by optimizing against a DDI study with one arm where OAT activity was strongly inhibited by probenecid and one control arm. The PBPK model for probenecid was downloaded from the Open Systems Pharmacology repository and can be found at: https://github.com/Open-Systems-Pharmacology/Probenecid-Model. [292] Probenecid is a competitive inhibitor of OAT with an inhibition constant (K_I) of 5.41 µM; previous validation of this inhibition constant for prediction of the furosemide-probenecid DDI has been published. [292] In the DDI simulation of probenecid and the OAT substrates, the apparent Michaelis-Menten constant for OAT transport ($K_{M,app}$) was calculated as (Eq. 3-1):

$$Km_{app} = Km \times (1 + \frac{I}{K_I})$$

Eq. 3-1

where I represents the concentration of the competitive inhibitor, probenecid. [292]

Incorporating empirical data derived from probenecid-DDI PK studies follows a "middle-out" approach, which implements *in vitro* understanding of the PK (bottom-up) with observed clinical data (top-down). [309–311] Although this model development strategy differs slightly from "traditional" PBPK model development, it provides the most mechanistically accurate approach in the absence of a proper method to scale *in vitro* data for OAT transport to *in vivo*.

For uncertain parameters, numerical optimization was performed using the parameter identification tool in PK-Sim. A Monte Carlo method was used to search the parameter space for the optimal solution that minimized the sum of squared error on the simulated versus observed drug concentrations and fractions excreted to urine. Multiple optimization runs (6 to 10) were performed to confirm identifiability of a unique solution.

The models that were optimized using mean individuals were then expanded to simulate the PK in virtual populations for model verification. Datasets for model verification are presented in **Appendix B, Section 1-3** for each molecule. One hundred individuals were generated for each virtual population. Patient demographics were set according to those reported in each observed study population being simulated. User-defined variability was assigned to the renal transporter concentrations with a normal distribution and a coefficient of variation of 20%. [284,312] Verification was assessed using the average fold error (AFE) (Eq. 3-2) and absolute average fold (AAFE) error (Eq. 3-3) for each simulation. Acceptance was confirmed if AFE <30% (0.7-1.3) and AAFE ≤2. For data sets including individual patient samples, inter-individual variability in the population simulation was accepted if 85 to 95% of observed concentrations fell within the 90th prediction interval.

$$AFE = 10^{\frac{1}{N}\sum_i \log\left(\frac{predicted_i}{observed_i}\right)}$$

Eq. 3-2

$$AAFE = 10^{\frac{1}{N}\sum_i \left|\log\left(\frac{predicted_i}{observed_i}\right)\right|}$$

Eq. 3-3

Where $predicted_i$ and $observed_i$ correspond to predicted and observed plasma concentrations respectively.

3.3.3 PBPK Models for Chronic Kidney Disease

Final population models for healthy adults were carried forward for evaluation in CKD with modifications to account for the systemic changes in whole-body anatomy and physiology that occur throughout the course of the disease such as GFR, kidney volume, renal perfusion, hematocrit, and plasma protein concentrations. The methodology and evaluation of this modeling strategy has been published previously. [284] Additionally, nonrenal clearance (CL_{NR}) was scaled for various stages of CKD to account for inhibition or downregulation of liver enzymes due to chronic uremia throughout disease progression as outlined in the corresponding section. [311] Utilizing the CKD-PBPK modeling approach, we produced several PBPK models across stages 3-5 of CKD to evaluate the proposed parameterization for OAT activity in CKD.

Predictive accuracy for the extrapolation to CKD was assessed by a limit of 1.5-fold error (0.67-1.5) when comparing simulated exposures to observed data from literature. Exposure was quantified as the area under the curve extrapolated to infinity (AUC_∞). If AUC_∞ was not reported within the study, AUC_∞ was calculated by noncompartmental analysis. Additionally, predicted vs. observed half-lives were compared. The limit of 1.5-fold error for each PK parameter was used as the threshold for acceptable performance when extrapolating to vulnerable and diverse populations based on previous criteria used in recent years. [288,313]

Additionally, model performance against the conventional AUC scaling method was also explored. Scaling AUC_∞ from healthy individuals was conducted using equation 4 (Eq. 3-4):

$$AUC_{CKD} = \frac{BW_{CKD}}{BW_{Healthy}} \cdot AUC_{Healthy} \div \left[fe \cdot \frac{GFR_{CKD}}{GFR_{Healthy}} + (1 - fe) \right]$$

Eq. 3-4

where AUC is area under the curve extrapolated to infinity for CKD and healthy individuals respectively, BW is body weight, GFR is glomerular filtration rate, and *fe* is the fraction excreted to urine unchanged after intravenous dose. Within this assessment patients on dialysis were assumed to have a GFR of 5 mL/min/1.73m^2.

3.3.4 Organic Anion Transporter Parameterization

The utility of p-aminohippuric acid (PAH) as a diagnostic indicator of renal plasma flow and tubular excretion was first discovered in the 1940's by Homer-Smith *et al*. [314] Based on its physicochemical properties, PAH has since become recognized as a prototypical OAT substrate and has helped to define the OAT pathway of several drugs. [315–317] Numerous publications have since quantified the activity of OAT excretion in various stages of CKD by comparing the renal extraction ratio of PAH (EPAH%) to eGFR. [318–323] Individual patient data was extracted, and several exploratory analyses were conducted to describe the relationship between EPAH and eGFR, including the logarithmic of EPAH, LASSO regression and polynomial function. Ultimately, a Weibull function utilizing Poisson weighting and setting the intercept equivalent to zero was used to convey this relationship. Weighting of observed EPAH values was conducted to characterize the EPAH in patients with severe renal impairment. The resulting EPAH% vs. eGFR relationship is presented in **Figure 3-1**.

The final function of EPAH (y) and eGFR (x) was given by (Eq. 3-5):

$$EPAH\ (\%) = \left(1 - e^{\left(-\left(\frac{eGFR}{43.9}\right)^{0.9}\right)}\right) x\ 100\%$$

Eq. 3-5

This parameterization describes how OAT mediated secretory function declines through various stages of CKD due to a combination of transporter down regulation and competitive OAT inhibition from uremic solutes. [282,285,286]

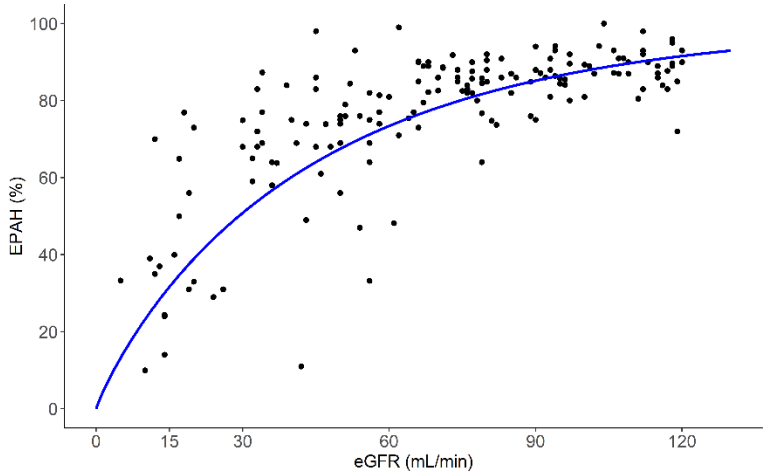


Figure 3-1. Parameterization of organic anion transporter 1and 3 functionality across varying stages of chronic kidney disease. Data investigating the relationship between p-aminohippuric acid extraction ratio (EPAH) and estimated GFR (eGFR) was extracted from several studies (black dots). [318–323] A Weibull function (blue-line) was determined to be the best representation of the relationship between EPAH and eGFR.

3.3.5 Non-Renal Clearance in CKD

Evolving data suggests that CKD reduces CLNR through various mechanisms. [324–326] Work conducted by Sayama *et al.* quantified the reduction in CLNR for several metabolic pathways. [311] The mean relative percentage (RP%) of CL_{NR} was 69% for moderate CKD (eGFR: 30-59 mL/min/1.73m^2) and 64% for severe CKD (eGFR: 15-29 mL/min/1.73m^2) compared to healthy individuals. [311] The mean RP was used to scale CL_{NR} in our PBPK simulations across the stages of CKD. It was assumed that mean RP of CL_{NR} for stage 5 CKD (GFR <15 mL/min/1.73m^2) was consistent with severe CKD (RP = 64%).

3.3.6 Sensitivity Analysis

A local sensitivity analysis was performed to test the importance of OAT activity for DDI potential in healthy adults and each stage of CKD. Simulations were built for mean male individuals at stage 3, 4, 5 (ESRD) and healthy conditions. All virtual subjects received a standard therapeutic dose of each drug (i.e., 400 mg IV for ciprofloxacin, 40 mg IV for furosemide, etc.). Organic anion transporter activity in each scenario was varied by 10% and the relative changes in AUC_∞ were reported as sensitivity coefficients. The sensitivity coefficient (S^p) for the effect of the parameter (p) on the PK output (PK) was calculated as the average of (Eq. 3-6):

$$S^p = \left| \frac{PK(p + 0.1 \times p) - PK(p)}{PK(p)} \right| \times \frac{100\%}{10\%}$$

Eq. 3-6

Therefore, a sensitivity coefficient of 1 means that a 10% change in the parameter value caused a ±10% change in the PK output, and a sensitivity coefficient of 0.1 means that a 10% change in the parameter value caused a ±1% change in the PK output.

3.4 Results

3.4.1 PBPK Models for Healthy Adults

Population PBPK models for four OAT substrate drugs were developed and verified to describe the mechanistic disposition in healthy adults with explicit contribution of OAT characterized using DDI modeling with probenecid. Detailed reports of model development and verification of meropenem, acyclovir and ciprofloxacin may be found in **Appendix B, Section 1-3.** Furosemide model development and verification was included from previous work by another group. [292] **Figure 3-2** shows the fitted concentration vs. time profiles for the DDI with probenecid for each drug.

Active tubular secretion mediated by OAT transport contributes to a significant percentage of renal clearance (CL_R) (60-98%) for each investigative drug. This DDI-PBPK modeling strategy enabled us to identify a unique solution for this process. Upon model simulation, all individual and population model simulations fell within the predefined acceptance criteria for model fit.

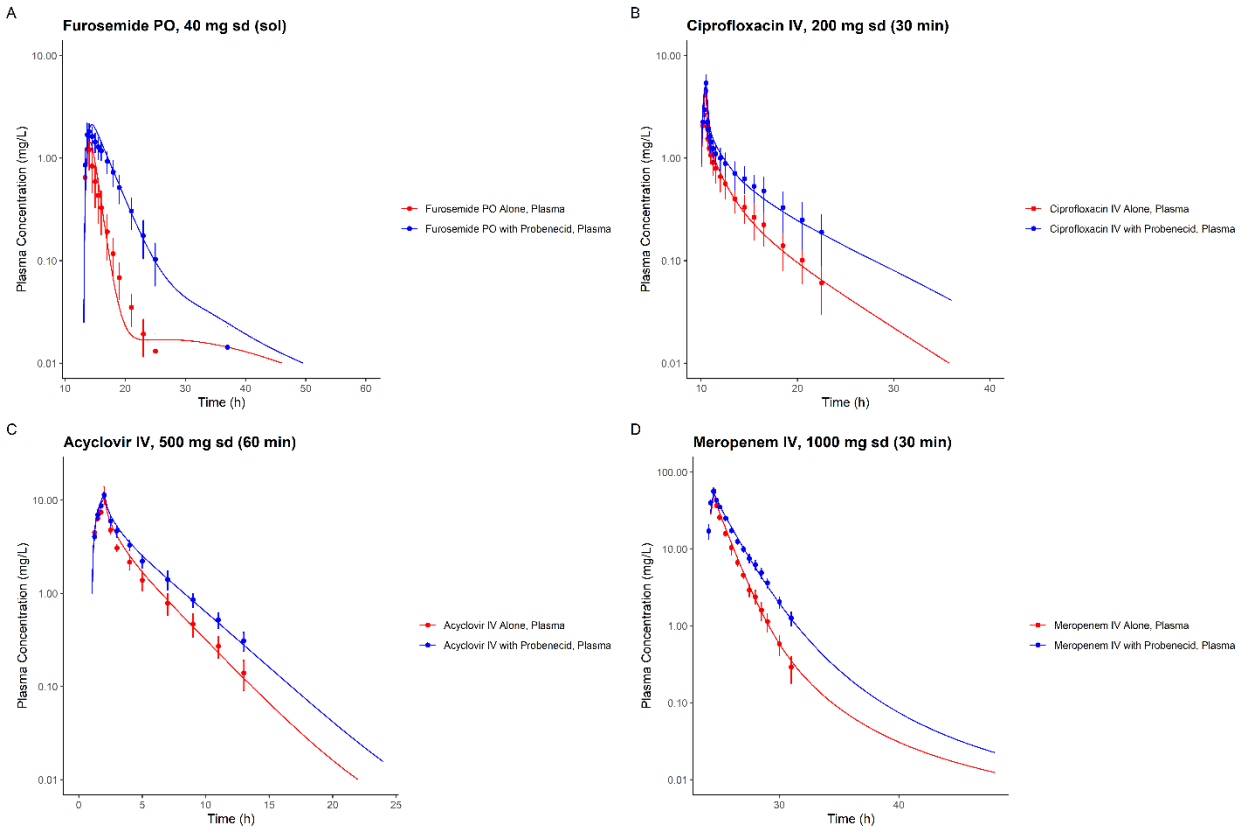


Figure 3-2. Simulated physiologically-based pharmacokinetic drug-drug interaction plasma concentration-time profiles after optimization compared to observed data for (A) furosemide, (B) ciprofloxacin, (C) acyclovir, and (D) meropenem. Observed data presented as mean (circles) with standard error of the mean (error bars) for each respective study. [296,297,327,328] The blue line represents the same dose of investigative drug administered after completion of probenecid dosing protocols. Details on dosing regimen and study populations may be found in each respective Appendix file (B1-3).
IV; intravenous, PO; by mouth, sd; single dose, sol; solution.

3.4.2 PBPK Models for Chronic Kidney Disease

Parameters for virtual individuals in the healthy populations were then modified to simulate the PK of OAT substrate drugs in various stages of CKD. Parameterization for CKD included a novel quantification of OAT activity, reduction in CL_{NR}, and foundational CKD physiological scaling. [284] To assess the accuracy of this approach and success of the OAT parameterization, predictions for exposure and half-life were compared to observed data from 8 clinical trials across CKD stages 3–5 (**Table 3-2**).

Table 3-2. Exposure predictions of drugs undergoing active tubular secretion via OAT in chronic kidney disease.

Study	Drug	Dose (mg)	GFR (mL/min) [range]	Observed AUC (mg·h/L)	Predicted AUC (mg·h/L)	Scaled AUC (mg·h/L)	Observed t ½ (h)	Predicted t ½ (h)
Stage 3								
Drusano *et al.* [329]	Ciprofloxacin	200 mg IV	39.84 [13.33-56.67]	12.36	12.36	10.98	7.70±1.22	8.57
Shah *et al.* [330]	Ciprofloxacin	400 mg IV every 12 hours	44.8 [31.3-59.9]	21.5	23.22	11.59	5.72	9.77
Chimata *et al.* [331]	Meropenem	500 mg IV	34.13 [32-37.3]	74.6±29	88.26	Healthy comparator not available	3.36±1.02	2.31
Christensson *et al.* [332]	Meropenem	500 mg IV	34±11.8	89.8±17.9	89.86	82.60	2.34	2.84
Leroy *et al.* [333]	Meropenem	500 mg IV	50.3±16.7 [30-80]	88±33.9	66.35	65.81	1.93±0.81	2.61
Stage 4								
Gladziwa *et al.* [334]	Furosemide	120 mg IV	16.7±5.5 [7-27]	47.2±15.6	60.05	Healthy comparator not available	4.6±3.0	2.81
Christensson *et al.* [332]	Meropenem	500 mg IV	17±8	156±63.8	128.88	99.89	3.82	5.24
Stage 5								
Drusano *et al.* [329]	Ciprofloxacin	200 mg IV	IHD	15.06	20.35	17.56	8.55±3.27	10.82
Shah *et al.* [330]	Ciprofloxacin	300 mg IV every 12 hours	14.5 [4.8-24.1]	30.1	25.86	19.18	8.33	11.75
Rane *et al.* [335]	Furosemide	80 mg IV	11±1	27.79	39.84	26.89	2.60	2.66
Chimata *et al* .[331]	Meropenem	500 mg IV	12.08 [4.3-21.5]	186.8±68.5	157.25	Healthy comparator not available	5.00±1.05	3.61
Christensson *et al.* [332]	Meropenem	500 mg IV	IHD	393±83.8	207.21	91.04	6.81	6.0

Leroy *et al.* [333]	Meropenem	500 mg IV	12.7±6.6 [2-30]	179±64.1	136.38	110.34	5.22±1.58	7.79
Leroy *et al.* [333]	Meropenem	500 mg IV	IHD	360±108	204.33	118.71	9.73±3.03	9.15
Laskin *et al.* [336]	Acyclovir	2.5 mg/kg IV	IHD	354.51[a] (µmol·h/L)	265.77[a] (µmol·h/L)	102.50	19.5±5.9	11.40

Data presented as mean ±SD (range)
Shaded region indicates failed predictions
[a]AUC calculated until last sampling time due to initiation of dialysis
AUC; area under the curve, GFR; glomerular filtration rate, h; hours, IHD; intermittent hemodialysis, IV; intravenous, t ½; half-life.

Mean AUC_{∞} was predicted within 1.5-fold error across all observed data sets except for two involving patients with ESRD undergoing intermittent hemodialysis (IHD) receiving meropenem (**Figure 3-6**). Within these data sets, predicted AUC_{∞} was within two-fold error of observed values. The meropenem-CKD model was able to accurately capture clearance processes in ESRD however significantly underpredicted maximum concentration (C_{max}) (**Figure 3-6)**. Of note, AUC_{∞} predictions were suitable for CKD stages 3 and 4 within the same trials. Similarly, C_{max} was underpredicted within our acyclovir-CKD model which may have contributed to underpredictions in AUC_{∞}.

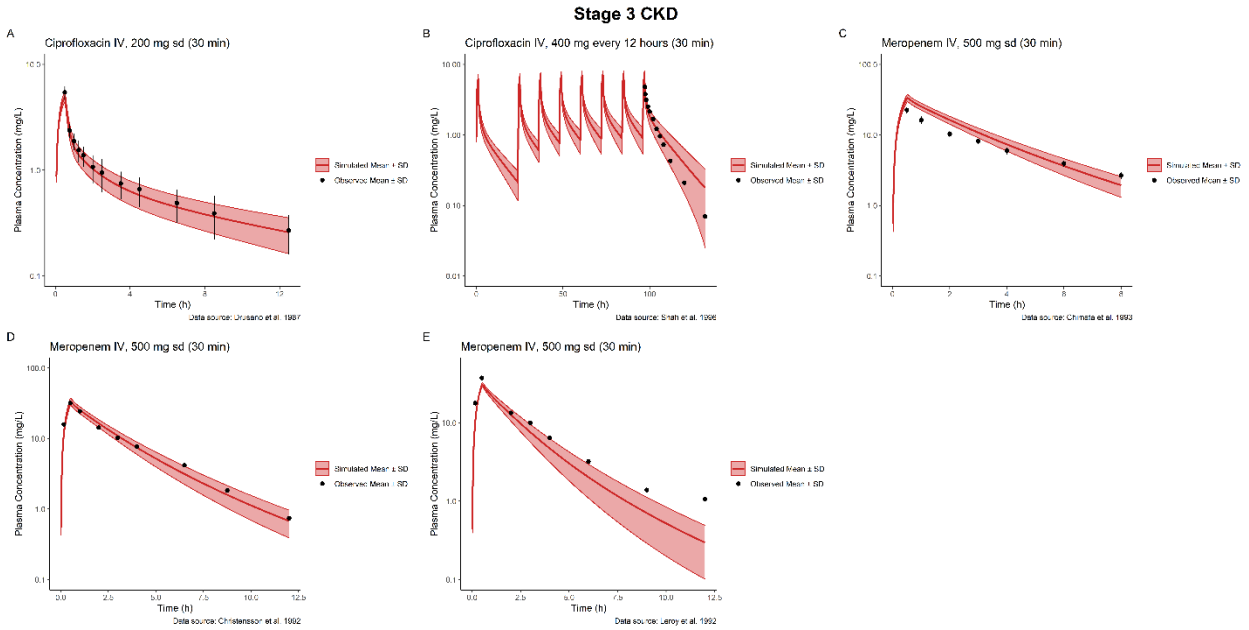


Figure 3-3. Simulated chronic kidney disease physiologically-based pharmacokinetic (CKD-PBPK) plasma concentration-time profiles compared to observed data for CKD stage 3. Observed data presented as mean (circles) with standard error of the mean (error bars) for each respective study. [329–333] The red line represents the simulated mean concentration-time profile facilitated by the population CKD-PBPK models in PK-Sim, while the shaded region indicates the corresponding standard deviation. Details on dosing regimen and study populations may be found in the Appendix B4.
IV; intravenous, sd; single dose, SD; standard deviation

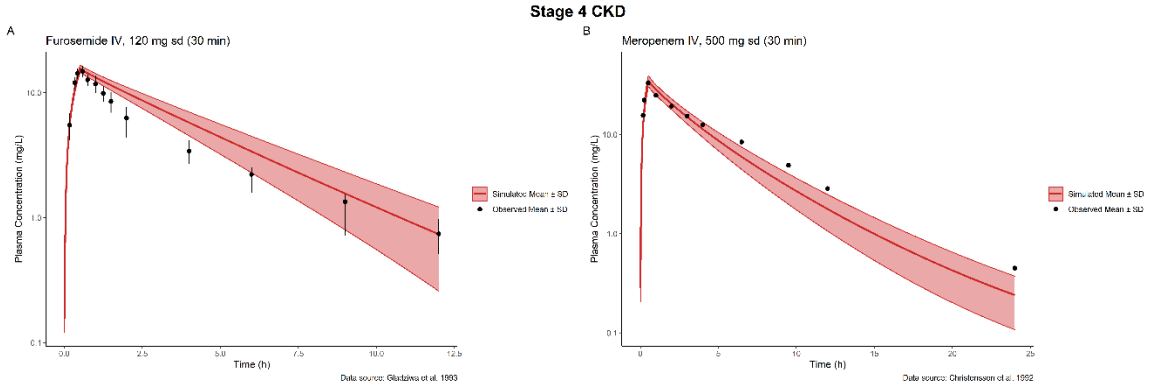


Figure 3-4. Simulated chronic kidney disease physiologically-based pharmacokinetic (CKD-PBPK) plasma concentration-time profiles compared to observed data for CKD stage 4. Observed data presented as mean (circles) with standard error of the mean (error bars) for each respective study. [332,334] The red line represents the simulated mean concentration-time profile facilitated by the population CKD-PBPK models in PK-Sim, while the shaded region indicates the corresponding standard deviation. Details on dosing regimen and study populations may be found in the Appendix B4.
IV; intravenous, sd; single dose, SD; standard deviation

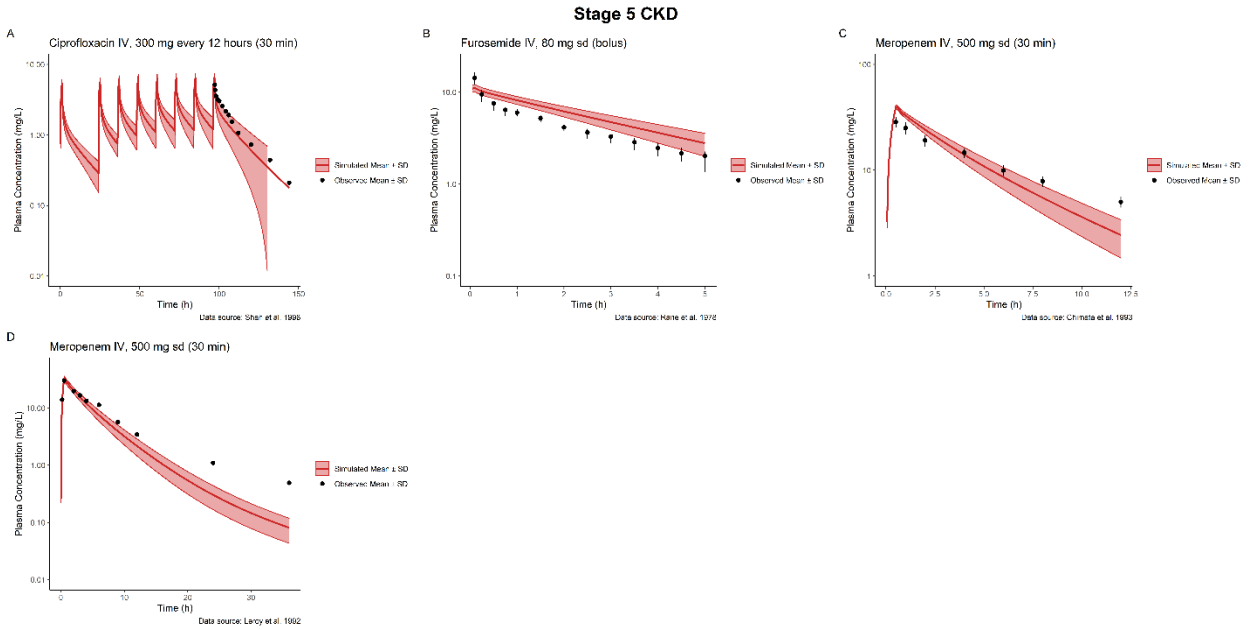


Figure 3-5. Simulated chronic kidney disease physiologically-based pharmacokinetic (CKD-PBPK) plasma concentration-time profiles compared to observed data for CKD stage 5 without administration of intermittent hemodialysis. Observed data presented as mean (circles) with standard error of the mean (error bars) for each respective study. [329,331,333,334] The red line represents the simulated mean concentration-time profile facilitated by the population CKD-PBPK models in PK-Sim, while the shaded region indicates the corresponding standard deviation. Details on dosing regimen and study populations may be found in the Appendix B4.

IV; intravenous, sd; single dose, SD; standard deviation

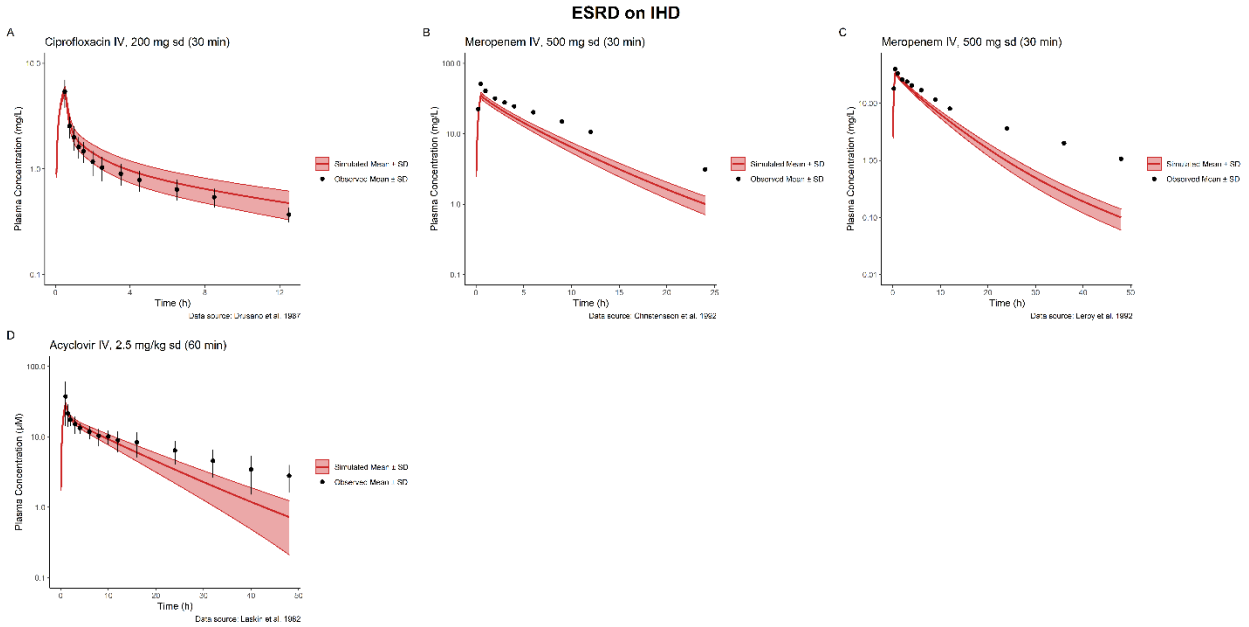


Figure 3-6. Simulated chronic kidney disease physiologically-based pharmacokinetic (CKD-PBPK) plasma concentration-time profiles compared to observed data for end stage renal disease on intermittent hemodialysis. Observed data presented as mean (circles) with standard error of the mean (error bars) for each respective study. [329,332,333,336] The red line represents the simulated mean concentration-time profile facilitated by the population CKD-PBPK models in PK-Sim, while the shaded region indicates the corresponding standard deviation. Details on dosing regimen and study populations may be found in the Appendix B4.
IV; intravenous, sd; single dose, SD; standard deviation

Of the remaining CKD-PBPK simulations, predicted AUC_{∞} fell within 1.5-fold error of observed values across all stages of CKD. Additionally, seven of the 15 predictive AUC_{∞} values were within a more rigorous 1.25-fold error (**Figure 3-7A.)**. Predicted elimination half-life within the CKD-PBPK simulations fell within 1.5-fold error for 11 of the 15 simulations. Predictive accuracy for elimination half-life resulted in an equal number of over and under-predictions.

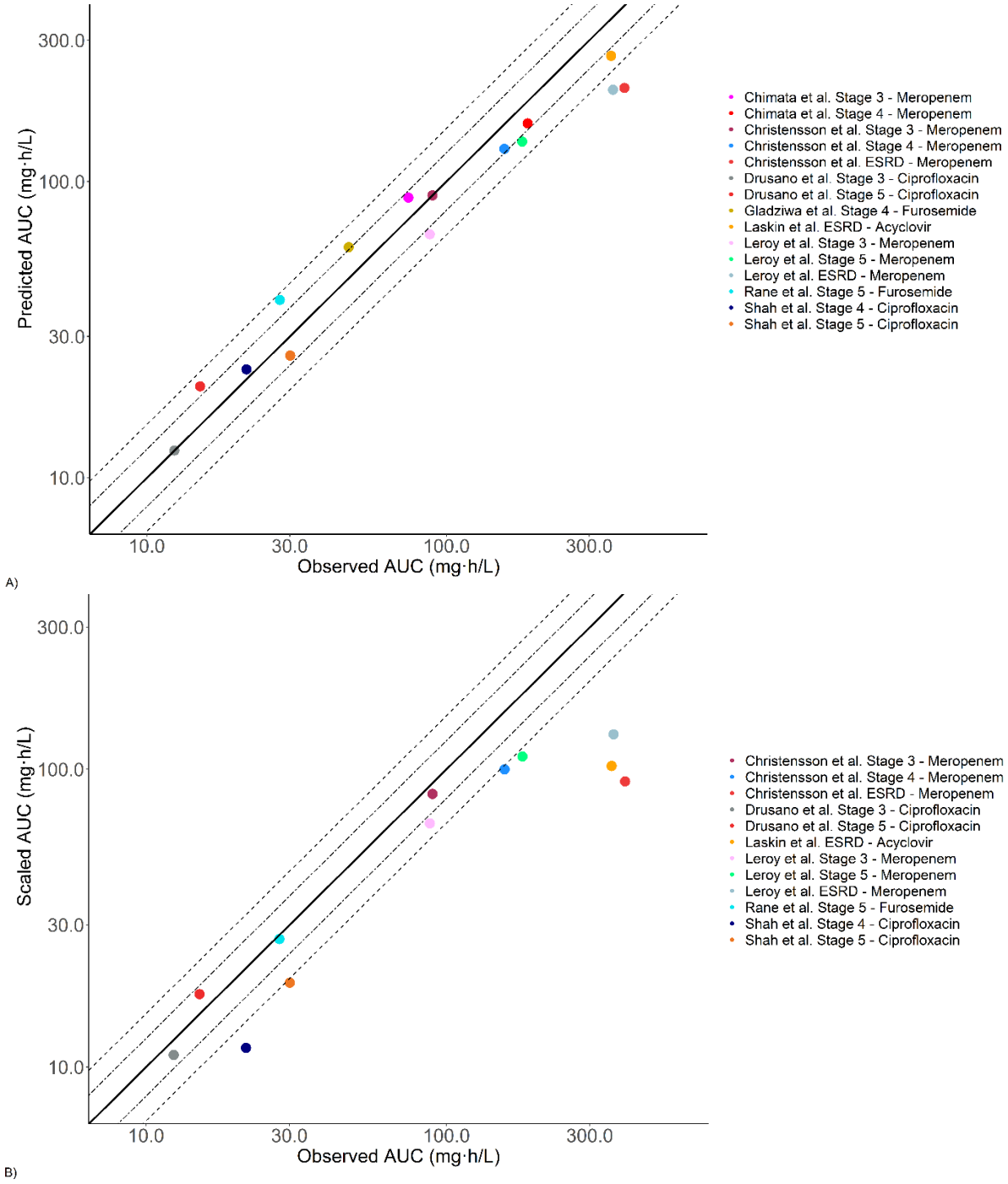


Figure 3-7 Predicted vs. observed area under the concentration-time curve extrapolated to infinity (AUC_{∞}) of included simulations using chronic kidney disease physiologically-based pharmacokinetic (CKD-PBPK) simulations (A) in comparison to conventional scaling methods (B). Dashed line represented 1.25-fold error, while the dotted line represents 1.5-fold error. *AUC_{∞}; area under the concentration-time curve extrapolated to infinity, ESRD; end stage renal disease.*

Overall, AUC_{∞} tended to be modestly underpredicted in 8 of the 15 simulations over the course of CKD progression. This trend was most notably witnessed with meropenem and acyclovir, both of which undergo large contributions of OAT mediated clearance. This error is largely driven by an inability to accurately capture C_{max} in these simulations, but the contribution of reduced apical transporter activity is plausible.

The conventional scaling method for predicting AUC failed to meet the 1.5-fold criteria in 7 of 12 empirical calculations (58%). Most notably, scaling predictions were unsuccessful in CKD stages 4 and 5. Comparisons of the conventional scaling method to observed values may be found in **Figure 3-7B.**

Representative PK profiles with interindividual variability may be found in Figures **3-3 to 3-6**. Overall, 85% of the simulated mean drug concentrations for CKD stages 3-5 fell within 1.5-fold of the corresponding observed drug concentrations used for model verification. Including simulations with ESRD between dialysis sessions, approximately 80% of simulated mean drug concentrations met acceptance criteria (**Appendix B5.**).

3.4.3 Sensitivity Analysis

Local sensitivity analyses for the four investigative drugs reveals the importance of OAT activity related to exposure in both healthy individuals and those across the stages of CKD (**Figure 3-8**). Organic anion transporter Km and V_{max} appear to be less influential on AUC_{∞} throughout CKD progression. Based upon this analysis, patients with CKD may be less vulnerable to OAT-mediated DDIs compared to healthy adults. A recent in vivo analysis determined that PAH clearance was reduced by nearly 50% in the subtotal nephrectomy rats compared to the healthy rat model in the presence of probenecid OAT mediated inhibition. [337] Due to OAT transporter downregulation and/or inhibition from uremic toxin accumulation, it is plausible that there are fewer available binding sites for inhibitors to occupy as CKD progresses. However, to our knowledge there is no clinical data in humans to support this theory and further research is needed to investigate this hypothesis.

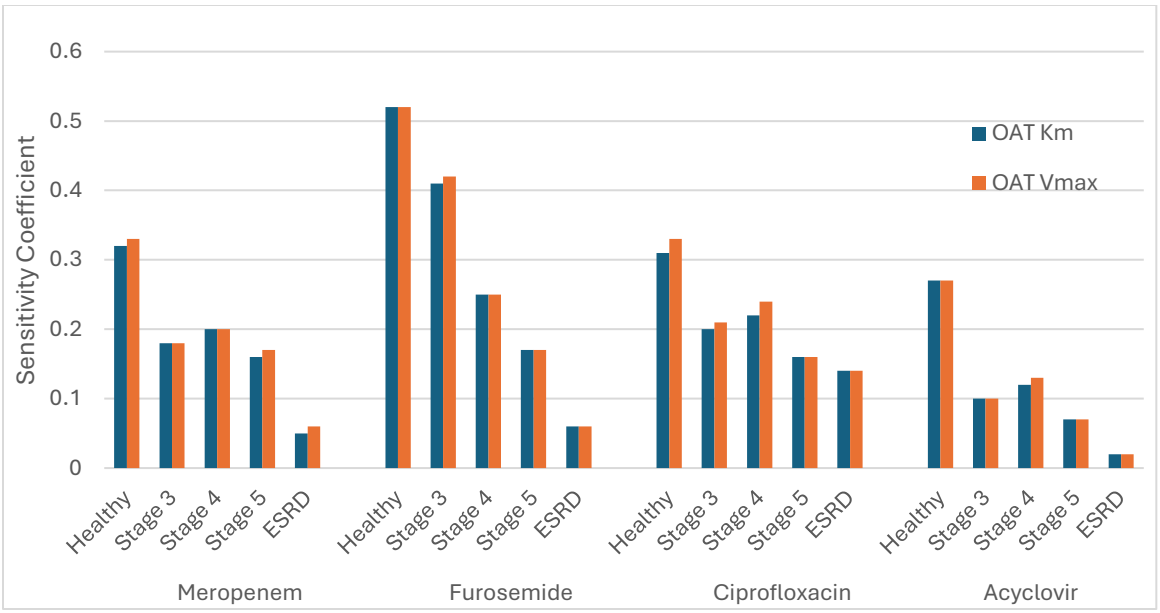


Figure 3-8. Local sensitivity analysis for organic anion transporter 1/3 drug-drug interaction potential in healthy individuals compared to chronic kidney disease for each investigative drug. OAT transporter K_M and V_{max} was varied by ±10% to analyze the relative change in area under the concentration-time curve extrapolated to infinity (AUC_∞).
ESRD; end stage renal disease on intermittent hemodialysis, Km; Michaelis-Menten constant, V_{max}; maximum rate of reaction.

3.4. Discussion

In this work, we demonstrated that PBPK models for CKD populations that additionally incorporated a new parameterization for impairment of OAT transporter secretory activity adequately described the PK of four renally cleared OAT substrates (fe_{urine} > 0.5) with a high contribution of active tubular secretion (> 60% to CL_R) in patients across various stages of CKD but struggled to capture PK in patients on IHD between dialysis sessions. Recent efforts have addressed the complexity of renal handling of drugs within CKD by incorporating physiological changes, as well as the competitive inhibition of uremic toxins and downregulation of metabolic enzymes and transporters. [288,338–341] The work conducted within this analysis builds upon this foundation and a previously validated CKD parameterization that has incorporated these physiological changes. [284] Successful predictions of exposure for the investigative drugs from real-world clinical trials supports the use of this PBPK modeling approach for OAT1/3 substrates.

Estimations of renal drug clearance approximated through creatinine clearance (Cockcroft-Gault) are based on the "intact nephron hypothesis". This theory suggests that the renal elimination processes, glomerular filtration, tubular secretion, and active reabsorption, decline proportionally with progression of CKD. [342–344] In other words, the theory suggests that the decline in CL_R of a drug that undergoes active tubular secretion is similar to one that does not. A recent analysis by Chapron *et al.* challenged this hypothesis by demonstrating that the method of scaling by GFR was unable to predict CL_R in CKD for half of the investigative drugs that were eliminated by tubular secretion, [344] most notably as CKD progressed. Our results confirmed this approach as 58% of CKD simulations failed to meet successful predictions of AUC_∞ using the conventional scaling method, a result that has been demonstrated previously. [284] The conventional scaling method provided reasonable predictions in early stages of CKD, however failed to meet acceptance criteria in more advanced stages (stage 4 & 5). Such a discrepancy was most notably witnessed with meropenem and acyclovir, two molecules with a large contribution of CL_R to total CL (>75%) and a large percentage of active tubular secretion accounting for CL_R (>75%). Therefore, caution should be warranted when incorporating the conventional scaling method to predict PK parameters of molecules with such characteristics in patients with advanced CKD. The results of this analysis highlight that characterization of active tubular secretion by parameterizing the effects of functional changes on OAT within CKD is of the upmost importance for accurately describing the PK within this population.

p-Aminohippuric acid CL_R may be used as an estimator of renal plasma flow due to its high extraction ratio in a healthy kidney, ability for free filtration from plasma, low protein binding and negligible tubular reabsorption. [315,345–347] In vitro, OAT1 has been identified as an efficient transporter for PAH. [348–350] Although, additional work has recorded limited and variable affinity of PAH for the OAT3 transporter, it is generally assumed that PAH has a greater affinity for the OAT1 transporter. [350,351] As such, utilizing PAH as a surrogate for OAT1/3 mediated renal secretion within our unique parameterization across the stages of CKD offers mechanistic and physiologic relevance. It should be noted, all data sets included within the OAT parameterization determined EPAH at steady state concentrations upon continuous infusion of PAH. This methodology ensures saturation of renal tubules and provides an accurate representation of PAH CL_R. [348,352] Through investigation of the relationship between EPAH and GFR, we determined that OAT mediated excretion was reduced by 27-49%, 50-69% and 70-

96% across CKD stages 3-5, respectively. Previous reports by Hsueh *et al*. from an analysis of 18 OAT substrates within CKD determined a median reduction of secretory clearance of 27% and 59% in moderate and severe staged CKD. [287] Our results coincide with these reported values.

Conclusions in this analysis are in accordance with previous work suggesting that reductions in OAT clearance should occur in addition to impairment of GFR and CL_{NR} processes in PBPK models of severe CKD. [287] However, the work presented here offers several key differences. First, this analysis uniquely incorporated DDI-PBPK modeling using probenecid within our base model construction following a "middle-out" approach to address the knowledge gaps in OAT transporter expression in the kidneys of patients with CKD. [281,311,341] DDI-PBPK modeling has served as a valuable tool in drug development to provide mechanistic insight into clinically relevant DDIs. [353–356] Incorporation of probenecid DDI-PBPK model simulations enabled identification of a unique solution for the contribution of OAT mediated renal excretion in total CL for each compound. Secondly, development of an OAT parametrization across stages of CKD through EPAH confirms that reducing CL_R in proportion to GFR is not sufficient to describe the PK of OAT substrates across all stages of CKD. Utilizing this approach increases generalizability as the OAT mediated renal excretion may be manipulated to further reflect the degree of renal impairment of the population of interest. Further research is essential to expand upon this analysis for alternative OAT substrates with varying contributions of tubular secretion on total CL.

The chronic state of inflammation and uremia throughout CKD has been cited as a contributing factor for the inhibition or downregulation of CL_{NR} processes within this population. [338,339,357,358] Increasing efforts have sought to quantify the decreases in CL_{NR} throughout CKD progression, however the degree of effect amongst pathways may be quite variable. [311,338,339] The four investigative drugs within this analysis undergo different mechanisms of CL_{NR}, however, all are predominantly renally cleared ($fe_{urine} > 0.5$). As a result, the effects of reduced CL_{NR} on simulated AUC_∞ appears to be minimal. Utilization of these scaling factors enabled accurate predictions of AUC_∞ with the investigative drugs across all stages of CKD, however further analyses are required to determine the validity in drugs that

undergo predominant CL_{NR}. Information on enzyme-specific pathways is preferred where applicable. [338,339]

The analysis is not without limitations. Using EPAH vs. eGFR for OAT parameterization allowed us to successfully predict the decline in OAT mediated secretion throughout CKD. However, as depicted in **Figure 3-1**, there is a paucity of data investigating this relationship in severe CKD. This may have over predicted the contribution of OAT secretion in stage 5 CKD for patients on IHD between dialysis sessions and could explain the trend to underpredict AUC_{∞} for meropenem and acyclovir. Future studies investigating EPAH in severe CKD may enhance the accuracy of model predictions.

Second, the four investigative drugs chosen within this analysis were all administered intravenously. While the findings for renal OAT are generalizable, there are additional uncertain factors that may need to be accounted for when simulating the oral PK of an OAT substrate drug in CKD. Chronic uremia throughout CKD progression may disrupt gastrointestinal physiology, leading to reductions in gastric emptying time, small and large intestinal transit times. [359,360] Additionally, many OAT substrates such as cephalexin, methotrexate, ciprofloxacin and rosuvastatin have been documented to also be substrates of the organic anion transporting polypeptide (OATP) family – transporters responsible for the absorption of relevant compounds from the intestinal lumen.[345,361] Reductions in the uptake of OATP substrates into hepatocytes have been documented in CKD, however the impact on oral bioavailability remains largely undefined. [339,362–364] Future research is needed to accurately describe any potential PK changes of orally administered OAT/OATP substrates in patients with CKD.

Third, in the analyses including patients with ESRD receiving IHD there was a tendency to over-predict CL_R resulting in an inability to meet acceptance criteria for two simulations (**Figure 3-6.**). It was assumed that apical transporter function on the renal tubule remains largely intact due to the inability to identify the specific transporter for each molecule and limited data supporting the functionality across CKD. [282] However, several in vivo animal studies suggest that apical transporters may be susceptible to uremic toxin inhibition and/or down-regulation as CKD progresses. [364–367] Contributions of such physiologic changes cannot be discounted within this population and further work is required to provide a more accurate representation of the renal drug handling of OAT substrates in the most severe stages of CKD.

Previous work has identified genetic polymorphisms amongst differing ethnicities which may have the potential to affect OAT activity by reducing the capacity for tubular secretion. [368–370] However, the results of such polymorphisms appear to have a negligible effect on CL_R and tubular secretion in healthy individuals. [371] The observed clinical PK studies in healthy and CKD patients to which PBPK models were constructed and validated did not report ethnicities of study participants. As a result, differences in physiology and PK based on ethnicities were not considered in the model. Further research is needed to confirm any potential contribution of genetic polymorphisms of OAT activity in those with CKD.

Finally, challenges in model verification were limited due to the lack of available individual subject data within CKD studies. All but one study by Laskin *et al.* included mean subject PK data used for model comparison (**Appendix B5**.). [336] However, when comparing range of exposures within individual-level data, the predicted mean exposure fell within the upper and lower limits (234– 498 μmol·h/L). Future work including individual PK data will allow for further assessment of model accuracy. Additionally, the model may be refined upon availability of clinical data to expand with additional compounds, incorporation of OAT polymorphisms, [372] or age differences to predict changes in PK for pediatric patients.

Dedicated PK studies in subjects with renal impairment offer many challenges due to the potential for toxic exposures and difficulties in recruitment. There is clear application for this work in drug development – assessing the PK of investigational drugs that are OAT substrates in patients with CKD ahead of clinical trials to assist with dose selection and clinical trial planning. When CKD effects on drug disposition are well characterized, CKD-PBPK models can be used to estimate drug-drug interactions in patients with CKD, or even estimate PK parameters across the disease spectrum in different ages, sexes and body weights that were not tested. There is also potential to supplement the clinical data collected from renal impairment trials so that the results are confirmatory, rather than exploratory. Fewer of these vulnerable subjects will be required to be enrolled in the studies.

3.5 Conclusion

Use of PBPK modeling within organ impairment to inform dose selection has not been supported with an adequate level of confidence from regulatory agencies such as the FDA and

EMA, especially in more advanced stages. [324,373] This work builds more evidence toward this end. Utilizing a unique PBPK-DDI model development approach and parameterizing OAT mediated excretion through EPAH, we were accurately able to predict exposure of four OAT substrates across the stages of CKD. However, the results should be interpreted with caution due to the limited number of drugs investigated, small sample sizes of included studies and similar PK characteristics between molecules (i.e. OAT substrates with a high contribution of active tubular secretion).

Although further refinement and verification may be needed for oral OAT substrates, the proposed workflow provides building block towards quantifying the effects of CKD disease progression on CL_R, and more specifically the contribution of OAT mediated tubular secretion to the elimination of major substrate drugs. The work herein adequately predicts the intravenous PK and renal handling of OAT substrates in patients with CKD but may under-predict concentrations in patients on IHD between dialysis sessions. A quantitative understanding of the reduction in OAT1/3-mediated excretion of drugs in varying stages of renal impairment will contribute to better predictive accuracy for PBPK models in drug development, assisting with clinical trial planning and potentially sparing this population from unnecessary toxic exposures.

Chapter 4: Anakinra Removal by Continuous Renal Replacement Therapy: An Ex-vivo Analysis

This chapter is reflective of an original manuscript published by the PhD candidate (Samuel Dubinsky) in *Critical Care Explorations*. All pertinent dialogue in this chapter was written by the PhD candidate, apart from section 4.3.6, which includes writing contributions from collaborators at the University of Utah.

Information regarding applicable letters of copyright permission is presented in the **Letters of Copyright Permission.**

4.1 Overview

Objectives: Patients with sepsis are at significant risk for multiorgan dysfunction, including the lungs and kidneys. To manage the morbidity associated with kidney impairment, continuous renal replacement therapy (CRRT) may be required. The extent of anakinra pharmacokinetics in CRRT remains unknown. The objectives of this study were to investigate the anakinra-circuit interaction and quantify the rate of removal from plasma.

Design: The anakinra-circuit interaction was evaluated using a closed loop ex-vivo CRRT circuit. CRRT was performed in three phases based upon method of solute removal: 1) hemofiltration, 2) hemodialysis, 3) hemodiafiltration. Standard control samples of anakinra were included to assess drug degradation.

Setting: University research laboratory.

Patients: None.

Interventions: Anakinra was administered to the CRRT circuit and serial pre-filter blood samples were collected along with time matched control and hemofiltrate samples. Each circuit was run in triplicate to assess inter-run variability. Concentrations of anakinra in each reference fluid were measured by enzyme-linked immunosorbent assay. Transmembrane filter clearance was estimated by the product of the sieving coefficient/dialysate saturation constant and circuit flow rates.

Measurements and Main Results: Removal of anakinra from plasma occurred within minutes for each CRRT modality. Average drug remaining (%) in plasma following anakinra administration was lowest with hemodiafiltration (34.9%). The average sieving coefficient was 0.34, 0.37 and 0.41 for hemodiafiltration, hemofiltration and hemodialysis respectively. Transmembrane clearance was fairly consistent across each modality with the highest during hemodialysis (5.53 mL/min), followed by hemodiafiltration (4.99 mL/min), and hemofiltration (3.94 mL/min). Percent drug remaining within the control samples (93.1%) remained consistent across each experiment, indicating negligible degradation within the blood.

Conclusions: The results of this analysis are the first to demonstrate that large molecule therapeutic proteins such as anakinra, are removed from plasma with modern CRRT technology.

Current dosing recommendations for patients with severe renal impairment may result in subtherapeutic anakinra concentrations in those receiving CRRT.

4.2 Introduction

Continuous renal replacement therapy has become the method of choice for renal support in critically ill patients due to its preferential effects on hemodynamic stability. [56,87] Solute removal occurs differently depending on the modality of CRRT which includes: continuous veno-venous hemofiltration (CVVH), continuous veno-venous hemodialysis (CVVHD) and continuous veno-venous hemodiafiltration (CVVHDF). The most important variables affecting drug pharmacokinetics during CRRT include volume of distribution (Vd), protein binding and molecular weight. [102–104] Intuitively, small molecules with a low Vd and high unbound fraction may be more susceptible to drug removal from systemic circulation when a CRRT circuit is utilized. [102–104] In addition to drug removal via filtration, adsorption of drug to circuit materials can be a mechanism of drug removal. Physicochemical properties that may predispose drugs to adsorption include lipophilicity (expressed as logP), protein binding and molecular charge. [102,103,117,127] However, predicting the pharmacokinetics of medications administered to this population is challenging as it requires a thorough understanding of the interplay between drug, circuit-specific properties and disease related factors. [103,374]

Anakinra, a recombinant human IL-1 receptor antagonist (IL-1 RA) received marketing approval by the US Food and Drug Administration for indications of rheumatoid arthritis and neonatal-onset multisystem inflammatory disease. [375,376] Interleukin-1 (IL-1), an endogenous pro-inflammatory cytokine, serves as a key contributor in the pathophysiology of hyperinflammatory conditions such as rheumatoid arthritis. [377] In addition to its role in chronic inflammatory conditions, IL-1 is implicated in the cytokine cascade and contributes to the pathophysiology of cytokine release syndromes (CRS) such as hemophagocytic lympohistiocytosis (HLH). [378,379] Although used off-label, anakinra has been recommended as a first line agent for the management of HLH [380–382] or CRS due to secondary HLH syndromes. [383–385]

Anakinra a large molecule (17 kDa), therapeutic protein has a small volume of distribution in healthy adults (3.32±0.62 L). [386] For chronic rheumatological conditions, doses

are administered subcutaneously however, intravenous administration is becoming more common to offset any potential impacts on absorption due to the presence of edema in patients with acute, hyperinflammatory conditions. [379] The apparent half-life of elimination is longer with subcutaneous dosing, than intravenous, with comparable clearance. [386,387] Renal elimination accounts for a large percentage of anakinra plasma clearance. [386–388] As a result, renal impairment has a significant impact on total clearance and adjustments of maintenance dosing regimens are recommended. [386]

Prior to receiving approval for use in chronic inflammatory diseases, anakinra was studied as an intriguing treatment alternative for acute, hyperinflammatory conditions including sepsis. [389–392] Release of inflammatory cytokines, such as IL-1 in response to circulating microbial toxins may result in sepsis induced organ dysfunction, including the lungs and kidneys. [72,74] Acute kidney injury (AKI) due to sepsis complications is one of the most common causes of AKI in critically ill patients, occurring in up to 50% of adults and 20% of children admitted to an intensive care unit. [69–71] Of these, a significant portion may require renal replacement therapy (RRT) to manage the morbidity associated with AKI. [56,87]

The extent of anakinra removal by different modalities of CRRT remains largely unknown. As anakinra remains a potential treatment alternative for patients with sepsis demonstrating hyperinflammatory phenotypes, [389–393] many of whom may require RRT, information regarding the anakinra-CRRT circuit interaction is of the utmost importance for designing safe and effective dosing regimens. Due to the physicochemical properties of anakinra (**Table 4-1.**) it is possible that with modern CRRT technology, significant removal from plasma may occur.

Table 4-1. Anakinra physicochemical properties and clearance mechanisms.

Drug	Compound Type	Molecular Weight (kDa)	Protein Binding (%)	Clearance Pathways
Anakinra	Protein	17.3 [394]	0	Renal & Non-renal [386–388]

kDa; kilodaltons.

We conducted this ex-vivo study to characterize the drug-circuit interaction of anakinra. We hypothesized that with the use of modernized hemofilters, and differing methods of solute removal (convection vs. diffusion), anakinra would be sufficiently removed from plasma across each CRRT modality.

4.2 Materials Methods

4.2.1 Institutional Review Board

As this study did not involve human subjects, institutional review board approval was not required.

4.2.2 Circuit Configuration

CRRT circuits were completed with the PRISMAX System (Baxter Healthcare) and HF1000 filter set (Baxter Healthcare) connected with a 500 mL EXACTAMIX EVA bag (Baxter Healthcare) (**Table 4-2.**) Each circuit configuration (**Figure 4-1.**) was run in triplicate to assess inter-run variability in anakinra concentrations. Upon each subsequent run, new hemofilters were used in addition to repriming the CRRT circuit with new blood volume to reduce any risk of hemofilter clotting.

Table 4-2. Continuous renal replacement therapy circuit components.

Component	Manufacturer	Model	Material
CRRT System	Baxter	PrisMax with TherMax heater	NA
Hemofilter	Baxter	HF1000 SA: 1.1m^2	PolyarylEtherSulfone hollow fibers, plasticized polyvinyl chloride tubing
Reservoir	Baxter	EXACTAMIX EVA, 500 mL	Ethylene vinyl acetate

CRRT; continuous renal replacement therapy, m^2; meters squared, mL; milliliters, NA; not applicable.

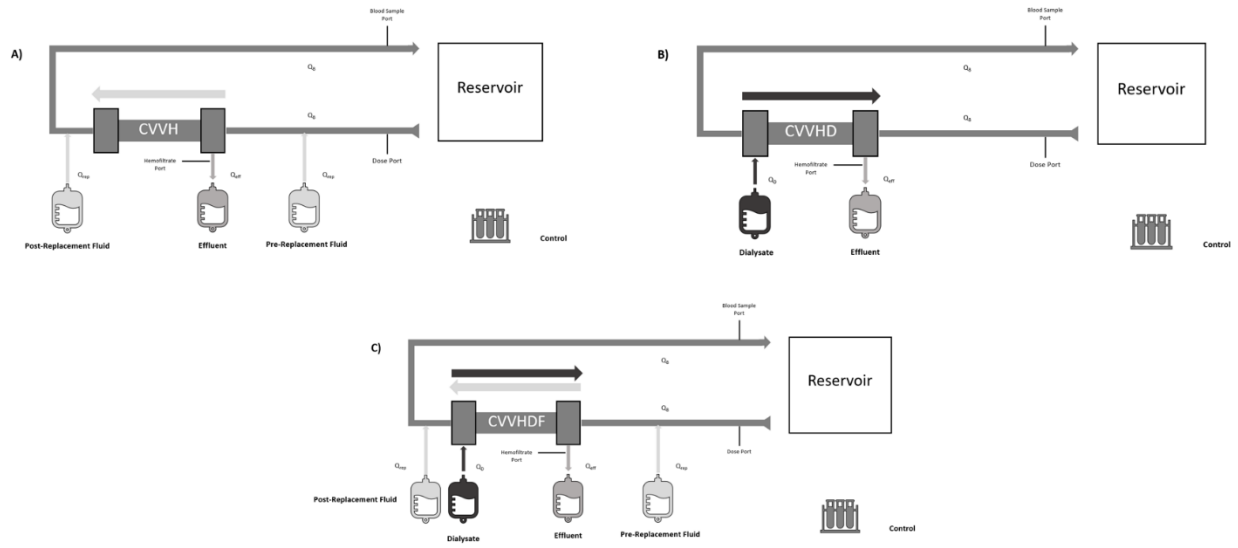


Figure 4-1. Illustration of the closed-loop ex-vivo continuous renal replacement (CRRT) circuit. Anakinra removal from plasma was determined with each modality of CRRT: A) continuous veno-venous hemofiltration (CVVH), B) continuous veno-venous hemodialysis (CVVHD), C) continuous veno-venous hemodiafiltration (CVVHDF). Standard control samples were analyzed with time matched plasma and hemofiltrate samples.
Q_B; blood flow (mL/min), Q_D; dialysate flow rate (mL/h), Q_{eff}; effluent flow rate (mL/h), Q_{rep}; replacement flow rate (mL/h).

4.3.3 Continuous Renal Replacement Therapy Circuit Setup

Each circuit was primed with a solution of 1 unit of human red blood cells (adenine saline added leukocytes reduced [~300 mL]), approximately 0.4 units of thawed human plasma frozen within 24 hours after phlebotomy (125 mL), Plasma-Lyte A crystalloid (150 mL), heparin sulfate (350 units), tomethamine (1.6 g), sodium bicarbonate (7 mEq), and human serum albumin (6.25 g). Albumin concentrations throughout experiments were targeted to achieve those similar to critically ill children (20-30 g/L). Maintenance of a physiologic pH (7.4; range: 7.08 – 7.63) was achieved with additional tromethamine. PrismaSate 4/2.5 dialysis solution (Baxter Healthcare) was used for pre-blood pump, dialysis, and replacement fluids for each circuit. Target volume of primed solution within each circuit was 500 mL. A description of the target concentrations of circuit solution components may be found in **Table 1** of **Appendix C**.

CRRT circuit prescriptions were as follows: 1)CVVH: blood flow rate (Q_B) 80 mL/min, pre-filter replacement fluid rate (Q_{pre}) 600 mL/h, post-filter replacement fluid rate (Q_{post}) 200 mL/h and total effluent rate (Q_{eff}) 800 mL/h; 2) CVVHD: Q_B 80 mL/min, dialysate fluid rate

(Q_D) 800 mL/h; 3)CVVHDF: Q_B 80 mL/min, Q_{pre} 300 mL/h, Q_{post} 100 mL/h, Q_{eff} 800 mL/h and Q_D 400 mL/h. Flow rates incorporated within the experiment were determined based upon a hypothetical child of approximately 10 kg as per consultation from Nephrologists within our institution. CRRT prescriptions for each modality are presented in **Table 4-2**. Setting the patient fluid removal rate (Q_{PFR}) to 0 L/h for each circuit ensured a consistent volume of recirculating blood was maintained over the course of the experiment. Blood was maintained at 37°C with the use of heating pads.

4.3.4 Control Setup

Six standard control samples of anakinra were included to determine drug degradation throughout the experiment. A total of 50 mL of primed blood solution was drawn from the primed CRRT circuit after approximately 5 minutes of circulation and before administration of the anakinra. The control sample was transferred into a PVC plastic tube and placed in a water bath maintained at 37°C.

4.3.5 Drug Administration and Sample Collection

Anakinra (Kineret) was administered (time = 0) in each CRRT circuit via an arterial port (**Figure 4-1.**). The circuit was dosed to achieve a therapeutic concentration of approximately 25 µg/mL. [386] A diluted anakinra solution was administered to the control tubes at time = -5 minutes to mimic circuit concentrations and placed within a rotator to mix for 5 minutes. The control sample was returned to the water bath for the duration of the experiment, except for sampling. Controls were inverted gently 5 times prior to sampling.

Samples were collected at the following time points: 1, 5, 15 and 30 minutes, 1, 2, 3, and 4 hours. Hemofiltrate samples were collected at each time point from the tubing prior to entering the effluent bag (**Figure 4-1.**). Physiologic pH of circuit blood was analyzed prior to anakinra administration and each subsequent hour with an i-STAT 1 Analyzer (Flextronics Manufacturing, Singapore) and EG6+ cartridge (Abbot, Abbot Park, IL) and adjusted as needed to maintain physiologic pH. Circuit blood and control samples were centrifuged (3000 rpm for 10 minutes at 4°C) immediately after collection. Plasma was pipetted and stored at -80°C. Hemofiltrate samples were stored at -80°C immediately following collection.

4.3.6 Drug Analysis

Anakinra concentrations were determined using a pre-validated ELISA kit for measuring IL-1 RA (Catalog# KAC1181; ThermoFisher Scientific, San Jose, CA). Calibrators were prepared in standard diluent buffer and analyzed in duplicate with every batch. The calibration curve ranged from 31.25 to 2000 pg/mL and was fit with a four-parameter sigmoidal curve. A two-step dilution process (first into phosphate-buffered saline, then into standard diluent) was used for the samples to bring them into the working range of the ELISA kit according to the expected concentration for the sample, with dilutions ranging from 12,500 to 37,500-fold. Samples were analyzed in duplicate wells, with sample data reflecting an average of those replicates if the % coefficient of variation (%CV) between the two wells was <20%. Samples were repeated in a subsequent analysis if the %CV>20%.

Percent of anakinra remaining in plasma was calculated at each time point using the following equation:

$$anakinra\ remaining\ (\%) = \frac{C_t}{C_i}\ x\ 100$$

Eq. 4-1

Where C_t is the concentration at time t and C_i is the concentration at time = 5 minutes for CRRT plasma and control samples. Additionally, passage of anakinra across the hemofilter in each respective CRRT system was calculated using the sieving coefficient (S_C) for CVVH and the dialysate saturation constant (S_D) for CVVHD and CVVHDF. Drug passage was determined from paired hemofiltrate/dialysate and plasma samples at each time point using the following equations:

Eq. 4-2

$$S_C = \frac{C_H}{C_P}$$

Eq. 4-3

$$S_D = \frac{C_D}{C_P}$$

Where C_H and C_D are concentrations in hemofiltrate and dialysate respectively, while C_P represents anakinra concentration in plasma.

Transmembrane clearance of anakinra was estimated for each modality using the following equations: [3,4]

Eq. 4-4

$$CL_{CVVH} = Q_f \; x \; S_C \; x \; CF$$

$$CF = \left(\frac{Q_{plasma}}{Q_{plasma} + Q_{pre}}\right)$$

$$Q_f = \left(Q_{pre} + Q_{post}\right) + Q_{PFR}$$

Eq. 4-5

$$CL_{CVVHD} = Q_D \; x \; S_D$$

Eq. 4-6

$$CL_{CVVHDF} = Q_{Eff} \; x \; S_D$$

$$Q_{Eff} = \left(Q_{pre} + Q_{post}\right) + Q_{PFR} + Q_D$$

Where Q_f represents the ultrafiltration rate. To account for pre-filter replacement fluid dilution a correction factor (CF) was applied when estimating the transmembrane clearance via convection (CL_{CVVH}). [102,103] In this equation Q_{plasma} represents the circuit plasma flow as determined by Q_b x 1-hematocrit. Flow rates incorporated in the transmembrane clearance equations (Eq.3-5) are presented in **Table 4-3**.

Table 4-3. Continuous renal replacement therapy circuit setup.

CRRT Modality	Blood Flow (mL/min)	Patient Fluid Removal Rate (mL/h)	Replacement Fluid Rate (mL/h)	Dialysis Fluid Rate (mL/h)	Total Effluent Rate (mL/h)
CVVH	80	0	Pre-filter: 600 Post-filter: 200	NA	800
CVVHD	80	0	NA	800	800
CVVHDF	80	0	Pre-filter: 300 Post-filter: 100	400	800

CRRT; continuous renal replacement therapy, CVVH; continuous veno-venous hemofiltration, CVVHD; continuous veno-venous hemodialysis, CVVHDF; continuous veno-venous hemodiafiltration, h; hours, mL; milliliters, min; minutes, NA; not applicable.

4.3.7 Statistical Analysis

An unpaired *t* test was used to analyze the effect of CRRT on recovery of anakinra in plasma. Percent recovery of anakinra in plasma for each circuit at time = 4 hours was compared to the recovery in the standard control experiments at the matching time point. Data is presented as the mean with the corresponding standard deviation.

4.3 Results

A total of 144 samples were taken for measurement of anakinra concentrations in plasma and hemofiltrate. Due to incomplete mixing of the CRRT circuits, anakinra concentrations at time = 1 minute were dropped from the analysis and Ci was calculated based on the 5-minute sample. For CVVH circuits, one replicate indicated a potentially longer delay in mixing than subsequent runs. Consequently, the percentage of drug remaining was calculated based on the 15-minute sample (C_i = concentration at time = 15 minutes) for CVVH circuits. Pharmacokinetic variable estimates, such as sieving coefficient and transmembrane clearance, for each CRRT circuit run are reported in **Table 2 & 3** of **Appendix C.**

4.3.1 CVVH Circuit

The average drug remaining (SD) was 79.7% (8.5) at 15 minutes and 5.86% (2.25) at 4 hours. Anakinra percent remaining in plasma was significantly different compared to the standard control at the completion of the experiment (p = <0.001). A graphical representation of the percent drug remaining in plasma and standard control is presented in **Figure 4-2**. The average sieving coefficient of anakinra over the course of the CVVH circuit analysis was 0.37

(0.12). The determined sieving coefficient was used to estimate a mean transmembrane clearance of 3.94 (0.86) mL/min (**Figure 4-3.**).

4.3.2 CVVHD Circuit

At time = 5 minutes the average percent of anakinra remaining was 71.2% (11.6) and 1.6% (0.6) at 4 hours. Similarly, the percent of drug remaining in plasma was significantly different compared to the standard control at 4 hours (p = <0.001). The determined dialysate saturation constant for anakinra was 0.41 (0.12), resulting in an estimated transmembrane clearance of 5.53 (1.67) mL/min (**Figure 4-3.**).

4.3.3 CVVHDF Circuit

Loss of anakinra occurred within minutes with hemodiafiltration, resulting in an average percent remaining in plasma at 5 minutes of 34.9% (8.8) and 1.2% (1.1) at 4 hours. The percent of anakinra remaining in plasma was significantly different compared to the standard control at the end of the experiment (p = <0.001). The average sieving coefficient was 0.34 (0.14), corresponding to an estimated transmembrane clearance of 4.99 (1.58) mL/min (**Figure 4-3**.).

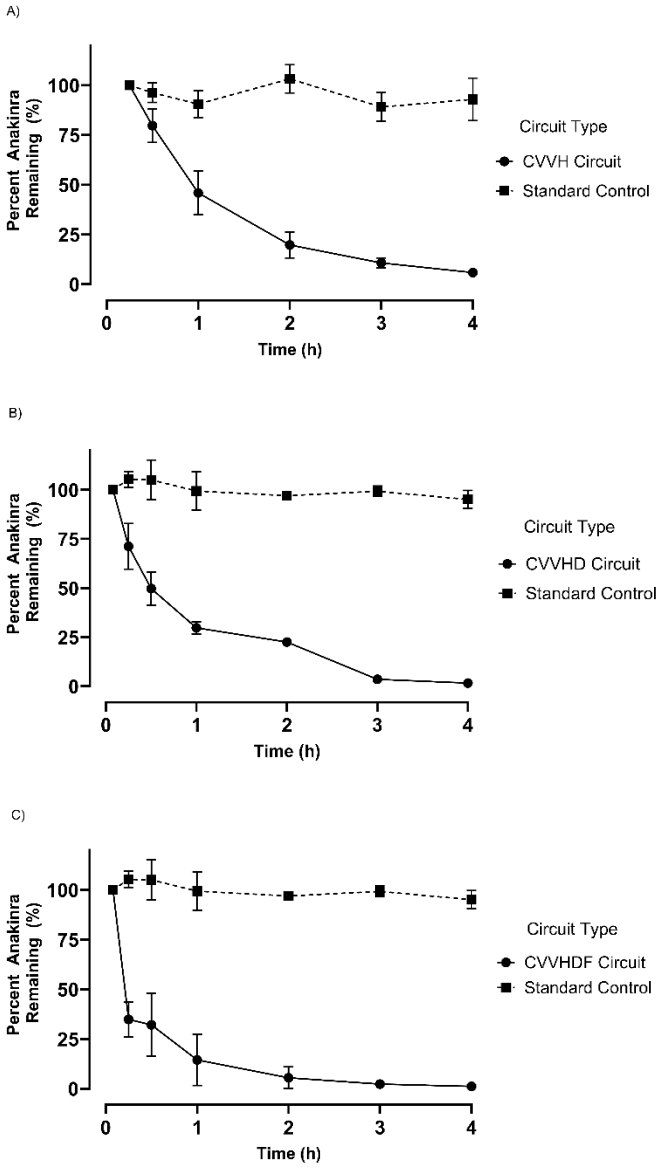


Figure 4-2. Percent anakinra remaining in plasma and standard control with standard deviation shown as error bars. Due to incomplete mixing of the circuit, anakinra percent remaining in plasma was determined at t= 15 minutes for A) hemofiltration (CVVH). Percent remaining in plasma was analyzed at time = 5 minutes for B) hemodialysis (CVVHD) and C) hemodiafiltration (CVVHDF).

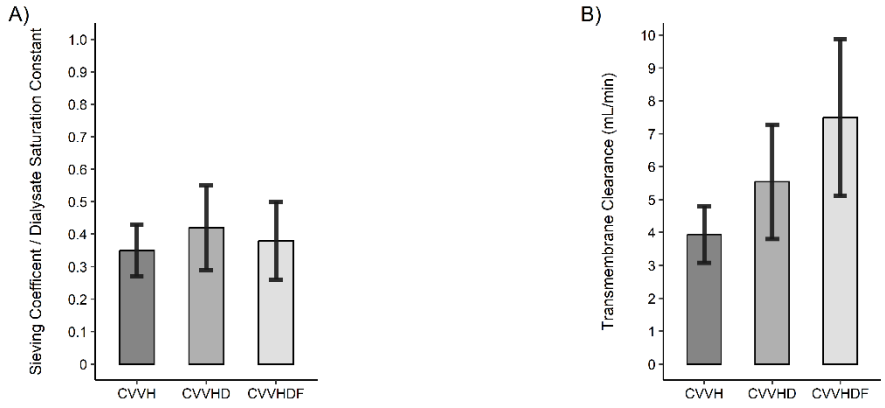


Figure 4-3. Graphical representation of the determined anakinra sieving coefficient / dialysate saturation constant (A) and estimated transmembrane clearance (B). All data presented as mean with error bars representing the standard deviation.
CVVH; continuous veno-venous hemofiltration, CVVHD; continuous veno-venous hemodiafiltration; CVVHDF; continuous veno-venous hemodiafiltration.

4.4 Discussion

The impact of CRRT on altering the drug disposition of small molecular weight drugs has been studied extensively, [89,102,103,105–107,374,395] however the effects on large molecular compounds, such as anakinra remains mostly unknown. We studied the pharmacokinetics of anakinra in a closed-loop CRRT circuit. Incorporating an ex-vivo study design enabled an independent assessment of the drug-circuit interaction from many of the additional factors that may impact drug pharmacokinetics in critically ill individuals such as hepatic dysfunction, circulatory function, drug-interactions, and fluid shifts. [19,23,31]

Ex-vivo CRRT analyses provide important information for the prediction of drug clearance. Such study designs allow for testing various permutations of CRRT flow rates, membranes, and methods of solute removal that may be used in clinical practice. Additionally, the ability to include multiple sampling times, drug redosing, and analyze drug clearance without potential risks associated with in-vivo studies highlight many of the advantages of ex-vivo studies. [396] Increasingly, clearance determined by ex-vivo CRRT circuits has been shown to have strong correlation with observed clinical data. [396–398] Therefore, valuable information on drug clearance can be obtained in the absence of clinical data to assist in designing dosing regimens for those requiring CRRT.

The drug-CRRT circuit interaction may alter the pharmacokinetics in one of two ways: 1) drug clearance by the circuit, either through convection, diffusion, or a combination of each or 2) drug adsorption to circuit components. Significant loss of anakinra occurred with each modality of CRRT, with concentrations of anakinra within hemofiltrate remaining consistent throughout (**Appendix C, Figure 2.**). The average sieving coefficient of anakinra was 0.37, 0.41 and 0.34 for CVVH, CVVHD, CVVHDF, respectively. Transmembrane clearance was similar across each modality (**Table 4-2.**), indicating that molecular weight has become a less influential parameter on estimating CRRT circuit removal with modernized "high-flux" membranes.

In this experiment it is important to understand that the percent of anakinra remaining in each circuit is dependent on the total volume of the blood pool. This experiment incorporated a CRRT prescription that was based upon a hypothetical 10 kg child. Children of this weight/age range typically have a total blood volume of approximately 80 mL/kg. As the age/weight of the patient increases, the CRRT prescription flow rates applied will also increase. Such increases in flow rates will affect the estimated transmembrane clearance values. Therefore, when applying the results of the percent anakinra remaining in plasma *in vivo*, it is imperative that one is familiar with the CRRT prescription and total volume of blood of the patient.

It is worth noting that transmembrane clearance was determined using the mean S_C and S_D over the course of the experiment multiplied by the corresponding flow rates. This equation may be considered less accurate compared to clearance determined by area under the curve via noncompartmental analyses, [399] as it suggests that transmembrane clearance is directly proportional to the CRRT flow rates and that S_C/S_D is static over time. However, the purpose of quantifying transmembrane clearance in this study was to compare across each CRRT modality and the values reported in **Table 4-2**. should be considered as an estimate, regardless of the method of quantification.

Although no adsorption analysis was conducted in the study, the consistently high concentrations within hemofiltrate and limited loss of drug in the standard controls indicate that removal of anakinra from plasma occurs significantly by filtration. Furthermore, adsorption was not expected to occur throughout the experiment due to the physicochemical properties of anakinra and the use of non-adsorptive membranes (PAES) throughout the experiment. [117]

Pharmacokinetic data on the use of anakinra in patients receiving RRT is sparse. The pharmacokinetic study by Yang et al was the first to describe the removal of anakinra by any modality of RRT. [386] In this study, patients receiving conventional intermittent hemodialysis (IHD) or peritoneal dialysis were included. Removal of anakinra by dialysis was less than 2.5% of the administered dose, indicating that anakinra plasma concentrations will not be altered by dialysis. [386] It was concluded that extending the dosing interval in patients with severe renal impairment or end-stage renal disease may be required to minimize anakinra toxicity.[386]

The results of this experiment differ from Yang et al. [386] We sought to investigate the rate of anakinra removal through each method of solute removal, hemofiltration, hemodialysis, and a combination of each. The removal of solutes via convection is molecular weight independent, as it utilizes a pressure gradient to remove molecules from plasma. [103,105,396] However, the extent of anakinra removal within this study utilizing a diffusion-based modality (CVVHD) does indicate that dialysis removes anakinra from plasma to a significant degree.

The differences in results between this study and that by Yang et al may be explained by different flow settings, duration of dialysis and most notably the use of modernized hemofilters. The molecular weight cut-off of modern CRRT circuit membranes is significantly larger than previous dialyzer membranes used in older IHD circuits. Modern “high-flux” membranes, as incorporated within the experiment are characterized by high porosity and have molecular weight cut-offs around 20-40 kDa. [102,104,400] Use of “high-flux” hemofilters may negate the expected difference in drug removal based upon method of solute removal, as they can deliver more effective hemodialysis. [396] Therefore, caution should be applied when interpreting the results of the study by Yang *et al.* when administering anakinra to patients receiving CRRT with modern synthetic hemofilters. Adjusting dosing regimens by decreasing the dose or increasing the dosing interval may result in subtherapeutic dosing regimens, however future studies evaluating the pharmacokinetics of anakinra in patients receiving CRRT are warranted.

Prior to market approval, anakinra was investigated as a treatment alternative for sepsis management due to targeting the IL-1 inflammatory cascade. [389–392] Although early studies provided equivocal results, more recent studies such as the PROVIDE trial will revisit the utility of anakinra as a efficacious agent in sepsis management. [393] It is important to note that dosing in this population has yet to be defined, as several protocols were trialed including continuous

infusions and intermittent bolus dosing. [389–391,393] However, it has been generally assumed that for severe AKI or those receiving RRT, anakinra doses should be reduced due to altered drug clearance and poor removal from RRT circuits. [386] Although not confirmatory based upon the ex-vivo study design, the results presented suggest that clearance of anakinra via CRRT does occur. Coupled with the fact that high dose anakinra is well tolerated, with limited side effects [389–391,401–404], dose reducing based on altered renal function in those receiving RRT may result in subtherapeutic concentrations. Further studies *in-vivo* are warranted to confirm.

In addition to potential uses for sepsis management, use of anakinra for managing CRS due to primary or secondary HLH and CAR-T cell complications continues to be explored. [379–385] Due to the inflammatory response triggered by cytokine release, incidence rates of AKI are high and a significant portion may require RRT. [405,406] Therefore, as anakinra continues to be investigated as a therapeutic alternative for managing complications of CRS, these results may become even more generalizable.

This study has limitations. Although incorporating different modalities of CRRT may be seen as a strength, fixed flow rates were utilized throughout the entirety of this experiment. Increasing flow rates may lead to greater reductions of drug from plasma for small molecules, [90,400] however the relationship between increasing flow rates and clearance of large molecules remains unknown. Therefore, future studies applying increasing flow rates are warranted. Secondly, the analysis was conducted using the HF1000 (PAES) hemofilter in each circuit run. Compared to alternative synthetic hemofilters, PAES hemofilters have reduced adsorptive capacity. [117,273] Although it was hypothesized that the adsorptive potential of anakinra would be low, this study does not rule out the possibility of adsorption when differing hemofilters are applied. Careful consideration of the composition of hemofilters is required when applying these results. Thirdly, a single intermittent bolus dose of anakinra was administered to the CRRT circuits. The current state of the literature has investigated several dosing strategies for both management of sepsis and CRS, including continuous infusions or intermittent bolus dosing twice to three times per day. Therefore, if alternative dosing strategies such as continuous infusions are to be applied, the risk of drug accumulation may exceed that of excess drug removal. Future ex-vivo study designs investigating transmembrane clearance of continuous infusion or multiple intermittent bolus dosing may be required. Finally, due to the discordance

between sample concentrations and the ELISA kit concentration range, significant dilutions of samples were required. Any slight error in analysis may be magnified, increasing the variability in concentrations observed within the study. This may explain the approximately 2-3 fold higher anakinra concentrations obtained within the plasma of the CVVHDF circuit. However, the percent recovery in plasma, SC and estimated transmembrane clearance remained consistent between each modality, unaffecting the results.

In vitro -in-vivo extrapolation (IVIVE) incorporates techniques to predict the pharmacokinetics related to absorption, distribution, metabolism, and elimination *in vitro* and quantifies the corresponding processes *in vivo*. [407,408] Information obtained from IVIVE predictive models allows for an assessment of drug pharmacokinetics and may serve as a valuable tool for clinical trial design. Similarly, quantification of drug clearance from an *ex-vivo* CRRT circuit may allow for extrapolation to clinical practice. Recently, the use of ex-vivo to in-vivo extrapolation through physiologically-based pharmacokinetic (PBPK) modeling with extracorporeal circuits has been informative in prospective prediction of drug pharmacokinetics in untested clinical scenarios. [144,150] Data from ex-vivo studies, such as those determined within this study, can be incorporated within a PBPK model to be used to predict the drug disposition in vivo and determine optimal dosing regimens for this vulnerable population.

4.5 Conclusion

In conclusion, this study is unique in that it is the first to investigate the pharmacokinetics of anakinra in a CRRT circuit. By incorporating a closed-loop ex-vivo study design, assessment of the anakinra-CRRT circuit interaction was conducted independent of many of the variables known to affect drug pharmacokinetics in the critically ill population. Throughout each CRRT modality, anakinra was significantly removed from plasma by filtration, with negligible adsorption to circuit components or degradation within the blood. The degree of loss of anakinra in the CRRT circuits suggests that administering renal dose adjustments may result in subtherapeutic concentrations when CRRT is applied. Incorporating the results into PBPK models may allow for optimal dose regimen design or aid in dose selection for future clinical trials.

Chapter 5: Cefazolin Removal via Pediatric Continuous Renal Replacement Therapy: An Ex-vivo Analysis

This chapter is reflective of an original manuscript in preparation by the PhD candidate (Samuel Dubinsky) for peer-reviewed journal publication. All pertinent dialogue in this chapter was written by the PhD candidate, except for **Section 5.3.5.** That included writing contributions from collaborators at the University of Utah.

5.1 Overview

Children with acute kidney injury requiring renal replacement therapy are at increased risk of nosocomial infections. As gram-positive bacteria are likely causal of these infections, antibiotics targeted against these organisms, such as cefazolin, are frequently administered to this population. Despite the high frequency of use, the extent of cefazolin pharmacokinetics in continuous renal replacement therapy (CRRT) remains unknown. Using a closed-loop continuous veno-venous hemodiafiltration (CVVHDF) circuit, the cefazolin-CRRT circuit interaction was evaluated. Serial pre-filter blood samples were collected, along with time matched control and hemofiltrate samples. The dialysate saturation constant was calculated and used to estimate cefazolin transmembrane clearance over the experiment. Upon completion of the experiment (t= 4 hours), approximately 90% of administered dose was removed from plasma. The average dialysate saturation constant was 0.31, corresponding to a transmembrane clearance of 4.08 mL/min. Cefazolin percent remaining within the control samples (93.90%), remained consistent across the experiment, indicating negligible degradation within the blood. The extent of loss of cefazolin within a closed-loop CVVHDF circuit highlights the importance of adapting dosing regimens to ensure adequate pharmacodynamic activity while limiting toxicity.

5.2 Introduction

Infections due to gram-positive bacteria continue to remain highly prevalent amongst critically ill individuals admitted to an intensive care unit. [409,410] Furthermore those with acute kidney injury (AKI) receiving renal replacement therapy (RRT) are at increased risk of nosocomial infections due to prolonged length of stay, exposure to invasive therapies or catheters, and exposure to frequent manipulation of vascular access catheters. [411,412] Thus, antibiotics with pharmacodynamic activity against gram-positive bacteria remain some of the most widely used antibiotics in these individuals.[413,414]

Cefazolin, a first-generation cephalosporin, exhibits high pharmacodynamic activity against gram positive organisms such as methicillin-susceptible Staphylococcus *aureus* (MSSA) and *Streptococcal* species. Cefazolin is hydrophilic, with a small molecular weight (476.50 g/mol) and high percentage bound to serum albumin. [415–417] It undergoes predominantly

renal clearance through both glomerular filtration and active tubular secretion, [418,419] therefore in those with AKI receiving RRT, careful consideration of dose adjustments is required to minimize the risk of therapeutic failure or adverse effects.

Continuous renal replacement therapy (CRRT) is widely used in the management of AKI in critically ill individuals due to its preferential effects on hemodynamic stability. [56,87] Drug removal may occur through the CRRT circuit or through adsorption onto circuit materials. [102–104,117] Drug clearance is variable and may be significantly altered, [103,374] increasing the risk of suboptimal exposure when standard dosing regimens are utilized. Estimating drug clearance by CRRT is complex due to the numerous permutations of circuit materials, modalities of solute removal and flow rates. Ex-vivo study designs allow for testing such permutations in circuit settings and the resulting clearance may be used to estimate that *in-vivo*. [90,396,398]

Despite being one of the most frequently prescribed antibiotics in children within an intensive care unit, [414] dosing recommendations for cefazolin in those receiving CRRT are largely based on expert opinion or adult extrapolation. Beyond the physiological and pharmacokinetic (PK) differences between adults and children, extrapolating adult drug dosing recommendations to pediatrics presents additional challenges due to the differences in blood flow, filtration and circuit settings that may affect drug clearance. The first step to informing dosing recommendations in this population is to obtain knowledge of the drug-circuit interaction. Therefore, the purpose of this study is to analyze the pharmacokinetics of cefazolin during a simulated pediatric CRRT circuit.

5.3 Materials and Methods

5.3.1 Circuit Configuration

Continuous veno-venous hemodiafiltration (CVVHDF) was applied within the *ex-vivo* analysis as it is the most commonly applied method of CRRT within a pediatric intensive care unit (PICU). [98] The CVVHDF circuit (**Figure 5-1**.) incorporated the PRISMAX System (Baxter Healthcare) and HF1000 filter set (Baxter Healthcare) connected with a 500 mL EXACTAMIX EVA bag (Baxter Healthcare). Three circuits were completed to assess inter-run variability in cefazolin concentrations. Upon each subsequent run, hemofilters were changed and the circuit was reprimed with new blood to reduce the risk of filter clotting.

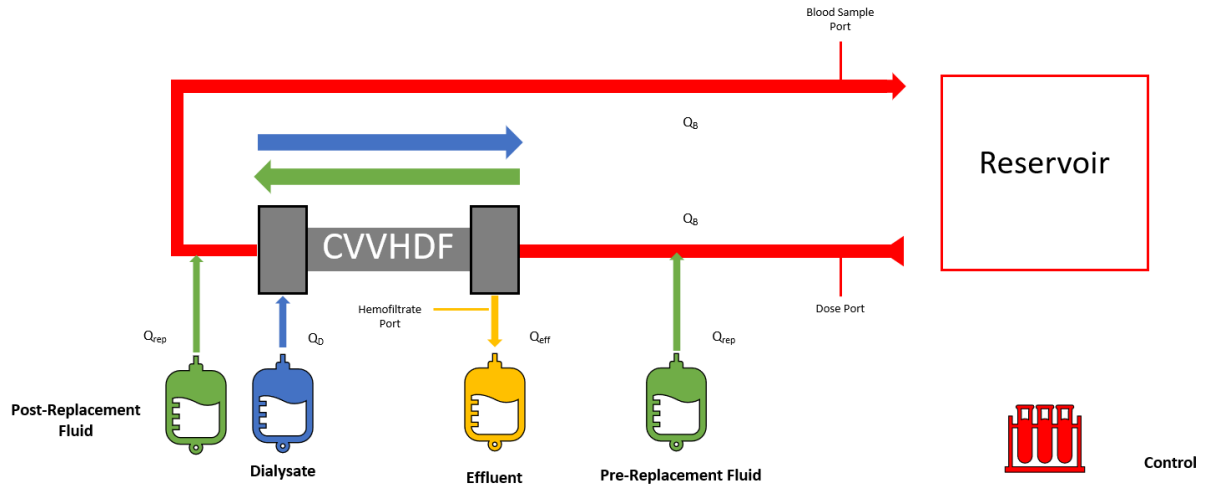


Figure 5-1. Illustration of the closed-loop ex-vivo CRRT circuit. Cefazolin removal from plasma was determined for continuous veno-venous hemodiafiltration (CVVHDF). Standard control samples were analyzed with time matched plasma and hemofiltrate samples.
Q_B; blood flow (mL/min), Q_D; dialysate flow rate (mL/h), Q_{eff}; effluent flow rate (mL/h), Q_{rep}; replacement flow rate (mL/h).

5.3.2 Continuous Renal Replacement Therapy Circuit Setup

Each CVVHDF circuit was primed with a solution of 1 unit of human red blood cells (adenine saline added leukocytes reduced [~300 mL]), ~ 0.4 units thawed human plasma frozen within 24 hours after phlebotomy (125 mL), Plasma-Lyte A crystalloid (~150 mL), heparin sulfate (350 units), tomethamine (1.6 g), sodium bicarbonate (7 mEq), human serum albumin (6.25 g). Albumin concentrations in the circuit solution was targeted to achieve those seen in critically ill children (20-30 g/L). Target volume of primed solution within each circuit was 500 mL. A description of the target concentrations of circuit solution components may be found in **Table 1.** of **Appendix D**.

Maintenance of physiologic pH (7.4; 7.22-7.65) was achieved with the addition of tromethamine. PrismaSATE 4/2.5 dialysis solution (Baxter Healthcare) was used for pre-blood pump, dialysis and replacement fluids. The CVVHDF prescription was as follows: blood flow rate (Q_B) 80 mL/min, dialysis fluid rate (Q_D) 400 mL/h, pre-blood pump replacement fluid rate (Q_{pre}) 300 mL/h, replacement fluid 100 mL/h delivered post filter (Q_{post}) and total effluent flow rate (Q_{Eff}) of 800 mL/h. Patient fluid removal (Q_{PFR}) was set to 0 mL/h to ensure a consistent volume of recirculating blood over the course of the experiment. The flow rates utilized over the

experiment were determined based upon a hypothetical child of approximately 10 kg, as per consultation from Nephrologists at our institution. CVVHDF prescription used throughout the entirety of this experiment is presented in **Table 5-2**. Blood was maintained at 37ºC with the use of heating pads.

Table 5-2. Continuous renal replacement therapy circuit setup.

CRRT Modality	Blood Flow (mL/min)	Patient Fluid Removal Rate (mL/h)	Replacement Fluid Rate (mL/h)	Dialysis Fluid Rate (mL/h)	Total Effluent Rate (mL/h)
CVVHDF	80	0	Pre-filter: 300 Post-filter: 100	400	800

CRRT; continuous renal replacement therapy, CVVHDF; continuous veno-venous hemodiafiltration, h; hours, mL; milliliters, min; minutes.

5.3.3 Control Setup

Three standard control samples of cefazolin were included to determine drug degradation throughout the experiment. A total of 50 mL of primed blood solution was drawn from the CVVHDF circuit after approximately 5 minutes of circulation and before the administration of cefazolin. The control sample was transferred into a PVC plastic tube (229,426, CELLTREAT, Pepperell, MA) and placed within a water bath maintained at 37ºC.

5.3.4 Drug Administration and Sample Collection

Cefazolin was administered at time = 0 via an arterial port downstream of the sampling port of the CVVHDF circuit (**Figure 5-1.**). Cefazolin was dosed to achieve a therapeutic concentration of approximately 250 mg/L. [415,419,420] Simultaneously, cefazolin was administered to the control tubes at time = -5 minutes and placed within a rotator to mix for 5 minutes. The control sample was returned to the water bath for the duration of the experiment, except for sampling. Controls were gently inverted five times prior to sampling.

Samples were collected at the following time points: 1, 5, 15, and 30 minutes, 1, 2, 3, and 4 hours. A hemofiltrate sample was collected at each time point from the tubing prior to entering the effluent bag (**Figure 5-1.**). Physiologic pH of circuit blood was analyzed each hour with an i-STAT 1 Analyzer (Flextronics Manufacturing, Singapore) and EG6+ cartridge (Abbot, Abbot

Park, IL) and adjusted if needed as described above. Blood samples were centrifuged (3000 rpm for 10 minutes at 4ºC) immediately after collection. Plasma was pipetted and stored at -80ºC. Hemofiltrate samples were stored at -80ºC immediately following collection.

5.3.5 Drug Analysis

Sample analysis for cefazolin in human plasma, and hemofiltrate (HF), utilized a simple, two-step dilution procedure followed by ultra-high-performance liquid chromatography (UHPLC) - electrospray ionization (ESI) - tandem mass spectrometry (UHPLC-ESI-MS/MS. Cefazolin-$^{13}C_2{}^{15}N$ was used as the internal standard. All reference materials were obtained from Toronto Research Chemicals (Toronto, Canada). The samples were first diluted 50-fold with mobile phase A (20 µL of sample plus 980 µL of aqueous mobile A). Then, 50 µL of the standards, QCs, blanks, and 50-fold diluted samples was aliquoted, followed by the addition of 50 µL of internal standard solution (5 µg/mL) plus 500 µL of mobile phase A. After mixing, 200 µL was transferred to autosampler vials, and 20 µL was injected for analysis by UHPLC-ESI-MS/MS. The LC system was a Waters Acquity UPLC® autosampler and pumping system interfaced with a Waters Quattro Premier XE™ triple quadrupole mass spectrometer. Chromatographic separation was performed on a Phenomenex (Torrance, CA) Kinetex EVO C18 column (2.1 x 50 mm, 1.7 µm particle size) using gradient elution flowing at 0.3 mL/min. The mobile phases were (A) 10 mM ammonium bicarbonate, pH 8, and (B) methanol, and initially equilibrated and held at 1% B for the first 1.5 minute of the gradient. The mobile phase composition was then linearly increased to 100% B at 2.0 minutes, where it was held for 2 minutes before being immediately returned to and equilibrated at initial conditions. The MS/MS was operated in the Selected Reaction Monitoring (SRM) mode under positive ionization conditions. For cefazolin and cefazolin-$^{13}C_2{}^{15}N$, the SRM transitions were mass/charge (collision energy) 455.0 to 323.1 (10 eV) and 458.0 to 326.1 (10 eV), respectively. The concentrations of cefazolin in the samples were determined from the ratio of the peak area of the analyte to the peak area of the internal standard, and comparison of this ratio with the calibration curve that was generated from the analysis of 2% human plasma in 10 mM ammonium bicarbonate, pH 8, to match the diluted study samples, fortified with known concentrations of the analyte and the internal standard.

Calibrators were prepared for each analytical run in 2% human plasma in 10 mM ammonium bicarbonate, pH 8, at nominal concentrations for cefazolin of 0.05, 0.1, 0.2, 0.5, 1, 2, 4, 6, 8, and 10 µg/mL. A double blank (matrix without internal standard) and zero sample (matrix with internal standard) were prepared for each run in the same matrix used for the calibrators. Quality Control samples (QCs) were also prepared in 2% human plasma in 10 mM ammonium bicarbonate, pH 8, at nominal concentrations of 0.15, 1.5, and 7.5 µg/mL and analysed in duplicate with each analytical run of study samples. The lower limit of quantitation (LLOQ) was 0.05 µg/mL which corresponds to a value of 2.5 µg/mL for the 50-fold diluted study samples. The upper limit of quantitation (ULOQ) was 10 µg/mL (500 µg/mL for the 50-fold diluted study samples).

Percent cefazolin remaining was calculated at each time point using the following equation:

$$Cefazolin\ Remaining\ (\%) = \frac{C_t}{C_i}\ x\ 100$$

Eq. 5-1

Where C_t is the concentration at time t and C_i is the concentration at time = 5 minutes for CVVHDF plasma and control samples. The dialysate saturation constant (S_D) was calculated to quantify the ability of cefazolin to cross the hemofilter. Drug passage was determined from paired hemofiltrate/dialysate and plasma samples at each time point using the following equation:

$$S_D = \frac{C_D}{C_P}$$

Eq. 5-2

Where C_D and C_P represent the cefazolin concentrations in dialysate and plasma, respectively.

Clearance of cefazolin across the circuit filter membrane was estimated by:

$$CL_{CVVHDF} = Q_{Eff}\ x\ S_D$$

$$Q_{Eff} = (Q_{pre} + Q_{post}) + Q_{PFR} + Q_D$$

Eq. 5-3

Where Q_{Eff} represents the effluent rate, Q_{pre} represents the pre-filter replacement fluid rate, Q_{post} represents the post-filter replacement fluid rate, Q_{PFR} represents the patient fluid removal rate and Q_D dialysate flow. [102,103]

5.3.6 Statistical Analysis

An unpaired *t* test was used to analyze the effect of CRRT on recovery of cefazolin in plasma. Percent recovery for each circuit a time = 4 hours was compared to the recovery in the standard control at the matching time point. Data is presented as the mean with corresponding standard deviation.

5.4 Results

A total of 48 samples of cefazolin in plasma and dialysate were analyzed. Concentrations at time = 1 minute were dropped from the analysis as they were below the LLOQ. Average percent of cefazolin remaining (standard deviation) in plasma at time = 15 minutes was 63.12% (12) and 10.35% (2.6) at 4 hours. Graphical representation of the percent of cefazolin remaining over time may be found in **Figure 5-2**.

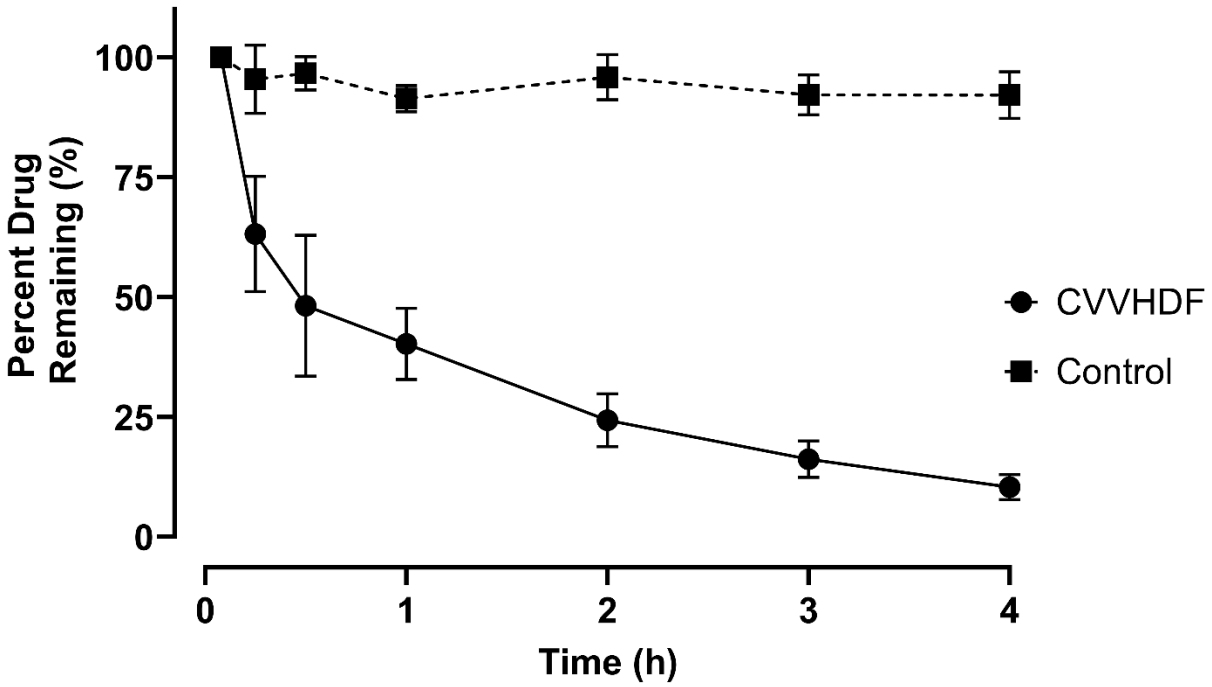


Figure 5-2. Percent cefazolin remaining in plasma and standard control with standard deviation shown as error bars. Percent remaining was analyzed at time = 5 minutes.
CVVHDF; continuous veno-venous hemodiafiltration.

The percent of cefazolin remaining in plasma was significantly different compared to the standard control at the completion of the experiment (p = <0.001). The average dialysate saturation constant over the course of the experiment was 0.31 (0.11), resulting in an estimated transmembrane clearance of 4.08 (1.41) mL/min. A visual representation of the average S_D over the course of the experiment may be found in **Figure 5-3.**, with a numerical representation reported in **Table 5-3**.

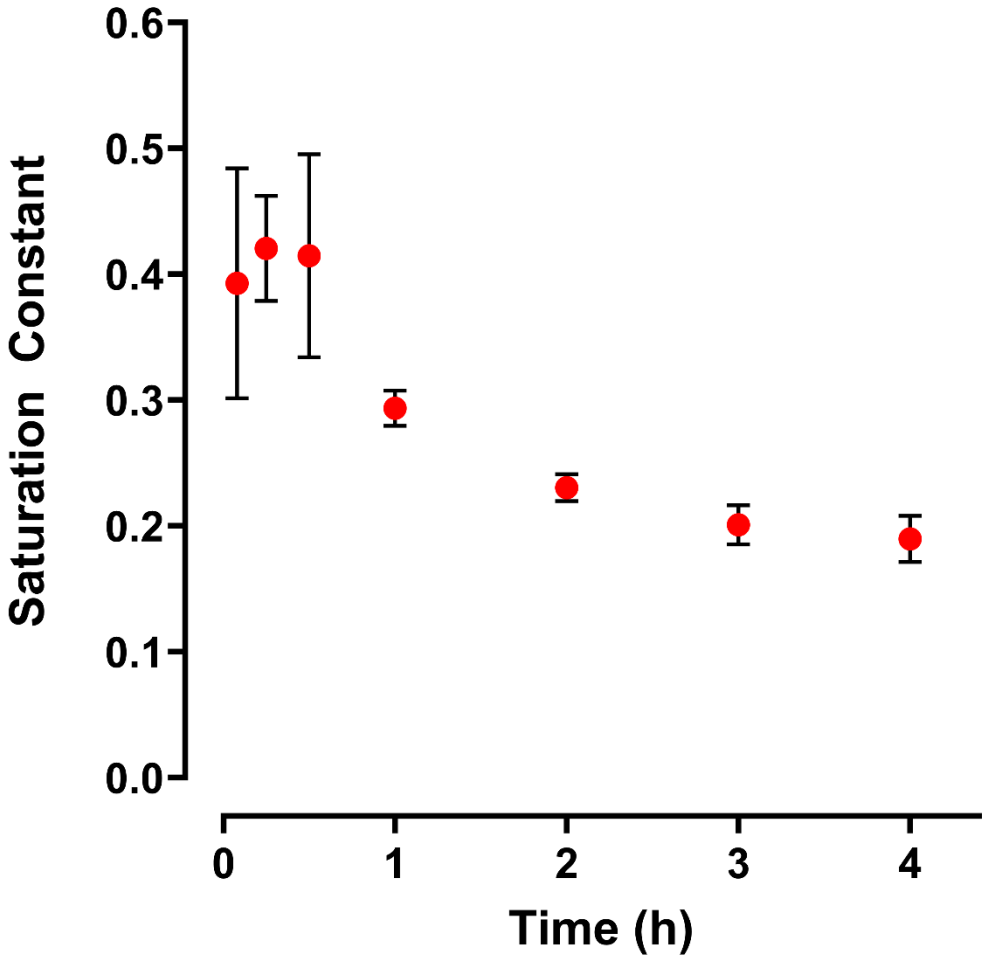


Figure 5-3. Graphical representation of the average (± standard deviation) cefazolin dialysate saturation constant over time.

Table 5-3. Cefazolin pharmacokinetic variables determined within a CVVHDF circuit. Data presented as mean, standard deviation and range.

Pharmacokinetic Variable	Mean	Standard Deviation	Range
Saturation coefficient	0.31	0.11	0.17 – 0.50
Transmembrane Clearance (mL/min)	4.08	1.41	2.25 – 6.69

5.5 Discussion

As advancements within pediatric critical care medicine continue to occur, the use of extracorporeal therapy such as CRRT is likely to have a significant role. Antibiotics are some of

the most frequently prescribed medications to critically ill children on CRRT, [154,395] therefore a thorough understanding of the drug-circuit interaction is of the utmost importance to ensuring optimal pharmacodynamic activity while minimizing toxicity. The objective of this study was two-fold. This study is the first to analyze the cefazolin-CRRT circuit interaction. Secondly, as CVVHDF is the most common method of CRRT applied within a PICU, [98] we sought to provide results that are generalizable and informative for clinicians.

In addition to CVVHDF, CRRT may also be employed with continuous veno-venous hemodialysis (CVVHD) or continuous veno-venous hemofiltration (CVVH). Solute removal occurs differently depending on the modality chosen, [56,102–104] however CVVHDF may be seen as a hybrid as it concurrently administers the dialysate flow of CVVHD with the ultrafiltration and use of replacement fluids in CVVH. Drug clearance is largely influenced by circuit characteristics (i.e. flow rates, membrane porosity) and drug physicochemical properties such as molecular weight, protein binding and lipophilicity. [89,105] It is worth noting that modern high-flux membranes, as incorporated within this study, may negate the effects of molecular weight on RRT clearance.[154]

The impact of CRRT on altering the PK of small molecular weight drugs has been studied extensively in both adults [89,102,103,105–107,374] and children [154,395]. The degree to which drugs are removed from the system are largely dependent upon the physicochemical properties. Drugs with low molecular weights, a high unbound fraction in plasma and those that undergo predominant renal clearance are most likely to have altered PK in individuals receiving CRRT. [89,105,395,421] As cefazolin shares many of these properties, drug clearance may be affected when CRRT is applied. Unexpectedly, the results from the *ex-vivo* analysis demonstrate that approximately 90% of the administered dose was removed upon the completion of the experiment (t = 4 hours).

The dialysate saturation constant (S_D) or sieving coefficient (S_C) allows for assessment of the ability for a molecule to pass across the hemofilter membrane. Molecules with a S_D or S_C approximating 1.0 suggest free passage across the circuit hemofilter. Although, the average cefazolin S_D was 0.31 within this experiment, substantial loss from plasma was noted. Interestingly, a range of SD was observed throughout the experiment (**Figure 5-3.**), indicating both between circuit and within circuit variability. This variability may be due to the unique

saturable protein binding of cefazolin to serum albumin. [415] Increases in the unbound fraction has been observed in both adults [415–417] and neonates [422,423] with the use of standard therapeutic doses. Compounded with the impact of critical illness on albumin concentrations, [21,23,424] interindividual variability in unbound concentrations and CRRT circuit clearance may be expected in this population. Therapeutic drug monitoring *in vivo* may allow for monitoring any potential variability and ensuring optimal pharmacodynamic activity. [425–427]

Therapeutic drug monitoring for antimicrobials can be used to maximize drug efficacy and minimize toxicity in an individual patient. This practice has been common for aminoglycosides and glycopeptides, however β-lactam therapeutic drug monitoring has yet to adopted as a routine intervention. [428–430] Due to the unequivocal results on patient outcomes and logistical challenges, the utility of β-lactam therapeutic drug monitoring in the intensive care unit has been debated. [431,432] However, amongst opposing views there does appear to be consensus that those receiving CRRT may be a population to benefit from therapeutic drug monitoring. [431–434] As this is largely reflective of the adult population, limited data in pediatrics demonstrate that β-lactam therapeutic drug monitoring in the PICU may be beneficial. [435] Although a limited number of children receiving CRRT were represented, one may suspect that this population would benefit from such approaches. However, further studies confirming its utility are important for widespread adoption amongst the clinical community.

The pharmacokinetics of drugs administered to critically ill children receiving CRRT have been previously described. [154,395] Unexpectedly, within these reviews no publications were identified investigating the use of cefazolin. Despite the high frequency of use, a large gap remains regarding published literature to guide clinicians in using safe and effective dosing regimens. [414] Available data describing clearance via RRT is limited to intermittent hemodialysis (IHD). Maynor *et al.* identified that approximately 60% of cefazolin was removed from plasma after four hours of IHD. [436] These results have been replicated in additional *in vitro* and *in vivo* studies in adults. [437–439] Several methodological and mechanistic differences preclude any comparison between our results and the previously published work, however, the reports herein suggest that cefazolin is adequately cleared by RRT, regardless of modality or circuit characteristics.

Although the results presented are the first to analyze cefazolin clearance from a pediatric CRRT circuit, they are not without limitations. First, a single modality with fixed flow rates was utilized over the course of the experiment. The use of modernized hemofilters has negated potential differences in circuit clearance between modalities when similar flow rates are applied. However, increasing flow rates may lead to increased clearance of small molecular weight drugs. [90,400] Future studies are warranted to assess the impact of increasing flow rates on cefazolin clearance. Second, the experimental design was conducted using the HF1000 (PAES) hemofilter within each circuit. Comparatively, PAES hemofilters have reduced adsorptive capacity to alternative synthetic hemofilters. [117,273] It was hypothesized that cefazolin would not undergo significant adsorption to circuit materials based upon its physicochemical properties. The results confirmed our hypothesis, as high concentrations of cefazolin were quantified in the hemofiltrate. As only one filter set was trialed within this experiment, extrapolating to filter sets with different compositions should be done cautiously. Third, a single intermittent bolus dose of cefazolin was administered to the CRRT circuits, the results may not be applied to alternative dosing strategies such as continuous or extended-interval infusions. As the use of continuous or extended-interval infusions for β-lactams becomes more prominent due to the potential for improved patient outcomes, [440–442] future studies will be required to quantify the risk of drug accumulation. Finally, despite evidence suggesting *ex-vivo* drug clearance may approximate that *in-vivo*, [90,398] the results in isolation should not be used to inform drug dosing recommendations. Due to the closed-circuit nature no metabolism is present and there is an inability to capture the physiological complexity of a critically ill individual. By incorporating the results of this experiment into a physiologically-based pharmacokinetic (PBPK) model, one may integrate the physiological changes associated with critical illness in addition to the PK of cefazolin to optimize drug dosing in this population more accurately.

5.6 Conclusion

In conclusion, this study quantifies the removal of cefazolin from a pediatric CRRT circuit. By incorporating a closed-loop ex-vivo study design, the cefazolin-CRRT circuit interaction was assessed independent of many of the variables known to affect drug PK in the critically ill population. Clearance of cefazolin was primarily attributed to hemodiafiltration with negligible amounts adsorbed to circuit components or degraded within the blood, suggesting

renally adjusted doses may result in subtherapeutic concentrations. Clearance of small molecules determined via closed-loop CRRT circuits may provide reasonable approximations to *in vivo* values.

Therefore, the results of this study provide the foundation to ensure optimal dosing regimens of cefazolin are utilized in this population. Incorporating ex-vivo results within a PBPK model will help guide clinicians to safe and effective use of cefazolin in this population.

Chapter 6: Physiologically-Based Pharmacokinetic Modelling in Critically Ill Children Receiving Anakinra While on Extracorporeal Life Support

This chapter is reflective of an original manuscript in preparation by the PhD candidate (Samuel Dubinsky) for peer-reviewed journal publication. All pertinent dialogue in this chapter was written by the PhD candidate.

6.1 Overview

Background and Objective:

Due to the pathophysiological changes associated with critical illness and the use of extracorporeal life-support (ECLS) such as continuous renal replacement therapy (CRRT) and extracorporeal membrane oxygenation (ECMO), the pharmacokinetics of drugs are often altered. The objective of this study was to develop a physiologically-based pharmacokinetic (PBPK) model for anakinra in children that accounts for the physiological changes associated with critical illness and ECLS technology to guide appropriate pharmacotherapy.

Methods:

A PBPK model for anakinra was first developed in healthy individuals prior to extrapolating to critically ill children receiving ECLS. To account for the impact of anakinra clearance by the dialysis circuit, a CRRT compartment was added to the pediatric PBPK model and parameterized using data from a previously published *ex-vivo* study. Additionally, an ECMO compartment was added to the whole-body structure to create the final anakinra ECLS-PBPK model. The final model structure was validated by comparing predicted concentrations with observed patient data. Due to limited information in guiding anakinra dosing in this population, *in-silico* dose simulations were conducted to provide baseline recommendations.

Results:

By accounting for changes in physiology and the addition of ECLS compartments, the final ECLS-PBPK model predicted the observed plasma concentrations in an adolescent receiving subcutaneous anakinra. Furthermore, dosing simulations suggest that anakinra exposure in adolescents receiving ECLS is similar to healthy counterparts.

Conclusion:

The anakinra ECLS-PBPK model developed in this study is the first to predict plasma concentrations in a population receiving simultaneous CRRT and ECMO. Dosing simulations provided may be used to inform anakinra use in critically ill children and guide future clinical trial planning.

6.2 Introduction

Sepsis may be defined as a life-threatening condition caused by a dysregulated host response to infection. [38] In children, sepsis is one of the leading causes of mortality and healthcare resource consumption across the world. [443–446] The high mortality risk can be attributed to refractory shock and/or multiple organ dysfunction syndrome (MODS), that includes failure of vital organs such as the lungs, kidneys and heart. [16,85,86,443]

Despite initiatives focused on early recognition and prompt pharmacotherapy, mortality rates remain high. Recent strategies have focused on distinguishing the heterogeneity in phenotypes of sepsis through classification of immune dysregulation. [392,393,447,448] These phenotypes may present as a state of immunoparalysis or hyperinflammation. In those with features of pronounced inflammation, pharmacologic agents targeted to mitigate the downstream effects of the cytokine storm may be beneficial in preventing or improving MODS and are the recent focus of ongoing clinical trials. [393,449]

As a result of the complications to vital organs, initiation of extracorporeal life support (ECLS) such as continuous renal replacement therapy (CRRT) and extracorporeal membrane oxygenation (ECMO) may be required. CRRT is a form of continuous dialysis that is often applied to critically ill individuals due to its preferential effects on hemodynamic stability. [56,87] In cases of respiratory or cardiac failure, ECMO is often needed for cardiopulmonary support. One of the many challenges associated with treating patients on ECLS is understanding the alterations in pharmacokinetics (PK) that may occur upon extracorporeal circuit initiation. Simplistically, drug PK may be altered through adsorption to circuit materials, and clearance via the ECLS circuits.

Anakinra, a recombinant human interleukin-1 receptor antagonist (IL-1 RA) is currently approved for use in patients with rheumatoid arthritis and neonatal onset multisystem inflammatory disease. [375,376] In addition to its role in chronic inflammatory conditions, IL-1 has been implicated in the cytokine storm cascade that contributes to the pathophysiology of acute cytokine release syndromes such as secondary hemophagocytic lymphohistiocytosis (sHLH) or macrophage activation syndrome (MAS). [383–385] Prior to receiving marketing

approval for use in chronic inflammatory diseases, anakinra was studied as an adjunct therapy for acute, hyperinflammatory conditions such as sepsis. [389–391] Despite the equivocal results in the early trials, Shakoory *et al*. revisited the hypothesis that anakinra may serve as a valuable treatment option in patients with sepsis experiencing hyperinflammatory features. [392] As anakinra continues to be investigated in this population, understanding the effect of ECLS on the PK will be essential to defining appropriate drug dosing regimens.

Physiologically-based pharmacokinetic (PBPK) modelling is a valuable tool that is uniquely positioned to predict drug PK in children receiving ECLS. [144,150] PBPK models are mechanistic and developed using drug physicochemical properties and known physiology. Therefore, extrapolations to different age-groups (adult to pediatric) or disease states (healthy to critically ill) can be made by accounting for age related processes or alterations in physiology known to affect drug PK. By mathematically describing the movement of drugs through each "organ" compartment, predicting drug exposure in patients on ECLS can be conducted by linking an ECLS compartment to the whole body structure. [144,150] This approach may allow for extrapolation to different age groups, new ECLS technology or circuit settings and provide meaningful dosing simulations in otherwise untested scenarios.

The purpose of this study was to create an ECLS-PBPK model of anakinra in critically ill children and assess model predictions to guide appropriate anakinra therapy. We leveraged our prior work describing anakinra-circuit interaction in isolated CRRT circuits [450] to build an ECLS-PBPK model to be evaluated with observed data from a prospective PK study. Additionally, dosing simulations across the pediatric age spectrum were conducted to investigate optimal dosing in children on ECLS and provide guidance for future clinical trial planning.

6.3 Methods

6.3.1 Software

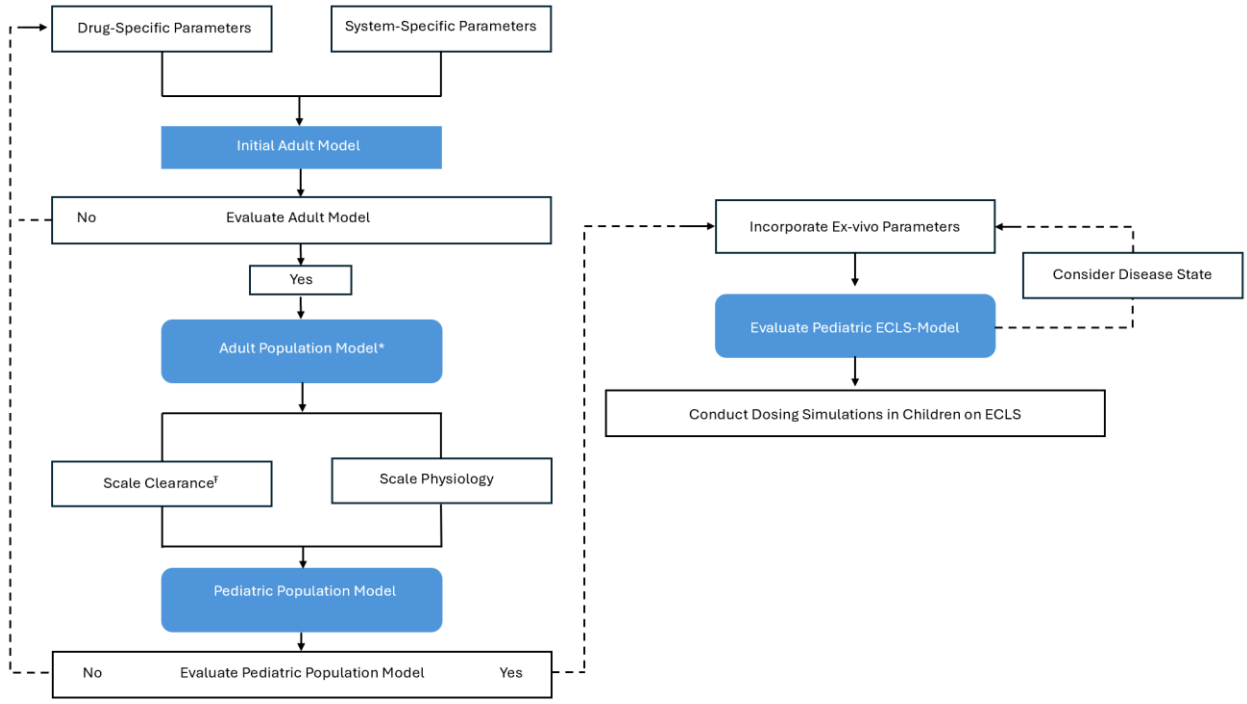
All PBPK modelling was carried out using PK-Sim version 11.0 as part of the Open Systems Pharmacology suite (www.open-systems-pharmacology.org) using the base model for large molecules and therapeutic proteins. [451] Parameter sets for healthy virtual individuals and populations were incorporated as described previously. [289,290] Alterations to the whole body PBPK model structure to incorporate modelling of subcutaneous (SC) dose administration

[2.2.2] and the addition of the ECLS compartments [2.4] were completed in MoBi version 11.0. Clinical data were digitized using WebPlot Digitizer version 4.7 (https://automeris.io/WebPlotDigitzer). Graphic illustrations were completed using GraphPad Prism version 10.1.2 (Boston, Massachusetts, USA) and R programming language version 4.1.1 (R Foundation for Statistical Computing, Vienna, Austria, 2019).

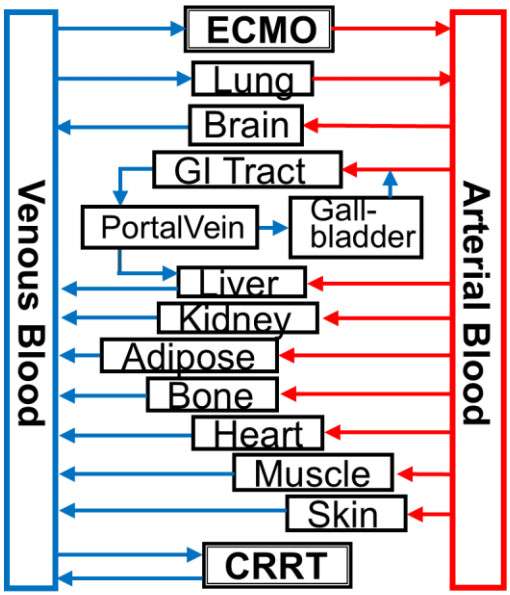
6.3.2 Model Building Workflow

The anakinra PBPK model was built using an established workflow for large molecules [144,277], while incorporating the base model for large molecules and therapeutic proteins. [451] First, an anakinra model was constructed in adults to gain confidence in the model structure prior to scaling to children. Models reflecting both intravenous (IV) and SC anakinra administration were created. Upon the adult model meeting acceptance criteria, age dependencies associated with anakinra PK were scaled to children.

Furthermore, as the pediatric PBPK model was evaluated using clinical PK data in children not on ECLS, the CRRT and ECMO compartments were added to the pediatric PBPK model to develop the final ECLS-PBPK model. The CRRT compartment was parameterized using data from our previously published *ex-vivo* study, [450] while the ECMO compartment was incorporated as reported by Watt *et al.*[144] Anakinra ECLS-PBPK model predictions were evaluated from data that were prospectively collected from the ongoing Opportunistic PK Study of Commonly Used Drugs in Children on ECLS (University of Utah Institutional Review Board Number: 00138310). A visual illustration of the anakinra PBPK model building process and structure used in this study may be found in **Figure 6-1.**



A)



B)

Figure 6-1. A visual illustration of the workflow and model structure for predicting anakinra pharmacokinetics in children receiving extracorporeal therapy using physiologically-based pharmacokinetic (PBPK) modelling. In this workflow, an adult PBPK model was constructed and validated (Step 1), prior to scaling to children (Step 2). Upon evaluation of the pediatric PBPK model, ex-vivo parameters were incorporated to the whole-body structure for verification of the final pediatric anakinra ECLS-PBPK model (Step 3).

[*]Adult population PBPK model simulations were evaluated in healthy individuals, and those with chronic kidney disease.
[Ŧ]Scaling of clearance consisted of age-related changes in glomerular filtration rate, while proteolysis was held constant from the adult model.

6.3.3 Adult PBPK Model

6.3.3.1 Adult Intravenous PBPK Model

In brief, the adult IV PBPK model was developed by collecting and appraising the physicochemical properties and PK characteristics of anakinra from the literature. The base model for large molecules and therapeutic proteins represents two-pore extravasation, endocytosis into vascular endothelium, binding to neonatal Fc receptor (FcRn) and lymph recirculation. [451] Due to what is currently known about anakinra PK, target-mediated drug disposition and binding to FcRn was not applicable. A detailed report of the model development and verification in healthy adults is available in the electronic supplementary material (**Appendix E, Section 1**), with the final model parameters presented in **Table 6-1**.

Table 6-1. Drug specific parameters and ADME of anakinra for PBPK model development.

	Used in naïve model	**Used in optimized model [range of optimized values]**
Drug Specific Parameters		
Molecule Weight (kDa)	17.3	17.3
Hydrodynamic Radius (nm)	2.16 [452,453]	2.16 [452,453]
Compound Type	Protein	Protein
Bioavailability (F)	0.8	0.8
Half-life of drug release (min)	0	212.07 [212.04 – 212.11]
ADME		
GFR Fraction	1	0.45
Proteolysis (CL_P; 1/min)	0	52.66 [29.65 – 68.45]

kDa; kilodaltons, nm; nanometres, min; minutes.

To account for the potential clearance pathways, non-specific proteolysis (CL_P) was incorporated within the liver and kidney, in addition to glomerular filtration, a method that has

been applied previously. [454] Adult model validation datasets may be found in **Appendix E, Section 1.2.4**.

6.3.3.2 Adult Subcutaneous PBPK Model

Anakinra IV administration is considered off-label, therefore a SC PBPK model was constructed in both adults and pediatrics. PBPK models for SC dosing of large molecules have been done with varying levels of complexity. [452,454–456] To represent the SC route of administration, a semi-mechanistic SC model was constructed by delivering the bioavailable dose (dose x F) as a bolus to the interstitial compartment of the skin. Validation of the SC PBPK model was carried forth prior to scaling to pediatrics. A full description of the anakinra SC model may be found in **Appendix E, Section 2.**

Yang *et al.* [386] demonstrated that across mild, moderate and severe stages of chronic kidney disease (CKD), anakinra total clearance upon administration of a SC dose was reduced by 16%, 50% and 70-75% respectively. Additionally, absolute bioavailability (F_{abs}) in those with end-stage renal disease (ESRD) receiving SC anakinra was determined to be 0.5. Although the pathophysiology differs between CKD and acute kidney injury (AKI), we incorporated a middle-out approach to quantify the reductions in total clearance across each CKD stage. Population simulations using the CKD-PBPK model structure developed by Malik *et al*.[284] were carried forward for evaluation of the observed data by Yang *et al*. [386] We assumed that the impact of severe CKD on total clearance would be similar to critically ill individuals with acute renal failure requiring CRRT. Additionally, both critical illness [34,35,457] and CKD [458,459] may impact the bioavailability of drugs administrated subcutaneously, therefore the absolute bioavailability determined in Yang *et al*. was applied within our ECLS-PBPK Model. A full description of the anakinra CKD-PBPK model development may be found in **Appendix E, Section 3.**

6.3.4 Pediatric PBPK Model

6.3.4.1 Pediatric Subcutaneous PBPK Model

Recent investigations by Malik *et al*. [460] have characterized the ontogeny of several physiological components that affect both volume of distribution at steady state (V_{ss}) and clearance of large molecules in children. In this work, ontogeny profiles were incorporated for

capillary surface area and lymph flow rates to reflect the SC route of administration. With respect to clearance, the ontogeny of anakinra proteolysis has yet to be fully elucidated in young children. It has been suggested that the proteolytic pathway of endogenous IL-1 RA remains intact and does not undergo any age-related alterations. [461,462] Due to the chemical structural similarities between endogenous IL-1RA and anakinra, it was assumed in the pediatric PBPK model that the CLP mechanism was consistent between adults and children. All additional parameters remained constant except those dependent on age (i.e. physiological parameters). Virtual populations reflecting the PK studies by Urien *et al*.,[463] and Ilowite *et al*.,[464] were created and used for evaluation purposes (**Table 6-2.**).

Table 6-2. Pharmacokinetic datasets for the pediatric subcutaneous anakinra model evaluation.

Reference	Ethnicity	Dose and Administration	N (male/female)	Age (years)	Weight (kg)	Height (cm)
Urien *et al*. [463]	European	2-10 mg/kg daily[a]	87 (52/32)[b]	7.6 [2.26-16.8][c]	21 [10-83][c]	NR
				8 [0.73-21][d]	21 [4.3-60][d]	
Ilowite *et al*. [464]	American	1 mg/kg daily[a]	24 (8/17)	10 [3-17][e]	36 [12-98][e]	NR

cm; centimetres, kg; kilograms; mg; milligram, NR; not reported, SC; subcutaneous

[a] Maximum dose of 100 mg

[b] Individuals included within pharmacokinetic analysis

[c] Data presented as median with [range] of patients with systemic-onset juvenile idiopathic arthritis included in final pharmacokinetic analysis

[d] Data presented as median with [range] of patients with cryopyrin-associated periodic syndromes included in the final pharmacokinetic analysis

[e] Data presented as mean with [range]

6.3.5 ECLS-PBPK Model

A CRRT model was implemented into MoBi for the purpose of simulating the removal of anakinra from the blood. The model was calibrated using the anakinra concentration measurements from our previously published *ex-vivo* experiments. [450] The CRRT compartment mathematically represents an “organ” compartment composed of a filter blood compartment, a dialysate compartment, and a reservoir compartment. Literature derived

parameter values for anakinra and manufacture specifications for the HF1000 filter set (Baxter Healthcare) were incorporated into the model. Uncertain parameters pertaining to anakinra degradation (δ) and the membrane diffusion coefficient (*D*) were optimized. Each modality of CRRT (CVVH, CVVD, CVVHDF) was simulated and the corresponding parameters were incorporated to be attached to the whole-body structure. An opportunistic PK study enrolling children on ECLS was conducted at Primary Children's Hospital (PCH), Salt Lake City, UT (University of Utah Institutional Review Board Number: 00138310). This study enrolled pediatric patients prescribed anakinra per standard of care and supported by ECMO and/or CRRT. Plasma samples were collected at times of routine lab draws.

As the observed data to which the model will be evaluated contained plasma concentrations from a patient on simultaneous ECMO, an additional compartment reflecting the ECMO circuit was integrated to the whole body PBPK model structure. Blood flow into and out of the ECMO compartment was assigned by partitioning pulmonary blood, with 80% allocated to the ECMO compartment and 20% allocated to the lungs. As no adsorption occurred within the ex-vivo CRRT study [450], it was assumed that no adsorption was present in the ECMO compartment. To account for potential edema and capillary leak syndrome that may occur in patients on ECMO, an edema factor of 30% was incorporated by increasing the total body weight by 30% and adding the increase in volume to the interstitial compartment of each organ. [144,465–467] Additionally, the interstitial:plasma protein ratio was increased to 1 to account for equalization of proteins due to capillary leak. [144,468] Population pediatric ECLS-PBPK model simulations were performed to be evaluated against the observed plasma concentrations collected from a 17 year old individual receiving anakinra 100 mg SC every 12 hours while on CVVHDF + ECMO. Details regarding CRRT prescription incorporated in final model may be found in **Appendix E, Section 4.**

6.3.6 Dosing Simulations

Variability in anakinra dosing may be seen for both chronic and acute conditions in adults [379,389–391,469] and pediatrics.[463,464,470–472] In pediatrics, Urien *et al.* suggest that average concentrations at steady state (C_{SS}) greater than 0.4 mg/L provides maximal effect on reducing the inflammatory marker C-reactive protein (CRP). [463] However, as this was

analytically derived in children with chronic inflammatory conditions, no such target has been identified in acute conditions. With respect to anakinra safety profiles, C_{SS} of 25.2±13.2 mg/L have been well tolerated in adults with inflammatory phenotypes of sepsis. [389] Therefore, we investigated the CSS of anakinra by simulating dosing protocols that have been trialed in pediatrics to compare to the aforementioned C_{SS} targets. Doses of 5 to 10 mg/kg/d divided every 12, 8 and 6 hours were simulated across the pediatric age spectrum. Weight-based doses were capped to a maximum of 100 mg per dose. For adolescents, fixed doses of 100 mg were simulated. CRRT settings in the model were adjusted for age as to what would be applied in the clinical setting. Details regarding CRRT prescriptions for each age group may be found in **Appendix E, Section 4.**

Product-label dose recommendations indicate that adjustments are required in those with renal impairment. [473] From the results of the *ex-vivo* study, we hypothesized that renal dose adjustments may not be necessary in those receiving CRRT due to the impact of the circuit on anakinra clearance. To investigate this further, predicted area under the curve (AUC) in adolescents receiving ECLS was compared to predictions in healthy individuals. Restrictions to adolescents were chosen due to data availability for evaluation purposes.

6.3.7 PBPK Model Acceptance Criteria

Verification of model accuracy was conducted using the average fold error (AFE; bias) and absolute average fold error (AAFE; precision) for each anakinra IV and SC simulation. Observed data was aggregated to mean or median concentrations. Acceptance was granted if AFE <30% (0.7-1.3) and AFFE ≤2 for simulated drug concentrations. Additionally, a comparison of relevant PK parameters between predicted vs. observed was conducted by calculating the fold error (**Eq. 6-1**). A fold-error of 2 (0.5-2) ensured successful model performance.

$$Fold\ Error = \frac{Predicted_{PKparameter}}{Observed_{PKparameter}}$$

Eq. 6-1

For data sets including individual patient samples, inter-individual variability was assessed by generating a prediction interval (5th-95th) and quantifying the number of observed concentrations that fell outside the prediction interval.

To assess the ECLS-PBPK model performance, a virtual population of 1000 adolescents was created to capture the demographics of the study participant. The number of observed concentrations was evaluated within the generated prediction interval.

6.4 Results

6.4.1 Adult IV PBPK Model

Optimal values determined for clearance, both renal (CL_R) and CL_P, were optimized in the adult IV PBPK model (**Table 6-1.**) using data from Yang *et al.* (**Appendix E, Section 1.2.2**). [386,387] Confidence in the adult model was established upon evaluation of the dose-escalation study by Granowitz *et al*. [474] Visual predictive checks of each dose reveal accurate predictions upon the observed concentration time profile (**Fig 6-2.**). Each dose except for the 3 mg/kg met our predefined criteria for AFE and AAFE. (**Appendix E, Section 1.2.4**)

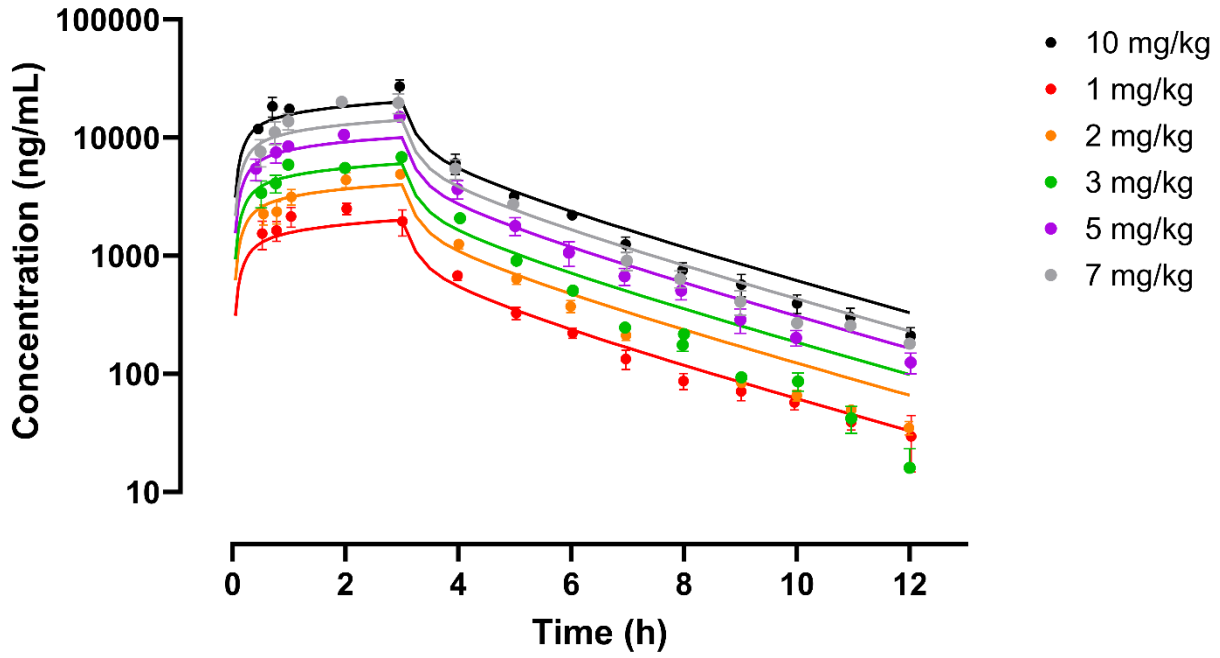


Figure 6-2. Anakinra IV PBPK model evaluation to observed concentrations from individuals in the study by Granowitz et al. [474] The solid line represents the average concentration vs. time profile of the virtual population while the observed data is presented as mean (circles) with standard deviation (error bars).

6.4.2 Adult Subcutaneous PBPK Model

The anakinra healthy adult SC PBPK model was developed using data from the PK study by Yang *et al*. (**Appendix E, Section 1.2.2**). [387] Successful evaluation was completed upon comparison from an independent data set from the PK study by Yang *et al*. (**Appendix E, Section 1.2.3)**. [386] Furthermore, AFE and AAFE fell within the predefined acceptance criteria and predicted maximum concentrations (C_{max}) and area under the concentration time curve extrapolated to infinity (AUC_{∞}) were within a 2-fold error compared to observed. (**Appendix E, Section 1.2.4**)

Virtual populations were constructed and evaluated for each stage of CKD (**Appendix E, Section 3.2.2**). Upon visual inspection (**Appendix E, Section 3.2.4**) CKD-PBPK model simulations accurately represent the observed concentration time profile across each stage, however, C_{max} was slightly overpredicted within the mild and moderate CKD simulations. Yet,

simulated C_{max}, time to maximum concentration (t_{max}) and area under the concentration time-curve extrapolated to infinity (AUC_{∞}) were within a 2-fold error of the average PK parameters from study participants (**Appendix E, Section 3.2.4)** The resulting impact of CL_P determined within the severe CKD stage was then carried forth to the final anakinra ECLS-PBPK model.

6.4.3 Pediatric Subcutaneous PBPK Model

The final adult anakinra SC PBPK model was scaled to pediatrics upon accounting for changes in age-related physiological parameters, ontogeny to capillary density and lymph flow rate. [460] Information pertaining to study design and demographics of the PK studies used for model evaluation may be found in **Table 6-2**. Age stratification and dosing details were not reported within these studies therefore ranges of the dosing protocols were applied to each simulation. Pediatric simulations showed good agreement between predicted vs observed concentrations as 70% and 75% of observed concentrations fell within the 5th-95th prediction interval from the study by Urien *et al*.,[463] and Ilowite *et al*.,[464] respectively. Visual representations of the pediatric population PBPK simulations may be found in **Figure 6-3.** and **Figure 6-4**.

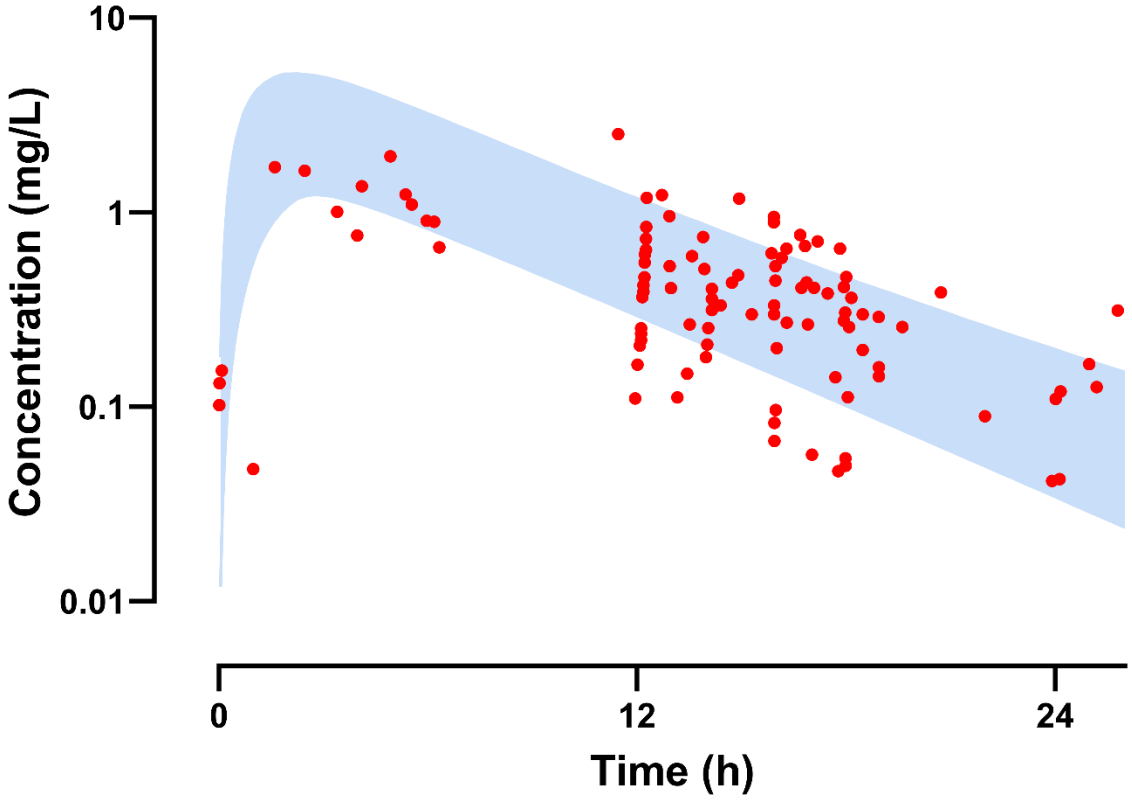


Figure 6-3. Predicted and observed plasma concentrations from the pediatric anakinra SC PBPK model. A virtual population (n=1000) individuals was created to correspond with the patient demographics in the pharmacokinetic study by Urien et al. [463] Individuals within this study received anakinra doses between 2-10 mg/kg daily, to a maximum of 100 mg. To simulate this, the 5th-95th prediction interval (shaded region) was simulated for the corresponding doses. Observed individual plasma concentrations is represented by the circles.

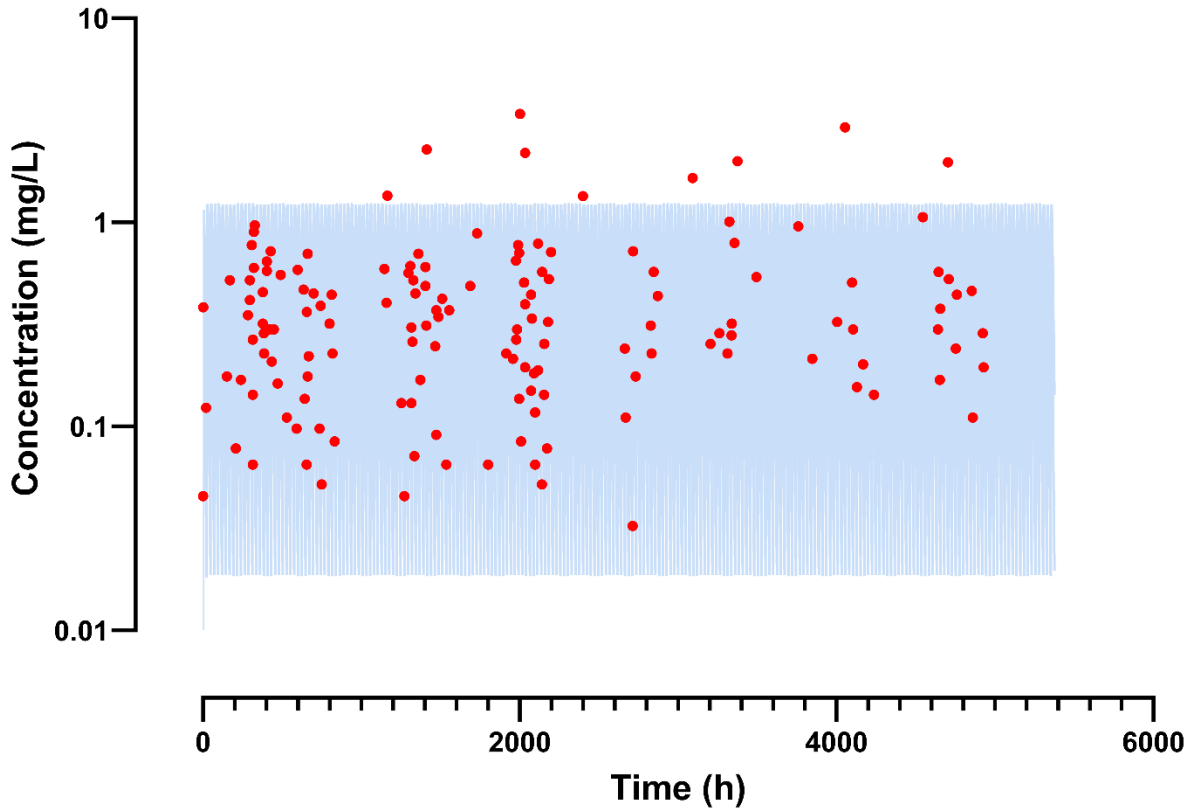


Figure 6-4. Predicted and observed plasma concentrations from the pediatric anakinra SC PBPK model. A virtual population (n=1000) individuals was created to correspond with the patient demographics in the pharmacokinetic study by Ilowite et al. [464] Individuals within this study received anakinra a dose of 1 mg/kg daily, to a maximum of 100 mg. To simulate this, the 5th-95th prediction interval (shaded region) was created for the corresponding dose. Observed individual plasma concentrations is represented by the circles.

6.4.4 ECLS-PBPK Model

The final pediatric SC ECLS-PBPK model was carried forth for evaluation upon fixing drug-specific parameters outlined in the adult model, accounting for the impact of renal impairment on clearance and applying the CRRT and ECMO compartments to the whole-body structure. The CRRT compartment was parameterized to the *ex-vivo* anakinra data previously reported (**Appendix E, Section 4.**). [450] As the observed concentrations were obtained from an individual receiving CVVHDF, this modality of CRRT was simulated while accounting for manufacture specifics in membrane surface area, thickness, filter fiber diameter and flow rates applied within the clinical setting. As outlined in **Figure 6-5.**, the addition of the CRRT

compartment to the whole-body structure improved model performance. Furthermore, accounting for the application of ECMO and potential associated edema led to successful predictions of the anakinra concentrations *in-vivo*.

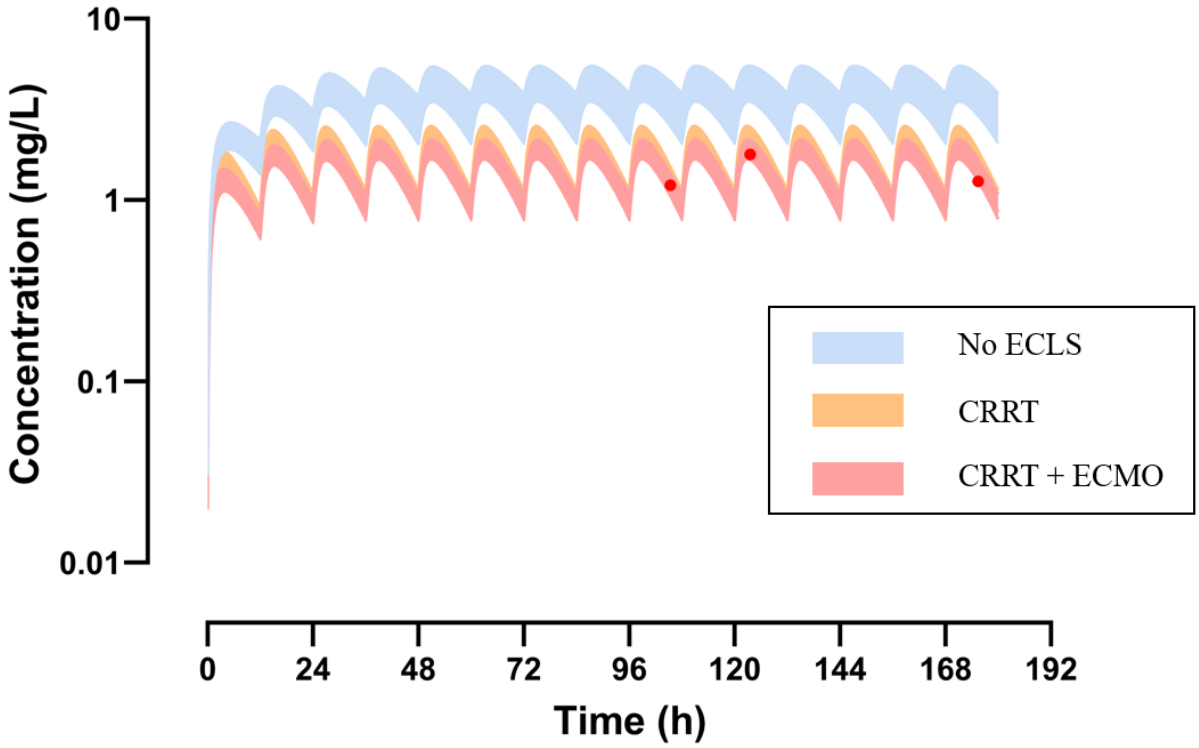


Figure 6-5. Predicted versus observed anakinra plasma concentrations of the final ECLS-PBPK model. Observed concentrations (red circles) were prospectively collected from the ongoing Opportunistic PK Study of Commonly Used Drugs in Children on ECLS for an adolescent receiving anakinra subcutaneous 100 mg every 12 hours, while be treated with simultaneous continuous renal replacement therapy (CRRT) and extracorporeal membrane oxygenation (ECMO). A virtual population (n=1000) was created, and a prediction interval (shaded region) was generated to predict the anakinra plasma concentrations. For visual representation, simulations were conducted with no extracorporeal life support (blue), with the addition of CRRT (orange) and with the addition of CRRT and ECMO (pink).
CRRT; continuous renal replacement therapy, ECLS; extracorporeal life-support, ECMO; extracorporeal membrane oxygenation, h; hours, µg/mL; microgram per mililitre.

6.4.5 Dosing Simulations

Dosing simulations were conducted for each age group, from neonates to adolescents. The *in-silico* simulations suggest that in neonates, divided doses of 10 mg/kg/d would be required to meet the C_{SS} for reduction in CRP (**Fig 6-6., A**). From infants to adolescents, each dose simulated met the suggested pharmacodynamic target. As illustrated in **Figure 6-6.**, each dosing protocol across each age bin fell well below the C_{SS} 25.2 mg/L safety threshold for anakinra. [389]

For comparison in adolescents, predicted AUC in those on ECLS was comparable to healthy individuals (**Fig 6-7.)**. The *in-silico* simulations further supports our hypothesis that renal dose adjustments may not be required due to the impact of CRRT on anakinra clearance.

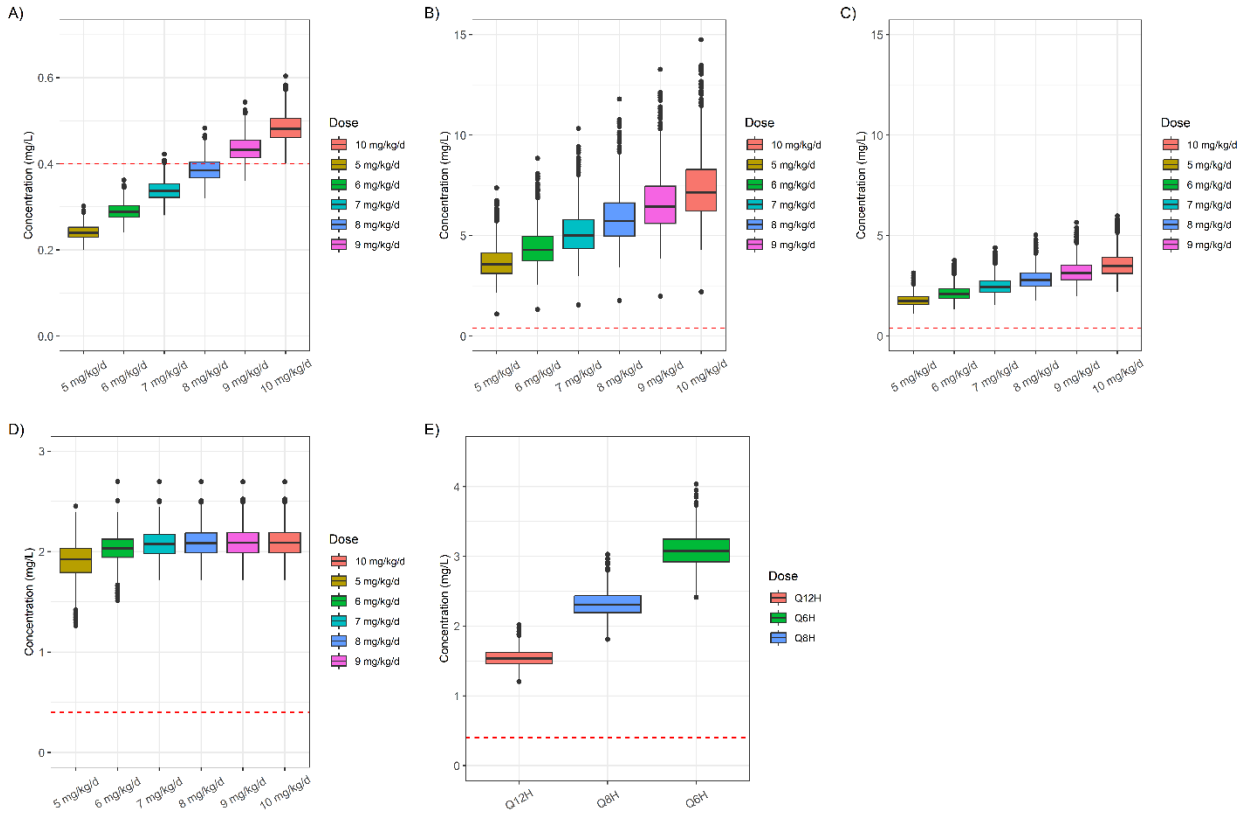


Figure 6-6. Anakinra ECLS-PBPK model dosing simulations to compare the area under the concentration time curve (AUC) at steady state in virtual adolescents receiving extracorporeal life-support (ECLS) to healthy adolescents. Virtual populations (n=1000) of adolescents (age:12-17) were created to simulate anakinra subcutaneous doses of 100 mg every 6-12 hours. The AUC at steady state was determined for those individuals receiving continuous renal replacement therapy (red), concurrent ECLS (continuous renal replacement therapy and extracorporeal membrane oxygenation; blue) and compared to a virtual population of healthy adolescents

(orange). The solid line represents the median, box represents the interquartile range, and the whiskers represent the 90th prediction interval.
AUC; area under the concentration time curve, ECLS; extracorporeal life-support, mg·h/L; milligram per hour per litre, Q6H; every 6 hours, Q8H; every 8 hours, Q12H; every 12 hours.

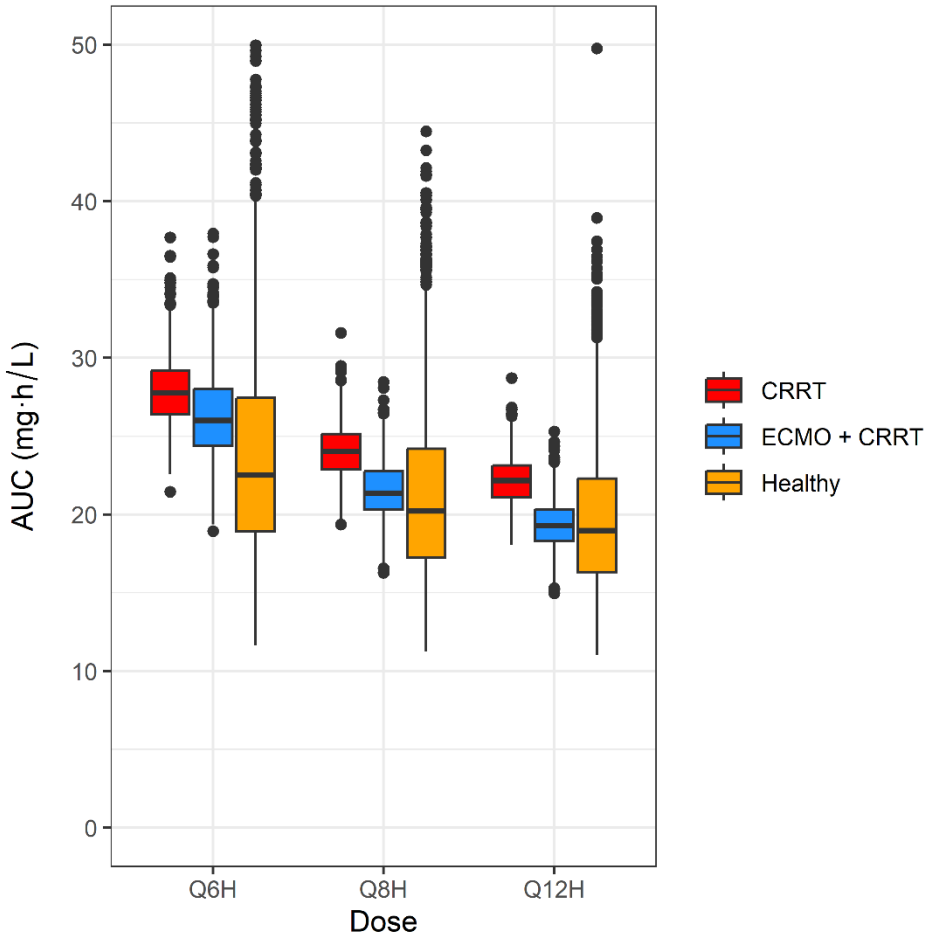


Figure 6-7. Anakinra ECLS-PBPK model dosing simulations to compare the area under the concentration time curve (AUC) at steady state in virtual adolescents receiving extracorporeal life-support (ECLS) to those who are not. Virtual populations (n=1000) of adolescents (age:12-17) were created to simulate anakinra subcutaneous doses of 100 mg every 6-12 hours. The AUC at steady state was determined for those individuals receiving continuous renal replacement therapy (red), concurrent ECLS (continuous renal replacement therapy and extracorporeal membrane oxygenation; red) and compared to a virtual population of adolescents who were not (blue). The solid line represents the median, box represents the interquartile range, and the whiskers represent the 90th prediction interval.
AUC; area under the concentration time curve, ECLS; extracorporeal life-support, mg·h/L; milligram per hour per litre, Q6H; every 6 hours, Q8H; every 8 hours, Q12H; every 12 hours.

6.5 Discussion

Appropriateness of drug dosing limits adverse events and ensures therapeutic success in the critical care setting. Due to the pathophysiological changes associated with critical illness and application of ECLS technologies, complex changes in drug PK may occur. The resulting alterations contribute to wide inter and intra-patient variability in drug PK and present challenges for clinicians in achieving appropriate pharmacotherapy. PK trials in pediatric patients receiving ECLS are pivotal to ensure safety and efficacy of dosing recommendations. However, in the current state of the literature [128,395], several limitations are presented. First, alterations in PK are drug and ECLS circuit specific as differences may arise in drug clearance via different modalities of CRRT. [102–106,395] Such differences require full PK studies to assess the impact of ECLS on the PK of each drug of interest. Secondly, ECLS technology is constantly advancing, therefore new dedicated PK studies are required upon the application of new technology. Within this approach, we sought out to address these limitations and improve generalizability amongst PK studies by integrating PBPK modelling.

The anakinra PBPK model was successfully validated upon IV and SC administration in adults prior to scaling to non-critically ill children. In the process of scaling to children, drug-specific parameters determined within the adult model were held constant, while system-specific model inputs were adjusted to the corresponding population of interest. The pediatric PBPK model successfully described the observed data from two independent data sets, upon application of different dosing strategies. [463,464] As the mechanism of proteolysis, in the kidney and potentially in the liver, remained constant between the adult and pediatric model further supports that this catabolic process may not endure any age-related changes. [461,462] Success in model performance in this population gave confidence in model structure prior to adding ECLS-specific compartments and modifications for disease states (i.e. renal impairment, edema).

The final pediatric ECLS-PBPK model was successful in capturing the observed anakinra concentrations obtained from the opportunistic PK study after the administration of a 100 mg SC dose every 12 hours, as 100% of the observed data fell within the 5th-95th prediction interval. A mechanistic description of anakinra clearance attributed to the CRRT circuit was conducted by

constructing a “CRRT organ” compartment attached to the whole-body structure. Parameterization of this compartment occurred by representing the movement of drug across the hemofilter using manufacture specifications in filter components. By defining the volume, flow rates and clearance attributed to the CVVHDF circuit, anakinra PK was predicted *in-vivo*. This modelling approach enables one to adjust CRRT circuit properties to manufacturer specifications, circuit flow rates or modality of solute removal and can be replicated upon the application of new technologies. As such, generalizability amongst populations is increased compared to traditional PK trials, providing a feasible solution to some of the current limitations.

Although ECLS-based PBPK modelling has been conducted previously, [144,150] the use of PBPK modelling to predict drug concentrations upon simultaneous CRRT and ECMO utilization in critically ill patients has yet to be established. Complications associated with sepsis increase the risk of MODS, with failure to vital organs such as the lungs and kidney being most common. [16,85,86,443] Therefore the resulting organ failure may require the need for simultaneous ECLS circuit administration. Additionally, ECMO use may contribute to exacerbating or the development of new renal impairment in these patients. [475–477] To offset these complications, the application of simultaneous CRRT-ECMO circuits in pediatric critical care settings is becoming more common. [478] Here within this approach, we successfully constructed the first ECLS-PBPK model to account for simultaneous CRRT and ECMO treatment. The addition of the ECMO compartment and edema disease state improved model performance as outlined in **Figure 6-5.** Although the addition of edema to the model structure is a simplistic representation of the true physiological response in critical illness, model performance was improved. Further characterizing the impact of ECMO use and fluid resuscitation on edema is critical for mechanistically describing drug PK in this population.

Drug dosing of anakinra for the management of acute inflammatory conditions has yet to be defined, as reported doses for adults [379,389–391,469] and pediatrics [463,464,470–472] are variable. Furthermore, the use of anakinra in pediatrics receiving ECLS is limited to small studies or case reports. [479–483] Upon successful predictions of anakinra concentrations in this population, we sought to investigate various dosing protocols to provide baseline recommendations that may be integrated into clinical practice. As illustrated in **Figure 6-6.**, each dose sustained C_{SS} well above the suggested 0.4 mg/L target necessary to maximize the

reductions in CRP for infants to adolescents. Interestingly, neonates required higher divided doses of 10 mg/kg/d to meet the C_{SS} threshold. The potential for overestimation of clearance attributed to CRRT for the *in-silico* simulations in this age group may explain these results, however the need for higher weight-based dosing in young children to prevent subtherapeutic exposure has been established for large molecules. [484–486] More specifically, the need for higher weight normalized doses of anakinra in children with lower age and body weight have been shown to maintain efficacy in those with systemic-onset juvenile idiopathic arthritis. [463,487] Further studies are warranted for confirmation, however the results presented suggest higher weight normalized doses of anakinra are required for effectiveness in younger aged children.

Extrapolation of the proposed dosing guidance in those with chronic illness, to patients with acute illness is limited by the absence of a therapeutic target in the acute setting. However, each simulated C_{SS} fell well below that reported by Fischer *et al*. [389], supporting the safety of the *in-silico* dose predictions. The need for anakinra dose titration to offset the inflammatory response is often required in the treatment of sHLH/MAS. [379,471,472] Therefore, starting with higher doses and tapering down based upon control of inflammation has been a common approach in practice. [379] The results of our *in-silico* dosing simulations suggest that this approach may be safely done in critically ill children experiencing MODS while on ECLS.

Current dosing recommendations for anakinra in those with severe renal impairment or those receiving renal replacement therapy suggest that total dose reduction via increasing the dosing interval is required. [386,473] As the result of our *ex-vivo* study demonstrated that anakinra is efficiently removed from plasma upon CRRT initiation, we hypothesized that renal dose adjustments may not be necessary for patients receiving CRRT. [450] To convey this, simulated doses in virtual adolescents receiving ECLS were compared to healthy adolescents with normal renal function (**Fig 6-7.**). The resulting simulations suggest that anakinra AUC would be similar between critically ill children with organ impairment on ECLS compared to adolescents with normal renal function. These simulations support the hypothesis that dose reductions in adolescents receiving ECLS are not required for treating acute inflammatory conditions. Further PK and clinical data in this population is necessary for confirming this hypothesis.

Despite being considered off-label, IV anakinra administration is being used to offset any potential variability in drug PK upon SC administration. Alterations in the PK of large molecules upon SC administration in critically ill patients is largely attributed to the redistribution of blood flow from peripheral tissues and edema. [31,34,36] Comparison of anakinra PK in healthy adults after the administration of a 100 mg IV or SC dose suggest that IV administration results in a significantly higher C_{max} and lower t_{max}, with similar AUC. As this was determined in healthy adults, extrapolating the similarities to the critically ill population is difficult. Our ECLS-PBPK model was evaluated upon data from an individual receiving SC anakinra, therefore no assessments of IV doses were available. However, to offset the potential variability in anakinra PK in this population, use of IV anakinra may become standard of care and further model evaluation will be essential.

Although successful predictions in anakinra PK were made, this study is not without limitations. First, the final ECLS-PBPK model was evaluated upon limited data. PBPK models are mechanistically constructed and can provide accurate predictions of drug PK when sampling is sparse. As anakinra drug concentrations were obtained from one individual, further validation of the *in-silico* dosing simulations across the age spectrum, different modalities of CRRT and flow rates are needed for complete model evaluation. In the absence of further data, confidence can be obtained in model accuracy due to the rigorous evaluation in healthy adults and pediatrics prior to extrapolating to critical illness. Secondly, a middle-out approach was applied to quantify the impact of renal dysfunction on anakinra clearance. Such approximations in those with severe CKD were carried forth to be used within the critically ill ECLS-PBPK model to simulate acute renal failure. The etiology and pathophysiology of acute vs chronic renal failure may differ substantially, however similarities in renal vasculature injury, tubular dysfunction and reductions in glomerular filtration may present similar reductions in the renal handling of drugs in the most severe stages of each. [488,489] Although this modelling approach provided a mechanistic representation to the impact of critical illness and organ failure on anakinra clearance, further information on the impact of different degrees of AKI on anakinra PK is necessary. Finally, the absolute bioavailability determined in severe CKD was applied in the critically ill population within these simulations. Both critical illness and CKD may impact the PK of drugs administered subcutaneously as a result of fluid accumulation and redistribution of blood flow from the peripheral tissues. [31,490–492] Although the model was evaluated with limited data, this

approximation appears to hold true. As more data is collected in acutely ill patients receiving SC anakinra, further evaluation on the bioavailability will be made.

6.6 Conclusion

In conclusion, the anakinra ECLS-PBPK model constructed in this study provides an approach to determining drug dosing in critically ill children experiencing MODS. By incorporating *ex-vivo* anakinra results and physiological alterations associated with critical illness, successful predictions of observed concentrations were made. Although the dosing regimen of anakinra in this population has yet to be determined, by accounting for the impact of drug clearance by the ECLS circuits, the dosing simulations presented within the study suggest that renally adjusted dosing regimens may not be required.

Incorporating ECLS-based compartments to the whole-body PBPK structure has been done previously, therefore this study gives confidence to the methodological approach and demonstrates the generalizability to different drugs and ECLS circuits. Additionally, this approach is the first to simultaneously incorporate both CRRT and ECMO compartments within a PBPK model. As the clinical application of concurrent ECLS circuits in the critical care setting becomes more common, this modelling approach provides a feasible solution in determining accurate dose predictions to guide bed-side dosing recommendations or assist with clinical trial planning by reducing the number of children enrolled in clinical trials.

Chapter 7: Defining safe and effective cefazolin dosing regimens for MSSA infections in the CNS: leveraging sparse real-world data and PBPK modeling

This chapter is reflective of an original manuscript in preparation by the PhD candidate (Samuel Dubinsky) for peer-reviewed journal publication. All pertinent dialogue in this chapter was written by the PhD candidate.

7.1 Overview

Infections in the central nervous system (CNS) are serious and carry a significant risk of mortality and morbidity. Use of cefazolin as a treatment alternative for CNS infections due to methicillin-susceptible *Staphylococcus aureus* (MSSA) has been debated due to the perceived inability of adequate concentrations at the site of infection. To leverage sparse observed cefazolin concentrations in the cerebrospinal fluid (CSF) and derive an understanding of the dose-exposure-response profile for MSSA infections in the CNS, physiologically-based pharmacokinetic (PBPK) modelling was used. The cefazolin CSF-PBPK model was successfully validated such that observed maximum and minimum CSF concentrations were accurately predicted. Additionally, the median predicted cefazolin CSF:plasma ratio was 4.51% compared to an observed value of 4.3%. *In-silico* simulations demonstrate that a continuous infusion of 10 g/day may be required to ensure 90% probability of target attainment (PTA) for an MIC $\leq$ 2 mg/L. Predicted plasma and CSF concentrations were well below concentrations associated with neurotoxicity. This study is the first to use sparse observed CNS data to develop an evaluated mechanistic model to describe the pharmacokinetics of cefazolin in the CSF. This work provides evidence in the safety and efficacy of cefazolin for the treatment of CNS infections attributed to MSSA with an evaluated model for use in future clinical trial planning.

7.2 Introduction

The penetration of antistaphylococcal β-lactams into the cerebrospinal fluid (CSF) and brain tissue has remained an area of interest for several years. Due to the perception of a more favourable physicochemical profile to improve penetration, [493,494] antistaphylococcal penicillin's such as intravenous oxacillin, nafcillin or cloxacillin are recommended for treatment of meningitis or ventriculitis due to methicillin susceptible *Staphylococcus aureus* (MSSA) by the Infectious Disease Society of America (IDSA). [495,496] Despite evidence indicating similar efficacy, and improved tolerability of cefazolin compared to antistaphylococcal penicillin's in the management of non-CSF infections, [497,498] guideline recommendations do not support cefazolin as an alternative for central nervous system (CNS) infections. [495] Therefore, in cases of an inability to administer antistaphylococcal penicillin's due to toxicity or anaphylaxis, one may be left to utilize non β-lactam alternatives such as vancomycin. Use of vancomycin in the treatment of MSSA in other clinical scenarios has been shown to be inferior. [499] Therefore revisitation of the use of cefazolin as a viable treatment option is imperative to ensure clinical success in this population.

Drug penetration in the CNS is dependent on several physicochemical properties such as molecular size, the degree of protein binding, lipophilicity and affinity for efflux drug transporters at the blood brain barrier. [500,501] The presumed inability of cefazolin to achieve therapeutic concentrations in the CSF is thought in part to be due to the relatively high protein binding (90%), low lipophilicity (logP= -0.24 to 0.3) and affinity for brain efflux pumps. [307,502–504] However, first generation cephalosporins, such as cefazolin, share many of the same physicochemical properties as recommended antistaphylococcal penicillin's.

Evidence supporting adequate cefazolin CNS penetration is largely limited to animal models and poorly sampled human studies. Recently, a case report and case series determined that administration of a cefazolin continuous infusion, guided by therapeutic drug monitoring, is both safe and efficacious in treating CNS infections. [494,505] Additionally, a pharmacokinetic (PK) study by Novak *et al.* [506] determined that the cohort-extrapolated median CSF to serum ratio was 8.4% in patients with external ventricular draining devices (EVD) receiving common infectious prophylactic doses. It was concluded that CSF concentrations may be adequate to meet pharmacodynamic endpoints with administration of standard therapeutic doses.

Challenges in conducting dedicated pharmacokinetic (PK) studies in this population are multifactorial due to the relatively low incidence rates of infections and invasive nature of lumbar puncture procedures. [495,496,507] This has resulted in limited data to support the use of cefazolin as a treatment alternative for active CNS infections. To leverage sparse observed cefazolin CSF concentrations and derive understanding of the dose-exposure-response profile for MSSA infections in the CNS, physiologically-based pharmacokinetic (PBPK) modelling can be used. These models characterize the PK of drugs based on mechanistic principles and known drug specific properties, with model structures defined by physiological compartments relevant to drug disposition, such as the CNS. [508] Because these models are not built on PK data, which in this case may be sparse, they can be developed with underlying mechanistic knowledge and subsequently validated with limited observed data. Validated models are often used for dose regimen design taking into account efficacy and safety. [145,509]

The primary objective of this study is to develop a PBPK model of cefazolin in adults that accurately predicts CSF concentrations. Such predictions will be then used to inform optimal dosing strategies based on known efficacy and safety thresholds for the treatment of meningitis or ventriculitis caused by MSSA. Impact of this modeling strategy will improve confidence in the use of cefazolin in this patient population and provide the framework for future clinical trial planning and/or product-label indications.

7.3 Methods

7.3.1 Software

The cefazolin adult intravenous (IV) PBPK model was constructed using PK-Sim version 11.1 as part of the Open Systems Pharmacology suite (www.open-systems-pharmacology.org). Parameter sets for healthy adults and aged persons in European and American populations have been described previously. [289,290] Clinical data was digitized using WebPlot Digitizer v4.6 (https://automeris.io/WebPlotDigitizer). Graphic illustrations were completed using R programming language version 4.1.1. (R Foundation for Statistical Computing, Vienna, Austria) and GraphPad Prism version 10.0.0 (Boston, Massachusetts, USA).

7.3.2 Healthy Adult Cefazolin PBPK Model Development

A PBPK model for IV cefazolin was constructed to mechanistically represent the PK in healthy adults. Briefly, the cefazolin model was developed by collecting and appraising the physicochemical properties and PK characteristics associated with distribution and clearance from the literature.

Clearance of cefazolin is predominantly attributed to renal clearance as most of the drug is excreted in urine unchanged (75-93%). [415,510] Renal tubular secretion dominates, as renal clearance far exceeds the glomerular filtration rate (GFR). [419,510] Organic anion transporters (OAT) are responsible for uptake into renal tubular epithelium and multi-drug resistance protein (MRP) transporters facilitate the efflux of cefazolin into tubular filtrate. [504,511] Information regarding expression and localization of renal transporters was extracted from Ivanyuk *et al*., [301] and Ci *et al*. [511]

A detailed report including input parameters and characteristics of the *in-vivo* PK studies used for model development may be found in **Appendix F, Section 1.** The cefazolin model constructed in this study was built upon the previously developed model by Dallmann *et al*., [504] while incorporating active tubular secretion and saturable protein binding. Additionally, an alternative cefazolin PBPK model constructed by Szeto *et al*. [512], which includes a slightly different interpretation of the data deserves reading.

7.3.3 Healthy Adult Cefazolin PBPK Model Evaluation

Verification of model accuracy was conducted using the average fold error (AFE; bias) and absolute average fold error (AAFE; precision). Acceptance was confirmed if AFE <30% (0.7-1.3) and AAFE ≤2 for simulated mean drug concentrations (**Appendix F, Section 1.2.1.4**). For data sets including individual patient samples, the predictions were considered acceptable if 85-95% of observed concentrations fell within the 90th prediction interval of a relevant population (**Appendix F, Section 1.2.1.4**).

7.3.4 Adult Cefazolin CSF-PBPK Model Development

In the PBPK model structure, the brain compartment is represented using the following four default subcompartments: blood, plasma, interstitial fluid, and intracellular compartments. With each compartment being linked to the whole-body structure through arterial and venous

blood. [513] The interstitial fluid compartment will be used as a surrogate for CSF cefazolin concentrations, a modeling strategy that has been done previously. [508,514,515] Drug permeability into the brain will be determined by Eq 7-1.

$$P = \left(\frac{MW_{eff} * 10^9}{366}\right)^{-6} * \frac{10^{logP}}{5} * 10^{-5}$$

Eq 7-1.

Where *P* is the specific organ permeability, MW_{eff} is the effective molecular weight, and logP is lipophilicity. [513] Due to limited data informing permeability into the brain, cefazolin permeability was optimized using the observed data from Grégoire *et al*. [505] (**Appendix F, Section 2.**)

Multiple drug transporters are located at the blood-brain barrier as a method of drug efflux back to systemic circulation. [501] Proteomic data indicates that both OAT and MRP4 are expressed at the blood-brain barrier. [516–518] Due to limited data on specific quantification of transporter expression, localization of OAT and MRP4 at the blood-brain barrier were incorporated within the model from the reverse transcriptase polymerase chain reaction (RT-PCR) dataset implemented within PK-Sim. [519] It was assumed that the maximum rate of transport (V_{max}) for OAT and MRP4 was consistent with the value quantified in the renal proximal tubule.

A local sensitivity analysis was performed to determine model parameters that influence the CSF $AUC_{dosing\ interval}$ at steady state upon doses of cefazolin IV 2000 mg every eight hours. Detailed methods describing the sensitivity analysis may be found in **Appendix F, Section 2.**

7.3.5 Adult Cefazolin CSF-PBPK Model Evaluation

The cefazolin adult CSF-PBPK model was evaluated using observed CSF concentrations from adults receiving cefazolin for the treatment of meningitis due to methicillin-susceptible *Staphylococcus* or prophylaxis. [494,506] Comparison of the directly measured maximum (C_{max}) and minimum (C_{min}), along with a 4 hour post-dose measurement of cefazolin CNS concentrations was completed. [506] Additionally, predicted CSF:plasma ratios (%) were

compared to observed data by Le Turnier *et al*. [494] A fold-error of 1.5 (0.67-1.5) (Eq. 7-2) was deemed acceptable.

$$Fold - Error = \frac{Predicted_{PKparameter}}{Observed_{PKparameter}}$$

Eq. 7-2

Demographics of the study participants used for cefazolin CSF model evaluation are presented in **Table 7-1**.

Table 7-1. Summary of pharmacokinetic studies used to evaluate the cefazolin-CSF PBPK model.

Novak *et al.* [506]		
	Observed Data	**Simulated Data**
Administration	Intravenous	Intravenous
Dose (mg)	2000 mg Q8H (n= 13/15)	2000 mg Q8H
n	15	1000
Age (y)	56 [51-60][a]	51-60[b]
Height (cm)	167.6 [163.9-172.7][a]	163.9-172.7[b]
Weight (kg)	71.7 [65-89][a]	65-89[b]
Sex (% female)	80	80
Le Turnier *et al.* [494]		
	Observed Data	**Simulated Data**
Administration	Intravenous	Intravenous
Daily Dose (mg/day)	8000 CI [7.88-8][a,c]	8000 CI
n	8	1000
Age (y)	58.4 [50.3-74]	50.3-74[b]
BMI (kg/m^2)	25.9 [24.2-26.9]	24.2-26.9[b]
Sex (% female)	25	25

BMI; body mass index, CI; continuous infusion, cm; centimetres, kg; kilograms, mg; milligrams, Q8H; every 8 hours, y; years.

[a] data presented as median [IQR]

[b] data presented as range

[c]All study participants in cefazolin cohort received dose as a continuous infusion

7.3.6 Dose-Exposure Assessment

Cephalosporins are classified as time-dependent antibiotics with several *in vitro* and animal studies determining that the amount of time the free drug concentration exceeds the minimum inhibitory concentration (MIC) in plasma (*f*T>MIC) is the best predictor of bacterial

killing and response. [425–427] Although these targets may differ slightly for drug-bacteria combinations, it is generally assumed that for cephalosporins a *f*T>MIC of 35-40% and a *f*T>MIC of 60-70% provides bacteriostatic and near-maximal bactericidal effects, respectively. [425–427] Additionally, higher pharmacodynamic targets (*f*T>MIC 100%) have been suggested to improve patient outcomes in those with severe infections. [520] Data on pharmacodynamic targets at the site of infection are unavailable and, as a result, plasma targets were used.

The Clinical and Laboratory Standards Institute (CLSI) and the European Committee on Antimicrobial Susceptibility Testing (EUCAST) have eliminated cefazolin MIC breakpoints for Staphylococcus *aureus*, however, utilize oxacillin as a surrogate. [521] EUCAST $MIC_{50/90}$ for MSSA are 0.5 mg/L and 1 mg/L, respectively, with an epidemiological cut off of 2 mg/L. [522] Therefore, MIC distributions of 0.0625-2 mg/L were examined within the pharmacodynamic assessments. A probability of target attainment (PTA) of 90% towards a 100% *f*T>MIC was deemed acceptable within the dosing simulations.

7.3.7 Safety Assessment

Cefazolin at product-labeled doses is generally well-tolerated, however in cases of excessive dosing or accumulation due to altered clearance, concern for neurotoxicity remains. Small case-reports imply that plasma trough concentrations ≥300 mg/L and CSF trough concentrations ≥30 mg/L were associated with neurotoxicity such as seizures. [523–525] The safety of the simulated dosing protocols were assessed by comparing concentrations that define safety with population based trough concentrations. The 90th percentile of steady state trough concentrations in plasma and CSF below safety limits will ensure that 90% of the virtual population will have cefazolin concentrations below the toxic threshold in each reference fluid.

7.4 Results

7.4.1 Healthy Adult Cefazolin PBPK Model Evaluation

The cefazolin population PBPK model was validated using observed plasma concentrations from the PK studies by Smyth *et al*.,[415] and Philipson *et al*.[526] (**Appendix F, Section 1**). The developed model accurately captured the observed data, with the population simulations meeting AFE and AAFE criteria, (**Appendix F, Section 1.2.1.4**) when compared to

observed data by Smyth *et al*. [415] Additionally, 90% of the observed data from the study by Philipson *et al*. [526] fell within the 90th prediction interval of the population PBPK model.

7.4.2 Adult Cefazolin CSF-PBPK Model Evaluation

The final healthy adult cefazolin IV population PBPK model was carried forward to evaluate the CSF concentrations from two PK studies. First, a virtual population (n=1000) of adults was created to represent the study demographics in Novak *et al*. [506] (**Table 7-1.**). Participants received cefazolin IV 2000 mg every eight hours for prophylaxis due to insertion of an EVD. CSF samples were drawn at a median of 2.5 days after the administered dose. The cefazolin CSF-PBPK model successfully captured the directly measured maximum (11.5 mg/L) and minimum (0.78 mg/L) CSF concentrations. The median predicted CSF concentration 4-hour post dose concentration was 1.83 mg/L compared to the observed value of 1.87 mg/L, equating to a fold-error of 0.98 **(Figure 7-1.)**. Model predicted median cefazolin CSF $AUC_{dosing\ interval}$ of 20.93 mg·h/L was within a 1.25 fold-error compared to cohort extrapolated median observed value of 18.19 mg·h/L. Additionally, the cefazolin PBPK model successfully captured the observed plasma AUC, with a predicted $AUC_{dosing\ interval}$ of 446.22 mg·h/L compared to an observed value of 302.40 mg·h/L. [506]

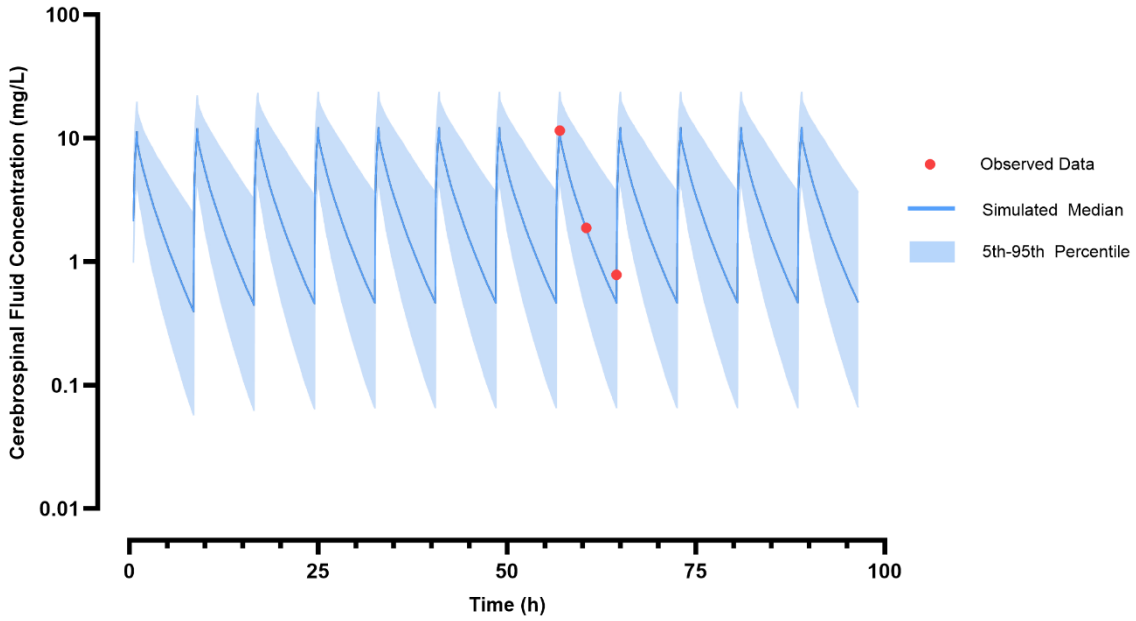


Figure 7-1. Population verification of the observed cefazolin cerebrospinal fluid (CSF) concentrations from individuals within the study by Novak *et al.* [506] CSF concentrations of cefazolin were obtained at a median of 2.5 days after the first administered dose from a dosing protocol of intravenous cefazolin administered every 8 hours. Predicted cefazolin maximum, minimum and 4-hour post dose cefazolin concentrations were compared to the observed values (circles). The solid line represents the median CSF concentrations with the shaded region representing the 5th-95th percentile of the virtual population.

To further evaluate the accuracy of the cefazolin CSF-PBPK model, a second comparison was made using CSF concentrations from participants in the case series by Le Turnier *et al*. [494] In this study, cefazolin was administered as a continuous infusion of 8 g/day for the treatment of proven meningitis with positive CSF cultures for *Staphylococcal* species. [494] Median observed CSF:plasma ratio was 4.3 %, while median model predicted CSF:plasma ratio of cefazolin was 4.51 %; a fold-error of 1.05. A visual representation of model predicted CSF concentrations compared to observed values is shown in **Figure 7-2**.

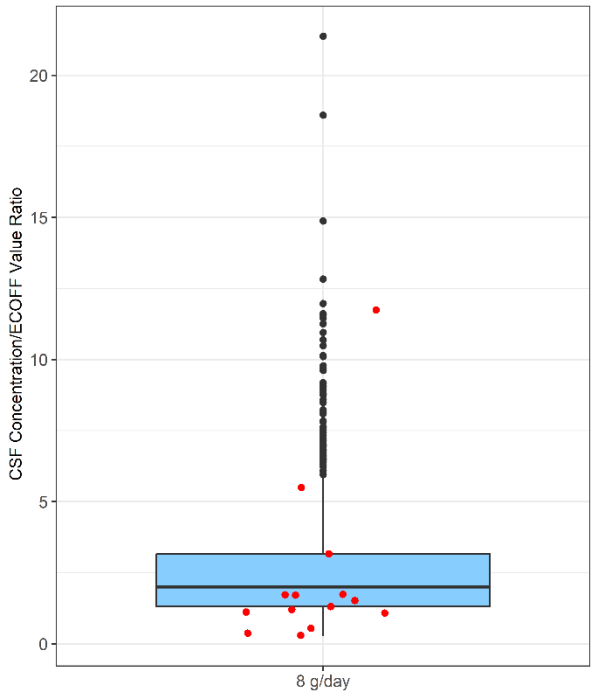


Figure 7-2. Population verification of the observed cefazolin cerebrospinal fluid (CSF) concentrations from individuals within the study by Le Turnier *et al*. [494] CSF concentrations of cefazolin (red dots) were obtained 24 hours after initiating a continuous infusion of 8 g/day. Data presented as a function of the EUCAST epidemiological cutoff (ECOFF) of 2 mg/L for methicillin-susceptible Staphylococcus aureus. The solid line represents the median, box represents the interquartile range, and the whiskers represent the 90th prediction interval.

Based on a local sensitivity analysis the most influential parameters on CSF exposure were brain permeability, transporter concentration expressed at the proximal tubule and blood brain barrier, fraction unbound and GFR. Results of the sensitivity analysis are presented in **Appendix F, Section 2.4.**

7.4.3 Dose-Exposure Assessment

To analyze the probability of target attainment (PTA) of cefazolin for CNS infections attributed to MSSA, several dosing protocols were simulated in a virtual populations with demographics as in Le Turnier *et al*. [494] A dosing protocol of 10g/day continuous infusion achieved 90% PTA for 100% fT>MIC to a MIC ≤ 2 mg/L. However, when evaluating the PTA using more conservative pharmacodynamic targets of 35-70% fT>MIC, [425–427] model predicted 90% PTA was achieved with standard infusion times (i.e. 30 minutes) of cefazolin IV 2000 mg every 8 hours for $MIC_{50/90}$ of 0.5 mg/L and 1.0 mg/L, respectively (**Appendix F,**

Section 3) . Visual illustrations of the PTA for the simulated cefazolin dosing protocols within each population are presented in **Figure 7-3.**, while the PTA to achieve 100% *f*T>MIC of each dose is presented in **Table 7-2.**

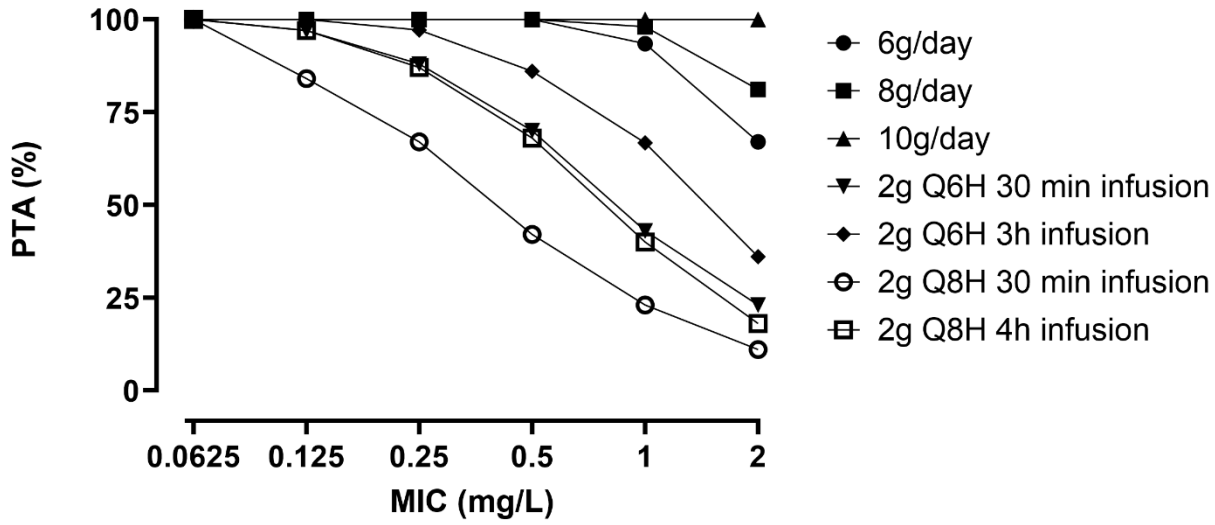


Figure 7-3. Target attainment of several cefazolin dosing protocols to reach 100% fT>MIC in the cerebrospinal fluid for the virtual population of participants from the study by Le Turnier *et al.* [494] A range of cefazolin MIC values for methicillin-susceptible Staphylococcus aureus (MSSA) were tested as per CLSI and EUCAST breakpoints. An epidemiological cutoff of 2.0 mg/L was incorporated. A probability of target attainment of 90% was deemed appropriate.

Table 7-2. Pharmacodynamic target attainment of simulated cefazolin dosing protocols for methicillin-susceptible Staphylococcus aureus. Data presented as the probability of target attainment in which the unbound cefazolin concentrations are 100% above the minimum inhibitory concentration (% fT>MIC) in the cerebrospinal fluid.

MIC (mg/L)	6g/day CI	8g/day CI	10g/day CI	2g Q6H 3h infusion	2g Q6H 30 min infusion	2g Q8H 4h infusion	2g Q8H 30 min infusion
0.0625	**100**	**100**	**100**	**100**	**100**	**100**	**100**
0.125	**100**	**100**	**100**	**100**	**97**	**97**	84
0.25	**100**	**100**	**100**	**97**	88	87	67
0.5	**100**	**100**	**100**	86	70	68	42
1.0	**93.4**	**98**	**100**	66.7	43	40	23
2.0	67	81.1	**100**	36	23	18	11

A Probability of target attainment of >90% to a 100% fT>MIC is represented in bold.
CI; continuous infusion, g; grams, h, hours, min; minutes, MIC; minimum inhibitory concentration, Q6H; every 6 hours, Q8H; every 8 hours.

7.4.4 Safety Assessment

Predicted trough concentrations in CSF and plasma from each dosing protocol fell well below the safety thresholds (**Table 7-4.)**. Potentially neurotoxic cefazolin CSF concentrations were not predicted in 90% of the virtual population for each simulated dose. A safety assessment using cefazolin IV 2000 mg every 6 hours with a 3-hour infusion time is presented in **Figure 7-4.**

Table 7-3. Cefazolin safety assessment. Data presented as trough concentrations of the 90th percentile within the virtual population for cerebrospinal fluid and plasma.

Dosing Regimen	CSF Concentration (mg/L)	Plasma Concentration (mg/L)
6g/day CI	6.65	106.82
8g/ day CI	9.62	148.81
10g/day CI	13.05	194.90
2g Q6H 3h infusion	5.58	91.68
2g Q6H 30 min infusion	3.93	67.24
2g Q8H 4h infusion	3.25	55.24
2g Q8H 30 min infusion	2.08	35.81

CI; continuous infusion, CSF; cerebrospinal fluid, g; grams, h, hours, min; minutes, Q6H; every 6 hours, Q8H; every 8 hours.

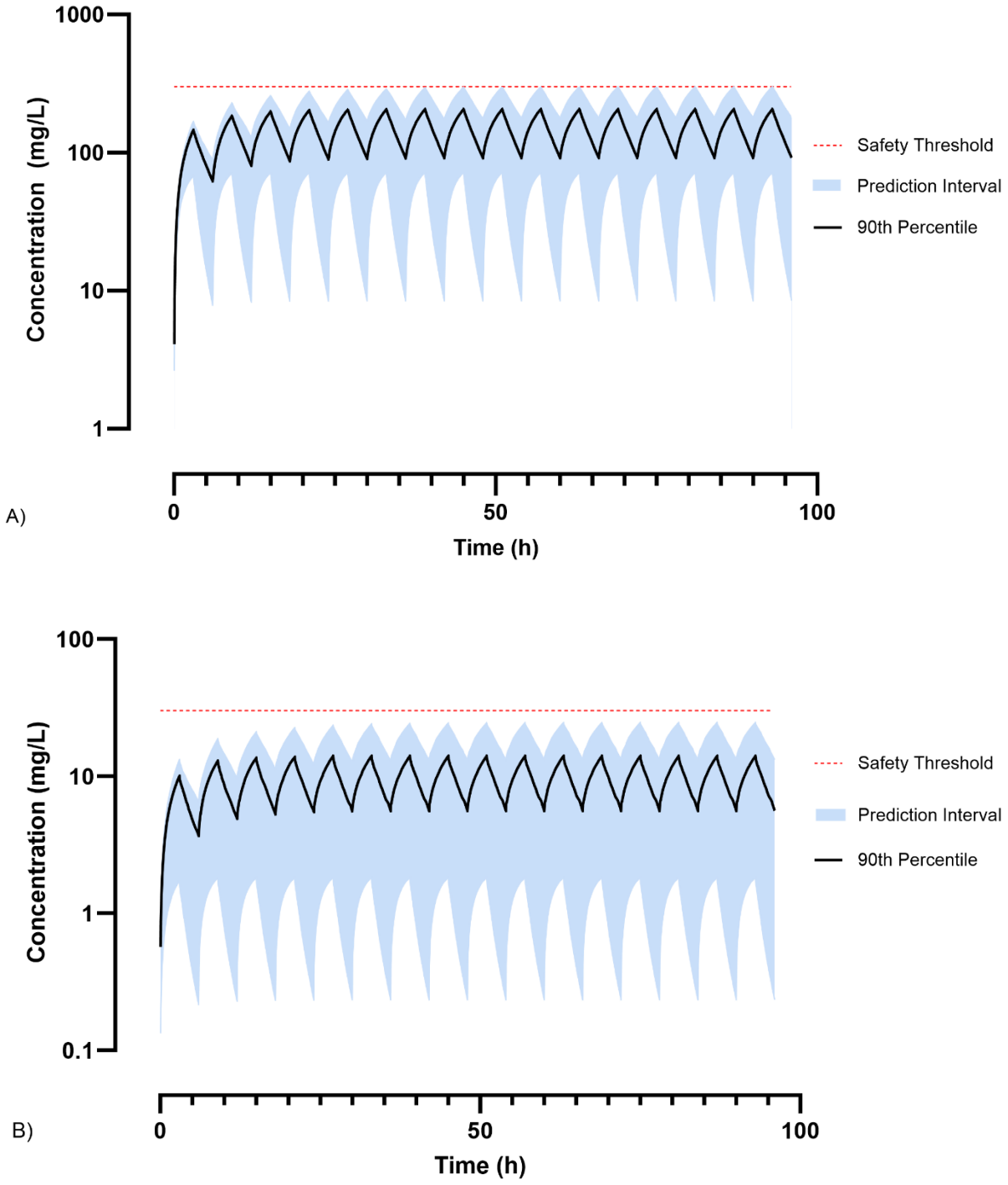


Figure 7-3. Visual illustration of cefazolin safety assessment. A simulated dose of cefazolin IV every 6 hours after a 3-hour infusion time was conducted for illustration purposes. The simulated trough in plasma (A) and cerebrospinal fluid (B) was evaluated to neurotoxicity threshold suggested to increase the likelihood of cefazolin induced neurotoxicity (dotted red line). The simulated range of plasma concentrations may be shown in the shaded region, with the solid black line representative of the 90th percentile in each reference fluid.

7.5 Discussion

CNS infections are serious and carry a significant risk of mortality and morbidity. [527] Adequate treatment requires timely administration of antimicrobials tailored against likely organisms. In addition to prompt initiation, sufficient antimicrobial concentration at the site of infection is critical. Penetration of drug from plasma to the CSF is dependant on several physicochemical properties such as molecular weight, lipophilicity, plasma protein binding, or whether the drug is a substrate of efflux transporters at the blood brain barrier. [501] Concerns for use of cefazolin as a treatment alternative for CNS infections is thought in part to be due to less favourable physicochemical characteristics compared to antistaphylococcal penicillin's. However, cefazolin and antistaphylococcal penicillin's are largely similar in their lipophilicity, degree of protein binding, [528] and are both substrates of drug-efflux transporters located at the blood-brain barrier. [301,516–518]

Despite these similarities, minimal CSF concentration comparisons have been reported. The first study to analyze potential differences in brain tissue concentrations was conducted by Frame *et al.* Average brain tissue concentrations of cefazolin (10.6 μg/g) were noticeably higher than nafcillin (2.7 μg/g) and methicillin (2.0 μg/g) after administration of a single IV dose in patients undergoing a craniotomy. [529] Furthermore, Le Turnier *et al.* noted a higher CSF:plasma ratio for cefazolin compared to cloxacillin in their study population. [494] With the resemblances in physicochemical properties in addition to the higher concentrations of cefazolin in the CSF [494] and brain tissue [529] than antistaphylococcal penicillin's, the longstanding dogma of inadequate cefazolin concentrations in the CNS should be refuted.

Drug associated characteristics play a significant role in determining penetration across the blood brain barrier into the CSF. In addition, the disposition of drug into the CNS may also be defined by host related physiological changes. Disruption of the blood brain barrier is an important component of the pathophysiology of CNS infections, resulting in increased permeability. Pathogens may affect the barrier integrity by direct toxic affects or triggering increased expression of inflammatory cytokines in response to infection. [530–532] Furthermore, increased cytokine production may inhibit several efflux pumps known to remove β-lactams out of the CSF. [533,534] Implications of this host-response results in higher drug concentrations due

inflammation compared to an intact blood-brain-barrier. [535,536] The presence of meningeal inflammation renders the drug-specific properties less important in governing drug entry into the CNS. [501] As incorporated in the model, cefazolin is a substrate for the OAT and MRP active transport systems.[504,511] both of which have been shown to be localized at the blood-brain barrier. [516–518] This physiological response was accounted for in model development through optimization due to limited *in-vitro* and *in-vivo* data to quantify to impact of inflammation on achieving cefazolin concentrations in the CNS. More information gained may allow for "infection-related" factors to scale the brain permeability constants within the model. Future research on the impact of infection on initial cefazolin CSF concentrations, and over the course of treatment is critical for further model refinement and design of dosing regimens in this population.

Limited clinical data on the use of cefazolin for CNS infections due to MSSA is available. An initial case report of a patient with MSSA (MIC = 0.5 mg/L) ventriculitis was successfully treated with an initial cefazolin dose of 10 g/day as a continuous infusion, followed by 8 g/day. [505] Median CSF concentrations were 11.9 mg/L and 6.1 mg/L, respectively. Despite the administration of high dose cefazolin, no adverse effects in this patient were reported. Furthermore, a case-series by Le Turnier *et.al* investigated the use of a cefazolin continuous infusion (8g/day) to patients with CSF-culture confirmed *Staphylococcal* meningitis. [494] All patients in the cefazolin cohort were successfully treated, with no recurrence of infection. The elevated CSF concentrations reported by Le Turnier *et al.*[494] were higher than what was reported by Novak *et al*, [506] suggesting a relationship between administered dose and/or brain permeability to CSF concentrations. This hypothesis was further confirmed within our sensitivity analysis, as both administered dose and brain permeability were highly influential on the CSF $AUC_{\text{dosing interval}}$ (**Appendix F, Section 2.4.**) Despite differences in dosing strategies and cefazolin concentrations, each study suggested pharmacodynamic targets for MSSA would be achieved.

One of the objectives of this study was to provide a pharmacodynamic analysis to investigate doses that would achieve adequate concentrations in the CSF. Using a predetermined pharmacodynamic target of 100% fT>MIC for a MIC ≤ 2.0 mg/L, a continuous infusion of cefazolin 10g/day was required to ensure a 90% PTA in the virtual population (**Table 7-2.**).

However, the *in-silico* simulations imply that more conservative pharmacodynamic targets (35-70% fT>MIC) may be achievable with standard cefazolin doses to a MIC ≤ 1.0 mg/L. Recommendations from a recent narrative review suggest doses of cefazolin IV 2 g every 6 hours or as a continuous infusion of 8-10 g/day may be required to effectively treat CNS infections due to MSSA. [528] Our results support these recommendations to a MIC ≤ 1.0 mg/L, however to ensure >90% PTA of 100% *f*T>MIC to an MIC ≤ 2.0 mg/L a continuous infusion of 10 g/day would be recommended. (**Table 7-2.**). As infections in the CNS are serious, we encourage targeting more aggressive pharmacodynamic endpoints to ensure clinical success. Therefore, knowledge of the MIC is prudent to ensuring successful pharmacotherapy with cefazolin in this patient population.

The extrapolation of pharmacodynamic targets from plasma to tissue-specific sites in this analysis are worth mentioning, and further research is required to ensure that this holds true. [537–539] In an experimental rabbit meningitis model, β-lactams maintained their time-dependent activity in the CSF similar to that in plasma. [540] Optimization of fT>MIC for β-lactams in plasma can occur with the use of continuous infusions. [440–442] Although comparisons of continuous infusions to standard bolus doses for increasing pharmacodynamic targets in the CNS are limited, Huang *et al*. demonstrated that the AUC_{CSF}/AUC_{plasma} ratio of cefepime was increased with a continuous infusion compared to intermittent dosing. [541] Until further data supports alternative pharmacodynamic targets in specific sites of infection, extrapolating PTA from plasma is reasonable and optimizing fT>MIC with continuous infusion appears to be superior.

Safe use of cefazolin as a therapeutic alternative for CNS infections has been in question for decades due to concern for neurotoxicity at elevated doses. High concentrations of cephalosporins within the CNS lowers the seizure threshold through competitive antagonism of the $GABA_A$ receptors in a dose-dependant manner. [542,543] Cefazolin is believed to be the most likely of the class to induce seizure activity, however case-reports include intraventricular administration [544] or excess dose in those with altered renal clearance. [523–525] Predicted trough concentrations were all well below reported CSF and plasma concentrations in those experiencing neurotoxicity (**Table 7-3**.). [523–525] Further, GFR significantly impacted cefazolin exposure in both plasma and CSF upon the sensitivity analysis (**Appendix F, Section**

2.4.), therefore caution is to be applied in patients with altered renal clearance. Investigations in patients with renal impairment is critical to ensure safety in this population.

Limitations to the cefazolin-PBPK model included few CNS PK studies for development and evaluation. Ideally, multiple observed data sets of cefazolin CNS concentrations would be available. This however highlights the advantages of a PBPK approach as sparse observed data is used to confirm model predictions, making use of various data sources to further understanding. Secondly, permeability of the blood brain barrier is highly variable and presence of meningeal inflammation due to infection is a significant determinant of drug penetration. [501,545] Brain permeability was an important parameter defining CNS exposure and further refinement in different populations will be needed. Finally, the model assumed that cefazolin active transport for OAT and MRP4 at the blood brain barrier was equated to that in the renal proximal tubule. Until further *in vitro* or *in vivo* data is available, these assumptions are reasonable.

7.6 Conclusion

Previous PBPK models have been able to predict the PK of cefazolin in different populations. [504,512] Although successful in describing concentrations in plasma, absence of a mechanistic quantification of cefazolin-transporter activity and saturable protein binding limit the generalizability of these models in describing the disposition of drug into different physiological compartments, such as the CNS. By incorporating and evaluating these unique properties throughout model development, the cefazolin-CSF PBPK model within this study provides a mechanistic representation of penetration into the CSF, resulting in accurate predictions of drug concentrations. [494,506]

In conclusion, this study provides the first cefazolin PBPK model to predict drug concentrations in the CSF compartment for adults. Additionally, pharmacodynamic and safety assessments were implemented across several different dosing regimens to optimize the fT>MIC in the treatment of MSSA associated CNS infections. PBPK modeling offers several advantages in this population as it can provide accurate assessments with limited samples due to a mechanistic understanding of drug PK. The results presented should be seen as a call for future research. Uncertainty remains in several aspects of the model and the potential for variability in cefazolin concentrations warrants more data to confirm safe and effective use. As the PBPK

model provides a mechanistic understanding of drug transport into, and out of the CNS, the model may be adapted to different populations including those with organ impairment or the pediatric population.

Chapter 8: Discussion, Conclusions, and Future Directions

8.1 Discussion

This thesis aims to advance knowledge of PK for medications in the critically ill population and apply principles in PBPK to improve dose optimization and support clinical trial planning. Critical illness is heterogeneous in nature, and by extension the impact on PK can be variable. Therefore, each chapter of this thesis describes the efforts towards improving our understanding of pathophysiology and PK associated with critical illness to support the improvement of pharmacotherapy.

As outlined in Chapter 1, the pathophysiological response may have varying impacts on drug PK. Not only does this result in wide interindividual variability in PK, but due to the unstable nature of critically ill patients, one may also expect a significant degree of intraindividual variability. [432,433,520,546] This poses extreme challenges to the clinical and research community in ensuring success in pharmacotherapy, while minimizing adverse effects. Large initiatives have been put forward to advance our understanding of the variability in PK amongst critically ill adults, [107,520,547] however significant gaps in children remain. The work here in this thesis builds upon these initiatives and presents a methodological approach to support bedside dosing recommendations or future clinical trial planning.

In Chapter 2, an extensive systematic review was conducted to analyze the literature of PK in critically ill children receiving CRRT. The objective of this chapter was multifactorial. First, it serves as a reference for clinicians to incorporate in their daily practice. Using a comprehensive search strategy, this review identified 45 studies, totaling approximately 600 children receiving CRRT and 33 different medications. This collection of all relevant studies resulted in the largest undertaking of a comprehensive review in critically ill children receiving CRRT currently published. All pertinent information on patient physiology and CRRT specifications were reported alongside PK parameters and suggested dosing guidance. Collating the data in this way ensures a patient-specific approach can be taken when applying the results. Prior to this publication, dosing guidance for children receiving CRRT were on the basis of adult extrapolation or lacked individualization to circuit specific properties (i.e. flow rates, modality etc.). [154] Furthermore, when assessing commonly used dosing references (i.e. Lexi-Comp),

only a minority of drugs have recommendations based on pediatric specific-CRRT studies. [414] Second, conclusions were drawn to assess potential differences in V_d and CL between critically ill children receiving CRRT and those who were not. Unexpectedly, V_d and CL were largely similar between the populations. This finding was most pronounced with small, hydrophilic molecules that undergo predominant renal clearance. [166,178,193,267–270] This review highlights that drugs with the aforementioned physicochemical and PK characteristics are most likely to have altered PK in this population. Knowledge of these characteristics is prudent to ensure appropriate pharmacotherapy. Finally, the quality of reporting of each study was assessed through the ClinPK tool. Overall, the reporting was generally poor and crucial information pertaining to PK variability was often absent.

Children receiving extracorporeal therapy represent an extremely vulnerable, and under-researched population. As Chapter 2 conveys, more work is required amongst the research community to fulfill this unmet, public health need. Contributions such as these enable synthesis of current literature and enable an amplification of the gaps in research. Additionally, the results of the quality of reporting should be seen as a call to the community that a higher standard must be met when conducting and reporting the results of such studies to our peers.

Furthermore, the contributions of this work were highlighted at the Pediatric Paracorporeal and Extracorporeal Therapies Summit in 2022. [548] Disseminating the results at large clinical congresses begins the conversation towards addressing the current state of research in this population. It is of great importance that the next phase of this work focuses on addressing these unmet needs and incorporating unique methods to improve our efficiency in how we conduct these studies to incentivize researchers to expand upon their efforts to improve patient care.

In Chapter 3, PBPK modelling was used to advance knowledge in how renal drug transporters may be altered over the course of CKD. Equations used to approximate GFR in guiding renal dose adjustments are based upon the “intact nephron hypothesis”, suggesting that the processes that govern renal clearance decline in parallel to GFR. [340,342,343] However, recent efforts have refuted this hypothesis suggesting that the decline in renal transporter activity is disproportionate to the decline in GFR in the most severe stages of CKD. [287] The results presented in Chapter 3 support these recent findings and highlight how the pathophysiology of

CKD may impact renal clearance processes differently. By parameterizing OAT transport function through the PAH extraction ratio, successful predictions of drug PK for OAT substrates were made across each stage of CKD. This mathematically derived relationship determined that the OAT functionality was reduced by 27-49%, 50-69% and 70-96% across CKD stages 3, 4, and 5, respectively.

There is a clear application of PBPK in patients with CKD for the purpose of clinical trial planning of new investigational compounds. Using this modelling approach provides insight into the corresponding impact of drug PK due to pathophysiology. Utilizing these methods expands upon population-based approaches as they give mechanistic insight to the processes that govern drug PK. Additionally, this approach enables assessments of potential drug-drug interactions in patients with CKD, currently an underrepresented area of study. This derivation of OAT decline can be transferable to new compounds to guide clinical trial planning or supplement clinical data so that the results are confirmatory, rather than exploratory.

Although Chapter 3 furthers our understanding of the impact of CKD on OAT activity, more work is needed. As outlined in **Figure 3-1**, there was a paucity of data to inform the PAH extraction ratio in the most severe stages of CKD. As this subset of the population is of the most interest, uncertainty does remain in the model structure. Inherently, studies in populations with advanced disease are difficult to conduct. Therefore, leveraging further *in-vitro* and animal studies to gain insight into how OAT transporters may be impaired in the most advanced stages of CKD could supplement this work. Although, these translational approaches will require further model evaluation. Additionally, as this methodologically approach was evaluated on OAT substrates that undergo a large contribution of tubular secretion to renal clearance it cannot be stated that this relationship holds true in weak OAT substrates. Further confirmation will be necessary.

The entirety of this thesis focuses on advancing pharmacotherapy in critical illness by applying PBPK strategies. Although the focus of Chapter 3 is on CKD, several parallels can be drawn. Kidney disease, whether acute or chronic, can have direct effects on renal OAT function by reductions in expression, function, localization or through inhibition. [282,285,286,549–551] In the critical care setting, AKI is complex and the etiology is often multifactorial due to poor perfusion to the kidneys or direct insult from drugs and/or endotoxins. [67,552] Rat models

simulating perfusion associated or drug-induced (i.e. gentamicin) AKI, reveal that OAT protein expression is significantly reduced. [550,551,553] Similar reductions in protein expression were also shown in animal models simulating chronic renal failure. [364,549,554,555] The degree of impact on OAT expression between the two forms of kidney injury (acute vs. chronic) has yet to be compared, however it does appear that the physiological response may have a similar impact at the cellular level. As the reductions in OAT activity were mechanistically derived from PAH extraction ratios in varying degrees of renal impairment, applying this parameterization into PBPK models of OAT substrates in patients with AKI seems physiologically relevant. This Chapter highlights the advantages of PBPK, as not only a resource to predict drug PK in otherwise untested scenarios, but as a methodological approach to understanding the implications of disease on pharmacology and PK.

The overall workflow presented in this thesis for applying PBPK to optimize pharmacotherapy in critically ill patients receiving ECLS follows a similar approach as presented by Watt *et al*. [144] This approach has three phases: 1) analysis of the drug-circuit via closed-loop ECLS circuit studies (ex-vivo), 2) development of a PBPK model of the drug of interest in the target population (adult vs. pediatric), 3) attaching an "ECLS" organ compartment to the whole-body PBPK structure. Chapters 4 and 5, focus on phase one, through the investigation of the CRRT circuit interaction of anakinra and cefazolin, respectively.

Chapter 4 provides a description of an ex-vivo analysis of anakinra, while incorporating each modality of CRRT. As outlined in Chapter 1, small, hydrophilic molecules with high unbound fractions in plasma are generally subjected to significant clearance via the CRRT circuit. However, the drug-circuit interaction for therapeutic proteins is largely unknown. This Chapter is the first to demonstrate that modern CRRT circuit technology can remove anakinra from plasma to a certain degree. Upon completion of the 4-hour experiment, approximately 5% of anakinra remained in plasma. The S_C and S_D ranged from 0.34 to 0.41, indicating an ability for anakinra to pass across the semipermeable membrane. Although, the methods presented do not enable full conclusions on the adsorption potential of anakinra, the consistently high drug concentrations in hemofiltrate indicate clearance by the circuit is the driving mechanism of drug removal from plasma (**Appendix C; Figure 2.**). While clearance determined via *ex-vivo* studies do not fully enable a direct extrapolation to CL_{total} *in-vivo* due to the absence of metabolism or

CL_{NR}, several conclusions from this analysis can be drawn. First, as modern CRRT technology incorporates “high-flux” hemofilters, the ability for drug removal of compounds approaching a molecular weight of 40 kDa is apparent. [102,104,400] As anakinra has a molecular weight of 17 kDa, the degree of removal found in this study is not unexpected. Second, currently approved dose recommendations for anakinra in those with renal impairment, including those receiving RRT, advise dose adjustments are required to avoid unnecessary exposure. These recommendations are solely based off data from Yang *et al.,* [386] which found negligible removal of anakinra by IHD. The results in Chapter 4 highlight how the mechanistic and circuit component differences of modern CRRT circuit technology forgo any direct extrapolation of these recommendations. Although in isolation, guidance on anakinra dosing in those receiving CRRT cannot be made from this study, the results do support that renal dose adjustments may not be necessary.

Chapter 5 provides another *ex-vivo* CRRT analysis where cefazolin was selected as the drug of interest. Infection amongst patients in the ICU are highly prevalent, with approximately 70% requiring antibiotics. [409,556] Upwards of 50% of infections are attributed to gram-positive bacteria. [413,414] Therefore, it is unsurprising that antibiotics with pharmacodynamic activity against gram-positive bacteria are some of the most prescribed to this population. [409,556] Despite its high frequency of use, limited data to guide dosing is available for adults, [374] while being nonexistent in children. In a collaboration with the Children’s Hospital of Philadelphia, cefazolin was one of the most frequently prescribed antibiotics to children receiving CRRT that had no pediatric-specific CRRT dosing recommendations in the literature. [414] To support evidence-based dosing guidance, Chapter 5 provides the first pediatric-specific CRRT *ex-vivo* study of cefazolin. Unexpectedly, 90% of the administered dose was removed within 4 hours. The variability of S_D was an interesting finding from this study, as it ranged from 0.17-0.5. This variability may be attributed to the uniqueness of cefazolin’s saturable protein binding to albumin. [415–417,422,423] Concentrations expected to be achieved in plasma after standard therapeutic doses may enable saturation to albumin binding sites, increasing the unbound fraction over the course of the dosing interval. The impact of this phenomenon may result in wide inter- and intra-patient variability in CL_{RRT}. Furthermore, these results highlight the importance of sampling time when analyzing the S_C or S_D of a particular compound. [557] It

is imperative that study results are transparent and that readers critically examine the sampling time when comparing differences in S_C and/or S_D.

A novel contribution of this thesis was including ECLS (i.e. CRRT & ECMO) compartments to the whole-body PBPK model. Chapter 6 outlines this methodological approach, integrating the results of the anakinra ex-vivo experiment (Chapter 4) to a PBPK model in critically ill children. Model development for anakinra was robust, and several factors were considered. First, a PBPK model for adults was successfully established prior to scaling to children. Developing PBPK models in adults furthers our understanding of drug PK as there is often more robust data to work with, and all potential clearance processes have undergone full maturation. For anakinra, mass-balance studies suggest a non-specific proteolysis that occurs in the kidney and liver. [386,388]. The pediatric model accounted for developmental differences in physiology, however, proteolysis was consistent with adults based on our current understanding. [461,462] Characterizing the proteolytic pathway for the purpose of defining the maturational component is prudent and will be subjected to future work when younger children are considered.

Second, knowledge gained from methods in CKD-PBPK modelling (Chapter 2) were applied to define the impact of kidney failure on the non-renal proteolytic pathways of anakinra. The impact of renal impairment on drug clearance is evident beyond the kidney. Chronic states of inflammation or endotoxin accumulation may induce downregulation and/or inhibition of metabolizing pathways in the liver. [338,339,357,358] By developing a CKD-PBPK model for anakinra, the impact of renal impairment on the proteolysis was quantified. This “middle-out” approach enabled new insight into anakinra PK and was incorporated into the full ECLS-PBPK model. This strategy generates the hypothesis as to whether scaling factors of CL_{NR} from CKD can be incorporated into future critical illness PBPK models. Finally, When the CRRT compartment was informed by the ex-vivo study, the model was able to mechanistically describe anakinra disposition in each modality of CRRT.

The anakinra ECLS-PBPK model was successfully validated with prospective data from critically ill children receiving simultaneous ECMO and CRRT. With the confidence gained in model predictions, *in-silico* dosing simulations were performed to provide guidance for baseline dosing recommendations in children receiving anakinra while on ECLS. As the

pharmacodynamic endpoint for anakinra in the management of inflammatory phenotypes has yet to be determined, the model simulations suggest that currently recommended doses of 5-10 mg/kg/d divided every 6-12 hours are adequate. Furthermore, anakinra AUC in the virtual population receiving ECLS was largely similar to those who were not. This *in-silico* approach suggests that anakinra may be safely administered to children receiving ECLS at current standard doses. It is the intention that the work herein will be used in guiding clinical trial design in children receiving anakinra.

The final Chapter of this thesis moves beyond the critically ill individual receiving ECLS and describes PBPK modelling efforts to predict drug concentrations in different organ compartments. Chapter 7 provides a mechanistic representation of cefazolin drug concentrations in the CNS. Use of cefazolin as a viable treatment option in patients with CNS infections attributed to MSSA has been controversial due to the presumed inability of adequate concentrations at the site of infection. However, recent PK and clinical data has refuted this historical concept. [494,505,506] Upon successful evaluations, a pharmacodynamic assessment was performed to suggest doses that would be effective against MSSA (MIC $\leq$ 2.0 mg/L) and safe based upon suspected neurotoxicity threshold. The *in-silico* dosing recommendations coincide with recent clinical data, [494,505] and those recommendations from a comprehensive narrative review on this subject matter. [528] This Chapter outlines the benefit of PBPK when data is sparse and provides another application of its use in the critical care setting.

Proteomic data on protein expression was incorporated for drug-efflux transporters OAT3 and MRP4 during model development. As cefazolin is a substrate of each transporter, the degree of CNS penetration may be influenced by the amount of expression at the site of the blood-brain-barrier. This concept was further supported by our sensitivity analysis, suggesting that the expression of each transporter contributes to the AUC_{CSF} of cefazolin. Such concepts may be further confirmed from an animal study conducted by Dacey *et al*., investigating the impact of meningeal inflammation and probenecid administration on the CSF penetration of several OAT substrate antibiotics (i.e. penicillin's, cephalosporins). [533] In this study, both meningeal inflammation and OAT inhibition via probenecid increased the CSF concentrations of penicillin compared to control. Furthermore, the influence of probenecid OAT inhibition was more pronounced in the rabbit meningitis models, suggesting that OAT mediated drug-efflux is more

important to CNS penetration in the presence of infection. Although, variability in this effect should be noted as active infection may also contribute to reductions in drug-efflux activity. [533,534] Studies with cefazolin involving meningitis animal models in the presence of probenecid are required to ensure that this holds true as differences in transporter affinity may be seen between cephalosporins and penicillins. [558,559]

8.2 Conclusion

This thesis seeks to advance the existing knowledge of PK in critically ill individuals by leveraging different collaborators and incorporating heterogeneous patient populations. Each Chapter reflects efforts towards improving pharmacotherapy in this clinical setting. Beginning with identifying underrepresented patient populations (i.e. critically ill children receiving CRRT), and commences with how methods in PBPK can efficiently support these research gaps. Each Chapter of this thesis is dedicated to advancing an understanding of drug PK in critically ill patients and proposes a translatable approach that can be applied to different drugs, patients, and new ECLS technology.

PK studies are vital to informing drug dosing in vulnerable patient populations. Several components are included, and an appropriate study design is essential to ensure validity of the results. Barriers are presented when designing PK studies in critically ill patients, including sufficient sample size, blood sampling strategies and PK analysis. Furthermore, variability in institutional protocols for ECLS implementation may result in multiple drug-circuit permutations and limit the generalizability of traditional PK trials. Blood sample collection may also present barriers, as obtaining robust samples across a dosing interval in a highly unstable patient is often impractical, and not advised. [560] This concern is most pronounced in critically ill neonates or young children, where blood volume is reduced compared to adult counterparts. [561] By incorporating PBPK strategies as presented in this thesis, many of these limitations can be overcome. As PBPK models incorporate a mechanistic understanding of drug PK in healthy individuals, applying “disease” related physiological alterations makes extrapolations to special populations possible. The mechanistic nature, or “bottom-up” approach enables valid model predictions when observed data is sparse. As such, a limited number of patients, with a limited number of samples can be incorporated into PBPK modelling studies to assess population-level variability in drug PK and support drug dosing or clinical trial planning.

Globally, several initiatives are ongoing to advance knowledge of drug PK in critically ill patients. Initiatives such as the Sampling Antibiotics in Renal Replacement Therapy (SMARRT) study collaborators and the Antibiotic, Sedative and Analgesic Pharmacokinetics during Extracorporeal Membrane Oxygenation (ASAP-ECMO) study group in adults focuses on optimizing drug delivery of antimicrobials to critically ill adults receiving ECLS. [547,562] Modelling and simulation is integral to these initiatives, and although PBPK has yet to be widely used across these studies, the methods herein may fill a vital role. Initiatives such as the Pediatric Trials Network (PTN) and the Collaborative Pediatric Critical Care Research Network (CPCCRN), have dedicated research to improving critical care practices in children. PBPK is an extremely resourceful tool to supplement these initiatives, as it can facilitate optimal trial design by improving efficiency in sample time and reducing the number of children required for successful model predictions. Secondly, PBPK enables extrapolation between populations. This is pivotal for the pediatric population and may provide first-in-dose predictions to inform future studies. Utilization of PBPK for improving drug delivery in critical care is at its early stages, however as outlined in this thesis, its potential will ensure a more refined approach to advancing pharmacotherapy in this population.

8.3 Future Directions

Interest in the PK alterations associated with critical illness has been growing over the past two decades. Dedicated research in this patient population has seen a shift from traditional PK studies to integrating methods of pharmacometrics to support drug dosing. Publications incorporating PopPK have seen a significant uptake in recent years. This was evident in our search strategy focused on children in Chapter 1, as 27% of studies included a PopPK analysis published after 2010. Regulatory agencies, such as the FDA and EMA, acknowledge the potential of pharmacometrics in supporting regulatory approval for drug development. [373,563–565] Several advantages are noted, which have been articulated throughout this thesis. These advantages are directly translatable to the clinical setting and may improve drug utilization for critically ill patients. Several advancements were made towards this fact, however future research will be directed to support our understanding of key components within this thesis.

In Chapter 1, despite the comprehensive review of what is currently known for drug PK in children receiving CRRT, several gaps remain. Specifically, reporting consistencies from PK

trials were generally poor. Initiatives such as the ClinPK tool and the Grading and Assessment of Pharmacokinetic-Pharmacodynamic Studies (GAPPS) tool have been proposed to ensure transparency in clinical PK trials and to grade the strength of evidence to support clinical decision-making. [158,566] An area of continual need will be to further incentivize researchers conducting PK trials in those receiving ECLS to report specifications (i.e. flow rates, circuit components etc.) to improve generalizability and ensure direct translation to the readers population of interest. Although the ClinPK tool assesses reporting for studies involving ECLS, more specific assessment tools may be required. [103] As the role of pharmacometrics has increased in drug development, regulatory bodies have proposed guidance in reporting for PopPK, [567–569] and PBPK studies. [570,571] These methods have become more apparent in the clinical setting to support bed-side dose recommendations, therefore ongoing knowledge translation is of the utmost importance to ensure appropriate assessments of available evidence. Therefore, tools to evaluate and weigh available evidence are prudent to ensure end-users are applying such models correctly and to promote high-quality decision making in support of patient care.

Although Chapter 2 focuses on using PBPK to inform drug dosing in chronic diseases, key components are applicable to the critical care setting. First, this Chapter incorporates a statistical description of how the excretion of the exogenous biomarker, PAH, may be impacted over the course of CKD. Biomarkers are at the forefront of personalized medicine, and advancements in analytical methods have enabled real-time monitoring achievable. In addition to use as a clinical-monitoring tool, the use of endogenous biomarkers (beyond SCr), as covariates in PopPK modelling is increasing. [572,573] Due to the mechanistic nature of PBPK models, the use of endogenous biomarkers to inform DDI potential, disease-related impairments in PK, or maturational components are plausible. Recently, Tan *et al*. described a PBPK model incorporating 4-pyridoxic acid (PDA), an endogenous substrate of OAT, for the purpose of assessing DDI-potential in CKD. [574] Real-time monitoring of PDA and characterizing its trajectory over the course of critical illness may enable a more mechanistic description of the renal handling of OAT substrates in this populations. Second, the chronic state of inflammation and accumulation of uremic toxins impacts CL_{NR} in CKD. As previously stated, similarities may be seen in the physiological response to critical illness in cases of hyperinflammatory phenotypes and/or acute renal failure. Future work dedicated towards PBPK modelling of drugs that are

predominantly cleared via non-renal pathways will be needed to confirm if scaling factors applied in the CKD-PBPK holds true. Based on what is currently known, this assumption has physiologic relevance.

In collaboration with the Children's Hospital of Philadelphia, several drugs were identified with little to no pediatric-specific CRRT dosing guidance for antimicrobials. [414] This finding was mirrored in Chapter 2, indicating significant work is required amongst the research community to bridge the knowledge gap. Chapters 4 through 7, present a feasible solution to advancing our understanding of drugs with little to no PK data. Future work can target drugs that are commonly used with limited dosing guidance, as this will be most impactful to clinicians in their practice setting. Furthermore, although Chapter 6 provides a robust anakinra ECLS-PBPK model in critically ill children, the results should be seen as a starting point to inform future clinical trial planning. Limited data was available for model evaluation, therefore on-going prospective PK collection across the age spectrum is essential to gain confidence in predictions. As discussed in the Chapter, administration of SC anakinra may become obsolete due to the impact of edema and inflammation on absorption. IV administration may become the standard of care for this indication, therefore further refinement in the final model will be necessary upon data collection in those receiving IV anakinra.

Finally, Chapter 7 moves away from drug alterations in patients receiving ECLS and applied concepts in PBPK to assist dose optimization for those with severe CNS infections. Recent publications have supported the notion that cefazolin achieves adequate concentrations at the site of infection. [494,505,506] Chapter 7, further supports these findings and provides a pharmacodynamic analysis to investigate dose. It is worth mentioning that the model is evaluated from limited data, and further evaluations are essential. Furthermore, due to variability in inflammation affecting blood-brain barrier permeability, more work is needed to further characterize how this response to infection not only affects cefazolin penetration but affects the penetration of additional antimicrobials. *In-vitro* studies utilizing MDCKII-MDR1 cell lines or animal models may be used to quantify the impact of inflammation on blood-brain barrier permeability or the activity of drug-efflux transporters that can be incorporated into PBPK models. [575–578] As drug penetration is highly dependent on drug physicochemical properties and physiology, specific "meningitis" PBPK models are possible with future *in-vitro* and *in-vivo*

studies. The work herein has led to an ongoing collaboration with the University Health Network. It is a privilege to be a part of these ongoing efforts to advance knowledge of drug PK in those with CNS infections.

Letters of Copyright Permission

SPRINGER NATURE LICENSE
TERMS AND CONDITIONS

Jun 10, 2024

This Agreement between University of Waterloo -- Samuel Dubinsky ("You") and Springer Nature ("Springer Nature") consists of your license details and the terms and conditions provided by Springer Nature and Copyright Clearance Center.

License Number	5774520392460
License date	Apr 22, 2024
Licensed Content Publisher	Springer Nature
Licensed Content Publication	Clinical Pharmacokinetics
Licensed Content Title	Pharmacokinetics of Commonly Used Medications in Children Receiving Continuous Renal Replacement Therapy: A Systematic Review of Current Literature
Licensed Content Author	Samuel Dubinsky et al
Licensed Content Date	Nov 30, 2021
Type of Use	Thesis/Dissertation
Requestor type	academic/university or research institute
Format	electronic
Portion	full article/chapter
Will you be translating?	no

Circulation/distribution	1 - 29
Author of this Springer Nature content	yes
Title of new work	Pharmacokinetics of Commonly Used Medications in Children Receiving Continuous Renal Replacement Therapy: A Systematic Review of Current Literature
Institution name	University of Waterloo School of Pharmacy
Expected presentation date	Jun 2024
Requestor Location	University of Waterloo 10 Victoria St S Kitchener, ON N2G1C5 Canada Attn: University of Waterloo
Total	0.00 CAD

Terms and Conditions

Springer Nature Customer Service Centre GmbH Terms and Conditions

The following terms and conditions ("Terms and Conditions") together with the terms specified in your [RightsLink] constitute the License ("License") between you as Licensee and Springer Nature Customer Service Centre GmbH as Licensor. By clicking 'accept' and completing the transaction for your use of the material ("Licensed Material"), you confirm your acceptance of and obligation to be bound by these Terms and Conditions.

1. Grant and Scope of License

1. 1. The Licensor grants you a personal, non-exclusive, non-transferable, non-sublicensable, revocable, world-wide License to reproduce, distribute, communicate to the public, make available, broadcast, electronically transmit or create derivative works using the Licensed Material for the purpose(s) specified in your RightsLink Licence Details only. Licenses are granted for the specific use requested in the order and for no other use, subject to these Terms and Conditions. You acknowledge and agree that the rights granted to you under this License do not include the right to modify, edit, translate, include in collective works, or create derivative works of the Licensed Material in whole or in part unless expressly stated in your RightsLink

Licence Details. You may use the Licensed Material only as permitted under this Agreement and will not reproduce, distribute, display, perform, or otherwise use or exploit any Licensed Material in any way, in whole or in part, except as expressly permitted by this License.

1. 2. You may only use the Licensed Content in the manner and to the extent permitted by these Terms and Conditions, by your RightsLink Licence Details and by any applicable laws.

1. 3. A separate license may be required for any additional use of the Licensed Material, e.g. where a license has been purchased for print use only, separate permission must be obtained for electronic re-use. Similarly, a License is only valid in the language selected and does not apply for editions in other languages unless additional translation rights have been granted separately in the License.

1. 4. Any content within the Licensed Material that is owned by third parties is expressly excluded from the License.

1. 5. Rights for additional reuses such as custom editions, computer/mobile applications, film or TV reuses and/or any other derivative rights requests require additional permission and may be subject to an additional fee. Please apply to journalpermissions@springernature.com or bookpermissions@springernature.com for these rights.

2. Reservation of Rights

Licensor reserves all rights not expressly granted to you under this License. You acknowledge and agree that nothing in this License limits or restricts Licensor's rights in or use of the Licensed Material in any way. Neither this License, nor any act, omission, or statement by Licensor or you, conveys any ownership right to you in any Licensed Material, or to any element or portion thereof. As between Licensor and you, Licensor owns and retains all right, title, and interest in and to the Licensed Material subject to the license granted in Section 1.1. Your permission to use the Licensed Material is expressly conditioned on you not impairing Licensor's or the applicable copyright owner's rights in the Licensed Material in any way.

3. Restrictions on use

3. 1. Minor editing privileges are allowed for adaptations for stylistic purposes or formatting purposes provided such alterations do not alter the original meaning or intention of the Licensed Material and the new figure(s) are still accurate and representative of the Licensed Material. Any other changes including but not limited to, cropping, adapting, and/or omitting material that affect the meaning, intention or moral rights of the author(s) are strictly prohibited.

3. 2. You must not use any Licensed Material as part of any design or trademark.

3. 3. Licensed Material may be used in Open Access Publications (OAP), but any such reuse must include a clear acknowledgment of this permission visible at the same time as the figures/tables/illustration or abstract and which must indicate that the Licensed Material is not part of the governing OA license but has been reproduced with permission. This may be indicated according to any standard referencing system but must include at a minimum 'Book/Journal title, Author, Journal Name (if applicable), Volume (if applicable), Publisher, Year, reproduced

with permission from SNCSC'.

4. STM Permission Guidelines

4. 1. An alternative scope of license may apply to signatories of the STM Permissions Guidelines ("STM PG") as amended from time to time and made available at https://www.stm-assoc.org/intellectual-property/permissions/permissions-guidelines/.

4. 2. For content reuse requests that qualify for permission under the STM PG, and which may be updated from time to time, the STM PG supersede the terms and conditions contained in this License.

4. 3. If a License has been granted under the STM PG, but the STM PG no longer apply at the time of publication, further permission must be sought from the Rightsholder. Contact journalpermissions@springernature.com or bookpermissions@springernature.com for these rights.

5. Duration of License

5. 1. Unless otherwise indicated on your License, a License is valid from the date of purchase ("License Date") until the end of the relevant period in the below table:

Reuse in a medical communications project	Reuse up to distribution or time period indicated in License
Reuse in a dissertation/thesis	Lifetime of thesis
Reuse in a journal/magazine	Lifetime of journal/magazine
Reuse in a book/textbook	Lifetime of edition
Reuse on a website	1 year unless otherwise specified in the License
Reuse in a presentation/slide kit/poster	Lifetime of presentation/slide kit/poster. Note: publication whether electronic or in print of presentation/slide kit/poster may require further permission.
Reuse in conference proceedings	Lifetime of conference proceedings
Reuse in an annual report	Lifetime of annual report
Reuse in training/CME materials	Reuse up to distribution or time period indicated in License
Reuse in newsmedia	Lifetime of newsmedia
Reuse in coursepack/classroom materials	Reuse up to distribution and/or time period indicated in license

6. Acknowledgement

6. 1. The Licensor's permission must be acknowledged next to the Licensed Material in print. In electronic form, this acknowledgement must be visible at the same time as the figures/tables/illustrations or abstract and must be hyperlinked to the journal/book's homepage.

6. 2. Acknowledgement may be provided according to any standard referencing system and at a minimum should include "Author, Article/Book Title, Journal name/Book imprint, volume, page number, year, Springer Nature".

7. Reuse in a dissertation or thesis

7. 1. Where 'reuse in a dissertation/thesis' has been selected, the following terms apply: Print rights of the Version of Record are provided for; electronic rights for use only on institutional repository as defined by the Sherpa guideline (www.sherpa.ac.uk/romeo/) and only up to what is required by the awarding institution.

7. 2. For theses published under an ISBN or ISSN, separate permission is required. Please contact journalpermissions@springernature.com or bookpermissions@springernature.com for these rights.

7. 3. Authors must properly cite the published manuscript in their thesis according to current citation standards and include the following acknowledgement: '*Reproduced with permission from Springer Nature*'.

8. License Fee

You must pay the fee set forth in the License Agreement (the "License Fees"). All amounts payable by you under this License are exclusive of any sales, use, withholding, value added or similar taxes, government fees or levies or other assessments. Collection and/or remittance of such taxes to the relevant tax authority shall be the responsibility of the party who has the legal obligation to do so.

9. Warranty

9. 1. The Licensor warrants that it has, to the best of its knowledge, the rights to license reuse of the Licensed Material. **You are solely responsible for ensuring that the material you wish to license is original to the Licensor and does not carry the copyright of another entity or third party (as credited in the published version).** If the credit line on any part of the Licensed Material indicates that it was reprinted or adapted with permission from another source, then you should seek additional permission from that source to reuse the material.

9. 2. EXCEPT FOR THE EXPRESS WARRANTY STATED HEREIN AND TO THE EXTENT PERMITTED BY APPLICABLE LAW, LICENSOR PROVIDES THE LICENSED MATERIAL "AS IS" AND MAKES NO OTHER REPRESENTATION OR WARRANTY. LICENSOR EXPRESSLY DISCLAIMS ANY LIABILITY FOR ANY CLAIM ARISING FROM OR OUT OF THE CONTENT, INCLUDING BUT NOT LIMITED TO ANY ERRORS, INACCURACIES, OMISSIONS, OR DEFECTS CONTAINED THEREIN, AND ANY IMPLIED OR EXPRESS WARRANTY AS TO MERCHANTABILITY OR FITNESS FOR A PARTICULAR PURPOSE. IN NO EVENT SHALL LICENSOR BE LIABLE TO YOU OR ANY OTHER PARTY OR ANY OTHER PERSON OR FOR ANY SPECIAL, CONSEQUENTIAL, INCIDENTAL, INDIRECT, PUNITIVE, OR EXEMPLARY DAMAGES, HOWEVER CAUSED, ARISING OUT OF OR IN CONNECTION WITH THE DOWNLOADING, VIEWING OR USE OF THE LICENSED MATERIAL REGARDLESS OF THE FORM OF ACTION, WHETHER FOR BREACH OF CONTRACT, BREACH OF WARRANTY, TORT, NEGLIGENCE, INFRINGEMENT OR OTHERWISE

(INCLUDING, WITHOUT LIMITATION, DAMAGES BASED ON LOSS OF PROFITS, DATA, FILES, USE, BUSINESS OPPORTUNITY OR CLAIMS OF THIRD PARTIES), AND WHETHER OR NOT THE PARTY HAS BEEN ADVISED OF THE POSSIBILITY OF SUCH DAMAGES. THIS LIMITATION APPLIES NOTWITHSTANDING ANY FAILURE OF ESSENTIAL PURPOSE OF ANY LIMITED REMEDY PROVIDED HEREIN.

10. Termination and Cancellation

10. 1. The License and all rights granted hereunder will continue until the end of the applicable period shown in Clause 5.1 above. Thereafter, this license will be terminated and all rights granted hereunder will cease.

10. 2. Licensor reserves the right to terminate the License in the event that payment is not received in full or if you breach the terms of this License.

11. General

11. 1. The License and the rights and obligations of the parties hereto shall be construed, interpreted and determined in accordance with the laws of the Federal Republic of Germany without reference to the stipulations of the CISG (United Nations Convention on Contracts for the International Sale of Goods) or to Germany´s choice-of-law principle.

11. 2. The parties acknowledge and agree that any controversies and disputes arising out of this License shall be decided exclusively by the courts of or having jurisdiction for Heidelberg, Germany, as far as legally permissible.

11. 3. This License is solely for Licensor's and Licensee's benefit. It is not for the benefit of any other person or entity.

Questions? For questions on Copyright Clearance Center accounts or website issues please contact springernaturesupport@copyright.com or +1-855-239-3415 (toll free in the US) or +1-978-646-2777. For questions on Springer Nature licensing please visit https://www.springernature.com/gp/partners/rights-permissions-third-party-distribution

Other Conditions:

Version 1.4 - Dec 2022

Questions? customercare@copyright.com.

(INCLUDING, WITHOUT LIMITATION, DAMAGES BASED ON LOSS OF PROFITS, DATA, FILES, USE, BUSINESS OPPORTUNITY OR CLAIMS OF THIRD PARTIES), AND WHETHER OR NOT THE PARTY HAS BEEN ADVISED OF THE POSSIBILITY OF SUCH DAMAGES. THIS LIMITATION APPLIES NOTWITHSTANDING ANY FAILURE OF ESSENTIAL PURPOSE OF ANY LIMITED REMEDY PROVIDED HEREIN.

10. Termination and Cancellation

10. 1. The License and all rights granted hereunder will continue until the end of the applicable period shown in Clause 5.1 above. Thereafter, this license will be terminated and all rights granted hereunder will cease.

10. 2. Licensor reserves the right to terminate the License in the event that payment is not received in full or if you breach the terms of this License.

11. General

11. 1. The License and the rights and obligations of the parties hereto shall be construed, interpreted and determined in accordance with the laws of the Federal Republic of Germany without reference to the stipulations of the CISG (United Nations Convention on Contracts for the International Sale of Goods) or to Germany´s choice-of-law principle.

11. 2. The parties acknowledge and agree that any controversies and disputes arising out of this License shall be decided exclusively by the courts of or having jurisdiction for Heidelberg, Germany, as far as legally permissible.

11. 3. This License is solely for Licensor's and Licensee's benefit. It is not for the benefit of any other person or entity.

Questions? For questions on Copyright Clearance Center accounts or website issues please contact springernaturesupport@copyright.com or +1-855-239-3415 (toll free in the US) or +1-978-646-2777. For questions on Springer Nature licensing please visit https://www.springernature.com/gp/partners/rights-permissions-third-party-distribution

Other Conditions:

Version 1.4 - Dec 2022

Questions? customercare@copyright.com.

6. 2. Acknowledgement may be provided according to any standard referencing system and at a minimum should include "Author, Article/Book Title, Journal name/Book imprint, volume, page number, year, Springer Nature".

7. Reuse in a dissertation or thesis

7. 1. Where 'reuse in a dissertation/thesis' has been selected, the following terms apply: Print rights of the Version of Record are provided for; electronic rights for use only on institutional repository as defined by the Sherpa guideline (www.sherpa.ac.uk/romeo/) and only up to what is required by the awarding institution.

7. 2. For theses published under an ISBN or ISSN, separate permission is required. Please contact journalpermissions@springernature.com or bookpermissions@springernature.com for these rights.

7. 3. Authors must properly cite the published manuscript in their thesis according to current citation standards and include the following acknowledgement: *'Reproduced with permission from Springer Nature'.*

8. License Fee

You must pay the fee set forth in the License Agreement (the "License Fees"). All amounts payable by you under this License are exclusive of any sales, use, withholding, value added or similar taxes, government fees or levies or other assessments. Collection and/or remittance of such taxes to the relevant tax authority shall be the responsibility of the party who has the legal obligation to do so.

9. Warranty

9. 1. The Licensor warrants that it has, to the best of its knowledge, the rights to license reuse of the Licensed Material. **You are solely responsible for ensuring that the material you wish to license is original to the Licensor and does not carry the copyright of another entity or third party (as credited in the published version).** If the credit line on any part of the Licensed Material indicates that it was reprinted or adapted with permission from another source, then you should seek additional permission from that source to reuse the material.

9. 2. EXCEPT FOR THE EXPRESS WARRANTY STATED HEREIN AND TO THE EXTENT PERMITTED BY APPLICABLE LAW, LICENSOR PROVIDES THE LICENSED MATERIAL "AS IS" AND MAKES NO OTHER REPRESENTATION OR WARRANTY. LICENSOR EXPRESSLY DISCLAIMS ANY LIABILITY FOR ANY CLAIM ARISING FROM OR OUT OF THE CONTENT, INCLUDING BUT NOT LIMITED TO ANY ERRORS, INACCURACIES, OMISSIONS, OR DEFECTS CONTAINED THEREIN, AND ANY IMPLIED OR EXPRESS WARRANTY AS TO MERCHANTABILITY OR FITNESS FOR A PARTICULAR PURPOSE. IN NO EVENT SHALL LICENSOR BE LIABLE TO YOU OR ANY OTHER PARTY OR ANY OTHER PERSON OR FOR ANY SPECIAL, CONSEQUENTIAL, INCIDENTAL, INDIRECT, PUNITIVE, OR EXEMPLARY DAMAGES, HOWEVER CAUSED, ARISING OUT OF OR IN CONNECTION WITH THE DOWNLOADING, VIEWING OR USE OF THE LICENSED MATERIAL REGARDLESS OF THE FORM OF ACTION, WHETHER FOR BREACH OF CONTRACT, BREACH OF WARRANTY, TORT, NEGLIGENCE, INFRINGEMENT OR OTHERWISE

with permission from SNCSC'.

4. STM Permission Guidelines

4. 1. An alternative scope of license may apply to signatories of the STM Permissions Guidelines ("STM PG") as amended from time to time and made available at https://www.stm-assoc.org/intellectual-property/permissions/permissions-guidelines/.

4. 2. For content reuse requests that qualify for permission under the STM PG, and which may be updated from time to time, the STM PG supersede the terms and conditions contained in this License.

4. 3. If a License has been granted under the STM PG, but the STM PG no longer apply at the time of publication, further permission must be sought from the Rightsholder. Contact journalpermissions@springernature.com or bookpermissions@springernature.com for these rights.

5. Duration of License

5. 1. Unless otherwise indicated on your License, a License is valid from the date of purchase ("License Date") until the end of the relevant period in the below table:

Reuse in a medical communications project	Reuse up to distribution or time period indicated in License
Reuse in a dissertation/thesis	Lifetime of thesis
Reuse in a journal/magazine	Lifetime of journal/magazine
Reuse in a book/textbook	Lifetime of edition
Reuse on a website	1 year unless otherwise specified in the License
Reuse in a presentation/slide kit/poster	Lifetime of presentation/slide kit/poster. Note: publication whether electronic or in print of presentation/slide kit/poster may require further permission.
Reuse in conference proceedings	Lifetime of conference proceedings
Reuse in an annual report	Lifetime of annual report
Reuse in training/CME materials	Reuse up to distribution or time period indicated in License
Reuse in newsmedia	Lifetime of newsmedia
Reuse in coursepack/classroom materials	Reuse up to distribution and/or time period indicated in license

6. Acknowledgement

6. 1. The Licensor's permission must be acknowledged next to the Licensed Material in print. In electronic form, this acknowledgement must be visible at the same time as the figures/tables/illustrations or abstract and must be hyperlinked to the journal/book's homepage.

Licence Details. You may use the Licensed Material only as permitted under this Agreement and will not reproduce, distribute, display, perform, or otherwise use or exploit any Licensed Material in any way, in whole or in part, except as expressly permitted by this License.

1. 2. You may only use the Licensed Content in the manner and to the extent permitted by these Terms and Conditions, by your RightsLink Licence Details and by any applicable laws.

1. 3. A separate license may be required for any additional use of the Licensed Material, e.g. where a license has been purchased for print use only, separate permission must be obtained for electronic re-use. Similarly, a License is only valid in the language selected and does not apply for editions in other languages unless additional translation rights have been granted separately in the License.

1. 4. Any content within the Licensed Material that is owned by third parties is expressly excluded from the License.

1. 5. Rights for additional reuses such as custom editions, computer/mobile applications, film or TV reuses and/or any other derivative rights requests require additional permission and may be subject to an additional fee. Please apply to journalpermissions@springernature.com or bookpermissions@springernature.com for these rights.

2. Reservation of Rights

Licensor reserves all rights not expressly granted to you under this License. You acknowledge and agree that nothing in this License limits or restricts Licensor's rights in or use of the Licensed Material in any way. Neither this License, nor any act, omission, or statement by Licensor or you, conveys any ownership right to you in any Licensed Material, or to any element or portion thereof. As between Licensor and you, Licensor owns and retains all right, title, and interest in and to the Licensed Material subject to the license granted in Section 1.1. Your permission to use the Licensed Material is expressly conditioned on you not impairing Licensor's or the applicable copyright owner's rights in the Licensed Material in any way.

3. Restrictions on use

3. 1. Minor editing privileges are allowed for adaptations for stylistic purposes or formatting purposes provided such alterations do not alter the original meaning or intention of the Licensed Material and the new figure(s) are still accurate and representative of the Licensed Material. Any other changes including but not limited to, cropping, adapting, and/or omitting material that affect the meaning, intention or moral rights of the author(s) are strictly prohibited.

3. 2. You must not use any Licensed Material as part of any design or trademark.

3. 3. Licensed Material may be used in Open Access Publications (OAP), but any such reuse must include a clear acknowledgment of this permission visible at the same time as the figures/tables/illustration or abstract and which must indicate that the Licensed Material is not part of the governing OA license but has been reproduced with permission. This may be indicated according to any standard referencing system but must include at a minimum 'Book/Journal title, Author, Journal Name (if applicable), Volume (if applicable), Publisher, Year, reproduced

Circulation/distribution	1 - 29
Author of this Springer Nature content	yes
Title of new work	Pharmacokinetics of Commonly Used Medications in Children Receiving Continuous Renal Replacement Therapy: A Systematic Review of Current Literature
Institution name	University of Waterloo School of Pharmacy
Expected presentation date	Jun 2024
Requestor Location	University of Waterloo 10 Victoria St S Kitchener, ON N2G1C5 Canada Attn: University of Waterloo
Total	0.00 CAD

Terms and Conditions

Springer Nature Customer Service Centre GmbH Terms and Conditions

The following terms and conditions ("Terms and Conditions") together with the terms specified in your [RightsLink] constitute the License ("License") between you as Licensee and Springer Nature Customer Service Centre GmbH as Licensor. By clicking 'accept' and completing the transaction for your use of the material ("Licensed Material"), you confirm your acceptance of and obligation to be bound by these Terms and Conditions.

1. Grant and Scope of License

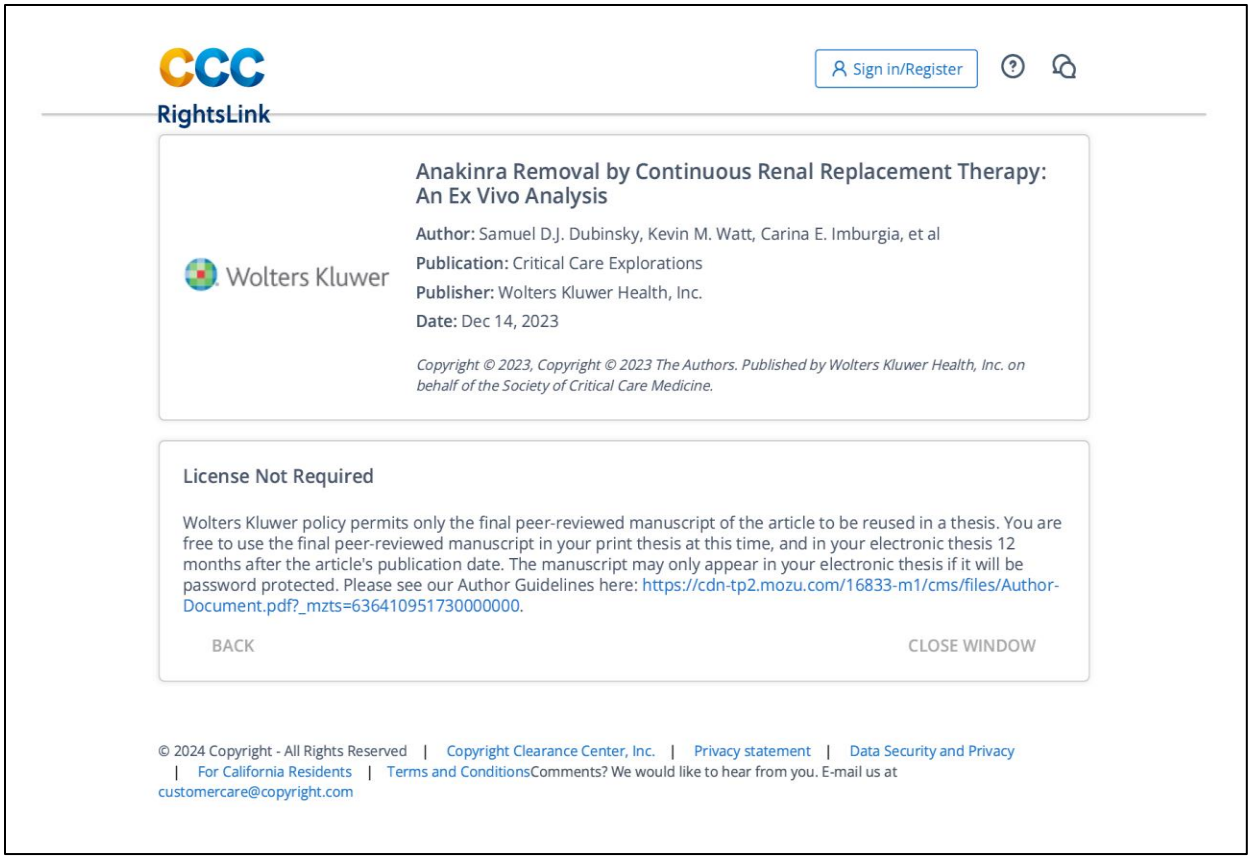
1. 1. The Licensor grants you a personal, non-exclusive, non-transferable, non-sublicensable, revocable, world-wide License to reproduce, distribute, communicate to the public, make available, broadcast, electronically transmit or create derivative works using the Licensed Material for the purpose(s) specified in your RightsLink Licence Details only. Licenses are granted for the specific use requested in the order and for no other use, subject to these Terms and Conditions. You acknowledge and agree that the rights granted to you under this License do not include the right to modify, edit, translate, include in collective works, or create derivative works of the Licensed Material in whole or in part unless expressly stated in your RightsLink

SPRINGER NATURE LICENSE
TERMS AND CONDITIONS

Jun 10, 2024

This Agreement between University of Waterloo -- Samuel Dubinsky ("You") and Springer Nature ("Springer Nature") consists of your license details and the terms and conditions provided by Springer Nature and Copyright Clearance Center.

License Number	5774520632997
License date	Apr 22, 2024
Licensed Content Publisher	Springer Nature
Licensed Content Publication	Clinical Pharmacokinetics
Licensed Content Title	Determining the Effects of Chronic Kidney Disease on Organic Anion Transporter1/3 Activity Through Physiologically Based Pharmacokinetic Modeling
Licensed Content Author	Samuel Dubinsky et al
Licensed Content Date	May 5, 2022
Type of Use	Thesis/Dissertation
Requestor type	academic/university or research institute
Format	print and electronic
Portion	full article/chapter
Will you be translating?	no


RightsLink
Sign in/Register
Anakinra Removal by Continuous Renal Replacement Therapy: An Ex Vivo Analysis
Author: Samuel D.J. Dubinsky, Kevin M. Watt, Carina E. Imburgia, et al
Publication: Critical Care Explorations
Publisher: Wolters Kluwer Health, Inc.
Date: Dec 14, 2023
Copyright © 2023, Copyright © 2023 The Authors. Published by Wolters Kluwer Health, Inc. on behalf of the Society of Critical Care Medicine.
License Not Required
Wolters Kluwer policy permits only the final peer-reviewed manuscript of the article to be reused in a thesis. You are free to use the final peer-reviewed manuscript in your print thesis at this time, and in your electronic thesis 12 months after the article's publication date. The manuscript may only appear in your electronic thesis if it will be password protected. Please see our Author Guidelines here: https://cdn-tp2.mozu.com/16833-m1/cms/files/Author-Document.pdf?_mzts=636410951730000000.
BACK
CLOSE WINDOW
© 2024 Copyright - All Rights Reserved | Copyright Clearance Center, Inc. | Privacy statement | Data Security and Privacy | For California Residents | Terms and ConditionsComments? We would like to hear from you. E-mail us at customercare@copyright.com

References

1. Maslove DM, Tang B, Shankar-Hari M, et al. Redefining critical illness. *Nat Med*. 2022;28(6):1141-1148. doi:10.1038/s41591-022-01843-x

2. Marshall JC, Bosco L, Adhikari NK, et al. What is an intensive care unit? A report of the task force of the World Federation of Societies of Intensive and Critical Care Medicine. *J Crit Care*. 2017;37:270-276. doi:10.1016/j.jcrc.2016.07.015

3. Guidelines for intensive care unit admission, discharge, and triage. Task Force of the American College of Critical Care Medicine, Society of Critical Care Medicine. *Crit Care Med*. 1999;27(3):633-638.

4. Vincent JL, Singer M, Marini JJ, et al. Thirty years of critical care medicine. *Crit Care*. 2010;14(3):311. doi:10.1186/cc8979

5. Vincent JL, Marshall JC, Namendys-Silva SA, et al. Assessment of the worldwide burden of critical illness: the intensive care over nations (ICON) audit. *Lancet Respir Med*. 2014;2(5):380-386. doi:10.1016/S2213-2600(14)70061-X

6. Abate SM, Assen S, Yinges M, Basu B. Survival and predictors of mortality among patients admitted to the intensive care units in southern Ethiopia: A multi-center cohort study. *Ann Med Surg 2012*. 2021;65:102318. doi:10.1016/j.amsu.2021.102318

7. CIHR. Care in Canadians. Accessed March 11, 2024. https://secure.cihi.ca/free_products/ICU_Report_EN.pdf

8. Sen-Crowe B, Sutherland M, McKenney M, Elkbuli A. A Closer Look Into Global Hospital Beds Capacity and Resource Shortages During the COVID-19 Pandemic. *J Surg Res*. 2021;260:56-63. doi:10.1016/j.jss.2020.11.062

9. Murthy S, Leligdowicz A, Adhikari NKJ. Intensive Care Unit Capacity in Low-Income Countries: A Systematic Review. *PLoS ONE*. 2015;10(1):e0116949. doi:10.1371/journal.pone.0116949

10. Pollack MM, Cuerdon TC, Getson PR. Pediatric intensive care units: results of a national survey. *Crit Care Med*. 1993;21(4):607-614. doi:10.1097/00003246-199304000-00023

11. Horak RV, Griffin JF, Brown AM, et al. Growth and Changing Characteristics of Pediatric Intensive Care 2001-2016. *Crit Care Med*. 2019;47(8):1135-1142. doi:10.1097/CCM.0000000000003863

12. Treble-Barna A, Beers SR, Houtrow AJ, et al. PICU-Based Rehabilitation and Outcomes Assessment: A Survey of Pediatric Critical Care Physicians. *Pediatr Crit Care Med J Soc Crit Care Med World Fed Pediatr Intensive Crit Care Soc*. 2019;20(6):e274-e282. doi:10.1097/PCC.0000000000001940

13. Canadian Institute for Health Information. Inpatient hospitalizations and average length of stay trends in Canada, 2003-2004 and 2004-2005. Published online November 2005. https://secure.cihi.ca/free_products/hmdb_analysis_in_brief_e.pdf.

14. Randolph AG, Gonzales CA, Cortellini L, Yeh TS. Growth of pediatric intensive care units in the United States from 1995 to 2001. *J Pediatr*. 2004;144(6):792-798. doi:10.1016/j.jpeds.2004.03.019

15. Randolph AG, Meert KL, O'Neil ME, et al. The feasibility of conducting clinical trials in infants and children with acute respiratory failure. *Am J Respir Crit Care Med*. 2003;167(10):1334-1340. doi:10.1164/rccm.200210-1175OC

16. Watson RS, Crow SS, Hartman ME, Lacroix J, Odetola FO. Epidemiology and Outcomes of Pediatric Multiple Organ Dysfunction Syndrome. *Pediatr Crit Care Med J Soc Crit Care Med World Fed Pediatr Intensive Crit Care Soc*. 2017;18(3_suppl Suppl 1):S4-S16. doi:10.1097/PCC.0000000000001047

17. Krmpotic K, Lobos AT. Clinical profile of children requiring early unplanned admission to the PICU. *Hosp Pediatr*. 2013;3(3):212-218. doi:10.1542/hpeds.2012-0081

18. Typpo KV, Petersen NJ, Hallman DM, Markovitz BP, Mariscalco MM. Day 1 multiple organ dysfunction syndrome is associated with poor functional outcome and mortality in the pediatric intensive care unit. *Pediatr Crit Care Med J Soc Crit Care Med World Fed Pediatr Intensive Crit Care Soc*. 2009;10(5):562-570. doi:10.1097/PCC.0b013e3181a64be1

19. Udy AA, Roberts JA, Lipman J. Clinical implications of antibiotic pharmacokinetic principles in the critically ill. *Intensive Care Med*. 2013;39(12):2070-2082. doi:10.1007/s00134-013-3088-4

20. Udy AA, Roberts JA, De Waele JJ, Paterson DL, Lipman J. What's behind the failure of emerging antibiotics in the critically ill? Understanding the impact of altered pharmacokinetics and augmented renal clearance. *Int J Antimicrob Agents*. 2012;39(6):455-457. doi:10.1016/j.ijantimicag.2012.02.010

21. Boucher BA, Wood GC, Swanson JM. Pharmacokinetic changes in critical illness. *Crit Care Clin*. 2006;22(2):255-271, vi. doi:10.1016/j.ccc.2006.02.011

22. Martinez MN, Amidon GL. A mechanistic approach to understanding the factors affecting drug absorption: a review of fundamentals. *J Clin Pharmacol*. 2002;42(6):620-643. doi:10.1177/00970002042006005

23. Roberts JA, Lipman J. Pharmacokinetic issues for antibiotics in the critically ill patient. *Crit Care Med*. 2009;37(3):840-851; quiz 859. doi:10.1097/CCM.0b013e3181961bff

24. Sepsis produces early depression of gut absorptive capacity: restoration with diltiazem treatment - PubMed. Accessed March 12, 2024. https://pubmed.ncbi.nlm.nih.gov/1636786/

25. Johnston JD, Harvey CJ, Menzies IS, Treacher DF. Gastrointestinal permeability and absorptive capacity in sepsis. *Crit Care Med*. 1996;24(7):1144-1149. doi:10.1097/00003246-199607000-00013

26. Vinarov Z, Abdallah M, Agundez JAG, et al. Impact of gastrointestinal tract variability on oral drug absorption and pharmacokinetics: An UNGAP review. *Eur J Pharm Sci Off J Eur Fed Pharm Sci*. 2021;162:105812. doi:10.1016/j.ejps.2021.105812

27. Nguyen NQ, Ng MP, Chapman M, Fraser RJ, Holloway RH. The impact of admission diagnosis on gastric emptying in critically ill patients. *Crit Care Lond Engl*. 2007;11(1):R16. doi:10.1186/cc5685

28. Tansley G, Hall R. Pharmacokinetic considerations for drugs administered in the critically ill. *Br J Hosp Med Lond Engl 2005*. 2015;76(2):89-94. doi:10.12968/hmed.2015.76.2.89

29. Smith BS, Yogaratnam D, Levasseur-Franklin KE, Forni A, Fong J. Introduction to drug pharmacokinetics in the critically ill patient. *Chest*. 2012;141(5):1327-1336. doi:10.1378/chest.11-1396

30. Tarling MM, Toner CC, Withington PS, Baxter MK, Whelpton R, Goldhill DR. A model of gastric emptying using paracetamol absorption in intensive care patients. *Intensive Care Med*. 1997;23(3):256-260. doi:10.1007/s001340050325

31. Morales Castro D, Dresser L, Granton J, Fan E. Pharmacokinetic Alterations Associated with Critical Illness. *Clin Pharmacokinet*. 2023;62(2):209-220. doi:10.1007/s40262-023-01213-x

32. Gertz M, Harrison A, Houston JB, Galetin A. Prediction of human intestinal first-pass metabolism of 25 CYP3A substrates from in vitro clearance and permeability data. *Drug Metab Dispos Biol Fate Chem*. 2010;38(7):1147-1158. doi:10.1124/dmd.110.032649

33. Dixon J, Lane K, Macphee I, Philips B. Xenobiotic metabolism: the effect of acute kidney injury on non-renal drug clearance and hepatic drug metabolism. *Int J Mol Sci*. 2014;15(2):2538-2553. doi:10.3390/ijms15022538

34. Priglinger U, Delle Karth G, Geppert A, et al. Prophylactic anticoagulation with enoxaparin: Is the subcutaneous route appropriate in the critically ill? *Crit Care Med*. 2003;31(5):1405-1409. doi:10.1097/01.CCM.0000059725.60509.A0

35. Dörffler-Melly J, de Jonge E, Pont AC, et al. Bioavailability of subcutaneous low-molecular-weight heparin to patients on vasopressors. *Lancet Lond Engl*. 2002;359(9309):849-850. doi:10.1016/s0140-6736(02)07920-5

36. Cihlar R, Sramek V, Papiez A, Penka M, Suk P. Pharmacokinetic Comparison of Subcutaneous and Intravenous Nadroparin Administration for Thromboprophylaxis in Critically Ill Patients on Vasopressors. *Pharmacology*. 2020;105(1-2):73-78. doi:10.1159/000502847

37. Smith DA, Beaumont K, Maurer TS, Di L. Volume of Distribution in Drug Design. *J Med Chem*. 2015;58(15):5691-5698. doi:10.1021/acs.jmedchem.5b00201

38. Singer M, Deutschman CS, Seymour CW, et al. The Third International Consensus Definitions for Sepsis and Septic Shock (Sepsis-3). *JAMA*. 2016;315(8):801-810. doi:10.1001/jama.2016.0287

39. Dolmatova EV, Wang K, Mandavilli R, Griendling KK. The effects of sepsis on endothelium and clinical implications. *Cardiovasc Res*. 2020;117(1):60-73. doi:10.1093/cvr/cvaa070

40. Nuytinck HK, Offermans XJ, Kubat K, Goris JA. Whole-body inflammation in trauma patients. An autopsy study. *Arch Surg Chic Ill 1960*. 1988;123(12):1519-1524. doi:10.1001/archsurg.1988.01400360089016

41. Hanes SD, Wood GC, Herring V, et al. Intermittent and continuous ceftazidime infusion for critically ill trauma patients. *Am J Surg*. 2000;179(6):436-440. doi:10.1016/s0002-9610(00)00388-3

42. Ronchera-Oms CL, Tormo C, Ordovás JP, Abad J, Jiménez NV. Expanded gentamicin volume of distribution in critically ill adult patients receiving total parenteral nutrition. *J Clin Pharm Ther*. 1995;20(5):253-258. doi:10.1111/j.1365-2710.1995.tb00659.x

43. Gous AG, Dance MD, Lipman J, Luyt DK, Mathivha R, Scribante J. Changes in vancomycin pharmacokinetics in critically ill infants. *Anaesth Intensive Care*. 1995;23(6):678-682. doi:10.1177/0310057X9502300603

44. Pea F, Viale P, Furlanut M. Antimicrobial therapy in critically ill patients: a review of pathophysiological conditions responsible for altered disposition and pharmacokinetic variability. *Clin Pharmacokinet*. 2005;44(10):1009-1034. doi:10.2165/00003088-200544100-00002

45. Pinder M, Bellomo R, Lipman J. Pharmacological principles of antibiotic prescription in the critically ill. *Anaesth Intensive Care*. 2002;30(2):134-144. doi:10.1177/0310057X0203000203

46. Vincent JL, Dubois MJ, Navickis RJ, Wilkes MM. Hypoalbuminemia in Acute Illness: Is There a Rationale for Intervention?: A Meta-Analysis of Cohort Studies and Controlled Trials. *Ann Surg*. 2003;237(3):319. doi:10.1097/01.SLA.0000055547.93484.87

47. Melia D, Post B. Human albumin solutions in intensive care: A review. *J Intensive Care Soc*. 2021;22(3):248-254. doi:10.1177/1751143720961245

48. Edwards DJ, Lalka D, Cerra F, Slaughter RL. Alpha1-acid glycoprotein concentration and protein binding in trauma. *Clin Pharmacol Ther*. 1982;31(1):62-67. doi:10.1038/clpt.1982.10

49. Hsiao SY, Lai YR, Kung CT, et al. α-1-Acid Glycoprotein Concentration as an Outcome Predictor in Adult Patients with Sepsis. *BioMed Res Int*. 2019;2019:3174896. doi:10.1155/2019/3174896

50. Benedetti MS, Whomsley R, Poggesi I, et al. Drug metabolism and pharmacokinetics. *Drug Metab Rev*. 2009;41(3):344-390. doi:10.1080/10837450902891295

51. Benet LZ, Zia-Amirhosseini P. Basic principles of pharmacokinetics. *Toxicol Pathol*. 1995;23(2):115-123. doi:10.1177/019262339502300203

52. Griffith DM, Lewis S, Rossi AG, et al. Systemic inflammation after critical illness: relationship with physical recovery and exploration of potential mechanisms. *Thorax*. 2016;71(9):820-829. doi:10.1136/thoraxjnl-2015-208114

53. Ewoldt TM, Abdulla A, Hunfeld N, et al. The impact of sepsis on hepatic drug metabolism in critically ill patients: a narrative review. *Expert Opin Drug Metab Toxicol*. 2022;18(6):413-421. doi:10.1080/17425255.2022.2106215

54. Stanke-Labesque F, Gautier-Veyret E, Chhun S, Guilhaumou R. Inflammation is a major regulator of drug metabolizing enzymes and transporters: Consequences for the personalization of drug treatment. *Pharmacol Ther*. 2020;215:107627. doi:10.1016/j.pharmthera.2020.107627

55. Lea-Henry TN, Carland JE, Stocker SL, Sevastos J, Roberts DM. Clinical Pharmacokinetics in Kidney Disease. *Clin J Am Soc Nephrol CJASN*. 2018;13(7):1085-1095. doi:10.2215/CJN.00340118

56. Tandukar S, Palevsky PM. Continuous Renal Replacement Therapy: Who, When, Why, and How. *Chest*. 2019;155(3):626-638. doi:10.1016/j.chest.2018.09.004

57. De Zan F, Amigoni A, Pozzato R, Pettenazzo A, Murer L, Vidal E. Acute Kidney Injury in Critically Ill Children: A Retrospective Analysis of Risk Factors. *Blood Purif*. 2020;49(1-2):1-7. doi:10.1159/000502081

58. Blanco VE, Hernandorena CV, Scibona P, Belloso W, Musso CG. Acute Kidney Injury Pharmacokinetic Changes and Its Impact on Drug Prescription. *Healthcare*. 2019;7(1):10. doi:10.3390/healthcare7010010

59. Melo F de AF, Macedo E, Fonseca Bezerra AC, et al. A systematic review and meta-analysis of acute kidney injury in the intensive care units of developed and developing countries. *PloS One*. 2020;15(1):e0226325. doi:10.1371/journal.pone.0226325

60. Kaddourah A, Basu RK, Bagshaw SM, Goldstein SL, AWARE Investigators. Epidemiology of Acute Kidney Injury in Critically Ill Children and Young Adults. *N Engl J Med*. 2017;376(1):11-20. doi:10.1056/NEJMoa1611391

61. Basu RK, Kaddourah A, Goldstein SL, AWARE Study Investigators. Assessment of a renal angina index for prediction of severe acute kidney injury in critically ill children: a multicentre, multinational, prospective observational study. *Lancet Child Adolesc Health*. 2018;2(2):112-120. doi:10.1016/S2352-4642(17)30181-5

62. Bellomo R, Ronco C, Kellum JA, Mehta RL, Palevsky P, Acute Dialysis Quality Initiative workgroup. Acute renal failure - definition, outcome measures, animal models, fluid therapy and information technology needs: the Second International Consensus Conference of the Acute Dialysis Quality Initiative (ADQI) Group. *Crit Care Lond Engl*. 2004;8(4):R204-212. doi:10.1186/cc2872

63. Mehta RL, Kellum JA, Shah SV, et al. Acute Kidney Injury Network: report of an initiative to improve outcomes in acute kidney injury. *Crit Care*. 2007;11(2):R31. doi:10.1186/cc5713

64. Kidney disease: improving global outcomes. Acute Kidney Injury. 2012. https://kdigo.org/wp-content/uploads/2016/10/KDIGO-2012-AKI-Guideline-English.pdf.

65. Section 2: AKI Definition. *Kidney Int Suppl*. 2012;2(1):19-36. doi:10.1038/kisup.2011.32

66. Akcan-Arikan A, Zappitelli M, Loftis LL, Washburn KK, Jefferson LS, Goldstein SL. Modified RIFLE criteria in critically ill children with acute kidney injury. *Kidney Int*. 2007;71(10):1028-1035. doi:10.1038/sj.ki.5002231

67. Pickkers P, Darmon M, Hoste E, et al. Acute kidney injury in the critically ill: an updated review on pathophysiology and management. *Intensive Care Med*. 2021;47(8):835-850. doi:10.1007/s00134-021-06454-7

68. Garofalo AM, Lorente-Ros M, Goncalvez G, et al. Histopathological changes of organ dysfunction in sepsis. *Intensive Care Med Exp*. 2019;7(Suppl 1):45. doi:10.1186/s40635-019-0236-3

69. Fitzgerald JC, Basu RK, Akcan-Arikan A, et al. Acute Kidney Injury in Pediatric Severe Sepsis: An Independent Risk Factor for Death and New Disability. *Crit Care Med*. 2016;44(12):2241-2250. doi:10.1097/CCM.0000000000002007

70. Bagshaw SM, George C, Bellomo R, ANZICS Database Management Committee. Early acute kidney injury and sepsis: a multicentre evaluation. *Crit Care Lond Engl*. 2008;12(2):R47. doi:10.1186/cc6863

71. Kolhe NV, Stevens PE, Crowe AV, Lipkin GW, Harrison DA. Case mix, outcome and activity for patients with severe acute kidney injury during the first 24 hours after admission to an adult, general critical care unit: application of predictive models from a secondary analysis of the ICNARC Case Mix Programme database. *Crit Care Lond Engl*. 2008;12 Suppl 1(Suppl 1):S2. doi:10.1186/cc7003

72. Kellum JA, Prowle JR. Paradigms of acute kidney injury in the intensive care setting. *Nat Rev Nephrol*. 2018;14(4):217-230. doi:10.1038/nrneph.2017.184

73. Langenberg C, Gobe G, Hood S, May CN, Bellomo R. Renal histopathology during experimental septic acute kidney injury and recovery. *Crit Care Med*. 2014;42(1):e58-67. doi:10.1097/CCM.0b013e3182a639da

74. Gomez H, Ince C, De Backer D, et al. A unified theory of sepsis-induced acute kidney injury: inflammation, microcirculatory dysfunction, bioenergetics, and the tubular cell adaptation to injury. *Shock Augusta Ga*. 2014;41(1):3-11. doi:10.1097/SHK.0000000000000052

75. Mariano F, Cantaluppi V, Stella M, et al. Circulating plasma factors induce tubular and glomerular alterations in septic burns patients. *Crit Care Lond Engl*. 2008;12(2):R42. doi:10.1186/cc6848

76. Mehta RL, Bouchard J, Soroko SB, et al. Sepsis as a cause and consequence of acute kidney injury: Program to Improve Care in Acute Renal Disease. *Intensive Care Med*. 2011;37(2):241-248. doi:10.1007/s00134-010-2089-9

77. Molitoris BA, Sutton TA. Endothelial injury and dysfunction: role in the extension phase of acute renal failure. *Kidney Int*. 2004;66(2):496-499. doi:10.1111/j.1523-1755.2004.761_5.x

78. Devarajan P. Update on mechanisms of ischemic acute kidney injury. *J Am Soc Nephrol JASN*. 2006;17(6):1503-1520. doi:10.1681/ASN.2006010017

79. Schetz M, Dasta J, Goldstein S, Golper T. Drug-induced acute kidney injury. *Curr Opin Crit Care*. 2005;11(6):555-565. doi:10.1097/01.ccx.0000184300.68383.95

80. Nash K, Hafeez A, Hou S. Hospital-acquired renal insufficiency. *Am J Kidney Dis Off J Natl Kidney Found*. 2002;39(5):930-936. doi:10.1053/ajkd.2002.32766

81. Faught LN, Greff MJE, Rieder MJ, Koren G. Drug-induced acute kidney injury in children. *Br J Clin Pharmacol*. 2015;80(4):901-909. doi:10.1111/bcp.12554

82. *de Broe ME, Porter GA, Bennet WM, Verpooten GA. Clinical nephrotoxins. 2nd ed. Springer Netherlands; 2003.*

83. Vincent JL, Sakr Y, Sprung CL, et al. Sepsis in European intensive care units: results of the SOAP study. *Crit Care Med*. 2006;34(2):344-353. doi:10.1097/01.ccm.0000194725.48928.3a

84. Soo A, Zuege DJ, Fick GH, et al. Describing organ dysfunction in the intensive care unit: a cohort study of 20,000 patients. *Crit Care Lond Engl*. 2019;23(1):186. doi:10.1186/s13054-019-2459-9

85. Weiss SL, Peters MJ, Alhazzani W, et al. Surviving Sepsis Campaign International Guidelines for the Management of Septic Shock and Sepsis-Associated Organ Dysfunction in Children. *Pediatr Crit Care Med J Soc Crit Care Med World Fed Pediatr Intensive Crit Care Soc*. 2020;21(2):e52-e106. doi:10.1097/PCC.0000000000002198

86. Leteurtre S, Martinot A, Duhamel A, et al. Validation of the paediatric logistic organ dysfunction (PELOD) score: prospective, observational, multicentre study. *Lancet Lond Engl*. 2003;362(9379):192-197. doi:10.1016/S0140-6736(03)13908-6

87. Ricci Z, Goldstein SL. Pediatric Continuous Renal Replacement Therapy. *Contrib Nephrol*. 2016;187:121-130. doi:10.1159/000442370

88. Tolwani A. Continuous renal-replacement therapy for acute kidney injury. *N Engl J Med*. 2012;367(26):2505-2514. doi:10.1056/NEJMct1206045

89. Pea F, Viale P, Pavan F, Furlanut M. Pharmacokinetic considerations for antimicrobial therapy in patients receiving renal replacement therapy. *Clin Pharmacokinet*. 2007;46(12):997-1038. doi:10.2165/00003088-200746120-00003

90. Jamal JA, Udy AA, Lipman J, Roberts JA. The impact of variation in renal replacement therapy settings on piperacillin, meropenem, and vancomycin drug clearance in the critically ill: an analysis of published literature and dosing regimens*. *Crit Care Med*. 2014;42(7):1640-1650. doi:10.1097/CCM.0000000000000317

91. Purohit PJ, Elkomy MH, Frymoyer A, et al. Antimicrobial Disposition During Pediatric Continuous Renal Replacement Therapy Using an Ex Vivo Model. *Crit Care Med*. 2019;47(9):e767-e773. doi:10.1097/CCM.0000000000003895

92. Ronco C, Clark WR. Haemodialysis membranes. *Nat Rev Nephrol*. 2018;14(6):394-410. doi:10.1038/s41581-018-0002-x

93. O'Reilly P, Tolwani A. Renal replacement therapy III: IHD, CRRT, SLED. *Crit Care Clin*. 2005;21(2):367-378. doi:10.1016/j.ccc.2005.01.004

94. John JC, Taha S, Bunchman TE. Basics of continuous renal replacement therapy in pediatrics. *Kidney Res Clin Pract*. 2019;38(4):455-461. doi:10.23876/j.krcp.19.060

95. Weidhase L, de Fallois J, Haußig E, Kaiser T, Mende M, Petros S. Myoglobin clearance with continuous veno-venous hemodialysis using high cutoff dialyzer versus continuous veno-venous hemodiafiltration using high-flux dialyzer: a prospective randomized controlled trial. *Crit Care*. 2020;24:644. doi:10.1186/s13054-020-03366-8

96. Balgobin S, Morena M, Brunot V, et al. Continuous Veno-Venous High Cut-Off Hemodialysis Compared to Continuous Veno-Venous Hemodiafiltration in Intensive Care Unit Acute Kidney Injury Patients. *Blood Purif*. 2018;46(3):248-256. doi:10.1159/000489082

97. Rewa OG, Ortiz-Soriano V, Lambert J, et al. Epidemiology and Outcomes of AKI Treated With Continuous Kidney Replacement Therapy: The Multicenter CRRTnet Study. *Kidney Med*. 2023;5(6):100641. doi:10.1016/j.xkme.2023.100641

98. Daverio M, Cortina G, Jones A, et al. Continuous Kidney Replacement Therapy Practices in Pediatric Intensive Care Units Across Europe. *JAMA Netw Open*. 2022;5(12):e2246901. doi:10.1001/jamanetworkopen.2022.46901

99. Bugge JF. Pharmacokinetics and drug dosing adjustments during continuous venovenous hemofiltration or hemodiafiltration in critically ill patients. *Acta Anaesthesiol Scand*. 2001;45(8):929-934. doi:10.1034/j.1399-6576.2001.450802.x

100. Brunet S, Leblanc M, Geadah D, Parent D, Courteau S, Cardinal J. Diffusive and convective solute clearances during continuous renal replacement therapy at various dialysate and ultrafiltration flow rates. *Am J Kidney Dis Off J Natl Kidney Found*. 1999;34(3):486-492. doi:10.1016/s0272-6386(99)70076-4

101. Golper TA, Cigarran-Guldris S, Jenkins RD, Brier ME. The role of convection during simulated continuous arteriovenous hemodialysis. *Contrib Nephrol*. 1991;93:146-148. doi:10.1159/000420206

102. Pistolesi V, Morabito S, Di Mario F, Regolisti G, Cantarelli C, Fiaccadori E. A Guide to Understanding Antimicrobial Drug Dosing in Critically Ill Patients on Renal Replacement Therapy. *Antimicrob Agents Chemother*. 2019;63(8):e00583-19. doi:10.1128/AAC.00583-19

103. Choi G, Gomersall CD, Tian Q, Joynt GM, Freebairn R, Lipman J. Principles of antibacterial dosing in continuous renal replacement therapy. *Crit Care Med*. 2009;37(7):2268-2282. doi:10.1097/CCM.0b013e3181aab3d0

104. Bugge JF. Influence of renal replacement therapy on pharmacokinetics in critically ill patients. *Best Pract Res Clin Anaesthesiol*. 2004;18(1):175-187. doi:10.1016/j.bpa.2003.09.002

105. Hoff BM, Maker JH, Dager WE, Heintz BH. Antibiotic Dosing for Critically Ill Adult Patients Receiving Intermittent Hemodialysis, Prolonged Intermittent Renal Replacement Therapy, and Continuous Renal Replacement Therapy: An Update. *Ann Pharmacother*. 2020;54(1):43-55. doi:10.1177/1060028019865873

106. Li AMMY, Gomersall CD, Choi G, Tian Q, Joynt GM, Lipman J. A systematic review of antibiotic dosing regimens for septic patients receiving continuous renal replacement therapy: do current studies supply sufficient data? *J Antimicrob Chemother*. 2009;64(5):929-937. doi:10.1093/jac/dkp302

107. Roberts JA, Joynt GM, Lee A, et al. The Effect of Renal Replacement Therapy and Antibiotic Dose on Antibiotic Concentrations in Critically Ill Patients: Data From the Multinational Sampling Antibiotics in Renal Replacement Therapy Study. *Clin Infect Dis Off Publ Infect Dis Soc Am*. 2021;72(8):1369-1378. doi:10.1093/cid/ciaa224

108. Schetz M, Ferdinande P, Van den Berghe G, Verwaest C, Lauwers P. Pharmacokinetics of continuous renal replacement therapy. *Intensive Care Med*. 1995;21(7):612-620. doi:10.1007/BF01700172

109. Troyanov S, Cardinal J, Geadah D, et al. Solute clearances during continuous venovenous haemofiltration at various ultrafiltration flow rates using Multiflow-100 and HF1000 filters. *Nephrol Dial Transplant Off Publ Eur Dial Transpl Assoc - Eur Ren Assoc*. 2003;18(5):961-966. doi:10.1093/ndt/gfg055

110. Uchino S, Cole L, Morimatsu H, Goldsmith D, Bellomo R. Clearance of vancomycin during high-volume haemofiltration: impact of pre-dilution. *Intensive Care Med*. 2002;28(11):1664-1667. doi:10.1007/s00134-002-1495-z

111. Frazee EN, Kuper PJ, Schramm GE, et al. Effect of continuous venovenous hemofiltration dose on achievement of adequate vancomycin trough concentrations. *Antimicrob Agents Chemother*. 2012;56(12):6181-6185. doi:10.1128/AAC.00459-12

112. Hakim RM. Clinical implications of hemodialysis membrane biocompatibility. *Kidney Int*. 1993;44(3):484-494. doi:10.1038/ki.1993.272

113. Hakim RM, Fearon DT, Lazarus JM. Biocompatibility of dialysis membranes: effects of chronic complement activation. *Kidney Int*. 1984;26(2):194-200. doi:10.1038/ki.1984.155

114. Thomas M, Moriyama K, Ledebo I. AN69: Evolution of the world's first high permeability membrane. *Contrib Nephrol*. 2011;173:119-129. doi:10.1159/000328961

115. Clark WR, Gao D, Ronco C. Membranes for dialysis. Composition, structure and function. *Contrib Nephrol*. 2002;(137):70-77.

116. Kanji S, Roger C, Taccone FS, Muller L. Practical considerations for individualizing drug dosing in critically ill adults receiving renal replacement therapy. *Pharmacotherapy*. 2023;43(11):1194-1205. doi:10.1002/phar.2858

117. Onichimowski D, Ziółkowski H, Nosek K, Jaroszewski J, Rypulak E, Czuczwar M. Comparison of adsorption of selected antibiotics on the filters in continuous renal replacement therapy circuits: in vitro studies. *J Artif Organs Off J Jpn Soc Artif Organs*. 2020;23(2):163-170. doi:10.1007/s10047-019-01139-x

118. Shiraishi Y, Okajima M, Sai Y, Miyamoto K, Inaba H. Elimination of teicoplanin by adsorption to the filter membrane during haemodiafiltration: screening experiments for linezolid, teicoplanin and vancomycin followed by in vitro haemodiafiltration models for teicoplanin. *Anaesth Intensive Care*. 2012;40(3):442-449. doi:10.1177/0310057X1204000309

119. Vossen MG, Pferschy S, Milacek C, et al. In vivo / in vitro Correlation of Pharmacokinetics of Gentamicin, Vancomycin, Teicoplanin and Doripenem in a Bovine Blood Hemodialysis Model. *Front Pharmacol*. 2021;12:702455. doi:10.3389/fphar.2021.702455

120. González de Molina F, Martínez-Alberici M de LÁ, Ferrer R. Treatment with echinocandins during continuous renal replacement therapy. *Crit Care Lond Engl*. 2014;18(2):218. doi:10.1186/cc13803

121. Macedo E, Mehta RL. Continuous Dialysis Therapies: Core Curriculum 2016. *Am J Kidney Dis Off J Natl Kidney Found*. 2016;68(4):645-657. doi:10.1053/j.ajkd.2016.03.427

122. Baud FJ, Houzé P, Raphalen JH, et al. Diafiltration flowrate is a determinant of the extent of adsorption of amikacin in renal replacement therapy using the ST150®-AN69 filter: An in vitro study. *Int J Artif Organs*. 2020;43(12):758-766. doi:10.1177/0391398820911928

123. Burrell A, Kim J, Alliegro P, et al. Extracorporeal membrane oxygenation for critically ill adults. *Cochrane Database Syst Rev*. 2023;9(9):CD010381. doi:10.1002/14651858.CD010381.pub3

124. Makdisi G, Wang I wen. Extra Corporeal Membrane Oxygenation (ECMO) review of a lifesaving technology. *J Thorac Dis*. 2015;7(7):E166-E176. doi:10.3978/j.issn.2072-1439.2015.07.17

125. Cui Y, Zhang Y, Dou J, et al. Venovenous vs. Venoarterial Extracorporeal Membrane Oxygenation in Infection-Associated Severe Pediatric Acute Respiratory Distress Syndrome: A Prospective Multicenter Cohort Study. *Front Pediatr*. 2022;10:832776. doi:10.3389/fped.2022.832776

126. ELSO. *ECLS Registry Report: International Summary.* August 2017.

127. Wildschut ED, Ahsman MJ, Allegaert K, Mathot RAA, Tibboel D. Determinants of drug absorption in different ECMO circuits. *Intensive Care Med*. 2010;36(12):2109-2116. doi:10.1007/s00134-010-2041-z

128. Sutiman N, Koh JC, Watt K, et al. Pharmacokinetics Alterations in Critically Ill Pediatric Patients on Extracorporeal Membrane Oxygenation: A Systematic Review. *Front Pediatr*. 2020;8:260. doi:10.3389/fped.2020.00260

129. Shekar K, Roberts JA, Mcdonald CI, et al. Sequestration of drugs in the circuit may lead to therapeutic failure during extracorporeal membrane oxygenation. *Crit Care Lond Engl*. 2012;16(5):R194. doi:10.1186/cc11679

130. Shekar K, Roberts JA, Mcdonald CI, et al. Protein-bound drugs are prone to sequestration in the extracorporeal membrane oxygenation circuit: results from an ex vivo study. *Crit Care Lond Engl*. 2015;19(1):164. doi:10.1186/s13054-015-0891-z

131. Preston TJ, Hodge AB, Riley JB, Leib-Sargel C, Nicol KK. In Vitro Drug Adsorption and Plasma Free Hemoglobin Levels Associated With Hollow Fiber Oxygenators in the Extracorporeal Life Support (ECLS) Circuit. *J Extra Corpor Technol*. 2007;39(4):234-237.

132. Preston TJ, Ratliff TM, Gomez D, et al. Modified Surface Coatings and their Effect on Drug Adsorption within the Extracorporeal Life Support Circuit. *J Extra Corpor Technol*. 2010;42(3):199-202.

133. Cheng V, Abdul-Aziz MH, Roberts JA, Shekar K. Optimising drug dosing in patients receiving extracorporeal membrane oxygenation. *J Thorac Dis*. 2018;10(Suppl 5):S629-S641. doi:10.21037/jtd.2017.09.154

134. Shekar K, Fraser JF, Smith MT, Roberts JA. Pharmacokinetic changes in patients receiving extracorporeal membrane oxygenation. *J Crit Care*. 2012;27(6):741.e9-18. doi:10.1016/j.jcrc.2012.02.013

135. Choi M, Alvarez N, Tsypin Y, Sparks B, Hirose H. Blood Transfusion Requirements for Patients on Extracorporeal Membrane Oxygenation. *J Heart Lung Transplant*. 2020;39(4):S100. doi:10.1016/j.healun.2020.01.953

136. Millar JE, Fanning JP, McDonald CI, McAuley DF, Fraser JF. The inflammatory response to extracorporeal membrane oxygenation (ECMO): a review of the pathophysiology. *Crit Care*. 2016;20:387. doi:10.1186/s13054-016-1570-4

137. Ostermann M, Lumlertgul N. Acute kidney injury in ECMO patients. *Crit Care*. 2021;25:313. doi:10.1186/s13054-021-03676-5

138. Thongprayoon C, Cheungpasitporn W, Lertjitbanjong P, et al. Incidence and Impact of Acute Kidney Injury in Patients Receiving Extracorporeal Membrane Oxygenation: A Meta-Analysis. *J Clin Med*. 2019;8(7):981. doi:10.3390/jcm8070981

139. Raffaeli G, Pokorna P, Allegaert K, et al. Drug Disposition and Pharmacotherapy in Neonatal ECMO: From Fragmented Data to Integrated Knowledge. *Front Pediatr*. 2019;7:360. doi:10.3389/fped.2019.00360

140. Vet NJ, de Hoog M, Tibboel D, de Wildt SN. The effect of inflammation on drug metabolism: a focus on pediatrics. *Drug Discov Today*. 2011;16(9-10):435-442. doi:10.1016/j.drudis.2011.02.014

141. Nolin TD, Aronoff GR, Fissell WH, et al. Pharmacokinetic assessment in patients receiving continuous RRT: perspectives from the Kidney Health Initiative. *Clin J Am Soc Nephrol CJASN*. 2015;10(1):159-164. doi:10.2215/CJN.05630614

142. Schatz LM, Brinkmann A, Röhr A, et al. Systematic Evaluation of Pharmacokinetic Models for Model-Informed Precision Dosing of Meropenem in Critically Ill Patients Undergoing Continuous Renal Replacement Therapy. *Antimicrob Agents Chemother*. 67(5):e00104-23. doi:10.1128/aac.00104-23

143. Broeker A, Vossen MG, Thalhammer F, et al. An Integrated Dialysis Pharmacometric (IDP) Model to Evaluate the Pharmacokinetics in Patients Undergoing Renal Replacement Therapy. *Pharm Res*. 2020;37(6):96. doi:10.1007/s11095-020-02832-w

144. Watt KM, Cohen-Wolkowiez M, Barrett JS, et al. Physiologically Based Pharmacokinetic Approach to Determine Dosing on Extracorporeal Life Support: Fluconazole in Children on ECMO. *CPT Pharmacomet Syst Pharmacol*. 2018;7(10):629-637. doi:10.1002/psp4.12338

145. Rowland M, Peck C, Tucker G. Physiologically-based pharmacokinetics in drug development and regulatory science. *Annu Rev Pharmacol Toxicol*. 2011;51:45-73. doi:10.1146/annurev-pharmtox-010510-100540

146. Maharaj AR, Edginton AN. Physiologically Based Pharmacokinetic Modeling and Simulation in Pediatric Drug Development. *CPT Pharmacomet Syst Pharmacol*. 2014;3(11):e148. doi:10.1038/psp.2014.45

147. Wu Q, Peters SA. A Retrospective Evaluation of Allometry, Population Pharmacokinetics, and Physiologically-Based Pharmacokinetics for Pediatric Dosing Using Clearance as a Surrogate. *CPT Pharmacomet Syst Pharmacol*. 2019;8(4):220-229. doi:10.1002/psp4.12385

148. Johnson TN, Rostami-Hodjegan A, Tucker GT. Prediction of the clearance of eleven drugs and associated variability in neonates, infants and children. *Clin Pharmacokinet*. 2006;45(9):931-956. doi:10.2165/00003088-200645090-00005

149. Edginton AN, Zimmerman EI, Vasilyeva A, Baker SD, Panetta JC. Sorafenib Metabolism, Transport, and Enterohepatic Recycling: Physiologically Based Modeling and Simulation in Mice. *Cancer Chemother Pharmacol*. 2016;77(5):1039-1052. doi:10.1007/s00280-016-3018-6

150. Fuhr LM, Hanke N, Meibohm B, Lehr T. Effective Removal of Dabigatran by Idarucizumab or Hemodialysis: A Physiologically Based Pharmacokinetic Modeling Analysis. *Clin Pharmacokinet*. 2020;59(6):809-825. doi:10.1007/s40262-019-00857-y

151. Ronco C, Bellomo R, Homel P, et al. Effects of different doses in continuous veno-venous haemofiltration on outcomes of acute renal failure: a prospective randomised trial. *Lancet Lond Engl*. 2000;356(9223):26-30. doi:10.1016/S0140-6736(00)02430-2

152. Craig WA. Does the dose matter? *Clin Infect Dis Off Publ Infect Dis Soc Am*. 2001;33 Suppl 3:S233-237. doi:10.1086/321854

153. Roberts JA, Kruger P, Paterson DL, Lipman J. Antibiotic resistance--what's dosing got to do with it? *Crit Care Med*. 2008;36(8):2433-2440. doi:10.1097/CCM.0b013e318180fe62

154. Veltri MA, Neu AM, Fivush BA, Parekh RS, Furth SL. Drug dosing during intermittent hemodialysis and continuous renal replacement therapy : special considerations in pediatric patients. *Paediatr Drugs*. 2004;6(1):45-65. doi:10.2165/00148581-200406010-00004

155. Dubinsky S. PROSPERO 2021 CRD42021250070. Pharmacokinetics of commonly used medications in children receiving continuous renal replacement therapy: a systematic review of current literature.

156. Covidence systematic review software, Veritas Health Innovation, Melbourne, Australia. Available at www.covidence.org.

157. Higgins JPT, Thomas J, Chandler J, *et.al*. Cochrane handbook for systematic reviews of interventions version 6.2 (updated February 2021). Cochrane, 2021. Available from www.training.cochrane.org/handbookCochrane handbook.

158. Kanji S, Hayes M, Ling A, et al. Reporting Guidelines for Clinical Pharmacokinetic Studies: The ClinPK Statement. *Clin Pharmacokinet*. 2015;54(7):783-795. doi:10.1007/s40262-015-0236-8

159. Page MJ, McKenzie JE, Bossuyt PM, et al. The PRISMA 2020 statement: an updated guideline for reporting systematic reviews. *BMJ*. 2021;372:n71. doi:10.1136/bmj.n71

160. Baird JS. The sieving coefficient and clearance of vasopressin during continuous renal replacement therapy in critically ill children. *J Crit Care*. 2010;25(4):591-594. doi:10.1016/j.jcrc.2010.03.005

161. Kleiber N, Mathôt RAA, Ahsman MJ, Wildschut ED, Tibboel D, de Wildt SN. Population pharmacokinetics of intravenous clonidine for sedation during paediatric extracorporeal membrane oxygenation and continuous venovenous hemofiltration. *Br J Clin Pharmacol*. 2017;83(6):1227-1239. doi:10.1111/bcp.13235

162. Michaličková D, Pokorná P, Tibboel D, Slanař O, Knibbe CAJ, Krekels EHJ. Rapid Increase in Clearance of Phenobarbital in Neonates on Extracorporeal Membrane Oxygenation: A Pilot Retrospective Population Pharmacokinetic Analysis. *Pediatr Crit Care Med J Soc Crit Care Med World Fed Pediatr Intensive Crit Care Soc*. 2020;21(9):e707-e715. doi:10.1097/PCC.0000000000002402

163. Nehus EJ, Mizuno T, Cox S, Goldstein SL, Vinks AA. Pharmacokinetics of meropenem in children receiving continuous renal replacement therapy: Validation of clinical trial simulations. *J Clin Pharmacol*. 2016;56(3):291-297. doi:10.1002/jcph.601

164. Mulla H, Lawson G, Peek GJ, Firmin RK, Upton DR. Plasma concentrations of midazolam in neonates receiving extracorporeal membrane oxygenation. *ASAIO J Am Soc Artif Intern Organs 1992*. 2003;49(1):41-47. doi:10.1097/00002480-200301000-00007

165. Tan WW, Watt KM, Boakye-Agyeman F, et al. Optimal Dosing of Meropenem in a Small Cohort of Critically Ill Children Receiving Continuous Renal Replacement Therapy. *J Clin Pharmacol*. 2021;61(6):744-754. doi:10.1002/jcph.1798

166. Wang Y, Li Z, Chen W, et al. Pharmacokinetics of meropenem in children with sepsis undergoing extracorporeal life support: A prospective observational study. *J Clin Pharm Ther*. 2021;46(3):754-761. doi:10.1111/jcpt.13344

167. Watt KM, Gonzalez D, Benjamin DK, et al. Fluconazole population pharmacokinetics and dosing for prevention and treatment of invasive Candidiasis in children supported with extracorporeal membrane oxygenation. *Antimicrob Agents Chemother*. 2015;59(7):3935-3943. doi:10.1128/AAC.00102-15

168. Watt KM, Benjamin DK, Cheifetz IM, et al. Pharmacokinetics and Safety of Fluconazole in Young Infants Supported with Extracorporeal Membrane Oxygenation. *Pediatr Infect Dis J*. 2012;31(10):1042-1047. doi:10.1097/INF.0b013e31825d3091

169. Wildschut ED, de Hoog M, Ahsman MJ, Tibboel D, Osterhaus ADME, Fraaij PLA. Plasma concentrations of oseltamivir and oseltamivir carboxylate in critically ill children on extracorporeal membrane oxygenation support. *PloS One*. 2010;5(6):e10938. doi:10.1371/journal.pone.0010938

170. Freter AE, Husayni TS, Reyes G. Pharmacokinetics of Catecholamines During Hemofiltration in Pediatric Patients. *J Cardiovasc Pharmacol Ther*. 1998;3(3):235-238. doi:10.1177/107424849800300306

171. Nehus EJ, Mouksassi S, Vinks AA, Goldstein S. Meropenem in children receiving continuous renal replacement therapy: clinical trial simulations using realistic covariates. *J Clin Pharmacol*. 2014;54(12):1421-1428. doi:10.1002/jcph.360

172. Rapp M, Urien S, Foissac F, et al. Population pharmacokinetics of meropenem in critically ill children with different renal functions. *Eur J Clin Pharmacol*. 2020;76(1):61-71. doi:10.1007/s00228-019-02761-7

173. Butragueño-Laiseca L, Troconiz IF, Grau S, et al. Finding the Dose for Ceftolozane-Tazobactam in Critically Ill Children with and without Acute Kidney Injury. *Antibiot Basel Switz*. 2020;9(12):887. doi:10.3390/antibiotics9120887

174. Yang M, Zhao L, Wang X, et al. Population Pharmacokinetics and Dosage Optimization of Linezolid in Critically Ill Pediatric Patients. *Antimicrob Agents Chemother*. 2023;95(5):e02504-20, AAC.02504-20. doi:10.1128/AAC.02504-20

175. Gist KM, Mizuno T, Goldstein SL, Vinks A. Retrospective Evaluation of Milrinone Pharmacokinetics in Children With Kidney Injury. *Ther Drug Monit*. 2015;37(6):792-796. doi:10.1097/FTD.0000000000000214

176. Moffett BS, Morris J, Munoz F, Arikan AA. Population pharmacokinetic analysis of vancomycin in pediatric continuous renal replacement therapy. *Eur J Clin Pharmacol*. 2019;75(8):1089-1097. doi:10.1007/s00228-019-02664-7

177. Stitt G, Morris J, Schmees L, Angelo J, Akcan Arikan A. Cefepime Pharmacokinetics in Critically Ill Pediatric Patients Receiving Continuous Renal Replacement Therapy. *Antimicrob Agents Chemother*. 2019;63(4):e02006-18. doi:10.1128/AAC.02006-18

178. Zylbersztajn BL, Izquierdo G, Santana RC, et al. Therapeutic Drug Monitoring of Vancomycin in Pediatric Patients With Extracorporeal Membrane Oxygenation Support. *J Pediatr Pharmacol Ther JPPT*. 2018;23(4):305-310. doi:10.5863/1551-6776-23.4.305

179. Thibault C, Massey SL, Naim MY, Abend NS, Zuppa AF. Population Pharmacokinetics of IV Phenobarbital in Neonates After Congenital Heart Surgery. *Pediatr Crit Care Med J Soc Crit Care Med World Fed Pediatr Intensive Crit Care Soc*. 2020;21(8):e557-e565. doi:10.1097/PCC.0000000000002341

180. Thibault C, Massey SL, Abend NS, Naim MY, Zoraian A, Zuppa AF. Population Pharmacokinetics of Phenobarbital in Neonates and Infants on Extracorporeal Membrane

Oxygenation and the Influence of Concomitant Renal Replacement Therapy. *J Clin Pharmacol*. 2021;61(3):378-387. doi:10.1002/jcph.1743

181. Aebi C, Headrick CL, McCracken GH, Lindsay CA. Intravenous ribavirin therapy in a neonate with disseminated adenovirus infection undergoing extracorporeal membrane oxygenation: pharmacokinetics and clearance by hemofiltration. *J Pediatr*. 1997;130(4):612-615. doi:10.1016/s0022-3476(97)70246-4

182. Armstrong DK, Hidalgo HA, Eldadah M. Vancomycin and tobramycin clearance in an infant during continuous hemofiltration. *Ann Pharmacother*. 1993;27(2):224-227. doi:10.1177/106002809302700219

183. Brüggemann RJM, Antonius T, Heijst A van, Hoogerbrugge PM, Burger DM, Warris A. Therapeutic drug monitoring of voriconazole in a child with invasive aspergillosis requiring extracorporeal membrane oxygenation. *Ther Drug Monit*. 2008;30(6):643-646. doi:10.1097/FTD.0b013e3181898b0c

184. Cies JJ, Moore WS, Conley SB, et al. Pharmacokinetics of Continuous Infusion Meropenem With Concurrent Extracorporeal Life Support and Continuous Renal Replacement Therapy: A Case Report. *J Pediatr Pharmacol Ther JPPT Off J PPAG*. 2016;21(1):92-97. doi:10.5863/1551-6776-21.1.92

185. Cies JJ, Moore WS, Miller K, et al. Therapeutic drug monitoring of continuous-infusion acylovir for disseminated herpes simplex virus infection in a neonate receiving concurrent extracorporeal life support and continuous renal replacement therapy. *Pharmacotherapy*. 2015;35(2):229-233. doi:10.1002/phar.1526

186. Cies JJ, Moore WS, Conley SB, et al. Continuous Infusion Vancomycin Through the Addition of Vancomycin to the Continuous Renal Replacement Therapy Solution in the PICU: A Case Series. *Pediatr Crit Care Med J Soc Crit Care Med World Fed Pediatr Intensive Crit Care Soc*. 2016;17(4):e138-145. doi:10.1097/PCC.0000000000000656

187. Lindsay CA, Bawdon R, Quigley R. Clearance of ticarcillin-clavulanic acid by continuous venovenous hemofiltration in three critically ill children, two with and one without concomitant extracorporeal membrane oxygenation. *Pharmacotherapy*. 1996;16(3):458-462.

188. Karsch K, Chen X, Miera O, et al. Pharmacokinetics of Oral and Intravenous Oseltamivir Treatment of Severe Influenza B Virus Infection Requiring Organ Replacement Therapy. *Eur J Drug Metab Pharmacokinet*. 2017;42(1):155-164. doi:10.1007/s13318-016-0330-9

189. Oualha M, Tréluyer JM, Moshous D, et al. Fluconazole Exposure in Plasma and Bile During Continuous Venovenous Hemodialysis. *Ther Drug Monit*. 2019;41(4):544-546. doi:10.1097/FTD.0000000000000641

190. Saito J, Shoji K, Oho Y, et al. Meropenem pharmacokinetics during extracorporeal membrane oxygenation and continuous haemodialysis: a case report. *J Glob Antimicrob Resist*. 2020;22:651-655. doi:10.1016/j.jgar.2020.04.029

191. Seto W, Trope AE, Gow RM. Propafenone disposition during continuous venovenous hemofiltration. *Ann Pharmacother*. 1999;33(9):957-959. doi:10.1345/aph.18359

192. Sargel CL, Aboud M, Forster A, et al. Intravenous Ribavirin for Parainfluenza and Respiratory Syncytial Virus in an Infant Receiving Extracorporeal Membrane Oxygenation and Continuous Renal Replacement Therapy. *J Pediatr Pharmacol Ther JPPT Off J PPAG*. 2018;23(4):337-342. doi:10.5863/1551-6776-23.4.337

193. Tang Girdwood S, Arbough T, Dong M, et al. Molecular Adsorbent Recirculating System Therapy with Continuous Renal Replacement Therapy Enhanced Clearance of Piperacillin in a Pediatric Patient and Led to Failure to Attain Pharmacodynamic Targets. *Pharmacotherapy*. 2020;40(10):1061-1068. doi:10.1002/phar.2462

194. Rosenborg S, Saraste L, Wide K. High Phenobarbital Clearance During Continuous Renal Replacement Therapy. *Medicine (Baltimore)*. 2014;93(7):e46. doi:10.1097/MD.0000000000000046

195. Dillon RC, Witcher R, Cies JJ, Moore WS, Chopra A. Pharmacokinetics of Peramivir in an Adolescent Patient Receiving Continuous Venovenous Hemodiafiltration. *J Pediatr Pharmacol Ther JPPT Off J PPAG*. 2017;22(1):60-64. doi:10.5863/1551-6776-22.1.60

196. Poli EC, Simoni C, André P, et al. Clindamycin clearance during Cytosorb® hemoadsorption: A case report and pharmacokinetic study. *Int J Artif Organs*. 2019;42(5):258-262. doi:10.1177/0391398819831303

197. Suzuki T, Suzuki T, Takatsuka H, Yamazaki S, Ishii I. Successful treatment of seizure disorder by evaluating phenobarbital clearance in a paediatric patient undergoing continuous haemodiafiltration. *J Clin Pharm Ther*. 2019;44(3):479-481. doi:10.1111/jcpt.12815

198. Eyler RF, Heung M, Pleva M, et al. Pharmacokinetics of oseltamivir and oseltamivir carboxylate in critically ill patients receiving continuous venovenous hemodialysis and/or extracorporeal membrane oxygenation. *Pharmacotherapy*. 2012;32(12):1061-1069. doi:10.1002/phar.1151

199. Cies JJ, Moore WS, Conley SB, Shea P, Enache A, Chopra A. Therapeutic Drug Monitoring of Continuous Infusion Doripenem in a Pediatric Patient on Continuous Renal Replacement Therapy. *J Pediatr Pharmacol Ther JPPT*. 2017;22(1):69-73. doi:10.5863/1551-6776-22.1.69

200. Churchwell MD, Pasko DA, Mueller BA. Daptomycin clearance during modeled continuous renal replacement therapy. *Blood Purif*. 2006;24(5-6):548-554. doi:10.1159/000097078

201. Kroh UF, Dinges GK, Lukasewitz P, Steinhäusser WU, Holl TJ, Lennartz H. Elimination of drugs by the new polyamide hemofilter FH77H during various in vitro conditions. *Blood Purif*. 1998;16(1):49-56. doi:10.1159/000014313

202. Harvey B, Johnson TN, Yeomanson D, Mulla H, Mayer AP. Ceftriaxone pharmacokinetic properties during continuous veno-veno haemofiltration using an in vitro adult, paediatric and neonatal model. *Perfusion*. 2014;29(1):32-38. doi:10.1177/0267659113497497

203. Watt KM, Hornik CP, Balevic SJ, et al. Pharmacokinetics of ticarcillin–clavulanate in premature infants. *Br J Clin Pharmacol*. 2019;85(5):1021-1027. doi:10.1111/bcp.13882

204. Burstein AH, Wyble LE, Gal P, et al. Ticarcillin-clavulanic acid pharmacokinetics in preterm neonates with presumed sepsis. *Antimicrob Agents Chemother*. 1994;38(9):2024-2028. doi:10.1128/AAC.38.9.2024

205. Fricke G, Doerck M, Hafner D, Horton R, Kresken M. The pharmacokinetics of ticarcillin/clavulanate acid in neonates. *J Antimicrob Chemother*. 1989;24 Suppl B:111-120. doi:10.1093/jac/24.suppl_b.111

206. Reed MD, Yamashita TS, Blumer JL. Pharmacokinetic-based ticarcillin/clavulanic acid dose recommendations for infants and children. *J Clin Pharmacol*. 1995;35(7):658-665. doi:10.1002/j.1552-4604.1995.tb04105.x

207. Zobell JT, Stockmann C, Young DC, et al. Population pharmacokinetic and pharmacodynamic modeling of high-dose intermittent ticarcillin-clavulanate administration in pediatric cystic fibrosis patients. *Clin Ther*. 2011;33(11):1844-1850. doi:10.1016/j.clinthera.2011.09.010

208. Schaefer B, Schmitt CP. The role of molecular adsorbent recirculating system dialysis for extracorporeal liver support in children. *Pediatr Nephrol Berl Ger*. 2013;28(9):1763-1769. doi:10.1007/s00467-012-2348-9

209. Cies JJ, Shankar V, Schlichting C, Kuti JL. Population pharmacokinetics of piperacillin/tazobactam in critically ill young children. *Pediatr Infect Dis J*. 2014;33(2):168-173. doi:10.1097/INF.0b013e3182a743c7

210. Béranger A, Benaboud S, Urien S, et al. Piperacillin Population Pharmacokinetics and Dosing Regimen Optimization in Critically Ill Children with Normal and Augmented Renal Clearance. *Clin Pharmacokinet*. 2019;58(2):223-233. doi:10.1007/s40262-018-0682-1

211. Zhao Y, Yao BF, Kou C, et al. Developmental Population Pharmacokinetics and Dosing Optimization of Cefepime in Neonates and Young Infants. *Front Pharmacol*. 2020;11:14. doi:10.3389/fphar.2020.00014

212. Capparelli E, Hochwald C, Rasmussen M, Parham A, Bradley J, Moya F. Population pharmacokinetics of cefepime in the neonate. *Antimicrob Agents Chemother*. 2005;49(7):2760-2766. doi:10.1128/AAC.49.7.2760-2766.2005

213. Lima-Rogel V, Medina-Rojas EL, Del Carmen Milán-Segovia R, et al. Population pharmacokinetics of cefepime in neonates with severe nosocomial infections. *J Clin Pharm Ther*. 2008;33(3):295-306. doi:10.1111/j.1365-2710.2008.00913.x

214. Shoji K, Bradley JS, Reed MD, van den Anker JN, Domonoske C, Capparelli EV. Population Pharmacokinetic Assessment and Pharmacodynamic Implications of Pediatric Cefepime Dosing for Susceptible-Dose-Dependent Organisms. *Antimicrob Agents Chemother*. 2016;60(4):2150-2156. doi:10.1128/AAC.02592-15

215. Reed MD, Yamashita TS, Knupp CK, Veazey JM, Blumer JL. Pharmacokinetics of intravenously and intramuscularly administered cefepime in infants and children. *Antimicrob Agents Chemother*. 1997;41(8):1783-1787.

216. Bradley JS, Ang JY, Arrieta AC, et al. Pharmacokinetics and Safety of Single Intravenous Doses of Ceftolozane/Tazobactam in Children With Proven or Suspected Gram-Negative Infection. *Pediatr Infect Dis J*. 2018;37(11):1130-1136. doi:10.1097/INF.0000000000002170

217. Sime FB, Udy AA, Roberts JA. Augmented renal clearance in critically ill patients: etiology, definition and implications for beta-lactam dose optimization. *Curr Opin Pharmacol*. 2015;24:1-6. doi:10.1016/j.coph.2015.06.002

218. Germovsek E, Lutsar I, Kipper K, et al. Plasma and CSF pharmacokinetics of meropenem in neonates and young infants: results from the NeoMero studies. *J Antimicrob Chemother*. 2018;73(7):1908-1916. doi:10.1093/jac/dky128

219. Du X, Li C, Kuti JL, Nightingale CH, Nicolau DP. Population pharmacokinetics and pharmacodynamics of meropenem in pediatric patients. *J Clin Pharmacol*. 2006;46(1):69-75. doi:10.1177/0091270005283283

220. Parker EM, Hutchison M, Blumer JL. The pharmacokinetics of meropenem in infants and children: a population analysis. *J Antimicrob Chemother*. 1995;36 Suppl A:63-71. doi:10.1093/jac/36.suppl_a.63

221. Ohata Y, Tomita Y, Nakayama M, Kozuki T, Sunakawa K, Tanigawara Y. Optimal dosage regimen of meropenem for pediatric patients based on pharmacokinetic/pharmacodynamic considerations. *Drug Metab Pharmacokinet*. 2011;26(5):523-531. doi:10.2133/dmpk.dmpk-11-rg-027

222. Ikawa K, Morikawa N, Ikeda K, Miki M, Kobayashi M. Population pharmacokinetics and pharmacodynamics of meropenem in Japanese pediatric patients. *J Infect Chemother Off J Jpn Soc Chemother*. 2010;16(2):139-143. doi:10.1007/s10156-009-0025-0

223. Kongthavonsakul K, Lucksiri A, Eakanunkul S, Roongjang S, Issaranggoon Na Ayuthaya S, Oberdorfer P. Pharmacokinetics and pharmacodynamics of meropenem in children with severe infection. *Int J Antimicrob Agents*. 2016;48(2):151-157. doi:10.1016/j.ijantimicag.2016.04.025

224. Cies JJ, Moore WS, Enache A, Chopra A. Population Pharmacokinetics and Pharmacodynamic Target Attainment of Meropenem in Critically Ill Young Children. *J Pediatr Pharmacol Ther JPPT*. 2017;22(4):276-285. doi:10.5863/1551-6776-22.4.276

225. Cannavino CR, Castaneda-Ruiz B, Redman R, et al. Safety and Tolerability of Doripenem in Hospitalized Children With Complicated Intra-Abdominal Infection, Complicated Urinary Tract Infections and Pneumonia. *Pediatr Infect Dis J*. 2015;34(11):1264-1267. doi:10.1097/INF.0000000000000859

226. Bragonier R, Brown NM. The pharmacokinetics and toxicity of once-daily tobramycin therapy in children with cystic fibrosis. *J Antimicrob Chemother*. 1998;42(1):103-106. doi:10.1093/jac/42.1.103

227. Beringer PM, Vinks AATMM, Jelliffe RW, Shapiro BJ. Pharmacokinetics of Tobramycin in Adults with Cystic Fibrosis: Implications for Once-Daily Administration. *Antimicrob Agents Chemother*. 2000;44(4):809-813.

228. Bates RD, Nahata MC, Jones JW, et al. Pharmacokinetics and safety of tobramycin after once-daily administration in patients with cystic fibrosis. *Chest*. 1997;112(5):1208-1213. doi:10.1378/chest.112.5.1208

229. Buijk SE, Mouton JW, Gyssens IC, Verbrugh HA, Bruining HA. Experience with a once-daily dosing program of aminoglycosides in critically ill patients. *Intensive Care Med*. 2002;28(7):936-942. doi:10.1007/s00134-002-1313-7

230. Barletta JF, Johnson SB, Nix DE, Nix LC, Erstad BL. Population pharmacokinetics of aminoglycosides in critically ill trauma patients on once-daily regimens. *J Trauma*. 2000;49(5):869-872. doi:10.1097/00005373-200011000-00013

231. Giachetto GA, Telechea HM, Speranza N, Oyarzun M, Nanni L, Menchaca A. Vancomycin pharmacokinetic-pharmacodynamic parameters to optimize dosage administration in critically ill children. *Pediatr Crit Care Med J Soc Crit Care Med World Fed Pediatr Intensive Crit Care Soc*. 2011;12(6):e250-254. doi:10.1097/PCC.0b013e3181fe4047

232. Moffett BS, Resendiz K, Morris J, Akcan-Arikan A, Checchia PA. Population Pharmacokinetics of Vancomycin in the Pediatric Cardiac Surgical Population. *J Pediatr Pharmacol Ther JPPT*. 2019;24(2):107-116. doi:10.5863/1551-6776-24.2.107

233. Marlowe KF, Chicella MF, Claridge TE, Pittman SW. An assessment of vancomycin pharmacokinetic variability in pediatric cardiology patients. *J Pediatr Pharmacol Ther JPPT Off J PPAG*. 2003;8(2):132-136. doi:10.5863/1551-6776-8.2.132

234. Zane NR, Reedy MD, Gastonguay MR, et al. A Population Pharmacokinetic Analysis to Study the Effect of Therapeutic Hypothermia on Vancomycin Disposition in Children Resuscitated From Cardiac Arrest. *Pediatr Crit Care Med J Soc Crit Care Med World Fed Pediatr Intensive Crit Care Soc*. 2017;18(7):e290-e297. doi:10.1097/PCC.0000000000001198

235. Silva DCB da, Seixas GTF, Araujo OR de, Arduini RG, Carlesse FA de MC, Petrilli AS. Vancomycin serum concentrations in pediatric oncologic/hematologic intensive care patients.

Braz J Infect Dis Off Publ Braz Soc Infect Dis. 2012;16(4):361-365. doi:10.1016/j.bjid.2012.06.011

236. Seixas GTF, Araujo OR, Silva DCB, Arduini RG, Petrilli AS. Vancomycin Therapeutic Targets and Nephrotoxicity in Critically Ill Children With Cancer. *J Pediatr Hematol Oncol*. 2016;38(2):e56-62. doi:10.1097/MPH.0000000000000470

237. Avedissian SN, Bradley E, Zhang D, et al. Augmented Renal Clearance Using Population-Based Pharmacokinetic Modeling in Critically Ill Pediatric Patients. *Pediatr Crit Care Med J Soc Crit Care Med World Fed Pediatr Intensive Crit Care Soc*. 2017;18(9):e388-e394. doi:10.1097/PCC.0000000000001228

238. Smith MJ, Gonzalez D, Goldman JL, et al. Pharmacokinetics of Clindamycin in Obese and Nonobese Children. *Antimicrob Agents Chemother*. 2017;61(4):e02014-16. doi:10.1128/AAC.02014-16

239. Li SC, Ye Q, Xu H, Zhang L, Wang Y. Population Pharmacokinetics and Dosing Optimization of Linezolid in Pediatric Patients. *Antimicrob Agents Chemother*. 2019;63(4):e02387-18. doi:10.1128/AAC.02387-18

240. McJunkin JE, Nahata MC, De Los Reyes EC, et al. Safety and pharmacokinetics of ribavirin for the treatment of la crosse encephalitis. *Pediatr Infect Dis J*. 2011;30(10):860-865. doi:10.1097/INF.0b013e31821c922c

241. Connor E, Morrison S, Lane J, Oleske J, Sonke RL, Connor J. Safety, tolerance, and pharmacokinetics of systemic ribavirin in children with human immunodeficiency virus infection. *Antimicrob Agents Chemother*. 1993;37(3):532-539.

242. Oo C, Barrett J, Hill G, et al. Pharmacokinetics and dosage recommendations for an oseltamivir oral suspension for the treatment of influenza in children. *Paediatr Drugs*. 2001;3(3):229-236. doi:10.2165/00128072-200103030-00005

243. Cies JJ, Wayne S. Moore II, Enache A, Chopra A. Peramivir for Influenza A and B Viral Infections: A Pharmacokinetic Case Series. *Pharmacotherapy*. 2019;39(11):1060. doi:10.1002/phar.2330

244. Sugaya N, Kohno S, Ishibashi T, Wajima T, Takahashi T. Efficacy, Safety, and Pharmacokinetics of Intravenous Peramivir in Children with 2009 Pandemic H1N1 Influenza A Virus Infection. *Antimicrob Agents Chemother*. 2012;56(1):369-377. doi:10.1128/AAC.00132-11

245. Muto C, Shoji S, Tomono Y, Liu P. Population pharmacokinetic analysis of voriconazole from a pharmacokinetic study with immunocompromised Japanese pediatric subjects. *Antimicrob Agents Chemother*. 2015;59(6):3216-3223. doi:10.1128/AAC.04993-14

246. Friberg LE, Ravva P, Karlsson MO, Liu P. Integrated population pharmacokinetic analysis of voriconazole in children, adolescents, and adults. *Antimicrob Agents Chemother*. 2012;56(6):3032-3042. doi:10.1128/AAC.05761-11

247. Karlsson MO, Lutsar I, Milligan PA. Population pharmacokinetic analysis of voriconazole plasma concentration data from pediatric studies. *Antimicrob Agents Chemother*. 2009;53(3):935-944. doi:10.1128/AAC.00751-08

248. Wadsworth JM, Milan AM, Anson J, Davison AS. Development of a liquid chromatography tandem mass spectrometry method for the simultaneous measurement of voriconazole, posaconazole and itraconazole. *Ann Clin Biochem*. 2017;54(6):686-695. doi:10.1177/0004563216686378

249. Brammer KW, Coates PE. Pharmacokinetics of fluconazole in pediatric patients. *Eur J Clin Microbiol Infect Dis Off Publ Eur Soc Clin Microbiol*. 1994;13(4):325-329. doi:10.1007/BF01974613

250. Wade KC, Wu D, Kaufman DA, et al. Population Pharmacokinetics of Fluconazole in Young Infants. *Antimicrob Agents Chemother*. 2008;52(11):4043-4049. doi:10.1128/AAC.00569-08

251. Piper L, Smith PB, Hornik CP, et al. Fluconazole Loading Dose Pharmacokinetics and Safety in Infants. *Pediatr Infect Dis J*. 2011;30(5):375-378. doi:10.1097/INF.0b013e318202cbb3

252. Debruyne D. Clinical pharmacokinetics of fluconazole in superficial and systemic mycoses. *Clin Pharmacokinet*. 1997;33(1):52-77. doi:10.2165/00003088-199733010-00005

253. Marsot A, Brevaut-Malaty V, Vialet R, Boulamery A, Bruguerolle B, Simon N. Pharmacokinetics and absolute bioavailability of phenobarbital in neonates and young infants, a population pharmacokinetic modelling approach. *Fundam Clin Pharmacol*. 2014;28(4):465-471. doi:10.1111/fcp.12042

254. van den Broek MPH, Groenendaal F, Toet MC, et al. Pharmacokinetics and clinical efficacy of phenobarbital in asphyxiated newborns treated with hypothermia: a thermopharmacological approach. *Clin Pharmacokinet*. 2012;51(10):671-679. doi:10.1007/s40262-012-0004-y

255. Shellhaas RA, Ng CM, Dillon CH, Barks JDE, Bhatt-Mehta V. Population pharmacokinetics of phenobarbital in infants with neonatal encephalopathy treated with therapeutic hypothermia. *Pediatr Crit Care Med J Soc Crit Care Med World Fed Pediatr Intensive Crit Care Soc*. 2013;14(2):194-202. doi:10.1097/PCC.0b013e31825bbbc2

256. Moffett BS, Weingarten MM, Galati M, et al. Phenobarbital population pharmacokinetics across the pediatric age spectrum. *Epilepsia*. 2018;59(7):1327-1333. doi:10.1111/epi.14447

257. Ramamoorthy C, Anderson GD, Williams GD, Lynn AM. Pharmacokinetics and side effects of milrinone in infants and children after open heart surgery. *Anesth Analg*. 1998;86(2):283-289. doi:10.1097/00000539-199802000-00011

258. Hornik CP, Yogev R, Mourani PM, et al. Population Pharmacokinetics of Milrinone in Infants, Children, and Adolescents. *J Clin Pharmacol*. 2019;59(12):1606-1619. doi:10.1002/jcph.1499

259. Eldadah MK, Schwartz PH, Harrison R, Newth CJ. Pharmacokinetics of dopamine in infants and children. *Crit Care Med*. 1991;19(8):1008-1011. doi:10.1097/00003246-199108000-00006

260. Habib DM, Padbury JF, Anas NG, Perkin RM, Minegar C. Dobutamine pharmacokinetics and pharmacodynamics in pediatric intensive care patients. *Crit Care Med*. 1992;20(5):601-608. doi:10.1097/00003246-199205000-00010

261. Potts AL, Larsson P, Eksborg S, Warman G, Lönnqvist PA, Anderson BJ. Clonidine disposition in children; a population analysis. *Paediatr Anaesth*. 2007;17(10):924-933. doi:10.1111/j.1460-9592.2007.02251.x

262. Xie HG, Cao YJ, Gauda EB, Agthe AG, Hendrix CW, Lee H. Clonidine clearance matures rapidly during the early postnatal period: a population pharmacokinetic analysis in newborns with neonatal abstinence syndrome. *J Clin Pharmacol*. 2011;51(4):502-511. doi:10.1177/0091270010370587

263. Payne K, Mattheyse FJ, Liebenberg D, Dawes T. The pharmacokinetics of midazolam in paediatric patients. *Eur J Clin Pharmacol*. 1989;37(3):267-272. doi:10.1007/BF00679782

264. Reed MD, Rodarte A, Blumer JL, et al. The single-dose pharmacokinetics of midazolam and its primary metabolite in pediatric patients after oral and intravenous administration. *J Clin Pharmacol*. 2001;41(12):1359-1369. doi:10.1177/00912700122012832

265. de Wildt SN, de Hoog M, Vinks AA, van der Giesen E, van den Anker JN. Population pharmacokinetics and metabolism of midazolam in pediatric intensive care patients. *Crit Care Med*. 2003;31(7):1952-1958. doi:10.1097/01.ccm.0000084806.15352.da

266. Ito S, Gow R, Verjee Z, et al. Intravenous and oral propafenone for treatment of tachycardia in infants and children: pharmacokinetics and clinical response. *J Clin Pharmacol*. 1998;38(6):496-501. doi:10.1002/j.1552-4604.1998.tb05786.x

267. Landersdorfer CB, Bulitta JB, Kirkpatrick CMJ, et al. Population Pharmacokinetics of Piperacillin at Two Dose Levels: Influence of Nonlinear Pharmacokinetics on the Pharmacodynamic Profile. *Antimicrob Agents Chemother*. 2012;56(11):5715-5723. doi:10.1128/AAC.00937-12

268. Mouton JW, van den Anker JN. Meropenem clinical pharmacokinetics. *Clin Pharmacokinet*. 1995;28(4):275-286. doi:10.2165/00003088-199528040-00002

269. Matzke GR, Zhanel GG, Guay DR. Clinical pharmacokinetics of vancomycin. *Clin Pharmacokinet*. 1986;11(4):257-282. doi:10.2165/00003088-198611040-00001

270. Arzuaga A, Isla A, Gascón AR, Maynar J, Corral E, Pedraz JL. Elimination of piperacillin and tazobactam by renal replacement therapies with AN69 and polysulfone hemofilters: evaluation of the sieving coefficient. *Blood Purif*. 2006;24(4):347-354. doi:10.1159/000092921

271. Golper TA. Drug removal during continuous hemofiltration or hemodialysis. *Contrib Nephrol*. 1991;93:110-116. doi:10.1159/000420197

272. Rumpf KW, Rieger J, Ansorg R, Doht B, Scheler F. Binding of antibiotics by dialysis membranes and its clinical relevance. *Proc Eur Dial Transpl Assoc Eur Dial Transpl Assoc*. 1977;14:607-609.

273. Michikoshi J, Matsumoto S, Miyawaki H, et al. Evaluation of Proteins and Cells that Adsorb to Dialysis Membranes Used in Continuous Hemodiafiltration: Comparison of AN69ST, Polymethylmethacrylate, and Polysulfone Membranes. *Blood Purif*. 2019;48(4):358-367. doi:10.1159/000501632

274. Vilay AM, Churchwell MD, Mueller BA. Clinical review: Drug metabolism and nonrenal clearance in acute kidney injury. *Crit Care*. 2008;12(6):235. doi:10.1186/cc7093

275. Lu H, Rosenbaum S. Developmental pharmacokinetics in pediatric populations. *J Pediatr Pharmacol Ther JPPT Off J PPAG*. 2014;19(4):262-276. doi:10.5863/1551-6776-19.4.262

276. Kearns GL, Abdel-Rahman SM, Alander SW, Blowey DL, Leeder JS, Kauffman RE. Developmental pharmacology--drug disposition, action, and therapy in infants and children. *N Engl J Med*. 2003;349(12):1157-1167. doi:10.1056/NEJMra035092

277. Edginton AN, Schmitt W, Willmann S. Development and evaluation of a generic physiologically based pharmacokinetic model for children. *Clin Pharmacokinet*. 2006;45(10):1013-1034. doi:10.2165/00003088-200645100-00005

278. Barker CIS, Standing JF, Kelly LE, et al. Pharmacokinetic studies in children: recommendations for practice and research. *Arch Dis Child*. 2018;103(7):695-702. doi:10.1136/archdischild-2017-314506

279. GBD Chronic Kidney Disease Collaboration. Global, regional, and national burden of chronic kidney disease, 1990-2017: a systematic analysis for the Global Burden of Disease Study 2017. *Lancet Lond Engl*. 2020;395(10225):709-733. doi:10.1016/S0140-6736(20)30045-3

280. Manley HJ, Cannella CA, Bailie GR, St Peter WL. Medication-related problems in ambulatory hemodialysis patients: a pooled analysis. *Am J Kidney Dis Off J Natl Kidney Found*. 2005;46(4):669-680. doi:10.1053/j.ajkd.2005.07.001

281. Morrissey KM, Stocker SL, Wittwer MB, Xu L, Giacomini KM. Renal transporters in drug development. *Annu Rev Pharmacol Toxicol*. 2013;53:503-529. doi:10.1146/annurev-pharmtox-011112-140317

282. Torres AM, Dnyanmote AV, Granados JC, Nigam SK. Renal and non-renal response of ABC and SLC transporters in chronic kidney disease. *Expert Opin Drug Metab Toxicol*. 2021;17(5):515-542. doi:10.1080/17425255.2021.1899159

283. Cheung KWK, Hsueh CH, Zhao P, et al. The Effect of Uremic Solutes on the Organic Cation Transporter 2. *J Pharm Sci*. 2017;106(9):2551-2557. doi:10.1016/j.xphs.2017.04.076

284. Malik PRV, Yeung CHT, Ismaeil S, Advani U, Djie S, Edginton AN. A Physiological Approach to Pharmacokinetics in Chronic Kidney Disease. *J Clin Pharmacol*. 2020;60 Suppl 1:S52-S62. doi:10.1002/jcph.1713

285. Droździk M, Oswald S, Droździk A. Impact of kidney dysfunction on hepatic and intestinal drug transporters. *Biomed Pharmacother Biomedecine Pharmacother*. 2021;143:112125. doi:10.1016/j.biopha.2021.112125

286. Masereeuw R, Mutsaers HAM, Toyohara T, et al. The kidney and uremic toxin removal: glomerulus or tubule? *Semin Nephrol*. 2014;34(2):191-208. doi:10.1016/j.semnephrol.2014.02.010

287. Hsueh CH, Yoshida K, Zhao P, et al. Identification and Quantitative Assessment of Uremic Solutes as Inhibitors of Renal Organic Anion Transporters, OAT1 and OAT3. *Mol Pharm*. 2016;13(9):3130-3140. doi:10.1021/acs.molpharmaceut.6b00332

288. Hsueh CH, Hsu V, Zhao P, Zhang L, Giacomini KM, Huang SM. PBPK Modeling of the Effect of Reduced Kidney Function on the Pharmacokinetics of Drugs Excreted Renally by Organic Anion Transporters. *Clin Pharmacol Ther*. 2018;103(3):485-492. doi:10.1002/cpt.750

289. Willmann S, Höhn K, Edginton A, et al. Development of a physiology-based whole-body population model for assessing the influence of individual variability on the pharmacokinetics of drugs. *J Pharmacokinet Pharmacodyn*. 2007;34(3):401-431. doi:10.1007/s10928-007-9053-5

290. Schlender JF, Meyer M, Thelen K, et al. Development of a Whole-Body Physiologically Based Pharmacokinetic Approach to Assess the Pharmacokinetics of Drugs in Elderly Individuals. *Clin Pharmacokinet*. 2016;55(12):1573-1589. doi:10.1007/s40262-016-0422-3

291. Schlender JF, Teutonico D, Coboeken K, et al. A Physiologically-Based Pharmacokinetic Model to Describe Ciprofloxacin Pharmacokinetics Over the Entire Span of Life. *Clin Pharmacokinet*. 2018;57(12):1613-1634. doi:10.1007/s40262-018-0661-6

292. Britz H, Hanke N, Taub ME, et al. Physiologically Based Pharmacokinetic Models of Probenecid and Furosemide to Predict Transporter Mediated Drug-Drug Interactions. *Pharm Res*. 2020;37(12):250. doi:10.1007/s11095-020-02964-z

293. Merrem (meropenem). Prescribing information. Boucherville, QC, Canada. Sandoz Canada INC. September 2017.

294. Arnal J, Gonzalez-Alvarez I, Bermejo M, et al. Biowaiver monographs for immediate release solid oral dosage forms: aciclovir. *J Pharm Sci*. 2008;97(12):5061-5073. doi:10.1002/jps.21392

295. DrugBank. Meropenem. https://go.drugbank.com/drugs/DB00760

296. Jaehde U, Sörgel F, Reiter A, Sigl G, Naber KG, Schunack W. Effect of probenecid on the distribution and elimination of ciprofloxacin in humans. *Clin Pharmacol Ther*. 1995;58(5):532-541. doi:10.1016/0009-9236(95)90173-6

297. Bax RP, Bastain W, Featherstone A, Wilkinson DM, Hutchison M, Haworth SJ. The pharmacokinetics of meropenem in volunteers. *J Antimicrob Chemother*. 1989;24 Suppl A:311-320. doi:10.1093/jac/24.suppl_a.311

298. de Miranda P, Good SS, Laskin OL, Krasny HC, Connor JD, Lietman PS. Disposition of intravenous radioactive acyclovir. *Clin Pharmacol Ther*. 1981;30(5):662-672. doi:10.1038/clpt.1981.218

299. Jd M, Sm T, Jd M. Evaluation of Proposed In Vivo Probe Substrates and Inhibitors for Phenotyping Transporter Activity in Humans. *J Clin Pharmacol*. 2016;56 Suppl 7. doi:10.1002/jcph.736

300. Shibayama T, Sugiyama D, Kamiyama E, Tokui T, Hirota T, Ikeda T. Characterization of CS-023 (RO4908463), a novel parenteral carbapenem antibiotic, and meropenem as substrates of human renal transporters. *Drug Metab Pharmacokinet*. 2007;22(1):41-47. doi:10.2133/dmpk.22.41

301. Ivanyuk A, Livio F, Biollaz J, Buclin T. Renal Drug Transporters and Drug Interactions. *Clin Pharmacokinet*. 2017;56(8):825-892. doi:10.1007/s40262-017-0506-8

302. Scotcher D, Billington S, Brown J, et al. Microsomal and Cytosolic Scaling Factors in Dog and Human Kidney Cortex and Application for In Vitro-In Vivo Extrapolation of Renal Metabolic Clearance. *Drug Metab Dispos Biol Fate Chem*. 2017;45(5):556-568. doi:10.1124/dmd.117.075242

303. Prasad B, Johnson K, Billington S, et al. Abundance of Drug Transporters in the Human Kidney Cortex as Quantified by Quantitative Targeted Proteomics. *Drug Metab Dispos Biol Fate Chem*. 2016;44(12):1920-1924. doi:10.1124/dmd.116.072066

304. Uchino H, Tamai I, Yabuuchi H, et al. Faropenem transport across the renal epithelial luminal membrane via inorganic phosphate transporter Npt1. *Antimicrob Agents Chemother*. 2000;44(3):574-577. doi:10.1128/AAC.44.3.574-577.2000

305. Willmann S, Lippert J, Schmitt W. From physicochemistry to absorption and distribution: predictive mechanistic modelling and computational tools. *Expert Opin Drug Metab Toxicol*. 2005;1(1):159-168. doi:10.1517/17425255.1.1.159

306. Rodgers T, Leahy D, Rowland M. Physiologically based pharmacokinetic modeling 1: predicting the tissue distribution of moderate-to-strong bases. *J Pharm Sci*. 2005;94(6):1259-1276. doi:10.1002/jps.20322

307. Rodgers T, Rowland M. Physiologically based pharmacokinetic modelling 2: predicting the tissue distribution of acids, very weak bases, neutrals and zwitterions. *J Pharm Sci*. 2006;95(6):1238-1257. doi:10.1002/jps.20502

308. Hsu V, de L T Vieira M, Zhao P, et al. Towards quantitation of the effects of renal impairment and probenecid inhibition on kidney uptake and efflux transporters, using physiologically based pharmacokinetic modelling and simulations. *Clin Pharmacokinet*. 2014;53(3):283-293. doi:10.1007/s40262-013-0117-y

309. Doki K, Neuhoff S, Rostami-Hodjegan A, Homma M. Assessing Potential Drug-Drug Interactions Between Dabigatran Etexilate and a P-Glycoprotein Inhibitor in Renal Impairment Populations Using Physiologically Based Pharmacokinetic Modeling. *CPT Pharmacomet Syst Pharmacol*. 2019;8(2):118-126. doi:10.1002/psp4.12382

310. Tsamandouras N, Rostami-Hodjegan A, Aarons L. Combining the "bottom up" and "top down" approaches in pharmacokinetic modelling: fitting PBPK models to observed clinical data. *Br J Clin Pharmacol*. 2015;79(1):48-55. doi:10.1111/bcp.12234

311. Sayama H, Takubo H, Komura H, Kogayu M, Iwaki M. Application of a Physiologically Based Pharmacokinetic Model Informed by a Top-Down Approach for the Prediction of Pharmacokinetics in Chronic Kidney Disease Patients. *AAPS J*. 2014;16(5):1018-1028. doi:10.1208/s12248-014-9626-3

312. Basit A, Radi Z, Vaidya VS, Karasu M, Prasad B. Kidney Cortical Transporter Expression across Species Using Quantitative Proteomics. *Drug Metab Dispos Biol Fate Chem*. 2019;47(8):802-808. doi:10.1124/dmd.119.086579

313. I M, Ma T. A Comparative Study Between Allometric Scaling and Physiologically Based Pharmacokinetic Modeling for the Prediction of Drug Clearance From Neonates to Adolescents. *J Clin Pharmacol*. 2019;59(2). doi:10.1002/jcph.1310

314. Smith HW, Finkelstein N, Aliminosa L, Crawford B, Graber M. The renal clearances of substituted hippuric acid derivatives and other aromatic acids in dog and man. *J Clin Invest*. 1945;24(3):388-404. doi:10.1172/JCI101618

315. Nigam SK, Bush KT, Martovetsky G, et al. The organic anion transporter (OAT) family: a systems biology perspective. *Physiol Rev*. 2015;95(1):83-123. doi:10.1152/physrev.00025.2013

316. Ullrich KJ, Rumrich G. Renal transport mechanisms for xenobiotics: chemicals and drugs. *Clin Investig*. 1993;71(10):843-848. doi:10.1007/BF00190334

317. Dantzler WH, Wright SH. The molecular and cellular physiology of basolateral organic anion transport in mammalian renal tubules. *Biochim Biophys Acta*. 2003;1618(2):185-193. doi:10.1016/j.bbamem.2003.08.015

318. Battilana C, Zhang HP, Olshen RA, Wexler L, Myers BD. PAH extraction and estimation of plasma flow in diseased human kidneys. *Am J Physiol*. 1991;261(4 Pt 2):F726-733. doi:10.1152/ajprenal.1991.261.4.F726

319. Bergstrom J, Bucht H, Ek J, Josephson B, Sundell H, Werko L. The renal extraction of para-aminohippurate in normal persons and in patients with diseased kidneys. *Scand J Clin Lab Invest*. 1959;11:361-375. doi:10.3109/00365515909060466

320. Bradley SE, Bradley GP, Tyson CJ, Curry JJ, Blake WD. Renal function in renal diseases. *Am J Med*. 1950;9(6):766-798. doi:10.1016/0002-9343(50)90292-0

321. Brodwall EK. Renal extraction of pah in renal disease. *Scand J Clin Lab Invest*. 1964;16:12-20. doi:10.3109/00365516409060477

322. Josephson B, Bucht H, Ek J, Werko L. Renal extraction, its depression, and the tubular storage of p-aminohippuric acid (PAH) in the healthy and in the diseased human kidney. *Scand J Clin Lab Invest*. 1952;4(1):1-14. doi:10.3109/00365515209060626

323. Cargill WH. The measurement of glomerular and tubular plasma flow in the normal and diseased human kidney. *J Clin Invest*. 1949;28(3):533-538. doi:10.1172/JCI102101

324. Zhang Y, Zhang L, Abraham S, et al. Assessment of the impact of renal impairment on systemic exposure of new molecular entities: evaluation of recent new drug applications. *Clin Pharmacol Ther*. 2009;85(3):305-311. doi:10.1038/clpt.2008.208

325. Zhang L, Xu N, Xiao S, et al. Regulatory perspectives on designing pharmacokinetic studies and optimizing labeling recommendations for patients with chronic kidney disease. *J Clin Pharmacol*. 2012;52(1 Suppl):79S-90S. doi:10.1177/0091270011415410

326. Yoshida K, Sun B, Zhang L, et al. Systematic and quantitative assessment of the effect of chronic kidney disease on CYP2D6 and CYP3A4/5. *Clin Pharmacol Ther*. 2016;100(1):75-87. doi:10.1002/cpt.337

327. Laskin OL, de Miranda P, King DH, et al. Effects of probenecid on the pharmacokinetics and elimination of acyclovir in humans. *Antimicrob Agents Chemother*. 1982;21(5):804-807.

328. Wiebe ST, Giessmann T, Hohl K, et al. Validation of a Drug Transporter Probe Cocktail Using the Prototypical Inhibitors Rifampin, Probenecid, Verapamil, and Cimetidine. *Clin Pharmacokinet*. 2020;59(12):1627-1639. doi:10.1007/s40262-020-00907-w

329. Drusano GL, Weir M, Forrest A, Plaisance K, Emm T, Standiford HC. Pharmacokinetics of intravenously administered ciprofloxacin in patients with various degrees of renal function. *Antimicrob Agents Chemother*. 1987;31(6):860-864. doi:10.1128/AAC.31.6.860

330. Shah A, Lettieri J, Blum R, Millikin S, Sica D, Heller AH. Pharmacokinetics of intravenous ciprofloxacin in normal and renally impaired subjects. *J Antimicrob Chemother*. 1996;38(1):103-116. doi:10.1093/jac/38.1.103

331. Chimata M, Nagase M, Suzuki Y, Shimomura M, Kakuta S. Pharmacokinetics of meropenem in patients with various degrees of renal function, including patients with end-stage renal disease. *Antimicrob Agents Chemother*. 1993;37(2):229-233. doi:10.1128/AAC.37.2.229

332. Christensson BA, Nilsson-Ehle I, Hutchison M, Haworth SJ, Oqvist B, Norrby SR. Pharmacokinetics of meropenem in subjects with various degrees of renal impairment. *Antimicrob Agents Chemother*. 1992;36(7):1532-1537. doi:10.1128/AAC.36.7.1532

333. Leroy A, Fillastre JP, Etienne I, Borsa-Lebás F, Humbert G. Pharmacokinetics of meropenem in subjects with renal insufficiency. *Eur J Clin Pharmacol*. 1992;42(5):535-538. doi:10.1007/BF00314864

334. Gladziwa U, Böhm R, Klotz U, Manuel-Rimbau M, Mann H, Sieberth HG. Pharmacokinetics of Furosemide in Patients with Chronic Renal Failure. *Drug Investig*. 1993;6(3):137-143. doi:10.1007/BF03259733

335. Rane A, Villeneuve JP, Stone WJ, Nies AS, Wilkinson GR, Branch RA. Plasma binding and disposition of furosemide in the nephrotic syndrome and in uremia. *Clin Pharmacol Ther*. 1978;24(2):199-207. doi:10.1002/cpt1978242199

336. Laskin OL, Longstreth JA, Whelton A, et al. Acyclovir kinetics in end-stage renal disease. *Clin Pharmacol Ther*. 1982;31(5):594-601. doi:10.1038/clpt.1982.83

337. Bush KT, Singh P, Nigam SK. Gut-derived uremic toxin handling in vivo requires OAT-mediated tubular secretion in chronic kidney disease. *JCI Insight*. 2020;5(7):e133817, 133817. doi:10.1172/jci.insight.133817

338. Tan ML, Yoshida K, Zhao P, et al. Effect of Chronic Kidney Disease on Nonrenal Elimination Pathways: A Systematic Assessment of CYP1A2, CYP2C8, CYP2C9, CYP2C19, and OATP. *Clin Pharmacol Ther*. 2018;103(5):854-867. doi:10.1002/cpt.807

339. Tan ML, Zhao P, Zhang L, et al. Use of Physiologically Based Pharmacokinetic Modeling to Evaluate the Effect of Chronic Kidney Disease on the Disposition of Hepatic CYP2C8 and OATP1B Drug Substrates. *Clin Pharmacol Ther*. 2019;105(3):719-729. doi:10.1002/cpt.1205

340. Follman KE, Morris ME. Prediction of the Effects of Renal Impairment on Clearance for Organic Cation Drugs that Undergo Renal Secretion: A Simulation-Based Study. *Drug Metab Dispos Biol Fate Chem*. 2018;46(5):758-769. doi:10.1124/dmd.117.079558

341. Rowland Yeo K, Aarabi M, Jamei M, Rostami-Hodjegan A. Modeling and predicting drug pharmacokinetics in patients with renal impairment. *Expert Rev Clin Pharmacol*. 2011;4(2):261-274. doi:10.1586/ecp.10.143

342. Bricker NS. On the meaning of the intact nephron hypothesis. *Am J Med*. 1969;46(1):1-11. doi:10.1016/0002-9343(69)90053-9

343. Dettli L. Drug dosage in renal disease. *Clin Pharmacokinet*. 1976;1(2):126-134. doi:10.2165/00003088-197601020-00004

344. Chapron A, Shen DD, Kestenbaum BR, Robinson-Cohen C, Himmelfarb J, Yeung CK. Does Secretory Clearance Follow Glomerular Filtration Rate in Chronic Kidney Diseases? Reconsidering the Intact Nephron Hypothesis. *Clin Transl Sci*. 2017;10(5):395-403. doi:10.1111/cts.12481

345. Momper JD, Yang J, Gockenbach M, Vaida F, Nigam SK. Dynamics of Organic Anion Transporter-Mediated Tubular Secretion during Postnatal Human Kidney Development and Maturation. *Clin J Am Soc Nephrol CJASN*. 2019;14(4):540-548. doi:10.2215/CJN.10350818

346. Toto RD. Conventional measurement of renal function utilizing serum creatinine, creatinine clearance, inulin and para-aminohippuric acid clearance. *Curr Opin Nephrol Hypertens*. 1995;4(6):505-509; discussion 503-504. doi:10.1097/00041552-199511000-00009

347. Dowling TC, Frye RF, Fraley DS, Matzke GR. Characterization of tubular functional capacity in humans using para-aminohippurate and famotidine. *Kidney Int*. 2001;59(1):295-303. doi:10.1046/j.1523-1755.2001.00491.x

348. Sweet DH, Miller DS, Pritchard JB, Fujiwara Y, Beier DR, Nigam SK. Impaired organic anion transport in kidney and choroid plexus of organic anion transporter 3 (Oat3 (Slc22a8)) knockout mice. *J Biol Chem*. 2002;277(30):26934-26943. doi:10.1074/jbc.M203803200

349. Eraly SA, Vallon V, Vaughn DA, et al. Decreased renal organic anion secretion and plasma accumulation of endogenous organic anions in OAT1 knock-out mice. *J Biol Chem*. 2006;281(8):5072-5083. doi:10.1074/jbc.M508050200

350. Rizwan AN, Krick W, Burckhardt G. The chloride dependence of the human organic anion transporter 1 (hOAT1) is blunted by mutation of a single amino acid. *J Biol Chem*. 2007;282(18):13402-13409. doi:10.1074/jbc.M609849200

351. Burckhardt G, Bahn A, Wolff NA. Molecular physiology of renal p-aminohippurate secretion. *News Physiol Sci Int J Physiol Prod Jointly Int Union Physiol Sci Am Physiol Soc*. 2001;16:114-118. doi:10.1152/physiologyonline.2001.16.3.114

352. Schumann L, Wüstenberg PW. An improved method to determine renal function using inulin and p-aminohippurate (PAH) steady-state kinetic modeling. *Clin Nephrol*. 1990;33(1):35-40.

353. Hanke N, Frechen S, Moj D, et al. PBPK Models for CYP3A4 and P-gp DDI Prediction: A Modeling Network of Rifampicin, Itraconazole, Clarithromycin, Midazolam, Alfentanil,

and Digoxin. *CPT Pharmacomet Syst Pharmacol*. 2018;7(10):647-659. doi:10.1002/psp4.12343

354. Center for Drug Evalatuion and Research. Clinical Pharmacology and Biopharmaceutics Revew: Olumiant. Published December 2017. Accessed September 2021.Baricitinib clinical https://www.accessdata.fda.gov/drugsatfda_docs/nda/2018/207924Orig1s000ClinPharmR.pdf.

355. Posada MM, Bacon JA, Schneck KB, et al. Prediction of renal transporter mediated drug-drug interactions for pemetrexed using physiologically based pharmacokinetic modeling. *Drug Metab Dispos Biol Fate Chem*. 2015;43(3):325-334. doi:10.1124/dmd.114.059618

356. Salerno SN, Carreño FO, Edginton AN, Cohen-Wolkowiez M, Gonzalez D. Leveraging Physiologically Based Pharmacokinetic Modeling and Experimental Data to Guide Dosing Modification of CYP3A-Mediated Drug-Drug Interactions in the Pediatric Population. *Drug Metab Dispos Biol Fate Chem*. 2021;49(9):844-855. doi:10.1124/dmd.120.000318

357. Nolin TD, Frye RF, Matzke GR. Hepatic drug metabolism and transport in patients with kidney disease. *Am J Kidney Dis Off J Natl Kidney Found*. 2003;42(5):906-925. doi:10.1016/j.ajkd.2003.07.019

358. Decker BS, O'Neill KD, Chambers MA, et al. Hemodialysis does not alter in vitro hepatic CYP3A4 and CYP2D6 metabolic activity in uremic serum. *Clin Pharmacol Adv Appl*. 2013;5:193-199. doi:10.2147/CPAA.S54381

359. Hirako M, Kamiya T, Misu N, et al. Impaired gastric motility and its relationship to gastrointestinal symptoms in patients with chronic renal failure. *J Gastroenterol*. 2005;40(12):1116-1122. doi:10.1007/s00535-005-1709-6

360. Vaziri ND, Yuan J, Nazertehrani S, Ni Z, Liu S. Chronic kidney disease causes disruption of gastric and small intestinal epithelial tight junction. *Am J Nephrol*. 2013;38(2):99-103. doi:10.1159/000353764

361. Shitara Y, Maeda K, Ikejiri K, Yoshida K, Horie T, Sugiyama Y. Clinical significance of organic anion transporting polypeptides (OATPs) in drug disposition: their roles in hepatic clearance and intestinal absorption. *Biopharm Drug Dispos*. 2013;34(1):45-78. doi:10.1002/bdd.1823

362. Nolin TD, Frye RF, Le P, et al. ESRD impairs nonrenal clearance of fexofenadine but not midazolam. *J Am Soc Nephrol JASN*. 2009;20(10):2269-2276. doi:10.1681/ASN.2009010082

363. Thomson BKA, Nolin TD, Velenosi TJ, et al. Effect of CKD and dialysis modality on exposure to drugs cleared by nonrenal mechanisms. *Am J Kidney Dis Off J Natl Kidney Found*. 2015;65(4):574-582. doi:10.1053/j.ajkd.2014.09.015

364. Naud J, Michaud J, Beauchemin S, et al. Effects of chronic renal failure on kidney drug transporters and cytochrome P450 in rats. *Drug Metab Dispos Biol Fate Chem*. 2011;39(8):1363-1369. doi:10.1124/dmd.111.039115

365. Mónica Torres A, Mac Laughlin M, Muller A, Brandoni A, Anzai N, Endou H. Altered renal elimination of organic anions in rats with chronic renal failure. *Biochim Biophys Acta*. 2005;1740(1):29-37. doi:10.1016/j.bbadis.2005.03.002

366. Deguchi T, Takemoto M, Uehara N, Lindup WE, Suenaga A, Otagiri M. Renal clearance of endogenous hippurate correlates with expression levels of renal organic anion transporters in uremic rats. *J Pharmacol Exp Ther*. 2005;314(2):932-938. doi:10.1124/jpet.105.085613

367. Nishihara K, Masuda S, Ji L, Katsura T, Inui KI. Pharmacokinetic significance of luminal multidrug and toxin extrusion 1 in chronic renal failure rats. *Biochem Pharmacol*. 2007;73(9):1482-1490. doi:10.1016/j.bcp.2006.12.034

368. Xu G, Bhatnagar V, Wen G, Hamilton BA, Eraly SA, Nigam SK. Analyses of coding region polymorphisms in apical and basolateral human organic anion transporter (OAT) genes [OAT1 (NKT), OAT2, OAT3, OAT4, URAT (RST)]. *Kidney Int*. 2005;68(4):1491-1499. doi:10.1111/j.1523-1755.2005.00612.x

369. Stephens JC, Schneider JA, Tanguay DA, et al. Haplotype variation and linkage disequilibrium in 313 human genes. *Science*. 2001;293(5529):489-493. doi:10.1126/science.1059431

370. Marzolini C, Tirona RG, Kim RB. Pharmacogenomics of the OATP and OAT families. *Pharmacogenomics*. 2004;5(3):273-282. doi:10.1517/phgs.5.3.273.29831

371. Nishizato Y, Ieiri I, Suzuki H, et al. Polymorphisms of OATP-C (SLC21A6) and OAT3 (SLC22A8) genes: consequences for pravastatin pharmacokinetics. *Clin Pharmacol Ther*. 2003;73(6):554-565. doi:10.1016/S0009-9236(03)00060-2

372. Lozano E, Briz O, Macias RIR, Serrano MA, Marin JJG, Herraez E. Genetic Heterogeneity of SLC22 Family of Transporters in Drug Disposition. *J Pers Med*. 2018;8(2):14. doi:10.3390/jpm8020014

373. Wagner C, Zhao P, Pan Y, et al. Application of Physiologically Based Pharmacokinetic (PBPK) Modeling to Support Dose Selection: Report of an FDA Public Workshop on PBPK. *CPT Pharmacomet Syst Pharmacol*. 2015;4(4):226-230. doi:10.1002/psp4.33

374. Heintz BH, Matzke GR, Dager WE. Antimicrobial dosing concepts and recommendations for critically ill adult patients receiving continuous renal replacement therapy or intermittent hemodialysis. *Pharmacotherapy*. 2009;29(5):562-577. doi:10.1592/phco.29.5.562

375. Cohen S, Hurd E, Cush J, et al. Treatment of rheumatoid arthritis with anakinra, a recombinant human interleukin-1 receptor antagonist, in combination with methotrexate: results of a twenty-four-week, multicenter, randomized, double-blind, placebo-controlled trial. *Arthritis Rheum*. 2002;46(3):614-624. doi:10.1002/art.10141

376. Goldbach-Mansky R, Dailey NJ, Canna SW, et al. Neonatal-onset multisystem inflammatory disease responsive to interleukin-1beta inhibition. *N Engl J Med*. 2006;355(6):581-592. doi:10.1056/NEJMoa055137

377. Furst DE. Anakinra: review of recombinant human interleukin-I receptor antagonist in the treatment of rheumatoid arthritis. *Clin Ther*. 2004;26(12):1960-1975. doi:10.1016/j.clinthera.2004.12.019

378. Crayne CB, Albeituni S, Nichols KE, Cron RQ. The Immunology of Macrophage Activation Syndrome. *Front Immunol*. 2019;10:119. doi:10.3389/fimmu.2019.00119

379. Mehta P, Cron RQ, Hartwell J, Manson JJ, Tattersall RS. Silencing the cytokine storm: the use of intravenous anakinra in haemophagocytic lymphohistiocytosis or macrophage activation syndrome. *Lancet Rheumatol*. 2020;2(6):e358-e367. doi:10.1016/S2665-9913(20)30096-5

380. La Rosée P, Horne A, Hines M, et al. Recommendations for the management of hemophagocytic lymphohistiocytosis in adults. *Blood*. 2019;133(23):2465-2477. doi:10.1182/blood.2018894618

381. Halyabar O, Chang MH, Schoettler ML, et al. Calm in the midst of cytokine storm: a collaborative approach to the diagnosis and treatment of hemophagocytic lymphohistiocytosis and macrophage activation syndrome. *Pediatr Rheumatol Online J*. 2019;17(1):7. doi:10.1186/s12969-019-0309-6

382. Bauchmuller K, Manson JJ, Tattersall R, et al. Haemophagocytic lymphohistiocytosis in adult critical care. *J Intensive Care Soc*. 2020;21(3):256-268. doi:10.1177/1751143719893865

383. Carter SJ, Tattersall RS, Ramanan AV. Macrophage activation syndrome in adults: recent advances in pathophysiology, diagnosis and treatment. *Rheumatol Oxf Engl*. 2019;58(1):5-17. doi:10.1093/rheumatology/key006

384. Kumar B, Aleem S, Saleh H, Petts J, Ballas ZK. A Personalized Diagnostic and Treatment Approach for Macrophage Activation Syndrome and Secondary Hemophagocytic Lymphohistiocytosis in Adults. *J Clin Immunol*. 2017;37(7):638-643. doi:10.1007/s10875-017-0439-x

385. Rajasekaran S, Kruse K, Kovey K, et al. Therapeutic role of anakinra, an interleukin-1 receptor antagonist, in the management of secondary hemophagocytic lymphohistiocytosis/sepsis/multiple organ dysfunction/macrophage activating syndrome in critically ill children*. *Pediatr Crit Care Med J Soc Crit Care Med World Fed Pediatr Intensive Crit Care Soc*. 2014;15(5):401-408. doi:10.1097/PCC.0000000000000078

386. Yang BB, Baughman S, Sullivan JT. Pharmacokinetics of anakinra in subjects with different levels of renal function. *Clin Pharmacol Ther*. 2003;74(1):85-94. doi:10.1016/S0009-9236(03)00094-8

387. Yang BB, Gozzi P, Sullivan JT. Pharmacokinetics of Anakinra in Subjects of Heavier vs. Lighter Body Weights. *Clin Transl Sci*. 2019;12(4):371-378. doi:10.1111/cts.12622

388. Kim DC, Reitz B, Carmichael DF, Bloedow DC. Kidney as a major clearance organ for recombinant human interleukin-1 receptor antagonist. *J Pharm Sci*. 1995;84(5):575-580. doi:10.1002/jps.2600840511

389. Fisher CJ, Slotman GJ, Opal SM, et al. Initial evaluation of human recombinant interleukin-1 receptor antagonist in the treatment of sepsis syndrome: a randomized, open-label, placebo-controlled multicenter trial. *Crit Care Med*. 1994;22(1):12-21. doi:10.1097/00003246-199401000-00008

390. Fisher CJ, Dhainaut JF, Opal SM, et al. Recombinant human interleukin 1 receptor antagonist in the treatment of patients with sepsis syndrome. Results from a randomized, double-blind, placebo-controlled trial. Phase III rhIL-1ra Sepsis Syndrome Study Group. *JAMA*. 1994;271(23):1836-1843.

391. Opal SM, Fisher CJ, Dhainaut JF, et al. Confirmatory interleukin-1 receptor antagonist trial in severe sepsis: a phase III, randomized, double-blind, placebo-controlled, multicenter trial. The Interleukin-1 Receptor Antagonist Sepsis Investigator Group. *Crit Care Med*. 1997;25(7):1115-1124. doi:10.1097/00003246-199707000-00010

392. Shakoory B, Carcillo JA, Chatham WW, et al. Interleukin-1 Receptor Blockade Is Associated With Reduced Mortality in Sepsis Patients With Features of Macrophage Activation Syndrome: Reanalysis of a Prior Phase III Trial. *Crit Care Med*. 2016;44(2):275-281. doi:10.1097/CCM.0000000000001402

393. Leventogiannis K, Kyriazopoulou E, Antonakos N, et al. Toward personalized immunotherapy in sepsis: The PROVIDE randomized clinical trial. *Cell Rep Med*. 2022;3(11):100817. doi:10.1016/j.xcrm.2022.100817

394. Cvetkovic RS, Keating G. Anakinra. *BioDrugs Clin Immunother Biopharm Gene Ther*. 2002;16(4):303-311; discussion 313-314. doi:10.2165/00063030-200216040-00005

395. Dubinsky S, Watt K, Saleeb S, et al. Pharmacokinetics of Commonly Used Medications in Children Receiving Continuous Renal Replacement Therapy: A Systematic Review of Current Literature. *Clin Pharmacokinet*. 2022;61(2):189-229. doi:10.1007/s40262-021-01085-z

396. Churchwell MD. Use of an in vitro model of renal replacement therapy systems to estimate extracorporeal drug removal. *J Clin Pharmacol*. 2012;52(1 Suppl):35S-44S. doi:10.1177/0091270011415979

397. Jamal JA, Udy AA, Wallis SC, et al. Can we use an ex vivo continuous hemofiltration model to describe the adsorption and elimination of meropenem and piperacillin? *Int J Artif Organs*. 2015;38(8):419-424. doi:10.5301/ijao.5000422

398. Kalaria SN, Armahizer M, McCarthy P, Badjatia N, Gobburu JV, Gopalakrishnan M. Development and Use of an Ex-Vivo In-Vivo Correlation to Predict Antiepileptic Drug Clearance in Patients Undergoing Continuous Renal Replacement Therapy. *Pharm Res*. 2022;39(5):827-836. doi:10.1007/s11095-022-03287-x

399. Andrews L, Benken S, Tan X, Wenzler E. Pharmacokinetics and dialytic clearance of apixaban during in vitro continuous renal replacement therapy. *BMC Nephrol*. 2021;22(1):45. doi:10.1186/s12882-021-02248-7

400. Bouchard J, Roberts DM, Roy L, et al. Principles and operational parameters to optimize poison removal with extracorporeal treatments. *Semin Dial*. 2014;27(4):371-380. doi:10.1111/sdi.12247

401. Gueorguieva I, Clark SR, McMahon CJ, et al. Pharmacokinetic modelling of interleukin-1 receptor antagonist in plasma and cerebrospinal fluid of patients following subarachnoid haemorrhage. *Br J Clin Pharmacol*. 2008;65(3):317-325. doi:10.1111/j.1365-2125.2007.03026.x

402. Galea J, Ogungbenro K, Hulme S, et al. Intravenous anakinra can achieve experimentally effective concentrations in the central nervous system within a therapeutic time window: results of a dose-ranging study. *J Cereb Blood Flow Metab Off J Int Soc Cereb Blood Flow Metab*. 2011;31(2):439-447. doi:10.1038/jcbfm.2010.103

403. Galea J, Ogungbenro K, Hulme S, et al. Reduction of inflammation after administration of interleukin-1 receptor antagonist following aneurysmal subarachnoid hemorrhage: results of the Subcutaneous Interleukin-1Ra in SAH (SCIL-SAH) study. *J Neurosurg*. 2018;128(2):515-523. doi:10.3171/2016.9.JNS16615

404. Ogungbenro K, Hulme S, Rothwell N, Hopkins S, Tyrrell P, Galea J. Study design and population pharmacokinetic analysis of a phase II dose-ranging study of interleukin-1 receptor antagonist. *J Pharmacokinet Pharmacodyn*. 2016;43(1):1-12. doi:10.1007/s10928-015-9450-0

405. Aulagnon F, Lapidus N, Canet E, et al. Acute kidney injury in adults with hemophagocytic lymphohistiocytosis. *Am J Kidney Dis Off J Natl Kidney Found*. 2015;65(6):851-859. doi:10.1053/j.ajkd.2014.10.012

406. Kanduri SR, Cheungpasitporn W, Thongprayoon C, et al. Systematic Review of Risk factors and Incidence of Acute Kidney Injury Among Patients Treated with CAR-T Cell Therapies. *Kidney Int Rep*. 2021;6(5):1416-1422. doi:10.1016/j.ekir.2021.02.013

407. Kaur P, Jiang X, Duan J, Stier E. Applications of In Vitro-In Vivo Correlations in Generic Drug Development: Case Studies. *AAPS J*. 2015;17(4):1035-1039. doi:10.1208/s12248-015-9765-1

408. Rostami-Hodjegan A. Physiologically based pharmacokinetics joined with in vitro-in vivo extrapolation of ADME: a marriage under the arch of systems pharmacology. *Clin Pharmacol Ther*. 2012;92(1):50-61. doi:10.1038/clpt.2012.65

409. Vincent JL, Rello J, Marshall J, et al. International study of the prevalence and outcomes of infection in intensive care units. *JAMA*. 2009;302(21):2323-2329. doi:10.1001/jama.2009.1754

410. Vincent JL, Sakr Y, Singer M, et al. Prevalence and Outcomes of Infection Among Patients in Intensive Care Units in 2017. *JAMA*. 2020;323(15):1478-1487. doi:10.1001/jama.2020.2717

411. Parienti JJ, Dugué AE, Daurel C, et al. Continuous renal replacement therapy may increase the risk of catheter infection. *Clin J Am Soc Nephrol CJASN*. 2010;5(8):1489-1496. doi:10.2215/CJN.02130310

412. Hoste EAJ, Blot SI, Lameire NH, Vanholder RC, De Bacquer D, Colardyn FA. Effect of nosocomial bloodstream infection on the outcome of critically ill patients with acute renal failure treated with renal replacement therapy. *J Am Soc Nephrol JASN*. 2004;15(2):454-462. doi:10.1097/01.asn.0000110182.14608.0c

413. Rudnick W, Science M, Thirion DJG, et al. Antimicrobial use among adult inpatients at hospital sites within the Canadian Nosocomial Infection Surveillance Program: 2009 to 2016. *Antimicrob Resist Infect Control*. 2020;9(1):32. doi:10.1186/s13756-020-0684-2

414. Stitt G, Dubinsky S, Edginton A, et al. Antimicrobial Dosing Recommendations in Pediatric Continuous Renal Replacement Therapy: A Critical Appraisal of Current Evidence. *Front Pediatr*. 2022;10:889958. doi:10.3389/fped.2022.889958

415. Smyth RD, Pfeffer M, Glick A, Van Harken DR, Hottendorf GH. Clinical pharmacokinetics and safety of high doses of ceforanide (BL-S786R) and cefazolin. *Antimicrob Agents Chemother*. 1979;16(5):615-621. doi:10.1128/AAC.16.5.615

416. Vella-Brincat JWA, Begg EJ, Kirkpatrick CMJ, Zhang M, Chambers ST, Gallagher K. Protein binding of cefazolin is saturable in vivo both between and within patients. *Br J Clin Pharmacol*. 2007;63(6):753-757. doi:10.1111/j.1365-2125.2006.02827.x

417. Decroix MO, Zini R, Chaumeil JC, Tillement JP. Cefazolin serum protein binding and its inhibition by bilirubin, fatty acids and other drugs. *Biochem Pharmacol*. 1988;37(14):2807-2814. doi:10.1016/0006-2952(88)90044-5

418. Rein MF, Westervelt FB, Sande MA. Pharmacodynamics of cefazolin in the presence of normal and impaired renal function. *Antimicrob Agents Chemother*. 1973;4(3):366-371. doi:10.1128/AAC.4.3.366

419. Brown G, Zemcov SJ, Clarke AM. Effect of probenecid on cefazolin serum concentrations. *J Antimicrob Chemother*. 1993;31(6):1009-1011. doi:10.1093/jac/31.6.1009

420. Schmitz ML, Blumer JL, Cetnarowski W, Rubino CM. Determination of appropriate weight-based cutoffs for empiric cefazolin dosing using data from a phase 1 pharmacokinetics and safety study of cefazolin administered for surgical prophylaxis in

pediatric patients aged 10 to 12 years. *Antimicrob Agents Chemother*. 2015;59(7):4173-4180. doi:10.1128/AAC.00082-15

421. Joy MS, Matzke GR, Armstrong DK, Marx MA, Zarowitz BJ. A primer on continuous renal replacement therapy for critically ill patients. *Ann Pharmacother*. 1998;32(3):362-375. doi:10.1345/aph.17105

422. De Cock RFW, Smits A, Allegaert K, et al. Population pharmacokinetic modelling of total and unbound cefazolin plasma concentrations as a guide for dosing in preterm and term neonates. *J Antimicrob Chemother*. 2014;69(5):1330-1338. doi:10.1093/jac/dkt527

423. Smits A, Kulo A, Verbesselt R, et al. Cefazolin plasma protein binding and its covariates in neonates. *Eur J Clin Microbiol Infect Dis Off Publ Eur Soc Clin Microbiol*. 2012;31(12):3359-3365. doi:10.1007/s10096-012-1703-x

424. Soeters PB, Wolfe RR, Shenkin A. Hypoalbuminemia: Pathogenesis and Clinical Significance. *JPEN J Parenter Enteral Nutr*. 2019;43(2):181-193. doi:10.1002/jpen.1451

425. Drusano GL. Antimicrobial pharmacodynamics: critical interactions of "bug and drug." *Nat Rev Microbiol*. 2004;2(4):289-300. doi:10.1038/nrmicro862

426. Craig WA. Pharmacokinetic/pharmacodynamic parameters: rationale for antibacterial dosing of mice and men. *Clin Infect Dis Off Publ Infect Dis Soc Am*. 1998;26(1):1-10; quiz 11-12. doi:10.1086/516284

427. Craig WA. Interrelationship between pharmacokinetics and pharmacodynamics in determining dosage regimens for broad-spectrum cephalosporins. *Diagn Microbiol Infect Dis*. 1995;22(1-2):89-96. doi:10.1016/0732-8893(95)00053-d

428. Ulldemolins M, Vaquer S, Llauradó-Serra M, et al. Beta-lactam dosing in critically ill patients with septic shock and continuous renal replacement therapy. *Crit Care*. 2014;18(3):227. doi:10.1186/cc13938

429. Roberts JA, Norris R, Paterson DL, Martin JH. Therapeutic drug monitoring of antimicrobials. *Br J Clin Pharmacol*. 2012;73(1):27-36. doi:10.1111/j.1365-2125.2011.04080.x

430. Roberts JA, Ulldemolins M, Roberts MS, et al. Therapeutic drug monitoring of beta-lactams in critically ill patients: proof of concept. *Int J Antimicrob Agents*. 2010;36(4):332-339. doi:10.1016/j.ijantimicag.2010.06.008

431. Dilworth TJ, Schulz LT, Micek ST, Kollef MH, Rose WE. β-Lactam Therapeutic Drug Monitoring in Critically Ill Patients: Weighing the Challenges and Opportunities to Assess Clinical Value. *Crit Care Explor*. 2022;4(7):e0726. doi:10.1097/CCE.0000000000000726

432. Abdul-Aziz MH, Alffenaar JWC, Bassetti M, et al. Antimicrobial therapeutic drug monitoring in critically ill adult patients: a Position Paper. *Intensive Care Med*. 2020;46(6):1127-1153. doi:10.1007/s00134-020-06050-1

433. Roberts DM, Roberts JA, Roberts MS, et al. Variability of antibiotic concentrations in critically ill patients receiving continuous renal replacement therapy: a multicentre pharmacokinetic study. *Crit Care Med*. 2012;40(5):1523-1528. doi:10.1097/CCM.0b013e318241e553

434. Seyler L, Cotton F, Taccone FS, et al. Recommended β-lactam regimens are inadequate in septic patients treated with continuous renal replacement therapy. *Crit Care*. 2011;15(3):R137. doi:10.1186/cc10257

435. Cies JJ, Moore WS, Enache A, Chopra A. β-lactam Therapeutic Drug Management in the PICU. *Crit Care Med*. 2018;46(2):272-279. doi:10.1097/CCM.0000000000002817

436. Maynor LM, Carl DE, Matzke GR, et al. An in vivo-in vitro study of cefepime and cefazolin dialytic clearance during high-flux hemodialysis. *Pharmacotherapy*. 2008;28(8):977-983. doi:10.1592/phco.28.8.977

437. Fogel MA, Nussbaum PB, Feintzeig ID, Hunt WA, Gavin JP, Kim RC. Cefazolin in chronic hemodialysis patients: a safe, effective alternative to vancomycin. *Am J Kidney Dis Off J Natl Kidney Found*. 1998;32(3):401-409. doi:10.1053/ajkd.1998.v32.pm9740155

438. Marx MA, Frye RF, Matzke GR, Golper TA. Cefazolin as empiric therapy in hemodialysis-related infections: efficacy and blood concentrations. *Am J Kidney Dis Off J Natl Kidney Found*. 1998;32(3):410-414. doi:10.1053/ajkd.1998.v32.pm9740156

439. Sowinski KM, Mueller BA, Grabe DW, et al. Cefazolin dialytic clearance by high-efficiency and high-flux hemodialyzers. *Am J Kidney Dis Off J Natl Kidney Found*. 2001;37(4):766-776. doi:10.1016/s0272-6386(01)80126-8

440. Roberts JA, Abdul-Aziz MH, Davis JS, et al. Continuous versus Intermittent β-Lactam Infusion in Severe Sepsis. A Meta-analysis of Individual Patient Data from Randomized Trials. *Am J Respir Crit Care Med*. 2016;194(6):681-691. doi:10.1164/rccm.201601-0024OC

441. Vardakas KZ, Voulgaris GL, Maliaros A, Samonis G, Falagas ME. Prolonged versus short-term intravenous infusion of antipseudomonal β-lactams for patients with sepsis: a systematic review and meta-analysis of randomised trials. *Lancet Infect Dis*. 2018;18(1):108-120. doi:10.1016/S1473-3099(17)30615-1

442. Rhodes NJ, Liu J, O'Donnell JN, et al. Prolonged Infusion Piperacillin-Tazobactam Decreases Mortality and Improves Outcomes in Severely Ill Patients: Results of a Systematic Review and Meta-Analysis. *Crit Care Med*. 2018;46(2):236-243. doi:10.1097/CCM.0000000000002836

443. Fleischmann-Struzek C, Goldfarb DM, Schlattmann P, Schlapbach LJ, Reinhart K, Kissoon N. The global burden of paediatric and neonatal sepsis: a systematic review. *Lancet Respir Med*. 2018;6(3):223-230. doi:10.1016/S2213-2600(18)30063-8

444. Balamuth F, Weiss SL, Neuman MI, et al. Pediatric severe sepsis in U.S. children's hospitals. *Pediatr Crit Care Med J Soc Crit Care Med World Fed Pediatr Intensive Crit Care Soc*. 2014;15(9):798-805. doi:10.1097/PCC.0000000000000225

445. Odetola FO, Gebremariam A, Freed GL. Patient and hospital correlates of clinical outcomes and resource utilization in severe pediatric sepsis. *Pediatrics*. 2007;119(3):487-494. doi:10.1542/peds.2006-2353

446. Ruth A, McCracken CE, Fortenberry JD, Hall M, Simon HK, Hebbar KB. Pediatric severe sepsis: current trends and outcomes from the Pediatric Health Information Systems database. *Pediatr Crit Care Med J Soc Crit Care Med World Fed Pediatr Intensive Crit Care Soc*. 2014;15(9):828-838. doi:10.1097/PCC.0000000000000254

447. Carcillo JA, Halstead ES, Hall MW, et al. Three hypothetical inflammation pathobiology phenotypes and pediatric sepsis-induced multiple organ failure outcome. *Pediatr Crit Care Med J Soc Crit Care Med World Fed Pediatr Intensive Crit Care Soc*. 2017;18(6):513-523. doi:10.1097/PCC.0000000000001122

448. Seymour CW, Kennedy JN, Wang S, et al. Derivation, Validation, and Potential Treatment Implications of Novel Clinical Phenotypes for Sepsis. *JAMA*. 2019;321(20):2003-2017. doi:10.1001/jama.2019.5791

449. Dean JM. Evolution of the Collaborative Pediatric Critical Care Research Network (CPCCRN). *Pediatr Crit Care Med J Soc Crit Care Med World Fed Pediatr Intensive Crit Care Soc*. 2022;23(12):1049-1055. doi:10.1097/PCC.0000000000003098

450. Dubinsky SDJ, Watt KM, Imburgia CE, et al. Anakinra Removal by Continuous Renal Replacement Therapy: An Ex Vivo Analysis. *Crit Care Explor*. 2023;5(12):e1010. doi:10.1097/CCE.0000000000001010

451. Niederalt C, Kuepfer L, Solodenko J, et al. A generic whole body physiologically based pharmacokinetic model for therapeutic proteins in PK-Sim. *J Pharmacokinet Pharmacodyn*. 2018;45(2):235-257. doi:10.1007/s10928-017-9559-4

452. Gill KL, Gardner I, Li L, Jamei M. A Bottom-Up Whole-Body Physiologically Based Pharmacokinetic Model to Mechanistically Predict Tissue Distribution and the Rate of Subcutaneous Absorption of Therapeutic Proteins. *AAPS J*. 2016;18(1):156-170. doi:10.1208/s12248-015-9819-4

453. Liebner R, Mathaes R, Meyer M, Hey T, Winter G, Besheer A. Protein HESylation for half-life extension: synthesis, characterization and pharmacokinetics of HESylated anakinra. *Eur J Pharm Biopharm Off J Arbeitsgemeinschaft Pharm Verfahrenstechnik EV*. 2014;87(2):378-385. doi:10.1016/j.ejpb.2014.03.010

454. Pan X, Stader F, Abduljalil K, et al. Development and Application of a Physiologically-Based Pharmacokinetic Model to Predict the Pharmacokinetics of Therapeutic Proteins from Full-term Neonates to Adolescents. *AAPS J*. 2020;22(4):76. doi:10.1208/s12248-020-00460-1

455. Schaller S, Willmann S, Lippert J, et al. A Generic Integrated Physiologically based Whole-body Model of the Glucose-Insulin-Glucagon Regulatory System. *CPT Pharmacomet Syst Pharmacol*. 2013;2(8):e65. doi:10.1038/psp.2013.40

456. Glassman PM, Balthasar JP. Physiologically-based modeling of monoclonal antibody pharmacokinetics in drug discovery and development. *Drug Metab Pharmacokinet*. 2019;34(1):3-13. doi:10.1016/j.dmpk.2018.11.002

457. Malinoski D, Jafari F, Ewing T, et al. Standard prophylactic enoxaparin dosing leads to inadequate anti-Xa levels and increased deep venous thrombosis rates in critically ill trauma and surgical patients. *J Trauma*. 2010;68(4):874-880. doi:10.1097/TA.0b013e3181d32271

458. Macdougall IC, Robson R, Opatrna S, et al. Pharmacokinetics and pharmacodynamics of intravenous and subcutaneous continuous erythropoietin receptor activator (C.E.R.A.) in patients with chronic kidney disease. *Clin J Am Soc Nephrol CJASN*. 2006;1(6):1211-1215. doi:10.2215/CJN.00730306

459. Kaufman JS, Reda DJ, Fye CL, et al. Subcutaneous compared with intravenous epoetin in patients receiving hemodialysis. Department of Veterans Affairs Cooperative Study Group on Erythropoietin in Hemodialysis Patients. *N Engl J Med*. 1998;339(9):578-583. doi:10.1056/NEJM199808273390902

460. Malik PRV, Edginton AN. Integration of Ontogeny Into a Physiologically Based Pharmacokinetic Model for Monoclonal Antibodies in Premature Infants. *J Clin Pharmacol*. 2020;60(4):466-476. doi:10.1002/jcph.1540

461. Green EA, Metz D, Galinsky R, et al. Anakinra Pilot - a clinical trial to demonstrate safety, feasibility and pharmacokinetics of interleukin 1 receptor antagonist in preterm infants. *Front Immunol*. 2022;13:1022104. doi:10.3389/fimmu.2022.1022104

462. Cayabyab RG, Jones CA, Kwong KYC, et al. Interleukin-1beta in the bronchoalveolar lavage fluid of premature neonates: a marker for maternal chorioamnionitis and predictor of adverse neonatal outcome. *J Matern-Fetal Neonatal Med Off J Eur Assoc Perinat Med Fed Asia Ocean Perinat Soc Int Soc Perinat Obstet*. 2003;14(3):205-211. doi:10.1080/jmf.14.3.205.211

463. Urien S, Bardin C, Bader-Meunier B, et al. Anakinra pharmacokinetics in children and adolescents with systemic-onset juvenile idiopathic arthritis and autoinflammatory syndromes. *BMC Pharmacol Toxicol*. 2013;14:40. doi:10.1186/2050-6511-14-40

464. Ilowite N, Porras O, Reiff A, et al. Anakinra in the treatment of polyarticular-course juvenile rheumatoid arthritis: safety and preliminary efficacy results of a randomized multicenter study. *Clin Rheumatol*. 2009;28(2):129-137. doi:10.1007/s10067-008-0995-9

465. Anderson HL, Coran AG, Drongowski RA, Ha HJ, Bartlett RH. Extracellular fluid and total body water changes in neonates undergoing extracorporeal membrane oxygenation. *J Pediatr Surg*. 1992;27(8):1003-1007; discussion 1007-1008. doi:10.1016/0022-3468(92)90547-k

466. Vrancken SL, Heijst AF, Zegers M, et al. Influence of volume replacement with colloids versus crystalloids in neonates on venoarterial extracorporeal membrane oxygenation on fluid retention, fluid balance, and ECMO runtime. *ASAIO J Am Soc Artif Intern Organs 1992*. 2005;51(6):808-812. doi:10.1097/01.mat.0000183474.01675.3a

467. Selewski DT, Askenazi DJ, Bridges BC, et al. The Impact of Fluid Overload on Outcomes in Children Treated with Extracorporeal Membrane Oxygenation: a Multi-Centre Retrospective Cohort Study. *Pediatr Crit Care Med J Soc Crit Care Med World Fed Pediatr Intensive Crit Care Soc*. 2017;18(12):1126-1135. doi:10.1097/PCC.0000000000001349

468. Radke C, Horn D, Lanckohr C, et al. Development of a Physiologically Based Pharmacokinetic Modelling Approach to Predict the Pharmacokinetics of Vancomycin in Critically Ill Septic Patients. *Clin Pharmacokinet*. 2017;56(7):759-779. doi:10.1007/s40262-016-0475-3

469. Cavalli G, De Luca G, Campochiaro C, et al. Interleukin-1 blockade with high-dose anakinra in patients with COVID-19, acute respiratory distress syndrome, and hyperinflammation: a retrospective cohort study. *Lancet Rheumatol*. 2020;2(6):e325-e331. doi:10.1016/S2665-9913(20)30127-2

470. Yang J, Jain S, Capparelli EV, et al. Anakinra Treatment in Patients with Acute Kawasaki Disease with Coronary Artery Aneurysms: A Phase I/IIa Trial. *J Pediatr*. 2022;243:173-180.e8. doi:10.1016/j.jpeds.2021.12.035

471. Bami S, Vagrecha A, Soberman D, et al. The use of anakinra in the treatment of secondary hemophagocytic lymphohistiocytosis. *Pediatr Blood Cancer*. 2020;67(11):e28581. doi:10.1002/pbc.28581

472. Phadke O, Rouster-Stevens K, Giannopoulos H, Chandrakasan S, Prahalad S. Intravenous administration of anakinra in children with macrophage activation syndrome. *Pediatr Rheumatol Online J*. 2021;19(1):98. doi:10.1186/s12969-021-00585-3

473. Center for Drug Evalatuion and Research. Clinical Pharmacology and Biopharmaceutics Revew: Olumiant. Published December 2017. Accessed September 2021.Baricitinib clinical https://www.accessdata.fda.gov/drugsatfda_docs/nda/2018/207924Orig1s000ClinPharmR.pdf.

474. Granowitz EV, Porat R, Mier JW, et al. Pharmacokinetics, safety and immunomodulatory effects of human recombinant interleukin-1 receptor antagonist in healthy humans. *Cytokine*. 1992;4(5):353-360. doi:10.1016/1043-4666(92)90078-6

475. Antonucci E, Lamanna I, Fagnoul D, Vincent JL, De Backer D, Silvio Taccone F. The Impact of Renal Failure and Renal Replacement Therapy on Outcome During Extracorporeal Membrane Oxygenation Therapy. *Artif Organs*. 2016;40(8):746-754. doi:10.1111/aor.12695

476. Fleming GM, Sahay R, Zappitelli M, et al. The Incidence of Acute Kidney Injury and its Effect on Neonatal and Pediatric ECMO Outcomes: A multicenter report from the KIDMO

Study Group. *Pediatr Crit Care Med J Soc Crit Care Med World Fed Pediatr Intensive Crit Care Soc*. 2016;17(12):1157-1169. doi:10.1097/PCC.0000000000000970

477. Haneya A, Diez C, Philipp A, et al. Impact of Acute Kidney Injury on Outcome in Patients With Severe Acute Respiratory Failure Receiving Extracorporeal Membrane Oxygenation. *Crit Care Med*. 2015;43(9):1898-1906. doi:10.1097/CCM.0000000000001141

478. Gorga SM, Lima L, Askenazi DJ, et al. Fluid Balance Management Informs Renal Replacement Therapy Use During Pediatric Extracorporeal Membrane Oxygenation: A Survey Report From the Kidney Intervention During Extracorporeal Membrane Oxygenation Group. *ASAIO J Am Soc Artif Intern Organs 1992*. 2022;68(3):407-412. doi:10.1097/MAT.0000000000001471

479. Maniscalco V, Abu-Rumeileh S, Mastrolia MV, et al. The off-label use of anakinra in pediatric systemic autoinflammatory diseases. *Ther Adv Musculoskelet Dis*. 2020;12:1759720X20959575. doi:10.1177/1759720X20959575

480. Schwartz SP, Walker TC, Kihlstrom M, et al. Extracorporeal Membrane Oxygenation for COVID-19-Associated Multisystem Inflammatory Syndrome in a 5-year-old. *Am Surg*. 2022;88(2):174-176. doi:10.1177/0003134820983198

481. Maunier L, Charbel R, Lambert V, Tissières P, Group the C study. Anakinra in pediatric acute fulminant myocarditis. *Ann Intensive Care*. 2022;12. doi:10.1186/s13613-022-01054-0

482. Çağlayan Ş, Sönmez HE, Otar Yener G, et al. Anakinra treatment in multisystemic inflammatory syndrome in children (MIS-C) associated with COVID-19. *Front Pediatr*. 2022;10:942455. doi:10.3389/fped.2022.942455

483. Cloyd C, Sargel C. 1014: Anakinra dosing for macrophage activation syndrome during continuous renal replacement therapy. *Crit Care Med*. 2022;50(1):504. doi:10.1097/01.ccm.0000810380.26200.b7

484. Edlund H, Melin J, Parra-Guillen ZP, Kloft C. Pharmacokinetics and pharmacokinetic-pharmacodynamic relationships of monoclonal antibodies in children. *Clin Pharmacokinet*. 2015;54(1):35-80. doi:10.1007/s40262-014-0208-4

485. Malik P, Edginton A. Pediatric physiology in relation to the pharmacokinetics of monoclonal antibodies. *Expert Opin Drug Metab Toxicol*. 2018;14(6):585-599. doi:10.1080/17425255.2018.1482278

486. Zhang Y, Wei X, Bajaj G, et al. Challenges and considerations for development of therapeutic proteins in pediatric patients. *J Clin Pharmacol*. 2015;55 Suppl 3:S103-115. doi:10.1002/jcph.382

487. Quartier P, Allantaz F, Cimaz R, et al. A multicentre, randomised, double-blind, placebo-controlled trial with the interleukin-1 receptor antagonist anakinra in patients with systemic-onset juvenile idiopathic arthritis (ANAJIS trial). *Ann Rheum Dis*. 2011;70(5):747-754. doi:10.1136/ard.2010.134254

488. Ferenbach DA, Bonventre JV. Acute kidney injury and chronic kidney disease: from the laboratory to the clinic. *Nephrol Ther*. 2016;12(Suppl 1):S41-S48. doi:10.1016/j.nephro.2016.02.005

489. Sato Y, Takahashi M, Yanagita M. Pathophysiology of AKI to CKD progression. *Semin Nephrol*. 2020;40(2):206-215. doi:10.1016/j.semnephrol.2020.01.011

490. Lim K, McGregor G, Coggan AR, Lewis GD, Moe SM. Cardiovascular Functional Changes in Chronic Kidney Disease: Integrative Physiology, Pathophysiology and Applications of Cardiopulmonary Exercise Testing. *Front Physiol*. 2020;11:572355. doi:10.3389/fphys.2020.572355

491. Katulka EK, Hirt AE, Kirkman DL, Edwards DG, Witman MAH. Altered vascular function in chronic kidney disease: evidence from passive leg movement. *Physiol Rep*. 2019;7(8):e14075. doi:10.14814/phy2.14075

492. Ngo B, Rongey C, Hiscox B, Rendell M, Woodley D, Smogorzewski M. Skin blood flow in patients with stage 5 chronic kidney disease on hemodialysis. *J Ren Nutr Off J Counc Ren Nutr Natl Kidney Found*. 2010;20(5 Suppl):S89-94. doi:10.1053/j.jrn.2010.06.008

493. Chew R, Woods ML. Flucloxacillin does not achieve therapeutic cerebrospinal fluid levels against meticillin-sensitive Staphylococcus aureus in adults: A case report and review of the literature. *Int J Antimicrob Agents*. 2016;47(3):229-231. doi:10.1016/j.ijantimicag.2015.12.009

494. Le Turnier P, Gregoire M, Deslandes G, et al. Should we reconsider cefazolin for treating staphylococcal meningitis? A retrospective analysis of cefazolin and cloxacillin cerebrospinal fluid levels in patients treated for staphylococcal meningitis. *Clin Microbiol Infect Off Publ Eur Soc Clin Microbiol Infect Dis*. 2020;26(10):1415.e1-1415.e4. doi:10.1016/j.cmi.2020.04.046

495. Tunkel AR, Hasbun R, Bhimraj A, et al. 2017 Infectious Diseases Society of America's Clinical Practice Guidelines for Healthcare-Associated Ventriculitis and Meningitis. *Clin Infect Dis Off Publ Infect Dis Soc Am*. 2017;64(6):e34-e65. doi:10.1093/cid/ciw861

496. Tunkel AR, Hartman BJ, Kaplan SL, et al. Practice guidelines for the management of bacterial meningitis. *Clin Infect Dis Off Publ Infect Dis Soc Am*. 2004;39(9):1267-1284. doi:10.1086/425368

497. Shi C, Xiao Y, Zhang Q, et al. Efficacy and safety of cefazolin versus antistaphylococcal penicillins for the treatment of methicillin-susceptible Staphylococcus aureus bacteremia: a systematic review and meta-analysis. *BMC Infect Dis*. 2018;18(1):508. doi:10.1186/s12879-018-3418-9

498. Lecomte R, Bourreau A, Deschanvres C, et al. Comparative outcomes of cefazolin versus antistaphylococcal penicillins in methicillin-susceptible Staphylococcus aureus infective endocarditis: a post hoc analysis of a prospective multicentre French cohort study. *Clin*

Microbiol Infect Off Publ Eur Soc Clin Microbiol Infect Dis. 2021;27(7):1015-1021. doi:10.1016/j.cmi.2020.08.044

499. McDanel JS, Perencevich EN, Diekema DJ, et al. Comparative effectiveness of beta-lactams versus vancomycin for treatment of methicillin-susceptible Staphylococcus aureus bloodstream infections among 122 hospitals. *Clin Infect Dis Off Publ Infect Dis Soc Am*. 2015;61(3):361-367. doi:10.1093/cid/civ308

500. Nau R, Sörgel F, Prange HW. Lipophilicity at pH 7.4 and molecular size govern the entry of the free serum fraction of drugs into the cerebrospinal fluid in humans with uninflamed meninges. *J Neurol Sci*. 1994;122(1):61-65. doi:10.1016/0022-510x(94)90052-3

501. Nau R, Sörgel F, Eiffert H. Penetration of drugs through the blood-cerebrospinal fluid/blood-brain barrier for treatment of central nervous system infections. *Clin Microbiol Rev*. 2010;23(4):858-883. doi:10.1128/CMR.00007-10

502. Yoshimura F, Nikaido H. Diffusion of beta-lactam antibiotics through the porin channels of Escherichia coli K-12. *Antimicrob Agents Chemother*. 1985;27(1):84-92. doi:10.1128/AAC.27.1.84

503. Karalis V, Tsantili-Kakoulidou A, Macheras P. Quantitative structure-pharmacokinetic relationships for disposition parameters of cephalosporins. *Eur J Pharm Sci Off J Eur Fed Pharm Sci*. 2003;20(1):115-123. doi:10.1016/s0928-0987(03)00177-5

504. Dallmann A, Ince I, Solodenko J, et al. Physiologically Based Pharmacokinetic Modeling of Renally Cleared Drugs in Pregnant Women. *Clin Pharmacokinet*. 2017;56(12):1525-1541. doi:10.1007/s40262-017-0538-0

505. Grégoire M, Gaborit B, Deschanvres C, et al. High-Dosage Cefazolin Achieves Sufficient Cerebrospinal Diffusion To Treat an External Ventricular Drainage-Related Staphylococcus aureus Ventriculitis. *Antimicrob Agents Chemother*. 2019;63(2):e01844-18. doi:10.1128/AAC.01844-18

506. Novak AR, Krsak M, Kiser TH, et al. Pharmacokinetic Evaluation of Cefazolin in the Cerebrospinal Fluid of Critically Ill Patients. *Open Forum Infect Dis*. 2022;9(2):ofab649. doi:10.1093/ofid/ofab649

507. Kreppel D, Antoniadis G, Seeling W. Spinal hematoma: a literature survey with meta-analysis of 613 patients. *Neurosurg Rev*. 2003;26(1):1-49. doi:10.1007/s10143-002-0224-y

508. Gerhart JG, Watt KM, Edginton A, et al. Physiologically-Based Pharmacokinetic Modeling of Fluconazole Using Plasma and Cerebrospinal Fluid Samples From Preterm and Term Infants. *CPT Pharmacomet Syst Pharmacol*. 2019;8(7):500-510. doi:10.1002/psp4.12414

509. Edginton AN. Using Physiologically Based Pharmacokinetic Modeling for Mechanistic Insight: Cases of Reverse Translation. *Clin Transl Sci*. 2018;11(2):109-111. doi:10.1111/cts.12517

510. Brodwall EK, Bergan T, Orjavik O. Kidney transport of cefazolin in normal and impaired renal function. *J Antimicrob Chemother*. 1977;3(6):585-592. doi:10.1093/jac/3.6.585

511. Ci L, Kusuhara H, Adachi M, Schuetz JD, Takeuchi K, Sugiyama Y. Involvement of MRP4 (ABCC4) in the luminal efflux of ceftizoxime and cefazolin in the kidney. *Mol Pharmacol*. 2007;71(6):1591-1597. doi:10.1124/mol.106.031823

512. Szeto KX, Le Merdy M, Dupont B, Bolger MB, Lukacova V. PBPK Modeling Approach to Predict the Behavior of Drugs Cleared by Kidney in Pregnant Subjects and Fetus. *AAPS J*. 2021;23(4):89. doi:10.1208/s12248-021-00603-y

513. Bayer Technology Services. Computational systems biology software suite. PKSim ® and MOBI® manual. Version 11.1, SB Suite. Accessed June 6, 2023. <http://www.syste ms-biolo gy.com/produ cts/pk-sim.html >.

514. Burkat PM. Physiologically Based Pharmacokinetic and Pharmacodynamic Modeling of Diazepam: Unbound Interstitial Brain Concentrations Correspond to Clinical End Points. *J Clin Pharmacol*. 2022;62(10):1297-1309. doi:10.1002/jcph.2071

515. Mehta K, Narayanan N, Heysell SK, et al. Pharmacogenetic variability and the probability of site of action target attainment during tuberculosis meningitis treatment: A physiologically based pharmacokinetic modeling and simulations study. *Tuberc Edinb Scotl*. 2022;137:102271. doi:10.1016/j.tube.2022.102271

516. Uchida Y, Ohtsuki S, Katsukura Y, et al. Quantitative targeted absolute proteomics of human blood-brain barrier transporters and receptors. *J Neurochem*. 2011;117(2):333-345. doi:10.1111/j.1471-4159.2011.07208.x

517. Strazielle N, Ghersi-Egea JF. Physiology of blood-brain interfaces in relation to brain disposition of small compounds and macromolecules. *Mol Pharm*. 2013;10(5):1473-1491. doi:10.1021/mp300518e

518. Shawahna R, Uchida Y, Declèves X, et al. Transcriptomic and quantitative proteomic analysis of transporters and drug metabolizing enzymes in freshly isolated human brain microvessels. *Mol Pharm*. 2011;8(4):1332-1341. doi:10.1021/mp200129p

519. Nishimura M, Naito S. Tissue-specific mRNA expression profiles of human ATP-binding cassette and solute carrier transporter superfamilies. *Drug Metab Pharmacokinet*. 2005;20(6):452-477. doi:10.2133/dmpk.20.452

520. Roberts JA, Paul SK, Akova M, et al. DALI: defining antibiotic levels in intensive care unit patients: are current β-lactam antibiotic doses sufficient for critically ill patients? *Clin Infect Dis Off Publ Infect Dis Soc Am*. 2014;58(8):1072-1083. doi:10.1093/cid/ciu027

521. Bard JD, Hindler JA, Gold HS, Limbago B. Rationale for Eliminating Staphylococcus Breakpoints for β-Lactam Agents Other Than Penicillin, Oxacillin or Cefoxitin, and Ceftaroline. *Clin Infect Dis Off Publ Infect Dis Soc Am*. 2014;58(9):1287-1296. doi:10.1093/cid/ciu043

522. The European Committee on Antimicrobial Susceptibility Testing. Breakpoint tables for interpretation of MICs and zone diameters, version 10.0, 2020. Accessed October 2023.

523. Gardner ME, Fritz WL, Hyland RN. A Case Attributed to Cefazolin and a Review of the Literature. *Drug Intell Clin Pharm*. 1978;12(5):268-271. doi:10.1177/106002807801200501

524. Moore TD, Bechtel TP, Ayers LW. Effect of multidose therapy on cerebrospinal fluid penetration of cefazolin. *Am J Hosp Pharm*. 1981;38(10):1496-1499.

525. Bechtel TP, Slaughter RL, Moore TD. Seizures associated with high cerebrospinal fluid concentrations of cefazolin. *Am J Hosp Pharm*. 1980;37(2):271-273.

526. Philipson A, Stiernstedt G, Ehrnebo M. Comparison of the pharmacokinetics of cephradine and cefazolin in pregnant and non-pregnant women. *Clin Pharmacokinet*. 1987;12(2):136-144. doi:10.2165/00003088-198712020-00004

527. van de Beek D, de Gans J, Spanjaard L, Weisfelt M, Reitsma JB, Vermeulen M. Clinical features and prognostic factors in adults with bacterial meningitis. *N Engl J Med*. 2004;351(18):1849-1859. doi:10.1056/NEJMoa040845

528. Antosz K, Battle S, Chang J, Scheetz MH, Al-Hasan M, Bookstaver PB. Cefazolin in the treatment of central nervous system infections: A narrative review and recommendation. *Pharmacotherapy*. 2023;43(1):85-95. doi:10.1002/phar.2750

529. Frame PT, Watanakunakorn C, McLaurin RL, Khodadad G. Penetration of nafcillin, methicillin, and cefazolin into human brain tissue. *Neurosurgery*. 1983;12(2):142-147. doi:10.1227/00006123-198302000-00002

530. van Sorge NM, Doran KS. Defense at the border: the blood-brain barrier versus bacterial foreigners. *Future Microbiol*. 2012;7(3):383-394. doi:10.2217/fmb.12.1

531. Kim KS, Wass CA, Cross AS. Blood-brain barrier permeability during the development of experimental bacterial meningitis in the rat. *Exp Neurol*. 1997;145(1):253-257. doi:10.1006/exnr.1997.6458

532. Quagliarello VJ, Ma A, Stukenbrok H, Palade GE. Ultrastructural localization of albumin transport across the cerebral microvasculature during experimental meningitis in the rat. *J Exp Med*. 1991;174(3):657-672. doi:10.1084/jem.174.3.657

533. Dacey RG, Sande MA. Effect of probenecid on cerebrospinal fluid concentrations of penicillin and cephalosporin derivatives. *Antimicrob Agents Chemother*. 1974;6(4):437-441. doi:10.1128/AAC.6.4.437

534. von Wedel-Parlow M, Wölte P, Galla HJ. Regulation of major efflux transporters under inflammatory conditions at the blood-brain barrier in vitro. *J Neurochem*. 2009;111(1):111-118. doi:10.1111/j.1471-4159.2009.06305.x

535. Nau R, Seele J, Djukic M, Eiffert H. Pharmacokinetics and pharmacodynamics of antibiotics in central nervous system infections. *Curr Opin Infect Dis*. 2018;31(1):57-68. doi:10.1097/QCO.0000000000000418

536. Kearney BP, Aweeka FT. The penetration of anti-infectives into the central nervous system. *Neurol Clin*. 1999;17(4):883-900. doi:10.1016/s0733-8619(05)70171-7

537. Gonçalves-Pereira J, Póvoa P. Antibiotics in critically ill patients: a systematic review of the pharmacokinetics of β-lactams. *Crit Care Lond Engl*. 2011;15(5):R206. doi:10.1186/cc10441

538. Taccone FS, Laterre PF, Dugernier T, et al. Insufficient β-lactam concentrations in the early phase of severe sepsis and septic shock. *Crit Care Lond Engl*. 2010;14(4):R126. doi:10.1186/cc9091

539. Roberts JA, Roberts MS, Robertson TA, Dalley AJ, Lipman J. Piperacillin penetration into tissue of critically ill patients with sepsis--bolus versus continuous administration? *Crit Care Med*. 2009;37(3):926-933. doi:10.1097/CCM.0b013e3181968e44

540. Lutsar I, McCracken GH, Friedland IR. Antibiotic pharmacodynamics in cerebrospinal fluid. *Clin Infect Dis Off Publ Infect Dis Soc Am*. 1998;27(5):1117-1127, quiz 1128-1129. doi:10.1086/515003

541. Huang H, Huang S, Zhu P, Xi X. Continuous versus intermittent infusion of cefepime in neurosurgical patients with post-operative intracranial infections. *Int J Antimicrob Agents*. 2014;43(1):68-72. doi:10.1016/j.ijantimicag.2013.08.019

542. Sugimoto M, Uchida I, Mashimo T, et al. Evidence for the involvement of GABA(A) receptor blockade in convulsions induced by cephalosporins. *Neuropharmacology*. 2003;45(3):304-314. doi:10.1016/s0028-3908(03)00188-6

543. Fernández-Torre JL, Martínez-Martínez M, González-Rato J, et al. Cephalosporin-induced nonconvulsive status epilepticus: clinical and electroencephalographic features. *Epilepsia*. 2005;46(9):1550-1552. doi:10.1111/j.1528-1167.2005.16305.x

544. Manzella JP, Paul RL, Butler IL. CNS toxicity associated with intraventricular injection of cefazolin. Report of three cases. *J Neurosurg*. 1988;68(6):970-971. doi:10.3171/jns.1988.68.6.0970

545. Ultrastructural localization of albumin transport across the cerebral microvasculature during experimental meningitis in the rat. *J Exp Med*. 1991;174(3):657-672.

546. Kapralos I, Mainas E, Apostolopoulou O, et al. Population pharmacokinetics of anidulafungin in ICU patients assessing inter- and intrasubject variability. *Br J Clin Pharmacol*. 2021;87(3):1024-1032. doi:10.1111/bcp.14457

547. Shekar K, Roberts JA, Welch S, et al. ASAP ECMO: Antibiotic, Sedative and Analgesic Pharmacokinetics during Extracorporeal Membrane Oxygenation: a multi-centre study to

optimise drug therapy during ECMO. *BMC Anesthesiol*. 2012;12:29. doi:10.1186/1471-2253-12-29

548. Stitt G, Thibault C, Mueller BA, et al. Pharmacokinetic Research in Pediatric Extracorporeal Therapies: Current State and Future Directions. *Blood Purif*. 2024;53(6):520-526. doi:10.1159/000534828

549. Zhang J, Wang H, Fan Y, Yu Z, You G. Regulation of organic anion transporters: role in physiology, pathophysiology, and drug elimination. *Pharmacol Ther*. 2021;217:107647. doi:10.1016/j.pharmthera.2020.107647

550. Bischoff A, Bucher M, Gekle M, Sauvant C. PAH clearance after renal ischemia and reperfusion is a function of impaired expression of basolateral Oat1 and Oat3. *Physiol Rep*. 2014;2(2):e00243. doi:10.1002/phy2.243

551. Schneider R, Meusel M, Betz B, et al. Oat1/3 restoration protects against renal damage after ischemic AKI. *Am J Physiol Renal Physiol*. 2015;308(3):F198-208. doi:10.1152/ajprenal.00160.2014

552. Wang L, Sweet DH. Renal organic anion transporters (SLC22 family): expression, regulation, roles in toxicity, and impact on injury and disease. *AAPS J*. 2013;15(1):53-69. doi:10.1208/s12248-012-9413-y

553. Guo X, Meng Q, Liu Q, et al. JBP485 improves gentamicin-induced acute renal failure by regulating the expression and function of Oat1 and Oat3 in rats. *Toxicol Appl Pharmacol*. 2013;271(2):285-295. doi:10.1016/j.taap.2013.04.029

554. Komazawa H, Yamaguchi H, Hidaka K, Ogura J, Kobayashi M, Iseki K. Renal uptake of substrates for organic anion transporters Oat1 and Oat3 and organic cation transporters Oct1 and Oct2 is altered in rats with adenine-induced chronic renal failure. *J Pharm Sci*. 2013;102(3):1086-1094. doi:10.1002/jps.23433

555. Huo X, Liu K. Renal organic anion transporters in drug-drug interactions and diseases. *Eur J Pharm Sci Off J Eur Fed Pharm Sci*. 2018;112:8-19. doi:10.1016/j.ejps.2017.11.001

556. Vincent JL, Bihari DJ, Suter PM, et al. The prevalence of nosocomial infection in intensive care units in Europe. Results of the European Prevalence of Infection in Intensive Care (EPIC) Study. EPIC International Advisory Committee. *JAMA*. 1995;274(8):639-644.

557. Hulko M, Haug U, Gauss J, Boschetti-de-Fierro A, Beck W, Krause B. Requirements and Pitfalls of Dialyzer Sieving Coefficients Comparisons. *Artif Organs*. 2018;42(12):1164-1173. doi:10.1111/aor.13278

558. Takeda M, Babu E, Narikawa S, Endou H. Interaction of human organic anion transporters with various cephalosporin antibiotics. *Eur J Pharmacol*. 2002;438(3):137-142. doi:10.1016/s0014-2999(02)01306-7

559. Wolman AT, Gionfriddo MR, Heindel GA, et al. Organic anion transporter 3 interacts selectively with lipophilic β-lactam antibiotics. *Drug Metab Dispos Biol Fate Chem*. 2013;41(4):791-800. doi:10.1124/dmd.112.049569

560. Chant C, Wilson G, Friedrich JO. Anemia, transfusion, and phlebotomy practices in critically ill patients with prolonged ICU length of stay: a cohort study. *Crit Care Lond Engl*. 2006;10(5):R140. doi:10.1186/cc5054

561. O'Hara K, Martin JH, Schneider JJ. Barriers and Challenges in Performing Pharmacokinetic Studies to Inform Dosing in the Neonatal Population. *Pharm J Pharm Educ Pract*. 2020;8(1):16. doi:10.3390/pharmacy8010016

562. Roberts JA, Joynt GM, Lee A, et al. The Effect of Renal Replacement Therapy and Antibiotic Dose on Antibiotic Concentrations in Critically Ill Patients: Data From the Multinational Sampling Antibiotics in Renal Replacement Therapy Study. *Clin Infect Dis Off Publ Infect Dis Soc Am*. 2021;72(8):1369-1378. doi:10.1093/cid/ciaa224

563. Manolis E, Pons G. Proposals for model-based paediatric medicinal development within the current European Union regulatory framework. *Br J Clin Pharmacol*. 2009;68(4):493-501. doi:10.1111/j.1365-2125.2009.03484.x

564. Manolis E, Osman TE, Herold R, et al. Role of modeling and simulation in pediatric investigation plans. *Paediatr Anaesth*. 2011;21(3):214-221. doi:10.1111/j.1460-9592.2011.03523.x

565. Zhao P, Zhang L, Grillo JA, et al. Applications of physiologically based pharmacokinetic (PBPK) modeling and simulation during regulatory review. *Clin Pharmacol Ther*. 2011;89(2):259-267. doi:10.1038/clpt.2010.298

566. Gastine S, Rashed AN, Hsia Y, et al. GAPPS (Grading and Assessment of Pharmacokinetic-Pharmacodynamic Studies) a critical appraisal system for antimicrobial PKPD studies - development and application in pediatric antibiotic studies. *Expert Rev Clin Pharmacol*. 2019;12(12):1091-1098. doi:10.1080/17512433.2019.1695600

567. Dykstra K, Mehrotra N, Tornøe CW, et al. Reporting guidelines for population pharmacokinetic analyses. *J Pharmacokinet Pharmacodyn*. 2015;42(3):301-314. doi:10.1007/s10928-015-9417-1

568. Guidance for Industry: Population Pharmacokinetics. US Food and Drug Administration website. Available at https://www.fda.gov/regulatory-information/search-fda-guidance-documents/population-pharmacokinetics. Accessed March 17, 2024.

569. Guideline on Reporting The Results of Population Pharmacokinetic Analyses. European Medicines Agency website. Available at https://www.ema.europa.eu/en/reporting-results-population-pharmacokinetic-analyses-scientific-guideline. Accessed March 17, 2024.

570. Physiologically Based Pharmacokinetic Analyses - Format and Content Guidance for Industry. US Food and Drug Administration website. Available at

https://www.fda.gov/regulatory-information/search-fda-guidance-documents/physiologically-based-pharmacokinetic-analyses-format-and-content-guidance-industry. Accessed March 17, 2024.

571. Guideline on The Reporting of Physiologically Based Pharmacokinetic (PBPK) Modelling and Simulation. European Medicines Agency website. Available at https://www.ema.europa.eu/en/reporting-physiologically-based-pharmacokinetic-pbpk-modelling-simulation-scientific-guideline. Accessed March 17, 2024.

572. Hansel J, Mannan F, Robey R, et al. Covariates in population pharmacokinetic studies of critically ill adults receiving β-lactam antimicrobials: a systematic review and narrative synthesis. *JAC-Antimicrob Resist*. 2024;6(1):dlae030. doi:10.1093/jacamr/dlae030

573. Ahmad A, Ogungbenro K, Kunze A, et al. Population pharmacokinetic modeling and simulation to support qualification of pyridoxic acid as endogenous biomarker of OAT1/3 renal transporters. *CPT Pharmacomet Syst Pharmacol*. 2021;10(5):467-477. doi:10.1002/psp4.12610

574. Tan SPF, Willemin ME, Snoeys J, et al. Development of 4-Pyridoxic Acid PBPK Model to Support Biomarker-Informed Evaluation of OAT1/3 Inhibition and Effect of Chronic Kidney Disease. *Clin Pharmacol Ther*. 2023;114(6):1243-1253. doi:10.1002/cpt.3029

575. Langthaler K, Jones CR, Saaby L, Bundgaard C, Brodin B. Application of a new MDCKII-MDR1 cell model to measure the extent of drug distribution in vitro at equilibrium for prediction of in vivo unbound brain-to-plasma drug distribution. *Fluids Barriers CNS*. 2024;21(1):11. doi:10.1186/s12987-023-00495-4

576. Jiang L, Kumar S, Nuechterlein M, et al. Application of a high-resolution in vitro human MDR1-MDCK assay and in vivo studies in preclinical species to improve prediction of CNS drug penetration. *Pharmacol Res Perspect*. 2022;10(1):e00932. doi:10.1002/prp2.932

577. Wang Q, Rager JD, Weinstein K, et al. Evaluation of the MDR-MDCK cell line as a permeability screen for the blood-brain barrier. *Int J Pharm*. 2005;288(2):349-359. doi:10.1016/j.ijpharm.2004.10.007

578. Avedissian SN, Pais G, Joshi MD, Rhodes NJ, Scheetz MH. A Translational Pharmacokinetic Rat Model of Cerebral Spinal Fluid and Plasma Concentrations of Cefepime. *mSphere*. 2019;4(1):e00595-18. doi:10.1128/mSphere.00595-18

579. Papp-Wallace KM, Endimiani A, Taracila MA, Bonomo RA. Carbapenems: past, present, and future. *Antimicrob Agents Chemother*. 2011;55(11):4943-4960. doi:10.1128/AAC.00296-11

580. Zhanel GG, Johanson C, Embil JM, et al. Ertapenem: review of a new carbapenem. *Expert Rev Anti Infect Ther*. 2005;3(1):23-39. doi:10.1586/14787210.3.1.23

581. Nix DE, Goodwin SD, Peloquin CA, Rotella DL, Schentag JJ. Antibiotic tissue penetration and its relevance: models of tissue penetration and their meaning. *Antimicrob Agents Chemother*. 1991;35(10):1947-1952.

582. Craig WA. The pharmacology of meropenem, a new carbapenem antibiotic. *Clin Infect Dis Off Publ Infect Dis Soc Am*. 1997;24 Suppl 2:S266-275. doi:10.1093/clinids/24.supplement_2.s266

583. Zhanel GG, Wiebe R, Dilay L, et al. Comparative review of the carbapenems. *Drugs*. 2007;67(7):1027-1052. doi:10.2165/00003495-200767070-00006

584. Moon YS, Chung KC, Gill MA. Pharmacokinetics of meropenem in animals, healthy volunteers, and patients. *Clin Infect Dis Off Publ Infect Dis Soc Am*. 1997;24 Suppl 2:S249-255. doi:10.1093/clinids/24.supplement_2.s249

585. Blumer JL. Meropenem: evaluation of a new generation carbapenem. *Int J Antimicrob Agents*. 1997;8(2):73-92. doi:10.1016/s0924-8579(96)00347-0

586. Takeuchi Y, Sunagawa M, Isobe Y, Hamazume Y, Noguchi T. Stability of a 1 beta-methylcarbapenem antibiotic, meropenem (SM-7338) in aqueous solution. *Chem Pharm Bull (Tokyo)*. 1995;43(4):689-692. doi:10.1248/cpb.43.689

587. Ljungberg B, Nilsson-Ehle I. Pharmacokinetics of meropenem and its metabolite in young and elderly healthy men. *Antimicrob Agents Chemother*. 1992;36(7):1437-1440.

588. Wise R, Logan M, Cooper M, Ashby JP, Andrews JM. Meropenem pharmacokinetics and penetration into an inflammatory exudate. *Antimicrob Agents Chemother*. 1990;34(8):1515-1517. doi:10.1128/AAC.34.8.1515

589. Kelly HC, Hutchison M, Haworth SJ. A comparison of the pharmacokinetics of meropenem after administration by intravenous injection over 5 min and intravenous infusion over 30 min. *J Antimicrob Chemother*. 1995;36 Suppl A:35-41. doi:10.1093/jac/36.suppl_a.35

590. Krueger WA, Bulitta J, Kinzig-Schippers M, et al. Evaluation by Monte Carlo Simulation of the Pharmacokinetics of Two Doses of Meropenem Administered Intermittently or as a Continuous Infusion in Healthy Volunteers. *Antimicrob Agents Chemother*. 2005;49(5):1881-1889. doi:10.1128/AAC.49.5.1881-1889.2005

591. de Miranda P, Good SS, Krasny HC, Connor JD, Laskin OL, Lietman PS. Metabolic fate of radioactive acyclovir in humans. *Am J Med*. 1982;73(1A):215-220. doi:10.1016/0002-9343(82)90094-8

592. Liu XI, Momper JD, Rakhmanina N, et al. Physiologically Based Pharmacokinetic Models to Predict Maternal Pharmacokinetics and Fetal Exposure to Emtricitabine and Acyclovir. *J Clin Pharmacol*. 2020;60(2):240-255. doi:10.1002/jcph.1515

593. Laskin OL, Longstreth JA, Saral R, de Miranda P, Keeney R, Lietman PS. Pharmacokinetics and tolerance of acyclovir, a new anti-herpesvirus agent, in humans. *Antimicrob Agents Chemother*. 1982;21(3):393-398.

594. Vergin H, Kikuta C, Mascher H, Metz R. Pharmacokinetics and bioavailability of different formulations of aciclovir. *Arzneimittelforschung*. 1995;45(4):508-515.

595. Cheung KWK, van Groen BD, Spaans E, et al. A Comprehensive Analysis of Ontogeny of Renal Drug Transporters: mRNA Analyses, Quantitative Proteomics, and Localization. *Clin Pharmacol Ther*. 2019;106(5):1083-1092. doi:10.1002/cpt.1516

596. Maharaj AR, Wu H, Hornik CP, et al. Simulated Assessment of Pharmacokinetically Guided Dosing for Investigational Treatments of Pediatric Patients With Coronavirus Disease 2019. *JAMA Pediatr*. 2020;174(10):e202422. doi:10.1001/jamapediatrics.2020.2422

597. Wise R, Lockley RM, Webberly M, Dent J. Pharmacokinetics of intravenously administered ciprofloxacin. *Antimicrob Agents Chemother*. 1984;26(2):208-210.

598. Emmanouel DS, Lindheimer MD, Katz AI. Role of the kidney in hormone metabolism and its implications in clinical medicine. *Klin Wochenschr*. 1980;58(19):1005-1012. doi:10.1007/BF01476870

599. Maack T, Johnson V, Kau ST, Figueiredo J, Sigulem D. Renal filtration, transport, and metabolism of low-molecular-weight proteins: a review. *Kidney Int*. 1979;16(3):251-270. doi:10.1038/ki.1979.128

600. Nielsen JT. Handling of proteins in isolated and in vitro perfused proximal tubules from rabbit kidney. *Dan Med Bull*. 1990;37(3):197-210.

601. Meibohm B, Zhou H. Characterizing the impact of renal impairment on the clinical pharmacology of biologics. *J Clin Pharmacol*. 2012;52(1 Suppl):54S-62S. doi:10.1177/0091270011413894

602. Czock D, Keller F, Seidling HM. Pharmacokinetic predictions for patients with renal impairment: focus on peptides and protein drugs. *Br J Clin Pharmacol*. 2012;74(1):66-74. doi:10.1111/j.1365-2125.2012.04172.x

603. Weis S, Kesselmeier M, Davis JS, et al. Cefazolin versus anti-staphylococcal penicillins for the treatment of patients with Staphylococcus aureus bacteraemia. *Clin Microbiol Infect Off Publ Eur Soc Clin Microbiol Infect Dis*. 2019;25(7):818-827. doi:10.1016/j.cmi.2019.03.010

604. Zappala AF, Holl WW, Post A. Cefazolin. In: Florey K, editor. Analytical profiles of drug substances. New York: Academic Press; 1975. p. 1–20.

605. Sakurai Y, Motohashi H, Ueo H, et al. Expression levels of renal organic anion transporters (OATs) and their correlation with anionic drug excretion in patients with renal diseases. *Pharm Res*. 2004;21(1):61-67. doi:10.1023/b:pham.0000012153.71993.cb

606. 5 Human Albumin. *Transfus Med Hemother*. 2009;36(6):399-407.

607. Uchida Y, Kamiie J, Ohtsuki S, Terasaki T. Multichannel liquid chromatography-tandem mass spectrometry cocktail method for comprehensive substrate characterization of multidrug resistance-associated protein 4 transporter. *Pharm Res*. 2007;24(12):2281-2296. doi:10.1007/s11095-007-9453-7

Appendix A

Supplementary Material for Chapter 2

1. Search Strategy

Table 1.0. Overview of final search strategy with included databases and syntax.

Database	Search Syntax
PubMed	(pharmacokinetics[mesh] OR pharmacokinetic*[tw] OR “drug kinetic*”[tw] OR ADME[tw] OR “biological availability”[tw] OR “area under curve”[tw] OR biotransformation[tw] OR "drug clearance"[tw] OR “metabolic clearance rate”[tw] OR “drug absorption”[tw] OR “tissue distribution”[tw] OR "volume of distribution"[tw] OR “drug elimination”[tw] OR “drug liberation”[tw] OR “drug metabolism”[tw] OR "drug dose"[tw] OR “therapeutic equivalency”[tw]) **AND** (infant, newborn[mesh] OR child[mesh] OR pediatrics[mesh] OR neonat*[tw] OR infant*[tw] OR newborn*[tw] OR pediatric*[tw] OR paediatric*[tw] OR child*[tw]) **AND** (renal replacement therapy[mesh] OR hemodialys*[tw] OR “peritoneal dialysis”[tw] OR “extracorporeal dialysis”[tw] OR hemodiafiltration[tw] OR hemofiltration[tw] OR "renal replacement therapy"[tw] OR “kidney replacement therapy”[tw] OR "continuous renal replacement therapy"[tw] OR "continuous veno-venous hemodialysis"[tw] OR "continuous veno-venous hemofiltration"[tw] OR "continuous veno-venous hemodiafiltration”[tw] OR “intensive care”[mesh] OR “critical care”[tw] OR “ICU”[tw] OR “PICU”[tw] OR “NICU”[tw])
EMBASE	1. exp pharmacokinetics/ 2. exp bioavailability/ 3. exp area under the curve/ 4. (pharmacokinetic* or drug kinetic* or ADME or biological availability or area under curve or biotransformation or drug clearance or metabolic clearance rate or drug absorption or tissue distribution or volume of distribution or drug elimination or drug liberation or drug metabolism or drug dose or therapeutic equivalency).tw. 5. 1 or 2 or 3 or 4 6. exp newborn/ 7. exp child/ 8. (neonat* or infant* or newborn* or pediatric* or paediatric* or child*).tw. 9. 6 or 7 or 8 10. exp renal replacement therapy/ 11. (hemodialys* or peritoneal dialysis or extracorporeal dialysis or hemodiafiltration or hemofiltration or renal replacement therapy or kidney replacement therapy or continuous renal replacement therapy or

	continuous veno venous hemodialysis or continuous veno venous hemofiltration or continuous veno venous hemodiafiltration).tw. 12. 10 or 11 13. 5 and 9 and 12 14. limit 13 to english language
Cochrane Library	(pharmacokinetic* OR “drug kinetic*” OR ADME OR “biological availability” OR “area under curve” OR biotransformation OR "drug clearance" OR “metabolic clearance rate” OR “drug absorption” OR “tissue distribution” OR "volume of distribution" OR “drug elimination” OR “drug liberation” OR “drug metabolism” OR "drug dose" OR “therapeutic equivalency”):ti,ab,kw (neonat* OR infant* OR newborn* OR pediatric* OR paediatric* OR child*):ti,ab,kw (hemodialys* OR "peritoneal dialysis" OR "extracorporeal dialysis" OR hemodiafiltration OR hemofiltration OR "renal replacement therapy" OR "kidney replacement therapy" OR "continuous renal replacement therapy" OR "continuous veno venous hemodialysis" OR "continuous veno venous hemofiltration" OR "continuous veno venous hemodiafiltration"):ti,ab,kw

2. ClinPK Checklist

Table A-2. ClinPK checklist of included studies.

	Checklist Item	
	Title/Abstract	
1	The title identifies the drug(s) and patient population(s) studies	40/45 (89%) [91,118,160–187,189,190,192,195–201]
2	The abstract minimally includes the name of the drugs studied, the route of administration, the population in whom it was studied and the results of the primary objective and major clinical pharmacokinetic findings.	40/45 (89%) [91,118,160–182,184–186,188–201]
	Background	
3	Pharmacokinetic data (i.e., absorption, distribution, metabolism, excretion) that is known and relevant to the drugs being studied is described	26/45 (58%) [91,118,161–168,171–175,178–180,184,186,190,193,194,200,202]
4	An explanation of the study rationale is provided	44/45 (98%) [91,118,160–182,184–202]
5	Specific objectives or hypothesis is provided	44/45 (98%) [91,118,160–182,184–202]
	Methods	

6	Eligibility criteria of study participants are described	29/45 (64%) [160–168,170,172–180,184–188,190,192,193,197,200]
7	Co-administration (or lack thereof) of study drug(s) with other potentially interacting drugs or food within this study is described.	15/45 (33%) [118,161,162,165,178–180,183,184,190,192,193,196,199,200]
8	Drug preparation and administration characteristics including dose, route, formulation, infusion duration (if applicable) and frequency are described.	33/45 (73%) [91,118,160–167,169–174,176,178,181,183,184,186,188–193,195,198–201]
9	Body fluid or tissue sampling (timing, frequency and storage) for quantitative drug measurement is described.	38/45 (84%) [91,118,160–170,172–176,178,180,181,183–193,195,198,199,201,202]
10	Validation of quantitative bioanalytical methods used in the study are referenced or describe if applicable.	40/45 (89%) [91,118,160–165,167–170,172–176,178,180–195,198–202]
11	Pharmacokinetic modelling methods and software used are described, including assumptions made regarding the number of compartments and order of kinetics (zero, first or mixed).	26/45 (58%) [91,160–165,167,168,171–176,180,180,183,187–189,193,196,198,201,202]
12	For population pharmacokinetic studies, covariates incorporated into pharmacokinetic models are identified and described.	11/45 (24%) [161,162,165,167,171–174,176,179,180]
13	Formulas for calculated variables (such as creatinine clearance, body surface area, AUC, and adjusted body weight) are provided or referenced.	27/45 (60%) [160–163,165,166,168,171,173,174,176–184,186,188,191,192,197–199,202]
14	The specific body weight used in drug dosing and pharmacokinetic calculations are reported (i.e., ideal body weight vs. actual body weight vs. adjusted body weight).	24/45 (53%) [160–163,165–167,171–174,176–182,184,186,188,197–199]
15	Statistical methods including software used are described.	20/45 (44%) [91,160–168,171–174,176,179,180,186,200,201]
	Results	
16	Study withdrawals or subjects lost to follow-up (or lack thereof) are reported.	9/45 (20%) [160,163,165–168,176,179,180]

17	Quantification of missing or excluded data is provided if applicable.	9/45 (20%) [91,163,164,166,176,179,180,191]
18	All relevant variables that may explain inter- and intra-patient pharmacokinetic variability (including: age, sex, end-organ function, ethnicity, weight or BMI, health status or severity of illness, and pertinent co-morbidities) are provided with appropriate measures of variance.	17/45 (38%) [161–163,165–167,171,172,174,176–180,182,183,186]
19	Results of pharmacokinetic analyses are reported with appropriate measures of precision (such as range or 95% confidence interval)	17/45 (38%) [91,118,162,163,165–168,176,177,180,182,183,186,189,198,200]
20	Studies in patients receiving extracorporeal drug removal (i.e., dialysis) should report the mode of drug removal, type of filters used, duration of therapy and relevant flow rates.	18/45 (40%) [91,118,163,166,171,176,177,184,186,189–191,194,195,197,200–202]
21	In studies of drug bioavailability comparing two formulations of the same drug, F (bioavailability), AUC, Cmax (maximal concentration) and Tmax (time to maximal concentration) should be reported.	1/45 (2%) [182]
	Discussion/Conclusion	
22	Study limitations describing potential sources of bias and imprecision where relevant should be described.	39/45 (87%) [118,161–169,171–180,182–189,191–200,202]
23	The relevance of study findings (applicability, external validity) is described	41/45 (91%) [91,160–180,182–184,186–202]
	Other Information	
24	Funding sources and conflicts of interest for the authors are disclosed.	35/45 (78%) [91,118,160–169,171–180,184,188,190–193,195–197,199–202]

Appendix B

Supplementary Material for Chapter 3

1. Building a Physiologically-Based Pharmacokinetic Model for Meropenem in Healthy Adults

1.1 Introduction

Meropenem, a small molecule antibiotic, was first approved by the Food and Drug Administration (FDA) in 1996 for use in skin and soft tissue infections, intra-abdominal infections, and bacterial meningitis. [293] A key contributor to the antibacterial effect of carbapenems is the ability to bind to, and inhibit multiple penicillin-binding proteins, essential proteins in bacterial cell wall synthesis. [579] The pharmacokinetics (PK) of meropenem are similar to other members of the β-lactam family. Meropenem exhibits very low protein binding, approximately 2% and has a volume of distribution (Vd) at steady state of 21L in healthy adults (~0.23-0.35 L/kg), occupying the interstitial space. [268,580,581] The metabolism and excretion of meropenem largely occurs within the renal system. PK studies have shown that 60-80% of the parent compound is found within the urine unchanged, with the remaining portion being converted to an inactive metabolite (ICI 213, 689). [331,582,583] The metabolism of meropenem has yet to be fully elucidated however it has been shown to under inactivation via renal dehydropeptidase-1 (DHP-1), with potential contribution of hydrolysis within the plasma. [331,583,584] Several of the pre-clinical studies have demonstrated that renal clearance via active tubular secretion through basolateral organic anion transport 1,3 (OAT) largely contributes to total renal clearance. [331,332] The apical transporter responsible for efflux of meropenem within the renal tubule to the filtrate still remains unknown however it has been theorized to be a substrate for sodium-dependent phosphate transporter type- 1. [304]

In this report, the building and verification of a PBPK model for intravenous meropenem in healthy adults is presented.

1.2 Methods and Results

1.2.1 Modelling Strategy

PBPK modelling and simulation were performed using PK-Sim version 9.1. Fifteen organs and two blood organs (17 compartments) were included in the standard model to represent a virtual adult.

1.2.2 Intravenous model construction

The process for creating the PBPK model for a healthy adult is described here. **Table 1**. presents the drug-specific parameters of meropenem and the values used for the naïve model.

Table 1. Physicochemical properties and ADME of meropenem for IV model construction

	Used in naïve model	**Used in optimized model [range of optimized values]**
Physicochemical Properties		
Octanol:water coefficient (logP)	-0.69 log units [295] -3.132 log units [585]	**-1.21 log units** [-1.21- -1.21]
Fraction unbound in plasma (f_u)	0.98 [268,293]	0.98
Molecular weight (MW)	383.463 g/mol [295]	383.463 g/mol
pKa (acid) **pKa (base)**	2.9 [586] 7.4 [586]	2.9 7.4
Water solubility	5.63 mg/mL [295]	
ADME		
Partition coefficient	Rodgers and Rowland	Rodgers and Rowland
Cell permeability	Charge dependent Schmitt	Charge dependent Schmitt
Renal DHP-1 enzyme concentration	1.0 µM (fixed)	1.0 µM
Renal DHP-1 K_M	2 mM [300]	2000 µM
Renal DHP-1 specific clearance	0 µmol/L/min	**89.21 µmol/L/min** [88.99-89.90]
GFR fraction	1.0	1.0
OAT3 concentration	0.0917 µM [292]	0.0917 µM
OAT3 K_M	847 µM [300]	847 µM
OAT3 Vmax	0 µmol/L/min	**1262.57 µmol/L/min** [1248.49-1268.14]
Apical Transporter concentration	1.0 µM (fixed)	1.0 µM
Apical Transporter K_M	770 µM [304]	770 µM
Apical Transporter Vmax	0 µmol/L/min	**116.11 µmol/L/min** [115.67-117.16]

The Rodgers and Rowland method for predicting partition coefficients and the Charge-dependent Schmitt method for calculating cellular permeability were selected based on visual model performance for curve shape.

Since metabolism of meropenem occurs through non-specific hydrolysis of β-lactam ring in plasma and renal metabolism via DHP-1, DHP-1 metabolism was assumed to be sole contributor.

The *in vitro* Michaelis-Menten constant (K_M) for DHP-1 was determined through the analysis by Shibayama *et.al.* [300] This value (2 mM) was fixed within the final model, while the maximum rate of metabolism (Vmax) was optimized.

The GFR fraction for a healthy individual was set to 1.0 allowing passive filtration to occur at the maximal filtration rate (GFR x f_u).

Active tubular secretion was parameterized by adding an OAT3 transporter on the basolateral side of the kidney cells and adding a generic transporter (TS) on the apical side of the kidney cells. Meropenem efflux via apical transport through kidney cells remains undefined, therefore assumptions were made in the final model building process. Farapenem, another carbapenem antibiotic, incorporates a similar renal clearance process as meropenem. It has been shown that farapenem is a substrate for the apical sodium-dependent phosphate transporter type 1, which is responsible for the efflux of farapenem from the renal tubule cells into the filtrate. [304] Hypotheses suggest that meropenem follows as similar efflux process. As such, the Michaelis-Menten constant for farapenem (770 μM) was utilized within the final model, while optimizing Vmax.

Transport by OAT3 was identified by optimizing against a drug-drug interaction (DDI) study measuring intravenous meropenem administered an hour after completion of an oral probenecid (strong OAT3 inhibitor) administration schedule. [297] The model for probenecid was downloaded from the Open Systems Pharmacology repository and can be found at: https://github.com/Open-Systems-Pharmacology/Probenecid-Model. It has been previously validated for predicting OAT1/3-mediated DDIs using furosemide as a model substrate. [292] Probenecid is a competitive inhibitor of OAT3 with an *in vitro* inhibition constant (K_I) of 5.41 μM. [292] In the competitive inhibition framework, the inhibitor binds reversibly and competes with substrate for free transporter. Inhibition constant (K_I) represents the dissociation constant for the transporter-inhibitor complex. In the DDI simulation of probenecid and meropenem, the apparent Michaelis-Menten constant for OAT3 transport ($K_{M,app}$) was calculated as:

$$K_{M,app} = K_M \times (1 + \frac{I}{K_I})$$

where I represents the concentration of the inhibitor, probenecid.

Multiple data sets were used within the IV model building process, containing data with meropenem administered alone and in combination with oral probenecid. Meropenem lipophilicity (logP), renal DHP-1 specific clearance, the maximum rate of OAT3 mediated transport and the maximum rate of apical transport were optimized using the parameter identification tool. The optimization was conducted using a Monte-Carlo approach to explore the parameter space. Upon completion of Monte-Carlo optimization, a Levenberg-Marquardt optimization strategy was conducted on ten randomized starting values to assess identifiability of a unique solution. There was minimal variability in optimized parameter values across the final

10 solutions as presented in Table 1, which suggests strong identifiability of a unique solution. A comparison of the fitted IV simulation to the observed data from Bax *et. al* [297] and Ljungberg *et.al* [587] is presented in Figure 1.

Table 2. Pharmacokinetic datasets of meropenem IV model construction

Reference	Ethnicity	Dose and Administration	N	Age (years)[a]	Weight (kg)[a]	Height (cm)[a]
Bax *et. al* [297]	White European Males	500 mg IV x 1 dose 1000 mg IV x 1 dose	6	26 [19-45]	74 [68-87]	179 [170-184]
Bax *et. al* [297]	White European Males	Probenacid PO 500 mg at 9AM, 6PM, 11PM the day before and 9AM the day of the study. Meropenem IV 1000 mg IV x 1 dose 1hr after probenecid protocol	6	26 [19-45]	74 [68-87]	179 [170-184]
Ljungberg *et. al* [587]	White European Males	500 mg IV x 1 dose	8	28.52 [20-34]	68.6	NR

[a]Data reported as mean [range], NR; not reported, IV; intravenous, PO; by mouth

1.2.3 Intravenous Model Verification

The optimized IV model was verified against additional data not used within the model building process (Table 3). The differences in patient demographics were incorporated within the IV model verification. As shown in Figure 2 and 3, the IV model provides a good representation of the pharmacokinetics of meropenem.

Table 3. Pharmacokinetic datasets for meropenem IV model verification

Reference	Ethnicity	Dose and Administration	N	Age (years)[a]	Weight (kg)[a]	Height (cm)[a]
Wise *et. al* [588]	White European Males	1000 mg IV x 1 dose	6	23.6 [23-31]	69.9 [63-80]	180 [169-187]
Kelly *et. al* [589]	White European Males	500 mg IV x 1 dose	5	28.8 [18-39]	82.1 [72.9-87.8]	177 [165-185]

[a]Data reported as mean [range]

1.2.4 Population Verification

A population PBPK simulation was performed to verify that the model can approximate both the mean and inter-individual variability in healthy individuals. Within this simulation, 1000 virtual individuals were generated, with each individual representing one full body parameter set for input within the PBPK model. The simulated profiles are presented in aggregate form with geometric mean and standard deviation to be compared against geometric mean and standard deviation measured within a pharmacokinetic study. The observed data from 16 individuals was extracted from Krueger *et.al* (Table 4). [590]

Table 4. Pharmacokinetic data set for meropenem IV model population verification

Reference	Ethnicity	Dose and Administration	N	Age (years)[a]	Weight (kg)[a]	Height (cm)[a]
Krueger *et.al* [590]	White European Males/Females	500 mg IV tid	8	21 [18-27]	67.1 [53-92]	NR
		1000 mg IV tid	8	24.4 [19-29]	66.1 [42.5-80.1]	

[a]Data reported as mean [range], NR; not reported

A virtual population of healthy adults (50% male, 50% female) was created within PK-Sim according to the demographics within Krueger *et.al.* [590] Inter-individual variability of the renal DHP-1 enzyme reference concentration was assigned to the rough average of metabolic enzymes within the PK-Sim database (lognormal distribution, 20% coefficient of variation). A log normal distribution with a geometric standard deviation of 1.53 was applied to OAT3 reference concentration. [303] Due to the lack of information describing the apical transport of meropenem, reference concentration of the generic transporter was assumed to have moderate variability of 35% coefficient of variation. Similar assumptions were applied to unknown parameters in previous published PBPK models of OAT3 substrates. [292]

Table 5.1. Demographic parameters for the virtual population receiving meropenem IV 1000 mg

Parameter	Value	
Population	European (ICRP)	
Number of Males		100
Number of Females		100
	Minimum	**Maximum**
Age	19 years	29 years
Weight	42.50 kg	80.10 kg

Table 5.2. Demographic parameters for the virtual population receiving meropenem IV 500 mg

Parameter	Value	
Population	European (ICRP)	
Number of Males		100
Number of Females		100
	Minimum	**Maximum**
Age	18 years	27 years
Weight	53 kg	92 kg

Figures 4 & 5 illustrate the population PBPK simulations for the final IV meropenem model after administration of 500 mg and 1000 mg doses. Visual inspections reveal that each model slightly underpredicts variability in volume of distribution and over-estimates variability clearance within the terminal phase.

1.3 Discussion and Conclusion

The final meropenem PBPK model adequately describes the pharmacokinetics of meropenem in a virtual population of healthy adults. The healthy model will be scaled to predict the pharmacokinetics in patients with renal impairment.

1.4 Figures

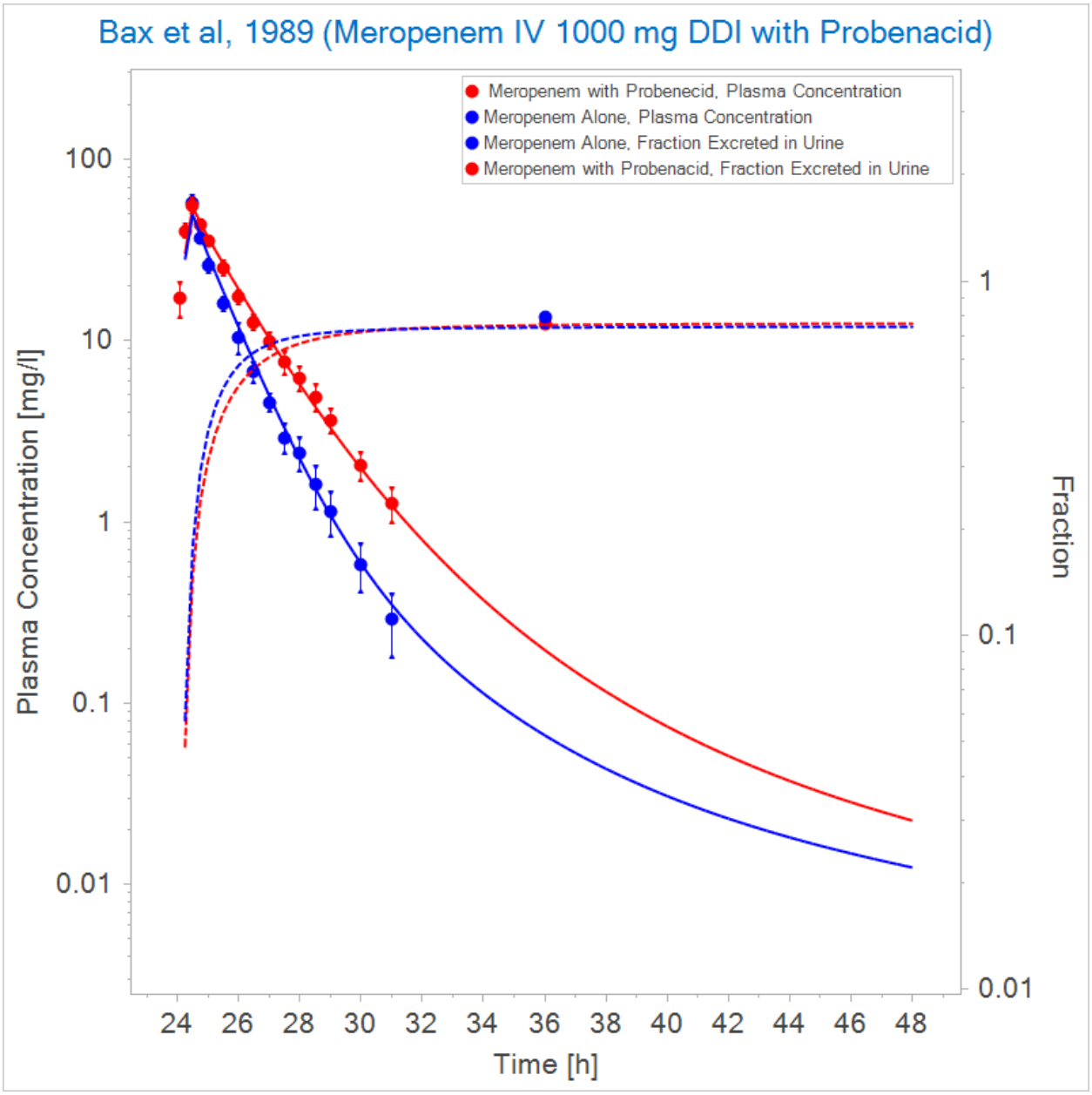


Figure 1. Simulation after optimization. Observed data reported as mean (circles) with standard error of the mean (error bars) from the study conducted by Bax *et.al*. [297] The solid blue line represents the simulated plasma concentration of meropenem 1000 mg administered by IV infusion over 30-minutes. The red line represents the simulated plasma concentration of the same dose of meropenem when administered 1-hour after completion of the probenecid administration protocol. Dashed lines represent the fraction of the IV dose excreted to urine respectively.

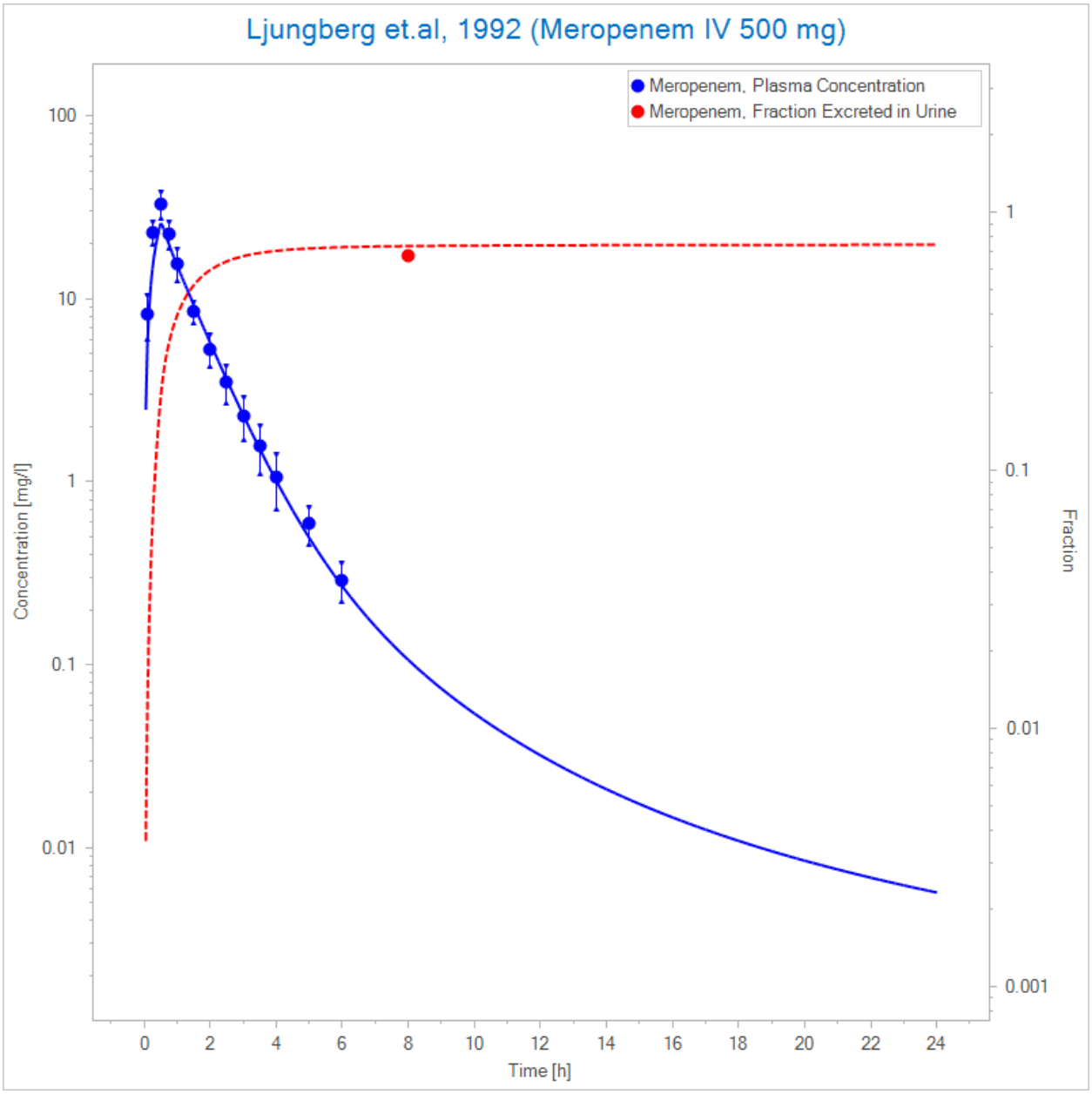


Figure 2. Simulation after optimization. Observed data reported as mean (circles) with standard error of the mean (error bars) from the study conducted by Ljunberg *et.al*. [587] The solid red line represents the simulated plasma concentration of meropenem 500 mg administered by IV infusion over 30-minutes. Dashed lines represent the fraction of the IV dose excreted to urine.

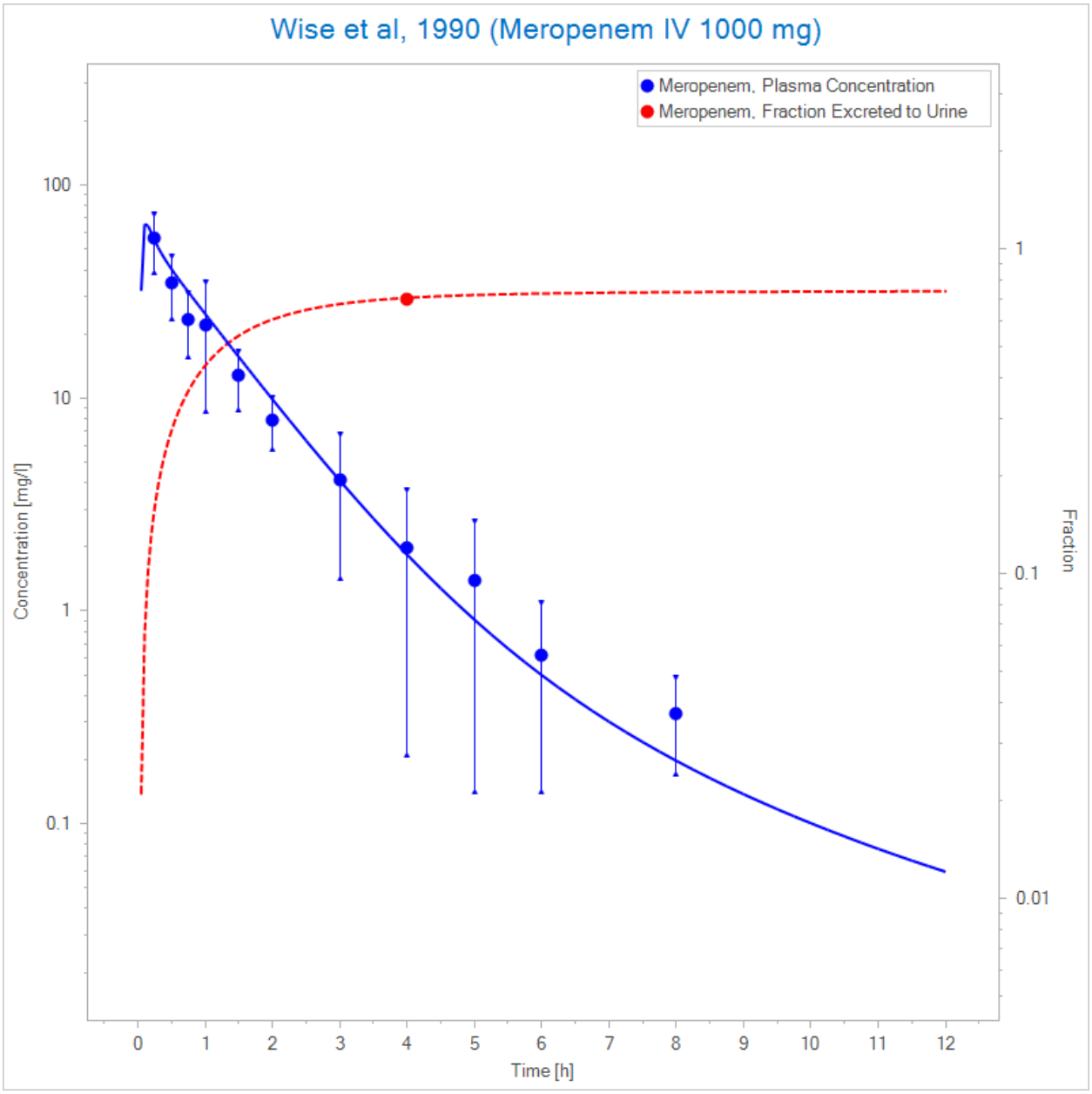


Figure 3. Simulation for independent verification of optimized model. Observed data reported as mean (circles) with standard error of the mean (error bars) from the study conducted by Wise *et.al*. [588] The solid red line represents the simulated plasma concentration of meropenem 500 mg administered by IV infusion over 5-minutes. Dashed lines represent the fraction of the IV dose excreted to urine.

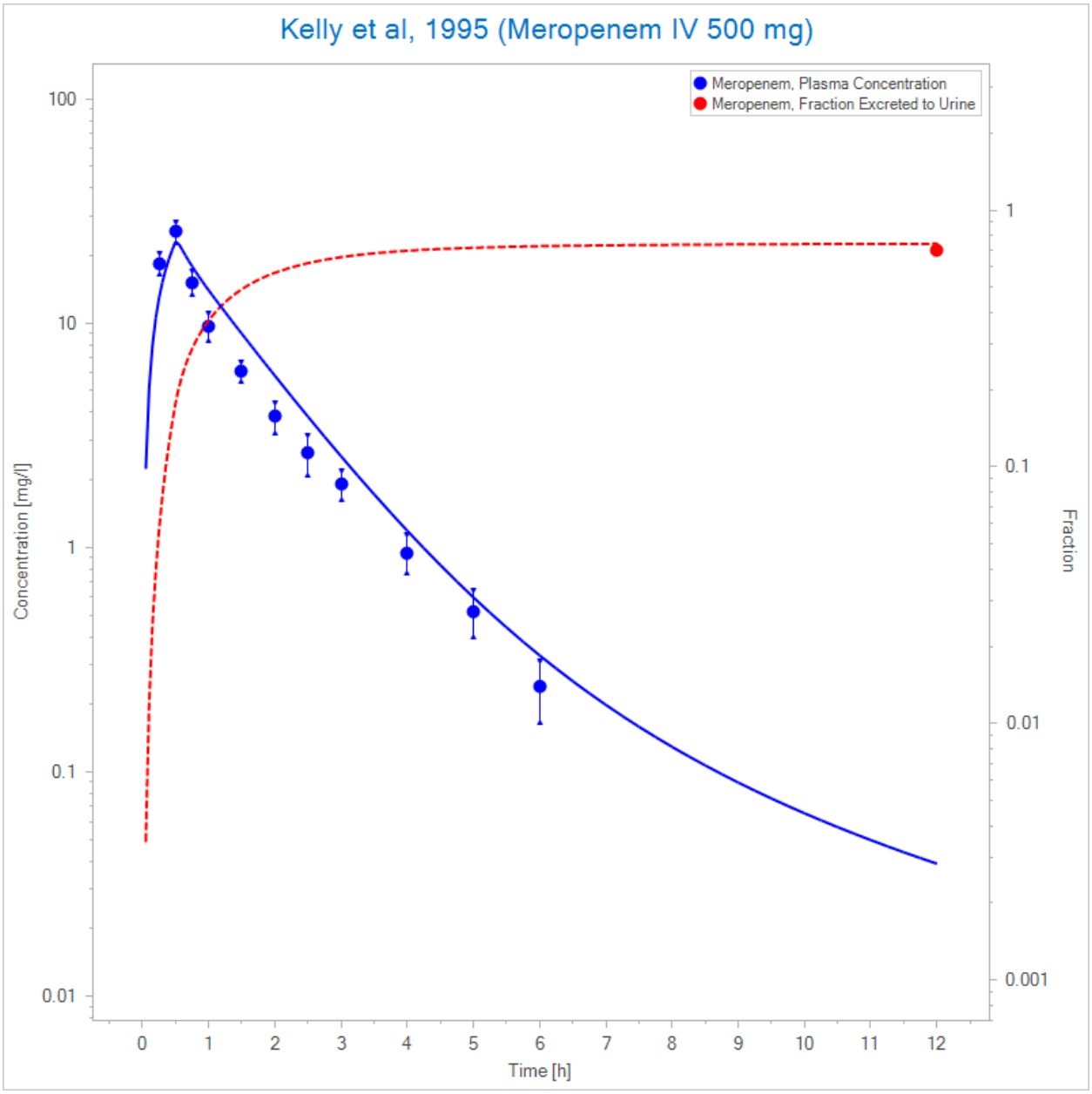


Figure 4. Simulation for independent verification of optimized model. Observed data reported as mean (circles) with standard error of the mean (error bars) from the study conducted by Kelly *et.al*. [589] The solid red line represents the simulated plasma concentration of meropenem 500 mg administered by IV infusion over 30-minutes. Dashed lines represent the fraction of the IV dose excreted to urine.

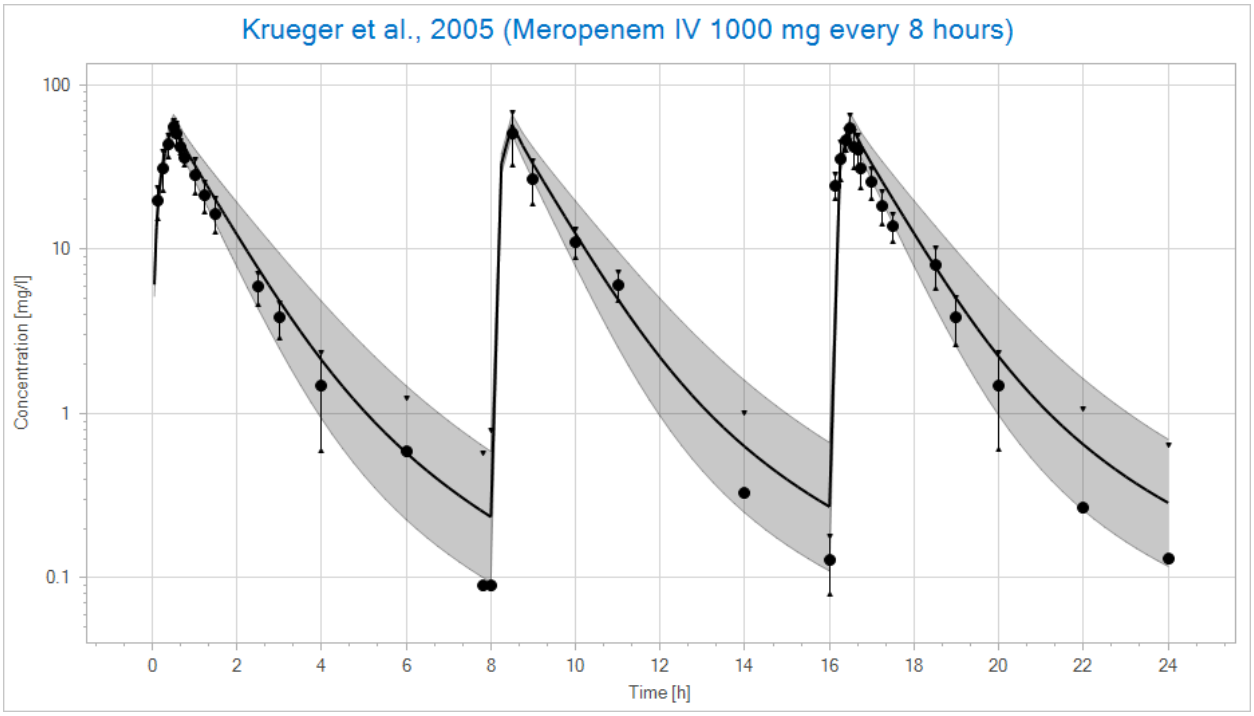


Figure 5. Population verification against the observed meropenem concentrations from individuals in the study by Krueger *et.al* [590] The solid line represents the simulated geometric mean and the shaded region represents the simulated geometric standard deviation of the virtual population. The observed data is presented as mean (circles) with arithmetic standard deviation (error bars).

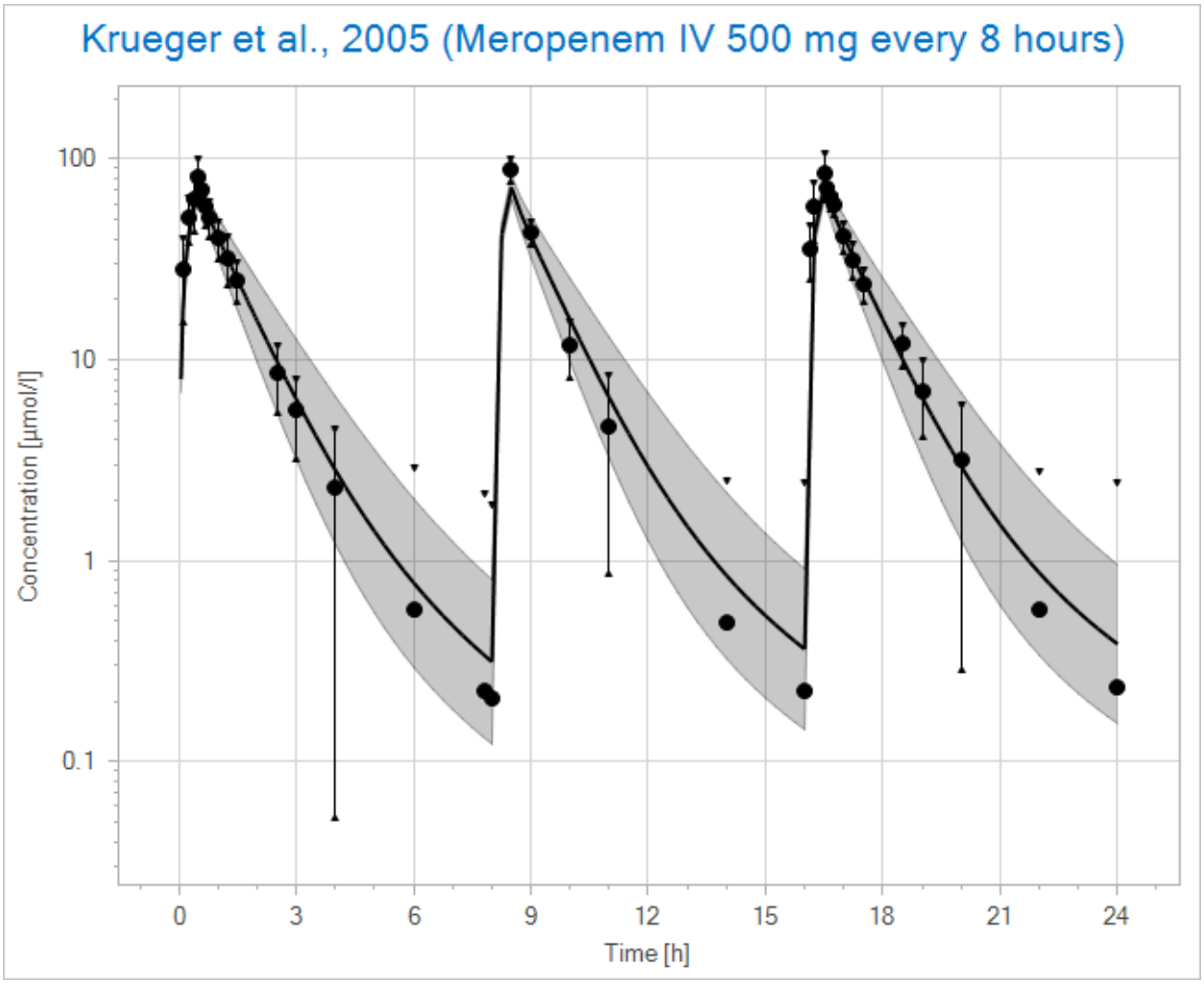


Figure 6. Population verification against the observed meropenem concentrations from individuals in the study by Krueger *et.al* [590] The solid line represents the simulated geometric mean and the shaded region represents the simulated geometric standard deviation of the virtual population. The observed data is presented as mean (circles) with arithmetic standard deviation (error bars).

2. Building a Physiologically-Based Pharmacokinetic Model for Acyclovir in Healthy Adults

2.1 Introduction

Acyclovir is a synthetic nucleoside analogue that is used as an antiviral medication. After intravenous administration, plasma concentrations of acyclovir decline in a biphasic manner. [294] The compound has low cellular permeability and low water solubility. Acyclovir is about 15% bound to plasma proteins. [591] The plasma half-life of acyclovir is 2 – 3.5 hours in healthy adults. [294,327] Most of the drug is excreted unchanged in the urine (62 – 91%). [298] Renal tubular secretion dominates, as renal clearance far exceeds the glomerular filtration rate. Organic anion transporters (OAT3) are responsible for uptake into renal tubular epithelium and MATE transporters are responsible for efflux into tubular filtrate. [301] The remainder of circulating acyclovir undergoes non-saturable metabolism with possible contributions from aldehyde dehydrogenase 2, presumed to occur in the liver. [591,592] One metabolite has been identified in urine, noted as CMMG, which accounts for 8.5 – 14.1% of an intravenous dose. [591] Less than 2% of an intravenous dose is excreted in feces as unchanged drug or metabolites. [298]

In this report, the building and verification of a PBPK model for intravenous acyclovir in healthy adults is presented. A recent PBPK model for acyclovir was released by Liu et al. with a slightly different interpretation of the data, which deserves reading. [592]

2.2 Methods and Results

2.2.1 Modelling Strategy

PBPK modelling and simulation were performed using PK-Sim version 9.1. Fifteen organs and two blood organs (= 17 compartments) were included in the standard model to represent a virtual adult.

2.2.2 Intravenous Model Construction

The process for creating the PBPK model for a healthy adult is described here. **Table 1** presents the drug-specific parameters of acyclovir and the values used for the naïve model.

Table 1. Physicochemical properties and ADME of acyclovir for IV model construction

	Used in naïve model	Used in optimized model [range of optimized values]
Physicochemical properties		
Octanol:water coefficient (logP)	-1.57 Log Units [294]	**-0.69 Log Units** [-0.69 – -0.69]
Fraction unbound in plasma (f_u)	0.85 [294]	0.85
Molecular weight (MW)	225.21 g/mol [294]	225.21
pKa (acid)	9.25 [294]	9.25
pKa (base)	2.27 [294]	2.27
Water solubility	2.5 mg/mL [294]	2.5 mg/mL
ADME		
Partition coefficient	Rodgers and Rowland	Rodgers and Rowland
Cell permeability	Charge-dependent Schmitt	Charge-dependent Schmitt
CMMG enzyme concentration	1.0 µM (fixed)	1.0 µM
CMMG specific clearance	0 L/min/µmol	**0.031 L/min/µmol** [0.031 – 0.031]
GFR fraction	1.0	1.0
OAT3 concentration	0.0917 µM [292]	0.0917 µM
OAT3 K_M	342.3 µM [299]	342.3 µM
OAT3 Vmax	0 mM/min	**25.75 mM/min** [25.70 – 26.19]
MATE concentration	1 µM (fixed)	1 µM
MATE K_M	3480 µM [299]	3480 µM
MATE Vmax	0 mM/min	**0.99 mM/min** [0.98 – 0.99]

The Rodgers and Rowland method for predicting partition coefficients and the Charge-dependent Schmitt method for calculating cellular permeability were selected based on visual model performance for curve shape.

First order metabolism was assumed to occur in the liver and was accomplished by adding a dummy enzyme termed ‘CMMG’ (after the major metabolite) in the intracellular space. The reference concentration was fixed to 1 µM and the specific clearance (L/min/µmol) was optimized using the parameter identification tool.

The GFR fraction for a healthy individual was set to 1.0 allowing passive filtration to occur at the maximal filtration rate (GFR x f_u).

Active tubular secretion was parameterized by adding an OAT3 transporter on the basolateral side of the kidney cells and adding a generic MATE transporter (representing MATE1, MATE2 and MATE2-K) on the apical side of the kidney cells. The *in vitro* Michaelis-Menten constants

(K_M) were available for both transporters from a review by Momper et al. [299] The maximum rates of transport for each transporter (Vmax) were optimized.

Transport by OAT3 was identified by optimizing against a drug-drug interaction (DDI) study measuring intravenous acyclovir administered an hour after 1 gram of oral probenecid, a potent OAT3 inhibitor. The model for probenecid was downloaded from the Open Systems Pharmacology repository and can be found at: https://github.com/Open-Systems-Pharmacology/Probenecid-Model. It has been previously validated for predicting OAT1/3-mediated DDIs using furosemide as a model substrate. [292] Probenecid is a competitive inhibitor of OAT3 with an *in vitro* inhibition constant (K_I) of 5.41 μM. [292] In the competitive inhibition framework, the inhibitor binds reversibly and competes with substrate for free transporter. Inhibition constant (K_I) represents the dissociation constant for the transporter-inhibitor complex. In the DDI simulation of probenecid and acyclovir, the apparent Michaelis-Menten constant for OAT3 transport ($K_{M,app}$) was calculated as:

$$K_{M,app} = K_M \times (1 + \frac{I}{K_I})$$

where I represents the concentration of the inhibitor, probenecid.

Table 2 presents the acyclovir datasets used for building the IV model, both alone and in combination with oral probenecid. The lipophilicity (logP), specific clearance of CMMG, the maximum rate of OAT3-mediated transport and the maximum rate of MATE-mediated transport were optimized using the parameter identification tool in PK-Sim. The optimization was carried out using a Levenberg-Marquardt approach for exploring the parameter space. Ten optimizations were run from randomized start values to assess identifiability of a unique solution. All ten runs converged to a unique solution. The run with the lowest error was selected as the final solution, and those values are presented in **Table 1**. The range of parameter values among the solutions is also reported to assess error, which was minimal. A comparison of the fitted IV simulation to the observed data from Laskin et al. is presented in **Figure 1**. [327]

Table 2. Pharmacokinetic datasets for acyclovir IV model construction

Study	Dose and administration	Cohort	N	Age (years)[a]	Weight (kg)[a]
Laskin et al. [327]	500 mg IV infusion over 60 min	Patients with malignancy and GFR ~90 mL/min/1.73m^2	3	47.3 [24 – 67]	79.1 [68 – 100]
Laskin et al. [327]	500 mg IV infusion over 60 min administered 1 h after probenecid 1 g by mouth	Patients with malignancy and GFR ~89 mL/min/1.73m^2	3	47.3 [24 – 67]	79.1 [68 – 100]

[a]Data reported as mean [range]

2.2.3 Intravenous Model Verification

The optimized IV model was verified against additional data not used in the model building process (**Table 3**). This data from another study by Laskin et al. was significantly heterogeneous from the model building datasets as it featured a dose escalation. [593] These subjects were more senior and had modestly lower renal function, which was accounted for by adjusting the GFR in the virtual individuals used for the simulation. **Figure 2** shows a good fit for describing the pharmacokinetics of acyclovir over increasing doses in these subjects.

Table 3. Pharmacokinetic datasets for acyclovir IV model verification

Study	Dose and administration	Cohort	N	Age (years)[a]	Weight (kg)[a]
Laskin et al. [593]	2.5 mg/kg IV infusion over 60 min	Patients with malignancy and GFR ~55.6 mL/min/1.73m^2	3	69 ± 10	86.2 ± 32.1
Laskin et al. [593]	5 mg/kg IV infusion over 60 min	Patients with malignancy and GFR ~56.9 mL/min/1.73m^2	3	64 ± 7	73.3 ± 16.5
Laskin et al. [593]	10 mg/kg IV infusion over 60 min	Patients with malignancy and GFR ~67.6 mL/min/1.73m^2	4	66 ± 9	63.7 ± 18.5
Laskin et al. [593]	15 mg/kg IV infusion over 60 min	Patients with malignancy and GFR ~114.1 mL/min/1.73m^2	3	40 ± 14	65.2 ± 3.8

[a]Data reported as mean ± SD

2.2.4 Population Verification

A population PBPK simulation was performed to verify that the model can approximate both the mean and the inter-individual variability in healthy individuals. In this workflow, 100 virtual individuals are generated, and each individual represents one full body parameter set for iterative input into the PBPK model. The resulting simulated profiles are presented in aggregate form with arithmetic mean and standard deviation to be compared against the arithmetic mean and standard deviation measured in a clinical trial. The observed data from 24 individuals was extracted from Vergin et al. (**Table 4**). [594]

Table 4. Pharmacokinetic dataset for acyclovir IV model population verification

Study	Dose and administration	Cohort	N	Age (years)[a]	Weight (kg)[a]
Vergin et al. [594]	250 mg IV infusion over 10 min	Healthy Male Volunteers	24	NR	NR

[a]Data reported as mean [range], NR = not reported

A virtual population of 100 healthy adults was created in PK-Sim to represent the study population from the dataset by Vergin et al. (**Table 5**). [289,594] Inter-individual variability in the 'CMMG' enzyme reference concentration was assigned to the rough average of metabolic enzymes in the PK-Sim database (lognormal distribution, 20% coefficient of variation). A log normal distribution with a geometric standard deviation of 1.53 was applied to OAT3 reference concentration. [303] Similarly the inter-individual variability in MATE reference concentration also extracted from the proteomic data by Cheung et al. (lognormal distribution, geometric SD, 1.48). [595,596]

Table 5. Demographic parameters for the virtual population

Parameter	Value	
Population	European (ICRP)	
Number of Males	100	
Number of Females	0	
	Minimum	**Maximum**
Age	18 years	45 years
BMI	18 $kg \cdot m^2$	30 $kg \cdot m^2$

Figure 3 presents the simulated concentration-time profiles for the population as compared to the observed concentrations across 24 subjects from the study by Vergin et al. [594] Visual inspection reveals that variability is under-estimated in the first hour after administration and over-estimated in the terminal phase.

2.3 Discussion and Conclusion

The final acyclovir PBPK model adequately describes the pharmacokinetics of acyclovir in virtual populations of healthy adults. The healthy model will be extrapolated to predict pharmacokinetics in patients with renal impairment.

2.4 Figures

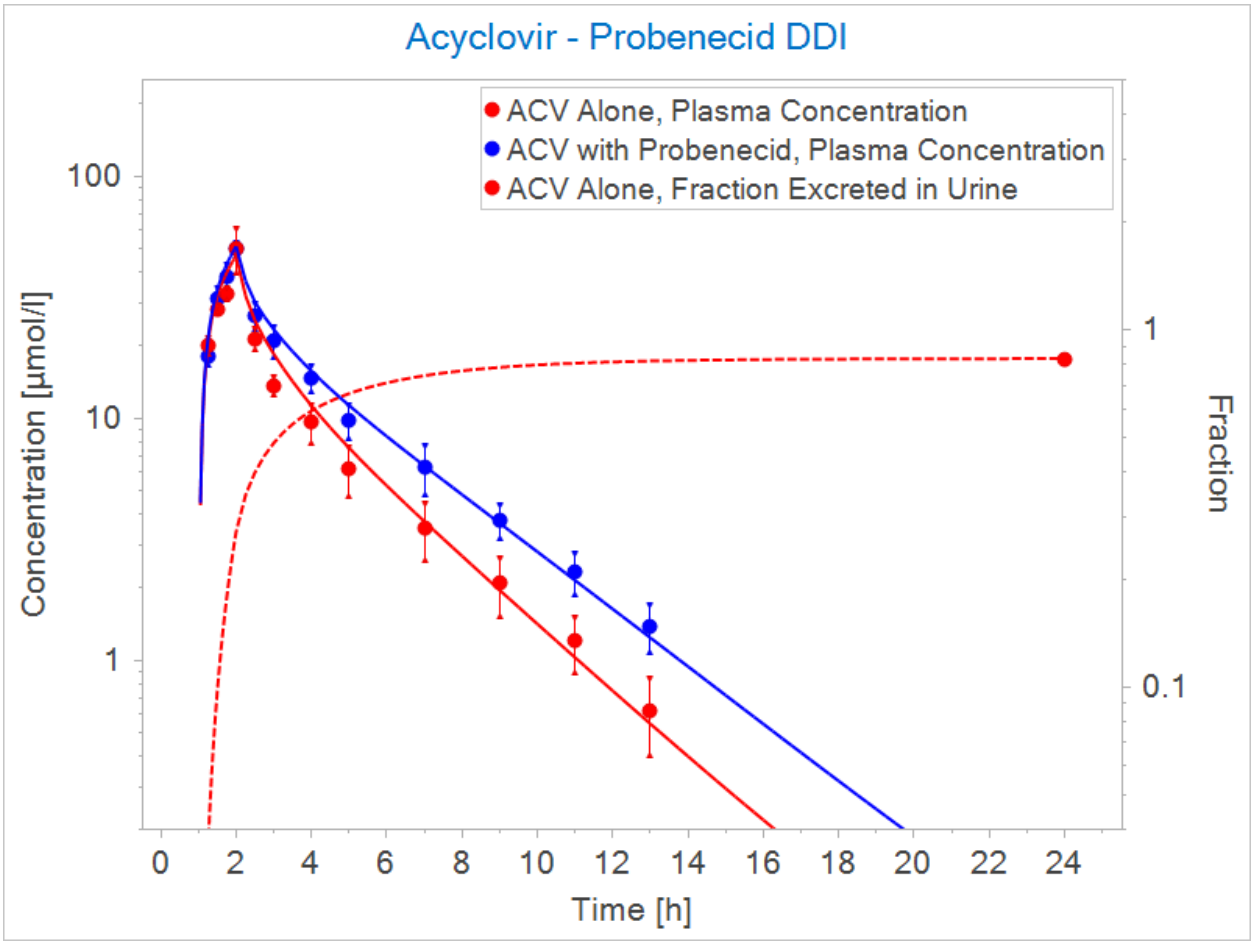


Figure 1. Simulation after optimization. Observed data reported as mean (circles) with standard error of the mean (error bars) from the study by Laskin et al. [327] The solid red line represents the simulated plasma concentration of acyclovir 500 mg administered by IV infusion over 60 minutes. The blue line represents the simulated plasma concentration of the same dose of acyclovir when administered 1 hour after probenecid 1 g PO. The dashed red line represents the simulated fraction of the IV dose excreted unchanged in urine (associate with the right axis).

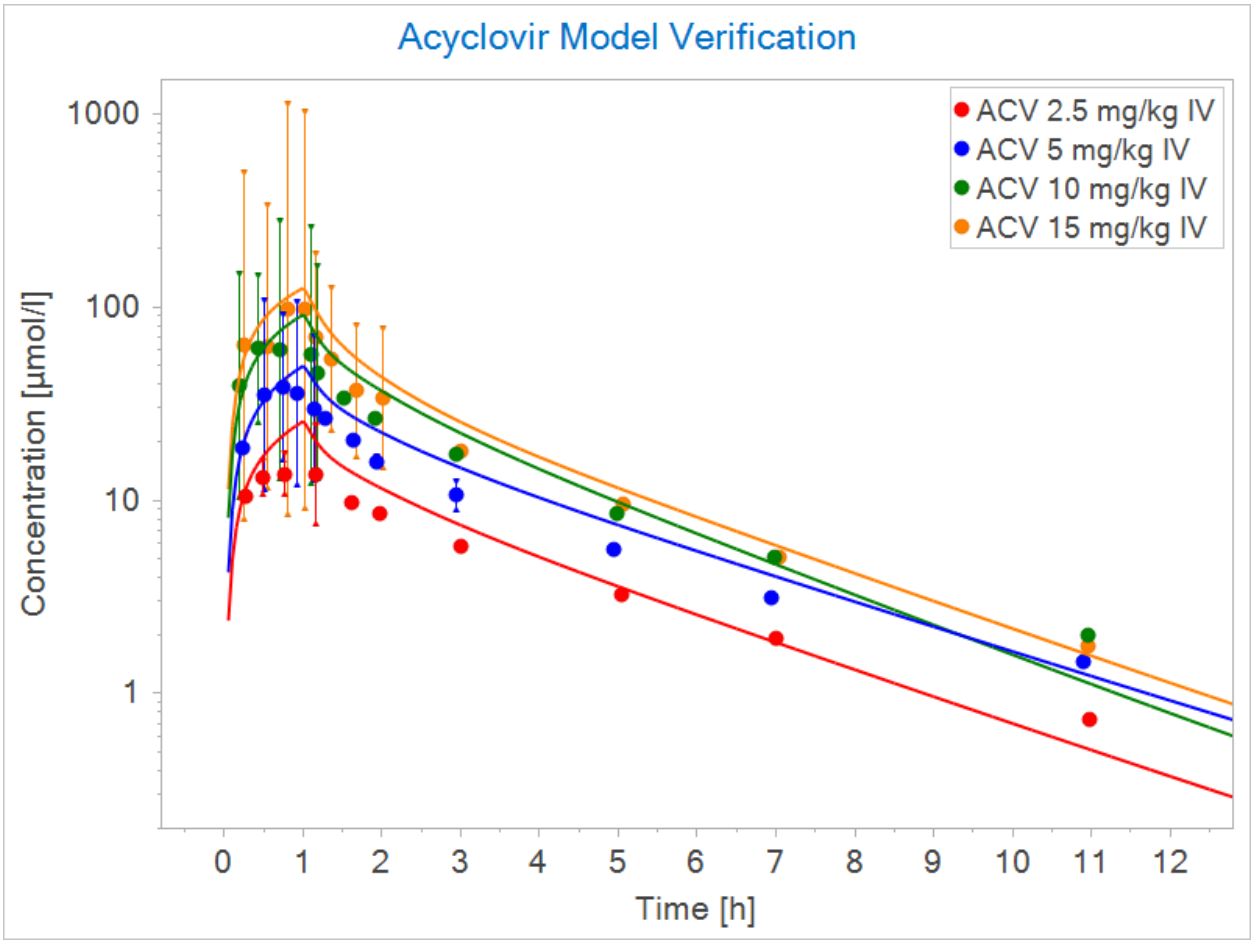


Figure 2. Simulation for independent verification of the optimized IV model. Observed data reported as mean (circles) with standard deviation (error bars) from the study by Laskin et al. [593] The solid coloured lines represent the simulated plasma concentration at increasing doses from 2.5 mg/kg IV to 15 mg/kg IV by infusion over 60 min.

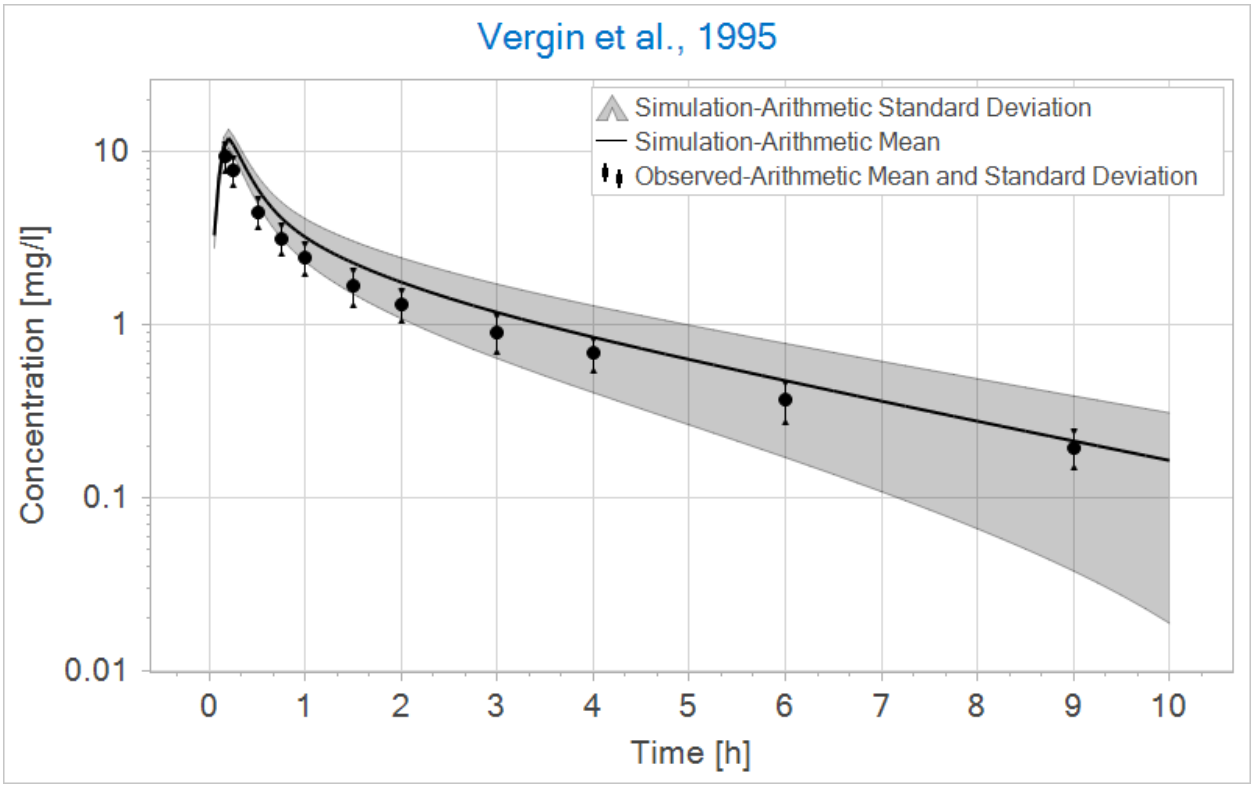


Figure 3. Population verification against the observed acyclovir concentrations from individuals in the study by Vergin et al. [594] The solid line represents the simulated arithmetic mean and the shaded region represents the simulated arithmetic standard deviation of the virtual population. The observed data is presented as mean (circles) with arithmetic standard deviation (error bars).

3. Building a Physiologically-Based Pharmacokinetic Model for Ciprofloxacin in Healthy Adults

3.1 Introduction

Ciprofloxacin is a widely used fluoroquinolone antibiotic. The compound is classified as a borderline BCS II/IV drug with moderate cellular permeability and low water solubility. The drug achieves some penetration into peripheral tissues. After intravenous administration, plasma concentrations decline in a biphasic manner. Ciprofloxacin is 60 – 80% unbound in plasma. The plasma half-life is 4 – 6 hours in healthy adults. Most of the drug is excreted unchanged in the urine (up to 70%). Net tubular secretion dominates since renal clearance exceeds the glomerular filtration rate. Organic anion transporters (OAT3) are responsible for uptake into renal tubular epithelium. An unknown combination of MATE-1, P-gp and BCRP transporters are likely responsible for efflux into tubular filtrate from the apical side of the tubular epithelium. Metabolism by CYP1A2 contributes to approximately 20% of total clearance. After intravenous administration, 12% of a ciprofloxacin dose can be recovered unchanged in feces, suggesting an important role of biliary excretion by presumably P-gp or BCRP transporters.

In this report, the building and verification of a PBPK model for intravenous ciprofloxacin in healthy adults is presented. Much of the work is based on a previous PBPK model for ciprofloxacin by Schlender et al. in 2018. [291]

3.2 Methods and Results

3.2.1 Modelling Strategy

PBPK modelling and simulation were performed using PK-Sim version 9.1. Fifteen organs and two blood organs (= 17 compartments) were included in the standard model to represent a virtual adult.

3.2.2 Intravenous Model Construction

The process for creating the PBPK model for a healthy adult is described here. **Table 1** presents the drug-specific parameters of ciprofloxacin and the values used for the naïve model.

Table 1. Physicochemical properties and ADME of ciprofloxacin for IV model construction

	Used in naïve model	Used in optimized model [range of optimized values]
Physicochemical properties		
Octanol:water coefficient (logP)	0.95 Log Units [291]	0.95 Log Units
Fraction unbound in plasma (f_u)	0.67 [291]	0.67
Molecular weight (MW)	331.30 g/mol [291]	331.30 g/mol
pKa (acid)	6.09 [291]	6.09
pKa (base)	8.62 [291]	8.62
Water solubility	38.4 mg/mL [291]	38.4 mg/mL
ADME		
Partition coefficient	PK-Sim Standard [291]	PK-Sim Standard
Cell permeability	PK-Sim Standard [291]	PK-Sim Standard
CYP1A2 enzyme concentration	1.8 µM	1.8 µM
CYP1A2 specific clearance	0 L/min/µmol	**0.027 L/min/µmol** [0.027 – 0.027]
GFR fraction	1.0	1.0
OAT3 concentration	0.0917 µM [292]	0.0917 µM
OAT3 K_M	70 µM [299]	70 µM
OAT3 Vmax	0 M/min	**5.96 M/min** [5.60 – 6.30]
APICAL concentration	1 µM (fixed)	1 µM
APICAL K_M	1000 µM	1000 µM
APICAL Vmax	0 µM/min	**58.39 µM/min** [55.45 – 61.62]
BILE concentration	1 µM (fixed)	1 µM
BILE K_M	1000 µM	1000 µM
BILE Vmax	0 µM/min	**49.61 µM/min** [49.16 – 50.00]

Each individual was set to express intracellular CYP1A2 in liver and minimally in gonads, kidney and lungs according to the RT-PCR data from the PK-Sim Gene Expression Database. A first order rate of metabolism was estimated using the parameter identification tool.

The GFR fraction for a healthy individual was set to 1.0 allowing passive filtration to occur at the maximal filtration rate (GFR x f_u).

Active tubular secretion was parameterized by adding an OAT3 transporter on the basolateral side of the kidney cells and adding a generic APICAL transporter (representing MATE1, P-gp and BCRP) on the apical side of the kidney cells. The *in vitro* Michaelis-Menten constant (K_M) was available for OAT3 from a review by Momper et al. [299] The Michaelis-Menten constant for the generic APICAL transporter (K_M) was fixed to a high value of 1000 µM to enable first

order secretion in the absence of any other data. The maximum rates of transport for each transporter (Vmax) were optimized.

Transport by OAT3 was identified by optimizing against a drug-drug interaction (DDI) study measuring intravenous ciprofloxacin administered with and without multiple oral administration of probenecid, a potent OAT3 inhibitor. The model for probenecid was downloaded from the Open Systems Pharmacology repository and can be found at: https://github.com/Open-Systems-Pharmacology/Probenecid-Model. It has been previously validated for predicting OAT1/3-mediated DDIs using furosemide as a model substrate. [292] Probenecid is a competitive inhibitor of OAT3 with an *in vitro* inhibition constant (K_I) of 5.41 μM. [292] In the competitive inhibition framework, the inhibitor binds reversibly and competes with substrate for free transporter. Inhibition constant (K_I) represents the dissociation constant for the transporter-inhibitor complex. In the DDI simulation of probenecid and ciprofloxacin, the apparent Michaelis-Menten constant for OAT3 transport ($K_{M,app}$) was calculated as:

$$K_{M,app} = K_M \times (1 + \frac{I}{K_I})$$

where I represents the concentration of the inhibitor, probenecid.

Biliary excretion of unchanged ciprofloxacin into feces was accomplished by adding a generic BILE transporter on the apical side of the liver cells. This generic transporter represents the effects of P-gp and/or BCRP. In the same way as for the generic renal transporter, the Michaelis-Menten constant for the generic BILE transporter (K_M) was fixed to a high value of 1000 μM to enable first order secretion and the maximum rate of transport (Vmax) was optimized. Enterohepatic recirculation was assumed not to occur.

Table 2 presents the ciprofloxacin datasets used for building the IV model, both alone and in combination with oral probenecid. Distribution related parameter were fixed based on the work done by Schlender et al. [291] The CYP1A2 specific clearance, the maximum rate of OAT3-mediated transport, the maximum rate of renal APICAL transport and the maximum rate of BILE transport were optimized using the parameter identification tool in PK-Sim. The optimization was carried out using a Levenberg-Marquardt approach for exploring the parameter space. Ten optimizations were run from randomized start values to assess identifiability of a unique solution. All ten runs converged to a unique solution. The run with the lowest error was selected as the final solution, and those values are presented in **Table 1**. The range of parameter values among the solutions is also reported to assess error, which was minimal. A comparison of the fitted IV simulation to the observed data from Jaehde et al. is presented in **Figure 1**. [296]

Table 2. Pharmacokinetic datasets for ciprofloxacin IV model construction

Study	Dose and administration	Cohort	N	Age (years)[a]	Weight (kg)[a]
Jaehde et al. [296]	200 mg IV infusion over 30 min	Healthy male and female subjects	12	29.3 ± 5.7 [21 – 38]	67.1 ± 11.6
Jaehde et al. [296]	200 mg IV infusion over 30 min with multiple oral administration of probenecid	Healthy male and female subjects	12	29.3 ± 5.7 [21 – 38]	67.1 ± 11.6

[a]Data reported as mean ± SD [range]

3.2.3 Intravenous Model Verification

The optimized IV model was verified against additional data not used in the model building process (**Table 3**). This data from Shah et al. was significantly heterogeneous from the model building datasets as it featured multiple dose administration of ciprofloxacin at 400 mg. [330] **Figure 2** shows a good fit for describing the pharmacokinetics of ciprofloxacin after multiple dose administration.

Table 3. Pharmacokinetic dataset for ciprofloxacin IV model verification

Study	Dose and administration	Cohort	N	Age (years)[a]	Weight (kg)[a]
Shah et al. [330]	400 mg IV infusion over 60 min every 8 hours	Healthy males with normal renal function (GFR > 90 mL/min/1.73m^2)	10	39.1 [32 – 46]	87 [65 – 99]

[a]Data reported as mean [range]

3.2.4 Population Verification

A population PBPK simulation was performed to verify that the model can approximate both the mean and the inter-individual variability in healthy individuals. In this workflow, 100 virtual individuals are generated, and each individual represents one full body parameter set for iterative input into the PBPK model. The resulting simulated profiles are presented in aggregate form with geometric mean and 5th – 95th prediction interval to be compared against the spread of individual concentration-time data measured in a clinical trial. The observed data from six individuals was extracted from Wise et al. (**Table 4**). [597]

Table 4. Pharmacokinetic dataset for ciprofloxacin IV model population verification

Study	Dose and administration	Cohort	N	Age (years)[a]	Weight (kg)[a]
Wise et al. [597]	100 mg IV injection	Healthy male subjects	6	29.2 [23 – 42]	78.5 [65 – 85]

[a]Data reported as mean [range]

A virtual population of 100 healthy adults was created in PK-Sim to represent the study population from the dataset by Wise et al. (**Table 5**). [289,597] Inter-individual variability in CYP1A2 is defined by default in PK-Sim ('Ontogeny/Variability like CYP1A2'). Inter-individual variability in OAT3 reference concentration was extracted from transporter proteomic data by Basit et al. (normal distribution, 20% coefficient of variation). [312] The APICAL and BILE transporters were assumed to follow the inter-individual variability of P-gp/MDR1, also extracted from the data by Basit et al. (normal distribution, 20% coefficient of variation). [312]

Table 5. Demographic parameters for the virtual population

Parameter	Value	
Population	European (ICRP)	
Number of Males	100	
Number of Females	0	
	Minimum	**Maximum**
Age	23 years	42 years
Height	169 cm	186 cm
Weight	65 kg	85 kg

Figure 3 presents the simulated concentration-time profiles for the population as compared to the observed concentration for six individuals from the study by Wise et al. [597] Visual inspection reveals that variability is under-estimated in the first hour after administration, but well-captured thereafter.

3.3 Discussion and Conclusion

The final ciprofloxacin PBPK model adequately describes the pharmacokinetics of ciprofloxacin in virtual populations of healthy adults receiving single and multiple intravenous doses by injection or infusion. The healthy model will be extrapolated to predict pharmacokinetics in patients with renal impairment.

3.4 Figures

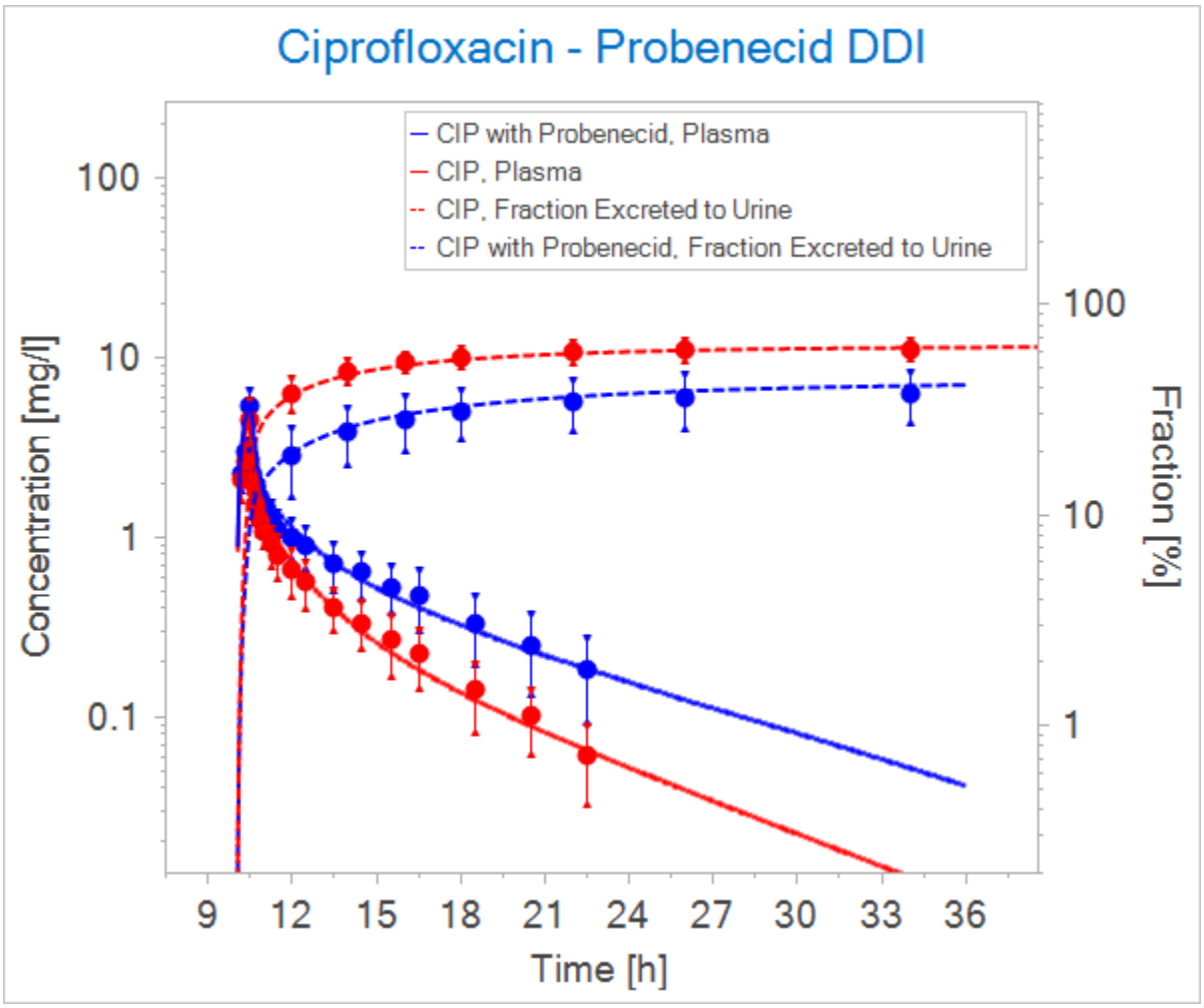


Figure 1. Simulation after optimization. Observed data reported as mean (circles) with standard deviation (error bars). The solid red line represents the simulated plasma concentration of ciprofloxacin 200 mg administered by IV infusion over 30 minutes. The solid blue line represents the simulated plasma concentration of the same dose of ciprofloxacin when given together with multiple oral administration of probenecid. The dashed lines represent the simulated fraction of the IV dose excreted unchanged in urine (associate with the right axis).

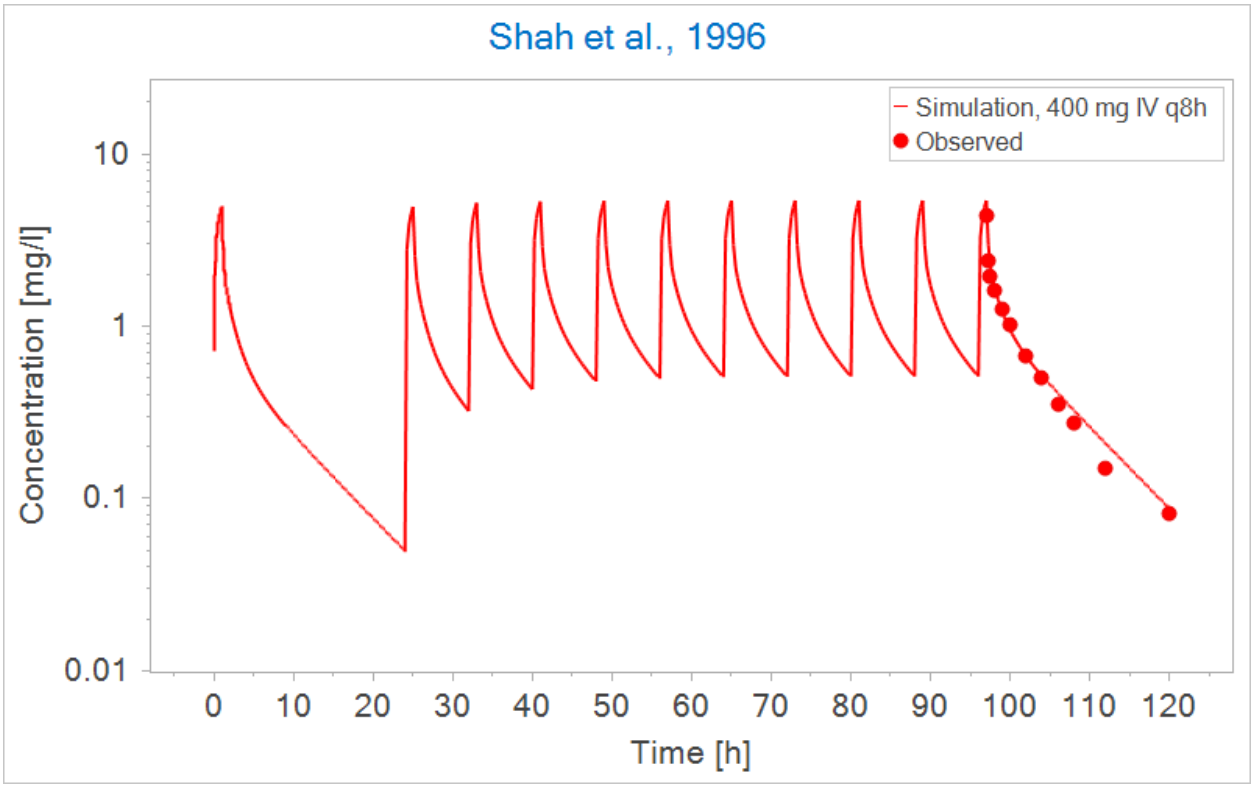


Figure 2. Simulation for independent verification of the optimized IV model. Observed data reported as mean (circles). The solid red line represents the simulated plasma concentration after multiple dose administration of ciprofloxacin 400 mg IV.

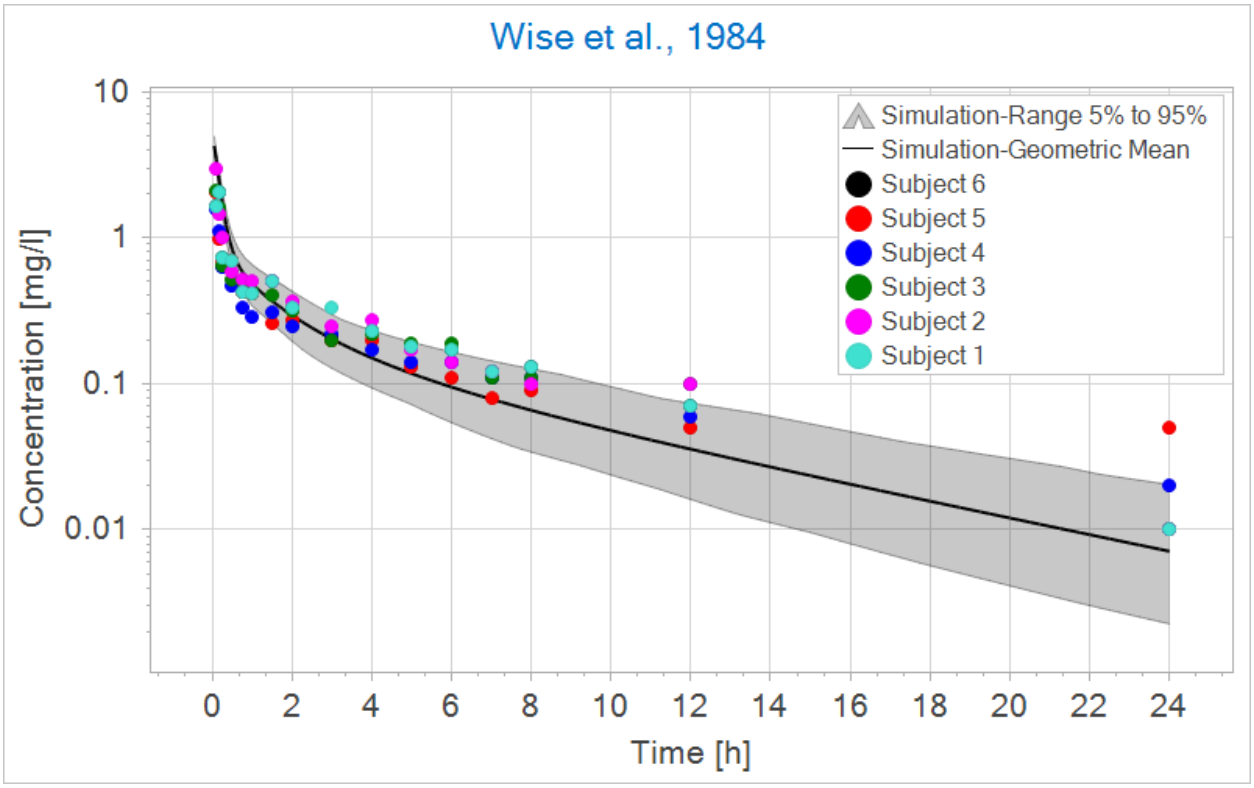


Figure 3. Population verification against the observed ciprofloxacin concentrations from individuals in the study by Wise et al. [597] The solid line represents the simulated geometric mean and the shaded region represents the simulated 5th and 95th percentile range of the virtual population. The observed data from individuals is presented as coloured circles.

4. Clinical Studies Incorporated in the CKD-PBPK Model Validation

4.1 Ciprofloxacin

Table 1. Ciprofloxacin pharmacokinetic studies in CKD used for CKD-PBPK model validation.

Study	Dose	Route	N	Age (y) [range]	Weight (kg) [range]	Female [%]	GFR (mL/min) [range]	Ethnicity
Drusano *et al.* [329]	200 mg	IV	11	43.6 [24-62]	75.9 [51.3-97.7]	9	39.84 [13.33-56.67]	NR
Drusano *et al.* [329]	200 mg	IV	8	45.5 [33-55]	68.9 [59.6-85.5]	0	IHD	NR
Shah *et al.* [330]	400 mg every 12 hours	IV	11	63 [32-64]	81.1 [61-119]	55	44.8 [31.3-59.9]	NR
Shah *et al.* [330]	300 mg every 12 hours	IV	10	51.7 [32-64]	76.9 [56-98]	60	14.5 [4.8-24.1]	NR

Data presented as mean [range]

GFR; glomerular filtration rate, IV; intravenous, IHD; intermittent hemodialysis, kg; kilograms, mL; millilitres, min; minutes, NR; not reported, y; years.

4.2 Acyclovir

Table 2. Acyclovir pharmacokinetic studies in CKD used for CKD-PBPK model validation.

Study	Dose	Route	N	Age ± SD (y) [range]	Weight [range]	Female [%]	GFR (mL/min)	Ethnicity
Laskin *et al.* [336]	2.5 mg/kg	IV	6	46 [30-72]	57.5 [48-74]	33	IHD	NR

Data presented as mean±SD [range]

GFR; glomerular filtration rate, IV; intravenous, IHD; intermittent hemodialysis, kg; kilograms, mL; millilitres, min; minutes, SD; standard deviation, y; years.

4.3 Meropenem

Table 3. Meropenem pharmacokinetic studies in CKD used for CKD-PBPK model validation.

Study	Dose	Route	N	Age ± SD (y) [range]	Weight ± SD (kg) [range]	Female [%]	GFR ± SD (mL/min) [range]	Ethnicity
Chimata *et* al. [331]	500 mg	IV	4	54.25 [48-61]	64.75 [43-85]	25	34.13 [32-37.3]	NR
Chimata *et al.* [331]	500 mg	IV	5	64.60 [46-76]	54 [50-58]	60	12.08 [4.3-21.5]	NR
Christensson *et al.* [332]	500 mg	IV	5	47±19.1 [18-68]	84±9.3	0	34±11.8	NR
Christensson *et al.* [332]	500 mg	IV	7	53±11.2 [35-66]	76±12.4	29	17±8	NR
Christensson *et al.* [332]	500 mg	IV	5	37±5.3 [32-45]	67±18.7	60	IHD	NR
Leroy *et al.* [333]	500 mg	IV	10	52.2±13.3	67±8.0	NR	50.3±16.7 [30-80]	NR
Leroy *et al.* [333]	500 mg	IV	10	51.3±14.3	64.4±8.5	NR	12.7±6.6 [2-30]	NR
Leroy *et al.* [333]	500 mg	IV	6	59.2±5.1	58.7±8.0	NR	IHD	NR

Data presented as mean±SD [range]

GFR; glomerular filtration rate, IV; intravenous, IHD; intermittent hemodialysis, kg; kilograms, mL; millilitres, min; minutes, NR; not reported, SD; standard deviation, y; years.

4.4 Furosemide

Table 4. Furosemide pharmacokinetic studies in CKD used for CKD-PBPK model validation.

Study	Dose	Route	N	Age (y) [range]	Weight (kg) [range]	Female [%]	GFR ± SD (mL/min) [range]	Ethnicity
Gladziwa *et al.* [334]	120 mg	IV	10	54.8 [31-69]	69.7 [55-82]	20	16.7±5.5 [7-27]	NR
Rane et al. [335]	80 mg	IV	6	[40-55]	81.6±6.4	NR	11±1	NR

Data presented as mean±SD [range]

GFR; glomerular filtration rate, IV; intravenous, kg; kilograms, NR; not reported, mL; millilitres, min; minutes, SD; standard deviation, y; years.

5. Chapter 3 Appendix Figures

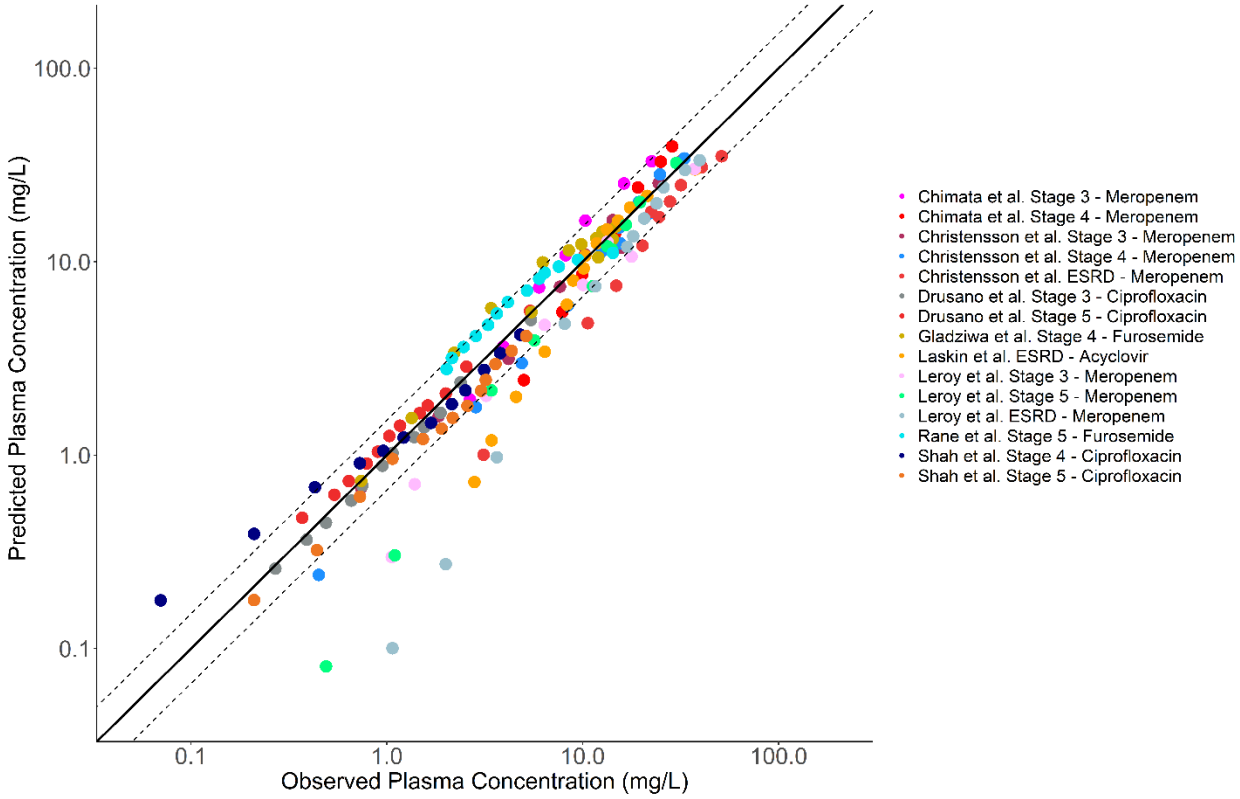


Figure 1. Predicted vs. observed plasma concentrations for all chronic kidney disease physiologically-based pharmacokinetic (CKD-PBPK) simulations. Dashed line represents 1.5-fold error.
ESRD; end stage renal disease.

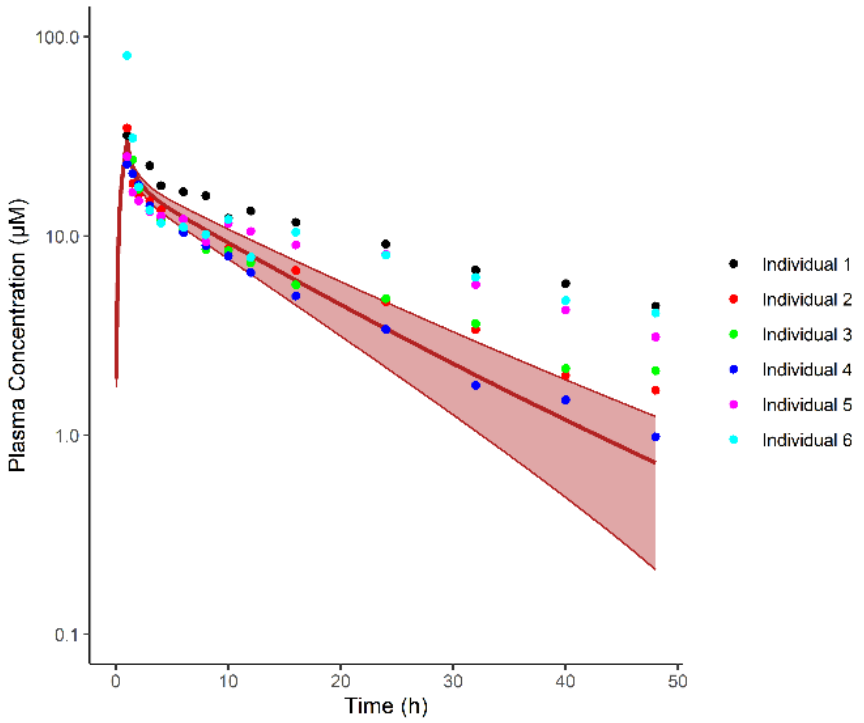
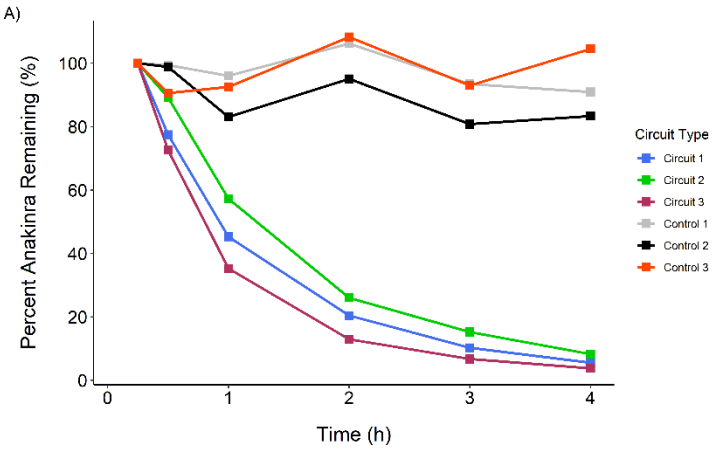


Figure 2. Simulated chronic kidney disease physiologically-based pharmacokinetic (CKD-PBPK) plasma concentration-time profiles of acyclovir compared to observed data for end stage renal disease on intermittent hemodialysis. Individual data presented as circles corresponding to each respective individual included within Laskin *et al*. [336] The red line represents the simulated mean concentration-time profile facilitated by the population CKD-PBPK model in PK-Sim ± the 90th prediction interval (shaded region). Details on dosing regimen and study population may be found in the **Appendix B4.2**.
h; hours, µM; micromolar.

Appendix C

Supplementary Material for Chapter 4

1. Supplementary Figures



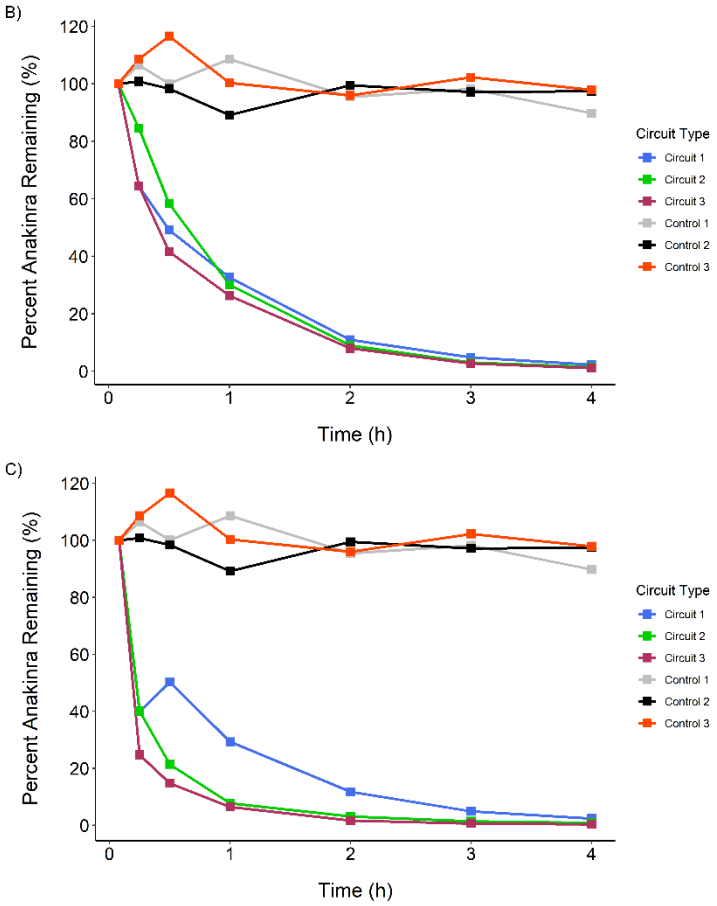
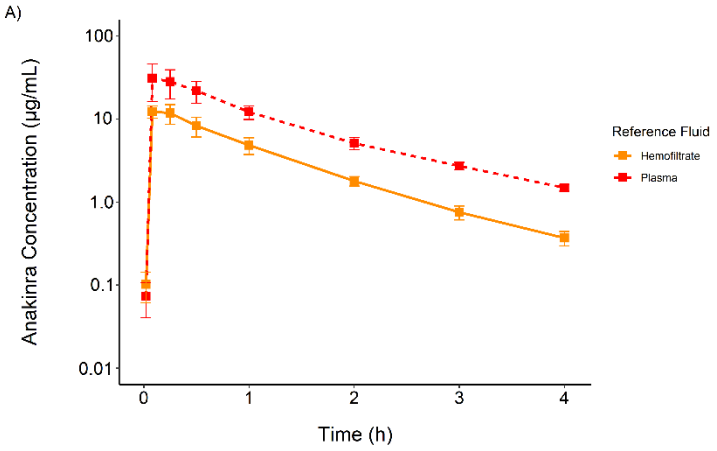


Figure 1. Percent anakinra remaining in plasma and standard control for each circuit run via A)hemofiltration (CVVH), B)hemodialysis (CVVHD) and C)hemodiafiltration (CVVHDF). Due to incomplete mixing of circuit #1 for CVVH, percent recovery of anakinra in plasma was determined at t = 15 minutes. Percent recovery in plasma was analyzed at t = 5 minutes for subsequent modalities of CRRT (CVVHD, CVVHDF).



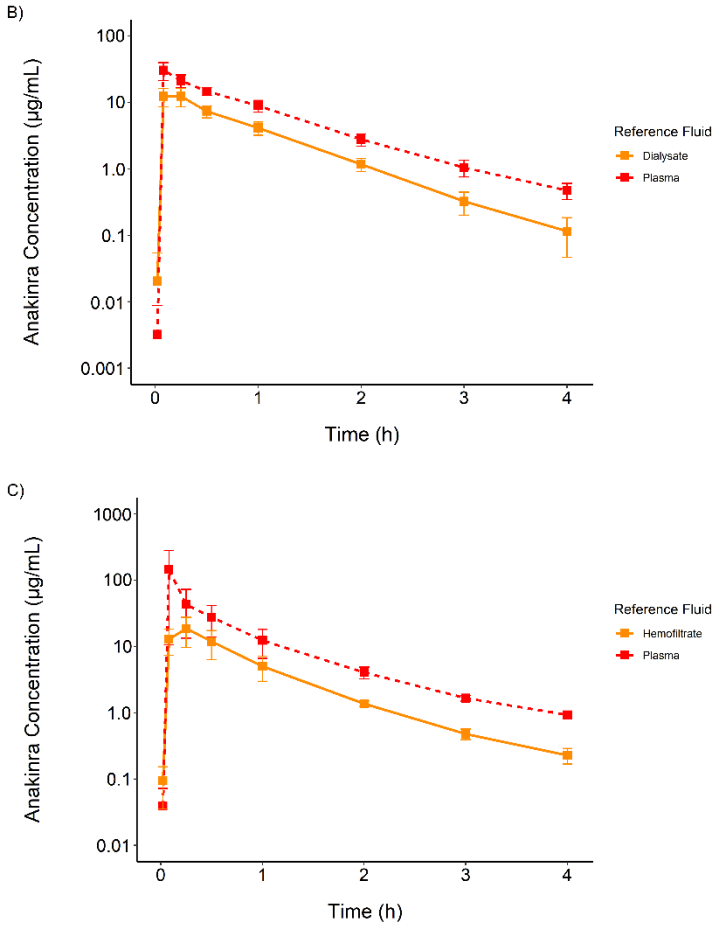


Figure 2. Average concentration of anakinra in plasma and hemofiltrate/dialysate over time. Standard deviation shown as error bars. Anakinra concentrations are presented for each CRRT modality: A) CVVH, B) CVVHD, C) CVVHDF. Graphical illustration transformed to logarithmic scale to aid in visual inspection.

2. Supplementary Tables

Table 1. Concentrations of key components within the CRRT circuit solution.

Sample	pH [7.35-7.45]	pCO2 (mmHg) [30-40]	pO2 (mmHg) [80-100]	HCO3 (mmol/L) [18-26]	Na (mEq/L) [135-145]	K (mEq/L) [3.5-5]	Hgb (g/L) [113-141]	HCT [0.31-0.41]
CVVHDF								
0	7.32±0.05	34.13±4.16	44.33±2.31	17.57±2.14	134.33±1.15	9	96.33±16.26	0.28±0.05
5	7.37±0.07	50.1±10.05	84.67±22.59	28.63±1.25	139.67±0.58	4.63±0.16	108.67±24.68	0.32±0.07
6	7.43±0.15	48.6±12.76	124.33±16.19	30.4±0.75	140.33±0.58	3.97±0.06	107.33±27.65	0.32±0.08
7	7.45±0.14	46.23±15.10	149.67±7.23	30.83±0.06	139.67±0.58	3.87±0.12	105.33±26.63	0.31±0.08
8	7.49±0.13	42.57±12.97	150.67±9.07	31.27±0.45	140±1.0	3.77±0.12	103±28.62	0.30±0.08
CVVH								
0	7.21±0.11	37.17±13.36	38.67±2.08	14.4±2.46	132.33±1.53	9	110±11.53	0.33±0.04
5	7.26±0.07	61.47±12.76	71±36.04	27.4±1.87	138±1.73	5.27±0.29	108.67±9.07	0.32±0.03
6	7.28±0.16	66.27±24.57	94.67±48.95	29.6±1.82	138.67±1.15	4.1±0.10	110±5.57	0.32±0.02
7	7.36±0.22	59.87±27.98	115.33±53.15	31±2.10	139±1.73	3.87±0.06	109±7	0.32±0.02
8	7.33±0.11	62.9±16.18	135.33±32.47	32.73±0.59	138.33±0.58	3.8	106.67±10.78	0.32±0.03
CVVHD								
0	7.30±0.11	37.6±9.35	53±23.89	18.4±3.33	137±2.65	8.2±0.98	85±12.12	0.25±0.04
5	7.25±0.12	69.53±19.62	109.33±52.84	29.47±1.02	139±1	4.47±0.32	86±8.5	0.25±0.03
6	7.26±0.1	71.53±17.09	122±51.16	31.5±1.15	138.33±0.58	3.97±0.06	86±7.21	0.24±0.03
7	7.18±0.17	85.67±29.76	133.33±40.82	30.63±0.46	138	3.8	8.73±5.1	0.26±0.02
8	7.23±0.13	77.9±22.87	144±23.64	31.93±1.10	138.33±0.58	3.8	86±7.21	0.25±0.03

Data presented as mean ± standard deviation.
Normal reference range values inserted within brackets.
CVVH; continuous veno-venous hemofiltration, CVVHD; continuous veno-venous hemodialysis, CVVHDF; continuous veno-venous hemodiafiltration, HCT; hematocrit, HCO3; bicarbonate, Hgb; hemoglobin, K; potassium, mEq/L; milliequivalent per litre, mm/Kg; millimetres of mercury, mmol/L; millimoles per litre; Na; sodium, pCO2; partial pressure of carbon dioxide, PO2; partial pressure of oxygen.

Table 2. Anakinra sieving coefficient/dialysate saturation constant determined through each CRRT modality. Data presented as mean, standard deviation and range.

CRRT Modality	Sieving/Saturation Coefficient	Standard Deviation	Range
CVVH	0.37	0.12	0.21 – 0.79
CVVHD	0.41	0.12	0.1 – 0.63
CVVHDF	0.34	0.14	0.06 – 0.72

CVVH; continuous veno-venous hemofiltration, CVVHD; continuous veno-venous hemodialysis, CVVHDF; continuous veno-venous hemodiafiltration.

Table 3. Estimated anakinra transmembrane clearance for each CRRT modality. Data presented as mean, standard deviation and range.

CRRT Modality	Transmembrane Clearance (mL/min)	Standard Deviation (mL/min)	Range (mL/min)
CVVH	3.94	0.86	2.46 – 5.96
CVVHD	5.53	1.67	1.34 – 8.34
CVVHDF	4.99	1.58	2.39 – 9.54

CVVH; continuous veno-venous hemofiltration, CVVHD; continuous veno-venous hemodialysis, CVVHDF; continuous veno-venous hemodiafiltration, mL; millilitres, min; minutes.

Table 4. Anakinra concentrations obtained within the ex-vivo CRRT analysis.

Time	Mean Plasma Concentration ± SD (µg/mL)	Mean Hemofiltrate Concentration ± SD (µg/mL)	Mean Control Concentration ± SD (µg/mL)
		CVVHDF	
1 min	0.039±0.03	0.094±0.06	58.81±30.87
5 min	144.95±134.29	12.87±5.51	59.66±29.17
15 min	43.01±29.63	18.69±9.01	63.15±32.44
30 min	27.72±13.78	11.90±5.52	64.40±37.51
1 h	12.37±5.74	5.04±2.06	58.73±28.88
2h	4.07±0.82	1.37±0.13	57.84±27.94
3h	1.66±0.17	0.48±0.09	59.63±30.69
4h	0.93±0.12	0.23±0.06	57.43±29.83
Time		**CVVH**	
1 min	0.07±0.03	0.102±0.05	53.9±15.25
5 min	31.23±14.91	12.34±2.05	51.3±12.90
15 min	29.78±10.89	11.83±3.16	49.8±10.16
30 min	21.93±6.54	8.32±2.24	50.2±10.94
1 h	12.19±2.26	4.84±1.11	45.5±12.10
2h	5.13±0.87	1.79±0.23	51.8±13.57
3h	2.72±0.28	0.75±0.15	44.8±12.20
4h	1.49±0.14	0.37±0.07	46.8±13.58
Time		**CVVHD**	
1 min	0.003±0.006	0.02±0.03	34.9[a]
5 min	30.66±9.22	12.42±3.77	40.2[a]
15 min	21.38±4.70	12.43±3.76	37.1[a]
30 min	14.76±2.06	7.40±1.53	34.6[a]
1 h	8.94±1.83	4.15±0.94	38.2[a]
2h	2.79±0.58	1.17±0.26	31.8[a]
3h	1.05±0.30	0.325±0.12	27.7[a]
4h	0.47±0.13	0.12±0.07	27.4[a]

[a]Due to negligible drug degradation, analysis of control anakinra concentrations for circuit 2 and 3 of CVVHD were not conducted.

CVVH; continuous veno-venous hemofiltration, CVVHD; continuous veno-venous hemodialysis, CVVHDF; continuous veno-venous hemodiafiltration, h; hours, min; minutes, SD; standard deviation, µg/mL; microgram per mililitre.

Appendix D

Supplementary Material for Chapter 5

1. Supplementary Figures

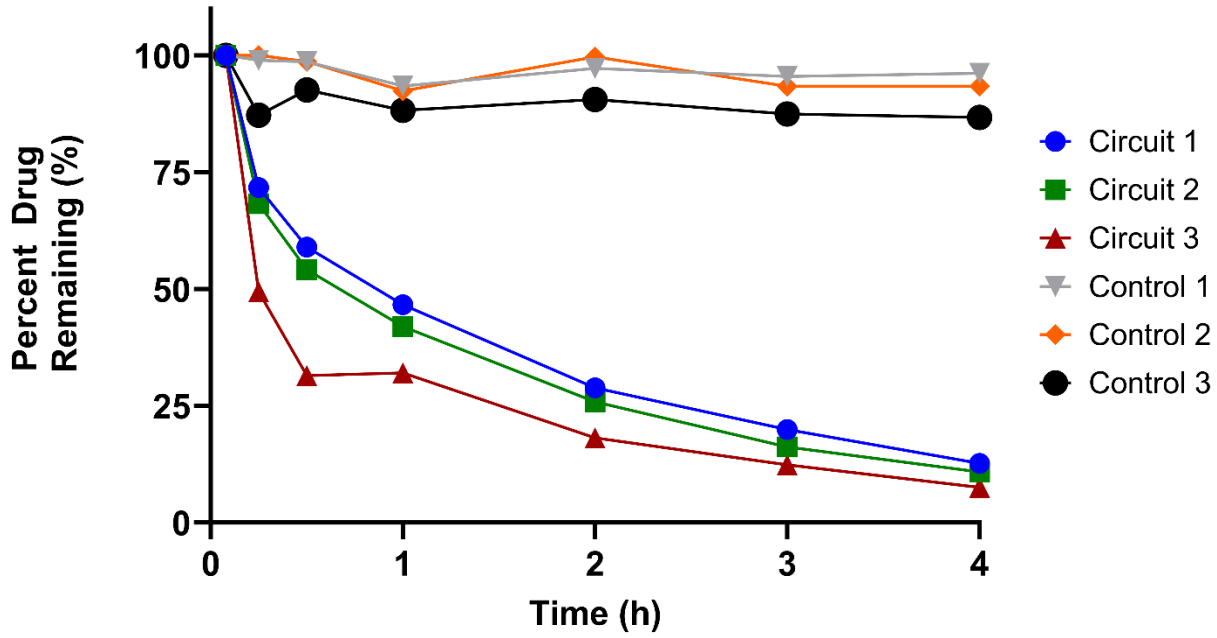


Figure 1. Percent cefazolin remaining in plasma and standard control for each circuit run within a closed-loop CVVHDF ex-vivo circuit. Percent cefazolin remaining in plasma and control was analyzed at time = 5 minutes.

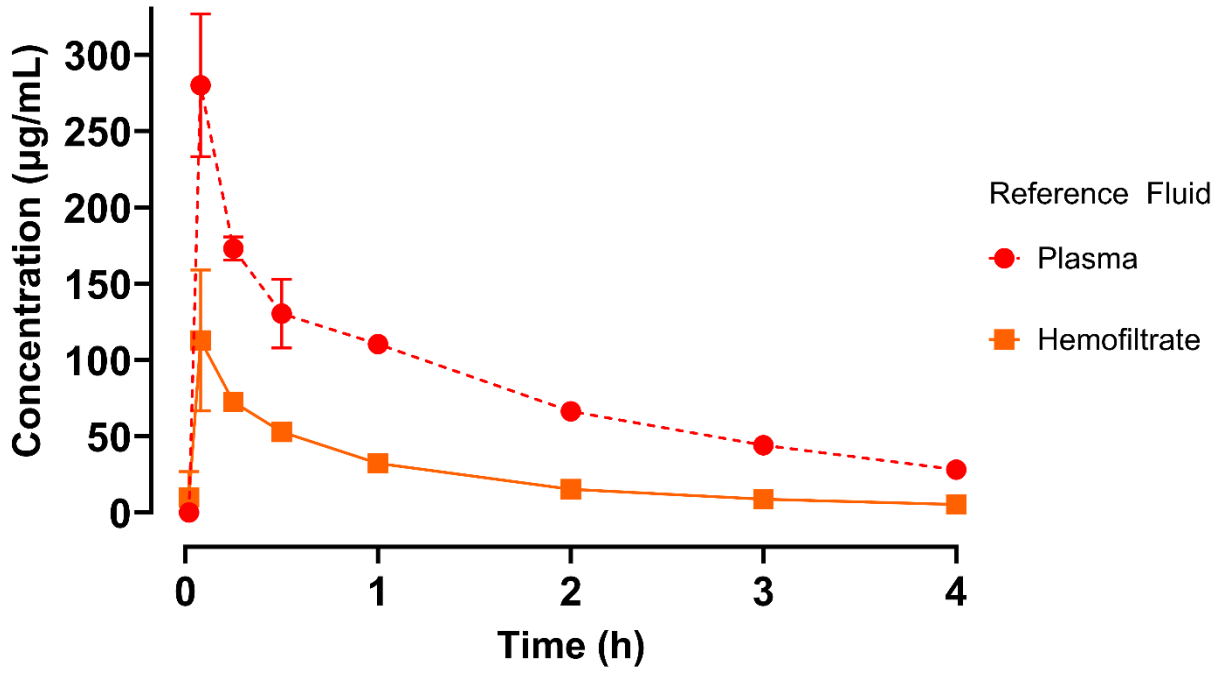


Figure 2. Average concentration of cefazolin in plasma and hemofiltrate over time within a closed-loop CVVHDF ex-vivo circuit. Standard deviation shown as error bars.

2. Supplementary Tables

Table 1.0 Concentrations of key components within the CRRT circuit solution.

Sample	pH [7.35-7.45]	pCO2 (mmHg) [30-40]	pO2 (mmHg) [80-100]	HCO3 (mmol/L) [18-26]	Na (mEq/L) [135-145]	K (mEq/L) [3.5-5]	Hgb (g/L) [113-141]	HCT [0.31-0.41]
0	7.38±0.08	35.27±8.43	52.33±34.36	20.7±3.59	137.67±1.53	9	90.33±4.04	0.27±0.01
5	7.41±0.11	47.13±15.21	93.67±48.01	28.77±2.49	140±1.0	4.77±0.15	100.67±5.13	0.30±0.02
6	7.42±0.17	48.53±20.52	115.33±35.47	30.7±1.76	140±1.0	3.97±0.06	99.67±4.04	0.29±0.01
7	7.46±0.20	47.3±23.48	134.67±19.14	30.67±0.15	140±1.0	3.8	98.67±3.51	0.29±0.01
8	7.47±0.22	48.43±26.30	147.67±10.79	32.47±1.0	138.33±2.1	3.8	99	0.29

Data presented as mean ± standard deviation.
Normal reference range values inserted within the brackets.
HCT; hematocrit, HCO3; bicarbonate, Hgb; hemoglobin, K; potassium, mEq/L; milliequivalent per litre, mm/Kg; millimetres of mercury, mmol/L; millimoles per litre; Na; sodium, pCO2; partial pressure of carbon dioxide, PO2; partial pressure of oxygen.

Table 2.0 Cefazolin concentrations obtained within the ex-vivo CRRT analysis.

Time	Mean Plasma Concentration ± SD (µg/mL)	Mean Hemofiltrate Concentration ± SD (µg/mL)	Mean Control Concentration ± SD (µg/mL)
		CVVHDF	
1 min	<LLOQ	29.5±17.03	314.33±36.67
5 min	280±46.81	112.83±46.26	327.33±55.52
15 min	173±7.55	72.53±4.45	309.67±28.29
30 min	130.33±22.51	52.83±2.20	315±41.21
1 h	110.33±5.77	32.33±0.81	298±40.95
2 h	66.27±5.96	15.23±0.73	312±37.72
3 h	44.12±5.05	8.83±0.60	300±36.50
4 h	28.20±3.38	5.31±0.20	299.67±34.12

CVVHDF; continuous veno-venous hemodiafiltration, LLOQ; lower limit of quantification h; hours, min; minutes, SD; standard deviation, µg/mL; microgram per millilitre.

Appendix E

Supplementary Material for Chapter 6

1. Building a PBPK Model for Intravenous Anakinra in Healthy Adults

1.1 Introduction

Anakinra is a recombinant, non-glycosylated version of the human interleukin-1 (IL-1) receptor antagonist that competitively inhibits the binding of IL-1.[377] Anakinra has been approved for use for indications of rheumatoid arthritis and neonatal-onset multisystem inflammatory disease. [375,376] Additionally, anakinra has been used off-label for management of cytokine release syndrome secondary to hemophagocytic lymphohistiocytosis (HLH) or chimeric antigen receptor (CAR) T-cell therapy, [380–385] sepsis [389–392] and subarachnoid hemorrhage. [401,402]

Due to the molecular size (17.3 kDa), it can be filtered at the glomerulus and the kidney is responsible for approximately 80% of total clearance. [386,388] Furthermore, pharmacokinetic (PK) studies support the impact of renal clearance on total clearance. [386] Based upon the investigations by Yang *et al*. [386] in subjects with chronic kidney disease (CKD), it was demonstrated that in the absence of glomerular filtration (CrCL = 0) a non-renal clearance was present. Although a mechanism for non-renal clearance has yet to be defined, it has been suggested in mass-balance rat studies that the liver may be another clearing organ. [388] Due to the negligible amount of unchanged drug found in urine, [388] it has been suggested that anakinra may be subsequently reabsorbed from the proximal tubule after glomerular filtration and undergo proteolysis. [386,598–601]

In this report, the building and verification of a PBPK model for intravenous anakinra in healthy adults is presented. The anakinra model incorporated the large, molecule two-pore model structure implemented in PK-Sim. [451] An alternate anakinra PBPK model was constructed by Pan *et al*., [454] which included a slightly different interpretation of the data that deserves reading.

1.2. Methods and Results

1.2.1 Modelling Strategy

PBPK modelling and simulation were performed using PK-Sim version 11.0. Fifteen organs and two blood compartments were included in the large molecule, two-pore model structure to represent a virtual adult. [451]

1.2.2 Intravenous Model Construction

The process for developing the anakinra PBPK model in healthy adults is described here. **Table 1.0** presents the drug-specific parameters for anakinra used within the final model.

Table 1.0. Drug specific parameters and ADME of anakinra for IV model development.

	Used in naïve model	**Used in optimized model [range of optimized values]**
Drug Specific Parameters		
Molecule Weight (kDa)	17.3	17.3
Hydrodynamic Radius (nm)	2.16 [452,453]	2.16 [452,453]
Compound Type	Protein	Protein
ADME		
GFR Fraction	1	0.45
Non-renal clearance (1/min)	0	52.66 [29.65 – 68.45]

kDa; kilodaltons, nm; naometres, min; minutes.

For the purpose of the anakinra PBPK model, Organ-specific partition coefficients were calculated with the PK-Sim standard, Schmitt, or the Rodgers and Rowland algorithms. [305–307] To account for possible reabsorption within the proximal tubule, an input for the fraction of tubular reabsorption is required. PK-Sim calculates the glomerular filtration fraction as follows (Eq.1):

Eq.1

$$Glomerular\ Filtration\ Fraction = \frac{Empiric\ Renal\ Clearance}{Expected\ Renal\ Clearance}$$

Where empiric renal clearance equals the renal plasma clearance in the literature and the expected renal clearance is the clearance expected in the absence of any reabsorption. As limited data was available to assess renal plasma clearance in humans, the glomerular filtration fraction was optimized.

To account for the potential non-renal clearance pathways, non-specific metabolism (non-renal clearance; CL_{NR}) was incorporated within the liver and kidney, a method that has been applied previously. [454] Both CLNR and glomerular filtration fraction were optimized based upon observed data using the Monte-Carlo method to search the parameter space. The optimized model was then used to generate population predictions of concentration vs. time profiles of virtual populations (n=1000) to be evaluated within independent data sets not used in the model building process. **Table 2.0** presents the data sets incorporated for model development.

Table 2.0 Pharmacokinetic datasets of intravenous anakinra for model construction.

Reference	Ethnicity	Dose and Administration	N (male/female)	Age (years)	Weight (kg)	Height (cm)
Yang *et al* [386]	American	1 mg/kg IV as a 1-minute infusion[a]	12 (12/0)	27 [19-34][b]	82 [62-92][b]	177 [169-183][b]
Yang *et al* [387]	American	1 mg/kg IV as a 1-minute infusion[a]	8 (2/6)	48.4±12.3	66.3±13.2	161.4±8.9

cm; centimetres, IV; intravenous, kg; kilograms
[a] Administered as a single dose
[b] Data presented as median [range]
[c] Data presented as mean ± standard deviation

A comparison of the fitted IV simulation to the observed data is presented in **Figure 1.0.**

1.2.3 Intravenous Model Evaluation

Verification of model accuracy was conducted using the average fold error (AFE; bias) and absolute average fold error (AAFE; precision) for the anakinra simulations. Acceptance was confirmed if AFE <30% (0.7-1.3) and AAFE ≤2 for simulated drug concentrations.

Eq.2

$$AFE = 10^{\frac{1}{N}\sum_i \log\left(\frac{predicted_i}{observed_i}\right)}$$

Eq. 3

$$AAFE = 10^{\frac{1}{N}\sum_i \left|\log\left(\frac{predicted_i}{observed_i}\right)\right|}$$

Where $predicted_i$ and $observed_i$ correspond to predicted and observed plasma concentrations respectively. For data sets including individual patient samples, inter-individual variability in the population simulation was accepted if ≥ 80% of observed concentrations fall within the generated prediction interval (5th to 95th).

1.2.4 Intravenous Model Verification

The optimized IV model was validated against independent data not used within the model building process (**Table 3.0**). This data was obtained from the study by Granowitz *et al*. [474] which include a dose escalation and multiple dose analysis. **Figure 2.0** illustrates good model performance on the visual predictive check over each dose escalation. All simulations met the predefined model acceptance criteria of AFE and AAFE, expect for those virtual individuals receiving anakinra IV 3 mg/kg as the AFE was slightly greater (**Table 4.0**).

Table 3.0 Pharmacokinetic datasets of intravenous anakinra for model verification.

Reference	Ethnicity	Dose and Administration (N)[a]	N (male/female)	Age (years) [range]	Weight (kg) [range]	Height (cm) [range]
Granowitz *et al*. [474]	American	1 mg/kg IV (3) 2 mg/kg IV (6) 3 mg/kg IV (4) 5 mg/kg IV (4) 7 mg/kg IV (4) 10 mg/kg IV (4)	29 (29/0)	[18-30]	NR[b]	NR[b]

cm; centimetres, IV; intravenous, kg; kilograms; NR, not reported
[a] Anakinra administered as a 3-hour intravenous infusion
[b] Data not reported by study authors therefore population means as produced by PK-Sim were incorporated

Table 4.0. Anakinra IV PBPK Model Evaluation

Reference	Dose	Average Fold Error	Absolute Average Fold Error
Granowitz *et al*. [474]	1 mg/kg IV	0.97	1.19
	2 mg/kg IV	1.28	1.38
	3 mg/kg IV	**1.54**	1.67
	5 mg/kg IV	1.06	1.22
	7 mg/kg IV	1.04	1.32
	10 mg/kg IV	1.14	1.28

1.2.5 Population Verification

A population PBPK simulation was performed to ensure that the model can approximate the mean and inter-individual variability in healthy individuals. In this workflow, 1000 virtual individuals were generated. Each individual represents one full body parameter set for iterative input into the PBPK model. Data sets used for population PBPK model evaluation may be found in **Table 5.0.**

Table 5.0. Pharmacokinetic datasets for intravenous anakinra model population verification.

Reference	Ethnicity	Dose and Administration	N (male/female)	Age (years)	Weight (kg)	Height (cm) [range]
Galea *et al* [402]	European	1) 100 mg IV bolus followed by 4 mg/kg/h infusion 2) 200 mg IV bolus followed by 2 mg/kg/h infusion 3) 300 mg IV bolus followed by 2 mg/kg/h infusion 4) 400 mg IV bolus followed by 6 mg/kg/h infusion 5) 500 mg IV bolus followed by 10 mg/kg/h	25 (17/28)	53[a] [37-76]	73[a] [58-110]	NR
Gueorguieva *et al* [401]	European	100 mg IV bolus followed by 2 mg/kg/h infusion	8 (6/2)	51[a] [39-69]	70[a] [64-150]	NR

cm; centimetres, IV; intravenous, kg; kilograms; NR, not reported
[a] Data reported as mean [range]

Figure 3.0 and **Figure 4.0** present the simulated concentration time profiles for the populations as compared to the observed concentrations from the studies by Galea *et al*. [402] and Gueorguieva *et al*., [401] respectively. Each simulation fell outside model acceptance criteria, as 68% and 70% of observed concentrations fell within the 5th to 95th prediction interval, respectively. As these patients received anakinra in the acute care setting after experiencing subarachnoid hemorrhage, over prediction in drug clearance may have limited successful predictions. No information pertaining to patient clinical status was reported. Therefore, despite not predicting ≥80% of observed concentrations, the population PBPK model was able to predict

a majority of the observed values upon different dosing strategies in a highly complex patient population.

1.3. Figures

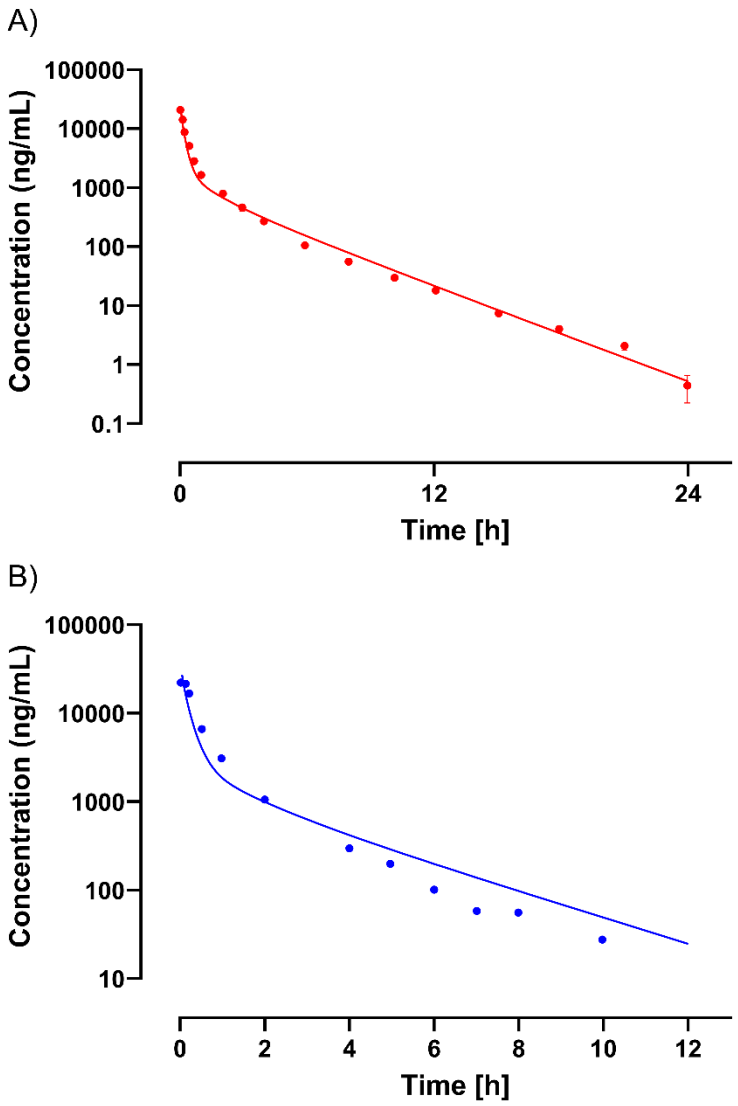


Figure 1.0. Simulation after optimization. Observed data reported as mean (circles) with standard error of the mean (error bars) from the studies conducted by Yang *et al*. [386] (A) and Yang *et al.* [387] (B). The solid red and blue lines represent the simulated plasma concentrations of anakinra IV 100 mg in a virtual individual representing the average demographics of study participants.
h; hour, ng/ml; nanogram per mililitre.

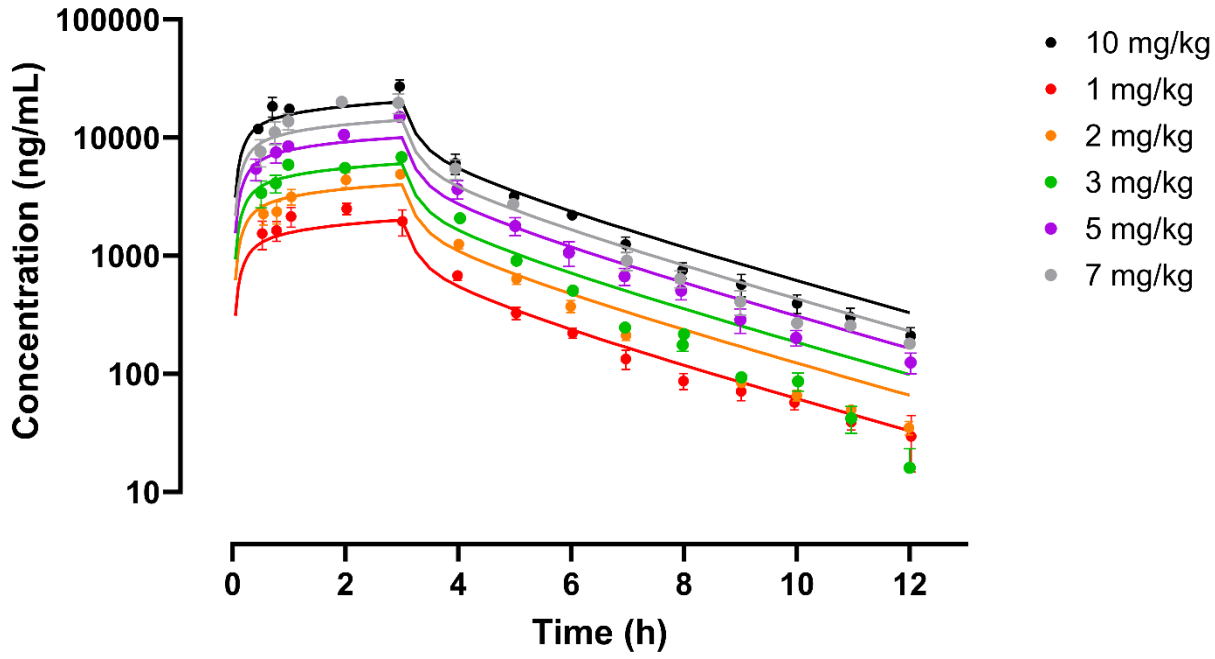


Figure 2.0. Anakinra IV PBPK model verification to observed concentrations from individuals in the study by Granowitz *et al*. [474] The solid line represents the average concentration vs. time profile of the virtual population while the observed data is presented as mean (circles) with standard deviation (error bars).

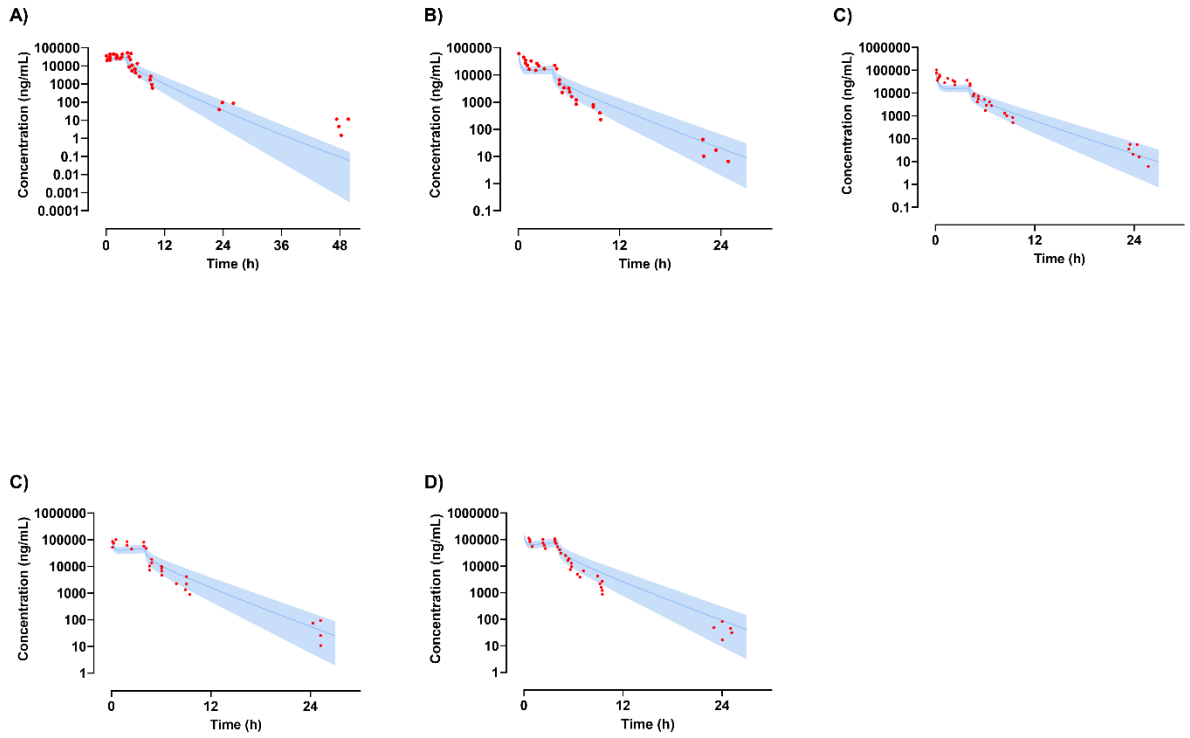


Figure 3.0. Population verification against the observed anakinra concentrations from individuals within the study by Galea *et al.* [402] The solid line represents the simulated arithmetic mean and the shaded region represents the simulated 5th to 95th prediction interval. Observed concentrations are presented as circles. Within this study five dosing regimens were administered: A) 100 mg IV bolus followed by 4 mg/kg/h infusion, B) 200 mg IV bolus followed by 2 mg/kg/h infusion, C) 300 mg IV bolus followed by 2 mg/kg/h infusion, D) 400 mg IV bolus followed by 6 mg/kg/h infusion, E) 500 mg IV bolus followed by a 10 mg/kg/h infusion.
h; hour, ng/mL; nanogram per mililitre.

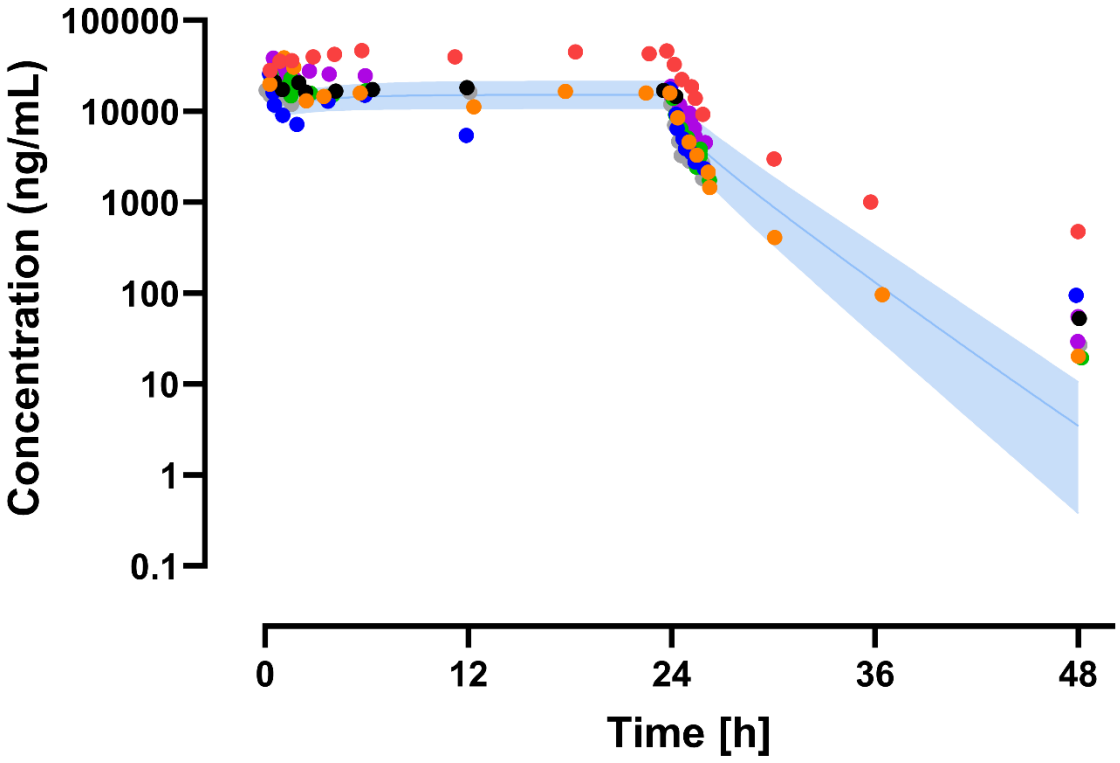


Figure 4.0. Population verification of the observed anakinra concentrations from individuals within the study by Gueorguieva *et al*. [401] The solid line represents the simulated arithmetic mean and the shaded region represents the simulated 5th to 95th prediction interval of the virtual population. The observed data from study individuals is presented as circles.

2. Building a PBPK Model for Subcutaneous Anakinra in Healthy Adults

2.1 Introduction

As anakinra is approved for us as a subcutaneous (SC) dose, a semi-mechanistic SC-PBPK model was developed. PBPK models representing SC dose administration have been previously constructed, [452,454–456,460] that include different levels of complexity. The purpose of developing a semi-mechanistic SC-PBPK model for anakinra was to carry forth this dosing strategy to be incorporated within the full ECLS-PBPK model.

2.2 Methods and Results

2.2.1 Modelling Strategy

PBPK modelling and simulation was performed using PK-Sim version 11.0. To account for SC dosing, the bioavailable dose (Dose x F) was applied as an IV administration to the interstitial compartment of the skin. This semi-mechanistic strategy enables anakinra to move to the lymph and blood by convection and diffusion. A similar modelling approach has been applied previously [454,460]. Variability in bioavailability (F) has been shown for anakinra in healthy adults, ranging from approximately 70-95%.[386,387] As such, bioavailability of anakinra was set to 0.8, while the half-life (t ½) of drug release was optimized based upon the data by Yang *et al*.[387] Parameters previously determined in the IV adult PBPK model remained fixed (**Table 1.0)**

2.2.2 Subcutaneous Model Construction

Data used to construct the anakinra SC-PBPK model was obtained from Yang *et al*. [387] A virtual individual corresponding to mean demographics of study participants was constructed for model development. Demographics corresponding to study participants may be found in **Table 2.0**. Half-life of drug release within the interstitial compartment of the skin was optimized upon the observed data set. The optimization incorporated the Monte-Carlo approach to explore the parameter space. Multiple optimization runs (6 to 10) were performed to confirm identifiability of an unique solution. The run with the lowest error was selected as the final solution as presented in **Table 1.0**. The optimized SC-PBPK model may be found in **Figure 1.0**.

Table 1.0. Drug specific parameters and ADME of anakinra for subcutaneous model development.

	Used in naïve model	Used in optimized model [range of optimized values]
Drug Specific Parameters		
Molecule Weight (kDa)	17.3	17.3
Hydrodynamic Radius (nm)	2.16 [452,453]	2.16 [452,453]
Compound Type	Protein	Protein
Bioavailability (F)	0.8	0.8
Half-life of drug release (min)	0	212.07 [212.04-212.11]
ADME		
GFR Fraction	1	0.45
Non-renal clearance (1/min)	0	52.66 [29.65 – 68.45]

kDa; kilodaltons, nm; nanometres, min; minutes.

Table 2.0 Pharmacokinetic datasets of subcutaneous anakinra for model construction.

Reference	Ethnicity	Dose and Administration	N (male/female)	Age (years)	Weight (kg)	Height (cm)
Yang *et al* [387]	American	100 mg SC[a]	8 (2/6)	48.4 [12.3][b]	66.3 [13.2][b]	161.4 [8.9][b]

cm; centimetres, kg; kilograms; SC; subcutaneous

[a] Administered as a single dose

[b] Data presented as mean [standard deviation]

2.2.3 Subcutaneous Model Evaluation

Verification of model accuracy was conducted using the average fold error (AFE; bias) and absolute average fold error (AAFE; precision) for the anakinra simulations. Acceptance was confirmed if AFE <30% (0.7-1.3) and AAFE ≤2 for simulated drug concentrations.

Eq. 1

$$AFE = 10^{\frac{1}{N}\sum_i \log\left(\frac{predicted_i}{observed_i}\right)}$$

Eq. 2

$$AAFE = 10^{\frac{1}{N}\sum_i \left|\log\left(\frac{predicted_i}{observed_i}\right)\right|}$$

Where $predicted_i$ and $observed_i$ correspond to predicted and observed plasma concentrations respectively. As Yang *et al*. [386] report relevant PK parameters, model predicted maximum concentrations (C_{max}), time to maximum concentration (t_{max}) and area-under the concentration time curve extrapolated to infinity (AUC_∞) were compared. A fold-error of ≤2 (Eq.3) was considered reasonable predictions.

Eq. 3

$$Fold - Error = \frac{Predicted_{PKparameter}}{Observed_{PKparameter}}$$

2.2.4 Subcutaneous Model Verification

The semi-mechanistic SC anakinra PBPK model was validated against independent data not used within the model building process. (**Table 3.0**.) A virtual population (n=1000) individuals was created with corresponding demographics of study participants in the study by Yang *et al*. [386] Each individual represents one full body parameter set for iterative input into the PBPK model. **Figure 2.0** illustrates reasonable model performance based upon the visual predictive check upon administration of a single SC anakinra dose of 100 mg. The constructed PBPK model overpredicted C_{max} in the study participants from Yang *et al*. [386], which is likely contributed to variability seen in bioavailability and absorption. This is evident in vastly different mean average C_{max} values between the two studies (1326 ng/mL vs. 773 ng/mL). However, despite the over prediction in both C_{max} and AUC_∞, each PK parameter fell within a two-fold error (**Table 4.0**). The final anakinra SC-PBPK model was then carried forth for predictions in the pediatric population.

Table 3.0 Pharmacokinetic datasets of subcutaneous anakinra for model construction.

Reference	Ethnicity	Dose and Administration	N (male/female)	Age (years)	Weight (kg)	Height (cm)
Yang *et al* [386]	American	100 mg SC[a]	6 (3/3)	46 [36-54][b]	72 [64-84][b]	166 [163-181][b]

cm; centimetres, kg; kilograms; SC; subcutaneous

[a] Administered as a single dose

[b] Data presented as median [range]

Table 4.0 Anakinra SC PBPK Model Evaluation

Reference	Dose	Average Fold Error	Absolute Average Fold Error
Yang *et al*. [386]	100 mg	1.30	1.62

Table 5.0 Anakinra SC PBPK Model Predictions of Pharmacokinetic Parameters

Reference	Predicted C_{max} (ng/mL)	Observed C_{max} (ng/mL)[a]	Predicted t_{max} (h)	Observed t_{max} (h) [a]	Predicted AUC_{∞} (ng·h/mL)	Observed AUC_{∞} (ng·h/mL) [a]
Yang *et al.* [386]	1491.89	773 (121)	**2.5**	5.24 (0.45)	13052.32	10200 (2080)

[a] Data presented as mean (standard deviation)

Bolded regions indicated failed predictions

2.3 Figures

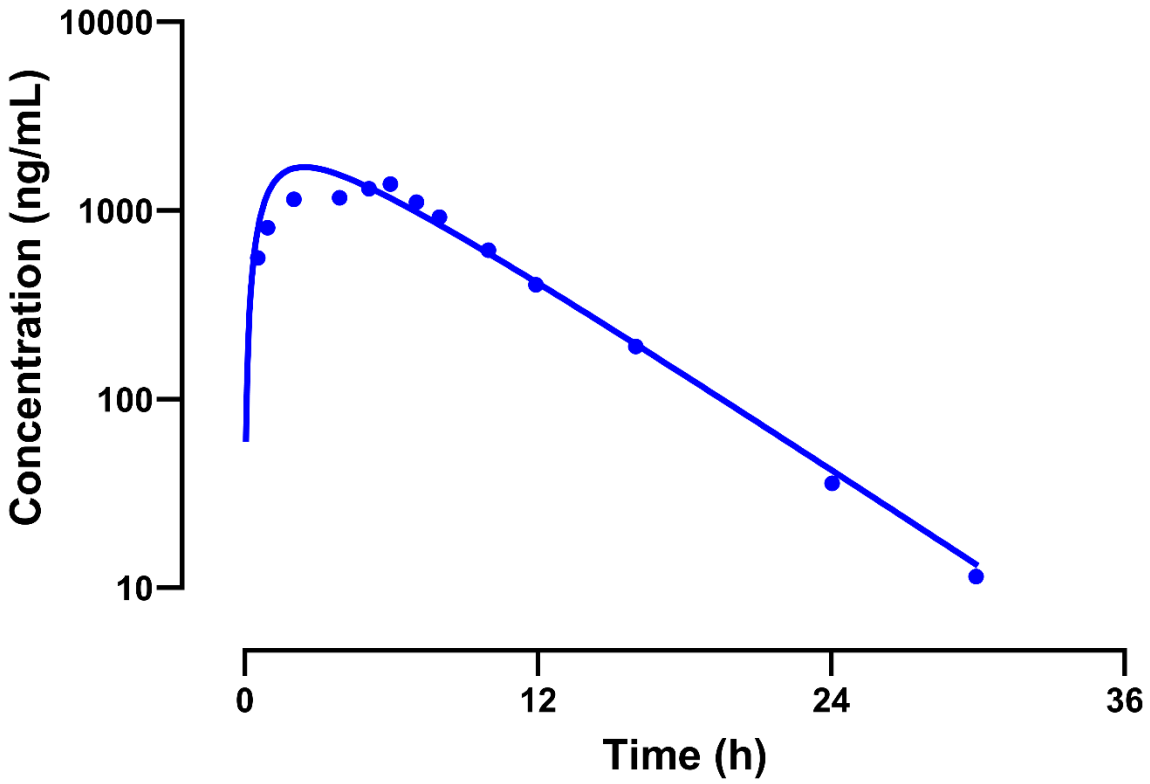


Figure 1.0 Simulation after optimization. Observed data reported as mean (circles) from study participants from Yang *et al.* [387] The solid blue line represents the simulated plasma concentrations of anakinra SC 100 mg in a virtual individual representing the average demographics of study participants.
h; hour, ng/ml; nanogram per mililitre.

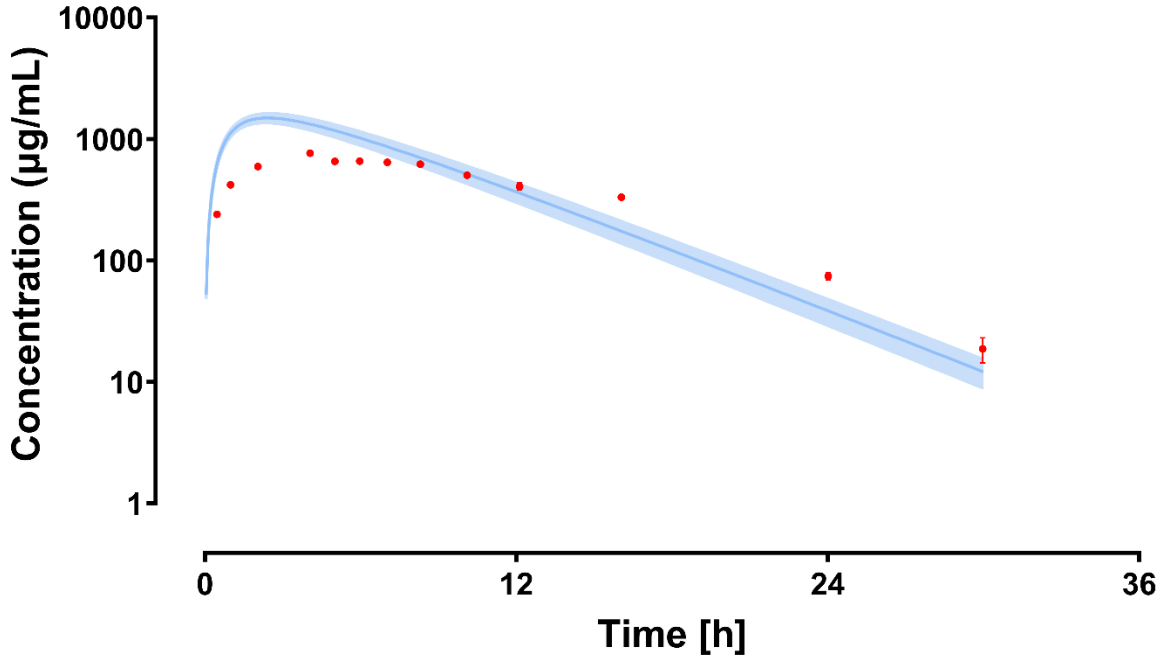


Figure 2.0 Population verification against the observed anakinra concentrations upon administration of a single 100 mg subcutaneous dose in individuals within the study by Yang *et al.* [386] The solid line represents the simulated arithmetic mean and the shaded region represents the simulated standard deviation. Observed concentrations are presented as circles (mean) with standard deviation (error bars).
h; hour, ng/mL; nanogram per mililitre.

3. Building a PBPK Model for Anakinra in Adults with Chronic Kidney Disease

3.1 Introduction

Anakinra is currently approved for subcutaneous (SC) administration and requires dosing adjustments based upon renal dysfunction. [386] In the pharmacokinetic study by Yang *et al*. it was concluded that in patients with a creatinine clearance (CrCL) less than 30 mL/min that doses should be administered every other day. The purpose of this semi-mechanistic PBPK modelling approach of subcutaneous anakinra in those with chronic kidney disease was to gain information regarding the impact of renal function on both renal clearance (CL_R) and non-renal clearance (CL_{NR}). These results were carried forth within the dosing strategies of the full ECLS-PBPK model.

3.2 Methods and Results

3.2.1 Modelling Strategy

PBPK modelling and simulation was performed using PK-Sim version 11.0. Similar to ESM 2, to account for SC dosing of anakinra, the bioavailable dose (Dose x F) was applied as an intravenous administration to the interstitial compartment of the skin. Renal clearance is estimated to account for approximately 80% of total clearance. Therefore, to assess the impact of kidney impairment on anakinra PK, PBPK simulations were conducted in each stage of chronic kidney disease (CKD). Parameters previously determined in the healthy adult IV and SC anakinra PBPK remained fixed (**Table 1.0**).

3.2.2 CKD PBPK Model Construction

Population CKD PBPK models were carried forth with modifications to account for systemic changes in whole-body anatomy and physiology such as glomerular filtration (GFR), kidney volume, renal perfusion, and hematocrit. The previously validated CKD-PBPK population by Malik *et al*. [284] was used for anakinra model assessments. It has been hypothesized that the

renal proteolysis of therapeutic proteins decreases in parallel to GFR. [602] However, recent efforts have tried to quantify this relationship and indicate a potential non-linear decline in clearance of therapeutic proteins in end-stage renal disease. Further complicating this matter, animal studies have identified the liver as a possible clearing organ. [388] It is currently unknown how the impacts of disease progression in CKD impacts proteolytic degradation of anakinra in other organ sites. To account for such decline in proteolysis, a middle-out approach was applied to match observed clearance (CL/F) across each stage of CKD in participants in the pharmacokinetic study by Yang *et al*. [386]

The bioavailability upon SC administration of large molecule compounds in advanced stages of CKD has been shown to be significantly reduced. [458,459] Furthermore, the absolute bioavailability determined in the study by Yang *et al.* for anakinra in patients with ESRD was 0.5. [386] No further assessments of absolute bioavailability could be made for CKD stages mild to moderate. Therefore, in the CKD simulations it was assumed the absolute bioavailability for CKD stages mild and moderate was consistent with healthy individuals (F=0.8), while an absolute bioavailability of 0.5 was applied to severe CKD dosing simulations. Demographics of study participants used for model construction may be found in **Table 2.0**.

Table 1.0. Drug specific parameters and ADME of anakinra for subcutaneous model development.

	Used in healthy model	Used in chronic kidney disease model
Drug Specific Parameters		
Molecule Weight (kDa)	17.3	17.3
Hydrodynamic Radius (nm)	2.16 [452,453]	2.16 [452,453]
Compound Type	Protein	Protein
Bioavailability (F)	0.8	0.8[a] 0.5[b]
Half-life of drug release (min)	0	212.07
ADME		
GFR Fraction	0.45	0.45
Non-renal clearance (1/min)	52.66	Mild: 0.11 Moderate: 0.04 Severe: 0.01

[a] absolute bioavailability applied to mild and moderate chronic kidney disease
[b] absolute bioavailability applied to severe chronic kidney disease
kDa; kilodaltons, nm; naometres, min; minutes.

Table 2.0 Pharmacokinetic datasets for the chronic kidney disease anakinra model construction.

Reference	CKD Stage	Dose and Administration	N (male/female)	Age (years)	Weight (kg)	Height (cm)
Yang *et al* [386]	Mild	100 mg SC[a]	6 (5/1)	49 [41-68][b]	87 [54-100][b]	180 [174-185][b]
	Moderate	100 mg SC[a]	6 (3/3)	68 [51-79][b]	92 [73-105][b]	171 [160-178][b]
	Severe	100 mg SC[a]	6 (4/2)	66 [45-76][b]	81 [60-105][b]	173 [159-175][b]

CKD; chronic kidney disease, cm; centimetres, kg; kilograms; SC; subcutaneous
[a] Administered as a single dose
[b] Data presented as mean [standard deviation]

3.2.3 CKD PBPK Model Evaluation

Verification of model accuracy was conducted using the average fold error (AFE; bias) and absolute average fold error (AAFE; precision) for the anakinra simulations. Acceptance was confirmed if AFE <30% (0.7-1.3) and AAFE ≤2 for simulated drug concentrations.

Eq. 1

$$AFE = 10^{\frac{1}{N}\sum_i \log\left(\frac{predicted_i}{observed_i}\right)}$$

Eq. 2

$$AAFE = 10^{\frac{1}{N}\sum_i \left|\log\left(\frac{predicted_i}{observed_i}\right)\right|}$$

Where $predicted_i$ and $observed_i$ correspond to predicted and observed plasma concentrations respectively. As Yang *et al*. [386] report relevant PK parameters, model predicted maximum concentrations (C_{max}), time to maximum concentration (t_{max}) and area-under the concentration time curve extrapolated to infinity (AUC_∞) were compared. A fold-error of ≤2 (Eq.3) was considered reasonable predictions.

Eq. 3

$$Fold - Error = \frac{Predicted_{PKparameter}}{Observed_{PKparameter}}$$

3.2.4 CKD PBPK Model Verification

The middle-out approach applied to the anakinra CKD-PBPK model was verified against observed data and pharmacokinetic parameters from the study by Yang *et al*. [386] A virtual population (n=1000) of individuals was created to correspond the demographics of those with each stage of CKD (**Table 2.0**). **Figure 1.0-3.0** indicate reasonable model performance based

upon the visual predictive check upon administration of a single SC anakinra 100 mg dose. The anakinra CKD PBPK model consistently overpredicted the maximum concentration (C_{max}) in CKD stages mild and moderate, however each predicted pharmacokinetic parameter still fell within a two-fold error compared to observed. As the absolute bioavailability was not known in CKD stages mild and moderate, it is hypothesized that the overprediction of C_{max} and underprediction of time to maximum concentration (t_{max}) was the result of mischaracterizing bioavailability in these stages. The final parameters used to assess the reduction in CL_{NR} will be carried forward in the final CRRT-PBPK model simulations.

Table 3.0 Anakinra CKD PBPK Model Evaluation.

Reference	CKD Stage	Average Fold Error	Absolute Average Fold Error
Yang *et al*. [386]	Mild	**1.51**	1.55
	Moderate	**1.45**	1.49
	Severe	1.10	1.26

Bolded regions indicated failed predictions.

Table 4.0 Anakinra SC PBPK Model Predictions of Pharmacokinetic Parameters.

CKD Stage	Predicted C_{max} (ng/mL)	Observed C_{max} (ng/mL)[a]	Predicted t_{max} (h)	Observed t_{max} (h) [a]	Predicted AUC_{∞} (ng·h/mL)	Observed AUC_{∞} (ng·h/mL) [a]
Mild	1837.89	984 (246)	3	4.48 (1.27)	18730.28	13000 (3940)
Moderate	2194.17	1320 (480)	3.50	5.24 (1.02)	27942.22	21100 (5900)
Severe	1837.82	1670 (434)	5	7.15 (1.73)	32532.47	33100 (5270)

[a] Data presented as mean (standard deviation)

3.3 Figures

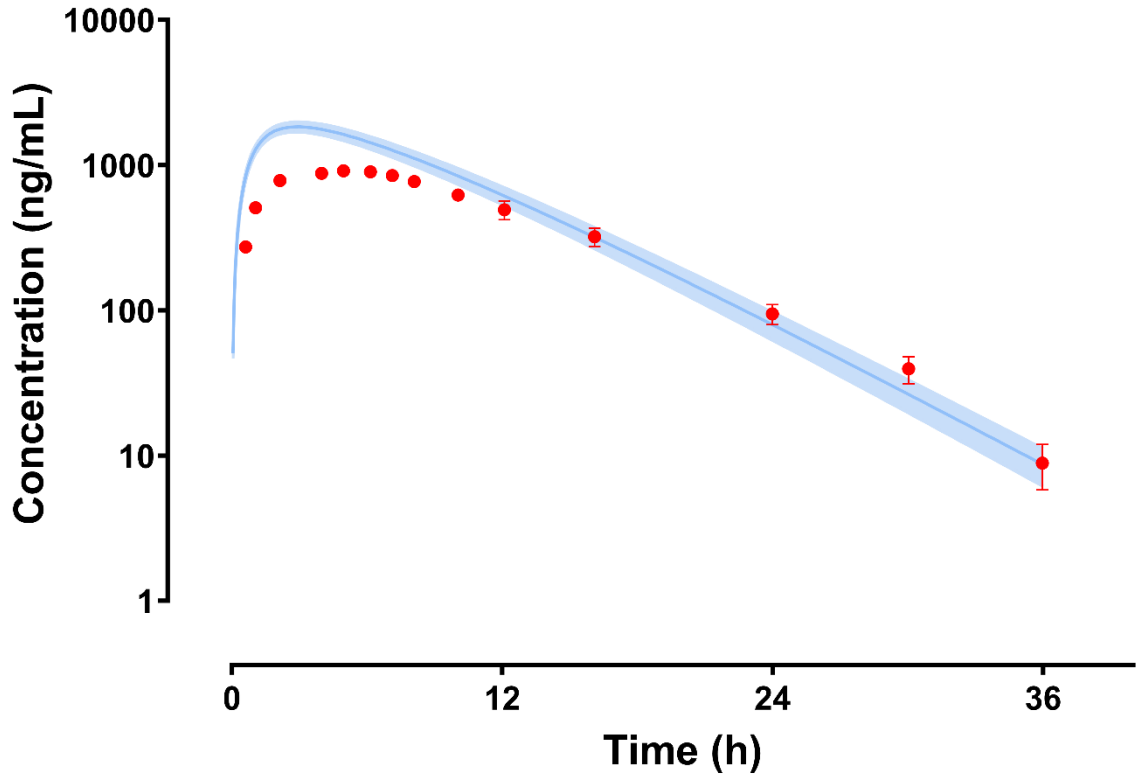


Figure 1.0 Population verification against the observed anakinra concentrations upon administration of a single 100 mg subcutaneous dose to individuals with mild chronic kidney disease within the study by Yang *et al.* [386] The solid line represents the simulated arithmetic mean and the shaded region represents the simulated standard deviation. Observed concentrations are presented as circles (mean) with standard deviation (error bars).
h; hour, ng/mL; nanogram per mililitre.

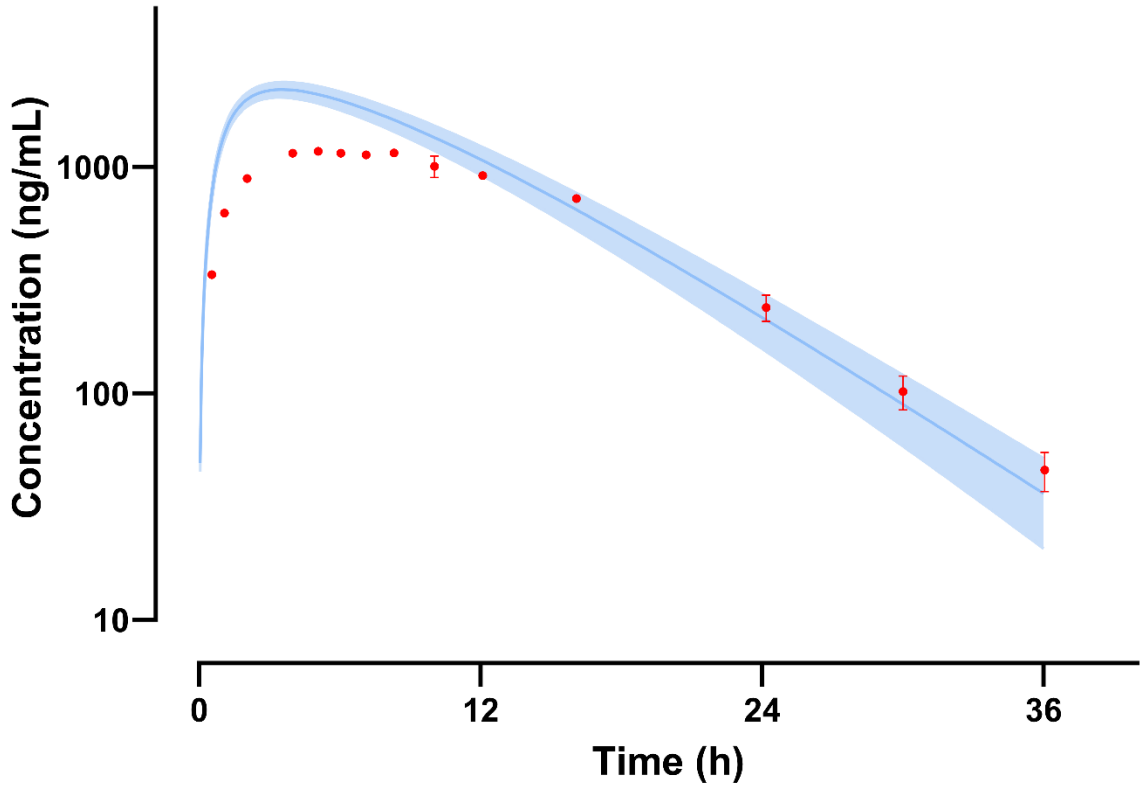


Figure 2.0 Population verification against the observed anakinra concentrations upon administration of a single 100 mg subcutaneous dose to individuals with moderate chronic kidney disease within the study by Yang *et al.* [386] The solid line represents the simulated arithmetic mean and the shaded region represents the simulated standard deviation. Observed concentrations are presented as circles (mean) with standard deviation (error bars).
h; hour, ng/mL; nanogram per mililitre.

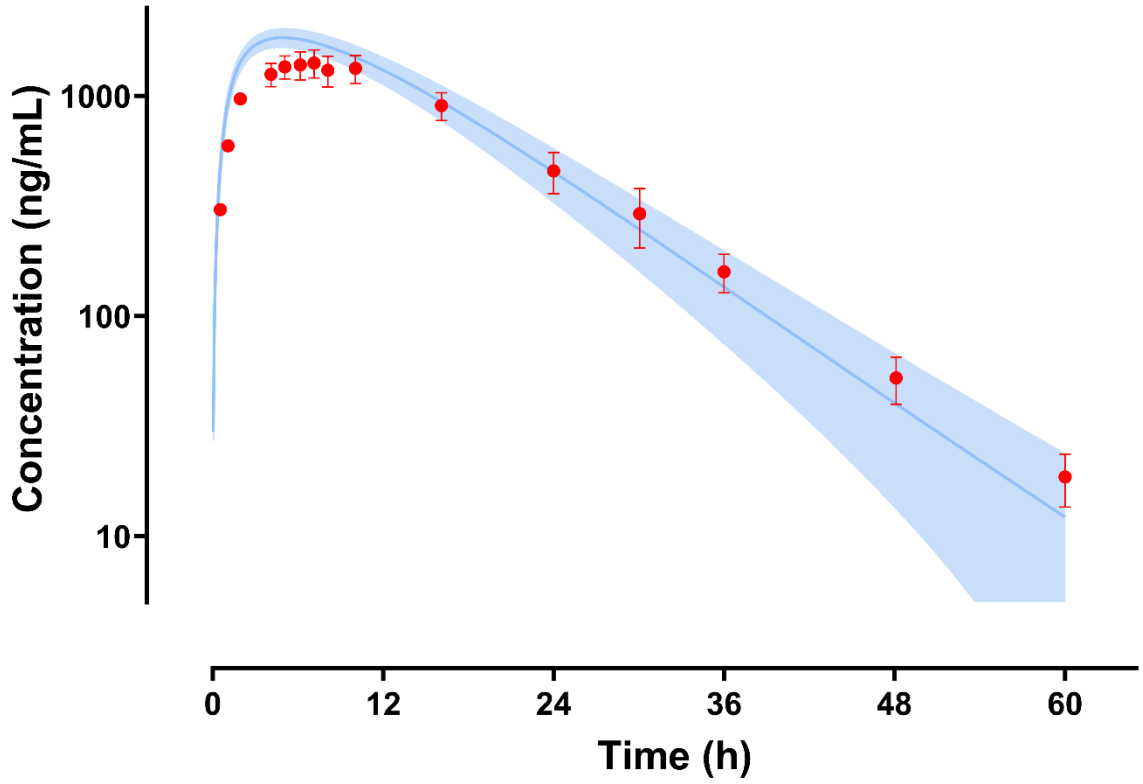


Figure 3.0 Population verification against the observed anakinra concentrations upon administration of a single 100 mg subcutaneous dose to individuals with severe chronic kidney disease within the study by Yang *et al.* [386] The solid line represents the simulated arithmetic mean and the shaded region represents the simulated standard deviation. Observed concentrations are presented as circles (mean) with standard deviation (error bars).
h; hour, ng/mL; nanogram per mililitre.

4. CRRT-PBPK Model Parameterization

4.1 Experimental Setup

Methods and data used to inform the CRRT-PBPK may be found in our previous *ex-vivo* study. [450] Information regarding CRRT circuit components and flow rates used throughout the *ex-vivo* study may be found in **Table 1** and **Table 2**, respectively.

Table 1. Continuous renal replacement therapy circuit components.

Component	Manufacturer	Model	Material
CRRT System	Baxter	PrisMax with TherMax heater	NA
Hemofilter	Baxter	HF1000 SA: 1.1m^2	PolyarylEtherSulfone hollow fibers, plasticized polyvinyl chloride tubing
Reservoir	Baxter	EXACTAMIX EVA, 500 mL	Ethylene vinyl acetate

CRRT; continuous renal replacement therapy, m^2; meters squared, mL; milliliters, NA; not applicable.

Table 2. Continuous renal replacement therapy circuit setup.

CRRT Modality	Blood Flow (mL/min)	Patient Fluid Removal Rate (mL/h)	Replacement Fluid Rate (mL/h)	Dialysis Fluid Rate (mL/h)	Total Effluent Rate (mL/h)
CVVH	80	0	Pre-filter: 600 Post-filter: 200	NA	800
CVVHD	80	0	NA	800	800
CVVHDF	80	0	Pre-filter: 300 Post-filter: 100	400	800

CRRT; continuous renal replacement therapy, CVVH; continuous veno-venous hemofiltration, CVVHD; continuous veno-venous hemodialysis, CVVHDF; continuous veno-venous hemodiafiltration, h; hours, mL; milliliters, min; minutes, NA; not applicable.

4.2 CRRT PBPK Model

A CRRT model was implemented in MoBi to simulate the removal of anakinra from plasma. The model was parameterized using the anakinra concentrations determined via a previously conducted *ex-vivo* study. [450] The CRRT system is mathematically represented by a model composed of three compartments: a filter blood compartment, a filter dialysate compartment and a reservoir compartment (**Figure 1**). Model parameters incorporated within the CRRT model development may be found in **Table 3**, with flow rates of each modality as detailed in **Table 2**. Parameters related to CRRT circuit components were included as per manufacturer (Baxter PrisMax HF 1000) specifications. Unknown parameters pertaining to anakinra degradation (δ) and membrane specific diffusion coefficients (*D*) were optimized upon the observed data. The results of each CRRT modality simulations after model parameterization are illustrated in **Figure 2**.

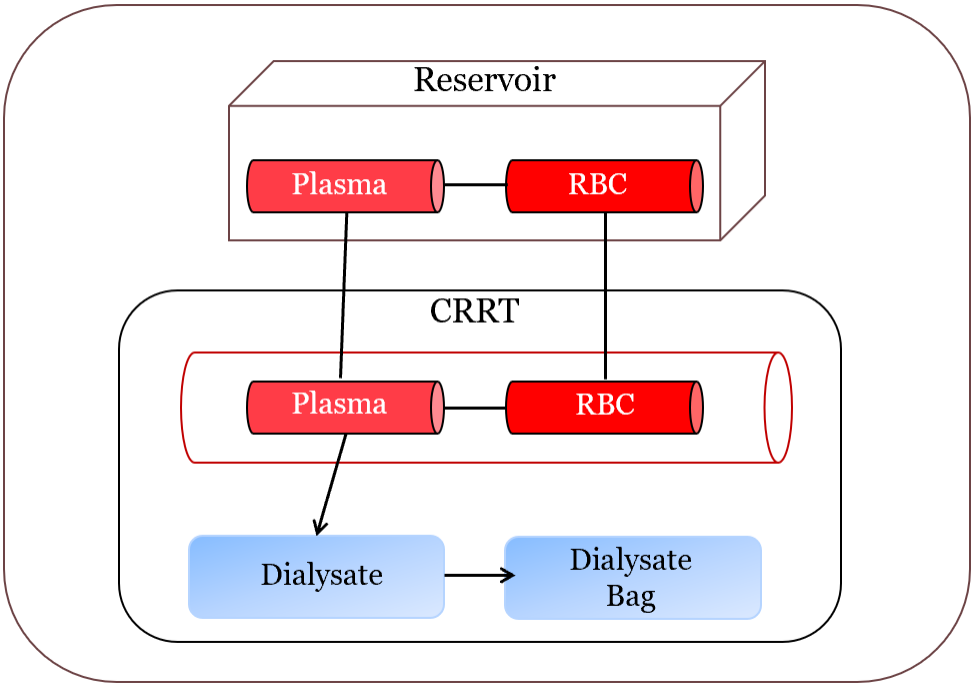
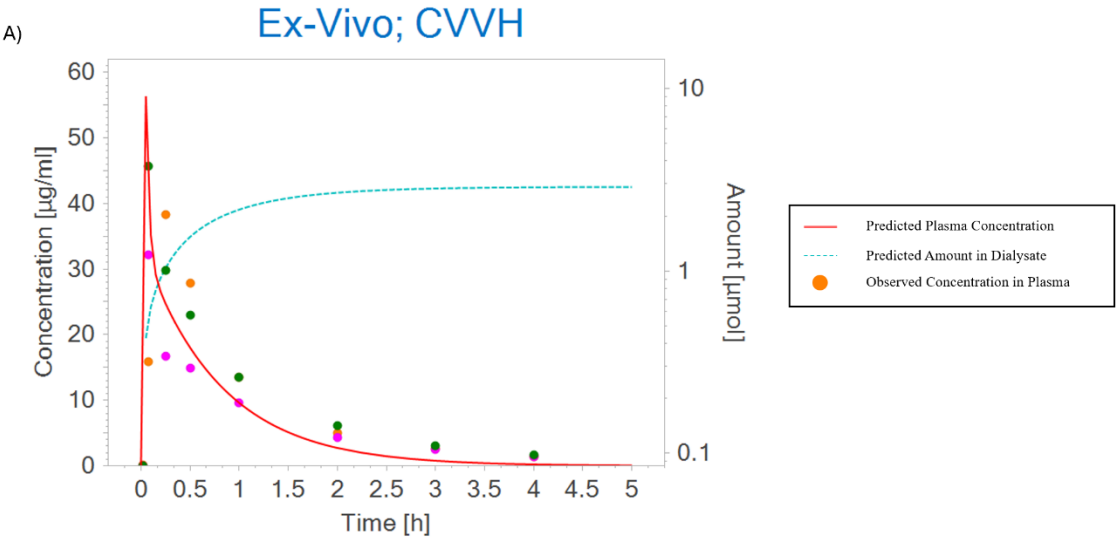


Figure 1. Continuous Renal Replacement Therapy (CRRT) circuit system utilized for physiologically-based pharmacokinetic model simulations.

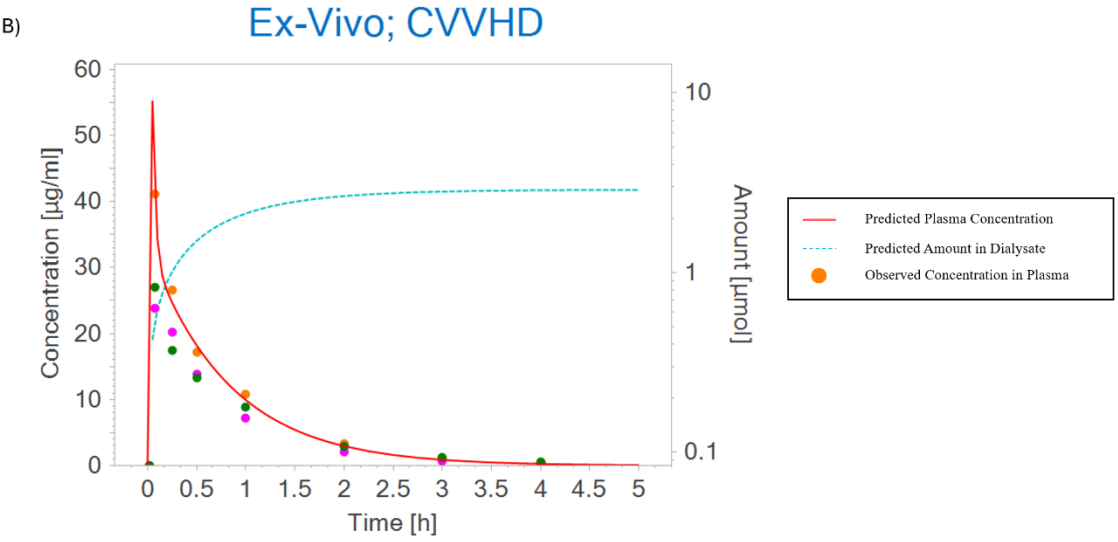
Table 3. Parameters incorporated in the CRRT model development.

Parameter	Used in Optimized CRRT Model
Membrane Surface Area	1.1 m^2 (PrisMax HF1000)
Membrane Thickness	50 µm (PrisMax HF1000)
Filter Fiber Diameter	215 µm (PrisMax HF1000)
Membrane Diffusion Coefficient (*D*)	8.39 cm^2/min (optimized)
Anakinra degradation in blood (δ)	3.70E-10 1/min (optimized)

A)



B)



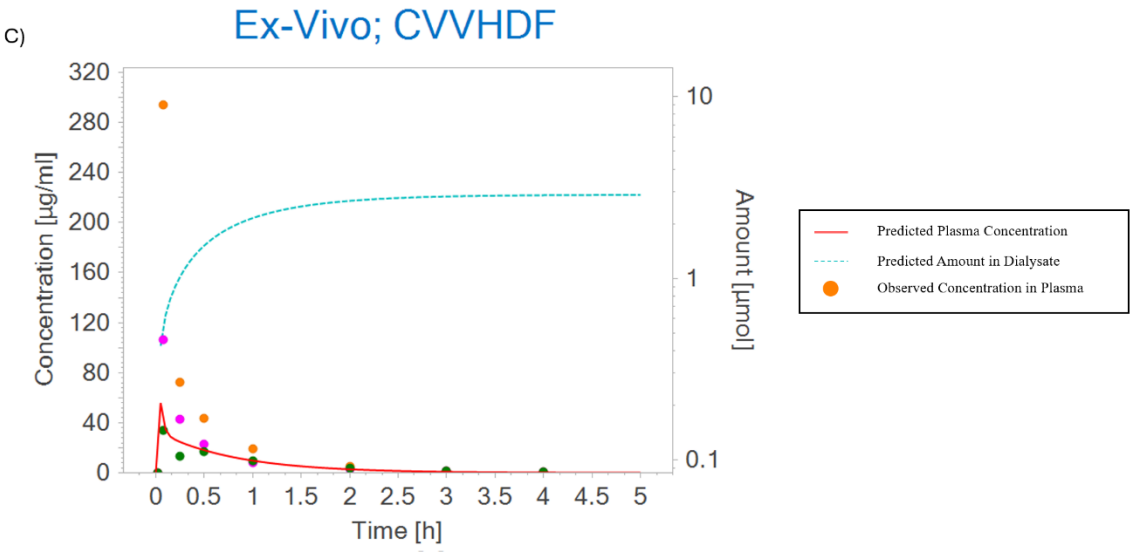


Figure 2. The continuous renal replacement therapy (CRRT) physiologically-based pharmacokinetic (PBPK) model development. The PBPK model was parameterized for each modality of CRRT, continuous veno-venous hemofiltration (CVVH; A), continuous veno-venous hemodialysis (CVVHD; B) and continuous veno-venous hemodiafiltration (CVVHDF; C) based upon the results from our previously published ex-vivo study. [450] Predicted plasma (red line) anakinra concentrations were compared to the observed values (circles), with the corresponding amount of anakinra flowing into the dialysate bag (blue dotted line). The final CRRT-PBPK ex-vivo model was then incorporated into the full pediatric PBPK model structure.

4.3 CRRT Circuit Settings for ECLS-PBPK Model Evaluation

Data from a 17-year-old individual receiving anakinra SC 100 mg every 12 hours was used for ECLS-PBPK model evaluation. This individual was simultaneously receiving CVVHDF and ECMO, the CRRT circuit settings applied were incorporated into the PBPK model. Details regarding circuit settings are shown in Table 4.

Table 4. Continuous renal replacement therapy circuit settings.

CRRT Modality	Blood Flow (mL/min)	Patient Fluid Removal Rate (mL/h)	Replacement Fluid Rate (mL/h)	Dialysis Fluid Rate (mL/h)	Total Effluent Rate (mL/h)
CVVHDF	150	300	Pre-filter: 0 Post-filter: 100	2000	2615*

CRRT; continuous renal replacement therapy, CVVHDF; continuous veno-venous hemodiafiltration, h; hours, mL; milliliters, min; minutes.
*Effluent dose of 50 mg/kg/hr was administered.

4.3 Pediatric ECLS-PBPK Model Dosing Simulations

To provide assessments of anakinra concentrations at steady state (C_{SS}) in children receiving CRRT several *in-silico* simulations were conducted. Predictions of C_{SS} at doses of 5-10 mg/kg/day divided were performed across the age spectrum. CRRT circuit settings used for each simulation may be found in **Table 5**.

Table 5. Representative CRRT prescriptions for each dosing age group incorporated within the anakinra ECLS-PBPK model simulations.

Age Group	BFR (mL/min)	DIA (mL/hr)	PBP (mL/hr)	REP (mL/hr)	UFR (mL/hr)
Neonates	20	900	0	0	120
Infants	30	500	68	100	55
Child	90	800	170	100	200
School Age	120	1300	270	100	270
Adolescents	150	2000	310	100	250

BFR; blood flow rate, DIA; dialysate flow rate, PBP; pre-blood pump flow rate, REP; replacement fluid flow rate, UFR; ultrafiltration flow rate.

Appendix F

Supplementary Material for Chapter 7

1. Building a PBPK Model for Cefazolin in Healthy Adults

1.1 Introduction

Cefazolin is a first-generation cephalosporin antibiotic used to treat infections caused by gram-positive bacteria, most notably those attributed to methicillin-susceptible *Staphylococcus aureus*. [603] The plasma protein binding of cefazolin is approximately 90%, however is unique in that it undergoes saturable protein binding at therapeutic doses. [415–417] The plasma elimination half-life of cefazolin is approximately 2 hours in healthy adults. [415,526] Most of the drug is excreted in urine unchanged (75-93%). [415,510] Renal tubular secretion dominates, as renal clearance far exceeds the glomerular filtration rate. [419,510] Organic anion transporters (OAT) are responsible for uptake into renal tubular epithelium and multi-drug resistance protein (MRP) transporters facilitate efflux into tubular filtrate. [511]

In this report, the building and verification of a PBPK model for intravenous cefazolin in healthy adults is presented. This cefazolin model was built upon a previously constructed model by Dallmann *et al*., while incorporating saturable protein binding and active tubular secretion. [504] An alternative cefazolin PBPK model was constructed by Szeto et al., which included a slightly different interpretation of the data that deserves reading. [512]

1.2 Methods and Results

1.2.1.1 Modelling Strategy

PBPK modelling and simulation were performed using PK-Sim version 11.0. Fifteen organs and two blood organs (= 17 compartments) were included in the standard model to represent a virtual adult.

1.2.1.2 Intravenous Model Construction

The process for creating the PBPK model for a healthy adult is described here. **Table 1** and **Table 2** present the drug-specific and system-dependent parameters for cefazolin values used within the naïve model.

Table 1.0. Physicochemical properties and ADME of cefazolin for IV model development

	Used in naïve model	**Used in optimized model [range of optimized values]**
Physicochemical Properties		
Octanol:water coefficient (logP)	-0.24 [502]	-0.24
Fraction unbound in plasma (f_u)	0.11 [503]	0.11
Molecular weight (MW)	455 g/mol [504,604]	455 g/mol
pKa (acid)	2.1 [292]	2.1
pKa (base)	NA	NA
Water solubility	0.350 mg/mL [504,604]	0.350 mg/mL
ADME		
Partition coefficient	Rodgers and Rowland	Rodgers and Rowland
Cell permeability	PK-Sim Standard	PK-Sim Standard
GFR fraction	1.0	1.0
OAT3 Concentration	0.0917 µM [292]	0.0917 µM
OAT3 K_M	117 µM [512,605]	117 µM
OAT3 Vmax	0 µmol/L/min	**158.98 µmol/L/min** [138.85 to 161.72]
MRP4 Concentration	0.02 µM [302,303]	0.02 µM
MRP4 K_M	81 µM [511]	81 µM
MRP4 Vmax	0 µmol/L/min	**194.57 µmol/L/min** [191.57 to 207.91]
Albumin Concentration	0.65 mmol/L [606]	0.65 mmol/L
Albumin dissociation constant (Kd)	55.82 µmol/L [415]	55.82 µmol/L
Albumin dissociation rate constant	0 1/min	**0.02 1/min** [0.02 to 0.02]

Table 2.0 System-dependent parameters used for cefazolin IV model development.

Transporter	Reference Concentration (Mean)	Reference Concentration (GeoSD)	Relative Expression	Localization	Direction	Half-life Liver (h)	Half-life Intestine (h)
OAT3	0.0917 [292]	1.53 [303]	RT-PCR [519]	Basolateral	Influx at renal tubules, efflux at blood brain barrier	36	23
MRP4	0.02 [302,303]	1.89 [303]	RT-PCR [519]	Apical at renal tubules; basolateral at blood brain barrier	Efflux	36	23

MRP4; multidrug resistance protein 4, OAT3; organic anion transporter 3, RT-PCR; reverse transcriptase polymerase chain reaction

The Rodgers and Rowland method for predicting partition coefficients and the PK-Sim Standard method for calculating cellular permeability were selected based on visual model performance and curve shape. The GFR fraction for a healthy individual was set to 1.0 allowing passive filtration to occur at the maximal filtration rate (GFR x f_u).

Active tubular secretion was parameterized by adding an OAT3 transporter on the basolateral side of the kidney cells and adding a MRP4 transporter on the apical side. The *in vitro* Michaelis-Menten constant (K_M) for MRP4 was extracted from the analysis by Ci *et al.* [511] To date, experiment K_M values for cefazolin on the OAT transporter are not available therefore it was approximated by the experimental inhibition constant (K_i) from *in vitro* measurements of ^{3}H-estrone sulfate uptake inhibition by cefazolin in HEK-292 cells. [605] Similar assumptions of OAT3 mediated uptake into renal tubule cells was conducted in the cefazolin PBPK model by Szeto *et al*. [512] The maximum rates of transport for each transporter (V_{max}) were optimized.

Active tubular secretion of cefazolin was identified by optimizing against a drug-drug interaction (DDI) study measuring intravenous cefazolin administered one hour after completion of an oral probenecid (strong OAT3 & MRP4 inhibitor) administration schedule. [419] The model for probenecid was downloaded for the Open Systems Pharmacology repository and can

be found at: https://github.com/Open-Systems-Pharmacology/Probenecid-Model. This model has been previously validated for predicting OAT1/3-mediated DDIs using furosemide as a model substrate. [292] Probenecid is a competitive inhibitor of OAT3 with an *in vitro* inhibition constant (K_I) of 5.41 µM. [292] In The DDI simulation of probenecid and cefazolin, the apparent Michaelis-Menten constant for OAT3 transport ($K_{M,app}$; Eq. 1) was calculated as:

$$K_{M,app} = K_M \times (1 + \frac{I}{K_I})$$

Eq. 1

Where *I* represents the concentration of the inhibitor, probenecid.

As previously mentioned, cefazolin is unique in that it undergoes saturable protein binding at plasma concentrations obtained at standard therapeutic doses. [415–417] To account for such processes, albumin was added as a protein binding partner within the healthy adult model with a reference concentration equal to 0.65 mmol/L and 100% expression in plasma (**Table 1**.). [[606]] A visual representation of the protein binding saturation regression adapted from Smyth *et al*. [415] may be found in **Figure 1**. The cefazolin dissociation constant from albumin (K_D) was obtained from Smyth *et al*., while the dissociation rate constant was optimized. Final parameters implemented within the healthy adult model may be found in **Table 1**.

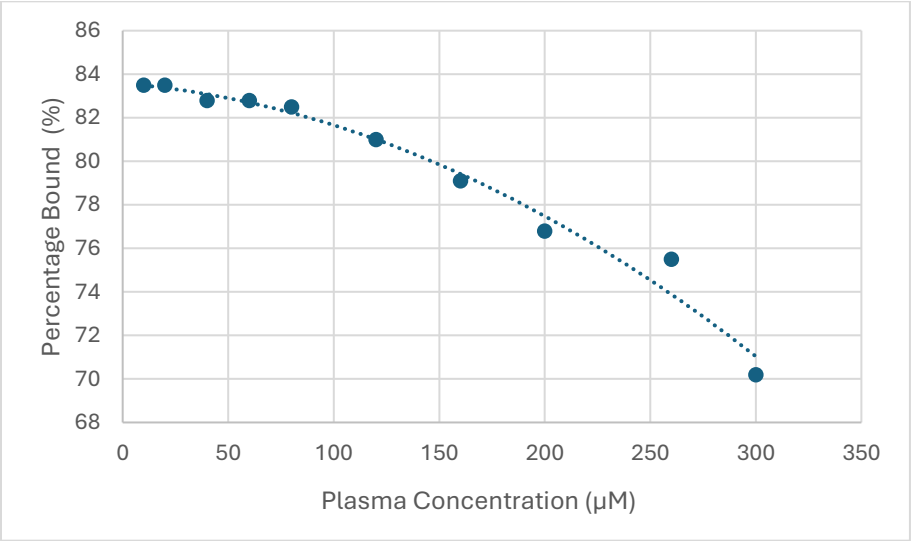


Figure 1. Plasma protein binding of cefazolin as adapted from Smyth *et al*. [415]

Table 3. presents the cefazolin datasets used for building the IV model. The maximum rate of OAT3-mediated transport and the maximum rate of MRP4-mediated transport were optimized using the parameter identification tool in PK-Sim. The optimization was performed using the Monte-Carlo method to search the parameter space for the optimal solution that minimized the sum of squared error on the simulated versus observed drug concentrations and fraction excreted to urine. Multiple Optimization runs (6 to 10) were performed to confirm identifiability of unique solution. The run with the lowest error was selected as the final solution, and those are presented in **Table 1.** The range of parameter values among the solutions is also reported to assess error, which was minimal. A comparison of the fitted IV simulation to the observed data from Brown *et al*. [419] is presented in **Figure 2**.

Table 3.0 Pharmacokinetic datasets of intravenous cefazolin for model construction

Reference	**Ethnicity**	**Dose and Administration**	**N**	**Age (years) [range]**	**Weight (kg) [range]**	**Height (cm) [range]**
Brown *et al*. [419]	North American200	2000 mg IV infusion over 10 min[a]	6	NR	NR	NR
Brown *et al*. [419]	Not reported	2000 mg IV infusion over 10 min[a] Probenecid PO 1000 mg administered 10 minutes prior to cefazolin	6	NR	NR	NR
Smyth *et al*.[415]	White American Males	2000 mg IV infusion over 30 min[a]	7	[21-35]	67±10[b]	NR

[a]Administered as sodium salt

[b]Data reported as mean ± standard deviation.

1.2.1.3 Intravenous Model Evaluation

Verification of model accuracy will be conducted using the average fold error (AFE; bias) (Eq 2.) and absolute average fold error (AAFE; precision) (Eq 3.) for each cefazolin simulation. Acceptance will be confirmed if AFE <30% (0.7-1.3) and AAFE ≤2 for simulated drug concentrations.

$$AFE = 10^{\frac{1}{N}\sum_i \log\left(\frac{predicted_i}{observed_i}\right)}$$

Eq. 2

$$AAFE = 10^{\frac{1}{N}\sum_i \left|\log\left(\frac{predicted_i}{observed_i}\right)\right|}$$

Eq. 3

Where $predicted_i$ and $observed_i$ correspond to predicted and observed plasma concentrations respectively. For data sets including individual patient samples, inter-individual variability in the population simulation will be accepted if 85-95% of observed concentrations fall within the 90th prediction interval.

Additionally, predictive accuracy of each simulation will be assessed by a limit of 1.5 fold error (0.67-1.5) when comparing simulated exposure to observed data from literature. Exposure will be quantified as the area under the concentration-time curve extrapolated to infinity (AUC_∞).

1.2.1.4 Intravenous Model Verification

The optimized IV model was verified against additional data not used in the model building process (**Table 4)**. This data was obtained from the study by Smyth *et al*. [415] which

included a dose escalation, and multiple dose analysis. **Figure 2** illustrates a good fit for describing the pharmacokinetics of cefazolin over increasing doses in these subjects. The predicted AUC_{∞} fell within a 1.25 fold-error to observed values across each cefazolin dose (**Table 6**).

Table 4.0 Pharmacokinetic datasets of intravenous cefazolin for model verification.

Reference	Ethnicity	Dose and Administration	N	Age (years) [range]	Weight (kg) [range]	Height (cm) [range]
Smyth *et al.*[415]	White American Males	2000 mg IV infusion over 30 min[a]	7	[21-35]	67±10[b]	NR
Smyth *et al.*[415]	White American Males	3000 mg IV infusion over 30 min[a]	7	[21-35]	67±10[b]	NR
Smyth *et al.*[415]	White American Males	4000 mg IV infusion over 30 min[a]	7	[21-35]	67±10[b]	NR

[a]Administered as sodium salt
[b]Data reported as mean ± standard deviation.

Table 5.0 Cefazolin IV Model Evaluation

Study	Dose	Average Fold Error	Absolute Average Fold Error
Smyth *et al.* [415]	2000 mg IV	0.95	1.15
	3000 mg IV	1.14	1.15
	4000 mg IV	1.22	1.22

Table 6.0 Exposure predictions of cefazolin IV model within healthy adults

Study	Dose	Predicted AUC	Observed AUC	Fold-Error
Smyth *et al.* [415]	2000 mg IV	472.09	509±75	0.93
Smyth *et al.* [415]	3000 mg IV	757.97	679±123	1.12
Smyth *et al.* [415]	4000 mg IV	1072.86	878±146	1.22
Philipson *et al.* [526]	500 mg IV	116.72	110±20.7	1.06

1.2.1.5 Population Verification

A population PBPK simulation was performed to verify that the model can approximate both the mean and inter-individual variability in healthy individuals. In this workflow, 1000 virtual individuals are generated, and each individual represents one full body parameter set for iterative input into the PBPK model. The resulting simulated profiles are presented in aggregate form with geometric mean and standard deviation to be compared with geometric mean and standard deviation measured in the clinical trial conducted by Smyth *et al*. [415] Additionally, a population PBPK simulation was constructed to verify that the model can approximate the pharmacokinetics in post-partum individuals within the study by Philipson *et al*. [526] The observed data used for population verification may be found in **Table 7**. A virtual population of 1000 healthy individuals were created in PK-Sim to represent the study population from Smyth *et al*. and Philipson *et al*. (**Table 8 & Table 9**). [289,415,526] Inter-individual variability in OAT3 and MRP4 reference concentration (**Table 2.**) was extracted from transporter proteomic data by Prasad *et al*. [303]

Table 7.0 Pharmacokinetic datasets for cefazolin intravenous model population verification

Reference	Ethnicity	Dose and Administration	N	Age (years) [range]	Weight (kg) [range]	Height (cm) [range]
Smyth *et al*.[415]	White American Males	4000 mg IV every 12 hours administered as a 30 min infusion[a]	7	[21-35]	67±10[b]	NR
Philipson *et al*.[526]	European Females	500 mg IV infusion over 2 min[a]	7	NR	62.3±6.3 [53.4-72.7]	NR

[a]Administered as sodium salt
[b]Data reported as mean ± standard deviation.

Table 8.0 Demographic parameters for the virtual population representing Smyth *et al*. [415]

Parameter	Value	
Population	European (ICRP)	
Number of Males	1000	
Number of Females	0	
	Minimum	**Maximum**
Age	21 years	35 years
Weight	57 kg	77 kg

Table 9.0 Demographic parameters for the virtual population representing Philipson *et al*. [526]

Parameter	Value	
Population	European (ICRP)	
Number of Males	0	
Number of Females	1000	
	Minimum	**Maximum**
Age	20 years	40 years
Weight	53.4 kg	72.7 kg

Figure 4 and **Figure 5** present the simulated concentration-time profiles for the population as compared to the observed concentrations from the studies by Smyth *et al*. and Philipson *et al*., respectively. [414,474] Visual inspection reveals that the population variability of cefazolin is captured by the healthy adult model.

1.3 Figures

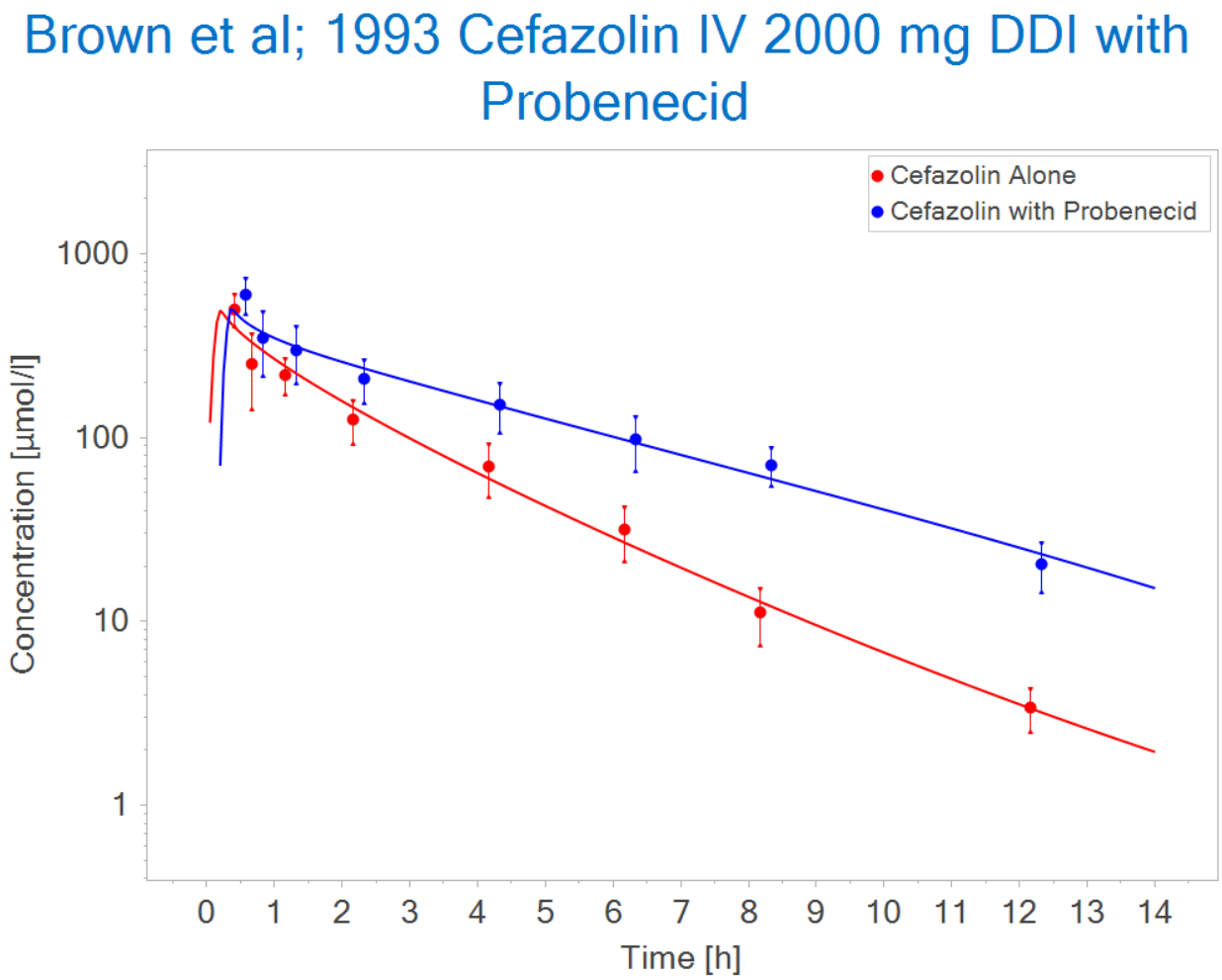


Figure 2. Simulation after optimization. Observed data reported as mean (circles) with standard error of the mean (error bars) from the study conducted by Brown *et al*. [419] The solid red ling represents the simulated plasma concentration of cefazolin IV 2000 mg infused over 10 minutes, while the blue line represents the same dose of cefazolin administered 1-hour after completion of the probenecid administration protocol.

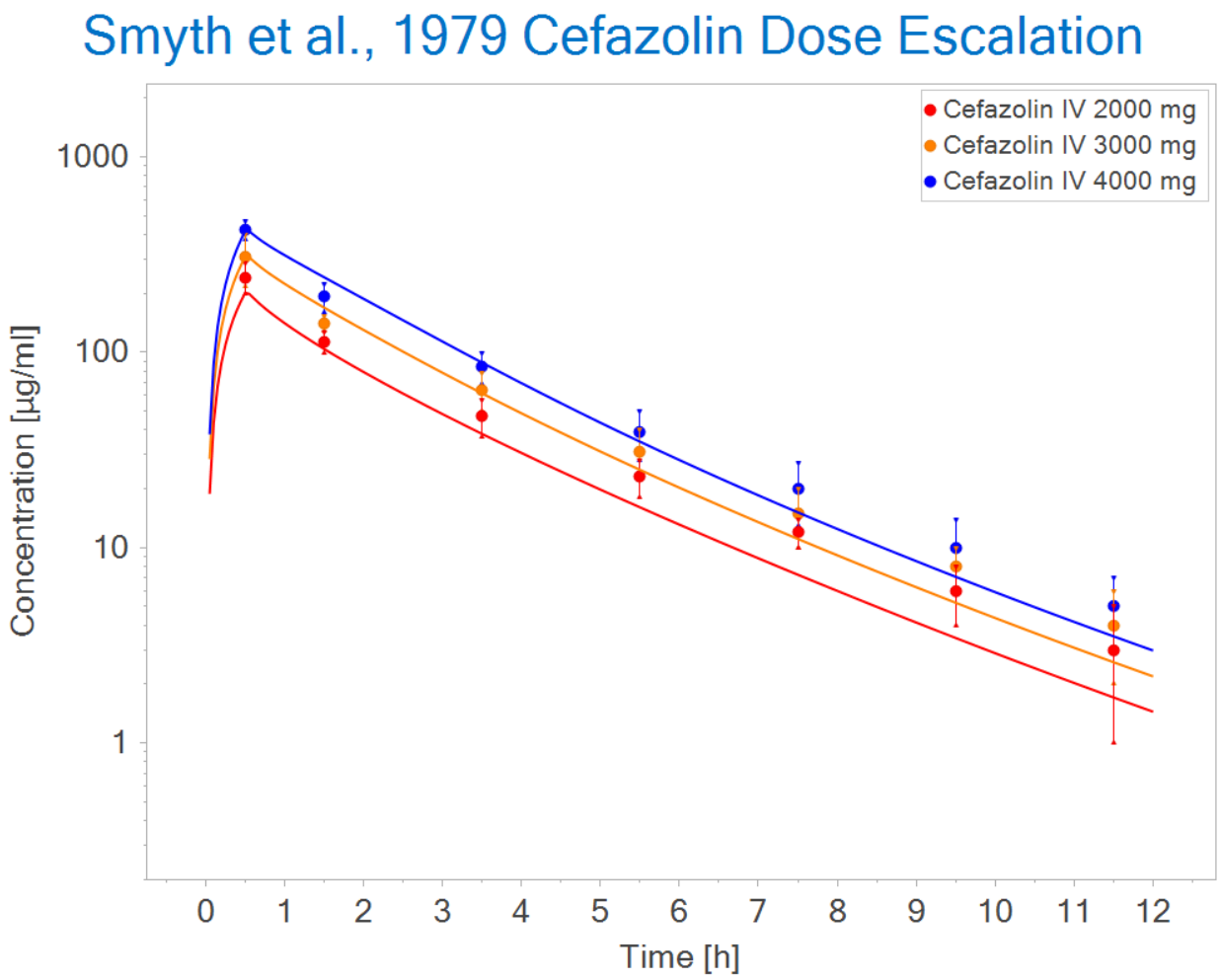


Figure 3. Cefazolin PBPK model verification against observed concentrations from individuals in the study by Smyth *et al*. [415] The solid line represents the concentration vs. time profile of the average individual while the observed data is presented as mean (circles) with standard deviation (error bars).

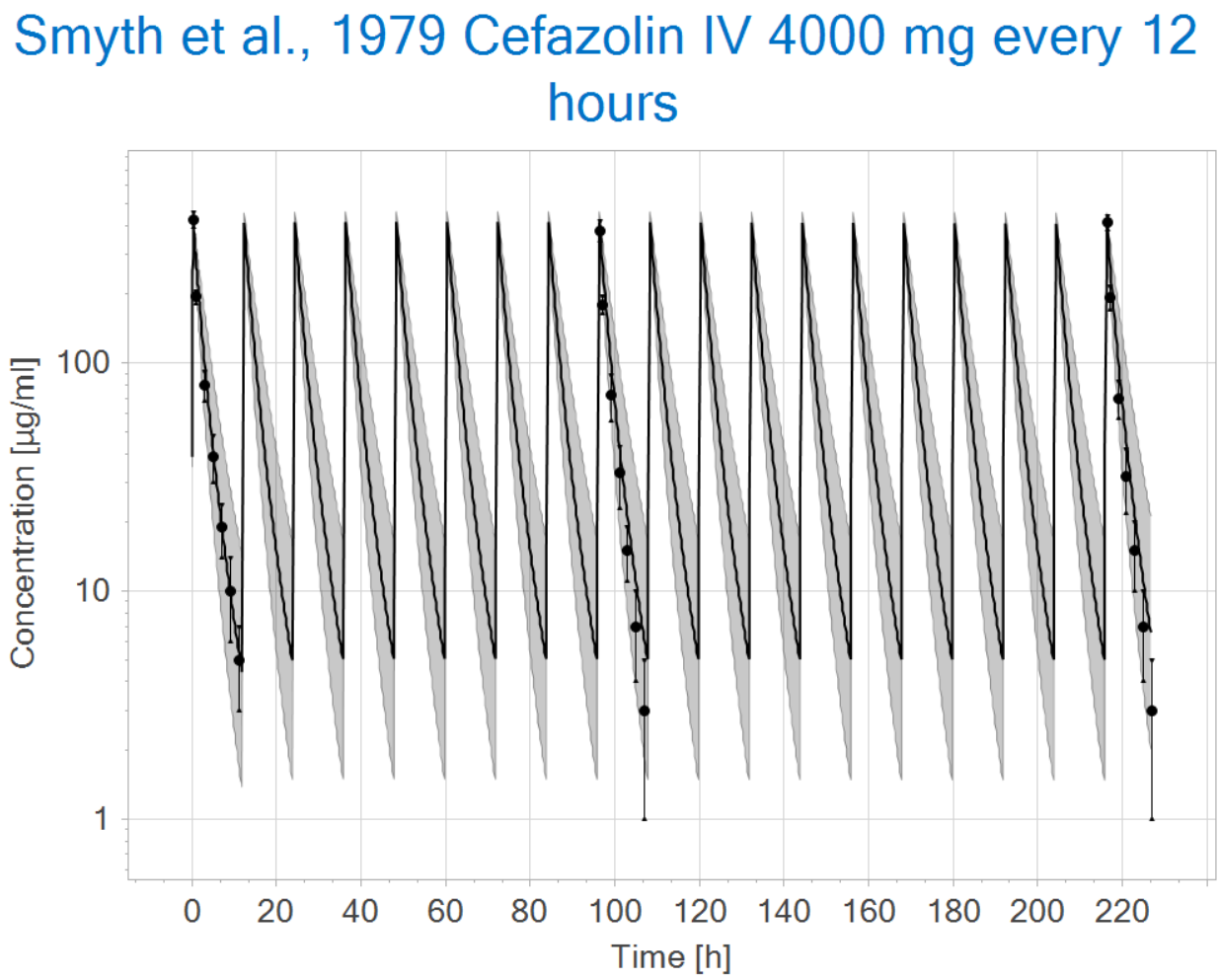


Figure 4. Population verification against the observed cefazolin concentrations from individuals within the study by Smyth *et al*. [415] The solid line represents the simulated geometric mean and the shaded region represents the simulated geometric standard deviations of the virtual population. The observed data is presented as mean (circles) with standard deviation (error bars).

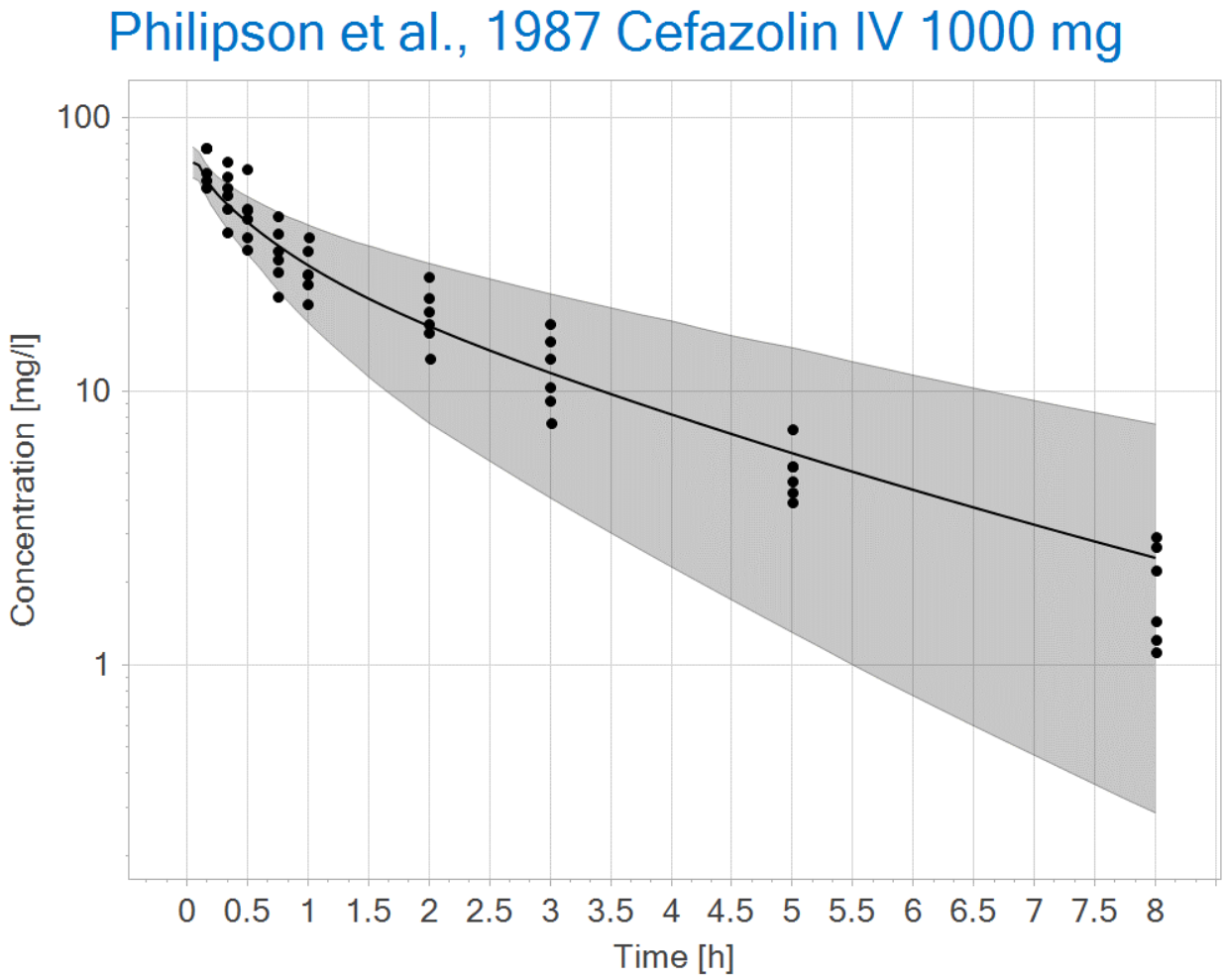


Figure 5. Population verification against the observed cefazolin concentrations from individuals within the study by Philipson *et al*. [526] The solid line represents the simulated geometric mean and the shaded region represents the simulated 5th to 95th percentile of the virtual population. The observed data is presented as mean (circles) values from study individuals.

2. Building a PBPK Model for Cefazolin Cerebrospinal Fluid Concentrations

2.1 Introduction

In this report, the parameterization of cefazolin cerebrospinal fluid (CSF) concentrations in adults is presented. The healthy adult cefazolin PBPK model (**Appendix F Section 1.**) was adapted with the purpose of determining the free-drug concentrations within the CSF.

2.2 Methods and Results

2.2.1 Modelling Strategy

PBPK modelling and simulation was performed using PK-Sim version 11.0. Fifteen organs and two blood organs (= 17 compartments) were included in the standard model to represent a virtual adult.

2.2.2 Cefazolin Cerebrospinal Fluid Model Construction

Within the healthy adult PBPK model, the brain will be subdivided into the four default compartments: blood, plasma, interstitial fluid, and intracellular compartments. The interstitial fluid compartment will be used as a surrogate to represent the CSF, a strategy that has been done previously. [508,514,515] Drug permeability into the brain was determined by Eq 1.

$$P = \left(\frac{MW_{eff} * 10^9}{366}\right)^{-6} * \frac{10^{logP}}{5} * 10^{-5}$$

Eq 1.

Where P is the specific organ permeability, MW_{eff} is the effective molecular weight, and logP is lipophilicity.[513] A virtual population of 1000 individuals will be constructed based upon the patient demographics within the cefazolin CSF pharmacokinetic studies. To obtain the permeability of cefazolin across the blood-brain barrier into the interstitial space a global optimization was performed using the parameter identification tool in PK-Sim with the observed data from Grégoire *et al* [505]. All model parameters determined in the healthy IV model were fixed during CSF model optimization.

As performed within the healthy adult cefazolin model, the optimization utilized the Monte-Carlo method to search the parameter space for the optimal solution that minimized the sum of

squatted error on the simulated versus observed drug concentrations within the CSF. Multiple Optimization runs (6 to 10) were performed to confirm identifiability of unique solution. The run with the lowest error was selected as the final solution. Data used in the construction of the cefazolin CSF model may be found in **Table 1**.

Cefazolin is a substrate for both OAT and MRP4 drug transporters. Multiple drug transporters are located at the blood-brain barrier as a method of drug efflux back to systemic circulation. [501] Proteomic data indicates that both OAT and MRP4 are localized at the blood-brain barrier. [516–518] Due to limited data on specific quantification of transporter expression, localization of OAT and MRP4 at the blood-brain barrier were incorporated within the model from the reverse transcriptase polymerase chain reaction dataset implemented within PK-Sim. [519] It was assumed that the maximum rate of transport (V_{max}) for OAT and MRP4 was consistent with the optimized value in the renal proximal tubule.

Table 1.0 Pharmacokinetic datasets of intravenous cefazolin for model construction

Reference	Ethnicity	Dose and Administration	N	Age (years) [range]	Weight (kg) [range]	Height (cm) [range]
Grégoire *et al* [505]	European	Cefazolin CI 10g/day for 6 days, then cefazolin CI 8g/day	1	42	67	NR

CI; continuous infusion, cm; centimetres, g; grams, kg; kilograms, NR; not reported.

2.2.3 Sensitivity Analysis

A local sensitivity analysis was performed to test influential parameters on cefazolin CSF concentrations. Parameters of interest included exposure between dosing intervals at steady state $AUC_{dosing\ interval}$ at steady state. Each parameter of interest included dose, brain permeability, drug transporter concentration (OAT & MRP4), lipophilicity (LogP), fraction unbound and glomerular filtration rate (GFR). Each parameter was varied by 10% and the relative changes in PK parameter of interest were reported as sensitivity coefficients. The sensitivity coefficient (S^P) for the effect of the parameter (p) on the PK output (PK) was calculates as the average of Eq 1.:

$$S^p = \left| \frac{PK(p + 0.1 \times p) - PK(p)}{PK(p)} \right| \times \frac{100\%}{10\%}$$

Eq.1

Therefore, a sensitivity coefficient of 1 means that a 10% change in the parameter value caused a ±10% change in the PK output, and a sensitivity coefficient of 0.1 means that a 10% change in the parameter value caused a ±1% change in the PK output. Simulations were built using a mean individual receiving a dose of cefazolin IV 2000 mg every 8 hours as reported by the study from Novak *et al*. [506]

2.3 Results and Discussion

Optimization of brain permeability with total and free concentrations of cefazolin from the study by Grégoire *et al*. yielded a unique solution of 2.71E-3 cm/min [2.71 to 2.72 E-3 cm/min] compared to the PK-Sim default value of 9.33E-7 cm/min. Additionally, the model was able to capture the plasma concentrations (**Figure 1.**) from the observed data. Although the model slightly over predicted total cefazolin concentrations and underpredicted free concentrations within the CSF, the optimization processes yielded a unique solution. Variability to blood brain barrier is to be expected and the identified parameter was incorporated into further model evaluations.

Local sensitivity analysis of the cefazolin CSF simulation revealed several parameters that highly influence drug concentrations within the CSF. Most notably, administered dose, brain permeability, fraction unbound, transporter concentration in the renal tubule and GFR impacted cefazolin CSF concentrations (**Figure 2.**).

Proteomic quantification of OAT and MRP4 at the human blood brain barrier indicates relatively low expression, raising the hypothesis that the efflux potential for cefazolin may be low. [516,607] The sensitivity analysis conducted within the cefazolin-CSF simulations supports this hypothesis for OAT, as the influence of the fraction expressed at the blood-brain barrier marginally impacted CSF concentrations. Further studies examining protein quantification and binding affinity for cefazolin to transporters at the blood brain barrier are warranted.

Brain permeability within the model was shown to be highly influential on cefazolin exposure within the CSF. In cases of infection, the blood brain barrier may become leaky due to an opening in the intercellular tight junctions. [501,545] Therefore, the presence of infection may result in increases in drug exposure compared to an intact blood brain barrier. Additionally, the functionality of drug-efflux transport systems may also be affected by infection. In an experimental model, the presence of meningeal inflammation due to meningitis weakened the influence of probenecid inhibition on drug-efflux transporters when penicillin G was administered by intracisternal injection. [533] As the fraction expressed of MRP4 at the blood-brain barrier influences cefazolin exposure within the CSF, there is potential for decreased functionality of drug transport out of the CSF in the presence of infection. Further *in vitro* and *in vivo* studies are warranted.

2.4 Figures

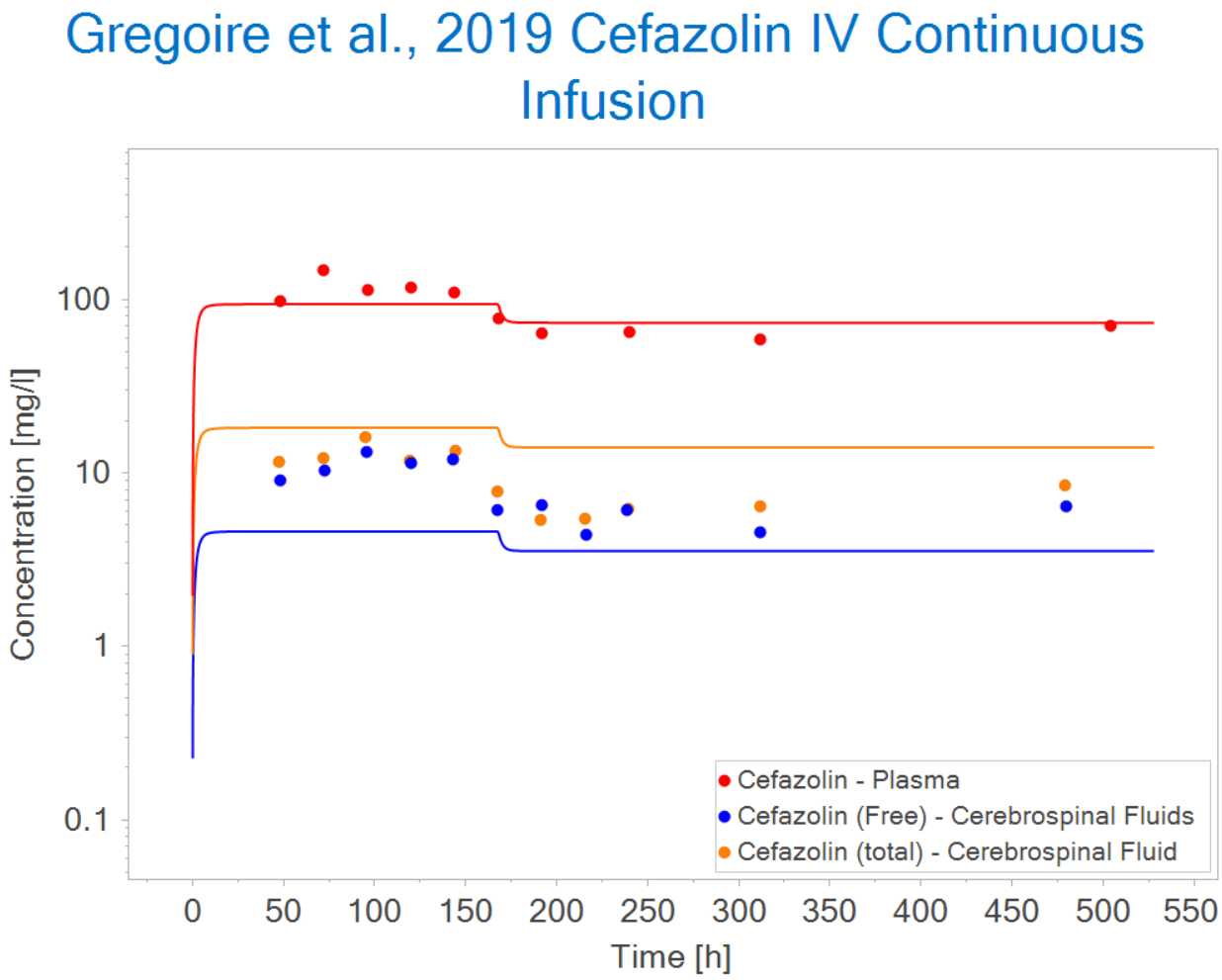


Figure 1. Simulation after optimization. Observed data reported as mean (circles) from the case report by Grégoire *et al*. [505] The solid red line represents the cefazolin plasma concentration from a continuous infusion of 10 g/day. After 6 days of therapy, the dose was reduced to a cefazolin continuous infusion of 8 g/day. The orange solid line represents the total cefazolin concentration in cerebrospinal fluid, while the blue solid line represents the free cefazolin concentration.

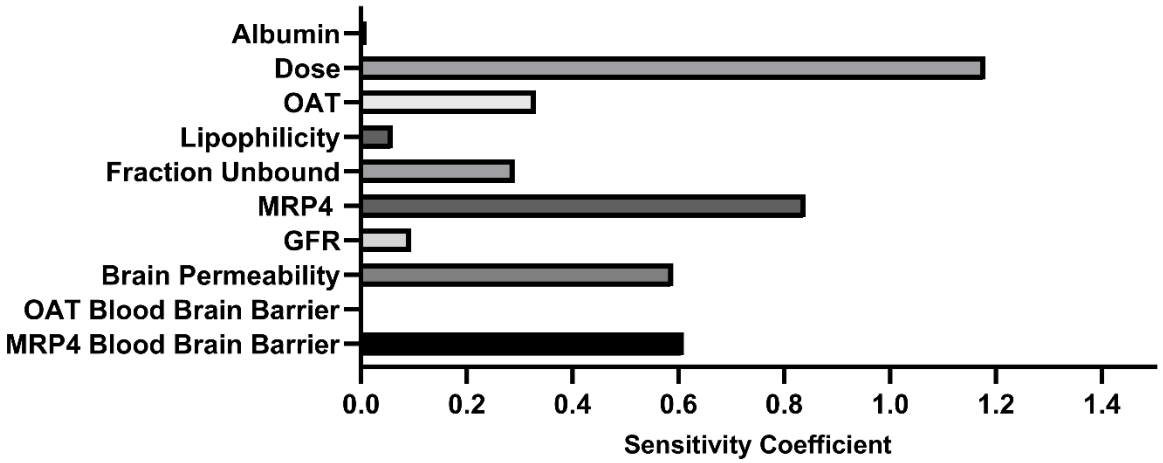


Figure 2. Local sensitivity analysis for cefazolin cerebrospinal fluid exposure was represented by the area under the curve between dosing intervals ($AUC_{dosing\ interval}$). All model parameters with varied by ±10% to analyze the relative changes in cefazolin $AUC_{dosing\ interval}$.

3. Additional Figures

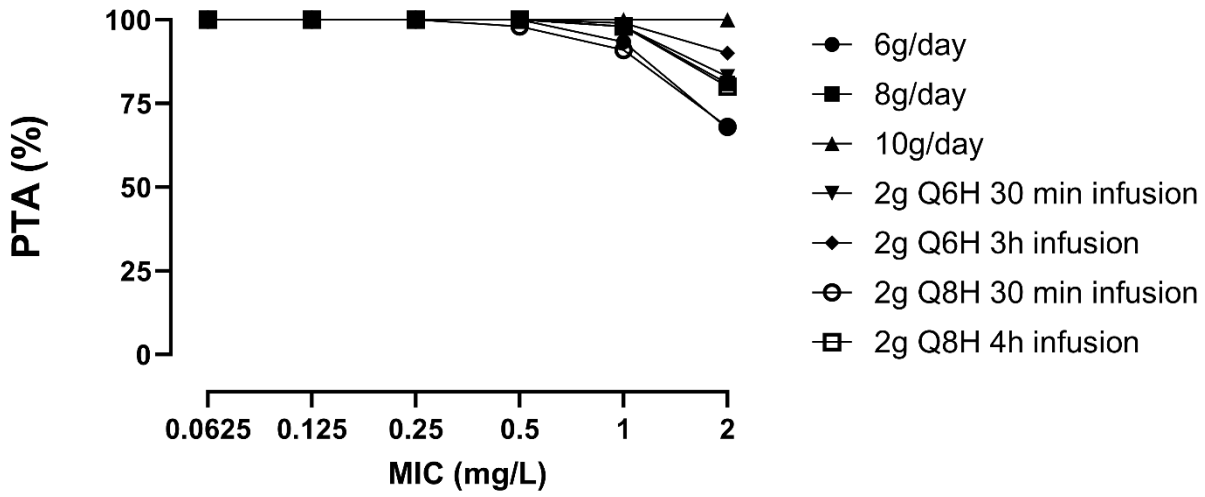


Figure 1.0 Target attainment of several cefazolin dosing protocols to reach 35% fT>MIC in the cerebrospinal fluid for the virtual population of participants from the study by Le Turnier *et al*. [2] A range of cefazolin MIC values for methicillin-susceptible *Staphylococcus* aureus (MSSA) were tested as per CLSI and EUCAST breakpoints. An epidemiological cutoff of 2.0 mg/L was incorporated. A probability of target attainment of 90% was deemed appropriate.

Table 1. Pharmacodynamic target attainment of simulated cefazolin dosing protocols for methicillin-susceptible *Staphylococcus aureus*. Data presented as the probability of target attainment in which the unbound cefazolin concentrations are 35% above the minimum inhibitory concentration (% fT>MIC) in the cerebrospinal fluid.

MIC (mg/L)	6g/day CI	8g/day CI	10g/day CI	2g Q6H 3h infusion	2g Q6H 30 min infusion	2g Q8H 4h infusion	2g Q8H 30 min infusion
0.0625	**100**	**100**	**100**	**100**	**100**	**100**	**100**
0.125	**100**	**100**	**100**	**100**	**100**	**100**	**100**
0.25	**100**	**100**	**100**	**100**	**100**	**100**	**100**
0.5	**100**	**100**	**100**	**100**	**100**	**100**	**98**
1.0	**93.4**	**98**	**100**	**99**	**98**	**98**	**91**
2.0	67	81.1	**100**	**90**	83	80	68

A Probability of target attainment of >90% to a 35% fT>MIC is represented in bold.
CI; continuous infusion, g; grams, h, hours, min; minutes, MIC; minimum inhibitory concentration, Q6H; every 6 hours, Q8H; every 8 hours.

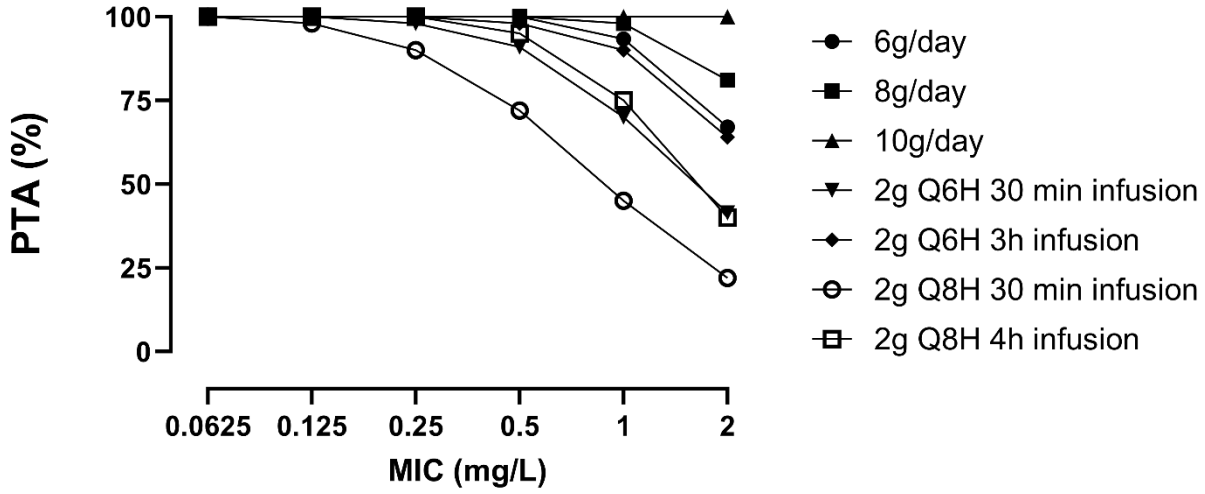


Figure 2.0 Target attainment of several cefazolin dosing protocols to reach 70% fT>MIC in the cerebrospinal fluid for the virtual population of participants from the study by Le Turnier *et al*. [2] A range of cefazolin MIC values for methicillin-susceptible *Staphylococcus* aureus (MSSA) were tested as per CLSI and EUCAST breakpoints. An epidemiological cutoff of 2.0 mg/L was incorporated. A probability of target attainment of 90% was deemed appropriate.

Table 2. Pharmacodynamic target attainment of simulated cefazolin dosing protocols for methicillin-susceptible *Staphylococcus aureus*. Data presented as the probability of target attainment in which the unbound cefazolin concentrations are 70% above the minimum inhibitory concentration (% fT>MIC) in the cerebrospinal fluid.

MIC (mg/L)	6g/day CI	8g/day CI	10g/day CI	2g Q6H 3h infusion	2g Q6H 30 min infusion	2g Q8H 4h infusion	2g Q8H 30 min infusion
0.0625	**100**	**100**	**100**	**100**	**100**	**100**	**100**
0.125	**100**	**100**	**100**	**100**	**100**	**100**	**98**
0.25	**100**	**100**	**100**	**100**	**98**	**100**	**90**
0.5	**100**	**100**	**100**	**98**	**91**	**95**	72
1.0	**93.4**	**98**	**100**	**90**	70	75	45
2.0	67	81.1	**100**	64	41.1	40	22

A Probability of target attainment of >90% to a 70% fT>MIC is represented in bold.
CI; continuous infusion, g; grams, h, hours, min; minutes, MIC; minimum inhibitory concentration, Q6H; every 6 hours, Q8H; every 8 hours.